SAPIENZA
UNIVERSITÀ DI ROMA

Thermal and dynamical response of solids within and beyond perturbation theory

Facoltà di Scienze Matematiche Fisiche e Naturali

Dottorato di Ricerca in Fisica – XXXVI Ciclo

Candidate

Giovanni Caldarelli

ID number 1718371

Thesis Advisor

Prof. Francesco Mauri

Prof. Lara Benfatto

Academic year 2023/2024

Thermal and dynamical response of solids within and beyond perturbation theory
Ph.D. thesis. Sapienza – University of Rome

This thesis has been typeset by LaTeX and the Sapthesis class.

Author's email: giovanni.caldarelli@uniroma1.it

Abstract

This thesis explores advanced aspects of lattice thermal transport and dynamical response in electronic systems, tackling unresolved questions in theoretical models of solid state physics.

We address the general theory of thermal transport, introducing a response formalism in the presence of a temperature gradient. Using a many-body Green's function approach, we compute the conductivity in ultralow thermal conductivity materials, accounting for the intraband transport of phonons. We obtain a new Kubo formula valid for strongly anharmonic systems, where conventional perturbative methods fail and phonon interactions are computed by exploiting self-consistent approaches. We derive an original expression of thermal conductivity obtained from first principles valid in self-consistent schemes, thereby advancing our understanding of heat transport near phase transitions.

We introduce a variational formulation for dynamical response functions in electronic systems including exchange interactions beyond the standard density functional theory picture. We demonstrate that this formulation yields a quadratic error dependence on the approximated electronic density matrix, enabling more accurate simulations of spectroscopic properties.

Contents

Introduction and overview

Condensed matter physics is rooted in the principles of quantum mechanics. Its foundational equations and the basic theory of solids have been firmly established and understood for about a century. As a consequence, much of recent theoretical effort in condensed matter focuses on applying known principles, with emphasis on developing innovative methods to address the computational challenges posed by the complexity of large-scale simulations. Advances in ab initio methods, combined with progress in computer architecture, have enabled researchers to perform highly accurate *in silico* experiments on crystals and molecules. These breakthroughs have established condensed matter physics as a key tool for materials science, offering unprecedented possibilities to expand the frontiers of modern technology.

However, despite our complete comprehension of its basic principles, solid-state physics presents several unresolved questions that challenge our understanding. In particular, the intricate nature of electronic response and transport phenomena in solids give rise to features that are not fully captured by current theoretical models. These aspects reveal that, even within well-defined frameworks, advancing our fundamental knowledge of condensed matter physics demands a theoretical effort to address concepts that still lie beyond our intellectual reach. In this thesis, we present our effort to grasp some of the high-hanging fruits of solid-state physics, namely the theory of thermal transport in strongly anharmonic crystals and the response of interacting electronic systems including exchange effects.

Heat conduction is one of the fundamental processes by which energy is transferred, and probably the transport phenomenon occurring in nature we witness the most. Nonetheless, the definition of flowing heat is somewhat more subtle that *e.g.* , the definition of the electrical current. Indeed, the latter is immediately defined in terms of the flux of its constituents, namely charged particles in motion under the action of an electric field. In contrast, the problem of heat transport has no such straightforward visualization. In solid-state physics we deal with systems composed by a regular array of atoms in which both electrons and the crystal lattice can participate to thermal transport. In metals the electrons are the main actors of thermal transport, whereas in electrical insulators and semiconductors the lattice of ions is responsible for heat conduction. In these systems, the phonons — *i.e.* the quantized excitations of the oscillations of the crystal lattice — behave as the heat carriers, moving heat as flowing vibrational energy. The fascinating aspect about thermal transport in solids is that even if so commonly experienced, it poses fundamental theoretical issues. How to derive the response function when the system is driven out of equilibrium by a temperature field? How can we describe the observables such as the heat flux in a quantum mechanical framework? What are the key mechanism that allow heat to flow in a solid? How do we describe heat transport in strongly anharmonic crystals where the main actors of heat transport are ill defined? Some of these questions were investigated and resolved, while others still remain open in the state of the art of the research in condensed matter.

The first Chapter of this thesis focuses on formulating a response formalism in the presence of a temperature gradient. Response functions are typically obtained assuming that an external field perturbs the equilbrium state of the system, entering as an external potential in the Hamiltonian. In the context of thermal transport, the temperature gradient plays the role of the perturbation. However, the temperature is a statistical property of the system, so it cannot be described by an external field. To describe the physical configuration of steady heat flow, we will employ a procedure based on the maximum entropy principle and a modified Liouville equation to formally account for irreversibility in the dynamics of thermal transport.[1,2] Even if specifically used in the derivation of a Kubo formula for thermal conductivity, our theoretical framework is applicable to the calculation of DC conductivities beyond thermal transport. Moreover, we will discuss how our formalism differs from standard derivation of the DC conductivity based on the adiabatic switching-on of an external "mechanical" potential that simulates the effects of a temperature field.

In the second Chapter, we employ a many-body Green's function formalism to compute thermal conductivity from the Kubo formula in materials with ultralow thermal conductivity. In the last few years, the technological interest in increasing the efficiency of thermoelectric energy-conversion devices,[3–5] or in optimizing thermal shields and thermal barrier coatings,[6–11] has stimulated intense research on materials with ultralow thermal conductivity. So-called complex crystals, defined as materials with a phonon spectrum featuring interband spacings smaller than the linewidths,[12,13] are promising candidates for these applications since their thermal conductivity is very low. More precisely, the thermal properties of complex crystals can be regarded as intermediate between those of simple crystals, where the interband spacings between phonon branches are much larger than their linewidths,[12,13] and those of glasses, where vibrational eigenstates are quasi-degenerate. In simple crystals, namely crystals with a unit cell of simple enough structure and weak anharmonicity, the picture of thermal transport describes the lattice as a phonon gas. Heat is carried by propagating phonon wavepackets moving through the system as free particles, eventually scattered by anharmonicity or disorder effects in a semiclassical picture framed by the theory of Peierls-Boltzmann Transport Equation[14] (PBTE). Ab-initio implementation of the PBTE model resulted in accurate quantitative predictions of thermal conductivity data in simple crystals.[15–25] This successful method fails spectacularly when applied to complex crystals.[26–32] The intermediate nature between a crystal and a glass of complex crystals has been related by several works[12,26,29,32–34] to the coexistence of Peierls-Boltzmann transport,[14,35,36] associated with intraband transport, and interband transport, dominant in amorphous media.[37,38] In fact, interband transport is enabled by large broadening of the phonon branches due to anharmonicity or disorder.

In order to account for both interband and intraband transport, we derive a full quantum description of heat transport using a many-body Green's function approach applicable to the case of complex crystals. We will explain analogies and differences between the various existing approaches,[12,33] with the goal of pointing to a consistent theoretical framework for the computation of lattice thermal conductivity. More specifically, we derive the thermal conductivity in the so-called dressed-bubble approximation, where the effects of anharmonicity and disorder are encoded via renormalized phonon spectral densities including all self-energy corrections. We provide a general expression able to describe thermal transport both in the low-damping regime, where phonon excitations are still well defined and interband transport is eventually relevant for densely spaced phonon bands, and in the overdamped

regime, where the phonon quasiparticle picture breaks down. Still, our dressed-bubble approximation consist in a particular truncation of the diagrammatic expansion around the fully anharmonic Born-Oppenheimer Hamiltonian, justified within perturbation theory. We show that our findings coincide with the expression obtained in some recent theoretical studies,[12,13] but slightly differ from others.[33,39] Despite formal differences between existing formulations, the numerical results for thermal conductivity are quantitatively very similar. We investigate two test cases: perovskite $CsPbBr_3$ and zirconate $La_2Zr_2O_7$, both materials with ultralow thermal conductivity. In these systems, we find that the different formulations lead to little or negligible numerical discrepancy, and the different approaches give successful predictions in agreement with experimental data. We then investigate the theoretical foundations for the consistency among the results obtained from different formulations, arguing if some invariance principle of transport coefficients lies behind such similarities.[40]

In the third Chapter, we develop a nonperturbative theoretical framework for lattice thermal transport. Anharmonicity becomes particularly relevant near structural phase transitions or at elevated temperatures, where traditional theoretical approaches struggle. Most established theoretical methods for studying lattice transport rely on perturbation theory,[12,15,41–47] treating anharmonicity as a small correction to an ideal network of harmonic oscillators. However, perturbative approaches are inapplicable in regimes of strong anharmonicity. In instances where the crystal structure is stabilized by thermal or quantum fluctuations, such as in the high-temperature phases of ferroelectric materials,[48,49] a standard perturbative calculation may yield imaginary phonon frequencies, giving a misleading indication of lattice instability. To address this limitation, modern strategies introduce self-consistency by solving lattice equations iteratively, thus capturing the full impact of anharmonicity nonperturbatively.[50–55] As an example, the self-consistent harmonic approximation (SCHA) is among the most advanced theoretical tools used to model crystals at the verge of structural instabilities.[50,56] In the SCHA, the density matrix of the interacting lattice is approximated with a Gaussian density matrix, describing the system as a set of effective harmonic oscillators. The interatomic force constant matrix and the equilibrium position of the ions are optimized to obtain the best estimate of the free energy of the fully anharmonic lattice of ions. As a result, the interatomic force constants acquire a temperature dependence, indicating the self-consistency of the model Hamiltonian that describes the system.

Nevertheless, in previous works the equations for thermal conductivity are derived within standard linear response, where the temperature variation is a small perturbation to a temperature-independent Hamiltonian.[44,57–59] As we will discuss in the first Chapter, within this approch the equations for thermal conductivity are derived assuming no temperature dependence of the lattice Hamiltonian, while self-consistent methods embed anharmonicity in temperature dependence of renormalized phonon frequencies and interatomic force constants. The introduction of self-consistency and temperature-dependent Hamiltonians in the thermal transport equations challenges the fundamental assumptions underlying such derivation of the linear response transport coefficients. Consequently, the common methodology of incorporating frequencies, scattering rates, and other lattice properties obtained from self-consistent schemes into the expressions for thermal conductivity based on linear response theory[49,60–64] lacks theoretical justification and thus predictive capabilities.

To formulate a theoretical approach suitable for studying thermal transport in strongly anharmonic crystals, we rephrase the formalism introduced in Chapter 1 for a self-consistent

framework. The maximum entropy principle and modified Liouville equation approach is particularly effective in treating self-consistent systems since it solely relies on manipulations of the density matrix and of the self-consistent Liouville operator that approximates the exact dynamics. We thus obtain a Kubo formula for thermal conductivity valid in time-dependent self-consistent dynamics. Then, we apply it to the dynamical extension of the self-consistent harmonic approximation. The idea behind the time-dependent self-consistent harmonic approximation (TD-SCHA) introduced in Ref. 65 is to constrain the ionic density matrix to be the most general Gaussian in Cartesian coordinates with time-dependent free parameters. In Ref. 65, a set of self-consistent equations of motion for the parameters of the Gaussian are derived by minimizing the quantum action.[65,66] However, the original formulation of the TD-SCHA is complex, necessitating an effort to gain a physical understanding of the parameters. We thus reformulate the TD-SCHA in the Wigner formalism, where the density matrix becomes a function of position and momentum in quantum-phase space. This approach makes the TD-SCHA equations more compact and intuitive. Most importantly, the Wigner formulation allows for a diagrammatic interpretation of the response functions obtained in TD-SCHA, granting a clear understanding of the variety of the anharmonic scatterings included in the theory and enabling easier comparisons with other existing theories of lattice dynamics.

We use this diagrammatic picture to interpret thermal conductivity as a two-phonon response function. Finally, by applying our newly formulated Kubo expression for self-consistent schemes, we find that thermal conductivity diverges in TD-SCHA. This limitation stems from an intrinsic shortcoming of the TD-SCHA itself: in the approximate self-consistent dynamics, the dressed-bubble diagrams —responsible for the natural decay of the heat-flux autocorrelation function and the resulting finite conductivity— are absent. Thus, while the TD-SCHA represents on of the most advanced first-principles approach to lattice dynamics, it still does not offer a fully nonperturbative model for thermal transport.

Our profound study of linear response in self-consistent schemes served us to face another theoretical challenge. In the fourth Chapter, we present a variational formulation of the dynamical response function in electronic systems within generalized TD-DFT with hybrid functionals, TD-HF and Bethe-Salpeter equation approaches. Following linear response theory,[67,68] the electronic response functions can be written in terms of a dressed (or screened) vertex and a bare (or unscreened) one. We refer to this formulation as 'bare-screen'. Nonetheless, if some approximations for the vertices are performed, the bare-screen structure yields results that are not the closest to the exact solution. It has been discussed in Ref. 69 for static perturbations, extended to time-dependent perturbations in Ref. 70 and recently confirmed in Ref. 71, that an exact rewriting of the response function in terms of dressed vertices corresponds to a variational formulation in terms of the electronic density. Within such formulation, any approximation of the self-consistent density, and hence of the self-consistent vertices, affects the value of the response function to the second order, contrary to the bare-screen case which is affected to the first order. We refer to this variational formulation as the 'screen-screen' approach.

Our goal is to extend the results of the Refs. 69 and 70 for a generic response function, and for a wider class of problems. In particular, we consider systems that can be described via generalized Kohn-Sham equations,[72] i.e. containing nonlocal electronic interactions. We operate neglecting retardation effects in the screening of the electronic interactions, as per the adiabatic approximation of time-dependent density functional theory (TD-DFT).[73–75] Several

theoretical schemes can be recovered as particular cases of our framework, such as time-dependent Hartree-Fock[76,77] (TD-HF), TD-DFT[73,74] with (global[78,79] or range separated[80–83] hybrid functionals), and the Bethe-Salpeter equation[84–86] (BSE) within the static-screened exchange (SX) approximation.[87] The central achievement of our work consists in obtaining an exact rewriting of the response function in terms of screened electronic vertices, that is variational with respect to the one-body electronic density-matrix. Our result is in close analogy to the screen-screen approach of Ref. 70, but valid for a wider class of electronic interactions and any linear response. In fact, the generality of this response formalism enables the investigation of virtually any type of electronic response, including the interatomic force constants used to compute phonons, and the electronic polarizability used to obtain optical or finite momentum transfer properties. We complement our study by presenting another formulation, referred to as 'screen*-screen', first introduced in Ref. 88 for DFT-like formalisms, and recently extended to the exact many-body response in Ref. 89. Here, the response function is rewritten exactly in terms of two vertices that are one the complex conjugate of the other. We show that the screen*-screen formulation is not variational in the density matrix, but it allows the rewriting of the imaginary part of the response function exactly as a generalized Fermi Golden Rule. Being positive definite, it can be used to justify semiclassical Boltzmann equation approaches, where the dissipation is viewed as a scattering probability.

We implement a computational procedure based on a set of self-consistent equations for the electronic density matrix to determine the response functions. The level of our approximation is equivalent to the SX+BSE methods, as developed e.g. in Refs. 90, 91. We illustrate our developments with an application to graphene, where excitonic effects are relevant in the description of several spectroscopic features.[92–100] In our practical application, we focus on the optical conductivity in the various formulations for the response function. We numerically demonstrate that the screen-screen approach is variational with respect to the electronic density matrix, while the others are not. As further proof, we show that when the optical conductivity is obtained using an approximated density matrix, the screen-screen approach approximates the exact optical conductivity with a quadratic error, while bare-screen and screen*-screen display a linear error.

Chapter 1

Lattice thermal transport in perturbative approaches

Introduction

One of the theoretical challenges presented by thermal transport is to formulate the response formalism in presence of a temperature gradient. Response functions are typically obtained assuming that an external field perturbs the equilbrium state of our system, entering as an external potential in the Hamiltonian. Physical quantities are then obtained performing a linear expansion with respect to the external field. In the context of thermal transport, the temperature gradient plays the role of the perturbation. However, the temperature is a statistical property of the system, so it cannot be described by an external field: we will discuss how the perturbation can be intended as "statistical", entering the system through the density matrix.[44] We will deal with open systems, so non-isolated systems in contact with a bath, which build up the temperature gradient and drive the system out of equilibrium. In this configuration, the non-equilibrium state can be maintained indefinitely; this is what we will refer to as a "steady state".[101] Thermal transport is treated by considering the system in a local equilibrium state, characterized by a nonuniform temperature profile. This is a valid assumption provided that temperature varies slowly on a scale larger than the microscopic relevant length, e.g. the lattice spacing.

In this Chapter, we formulate a theoretical approach suitable for studying thermal transport. To achieve this, we follow the footprints of the works by Zubarev,[102,103] formally deriving the state of local thermal equilibrium. We do so employing the Maximum Entropy Principle to obtain the steady state-density matrix in the presence of heat flow and a modified Liouville equation to formally account for irreversibility in the dynamics of thermal transport (cfr. 1 Sec. 20,[2] Sec. 2.1) In devising a modified Liouville equation, we establish a theoretical framework applicable to the calculation of DC conductivities beyond thermal transport. Moreover, we will discuss how our formalism differs from standard derivation of the DC conductivity based on the adiabatic switching-on of an external "mechanical" potential that simulates the effects of a temperature field.[44,57,104]

Chapter Overview

This Chapter is organized as follows: in Sec. 1.1 we provide a general introduction to thermal transport, discussing some subtleties that differentiate this intricate problem from standard response theory. In Sec. 1.2, we introduce the maximum entropy principle used to derive the local equilibrium and the steady-state density matrix from which the thermal conductivity can be computed. In Sec. 1.3 we calculate the steady-state density matrix solving a modified Liouville equation, introducing an approach that will serve us for the calculation of the Kubo formula for thermal conductivity in self-consistent dynamics. Finally, in Sec. 1.4 we draw some conclusions.

1.1 Situating thermal transport in linear response theory

Thermal transport occurs when heat flows in an inhomogeneous temperature field. The thermal conductivity $\kappa^{\mu\nu}$ is the ratio between the heat flux $\boldsymbol{J}$ and the temperature gradient $\boldsymbol{\nabla}T$

$$J^{\gamma} = -\sum_{\nu} \kappa^{\gamma\nu} \boldsymbol{\nabla}^{\nu} T \,, \tag{1.1.1}$$

where $\gamma, \nu{=}x, y, z$ are cartesian indices (bold lettering indicates cartesian vectors). In quantum mechanics, the heat flux $\boldsymbol{J}$ is the expectation value of the operator $\hat{\boldsymbol{J}}$ (a caret over a letter will be used to indicate quantum-mechanical operators)

$$\boldsymbol{J} = \mathrm{Tr}\left[\hat{\boldsymbol{J}}\hat{\rho}_{\mathrm{st}}\right], \tag{1.1.2}$$

where $\hat{\rho}_{\mathrm{st}}$ is the quantum statistical operator (density matrix) that describes the steady-state: a nonequilibrium state that features nonuniform temperature and steady currents.

The thermal conductivity is defined by computing $\hat{\rho}_{\mathrm{st}}$ at linear order in the gradient of the temperature field $T(\boldsymbol{x})$, considered as a perturbation. On general ground, this problem is analogous to the linear response to a static perturbation. The typical example is the current response to an electrostatic potential $\phi(\boldsymbol{x})$:

$$J_e^{\gamma} = -\sum_{\nu} \sigma^{\gamma\nu} \boldsymbol{\nabla}^{\nu} \phi \,, \tag{1.1.3}$$

where $\sigma^{\gamma\nu}$ is the (DC) electrical conductivity and $\boldsymbol{J}_e$ the electrical current. However, the derivation of $\kappa^{\mu\nu}$ is conceptually different from the standard derivation of the electrical conductivity in linear response to a static perturbation. In fact, in the case of a *mechanical* process, the static perturbation enters in the Hamiltonian of the system as $\hat{H}_{\mathrm{tot}}{=}\hat{H}{+}\hat{H}^{(1)}$ via an adiabatic switching-on hypothesis.[105,106] In this scheme, the state where the current is computed is reached at $t{=}0$ after the switching-on of the perturbation $\hat{H}^{(1)}$ from $t{=}{-}\infty$. In practical terms, one expands the density matrix $\hat{\rho}(t{=}0) \propto e^{-\beta(H+H^{(1)})}$ at linear order in $H^{(1)}$ with respect the unperturbed state $\hat{\rho}(t{=}{-}\infty){\propto}e^{-\beta\hat{H}}$ realized at $t{=}{-}\infty$ to get:

$$\boldsymbol{J}_e = \mathrm{Tr}\left[\hat{\boldsymbol{J}}_e(\hat{\rho}(t{=}0){-}\hat{\rho}(t{=}{-}\infty))\right] \simeq \mathrm{Tr}\left[\hat{\boldsymbol{J}}_e\hat{\rho}^{(1)}\right] \,, \tag{1.1.4}$$

where we defined $\hat{\rho}^{(1)} \simeq e^{-\beta(H+H^{(1)})}{-}e^{-\beta\hat{H}}$. An implication of the adiabatic switching-on hypothesis is that the state where the current is computed has *lower* entropy than the initial state: the drift current moves all the charges of the same sign towards the minimum of the potential $\phi(\boldsymbol{x})$, resulting in a more ordered configuration than the initial one.

In the case of thermal transport one does not have a mechanical perturbation. As it has been originally suggested in Ref. 1,2,107, the current can be derived in this case by a process of entropy maximization. We will discuss in details in this Section the theoretical procedure to derive the steady-state density matrix $\hat{\rho}_{\text{st}}$ in the presence of a thermal current from the maximum entropy principle (MEP) or equivalently in Sec. 1.3 from a modified Liouville equation. Exploiting the MEP, we show that the density matrix that describes the state of the system in presence of an inverse temperature field $\beta(\boldsymbol{x})=\frac{1}{k_B T(\boldsymbol{x})}$ is

$$\hat{\rho}_{\text{loc}} \propto e^{-\int \mathrm{d}\boldsymbol{x}\hat{h}(\boldsymbol{x})\beta(\boldsymbol{x})}\,, \tag{1.1.5}$$

where the energy density operator $\hat{h}(\boldsymbol{x})$ is defined through its relation with the Hamiltonian $\hat{H}$ via an integral over the volume V of the system as

$$\hat{H} = \int_V \mathrm{d}\boldsymbol{x}\, \hat{h}(\boldsymbol{x}) \tag{1.1.6}$$

(if not specified, spatial integrals are intended as performed over the volume V). As a local maximum of the entropy, we dub the state represented by $\hat{\rho}_{\text{loc}}$ in Eq. (1.1.5) a local equilbrium state. We will show that the local equilibrium state is not a constant of motion and it does not sustain currents; it is thus unable to describe the steady state we seek. Nonetheless, the steady state $\hat{\rho}_{\text{st}}$ can be obtained from the application of the MEP with the additional requirement of stationarity, *i.e.* $[\hat{\rho}_{\text{st}}, \hat{H}]=0$. In doing so, we will obtain a steady-state $\hat{\rho}_{\text{st}}$ that still retains the information on the local temperature $T(\boldsymbol{x})$, but with a modified energy density.

A key step in our formalism is to show that the steady state obtained from the MEP can also be written as the static solution of a modified Liouville equation.This result will allow us to extend in a compact and elegant way the same formalism to the case of the self-consistent approach to interacting systems, discussed in Chapter 3.

The modified Liouville equation describes a relaxation process that is conceptually different from the adiabatic switching-on of a mechanical perturbation. In fact, we will discuss how in the modified Liouville equation the steady-state is forced to relax to the local equilibrium state, with a dynamics that increases the entropy by construction. As per Eqs. (1.1.3)-(1.1.4), the thermal conductivity is obtained by computing the expectation value of the heat flux at linear order in the gradient $\boldsymbol{\nabla} T(\boldsymbol{x})$ of the temperature field, by expanding the steady state with respect to the local equilibrium state, *i.e.*

$$\boldsymbol{J} = \mathrm{Tr}\left[\hat{\boldsymbol{J}}(\hat{\rho}_{\text{st}}-\hat{\rho}_{\text{loc}})\right] \simeq -\sum_{\nu} \kappa^{\gamma\nu}\boldsymbol{\nabla}^{\nu} T\,. \tag{1.1.7}$$

As we will show, the local equilibrium $\hat{\rho}_{\text{loc}}$ is a state with *higher* entropy than the steady state. This is the opposite of what happens in the adiabatic switching-on approach encoded in Eq. (1.1.4), where the current-carrying state has lower entropy than the unperturbed state. In addition, the dynamics dictated by the modified Liouville equation, and encoded in Eq. (1.1.7), implies that the current is measured after that the system has evolved from the steady-state realized in the far past to the local equilibrium. In other words, the difference $\hat{\rho}_{\text{st}}-\hat{\rho}_{\text{loc}}$ in Eq. (1.1.7) corresponds to a difference $\hat{\rho}(t=-\infty)-\hat{\rho}(t=0)$:

$$\boldsymbol{J} = \mathrm{Tr}\left[\hat{\boldsymbol{J}}(\hat{\rho}(t=-\infty)-\hat{\rho}(t=0))\right] = \mathrm{Tr}\left[\hat{\boldsymbol{J}}(\hat{\rho}_{\text{st}}-\hat{\rho}_{\text{loc}})\right] \tag{1.1.8}$$

that has the *opposite* sign of what one usually obtains in the case of mechanical perturbation, see Eq. (1.1.4).

This subtle difference between the electrical and thermal transport has been often overlooked in the attempts present in the literature to derive the thermal conductivity by response to a fictious mechanical force. The idea, originally elaborated by Luttinger,[57] is to define a "mechanical proxy" that reproduces the effects of a thermal gradient. One then starts from the local density matrix $\hat{\rho}_{\text{loc}}$ of Eq. (1.1.5) and expand it at linear order in the temperature field $\beta(\boldsymbol{x})=\beta+\delta\beta(\boldsymbol{x})$ as $\hat{\rho}_{\text{loc}}\simeq e^{-\beta(\hat{H}+\hat{H}^{(1)})}$, thus defining a "thermal potential"

$$\begin{aligned}\hat{H}^{(1)}&=\beta^{-1}\int \mathrm{d}\boldsymbol{x}\,\delta\beta(\boldsymbol{x})\hat{h}(\boldsymbol{x})\\ &=\lim_{\epsilon\to 0^+}\beta^{-1}\int \mathrm{d}\boldsymbol{x}\,\delta\beta(\boldsymbol{x})\int_{-\infty}^{0}\mathrm{d}t\,e^{\epsilon t}\frac{\partial\hat{h}(\boldsymbol{x},t)}{\partial t}\,,\end{aligned} \tag{1.1.9}$$

where $\epsilon>0$ and the time-dependent density operator is expressed in the Heisenberg representation. However, this expansion and the following steps leading to Eq. (1.1.4), implicitly assume that the thermal current is computed as the equivalent of $\boldsymbol{J}=\mathrm{Tr}\left[\hat{\boldsymbol{J}}(\hat{\rho}_{\text{loc}}-\hat{\rho}^{(0)})\right]$, where $\hat{\rho}^{(0)}\propto e^{-\beta\hat{H}}$ is the density matrix of the average temperature field. As a matter of fact, this approach leads, at linear order in $\boldsymbol{\nabla}T$, to the opposite sign of Eq. (1.1.7), giving a negative thermal conductivity (explicitly proven in Appendix 1.A). To the best of our knowledge, this sign change has been mentioned in Ref. 108 but it has been overlooked in most of the previous derivations,[44,57,104] due to a compensation with an accidental errors in the intermediate analytical derivation leading to the definition of the thermal conductivity. It is worth noting that while at linear order the difference between a MEP approach to thermal transport and the use of a mechanical proxy is in a sign change, at next orders the expressions could become significantly different.[109] Finally, besides its conceptual problems, an approach based on a mechanical proxy cannot be implemented for self-consistent schemes, where the Hamiltonian displays an explicit temperature dependence, making it ambiguous the definition of a perturbative term $\hat{H}^{(1)}$ analogous to Eq. (1.1.9). This discussion motivates us to adopt the MEP and modified Liouville equation scheme to develop a solid theoretical framework for thermal transport, that will be extended to the case of self-consistent schemes in Chapter 3.

1.2 Maximum entropy principle formalism

1.2.1 Global equilibrium from the maximum entropy principle

To understand the basics of the applications of MEP to the derivation of the density matrix, we will follow Grandy[107] and the book by Zubarev[1] Sec. 20. Let us suppose that the available information on our system are the expectation values of a certain Heisenberg operator

$$\hat{F}(t)=\hat{U}^{\dagger}(t,t_0)\hat{F}(t_0)\hat{U}(t,t_0) \tag{1.2.1}$$

where $\hat{U}(t,t_0)$ is the evolution operator satifying

$$i\hbar\frac{\mathrm{d}\hat{U}(t,t_0)}{\mathrm{d}t}=\hat{H}(t)\hat{U}(t,t_0) \tag{1.2.2}$$

and subject to the initial condition $U(t_0,t_0)=1$ where $\hat{H}(t)$ is the Hamiltonian of the closed system. The time-evolution can also be described following the evolution of the density matrix

$$\hat{\rho}(t)=\hat{U}(t,t_0)\hat{\rho}(t_0)\hat{U}^{\dagger}(t,t_0)\,. \tag{1.2.3}$$

In our description of thermal transport, the Hamiltonian is the system Hamiltonian without any bath coupling, and does not depend explicitly on time, hence $\hat{U}(t,t_0)=e^{-\frac{i}{\hbar}(t-t_0)\hat{H}}$. Now let us suppose that all we know about our system is that the operator $\hat{F}$ has expectation value $f_0=\langle\hat{F}(t_0)\rangle=\mathrm{Tr}\left[\hat{\rho}\hat{F}(t_0)\right]$ at $t=t_0$. The statistical operator is the maximum of the entropy functional subject to the constraint

$$\tilde{S}[\rho]=-\,\mathrm{Tr}[\hat{\rho}\log\hat{\rho}]-\lambda_0\left(\mathrm{Tr}\left[\hat{\rho}\hat{F}(t_0)\right]-f_0\right) \tag{1.2.4}$$

which is formally solved (along with the normalization condition $\mathrm{Tr}[\hat{\rho}]=1$)[I] by

$$\begin{aligned}&\delta\tilde{S}=-\,\mathrm{Tr}\left[\delta\hat{\rho}\left(\log\hat{\rho}+\lambda_0\hat{F}(t_0)\right)\right]=0,\\&\hat{\rho}^{(0)}=\frac{1}{Z_0}e^{-\lambda_0\hat{F}(\tau_0)},\quad Z_0(\lambda_0)=\mathrm{Tr}\left[e^{-\lambda_0\hat{F}(t_0)}\right].\end{aligned} \tag{1.2.5}$$

The simplest practical application of this is the canonical ensemble, in which we assume that our information on the system is the expectation value of the energy E, *i.e.*

$$\tilde{S}[\rho]=-\,\mathrm{Tr}[\hat{\rho}\log\hat{\rho}]-\beta\left(\mathrm{Tr}\left[\hat{\rho}\hat{H}\right]-E\right) \tag{1.2.6}$$

which of course is maximized by

$$\hat{\rho}^{(0)}=\frac{1}{Z(\beta)}e^{-\beta\hat{H}}\,,\qquad Z(\beta)=\mathrm{Tr}\left[e^{-\beta\hat{H}}\right] \tag{1.2.7}$$

and the physical interpretation of the lagrangian multiplier (up to now just a mathematical entity) $\beta=\frac{1}{k_BT}$ is provided by the thermodynamical relations

$$-\frac{\partial\log Z(\beta)}{\partial\beta}=E\quad;\quad\frac{\partial S(\beta(E))}{\partial E}=\beta \tag{1.2.8}$$

where the Shannon entropy is reported without a tilde $S=-\,\mathrm{Tr}[\hat{\rho}\log\hat{\rho}]$.

1.2.2 Local equilibrium from the Maximum Entropy Principle

In the previous section we have discussed how to obtain the global equilibrium density matrix by using the MEP assuming that the sole information that we have on our system is its energy E. Here, we show how to utilize the MEP to combine more than one piece of information to obatin the local equilibrium condition. To derive the nonequilibrium density matrix, we employ the MEP as in Refs. 1,2,102,103. Within the MEP approach, we optimize the density matrix to maximize the entropy under the constraint of a nonuniform density variable.[1,2,101] If the constraint is imposed on the mass density, we obtain the density matrix describing mass transport. If it is imposed on the energy density, we obtain the density matrix describing a system with a nonuniform temperature profile, which is the situation

[I] Actually, the normalization condition is typically expressed as an extra Langrangian multiplier. Since it does not change much of the derivation, we will omit it for brevity.

where thermal transport occurs. Here we discuss the case of thermal transport; the case of mass transport is presented in Appendix 1.B to showcase the generality of our method.

To study thermal transport, we apply the MEP imposing a nonuniform energy density field $h(\boldsymbol{x})$. We seek the density matrix that maximizes entropy while satisfying the constraint that the expectation value of the energy density operator $\hat{h}(\boldsymbol{x})$ equals the energy density $h(\boldsymbol{x})$. This can be imposed via a set of local Langrangian multipliers $\beta(\boldsymbol{x})$ on the entropy functional $\tilde{S}[\rho]$:

$$\tilde{S}[\rho] = -\operatorname{Tr}[\hat{\rho}\log\hat{\rho}] - \int_V \mathrm{d}\boldsymbol{x}\,\beta(\boldsymbol{x})\left(\operatorname{Tr}\left[\hat{\rho}\hat{h}(\boldsymbol{x})\right] - h(\boldsymbol{x})\right) . \tag{1.2.9}$$

Eq. (1.2.9) is maximized by the solution

$$\begin{aligned} \hat{\rho}_{\text{loc}} &= \frac{1}{Z[\beta(\boldsymbol{x})]} e^{-\int \mathrm{d}\boldsymbol{x}\beta(\boldsymbol{x})\hat{h}(\boldsymbol{x})}, \\ Z[\beta(\boldsymbol{x})] &= \operatorname{Tr}\left[e^{-\int \mathrm{d}\boldsymbol{x}\beta(\boldsymbol{x})\hat{h}(\boldsymbol{x})}\right], \end{aligned} \tag{1.2.10}$$

where the Lagrange multiplier $\beta(\boldsymbol{x})$ represents the inverse of the temperature field, being the derivative of the entropy with respect to the local energy density.

$\hat{\rho}_{\text{loc}}$ in Eq. (1.2.10) can be understood as the description of the system in a state of "local" thermal equilibrium. This becomes evident via a procedure of "coarse-graining"[58] of the system over a characteristic length scale ℓ that is large as compared to the typical microscopic spacing a of the original discrete system, but small compared to the length scale λ_T over which the temperature varies, *i.e.* $a \ll \ell \ll \lambda_T$. This hierarchy of length scales allows[44,110] to define a continuous density operator $\hat{h}(\boldsymbol{x})$ as the convolution of the microscopic energy density $\hat{h}_a$, defined from the Hamiltonian

$$\hat{H} = \sum_a^{N_{\text{tot}}} \hat{h}_a , \tag{1.2.11}$$

with a smooth distribution Δ_ℓ as[35,110]

$$\hat{h}(\boldsymbol{x}) = \sum_a^N \hat{h}_a \Delta_\ell(\boldsymbol{x} - \hat{\boldsymbol{x}}_a) . \tag{1.2.12}$$

In (1.2.11), $\hat{h}_a$ is the operator that describes the energy associated with particle a, while N is the total number of components of the system. The function Δ_ℓ in (1.2.12) is peaked around $\boldsymbol{x}_a$ (the position of particle a), but it is spatially spread on a mesoscopic length $\ell \gg a$ large enough to allow one for a regularization of small-scale variations, needed to define spatial derivatives of the density (and current) operator. The additional condition $\lambda_T \gg \ell$ can be used to partition the system into $i = 1, \ldots, \mathcal{N}$ small spatial volumes of linear size ℓ where the temperature $T_i = \frac{1}{k_B \beta_i}$ can be assumed to be locally constant (cfr. Fig. 1.1). Within this condition, $\hat{\rho}_{\text{loc}}$ can be further approximated as the product of uncorrelated "local" canonical ensembles such that

$$\hat{\rho}_{\text{loc}} \simeq \prod_{i=1}^{\mathcal{N}} \hat{\rho}^i_{\text{loc}} = \prod_{i=1}^{\mathcal{N}} \frac{1}{Z[\beta_i]} e^{-\beta_i \hat{h}_i} , \tag{1.2.13}$$

Notice that Eq. (1.2.13) is not an exact equality, since in general local density operators do not commute $[\hat{h}_i, \hat{h}_j] \neq 0$. However, the decomposition becomes exact as $\mathcal{N} \to \infty$, and it is only

meant to motive the concept of local equilibrium in relation to the expression (1.2.10), whose derivation holds in general and does not require the factorization (1.2.13).

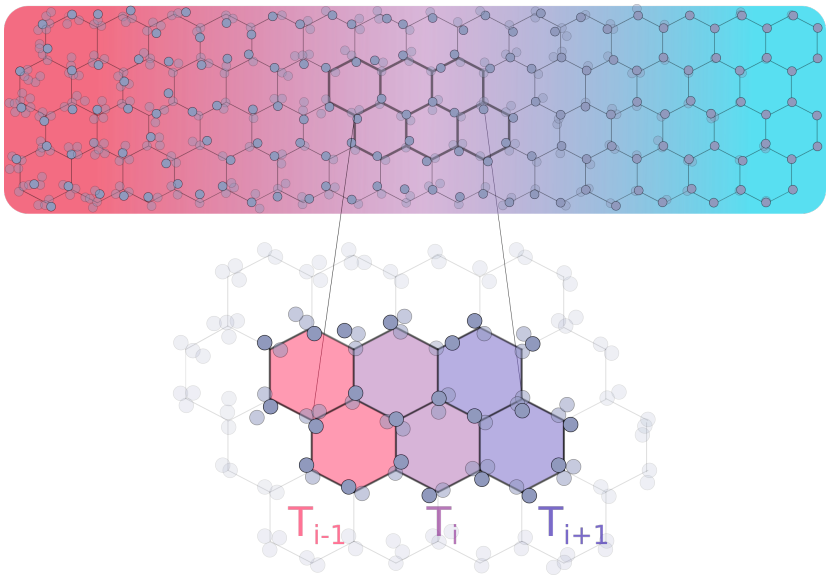

Figure 1.1. Pictorial visualization of local thermal equilibrium. The temperature field $T(\boldsymbol{x})$ can be thought as being obtained from a continuous limit of discretized subsystems, each at equilibrium with local temperature T_i on a mesoscopic scale [cfr. Eq. (1.2.13)].

Even though $\hat{\rho}_{\text{loc}}$ models a system with an inhomogeneous temperature field, it cannot describe a steady-state heat flow. In Appendix 1.B, we explicitly demonstrate that

$$\mathrm{Tr}\left[\hat{\boldsymbol{j}}(\boldsymbol{x})\hat{\rho}_{\text{loc}}\right] = 0\,, \tag{1.2.14}$$

where the current density $\hat{\boldsymbol{j}}(\boldsymbol{x})$ is linked to the heat flux $\hat{\boldsymbol{J}}$ and the energy density $\hat{h}(\boldsymbol{x})$ by

$$\hat{\boldsymbol{J}}(t) = \frac{1}{V}\int_V \mathrm{d}\boldsymbol{x}\, \hat{\boldsymbol{j}}(\boldsymbol{x},t), \tag{1.2.15}$$

$$\frac{\partial}{\partial t}\hat{h}(\boldsymbol{x},t) = -\boldsymbol{\nabla}\cdot\hat{\boldsymbol{j}}(\boldsymbol{x},t)\,, \tag{1.2.16}$$

where the evolution of the operators is intended in the Heisenberg scheme

$$\frac{\partial\hat{O}(t)}{\partial t} = \frac{i}{\hbar}[\hat{H},\hat{O}(t)] \;\Rightarrow \hat{O}(t) = e^{i\hat{H}/\hbar}\hat{O}e^{-i\hat{H}/\hbar}. \tag{1.2.17}$$

In fact, the steady-state density matrix $\hat{\rho}_{\text{st}}$ that sustain steady heat flow must be a solution of the Liouville equation

$$\frac{\partial\hat{\rho}(t)}{\partial t} + \frac{i}{\hbar}[\hat{H},\hat{\rho}(t)] = 0\,. \tag{1.2.18}$$

in the stationary case, *i.e.* with $\frac{\partial\hat{\rho}_{\text{st}}}{\partial t}=0$. As such, it must commute with the Hamiltonian $[\hat{H},\hat{\rho}_{\text{st}}]=0$. Since $\hat{\rho}_{\text{loc}}$ depends on the energy density $\hat{h}(\boldsymbol{x})$, which does not, in general, commute with the Hamiltonian, it follows that $\hat{\rho}_{\text{loc}}\neq\hat{\rho}_{\text{st}}$.

1.2.3 Steady state from the maximum entropy principle

The strategy employed to obtain the steady-state density matrix involves imposing an additional constraint on the variational calculation of entropy functional.[107,111,112] Specifically,

we not only maximize the entropy with a constraint on the nonuniform energy density $h(\boldsymbol{x})$, but also ensure that the variation maintains the density matrix stationary. Details of the derivation are presented in Appendix 1.C. We maximize the functional of Eq. (1.2.9) with the additional constraint

$$[\hat{\rho}_{\text{st}}, \hat{H}] = 0 \tag{1.2.19}$$

to be imposed on the infinitesimal variations $\delta\hat{\rho}$ on the density matrix, in the sense that the variations of $\hat{\rho}_{\text{st}}$ must be done in such a way as to satisfy Eq. (1.2.19) at all times. We are thus searching a local maximum of the entropy on the manifold of the statistical operators that commute with the Hamiltonian. Computing the variation of the functional $\tilde{S}$ in Eq. (1.2.9), we get

$$\delta\tilde{S} = -\operatorname{Tr}\left[\delta\hat{\rho}\left(\log\hat{\rho}_{\text{st}} + \int_V \mathrm{d}\boldsymbol{x}\,\beta(\boldsymbol{x})\hat{h}(\boldsymbol{x})\right)\right] = 0. \tag{1.2.20}$$

If the variation on the density matrix $\delta\hat{\rho}$ was completely arbitrary, Eq. (1.2.20) would result in the local equilibrium density matrix Eq. (1.2.10). Instead, the stationarity condition Eq. (1.2.19) imposes

$$[\hat{\rho}_{\text{st}} + \delta\hat{\rho}, \hat{H}] = 0 \quad \rightarrow \quad [\delta\hat{\rho}, \hat{H}] = 0 \tag{1.2.21}$$

so that the "displaced" density matrix $\hat{\rho}_{\text{st}} + \delta\hat{\rho}$ still possess the relevant features of a steady state.

We show in Appendix 1.C that the density matrix maximizing the entropy (1.2.9) along with the constraint (1.2.21) still features a nonuniform temperature $\beta(\boldsymbol{x})$, but the local operator $\hat{h}_d(\boldsymbol{x})$ contains only the diagonal elements of the energy density $\hat{h}(\boldsymbol{x})$ on the basis that diagonalizes the Hamiltonian $\hat{H}$, *i.e.*

$$\hat{\rho}_{\text{st}} = \frac{1}{Z_{st}} e^{-\int_V \mathrm{d}\boldsymbol{x}\beta(\boldsymbol{x})\hat{h}_d(\boldsymbol{x})}, \quad Z_{st} = \operatorname{Tr}\left[e^{-\int_V \mathrm{d}\boldsymbol{x}\beta(\boldsymbol{x})\hat{h}_d(\boldsymbol{x})}\right]. \tag{1.2.22}$$

As we demonstrate in Appendix 1.C, the diagonal operator $\hat{h}_d(\boldsymbol{x})$ admits an explicitly representation as:

$$\hat{h}_d(\boldsymbol{x}) = \hat{h}(\boldsymbol{x}) - \lim_{\epsilon\to 0^+}\int_{-\infty}^{0} \mathrm{d}t\, e^{\epsilon t}\frac{\partial}{\partial t}\hat{h}(\boldsymbol{x}, t)\,. \tag{1.2.23}$$

where $\epsilon{>}0$. The second term in the right-hand side of Eq. (1.2.23) strongly resembles the usual correction $H^{(1)}$ to the Hamiltonian $\hat{H}$ that is usually introduced in the case of a mechanical perturbation, see Eq. (1.1.9) above. Indeed, in analogy with this case it breaks the time-reversal symmetry of the local equilibrium density matrix for every finite ϵ, allowing a finite heat flux. However, in the MEP derivation such a perturbation crucially enters the steady-state density matrix $\hat{\rho}_{\text{st}}$ with a sign difference as compared to Eq. (1.1.9), that along with the prescription Eq. (1.1.7) determines the correct sign in the derivation of the thermal conductivity. To demonstrate it, let us start from the definition of current as the average value of the heat flux on the steady-state density matrix:

$$\boldsymbol{J} = \lim_{\epsilon\to 0^+}\operatorname{Tr}\left[\hat{\boldsymbol{J}}\hat{\rho}^{\epsilon}_{\text{st}}\right]. \tag{1.2.24}$$

To obtain the thermal conductivity we need to expand $\hat{\rho}_{\text{st}}$ at linear order in $\nabla\beta(\boldsymbol{x})$, where $\beta(\boldsymbol{x}){=}\beta{+}\delta\beta(\boldsymbol{x})$ and β is the average inverse temperature. To this aim, let us rewrite the pre-ϵ

limit steady-state density matrix Eq. (1.2.23) as

$$\begin{aligned}\hat{\rho}^{\epsilon}_{\text{st}} &= \frac{1}{Z_{st}}\exp\Big[-\int \mathrm{d}\boldsymbol{x}\,\beta(\boldsymbol{x})\hat{h}(\boldsymbol{x})-\hat{U}\Big],\\ \hat{U} &= \int \mathrm{d}\boldsymbol{x}\,\beta(\boldsymbol{x})\boldsymbol{\nabla}\cdot\widehat{\tilde{\boldsymbol{j}}}^{\epsilon}(\boldsymbol{x}) = -\int \mathrm{d}\boldsymbol{x}\,\nabla\beta(\boldsymbol{x})\cdot\widehat{\tilde{\boldsymbol{j}}}^{\epsilon}(\boldsymbol{x})\,.\end{aligned} \tag{1.2.25}$$

where we used the continuity equation Eq. (1.2.16) to replace the time derivative of the energy density with the gradient of the density current, and we introduced the short-hand notation

$$\widehat{\tilde{\boldsymbol{j}}}^{\epsilon}(\boldsymbol{x}) = \int_{-\infty}^{0}\mathrm{d}t\,e^{\epsilon t}\hat{\boldsymbol{j}}(\boldsymbol{x},t)\,. \tag{1.2.26}$$

In addition, the last equality of Eq. (1.2.25) has been omitting a surface, negligible in the thermodynamic limit. Eq. (1.2.25) admits a natural expansion of $\hat{\rho}_{\text{st}}$ around the local equilibrium solution $\hat{\rho}_{\text{loc}}$ in powers of $\nabla\beta$. This can be done by using the exponential operatorial identity[2,111,113] (proven in Appendix 1.D)

$$e^{-(\hat{A}+\hat{B})} = e^{-\hat{A}} - e^{-\hat{A}}\int_0^1 \mathrm{d}\sigma\,e^{\sigma\hat{A}}\hat{B}e^{-\sigma(\hat{A}+\hat{B})} \tag{1.2.27}$$

so that Eq. (1.2.25) reads:

$$\hat{\rho}^{\epsilon}_{\text{st}} = \hat{\rho}_{\text{loc}} - e^{-\int \mathrm{d}\boldsymbol{x}\beta(\boldsymbol{x})\hat{h}(\boldsymbol{x})}\int_0^1 \mathrm{d}\sigma\,e^{\sigma\int \mathrm{d}\boldsymbol{x}\beta(\boldsymbol{x})\hat{h}(\boldsymbol{x})}\hat{U}e^{-\sigma[\int \mathrm{d}\boldsymbol{x}\beta(\boldsymbol{x})\hat{h}(\boldsymbol{x})+\hat{U}]} \tag{1.2.28}$$

Since the second term of Eq. (1.2.28) is already of linear order in $\nabla\beta(\boldsymbol{x})$, one can replace everywhere in the remaining exponentials $\beta(\boldsymbol{x})$=β to get:

$$\begin{aligned}\hat{\rho}^{\epsilon}_{\text{st}} &= \hat{\rho}_{\text{loc}} - \hat{\rho}^{(0)}\int_0^1 \mathrm{d}\sigma\,e^{\sigma\beta\hat{H}}\hat{U}e^{-\sigma\beta\hat{H}}\\ &= \hat{\rho}_{\text{loc}} - \hat{\rho}^{(0)}T\int_0^{\beta}\mathrm{d}\lambda\,\hat{U}(-i\hbar\lambda)e^{-\sigma\beta\hat{H}}\\ &= \hat{\rho}_{\text{loc}} + \hat{\rho}^{(0)}T\int_{-\infty}^{0}dte^{\epsilon t}\int_0^{\beta}\mathrm{d}\lambda\int \mathrm{d}\boldsymbol{x}\,\boldsymbol{\nabla}\beta(\boldsymbol{x})\cdot\hat{\boldsymbol{j}}(-t-i\hbar\lambda)\\ &= \hat{\rho}_{\text{loc}} - \hat{\rho}^{(0)}\frac{V}{T}\int_0^{\infty}dte^{-\epsilon t}\int_0^{\beta}\mathrm{d}\lambda\,\boldsymbol{\nabla}T\cdot\hat{\boldsymbol{J}}(-t-i\hbar\lambda)\end{aligned} \tag{1.2.29}$$

where we defined the density matrix of the global thermal equilibrium as

$$\hat{\rho}^{(0)} = \frac{1}{Z[\beta]}e^{-\beta\hat{H}}\,,\qquad Z[\beta] = \mathrm{Tr}\Big[e^{-\beta\hat{H}}\Big]\,. \tag{1.2.30}$$

and we used the Heisenberg representation (1.2.17) for the operators. In addition, in the last step of Eq. (1.2.29) we assumed an uniform temperature gradient. In principle, to get the current at linear order in $\boldsymbol{\nabla}T$ one should expand in Eq. (1.2.25) also the $1/Z_{st}$

normalization factor. However, once replaced into Eq. (1.2.24), the expansion of the inverse partition function leads to the product of the uncorrelated density operators with respect to the $\boldsymbol{\nabla} T{=}0$ term of the expansion, that according to Eq. (1.2.29) is the local equilibrium density matrix. Since we already demonstrated that $\mathrm{Tr}\left[\hat{\boldsymbol{J}}\hat{\rho}_{\mathrm{loc}}\right]{=}0$, the term coming from the expansion of the normalization constant is zero. From the decomposition Eq. (1.2.29) one immediately obtains for the average current computed on the steady state:

$$\begin{aligned} J(\epsilon)^{\mu} &= \mathrm{Tr}\left[\hat{J}^{\mu}\hat{\rho}^{\epsilon}_{st}\right] \\ &\simeq -\frac{V}{T}\int_0^{\infty}\mathrm{d}t\, e^{-\epsilon t}\int_0^{\beta}\mathrm{d}\lambda\,\mathrm{Tr}\Big[\hat{\rho}^{(0)}\hat{J}^{\mu}(0)\hat{J}^{\nu}(-t{-}i\hbar\lambda)\Big]\nabla^{\nu}T \end{aligned} \tag{1.2.31}$$

from which it immediately follows the usual Kubo formula for thermal conductivity.[1,58,110,113,114]

$$\kappa^{\gamma\nu} = \lim_{\epsilon\to 0^+}\frac{V}{T}\int_0^{\infty}\mathrm{d}t\, e^{-\epsilon t}\int_0^{\beta}\mathrm{d}\lambda\,\mathrm{Tr}\Big[\hat{\rho}^{(0)}\hat{J}^{\nu}(-t{-}i\hbar\lambda)\hat{J}^{\gamma}(0)\Big]. \tag{1.2.32}$$

1.3 Modified Liouville equation approach

In the derivation of Eq. (1.2.32), the time-dependence of the steady-state solution Eq. (1.2.22) appears as an artifact to represent the diagonal density operator via Eq. (1.2.23). A deeper understanding of the above result based on the time evolution of the density matrix from the steady state Eq. (1.2.22) to the local equilibrium $\hat{\rho}_{\mathrm{loc}}$ can be obtained by showing, as done in Appendix 1.C, that the pre-ϵ-limit expression $\rho^{\epsilon}_{\mathrm{st}}$ can be seen as the static solution of the modified Liouville equation developed by Zubarev,[102]

$$\frac{\partial\hat{\rho}^{\epsilon}(t)}{\partial t} + \frac{i}{\hbar}[\hat{H},\hat{\rho}^{\epsilon}(t)] = -\epsilon\left[\hat{\rho}^{\epsilon}(t) - \hat{\rho}_{\mathrm{loc}}(t)\right]\,. \tag{1.3.1}$$

In Eq. (1.3.1) we impose a relaxation timescale of ϵ^{-1} to simulate coupling with a thermal bath, that breaks time-reversal symmetry of the Liouville equation (1.2.18),[2,113] by allowing entropy production and irreversibility.[2,107,111,115] As discussed in Appendix 1.B, the absence of currents in the local equilibrium state $\hat{\rho}_{\mathrm{loc}}$ arises from time-reversal symmetry: the Liouville equation Eq. (1.2.18) describes the dynamics of a closed system in which the entropy is conserved. Therefore, solutions of the standard Liouville equation can not account for dissipative processes involving directional heat flow: energy excitations propagate back and forth in the system and result in zero net current over time. On the other hand, the modified Liouville equation brings in the ϵ term in equation Eq. (1.3.2) to break time reversal, introducing an effective coupling with a thermal bath and simulating entropy production. In the $\epsilon{\to}0^+$ and thermodynamical limit, the details of the coupling with the bath become irrelevant.[107]

In this Section we will show explicitly how the thermal conductivity Eq. (1.2.32) can be obtained from the solution of the modified Liouville equation (1.3.1). This derivation permits to express the time dependence of the leading term in $\hat{\rho}^{\epsilon}_{\mathrm{st}}$ via the formal action of the Liouville superoperator, providing a general solution that can be extended to the case of self-consistent problems. In addition, the modified Liouville equation allows to identify the time evolution of the density operator as a relaxation process from the steady-state $\hat{\rho}_{\mathrm{st}}$

realized at $t{=}-\infty$ to the local equilibirum $\hat{\rho}_{\rm loc}$ at $t{=}0$, as mentioned in Eq. (1.1.8) [II].

To derive the steady-state solution from the modified Liouville equation (1.3.1) let us first rewrite it as

$$\left(\frac{\partial}{\partial t}+\frac{i}{\hbar}\mathcal{L}\right)\hat{\rho}^{\epsilon}(t)=-\epsilon\left[\hat{\rho}^{\epsilon}(t)-\hat{\rho}_{\rm loc}(t)\right] \tag{1.3.2}$$

where $\epsilon{>}0$ and the Liouville superoperator acts as $\mathcal{L}\hat{\rho}{=}[\hat{H},\hat{\rho}]$, so that the Heisenberg evolution (1.2.1) is equivalently expressed as:

$$\frac{\partial\hat{O}(t)}{\partial t}=\frac{i}{\hbar}\mathcal{L}\hat{O}\quad\Rightarrow\hat{O}(t){=}e^{\frac{i}{\hbar}\mathcal{L}t}\hat{O} \tag{1.3.3}$$

To find the steady-state $\hat{\rho}_{\rm st}$, we look for stationary solutions $\frac{\partial\hat{\rho}}{\partial t}{=}0$ of Eq. (1.3.2). For finite ϵ, we integrate from time $-T$ to t (1.3.2), obtaining

$$e^{(\frac{i}{\hbar}\mathcal{L}+\epsilon)t}\hat{\rho}^{\epsilon}(t)-e^{-\frac{i}{\hbar}\mathcal{L}T}e^{-\epsilon T}\hat{\rho}^{\epsilon}(-T){=}\int_{-T}^{t}\mathrm{d}t'\epsilon e^{\epsilon t'}e^{\frac{i}{\hbar}\mathcal{L}t'}\hat{\rho}_{\rm loc}(t')\,. \tag{1.3.4}$$

In the $T{\to}\infty$ limit, the factor $e^{-\epsilon T}$ eliminates information about the initial conditions: the bath coupling implies memory loss. Notably, the two limits do not commute; if the limits are reversed, hence if $\epsilon{\to}0^{+}$ is done before $T{\to}\infty$, we get the unitary evolution of the initial state $\hat{\rho}(t){=}e^{\frac{i}{\hbar}\mathcal{L}(t-T)}\rho(-T)$ that does not encompass dissipative processes.[113]

Taking the $T{\to}\infty$ limit of Eq. (1.3.4) and integrating by parts we get

$$\hat{\rho}^{\epsilon}(t){=}\hat{\rho}_{\rm loc}(t){-}\int_{-\infty}^{t}\mathrm{d}t'\,e^{-\epsilon(t-t')}e^{-\frac{i}{\hbar}\mathcal{L}(t-t')}\left[\frac{\partial}{\partial t'}+\frac{i}{\hbar}\mathcal{L}\right]\hat{\rho}_{\rm loc}(t')\,. \tag{1.3.5}$$

Eq. (1.3.5) represents the formal solution of the modified Liouville equation Eq. (1.3.2), and allow us to derive the steady-state density matrix; by setting $\frac{\partial\hat{\rho}}{\partial t}{=}0$ and evaluating the solution at $t{=}0$, we get the steady state

$$\hat{\rho}^{\epsilon}_{\rm st}(0)=\hat{\rho}_{\rm loc}(0)-\int_{0}^{\infty}\mathrm{d}t\,e^{-\epsilon t}e^{-\frac{i}{\hbar}\mathcal{L}t}\frac{i}{\hbar}\mathcal{L}\hat{\rho}_{\rm loc}\,. \tag{1.3.6}$$

In Eq. (1.3.6), we can express the steady state as the difference between the solution of the modified Liouville equation and $\hat{\rho}_{\rm loc}(t{=}0)$, since the local equilibrium density matrix does not contribute to transport (Sec. 1.2.2, Appendix 1.B).

The main ingredients of Eq. (1.3.6) are the Liouville superoperator $\mathcal{L}$ that describes the internal dynamics of the system and the local equilibrium density matrix $\hat{\rho}_{\rm loc}$. We stress that the derivation of Eq. (1.3.6) is not specific to lattice thermal transport. When the relevant local equilibrium conditions — *e.g.* the electrochemical-local equilibrium for charge and mass transport [Eq. (1.B.2)] — and the appropriate Hamiltonian governing the dynamics are defined, the result Eq. (1.3.6) can describe the steady state for different transport phenomena.[101]

It is worth nothing that obtaining the steady-state with finite currents in the $\epsilon{\to}0^{+}$ com-

[II] Actually, it is not important that the local equilibrium $\hat{\rho}_{\rm loc}$ is established precisely at $t{=}0$, but rather that it is established after an infinite time with respect to the "steady-state". This will be more clear in introducing the modified Liouville equation, where the relaxation timescale from the steady state to the local equilibrium scale goes to infinity as ϵ goes to zero.

bined with the thermodynamical limit is similar to the problem of describing a ferromagnet with finite magnetic moment. In a ferromagnet, the Hamiltonian is symmetric upon reversal of the direction of the magnetic moments, while the state — *i.e.* the density matrix — possess a preferential orientation (namely, the direction of the magnetic moment). The state with positive (negative) magnetic moment is obtained by taking off the external magnetic field $h{\to}0^+$ ($h{\to}0^-$) that enforces the symmetry of the state after the thermodynamical limit.[116] In this sense, the existence of a steady state that sustains a heat flux can be intepreted as the spontaneous symmetry breaking of time-reversal symmetry of the Liouville equation.[2,115]

1.3.1 Derivation of thermal conductivity from the modified Liouville equation

To derive the thermal conductivity we proceed as before from Eq. (1.2.24), by expanding $\hat{\rho}^{\epsilon}_{st}$ in Eq. (1.3.6) at linear order in the temperature gradient, in full analogy with the procedure detailed in the previous Section. In particular, by defining $\beta(\boldsymbol{x}){=}\beta{+}\delta\beta(\boldsymbol{x})$ and by using the operatorial identity (1.2.27) we obtain at linear order in $\delta\beta(\boldsymbol{x})$

$$\hat{\rho}_{\text{loc}} \simeq \hat{\rho}^{(0)}{-}\hat{\rho}^{(0)} \int_0^\beta \mathrm{d}\lambda\, e^{\lambda\hat{H}} \int \mathrm{d}\boldsymbol{x}\, \frac{\delta\beta(\boldsymbol{x})}{\beta} \hat{h}(\boldsymbol{x}) e^{-\lambda\hat{H}}\,, \tag{1.3.7}$$

By using the definition of the time derivative of the operators in the Heisenberg scheme (1.2.17), Eq. (1.3.3) and the fact that $\mathcal{L}\hat{\rho}^{(0)}{=}0$, we can plug Eq. (1.3.7) into Eq. (1.3.6) obtaining

$$\hat{\rho}^{\epsilon}_{\text{st}}{=}\hat{\rho}^{(0)} \int_0^\infty \mathrm{d}t\, e^{-\epsilon t} e^{-\frac{i}{\hbar}\mathcal{L}t} \int_0^\beta \mathrm{d}\lambda \int \mathrm{d}\boldsymbol{x}\, \frac{\delta\beta(\boldsymbol{x})}{\beta} e^{\lambda\hat{H}} \frac{\partial}{\partial t} \hat{h}(\boldsymbol{x},0) e^{-\lambda\hat{H}}\,, \tag{1.3.8}$$

where $\hat{h}(\boldsymbol{x},0)$ is $\hat{h}(\boldsymbol{x})$ computed at $t{=}0$. Now using the continuity equation Eq. (1.2.16), integrating by parts and using the approximation of a uniform temperature gradient throughout the sample,[44,58] we get

$$\hat{\rho}^{\epsilon}_{\text{st}}{=}{-}\hat{\rho}^{(0)} \int_0^\infty \mathrm{d}t\, e^{-\epsilon t} e^{-\frac{i}{\hbar}\mathcal{L}t} \int_0^\beta \mathrm{d}\lambda\, e^{\lambda\hat{H}} \frac{\boldsymbol{\nabla} T}{\beta} \cdot V\hat{\boldsymbol{J}}(0) e^{-\lambda\hat{H}}\,. \tag{1.3.9}$$

The thermal conductivity is thus obtained by calculating the expectation value of the heat flux Eq. (1.2.24) with the steady-state density matrix Eq. (1.3.9) as

$$\kappa^{\gamma\nu}{=}\lim_{\epsilon\to 0^+} \frac{V}{T} \int_0^\infty \mathrm{d}t\, e^{-\epsilon t} \int_0^\beta \mathrm{d}\lambda\, \mathrm{Tr}\left[\hat{\rho}^{(0)} e^{-\frac{i}{\hbar}t\mathcal{L}} e^{-\lambda\hat{H}} \hat{J}^{\nu}(0) e^{\lambda\hat{H}} \hat{J}^{\gamma}(0)\right] \tag{1.3.10}$$

that can alternatively be expressed as Eq. (1.2.32) above since:

$$e^{-\frac{i}{\hbar}t\mathcal{L}} e^{-\lambda\hat{H}} \hat{J}^{\nu}(0) e^{\lambda\hat{H}} = \hat{J}^{\nu}(-t{-}i\hbar\lambda) \tag{1.3.11}$$

For finite ϵ, we can solve the time integral in Eq. (1.2.32) obtaining

$$\kappa^{\gamma\nu}(i\epsilon) = \frac{V}{T} \int_0^\beta \mathrm{d}\lambda\, \mathrm{Tr}\left[\hat{\rho}^{(0)} \frac{i}{i\hbar\epsilon - \mathcal{L}} \hat{J}^{\nu}(-i\hbar\lambda) \hat{J}^{\gamma}(0)\right] \tag{1.3.12}$$

in which the conductivity can be seen as the DC (ω=0) value of a complex conductivity $\kappa^{\gamma\nu}(\omega+i\epsilon)$, featuring the many-body propagator $[\hbar(\omega+i\epsilon) - \mathcal{L}]^{-1}$,[75,110] as in the standard result linear response to an external time-dependent Hamiltonian[104,106,117] [apart from a sign, cfr. Appendix 1.A].

It is worth mentioning that the same procedure used to derive Eq. (1.2.32) can be used to derive the Kubo formula for the electrical conductivity or Fick's law for mass diffusivity by setting the appropriate local equilibrium state with nonuniform electrochemical potential $\bar{\mu}(\boldsymbol{x})=\mu(\boldsymbol{x})+q\phi(\boldsymbol{x})$, where $\phi(\boldsymbol{x})$ is the electrostatic potential and q is the charge of the particles in the system [cfr. Eq. (1.B.2)].

1.4 Conclusions

In this Chapter, we have reviewed the essentials of Zubarev's maximum entropy principle plus modified Liouville equation approach to discuss response functions in nonequilibrium systems. We have discussed how it can be applied to derive the formal expression of the local equilibrium density matrix, which can then be used to derive the steady-state nonequilibrium operator. The latter is the central object in studying nonequilibrium systems since it describes that state that sustains currents, hence it can be used to compute the transport coefficients. We have shown how from this formalism a Kubo formula for thermal conductivity can be derived. The Kubo formula Eq. (2.1.1) has the same structure as the equivalent expression for electrical conductivity. However, the starting point of the derivation of the two is conceptually different. Electrical conductivity is typically derived as a response to an external electrical field, while here the perturbation consists in the presence of a temperature gradient, that characterizes the local equilibrium state. Due to its generality, this formalism can also be used to discuss electrical and mass transport (cfr. 1.B). Another important feature that we will exploit is that this procedure solely relies on manipulations of the density matrix and of the Liouville operators, providing a solid theoretical foundation for the application of self-consistent methods to transport phenomena. This will allow us to derive a Kubo formula of thermal conductivity that does not rely on any perturbative truncation of the Hamiltonian of the system. We will explore such an extension of the method in Chapter 3.

Appendices of Chapter 1

1.A Transport coefficients and adiabatic switching-on of a mechanical potential

In this Appendix, we discuss some of the complications of the standard methodology used to obtain the transport coefficients in linear response theory. The approach outlined by the seminal paper of Luttinger[57] and revised by Mahan[104] consist in considering an adiabatic switched on perturbation of the form

$$\hat{H}_{tot}(t) = \hat{H} + e^{\epsilon t}\hat{H}^{(1)} \tag{1.A.1}$$

and supposing that the density matrix evolves from equilibrium accordingly as

$$\hat{\rho}(t) = \hat{\rho}^{(0)} + e^{\epsilon t}\hat{\rho}^{(1)}\,, \tag{1.A.2}$$

where $\hat{\rho}^{(0)}$ is the equilibrium density matrix that features the hamiltonian $\hat{H}$ [Eq. (3.1.2)]. In Eq. (1.A.1), the perturbation has the form

$$\hat{H}^{(1)} = \int \mathrm{d}\boldsymbol{x}\, \psi(\boldsymbol{x})\hat{d}(\boldsymbol{x}) \tag{1.A.3}$$

where $\psi(\boldsymbol{x})$ is the external field that couples to the density $\hat{d}(\boldsymbol{x})$, which is related to its current $\hat{i}(\boldsymbol{x})$ as

$$\frac{\partial \hat{d}(\boldsymbol{x},t)}{\partial t} + \boldsymbol{\nabla}\cdot\hat{i}(\boldsymbol{x},t) = 0\,. \tag{1.A.4}$$

For the case of electric transport, $\psi(\boldsymbol{x})$=$\phi(\boldsymbol{x})$ is the electrostatic potential, while $\hat{d}(\boldsymbol{x})$=$q\hat{n}(\boldsymbol{x})$ is the charge density. For thermal transport, as seen in Eq. (1.1.9), $\psi(\boldsymbol{x})$=$\frac{\delta\beta(\boldsymbol{x})}{\beta}$ is the variation of the temperature field, while $\hat{d}(\boldsymbol{x})$=$\hat{h}(\boldsymbol{x})$ is the energy density. By expanding at linear order in the perturbation the Liouville equation

$$\frac{\partial\hat{\rho}(t)}{\partial t} + \frac{i}{\hbar}[\hat{H},\hat{\rho}(t)] = \frac{\partial\hat{\rho}(t)}{\partial t} + \frac{i}{\hbar}\mathcal{L}\hat{\rho}(t) = 0\,, \tag{1.A.5}$$

with $\hat{H}_{tot}$, one gets

$$(i\hbar\epsilon - \mathcal{L})\hat{\rho}^{(1)} = [\hat{H}^{(1)},\hat{\rho}^{(0)}]\,. \tag{1.A.6}$$

Using the Kubo identity[106] (proven in Appendix 1.D

$$[\hat{A}, e^{-\beta\hat{H}}] = e^{-\beta\hat{H}}\int_0^\beta \mathrm{d}\lambda\, e^{\lambda\hat{H}}\mathcal{L}\hat{A}e^{-\lambda\hat{H}}, \tag{1.A.7}$$

we get that Eq. (1.A.6) is solved by

$$\hat{\rho}^{(1)} = -\hat{\rho}^{(0)}\int_{-\infty}^{0}\mathrm{d}t\, e^{(\epsilon+\frac{i}{\hbar}\mathcal{L})t}\int_0^\beta \mathrm{d}\lambda\, e^{\lambda\hat{H}}\frac{i}{\hbar}\mathcal{L}\hat{H}^{(1)}e^{-\lambda\hat{H}}\,. \tag{1.A.8}$$

Using the definition of the Heisenberg evolution of the operators [Eq. (1.2.17)], we can express Eq. (1.A.8) as

$$\hat{\rho}^{(1)} = -\hat{\rho}^{(0)} \int_0^\infty \mathrm{d}t\, e^{-\epsilon t} e^{-\frac{i}{\hbar}\mathcal{L}t} \int_0^\beta \mathrm{d}\lambda \int \mathrm{d}\boldsymbol{x}\, \psi(\boldsymbol{x}) e^{\lambda \hat{H}} \frac{\partial}{\partial t} \hat{d}(\boldsymbol{x}, 0) e^{-\lambda \hat{H}} \tag{1.A.9}$$

Now using the continuity equation Eq. (1.A.4), integrating by parts and using the approximation of a uniform gradient $\boldsymbol{\nabla}\psi$ throughout the sample, we can express Eq. (1.A.9) as

$$\hat{\rho}^{(1)} = -\hat{\rho}^{(0)} \int_0^\infty \mathrm{d}t\, e^{-\epsilon t} e^{-\frac{i}{\hbar}\mathcal{L}t} \int_0^\beta \mathrm{d}\lambda\, e^{\lambda \hat{H}} V \boldsymbol{\nabla}\psi \cdot \hat{\boldsymbol{I}}(0) e^{-\lambda \hat{H}}\,, \tag{1.A.10}$$

where we have introduced the macroscopic current $\hat{\boldsymbol{I}}$ associated with the current density $\hat{i}$ expressed in Eq. (1.A.4). To obtain the transport coefficient, we compute the expectation value of the current $\hat{\boldsymbol{I}}$ at $t{=}0$ as

$$\begin{aligned} I^\gamma(0) &= \mathrm{Tr}\left[\hat{\rho}(0)\hat{I}^\gamma\right] \\ &= -V \sum_\nu \boldsymbol{\nabla}^\nu \psi \int_0^\infty \mathrm{d}t\, e^{-\epsilon t} \int_0^\beta \mathrm{d}\lambda\, \mathrm{Tr}\left[\hat{\rho}^{(0)} \hat{I}^\gamma \hat{I}^\nu(-t - i\hbar\lambda)\right]. \end{aligned} \tag{1.A.11}$$

In the case of electrical transport, $-\boldsymbol{\nabla}\psi{=}-\boldsymbol{\nabla}\phi$ is the electric field $\boldsymbol{\mathcal{E}}$, and Eq. (1.A.11) consists in the Kubo formula for electrical conductivity $J_e^\gamma{=}\sum_\nu \sigma^{\gamma\nu}\mathcal{E}^\nu$. However, in the case of thermal transport $-\boldsymbol{\nabla}\psi{=}-\boldsymbol{\nabla}\beta{=}\boldsymbol{\nabla}T$, and Eq. (1.A.11) gives the Fourier law $J^\gamma{=}\sum_\nu \kappa^{\gamma\nu}\boldsymbol{\nabla}^\nu T$ with the wrong sign.[108] Notice that even if slightly different, the derivation of thermal conductivity provided by Allen[44] gives the same sign of thermal conductivity [there is a misprint in the sign of the second term of Eq. (16) of Ref. 44, cfr. Eq. (1.2.27)].

Even if appears as a mathematical finesse, the complication just discussed actually has a deep physical meaning. In fact, if we come back to Eqs. (1.A.6)-(1.A.7), we can express the induced density matrix as

$$\hat{\rho}^{(1)} = \frac{1}{i\hbar\epsilon - \mathcal{L}} \mathcal{L}\hat{\rho}^{(0)} \int_0^\beta \mathrm{d}\lambda\, e^{\lambda \hat{H}} \hat{H}^{(1)} e^{-\lambda H} \tag{1.A.12}$$

so that the density matrix Eq. (1.A.2) at $t{=}0$ reads

$$\hat{\rho}(t{=}0){=}\hat{\rho}^{(0)} + \frac{1}{i\hbar\epsilon - \mathcal{L}} \mathcal{L}\hat{\rho}^{(0)} \int_0^\beta \mathrm{d}\lambda\, e^{\lambda \hat{H}} \hat{H}^{(1)} e^{-\lambda H} \tag{1.A.13}$$

which using Eq. (1.2.27), can be seen as

$$\hat{\rho}(t{=}0) = \frac{1}{Z} e^{-\beta(\hat{H} + \hat{H}^{(1)})} + \mathcal{O}(\epsilon)\,. \tag{1.A.14}$$

For the case of thermal transport, this tells us that the adiabatic switching-on of the thermal potential Eq. (1.1.9) basically describes the evolution from the global equilibrium $\hat{\rho}^{(0)}$ established in the infinite past to a local equilibrium regime at $t{=}0$

$$\hat{\rho}(t{=}{-}\infty) \propto e^{-\beta \hat{H}} \to \hat{\rho}(t{=}0) \propto e^{-\int \mathrm{d}\boldsymbol{x} \beta(\boldsymbol{x}) \hat{h}(\boldsymbol{x})}\,. \tag{1.A.15}$$

As can be easily understood, the local equilibrium condition has lower entropy than the global equilibrium, since the temperature field constrains the system to be in a more ordered phase (from hot to cold). In fact, if left isolated, the local equilibrium condition would eventually relax to the global equilbrium in a spontaneous transformation,[1] increasing the entropy.

In conclusion, while apt for the description of transport process where the currents are stimulated by mechanical forces, hence are driven in the direction of the minimum of the energy, the standard procedure of the adiabatic switching-on of the perturbation does not reproduce the evolution of the system in which entropy is produced.

1.B Mass transport and proof of absence of transport in local equilibrium

In this Appendix, we present the formulation of the local equilibrium density matrix apt to describe a system with a nonuniform density of particles, thus representing the physical situation for mass transport to occur. Moreover, we report the discussion delivered by Nakajima[101] about the impossibility to describe mass diffusion from a local equilibrium density matrix in presence of nonuniform particle distribution.

For the case of mass transport, the local equilibrium density matrix can be obtained from the MEP. The constraints to be imposed consist in the average value of the energy E (canonical ensemble), and the presence of a nonuniform particle density $n(\boldsymbol{x})$. The constrained optimization is performed with Lagrange multipliers β and $\mu(\boldsymbol{x})$, maximizing the functional

$$\begin{aligned}\tilde{S}[\rho]=&-\operatorname{Tr}[\hat{\rho}\log\hat{\rho}]-\beta\left(\operatorname{Tr}\left[\hat{\rho}\hat{H}\right]-E\right)\\&-\int \mathrm{d}\boldsymbol{x}\,\lambda(\boldsymbol{x})\left(\operatorname{Tr}[\hat{\rho}\hat{n}(\boldsymbol{x})]-n(\boldsymbol{x})\right)\end{aligned} \tag{1.B.1}$$

to obtain

$$\begin{aligned}\hat{\rho}_{\mathrm{loc}}^{el-chem}&=\frac{1}{Z\left[\beta,\lambda(\boldsymbol{x})\right]}e^{-\beta\hat{H}-\int \mathrm{d}\boldsymbol{x}\lambda(\boldsymbol{x})\hat{n}(\boldsymbol{x})}\,,\\ Z\left[\beta,\lambda(x)\right]&=\operatorname{Tr}\left[e^{-\beta\hat{H}-\int \mathrm{d}\boldsymbol{x}\lambda(\boldsymbol{x})\hat{n}(\boldsymbol{x})}\right]\,,\end{aligned} \tag{1.B.2}$$

where $\hat{n}(\boldsymbol{x})$ is the particle density operator. Unless specified otherwise, spatial integrals are conducted over the volume V of the system.

Eq. (1.B.2) describes an ensemble in contact with a bath that imposes a temperature $T=\frac{1}{k_B\beta}$ and an electrochemical potential $\lambda(\boldsymbol{x})=-\beta\bar{\mu}(\boldsymbol{x})=-\beta[\mu(\boldsymbol{x})+q\phi(\boldsymbol{x})]$, where q is the charge of the particles (the same for every particle) and $\phi(\boldsymbol{x})$ is the electrostatic potential.[111] This is understood from the thermodynamical relations with the entropy

$$\begin{aligned}-\frac{\partial\log Z}{\partial\beta}&=E\,,\quad &\frac{\partial S}{\partial E}&=\beta\,,\\ -\frac{\delta\log Z}{\delta\lambda(\boldsymbol{x})}&=n(\boldsymbol{x})\,,\quad &\frac{\delta S}{\delta n(\boldsymbol{x})}&=\lambda(\boldsymbol{x})\equiv-\beta\bar{\mu}(\boldsymbol{x})\,.\end{aligned} \tag{1.B.3}$$

In fact, a nonuniform distribution of particles is either obtained with a gradient of the chemical potential or, if the particles are charged, with an electrical field $\boldsymbol{\mathcal{E}}=-\boldsymbol{\nabla}\phi$.

$$\begin{aligned}\hat{\rho} &= \frac{1}{Z[\beta,\mu(\boldsymbol{x})]} e^{-\beta[\hat{H}-\int \mathrm{d}\boldsymbol{x}\mu(\boldsymbol{x})\hat{n}(\boldsymbol{x})]},\\ Z[\beta,\mu(\boldsymbol{x})] &= \mathrm{Tr}\left[e^{-\beta[\hat{H}-\int \mathrm{d}\boldsymbol{x}\mu(\boldsymbol{x})\hat{n}(\boldsymbol{x})]}\right] .\end{aligned} \tag{1.B.4}$$

The particle density operator is simply

$$\hat{n}(\boldsymbol{x},t) = \sum_a^N \delta(\boldsymbol{x}-\hat{\boldsymbol{x}}_a(t)) \tag{1.B.5}$$

where the sum runs over all the N particles of the system. From the continuity equation

$$\frac{\partial}{\partial t}\hat{n}(\boldsymbol{x},t) = -\boldsymbol{\nabla}\cdot\hat{\boldsymbol{j}}(\boldsymbol{x},t) \tag{1.B.6}$$

we get the particle current

$$\begin{aligned}&\frac{\partial}{\partial t}\hat{n}(\boldsymbol{x}) = \frac{1}{i\hbar}[\hat{n}(\boldsymbol{x}),\hat{H}] = \sum_a^N \frac{1}{i\hbar}\sum_\alpha [\delta(\boldsymbol{x}-\hat{\boldsymbol{x}}_a), \frac{\hat{p}_{a\alpha}^2}{2m_a}]\\ &= \frac{1}{2}\sum_a^N\sum_\alpha \frac{\hat{p}_{a\alpha}}{m_a}\frac{1}{i\hbar}[\delta(\boldsymbol{x}-\hat{\boldsymbol{x}}_a),\hat{p}_{a\alpha}] + \frac{1}{i\hbar}[\delta(\boldsymbol{x}-\hat{\boldsymbol{x}}_a),\hat{p}_{a\alpha}]\frac{\hat{p}_{a\alpha}}{m_a}\\ &= \tfrac{1}{2}\sum_a^N\sum_\alpha \frac{\hat{p}_{a\alpha}}{m_a}\frac{\partial}{\partial x_{a\alpha}}\delta(\boldsymbol{x}-\hat{\boldsymbol{x}}_a) + \text{h.c.}\\ &= -\boldsymbol{\nabla}\cdot\tfrac{1}{2}\sum_a^N[\frac{\hat{p}_a}{m_a}\delta(\boldsymbol{x}-\hat{\boldsymbol{x}}_a) + \delta(\boldsymbol{x}-\hat{\boldsymbol{x}}_a)\frac{\hat{p}_a}{m_a}] = -\boldsymbol{\nabla}\cdot\hat{\boldsymbol{j}}(\boldsymbol{x})\end{aligned} \tag{1.B.7}$$

where $\hat{\boldsymbol{p}}_a$ is the momentum of particle a, hence

$$\hat{\boldsymbol{j}}(\boldsymbol{x}) = \tfrac{1}{2}\sum_a^N[\frac{\hat{p}_a}{m_a}\delta(\boldsymbol{x}-\hat{\boldsymbol{x}}_a) + \delta(\boldsymbol{x}-\hat{\boldsymbol{x}}_a)\frac{\hat{p}_a}{m_a}] . \tag{1.B.8}$$

We then introduce the time-reversal operation $\hat{\mathcal{T}}$, that acts as

$$\hat{\mathcal{T}}\hat{\boldsymbol{x}}\hat{\mathcal{T}} = \hat{\boldsymbol{x}}, \quad \hat{\mathcal{T}}\hat{\boldsymbol{p}}\hat{\mathcal{T}} = -\hat{\boldsymbol{p}} \tag{1.B.9}$$

and satisfies $\hat{\mathcal{T}}^2$=1, $[\hat{\mathcal{T}},\hat{H}]$=0 in the nonmagnetic case. From (1.B.5) and (1.B.8) we understand that

$$\hat{\mathcal{T}}\hat{n}(\boldsymbol{x})\hat{\mathcal{T}} = \hat{n}(\boldsymbol{x}), \quad \hat{\mathcal{T}}\hat{\boldsymbol{j}}(\boldsymbol{x})\hat{\mathcal{T}} = -\hat{\boldsymbol{j}}(\boldsymbol{x}) . \tag{1.B.10}$$

Since $\hat{\rho}_{\text{loc}}$ only depends on $\hat{H}$ and $\hat{n}(\boldsymbol{x})$ that commute with $\hat{\mathcal{T}}$, it will commute with $\hat{\mathcal{T}}$ as well, i.e. $\hat{\mathcal{T}}\hat{\rho}_{\text{loc}}\hat{\mathcal{T}}$=$\hat{\rho}_{\text{loc}}$. It follows that

$$\begin{aligned}\boldsymbol{j}(\boldsymbol{x}) &= \mathrm{Tr}\Big[\hat{\rho}_{\text{loc}}\hat{\boldsymbol{j}}(\boldsymbol{x})\Big] \propto \mathrm{Tr}\Big[e^{-\beta[\hat{H}-\int \mathrm{d}\boldsymbol{x}\mu(\boldsymbol{x})\hat{n}(\boldsymbol{x})]}\hat{\boldsymbol{j}}(\boldsymbol{x})\Big]\\ &= \mathrm{Tr}\Big[\hat{\mathcal{T}}e^{-\beta[\hat{H}-\int \mathrm{d}\boldsymbol{x}\mu(\boldsymbol{x})\hat{n}(\boldsymbol{x})]}\hat{\mathcal{T}}\hat{\mathcal{T}}\hat{\boldsymbol{j}}(\boldsymbol{x})\hat{\mathcal{T}}\Big]\\ &= -\mathrm{Tr}\Big[\hat{\rho}_{\text{loc}}\hat{\boldsymbol{j}}(\boldsymbol{x})\Big] = 0\end{aligned} \tag{1.B.11}$$

which proves that no current is sustained by the local equilibrium state.

The proof outlined above is not tied to mass transport but consists in a general result for the

local equilibrium density matrix. It follows from the fact that $\hat{\rho}_{\text{loc}}$ depends on densities that are not conserved, i.e. do not commute with the Hamiltonian.[1,101,113,118] Since the conserved density $\hat{n}(\boldsymbol{x})$ and the correspondent current $\hat{\boldsymbol{j}}(\boldsymbol{x})$ are related from the continuity equation (1.B.6) by a time derivative, they possess opposite behaviour upon time reversal. This can be understood considering the fact that the time-reversal operator $\hat{\mathcal{T}}$ acts on complex numbers as complex conjugate operation, hence $\hat{\mathcal{T}}\frac{\partial}{\partial t}\hat{n}(\boldsymbol{x},t)\hat{\mathcal{T}}=\hat{\mathcal{T}}\frac{1}{i\hbar}[\hat{H},\hat{n}(\boldsymbol{x},t)]\hat{\mathcal{T}}=-\frac{\partial}{\partial t}\left(\hat{\mathcal{T}}\hat{n}(\boldsymbol{x},t)\hat{\mathcal{T}}\right)$ if $[\hat{\mathcal{T}},\hat{H}]=0$. The local equilibrium density matrix depends on the densities, hence it possess their symmetry upon time reversal (even). Since the expectation value of a current in a local equilibrium state consists in the trace of a product of operators with opposite symmetry on time reversal, it is zero

$$\begin{aligned}&\operatorname{Tr}\left[\hat{\rho}_{\text{loc}}(t)\hat{\boldsymbol{j}}(\boldsymbol{x},t)\right]=\operatorname{Tr}\left[\hat{\mathcal{T}}\hat{\rho}_{\text{loc}}(t)\hat{\mathcal{T}}\hat{\boldsymbol{j}}(\boldsymbol{x},t)\right]\\&=\operatorname{Tr}\left[\hat{\rho}_{\text{loc}}(t)\hat{\mathcal{T}}\hat{\boldsymbol{j}}(\boldsymbol{x},t)\hat{\mathcal{T}}\right]=-\operatorname{Tr}\left[\hat{\rho}_{\text{loc}}(t)\hat{\boldsymbol{j}}(\boldsymbol{x},t)\right]=0\end{aligned}\tag{1.B.12}$$

(cfr. 1 Sec. 20.5).

1.C Foundations of the modified Liouville equation from maximum entropy principle

In this Appendix, we discuss the details of the derivation of the steady-state density matrix through the application of the maximum entropy principle. Additionally, we demonstrate how this operator satisfies the modified Liouville equation Eq. (1.3.2) and we show how the standard Kubo formula for thermal conductivity is recovered with such approach.

Details on the derivation of the steady state from the maximum entropy principle

For this derivation, we will follow the works by Grandy[107,111] and Scalapino.[112] As discussed in the main text, to obtain the steady state $\hat{\rho}_{\text{st}}$ we maximize the functional

$$\tilde{S}[\rho_{\text{st}}]=-\operatorname{Tr}[\hat{\rho}_{\text{st}}\log\hat{\rho}_{\text{st}}]-\int_V \mathrm{d}\boldsymbol{x}\,\beta(\boldsymbol{x})\left(\operatorname{Tr}\left[\hat{\rho}_{\text{st}}\hat{h}(\boldsymbol{x})\right]-h(\boldsymbol{x})\right)\tag{1.C.1}$$

with the additional constraint

$$[\hat{\rho}_{\text{st}},\hat{H}]=0\tag{1.C.2}$$

to be imposed on the variations. The stationarity condition Eq. (1.2.19) can be rephrased as

$$[\hat{\rho}_{\text{st}}+\delta\hat{\rho},\hat{H}]=0\quad\rightarrow\quad[\delta\hat{\rho},\hat{H}]=0\tag{1.C.3}$$

as introduced in Eq. (1.2.21). Let us introduce a representation in which the Hamiltonian is diagonal, i.e. a complete set of eigenvectors $\{|E\nu\rangle\}$ of the Hamiltonian $\hat{H}\,|E\nu\rangle=E\,|E\nu\rangle$ where E is the energy eigenvalue, while ν denotes all the relevant quantum numbers other than the energy. The stationarity condition Eq. (1.C.3) can be rewritten as

$$\begin{aligned}\langle E\nu|[\delta\hat{\rho},\hat{H}]|E'\nu'\rangle&=0\\(E-E')\,\langle E\nu|\delta\hat{\rho}|E'\nu'\rangle&=0\end{aligned}\tag{1.C.4}$$

which implies that if $E\neq E'$, the variations are all zero $\langle E\nu|\delta\hat{\rho}|E'\nu'\rangle=0$, whereas if $E=E'$ the above condition is automatically satisfied and the variations $\langle E\nu|\delta\hat{\rho}|E'\nu'\rangle$ are uncos-

trained. Thus, in order to keep the density matrix stationary, we must perform variations in a degenerate subspace. Let us express Eq. (1.2.20) in the basis $\{|E\nu\rangle\}$:

$$\delta\tilde{S}=\sum_{EE',\nu\nu'}\langle E\nu|\delta\hat{\rho}|E'\nu'\rangle\,\langle E'\nu'|\log\hat{\rho}_{\text{st}}+\int_V \mathrm{d}\boldsymbol{x}\,\beta(\boldsymbol{x})\hat{h}(\boldsymbol{x})|E\nu\rangle\ . \tag{1.C.5}$$

From Eq. (1.C.4) we get that $\langle E\nu|\delta\hat{\rho}|E'\nu'\rangle=\delta_{EE'}\delta\rho^E_{\nu,\nu'}$, where $\delta\rho^E_{\nu,\nu'}$ are the unconstrained variations, hence

$$\delta\tilde{S}=\sum_{E,\nu\nu'}\delta\rho^E_{\nu,\nu'}\,\langle E\nu'|\log\hat{\rho}_{\text{st}}+\int_V \mathrm{d}\boldsymbol{x}\,\beta(\boldsymbol{x})\hat{h}(\boldsymbol{x})|E\nu\rangle=0. \tag{1.C.6}$$

Since the variations $\delta\rho^E_{\nu,\nu'}$ are unconstrained, their coefficients must be zero for all E,ν,ν'. If we define the diagonal part of the energy density as

$$\langle E\nu|\hat{h}_d|E'\nu'\rangle=\delta_{EE'}\,\langle E\nu|\hat{h}|E'\nu'\rangle \tag{1.C.7}$$

we see that Eq. (1.C.6) can be expressed as

$$\langle E\nu'|\log\hat{\rho}_{\text{st}}+\int_V \mathrm{d}\boldsymbol{x}\,\beta(\boldsymbol{x})\hat{h}_d(\boldsymbol{x})|E\nu\rangle=0 \tag{1.C.8}$$

from which we derive the structure of the steady-state density matrix

$$\begin{aligned}\hat{\rho}_{\text{st}}&=\frac{1}{Z_{st}}e^{-\int_V \mathrm{d}\boldsymbol{x}\beta(\boldsymbol{x})\hat{h}_d(\boldsymbol{x})}\ ,\\ Z_{st}&=\mathrm{Tr}\left[e^{-\int_V \mathrm{d}\boldsymbol{x}\beta(\boldsymbol{x})\hat{h}_d(\boldsymbol{x})}\right].\end{aligned} \tag{1.C.9}$$

which is the structure introduced in Eq. (1.2.22).

We now exploit Eq. (1.C.7) to derive an explicit operatorial structure for $\hat{h}_d$. Let us describe for a generic operator $\hat{O}$ its diagonal part as

$$\hat{O}_d=\hat{O}-\frac{i}{\hbar}[\hat{H},\hat{A}]\,. \tag{1.C.10}$$

The idea is that since $\hat{O}_d$ must commute with $\hat{H}$ and $\hat{O}$ in general does not, we are "removing" the part of $\hat{O}$ that does not commute with $\hat{H}$ (related to $\hat{A}$, still to be defined) to obtain $\hat{O}_d$. Now using Eq. (1.C.7), we get that if we evaluate the matrix element between different energy states $E\neq E'$

$$\begin{aligned}\langle E\nu|\hat{O}_d|E'\nu'\rangle=0&=\langle E\nu|\hat{O}|E'\nu'\rangle-\langle E\nu|\frac{i}{\hbar}[\hat{H},\hat{A}]|E'\nu'\rangle\\ \langle E\nu|\hat{A}|E'\nu'\rangle&=\frac{1}{\frac{i}{\hbar}(E-E')}\langle E\nu|\hat{O}|E'\nu'\rangle\end{aligned} \tag{1.C.11}$$

from which we can formally solve for $\hat{A}$ as

$$\hat{A}=\lim_{\epsilon\to0^+}\int_{-\infty}^{0}\mathrm{d}t\,e^{\epsilon t}e^{\frac{i}{\hbar}t\hat{H}}\hat{O}e^{-\frac{i}{\hbar}t\hat{H}} \tag{1.C.12}$$

which can be easily proved by direct evaluation of the matrix element $\langle E\nu|\hat{A}|E'\nu'\rangle$. Now using Heisenberg representation, we can express Eq. (1.C.12) as

$$\hat{A} = \lim_{\epsilon\to 0^+} \int_{-\infty}^{0} \mathrm{d}t\, e^{\epsilon t}\hat{O}(t) \tag{1.C.13}$$

and the diagonal part of the operator Eq. (1.C.10) can then be expressed as

$$\hat{O}_d = \hat{O} - \lim_{\epsilon\to 0^+} \int_{-\infty}^{0} \mathrm{d}t\, e^{\epsilon t}\frac{i}{\hbar}[\hat{H},\hat{O}(t)] = \hat{O} - \lim_{\epsilon\to 0^+} \int_{-\infty}^{0} \mathrm{d}t\, e^{\epsilon t}\frac{\partial}{\partial t}\hat{O}(t). \tag{1.C.14}$$

We can thus express the diagonal part of the energy density as

$$\hat{h}_d(\boldsymbol{x}) = \hat{h}(\boldsymbol{x}) - \lim_{\epsilon\to 0^+} \int_{-\infty}^{0} \mathrm{d}t\, e^{\epsilon t}\frac{\partial}{\partial t}\hat{h}(\boldsymbol{x},t) \tag{1.C.15}$$

which is the expression introduced in Eq. (1.2.23) Now we can express the steady-state density matrix Eq. (1.2.22) in terms of explicit operators

$$\hat{\rho}_{\mathrm{st}} = \frac{1}{Z_{st}}\exp\Big[-\int \mathrm{d}\boldsymbol{x}\,\beta(\boldsymbol{x})\hat{h}(\boldsymbol{x}) + \lim_{\epsilon\to 0^+}\int_{-\infty}^{0}\mathrm{d}t\, e^{\epsilon t}\int \mathrm{d}\boldsymbol{x}\,\beta(\boldsymbol{x})\frac{\partial}{\partial t}\hat{h}(\boldsymbol{x},t) \tag{1.C.16}$$

from which we understand how the steady-state operator differs from the local equilibrium density matrix Eq. (1.2.10) due to the presence of the extra term containing the integral of the energy density.

Derivation of the modified Liouville Equation and entropy considerations

Now let us show how the steady state obtained from the maximum entropy principle (1.C.16) satisfies the modified Liouville equation introduced in Eq. (1.3.2). Noting from Eq. (1.2.10) that $-\int \mathrm{d}\boldsymbol{x}\,\beta(\boldsymbol{x})\hat{h}(\boldsymbol{x}) = \log\hat{\rho}_{\mathrm{loc}}$ besides normalization constants, Eq. (1.C.16) can be expressed as

$$\hat{\rho}_{\mathrm{st}} = \exp\left[\log\hat{\rho}_{\mathrm{loc}} - \lim_{\epsilon\to 0^+}\int_{-\infty}^{0}\mathrm{d}t\, e^{\epsilon t}\frac{\partial}{\partial t}e^{i\mathcal{L}t}\log\hat{\rho}_{\mathrm{loc}}\right]. \tag{1.C.17}$$

If we consider the logarithm of the pre-ϵ-limit density matrix we get

$$\begin{aligned}
\log\hat{\rho}^{\epsilon}_{\mathrm{st}} &= \log\hat{\rho}_{\mathrm{loc}} - \int_{-\infty}^{0}\mathrm{d}t\, e^{\epsilon t}\frac{\partial}{\partial t}e^{\frac{i}{\hbar}\mathcal{L}t}\log\hat{\rho}_{\mathrm{loc}} \\
&= \log\hat{\rho}_{\mathrm{loc}} - \int_{-\infty}^{0}\mathrm{d}t\, e^{\epsilon t}e^{\frac{i}{\hbar}\mathcal{L}t}\frac{i}{\hbar}\mathcal{L}\log\hat{\rho}_{\mathrm{loc}} \\
&= \log\hat{\rho}_{\mathrm{loc}} - \frac{1}{\epsilon + i\mathcal{L}}\frac{i}{\hbar}\mathcal{L}\log\hat{\rho}_{\mathrm{loc}} \\
(\hbar\epsilon + i\mathcal{L})\log\hat{\rho}^{\epsilon}_{\mathrm{st}} &= (\hbar\epsilon + i\mathcal{L})\log\hat{\rho}_{\mathrm{loc}} - i\mathcal{L}\log\hat{\rho}_{\mathrm{loc}} \\
i\mathcal{L}\log\hat{\rho}^{\epsilon}_{\mathrm{st}} &= -\hbar\epsilon(\log\hat{\rho}^{\epsilon}_{\mathrm{st}} - \log\hat{\rho}_{\mathrm{loc}})
\end{aligned} \tag{1.C.18}$$

where the last line is precisely the expression of the modified Liouville equation Eq. (1.3.2) in the static case ($\frac{\partial \rho}{\partial t}=0$, no explicit time dependence) for $\log \hat{\rho}$.[2,113] It can be shown that we can impose the Liouville equation either on $\hat{\rho}$ or $\log \hat{\rho}$, since if one is subject to a dynamical equation, the other will be too.[1,2,113]

From the discussion just carried out, we can understand how the modified Liouville equation describes processes in which the entropy increases. In fact, if we recast Eq. (1.C.18) for the entropy operator $\hat{\sigma}=-\log \hat{\rho}$, we get

$$i\mathcal{L}\hat{\sigma}^{\epsilon}_{st} = \hbar\epsilon(\hat{\sigma}_{\rm loc} - \hat{\sigma}^{\epsilon}_{st}) \,. \tag{1.C.19}$$

From a simple statistical mechanics argument, we understand that the entropy of the steady state is lower that that of the local equilibrium state, *i.e.* the right-hand side of Eq. (1.C.19) is positive for $\epsilon>0$. In fact, in Sec. 1.C we have showed how the steady-state density matrix is obtained with the maximum entropy principle applied with an extra requirement with respect to the constraints used to derive the local equilibrium operator. The number of configurations that can represent local equilibrium is thus larger than those that represent the steady-state. Since the action of the Liouville operator describe the variation of the operator $\hat{\sigma}$, Eq. (1.C.19) implies that $\frac{\mathrm{d}S}{\mathrm{d}t}>0$. In other words, the introduction of the ϵ term in the modified Liouvile equation, forces the relaxation of the density matrix from the steady-state to the local equilbrium state. Since the steady-state has lower symmetry (time-reversal symmetry is broken) than the local equilbrium state, this process increases entropy.

Notice that the main difference between the approach of the maximum entropy principle for the steady-state and the one that starts from the modified Liouville equation Eq. (1.3.2) carried out in Sec. 1.3, is that in the latter an initial condition on the density matrix should be specified, while for the former it is not needed. In fact, the variational approach finds the stationary nonequilbrium state without any description on how this steady-state is established, while the modified Liouville equation consist in a differential equation in which the whole dynamics is described.

1.D Useful operatorial identities

Here we prove some of the key operatorial relations used in this Chapter.

Exponential expansion

Here we prove the proof of the expansion of the exponential operator

$$e^{-(\hat{A}+\hat{B})} = e^{-\hat{A}} - e^{-\hat{A}} \int_0^1 \mathrm{d}\sigma \, e^{\sigma\hat{A}}\hat{B}e^{-\sigma(\hat{A}+\hat{B})} \tag{1.D.1}$$

To prove it, we follow Zubarev[2] and Kubo[113] introducing the auxiliary function

$$K(\tau) = e^{\tau\hat{A}}e^{-\tau(\hat{A}+\hat{B})} \,. \tag{1.D.2}$$

Considering its derivative, we get

$$\frac{\partial K(\tau)}{\partial \tau} = \hat{A}e^{\tau\hat{A}}e^{-\tau(\hat{A}+\hat{B})} - (\hat{A}+\hat{B})e^{\tau\hat{A}}e^{-\tau(\hat{A}+\hat{B})} = -e^{\tau\hat{A}}\hat{B}e^{-\tau(\hat{A}+\hat{B})} \tag{1.D.3}$$

so that

$$\begin{aligned}\int_0^\tau \mathrm{d}\sigma\, \frac{\partial K(\sigma)}{\partial \sigma} = K(\tau) - K(0) = -\int_0^\tau \mathrm{d}\sigma\, e^{\sigma\hat{A}}\hat{B}e^{-\sigma(\hat{A}+\hat{B})} \\ e^{\tau\hat{A}}e^{-\tau(\hat{A}+\hat{B})} - 1 = -\int_0^\tau \mathrm{d}\sigma\, e^{\sigma\hat{A}}\hat{B}e^{-\sigma(\hat{A}+\hat{B})}\,.\end{aligned} \tag{1.D.4}$$

Multiplying times $e^{-\tau A}$ from the left both sides of the equation above and evaluating the case τ=1 we get (1.D.1).

Kubo identity

Here we prove the Kubo identity

$$[\hat{A}, e^{-\beta\hat{H}}] = e^{-\beta\hat{H}} \int_0^\beta \mathrm{d}\lambda\, e^{\lambda\hat{H}}[\hat{H}, \hat{A}]e^{-\lambda\hat{H}}\,. \tag{1.D.5}$$

Introducing a complete set $\{|n\rangle\}$ of eigenstates of the Hamiltonian $\hat{H}\,|n\rangle = E_n\,|n\rangle$, we can evaluate the left-hand side simply as

$$\langle m|[\hat{A}, e^{-\beta\hat{H}}]|n\rangle = \left(e^{-\beta E_n} - e^{-\beta E_m}\right)\,\langle m|\hat{A}|n\rangle\,. \tag{1.D.6}$$

The right-hand side of (1.D.5) instead reads

$$\begin{aligned}\langle m|e^{-\beta\hat{H}} \int_0^\beta \mathrm{d}\lambda\, e^{\lambda\hat{H}}[\hat{H}, \hat{A}]e^{-\lambda\hat{H}}|n\rangle = e^{-\beta E_m}\int_0^\beta \mathrm{d}\lambda\,(E_m - E_n)e^{\beta(E_m-E_n)}\,\langle m|\hat{A}|n\rangle \\ = e^{-\beta E_m}\left(e^{\beta(E_m-E_n)} - 1\right)\,\langle m|\hat{A}|n\rangle = \left(e^{-\beta E_n} - e^{-\beta E_m}\right)\,\langle m|\hat{A}|n\rangle\,,\end{aligned} \tag{1.D.7}$$

which finally proves (1.D.5).

Chapter 2

Many-body Green's function approach to lattice thermal transport

Introduction

In the last few years, the technological interest in increasing the efficiency of thermoelectric energy-conversion devices,[3–5] or in optimizing thermal shields and thermal barrier coatings,[6–11] has stimulated intense research on materials with ultralow thermal conductivity. So-called complex crystals, defined as materials with a phonon spectrum featuring interband spacings smaller than the linewidths,[12,13] are promising candidates for these applications since their thermal conductivity is very low (typically $\lesssim 1 \frac{\mathrm{W}}{m \cdot K}$ around room temperature). More precisely, the thermal properties of complex crystals can be regarded as intermediate between those of simple crystals, where the interband spacings between phonon branches are much larger than their linewidths,[12,13] and those of glasses, where vibrational eigenstates are quasi-degenerate. More specifically, while in simple crystals the thermal conductivity $\kappa(T)$ follows the typical[119] Peierls-Boltzmann $\kappa(T) \sim T^{-1}$ decay for $T \gg \theta_D$ (where θ_D is the Debye temperature), in complex crystals $\kappa(T)$ has a much milder asymptotic decay, which resembles the saturating trend typical of glasses.[37,120–122] Such intermediate behavior has been related by several works[12,26,29,32–34] to the coexistence of Peierls-Boltzmann intraband transport, dominant in simple crystals,[14,35,36] and interband [I]transport, dominant in glasses.[37]

The milestone work by Hardy[35] that generalized the heat-flux operator in a lattice for interband transport stimulated some theoretical work in the 1960s aiming at a formal description of both mechanisms within a Green-Kubo formalism,[123,124] but a quantitative comparison among the two mechanisms emerged only in recent times. The reason for such delay lies probably in the fact that the computing power needed to simulate systems in which interband transport is relevant was prohibitive for the time. In fact, it was not long ago that very accurate first-principle scattering rates to be used in thermal transport calculation became available.[15,43,125] Thus, a number of works have relied on these advances to study heat conduction from first-principles in crystals using the simplest numerically manageable model, the Peierls-Boltzmann equation for intraband transport, highlighting its accuracy in simple crystals[15–25] but also its failures in complex crystals.[26–32] As a result, these works have sparked interest in understanding how to describe accurately — and in a computationally affordable form — thermal transport. The most recent theoretical efforts[12,33,39,126] were thus

[I]Here the term "interband" for glasses is understood considering glasses as limiting cases of disordered but periodic crystals in the limit of infinitely large primitive cells

motivated by a quantitative estimate of interband effects, but they actually led to a broader perspective about the microscopic description of heat transport, highlighting the failures of Peierls-Boltzmann formulation in complex crystals,[12] where interband transitions emerge.

The existence of different approaches to account for interband transport raises the question of elucidating analogies and differences between them, and most importantly, benchmarking the differences in their predictions for the thermal conductivity. One can indeed identify two main sources for such differences.

The first one concerns the definition of the quantum heat current operator $\hat{\boldsymbol{j}}$, a well-known problem for the theoretical description of thermal transport.[127–129] Indeed, while in the case of the electrical current one can define the quantum current operator via the response to an external gauge field, in the case of the thermal current $\hat{\boldsymbol{j}}$ can only be defined via a continuity equation for the local energy density $\hat{h}$:

$$\frac{\partial \hat{h}(\boldsymbol{x},t)}{\partial t} + \boldsymbol{\nabla}\cdot\hat{\boldsymbol{j}}(\boldsymbol{x},t) = 0 \tag{2.0.1}$$

already introduced in (1.2.16). However, the identification of the local energy density $\hat{h}$ is not unique, since the local partition of the total energy density of the crystal can be done in different ways. This non-uniqueness is reflected in the definition of the heat current operator, and it has been used in Ref.[40] to formulate a so-called gauge-invariance principle for the thermal transport that is analogous to the well-known one for electrical current, *i.e.* different definitions of the thermal current that lead to the same physical result for the transport coefficients. As we shall see, this issue is deeply connected with the approximation scheme used to compute the thermal conductivity. Among the recently published works, the Green-Kubo approaches of Refs. 33, 126 relied on the original heat-flux definition proposed by Hardy,[35] where $\hat{h}(\boldsymbol{x},t)$ is essentially a coarse-grained version of the harmonic Hamiltonian expressed in terms of the ionic displacement operators and their conjugate momenta. On the other hand, a different approach used, where the heat flux is directly computed from a generalization of the BTE named Wigner transport equation (WTE), detailed in Refs. 12. This formulation exploits the Wigner transformation of the density matrix, which naturally suggests the introduction of bosonic operators which describe localized vibrational excitations. Even though in Refs. 12, 13 the corresponding quantum operator for the heat current is not explicitly given, from the form of the matrix elements of phonon velocities presented in[12] one can already infer a different structure for it with respect to the one given by Hardy.

A second apparent source of discrepancies between recent[33,39] and previous[123,124] works based on the Green-Kubo formalism concerns the implementation of interaction effects for phonons. Indeed, while the original papers[123,124] followed the standard route of implementing self-energy corrections in the frequency domain via a generalized phonon spectral function, in Ref. 33, 39 the calculations are done in the time-domain, with approximated schemes needed to assign frequency-independent lifetimes to each phonon mode. Even though the two approaches are expected to give the same final expressions in the limit where phonon broadening is sufficiently smaller than phonon energies, such a formal equivalence cannot be obtained, as we will see below, leaving open the question of a consistent derivation of thermal conductivity within the Green-Kubo approach.

The aim of the present Chapter is to derive a full quantum description of heat transport in the case of complex crystals using the many-body Green's function approach, and to explain analogies and differences between the various existing approaches, with the goal of pointing to a consistent theoretical framework for the computation of thermal conductivity

in crystals. More specifically, we derive the thermal conductivity in the so-called dressed-bubble approximation, where the effects of anharmonicity and disorder are encoded via renormalized phonon spectral densities including all self-energy corrections. The resulting expression of the thermal conductivity depends on the choice of the heat-flux operator. Here we focus on two specific choices for the heat flux: the one originally proposed by Hardy,[35] and used later in several works,[33,124,126] and the one obtained following the Wigner approach as proposed in Ref. 13. In both cases, we provide a general expression able to describe thermal transport both in the low-damping regime, where phonon excitations are still well defined and interband transport is eventually relevant for densely spaced phonon bands, and in the overdamped regime, where the phonon quasiparticle picture breaks down. To make a closer connection with the previous works, we show how some of the aforementioned results for thermal conductivity can be compared to our fully-quantum expression in the Lorentzian spectral function approximation (LSFA). The LSFA consists in approximating the imaginary part of the self-energy with its value computed at the (bare) phonon frequencies $\Omega(\boldsymbol{q})_s$ so that the spectral density reduces to a Lorentzian with full-width at half maximum $\Gamma(\boldsymbol{q})_s$. As we shall see, the two different heat fluxes yield conductivities differing exclusively in the contributions from interband processes. The heat flux derived by Hardy describes processes which are relevant for $\Omega(\boldsymbol{q})_s - \Omega(\boldsymbol{q})_{s'} \lesssim \Gamma(\boldsymbol{q})_s + \Gamma(\boldsymbol{q})_{s'}$, denoted as "resonant" in Ref.,[33] and processes relevant for $\Omega(\boldsymbol{q})_s + \Omega(\boldsymbol{q})_{s'} \lesssim \Gamma(\boldsymbol{q})_s + \Gamma(\boldsymbol{q})_{s'}$, denoted as "antiresonant". We show that the former give a sizeable contribution to the thermal conductivity, while the latter are typically negligible, as expected since phonon frequencies are always positive. Within the Wigner formulation[12,13] these antiresonant terms are absent. We show that using the Wigner heat flux in the LSFA yields exactly the result for the single-mode relaxation-time approximation (SMA) of the WTE reported in Ref. 13.

The recovery of the result for thermal conductivity presented in Ref. 12 from the present quantum formula supports the theoretical consistency of the Wigner formalism for thermal transport. In the case of the Hardy current operator the present result corresponds to the ones given in Ref. 123, 124, but differs from more recent derivations.[33,39] We show that such a discrepancy originates from the procedure used to implement the limit of frequency-independent phonon lifetimes within the real-time Green's function, and we show that this affects only the description of interband effects.

Despite formal differences between the thermal-conductivity expressions derived from the Hardy or the Wigner heat-flux operators, the numerical results are quantitatively very similar in the regime where the LSFA holds. We investigate two test cases: perovskite $CsPbBr_3$ and zirconate $La_2Zr_2O_7$, both materials with ultralow thermal conductivity. In these systems, we find that the different formulations for the heat flux lead to little or negligible numerical discrepancy, and both approaches give successful predictions in agreement with experimental data. Interestingly, we find that the same holds also for the results obtained via the real-time approximated scheme used in Refs. 33, 39. So, the formal discrepancies in the final expressions of thermal conductivity become quantitatively irrelevant for the systems under investigation.

We finally discuss the theoretical foundations for the consistency among the results obtained from the Hardy and Wigner heat fluxes, arguing that the gauge-invariance principle of transport coefficients[40] might not be sufficient to explain such a similarity, and suggesting that a consistent theoretical prescription on how to choose the heat flux is still missing. In this regard, we provide some plausibility arguments which point toward the Wigner heat flux as the most appropriate choice.

Chapter Overview

This Chapter is organized as follows: in Sec. 2.1 we show how to recast the Kubo formula for thermal conductivity in terms of the static limit of a finite-frequency response function, using the fluctuation-dissipation theorem. In Sec. 2.2 we present the definitions of the local energy operator used in the Hardy[35] and in the Wigner[12] formalism, and we describe how to derive the corresponding heat-flux operators following Hardy's original procedure.[35] In Sec. 2.3 we show how to compute thermal conductivity using the expressions that have been derived for the Hardy and Wigner heat-flux operators in the dressed-bubble approximation, which is analyzed as a perturbative diagrammatic expansion of finite-temperature Green's functions. Thereafter, the resulting expressions are discussed and compared, while addressing differences and analogies with the formulas already present in the literature.[12,33,123,124] Finally, in Sec. 2.4 we comment on the numerical results obtained in the LSFA, wondering if the agreement between the computed thermal conductivities obtained from the different definitions of the heat flux is a consequence of the gauge invariance of transport coefficients, and in Sec. 2.5 we present some closing remarks.

The content of this Chapter has been published in Phys. Rev. B 106, 024312 (2022).[110]

2.1 Kubo formula for thermal conductivity

In the linear-response regime the thermal conductivity at temperature T is an equilibrium property, and as such can be computed in the absence of an external perturbation acting on the system using the Kubo formula for thermal conductivity,

$$\kappa^{\gamma\sigma} = \lim_{\epsilon\to 0^+} \frac{V}{T} \int_0^\infty \mathrm{d}t\, e^{-\epsilon t} \int_0^\beta \mathrm{d}\lambda\, \mathrm{Tr}\Big[\hat{\rho}_0 \hat{J}^\sigma(0) \hat{J}^\gamma(+t+i\hbar\lambda)\Big] \tag{2.1.1}$$

that we have derived in Eq. (1.3.10).

In a crystal, Eq. (1.3.10) features the heat-flux operator $\hat{\boldsymbol{J}}$ as the volume integral of the microscopic current density $\hat{\boldsymbol{J}}$ defined in (1.2.15) normalized by the volume of the system $V{=}N_c\mathcal{V}$, obtained multiplying the number of primitive cells N_c by the primitive cell volume $\mathcal{V}$. Note that in the classical limit ($\hbar{\to}0$) Eq. (2.1.1) reduces to the usual expression of the Kubo formula for thermal conductivity as the time integral of the heat-flux auto-correlation function: $\kappa^{\gamma\sigma}{=}\frac{N_c\mathcal{V}}{k_B T^2}\int_0^\infty \mathrm{d}t\, \langle J^\gamma(t) J^\sigma(0)\rangle$. The angle brackets indicate the averaging in absence of thermal disturbances (*i.e.* at global equilibrium), thus for a generic operator $\hat{O}$ we have $\langle\hat{O}\rangle{=}\,\mathrm{Tr}\big[\hat{O}\hat{\rho}_0\big]$, where $\hat{\rho}_0$ is the canonical density matrix defined in Eq. (1.2.7).

The ordering of the cartesian components of the heat-flux operator does not matter, since the Onsager relations[130] imply that $\kappa^{\alpha\beta}{=}\kappa^{\beta\alpha}$. In complete analogy with the standard approach to the calculation of electrical conductivity,[67] Eq. (2.1.1) can be expressed as the static limit of a finite-frequency response function. Let us consider the current-current correlation function, together with its Fourier transform (frequency integrals will always be intended from $-\infty$ to $+\infty$)

$$S^{\gamma\sigma}(t) = \langle \hat{J}^\gamma(t) \hat{J}^\sigma(0)\rangle = \int \mathrm{d}\omega\, e^{-i\omega t} S^{\gamma\sigma}(\omega)\,; \tag{2.1.2}$$

this is related to the retarded response function

$$\chi^{\gamma\sigma}(t) = \frac{i}{\hbar}\theta(t)\langle[\hat{J}^{\gamma}(t), \hat{J}^{\sigma}(0)]\rangle \tag{2.1.3}$$

by the fluctuation-dissipation theorem[117] as follows

$$S^{\gamma\sigma}(\omega) = \frac{\hbar}{\pi}[n_T(\omega)+1]\mathrm{Im}\chi^{\gamma\sigma}(\omega+i0^+), \tag{2.1.4}$$

where $n_T(\omega)=(e^{\frac{\hbar\omega}{k_BT}}-1)^{-1}$ is the Bose-Einstein equilibrium distribution function at temperature T. Inserting (2.1.2) in (2.1.1) and calculating the integrals in λ and t yields

$$\kappa^{\alpha\beta}=\lim_{\epsilon\to0^+}\frac{N_c\mathcal{V}}{T}\int \mathrm{d}\omega\,\frac{i}{\omega+i\epsilon}\frac{1-e^{-\frac{\hbar\omega}{k_BT}}}{\hbar\omega}S^{\alpha\beta}(\omega)\,. \tag{2.1.5}$$

At this point we can use Eq. (2.1.4) in the latter equation and the well-known Sokhotski–Plemelj formula[131] $\lim_{\epsilon\to0^+}\frac{i}{\omega\pm i\epsilon}=i\mathcal{P}\frac{1}{\omega}\pm\pi\delta(\omega)$ to obtain

$$\kappa^{\gamma\sigma}=\lim_{\omega\to0}\frac{N_c\mathcal{V}}{T}\frac{\mathrm{Im}\chi^{\gamma\sigma}(\omega+i0^+)}{\omega}\,. \tag{2.1.6}$$

Note that when using the aforementioned result to solve the $\epsilon\to0$ limit one actually gets an imaginary part of thermal conductivity related to a Cauchy principal value integral (denoted with $\mathcal{P}$). But if Onsager relations hold — thus, if κ is a symmetric tensor — the expression (2.1.1) is purely real. In fact, the $\epsilon\to0$ limits yields $\mathrm{Im}\kappa^{\gamma\sigma}=\frac{V}{k_BT}\mathcal{P}\int\mathrm{d}\omega\,\frac{\mathrm{Im}\chi^{\gamma\sigma}(\omega+i0^+)}{\omega^2}$ which is zero since $\mathrm{Im}\chi^{\gamma\sigma}(\omega+i0^+)=-\mathrm{Im}\chi^{\sigma\gamma}(-\omega+i0^+)$ as can be easily shown with a spectral decomposition of the response function.

The advantage of the representation (2.1.6) over (2.1.1) is that the imaginary part of the retarded response function can be computed as the analytic continuation of the time-ordered imaginary-time response function, as we will see in Sec. 2.3. The response function formalism is the most convenient choice to implement perturbative calculations of thermal conductivity when accounting for interactions. In contrast, the formulation (2.1.1) is in practice feasible only in the so-called bubble approximation, as we will discuss in more detail in what follows and in the Appendix 2.C.

2.2 Heat-flux operator for a crystal lattice

Here we describe how to derive the heat-flux operators following Hardy's original procedure[35] starting from the definitions of the on-site energy operator used in the Hardy[35] and in the Wigner[12] formalism. In fact, to calculate the thermal conductivity from (2.1.6), a definition of the heat-flux operator for a lattice must be introduced. The standard picture of heat transport in crystals relies on the Peierls-Boltzmann transport equation in its linearized form (LBTE),[14] in which phonon interband effects are neglected. This model pictures the crystal lattice as a semiclassical gas of propagating phonon wavepackets that scatter like particles, and in this formalism, the heat-flux operator $\hat{\boldsymbol{J}}_P$ accounts for particle-like propagation via independent phonon bands

$$\hat{\boldsymbol{J}}_P=\frac{1}{N_c\mathcal{V}}\sum_{\boldsymbol{q},s}\hbar\Omega(\boldsymbol{q})_s\boldsymbol{v}(\boldsymbol{q})_s\hat{n}(\boldsymbol{q})_s, \tag{2.2.1}$$

where $\Omega(\boldsymbol{q})_s$ and $\boldsymbol{v}(\boldsymbol{q})_s{=}\boldsymbol{\nabla}_{\boldsymbol{q}}\Omega(\boldsymbol{q})_s$ are respectively the frequency and group velocity of phonon with quasi-momentum $\boldsymbol{q}$ and in band s, and the sum in $\boldsymbol{q}$ spans over the values of crystal momentum fixed by periodic boundary conditions contained in the first Brillouin zone. The heat flux is diagonal in the phonon band index, depending only on the phonon number operator $\hat{n}(\boldsymbol{q})_s{=}\hat{a}^\dagger(\boldsymbol{q})_s\hat{a}(\boldsymbol{q})_s$, where $\hat{a}^\dagger(\boldsymbol{q})_s$ ($\hat{a}(\boldsymbol{q})_s$) denote the creation (annihilation) operator of a phonon with wavevector $\boldsymbol{q}$ belonging to the band s.[119,132] Within the SMA, each phonon mode contributes individually to the lattice thermal conductivity, which reads[119]

$$\kappa_P^{\gamma\sigma}{=}\frac{1}{N_c\mathcal{V}}\sum_{\boldsymbol{q},s}C(\boldsymbol{q})_s v^\gamma(\boldsymbol{q})_s v^\sigma(\boldsymbol{q})_s\tau(\boldsymbol{q})_s \tag{2.2.2}$$

where $C(\boldsymbol{q})_s{=}\frac{\hbar^2\omega^2(\boldsymbol{q})_s}{k_BT^2}n_T(\omega(\boldsymbol{q})_s)[n_T(\omega(\boldsymbol{q})_s){+}1]$ is the contribution of the mode $(\boldsymbol{q},s)$ to the heat capacity of the lattice and $\tau(\boldsymbol{q})_s{=}\frac{1}{\Gamma(\boldsymbol{q})_s}$ is the phonon lifetime. Eq. (2.2.2) basically describes the thermal conductivity of a gas[44] of particles labeled by $(\boldsymbol{q},s)$, each characterized by specific heat $C(\boldsymbol{q})_s$, velocity $\boldsymbol{v}(\boldsymbol{q})_s$ and lifetime $\tau(\boldsymbol{q})_s$. As we shall see below, Eq. (2.2.2) consist in the intraband contribution to the thermal conductivity — *i.e.* the SMA limit for κ_P in Ref. 13— in the LSFA of the result derived from the fully quantum formula (2.1.6).

Here we want to describe thermal transport beyond Peierls-Boltzmann, *i.e.* accounting not only for intraband propagation but also for interband effects. Thus, a generalized definition of the heat flux that is non-diagonal in the phonon band indices is needed. In fact, while in normal crystals with well-separated and defined phonon bands diagonal heat-flux elements are dominant (since $\langle\hat{a}^\dagger(\boldsymbol{q})_s\hat{a}(\boldsymbol{q})_s\rangle{\gg}\langle\hat{a}^\dagger(\boldsymbol{q})_s\hat{a}(\boldsymbol{q})_{s'}\rangle$ for $s{\neq}s'$), when the phonon bands become close in energy phonons can not only propagate particle-like but also tunnel from one band to another other in a wave-like fashion. This happens in glasses and disordered solids, where the vibrational spectrum is quite dense featuring many quasi-degenerate modes,[44,120] and in complex crystals, where strong anharmonicity broadens the phonon bands and provides overlap between different states. In these cases, interband transitions are of paramount importance, giving significant or even dominant contributions to heat transport.[3,4,28] Interband effects are absent from the equations (2.2.1)-(2.2.2) derived from the LBTE, and in the following, we illustrate how these emerge from a wave-like interference between different vibrational modes. This physical picture is further detailed in Appendix 2.D.

The Hamiltonian that describes ionic motion for a crystal within the harmonic approximation reads

$$\hat{H}_0{=}\sum_{\boldsymbol{R}_l b\alpha}\frac{\hat{P}^2(\boldsymbol{R}_l)_{b\alpha}}{2M_b}{+}\frac{1}{2}\sum_{\substack{\boldsymbol{R}_l b\alpha\\ \boldsymbol{R}_{l'}b'\alpha'}}\phi_{\boldsymbol{R}_l b\alpha,\boldsymbol{R}_{l'}b'\alpha'}\hat{u}(\boldsymbol{R}_l)_{b\alpha}\hat{u}(\boldsymbol{R}_{l'})_{b'\alpha'}, \tag{2.2.3}$$

where the sum on $\boldsymbol{R}_l$ indicates the sum over the N_c primitive cells located at lattice sites $\boldsymbol{R}_l$, the index $b{=}1,\dots,N_{at}$ runs over all the atomic species inside the primitive cell of volume $\mathcal{V}$ and α denotes a cartesian direction. The equilibrium positions of the atoms inside the primitive cell are identified by the vectors $\boldsymbol{\tau}_b$, *i.e.* the equilibirum position of atom b inside the primitive cell $\boldsymbol{R}_l$ is $\boldsymbol{R}_l{+}\boldsymbol{\tau}_b$. The ionic displacement from the equilibrium position $\hat{u}$ and ionic momentum $\hat{P}$ are canonically conjugated variables satisfying the usual commutation rules

$$[\hat{u}(\boldsymbol{R}_l)_{b\alpha},\hat{P}(\boldsymbol{R}_{l'})_{b'\alpha'}]=i\hbar\delta_{\boldsymbol{R}_l,\boldsymbol{R}_{l'}}\delta_{b,b'}\delta_{\alpha,\alpha'}\,. \tag{2.2.4}$$

The interatomic force constant matrix ϕ is defined as the the second derivative of the Born-

Oppenheimer potential with respect to ionic displacements, which is symmetric and translational invariant[36]

$$\phi_{\boldsymbol{R}_l b\alpha,\boldsymbol{R}_{l'}b'\alpha'} = \phi_{\boldsymbol{R}_{l'}b'\alpha',\boldsymbol{R}_l b\alpha} = \phi_{(\boldsymbol{R}_l-\boldsymbol{R}_{l'})b\alpha,\boldsymbol{0}b'\alpha'} \,. \tag{2.2.5}$$

In our framework, we will consider the harmonic Hamiltonian (2.2.3) as the unperturbed Hamiltonian of the system, whereas the higher-order anharmonic terms will be considered as perturbations.

In order to derive the heat-flux operator, we follow the procedure originally derived by Hardy.[35] The starting point is the identification of a local energy field operator $\hat{h}(\boldsymbol{R}_l)_{b\alpha}$ that satisfies

$$\hat{H}_0 = \sum_{\boldsymbol{R}_l b\alpha} \hat{h}(\boldsymbol{R}_l)_{b\alpha} \,. \tag{2.2.6}$$

From there, the expression of the heat-flux operator is derived using the procedure discussed in Sec. 1.2.2 to obtain local operators from discrete ones and the continuity equation (1.2.16).

The identification of $\hat{h}(\boldsymbol{R}_l)_{b\alpha}$ from the structure of the Hamiltonian is non-trivial. In fact, there are an infinite number of ways to partition energy while satisfying the requirement (2.2.6). As a consequence of this arbitrariness, the resulting heat-flux operator is not uniquely defined. The definition of the generalized heat flux which is most commonly adopted is the one derived originally by Hardy,[35] which has been successfully implemented to calculate interband thermal transport phenomena in recent studies.[33,39,126] On the other hand, in Ref. 12 a different definition of heat-flux operator arises within the theoretical framework of the WTE. In the present section, the two different definitions of the heat-flux operator are compared and analyzed.

Nonetheless, as shown in Ref. 40, whenever two choices of the microscopic energy density differ by the divergence of a bounded vector field, they realize two equivalent "gauges" of the energy field and lead to the same result for the thermal conductivity (further discussion in Appendix 2.B). This gauge-invariance principle cannot be invoked, though, for local energies which do not differ by a divergence. We argue that this is the case for the two heat fluxes we discuss here, that do not seem to be connected by a gauge transformation in the sense of Ref. 40, even though the numerical results for thermal conductivity are quantitatively very close. We stress that both definitions of the local energy lead to harmonic heat fluxes, but with a different structure for the interband contribution, as alluded to above.

2.2.1 Hardy heat flux

In this Section, we present the procedure to derive the heat-flux operator originally proposed by Hardy in Ref. 35. The starting point is the definition of the local energy field; the one used by Hardy is the most natural choice given the structure of the Hamiltonian (2.2.3)

$$\hat{h}(\boldsymbol{R}_l)_{b\alpha} = \frac{\hat{P}^2(\boldsymbol{R}_l)_{b\alpha}}{2M_b} + \frac{1}{2}\sum_{\boldsymbol{R}_{l'}b'\alpha'} \phi_{\boldsymbol{R}_l b\alpha,\boldsymbol{R}_{l'}b'\alpha'}\hat{u}(\boldsymbol{R}_l)_{b\alpha}\hat{u}(\boldsymbol{R}_{l'})_{b'\alpha'} . \tag{2.2.7}$$

In order to derive the heat-flux operator from the continuity equation (1.2.16) one needs to introduce an energy density operator $\hat{h}(\boldsymbol{x})$, which is a continuous function of the space coordinate $\boldsymbol{x}$, such that its integral in space gives the harmonic Hamiltonian (2.2.3). To do so, we perform a convolution of the discrete operator (2.2.7) with a smooth normalized

distribution Δ_ℓ introduced in Eq. (1.2.12), obtaining

$$\hat{h}(\boldsymbol{x}) = \sum_{\boldsymbol{R}_l b\alpha} \hat{h}(\boldsymbol{R}_l)_{b\alpha} \Delta_\ell(\boldsymbol{x}-\boldsymbol{R}_l-\boldsymbol{\tau}_b), \tag{2.2.8}$$

In this case, $\Delta_\ell(\boldsymbol{x}-\boldsymbol{R}_l-\boldsymbol{\tau}_b)$ can be chosen as a function centered on the ionic equilibrium position $\boldsymbol{R}_l+\boldsymbol{\tau}_b$ and spatially spread over a mesoscopic length ℓ (*i.e.* $\ell \gg a$ where a is the microscopic bond length), such as $\Delta_\ell(\boldsymbol{x}-\boldsymbol{R}_l-\boldsymbol{\tau}_b)=\frac{1}{\ell^3\sqrt{\pi^3}}\exp\left[-\frac{|\boldsymbol{x}-\boldsymbol{R}_l-\boldsymbol{\tau}_b|^2}{\ell^2}\right]$.

The heat-flux operator can be now derived from (2.2.8) using the continuity equation (1.2.16) and the Heisenberg time-evolution equation for the energy density in the harmonic approximation:

$$-\boldsymbol{\nabla}\cdot\hat{\boldsymbol{j}}(\boldsymbol{x}) = \frac{\partial \hat{h}(\boldsymbol{x})}{\partial t} = -\frac{i}{\hbar}[\hat{h}(\boldsymbol{x}), \hat{H}_0]\,. \tag{2.2.9}$$

The total heat-flux operator is then obtained by inserting (2.2.8) in (2.2.9), performing a Taylor expansion of the function $\Delta_\ell(\boldsymbol{x}-\boldsymbol{R}_l-\boldsymbol{\tau}_b)$, and finally integrating the heat current density over the crystal volume and considering only the contribution from the lowest-order term of the aforementioned Taylor expansion. This procedure, outlined in Appendix 2.A, yields

$$\begin{aligned}\hat{\boldsymbol{J}} &= -\frac{i}{N_c\mathcal{V}\hbar}\sum_{\boldsymbol{R}_l b\alpha}(\boldsymbol{R}_l+\boldsymbol{\tau}_b)[\hat{h}(\boldsymbol{R}_l)_{b\alpha}, \hat{H}_0] \\ &= \frac{1}{2N_c\mathcal{V}}\sum_{\substack{\boldsymbol{R}_l b\alpha \\ \boldsymbol{R}_{l'} b'\alpha'}}(\boldsymbol{R}_l+\boldsymbol{\tau}_b-\boldsymbol{R}_{l'}-\boldsymbol{\tau}_{b'})\phi_{\boldsymbol{R}_l b\alpha,\boldsymbol{R}_{l'} b'\alpha'}\hat{u}(\boldsymbol{R}_l)_{b\alpha}\frac{\hat{P}(\boldsymbol{R}_{l'})_{b'\alpha'}}{M_{b'}}.\end{aligned} \tag{2.2.10}$$

Notice that, since we are interested in the heat flux $\hat{\boldsymbol{J}}$ which is the volume average of the current density $\hat{\boldsymbol{j}}(\boldsymbol{x})$, the microscopic details of the coarse-graining procedure are irrelevant, as testified by the fact that the expression of the heat flux reported above does not feature the characteristic length ℓ introduced to define the local energy density operator $\hat{h}(\boldsymbol{x})$ in Eq. (2.2.8).

The total heat flux (2.2.10) has been derived in real space relying on the assumption of being in the close-to-equilibrium regime, which is required to employ the momentum $\hat{P}(\boldsymbol{R}_l)_{b\alpha}$ and displacement $\hat{u}(\boldsymbol{R}_l)_{b\alpha}$ operators of atoms at well-defined positions in real space $\boldsymbol{R}_l+\boldsymbol{\tau}_b$. However, the evaluation of its expectation value does not necessarily require to employ a real-space representation, and for later convenience we recast it in reciprocal space, where translation-invariant quantities assume a block-diagonal form. To see this, let us recast Eq. (2.2.10) employing the standard phonon annihilation (creation) operators $\hat{a}(\boldsymbol{q})_s$ ($\hat{a}^\dagger(\boldsymbol{q})_s$), which are labeled by a wavevector $\boldsymbol{q}$ belonging to the first Brillouin zone and a mode index s,[119,132] and are related to the displacement and momentum operators via

$$\hat{a}(\boldsymbol{q})_s = \frac{1}{\sqrt{N_c}}\sum_{\boldsymbol{R}_l,b,\alpha} e^\star(\boldsymbol{q})_{s,b\alpha}\left[\frac{\hat{P}(\boldsymbol{R}_l)_{b\alpha}}{\sqrt{2\hbar\Omega(\boldsymbol{q})_s M_b}} - i\frac{\sqrt{\Omega(\boldsymbol{q})_s M_b}}{2\hbar}\hat{u}(\boldsymbol{R}_l)_{b\alpha}\right]e^{-i\boldsymbol{q}\cdot(\boldsymbol{R}_l+\boldsymbol{\tau}_b)}. \tag{2.2.11}$$

In Eq. (2.2.11), $\varepsilon(\boldsymbol{q})_{s,b\alpha}$ are the phonon polarization vectors and $\Omega(\boldsymbol{q})_s$ are the phonon frequencies. These quantities are obtained from the dynamical matrix

$$d(\boldsymbol{q})_{b\alpha,b'\alpha'} = \sum_{\boldsymbol{R}_l}\frac{\phi_{\boldsymbol{R}_l b\alpha,\boldsymbol{R}'_l b'\alpha'}}{\sqrt{M_b M_{b'}}}e^{-i\boldsymbol{q}\cdot(\boldsymbol{R}_l+\boldsymbol{\tau}_b-\boldsymbol{\tau}_{b'})} \tag{2.2.12}$$

by solving the eigenvalue equation $\Omega^2(\boldsymbol{q})_s\varepsilon(\boldsymbol{q})_{s,b\alpha}=\sum_{b'\alpha'} d(\boldsymbol{q})_{b\alpha,b'\alpha'}\varepsilon(\boldsymbol{q})_{s,b'\alpha'}$. Combining Eq. (2.2.11) and Eq. (2.2.4), it is straightforward to show that the phonon creation and annihilation operators satisfy the usual bosonic commutation rules

$$[\hat{a}(\boldsymbol{q})_s, \hat{a}^\dagger(\boldsymbol{q}')_{s'}] = \delta_{s,s'}\delta_{\boldsymbol{q},\boldsymbol{q}'} \, . \tag{2.2.13}$$

The usefulness of these phonon operators is to simplify the expression for the harmonic Hamiltonian (2.2.3) to a diagonal form

$$\hat{H}_0 = \sum_{\boldsymbol{q},s} \hbar\Omega(\boldsymbol{q})_s \left[\hat{a}^\dagger(\boldsymbol{q})_s\hat{a}(\boldsymbol{q})_s + \tfrac{1}{2}\right] , \tag{2.2.14}$$

as well as that of the heat flux (2.2.10) to a block-diagonal form

$$\hat{\boldsymbol{J}}=\frac{1}{N_c\mathcal{V}}\sum_{\boldsymbol{q},ss'} \hbar\Omega(\boldsymbol{q})_s\boldsymbol{v}(\boldsymbol{q})_{ss'}\tfrac{1}{2}\left[\hat{a}^\dagger(\boldsymbol{q})_s+\hat{a}(-\boldsymbol{q})_s\right]\left[\hat{a}(\boldsymbol{q})_{s'}-\hat{a}^\dagger(-\boldsymbol{q})_{s'}\right], \tag{2.2.15}$$

where the generalized phonon velocity $\boldsymbol{v}(\boldsymbol{q})_{ss'}$ is a $3N_{at}\times 3N_{at}$ matrix for every Cartesian component, defined as

$$\boldsymbol{v}(\boldsymbol{q})_{ss'}=\frac{1}{2\sqrt{\Omega(\boldsymbol{q})_s\Omega(\boldsymbol{q})_{s'}}}\varepsilon^*(\boldsymbol{q})_{s,b\alpha}\boldsymbol{\nabla}_{\boldsymbol{q}}d(\boldsymbol{q})_{b\alpha,b'\alpha'}\varepsilon(\boldsymbol{q})_{s',b'\alpha'} \, . \tag{2.2.16}$$

The diagonal $s=s'$ elements of this matrix are the usual phonon group velocities $\boldsymbol{v}(\boldsymbol{q})_{ss} = \boldsymbol{\nabla}_{\boldsymbol{q}}\Omega(\boldsymbol{q})_s$. Other properties of the velocity matrix (2.2.16) are

$$\boldsymbol{v}(\boldsymbol{q})_{ss'}=\boldsymbol{v}^*(\boldsymbol{q})_{s's}=-\boldsymbol{v}(-\boldsymbol{q})_{s's} \tag{2.2.17}$$

These relations follow directly from the properties of the dynamical matrix (2.2.12), which are consequence of the symmetries (2.2.5) of the interatomic force constants matrix. Note that the phase for the Fourier transform in Eqs.(2.2.11),(2.2.12) features the atomic equilibrium position $e^{-i\boldsymbol{q}\cdot(\boldsymbol{R}_l+\boldsymbol{\tau}_b)}$ ("Wallace convention"[132]) instead of just the primitive cell position $e^{-i\boldsymbol{q}\cdot\boldsymbol{R}_l}$ ("Ziman convention"[119]). Employing the Ziman or Wallace phase convention does not affect the eigenvalues of the dynamical matrix, but it can change the off-diagonal elements of the velocity matrix. The Wallace phase convention for the Fourier transform possesses the advantage of being independent of the choice of the crystal's unit cell and of yielding a thermal conductivity expression that is size consistent; further discussions and details are presented in Ref. 13.

Using the properties of the velocity matrix and phonon frequencies and considering the commutation rules (2.2.13), we can rearrange the Hardy heat-flux operator as the sum of a "resonant" heat-flux operator $\hat{\boldsymbol{J}}_R$ and a "antiresonant" heat-flux operator $\hat{\boldsymbol{J}}_A$, according to the terminology introduced in Ref. 33. They are defined as

$$\hat{\boldsymbol{J}} \;= \hat{\boldsymbol{J}}_R + \hat{\boldsymbol{J}}_A, \tag{2.2.18a}$$

$$\hat{\boldsymbol{J}}_R=\frac{\hbar}{N_c\mathcal{V}}\sum_{\boldsymbol{q},ss'}\frac{\Omega(\boldsymbol{q})_s+\Omega(\boldsymbol{q})_{s'}}{2}\boldsymbol{v}(\boldsymbol{q})_{ss'}\hat{a}^\dagger(\boldsymbol{q})_s\hat{a}(\boldsymbol{q})_{s'}, \tag{2.2.18b}$$

$$\hat{\boldsymbol{J}}_A=\frac{\hbar}{N_c\mathcal{V}}\sum_{\boldsymbol{q},ss'}\frac{\Omega(\boldsymbol{q})_s-\Omega(\boldsymbol{q})_{s'}}{4}\boldsymbol{v}(\boldsymbol{q})_{ss'}\left[\hat{a}(-\boldsymbol{q})_s\hat{a}(\boldsymbol{q})_{s'}-\hat{a}^\dagger(\boldsymbol{q})_s\hat{a}^\dagger(-\boldsymbol{q})_{s'}\right]. \tag{2.2.18c}$$

The resonant combination of operators $a^\dagger(\boldsymbol{q})_s a(\boldsymbol{q})_{s'}$ gives us a physical picture of a vertical

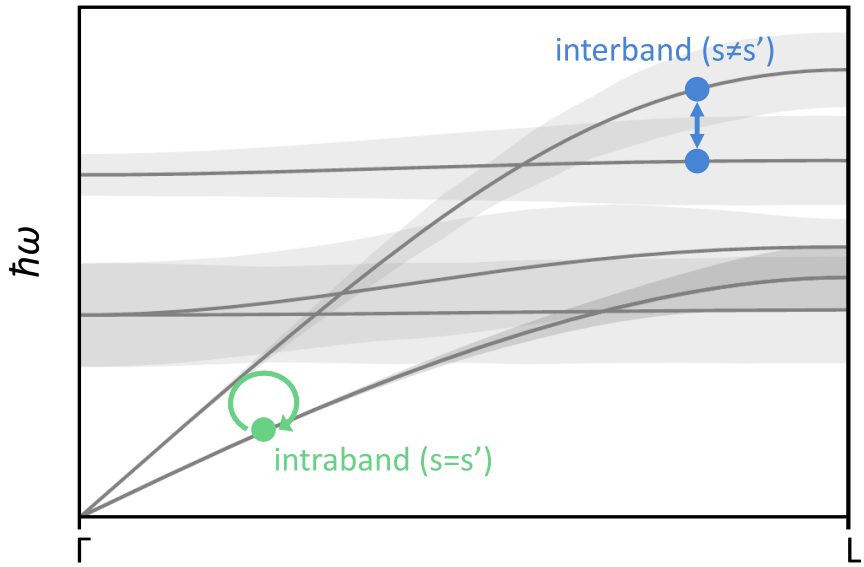

Figure 2.1. Pictorial representation of the intraband and interband transitions described by Hardy's resonant (2.2.18b) and Wigner (2.2.24) heat-flux operators. Solid lines represent phonon bands of a representative crystal, shaded areas represents finite phonon linewidths. The diagonal elements ($s{=}s'$) of the heat flux describe the particle-like intraband propagation of phonon wavepackets. The off-diagonal ($s{\neq}s'$) elements describe the interband tunneling of phonons between two different bands: while as $\Gamma(\boldsymbol{q})_s{\to}0$ these processes are only possible when an external perturbation provides the finite energy difference $\hbar\omega_\Delta{=}\hbar\Omega(\boldsymbol{q})_s{-}\hbar\Omega(\boldsymbol{q})_{s'}$; as $\Gamma(\boldsymbol{q})_s$ increases, the tunneling between the two states is possible even at $\hbar\omega_\Delta{=}0$.

transition (tunneling at equal crystal momentum $\boldsymbol{q}$) in which a mode s' is destroyed and a mode s is created (see Fig. 2.1 for a pictorial interpretation). In absence of degeneracies, the diagonal elements $s'{=}s$ represents a transition within the same band, while for $s'{\neq}s$ the transition involves different bands. The expectation value of the operators that realize the intraband transition $\langle a^\dagger(\boldsymbol{q})_s a(\boldsymbol{q})_s\rangle{=}n(\boldsymbol{q})_s$ can be interpreted as the population of the phonon mode $(\boldsymbol{q}, s)$, with definite energy, momentum and band, which corresponds to a particle-like excitation with precise nature. Instead, the interband terms $\langle a^\dagger(\boldsymbol{q})_s a(\boldsymbol{q})_{s'}\rangle$ describe the coherence between pairs of eigenstates, *i.e.* coupling between two different vibrational modes s, s' with the same wavevector $\boldsymbol{q}$, and cannot be directly interpreted as a vibrational excitation of definite nature. When two bands are degenerate, *i.e.* $\Omega(\boldsymbol{q})_s{=}\Omega(\boldsymbol{q})_{s'}$ for $s'{\neq}s$, one can exploit the freedom of diagonalizing at least one Cartesian component of the velocity operator in the degenerate subspace,[13,22] obtaining a zero interband contribution from perfectly degenerate vibrational modes and an intraband conductivity along such Cartesian direction exactly equivalent to the Peierls-Boltzmann conductivity discussed in Ref. 22. For these reasons we employ the convention of considering interband contributions to the conductivity to emerge exclusively from off-diagonal and non-degenerate velocity-operator elements. Since the temperature gradient is constant in time, a finite-frequency transition would not be allowed by the external perturbation, as evidenced by the fact that the thermal conductivity is defined as the $\omega{\to}0$ limit of the current-current correlation function (see Eq. (2.1.6)). As a consequence, a perfect crystal with no phonon damping $\Gamma(\boldsymbol{q})_s{=}0, \forall(\boldsymbol{q}, s)$ has infinite thermal conductivity, since no relaxation process can hinder the intraband thermal conduction (cf. Eq. (2.2.2)). As soon as phonon states get broadened by anharmonicity or disorder ($\Gamma(\boldsymbol{q})_s{\neq}0$),

intraband transport becomes limited to a finite value and the additional interband transport mechanisms become possible[II].

As mentioned in the introduction, this will be relevant whenever broadening of the phonon energy levels overcomes their energy difference, *i.e.* $\Gamma(\boldsymbol{q})_s+\Gamma(\boldsymbol{q})_{s'}\gtrsim\Omega(\boldsymbol{q})_s-\Omega(\boldsymbol{q})_{s'}$, as pictorially shown in Fig. 2.1. The antiresonant combination $a(\boldsymbol{q})_s a(\boldsymbol{q})_{s'}$ represents some sort of "pair tunneling" process, typical in the context of superfluidity,[134] where a condensate reservoir exists. However, in the case of phonons, there is no condensation so these processes are expected to be irrelevant, as indeed we will confirm via both analytical and numerical estimates.

We finally note that in the original work by Hardy[35] the heat-flux operator had also anharmonic terms. Such a difference is due to the choice done in Ref. 35 of centering the Δ_ℓ function of Eq. (2.2.8) on the instantaneous position of the ions $\boldsymbol{R}_l+\boldsymbol{\tau}_b+\hat{\boldsymbol{u}}(\boldsymbol{R}_l)_b$ rather than just on their equilibrium position, as we did. This would introduce anharmonic $\mathcal{O}(p^3)$ (convective) and $\mathcal{O}(u^3)$ (conductive) terms in the energy density, even if calculated from the harmonic on-site energy (2.2.7). As shown in Appendix 2.B, the resulting heat-flux operator differs by a total time derivative from the one given in Eqs. (2.2.18b)-(2.2.18c) (if mass diffusion is negligible[33]). Thus, owing to the gauge invariance principle for heat transport,[40] this term does not affect the total thermal conductivity of the system when the exact correlation function (2.1.2) is computed. However, when the correlation function (2.1.2) is computed within an approximation, such as the dressed-bubble approximation employed in this work, this additional term cannot be neglected *a priori*.

Nonetheless, as already argued in Ref. 35, at the level of the present approximation the anharmonic terms in the heat current lead to higher-order corrections; we then expect a negligible contribution to the thermal conductivity and will retain in what follows only the harmonic terms (2.2.18b)-(2.2.18c).

2.2.2 Wigner heat flux

In this Section, we show how the procedure outlined in Sec.2.2.1 for the derivation of the heat flux can be employed to obtain a new expression of the quantum-mechanical heat-flux operator which is in close connection with the Wigner formulation of thermal transport, developed in Refs. 12,13. The starting point is once again the identification of the local energy operator. The local energy operator (2.2.7) follows quite naturally from the expression of the harmonic Hamiltonian (2.2.3) in the representation of atomic momentum and displacement operators $\hat{P}$ and $\hat{u}$. Now let us show how a different representation of the harmonic Hamiltonian provides a different yet equally valid choice of the local energy, from which a different heat-flux operator follows. In Ref. 13 the bosonic operators in real space were introduced as a set of creation (annihilation) operators that describe the excitation (de-excitation) of space-dependent atomic vibrations, and they were shown to be suitable to describe an out-of-equilibrium solid with space-dependent vibrational energy. These operators are related to the atomic momentum and displacement operators via

$$\hat{a}(\boldsymbol{R}_l)_{b\alpha}=\frac{1}{\sqrt{2\hbar}}\sum_{\boldsymbol{R}_{l'}b'\alpha'}\Big(\sqrt[4]{G^{-1}}_{\boldsymbol{R}_l b\alpha,\boldsymbol{R}_{l'}b'\alpha'}\frac{\hat{P}(\boldsymbol{R}_{l'})_{b'\alpha'}}{\sqrt{M_{b'}}}-i\sqrt{M_b}\sqrt[4]{G}_{\boldsymbol{R}_l b\alpha,\boldsymbol{R}_{l'}b'\alpha'}\hat{u}(\boldsymbol{R}_{l'})_{b'\alpha'}\Big), \quad (2.2.19)$$

[II] It is worth specifying that this statement is formally valid for a 3D solid without long-range interatomic forces. When considering a system with reduced dimensionality, there are cases of anharmonic systems in 1 or 2D that possess a thermal conductivity diverging with system size, like the anharmonic chains with momentum-conserving potential described by the Fermi-Pasta-Ulam model[133]

where the n-th root of the matrix $G_{\boldsymbol{R}_l b\alpha,\boldsymbol{R}'_l b'\alpha'}=\frac{\phi_{\boldsymbol{R}_l b\alpha,\boldsymbol{R}'_l b'\alpha'}}{\sqrt{M_b M_{b'}}}$ is obtained as the inverse Fourier transform of the n-th root of the dynamical matrix (2.2.12),

$$\sqrt[n]{G}_{\boldsymbol{R}_l b\alpha,\boldsymbol{R}'_l b'\alpha'} = \frac{1}{N_c}\sum_{\boldsymbol{q}} \sqrt[n]{d(\boldsymbol{q})}_{b\alpha,b'\alpha'} e^{+i\boldsymbol{q}\cdot(\boldsymbol{R}_l+\boldsymbol{\tau}_b-\boldsymbol{R}'-\boldsymbol{\tau}_{b'})} \tag{2.2.20}$$

where $\sqrt[n]{d(\boldsymbol{q})}_{b\alpha,b'\alpha'} = \sum_s \omega^{\frac{2}{n}}(\boldsymbol{q})_s \varepsilon(\boldsymbol{q})_{s,b\alpha}\varepsilon^*(\boldsymbol{q})_{s,b'\alpha}$. One can easily show from Eq. (2.2.19) that these operators satisfy the usual bosonic commutation rules

$$[\hat{a}(\boldsymbol{R}_l)_{b\alpha}, \hat{a}^\dagger(\boldsymbol{R}'_l)_{b'\alpha'}] = \delta_{\boldsymbol{R}_l,\boldsymbol{R}'_l}\delta_{b,b'}\delta_{\alpha,\alpha'}, \tag{2.2.21}$$

which follow trivially from the commutation rules (2.2.13) and the properties of the phonon polarization vectors. Ref. 13 shows how the operator $\hat{a}^\dagger(\boldsymbol{R}_l)_{b\alpha}$ creates atomic vibrations along direction α and centered around the position $\boldsymbol{R}_l+\boldsymbol{\tau}_b$, thus it can be used (together with its adjoint) to describe space-dependent vibrations.

In terms of the bosonic operators in real space, the harmonic Hamiltonian reads

$$\hat{H}_0=\hbar\sum_{\substack{\boldsymbol{R}_l b\alpha\\ \boldsymbol{R}_{l'} b'\alpha'}}\sqrt{G}_{\boldsymbol{R}_l b\alpha,\boldsymbol{R}_{l'} b'\alpha'}[\hat{a}^\dagger(\boldsymbol{R}_l)_{b\alpha}\hat{a}(\boldsymbol{R}_{l'})_{b'\alpha'}+\frac{1}{2}\delta_{\boldsymbol{R}_l,\boldsymbol{R}_{l'}}\delta_{b,b'}\delta_{\alpha,\alpha'}]. \tag{2.2.22}$$

From Eq. (2.2.22), the local energy operator is naturally defined as

$$\hat{h}(\boldsymbol{R}_l)_{b\alpha}=\frac{\hbar}{2}\sum_{\boldsymbol{R}_{l'} b'\alpha'}\sqrt{G}_{\boldsymbol{R}_l b\alpha,\boldsymbol{R}_{l'} b'\alpha'}\hat{a}^\dagger(\boldsymbol{R}_l)_{b\alpha}\hat{a}(\boldsymbol{R}_{l'})_{b'\alpha'}+\text{h.c.}\,, \tag{2.2.23}$$

where the hermitian conjugate (h.c.) is added to enforce hermiticity of the local energy and heat-flux operators, whereas the zero-point energy term can be neglected since as a constant it cannot yield any heat flux. Given the definition of the local energy operator (2.2.23), we can apply the same procedure outlined in the previous Section to derive the heat-flux operator. As detailed in Appendix 2.A, its expression in terms of the standard phonon operators is

$$\hat{\boldsymbol{J}}=\frac{\hbar}{N_c\mathcal{V}}\sum_{\boldsymbol{q},ss'}\frac{\Omega(\boldsymbol{q})_s+\Omega(\boldsymbol{q})_{s'}}{2}\boldsymbol{v}(\boldsymbol{q})_{ss'}\hat{a}^\dagger(\boldsymbol{q})_s\hat{a}(\boldsymbol{q})_{s'} \tag{2.2.24}$$

where the velocity matrix is now defined as

$$\boldsymbol{v}(\boldsymbol{q})_{ss'} = \varepsilon^*(\boldsymbol{q})_{s,b\alpha}\boldsymbol{\nabla}_{\boldsymbol{q}}\sqrt{d(\boldsymbol{q})}_{b\alpha,b'\alpha'}\varepsilon(\boldsymbol{q})_{s',b'\alpha'}\,. \tag{2.2.25}$$

We will refer to this operator as the Wigner heat-flux operator, and accordingly to the local energy (2.2.23) as the Wigner local energy operator. This nomenclature is chosen to underline the analogies with the heat flux discussed in Wigner's phase-space formulation for thermal transport presented in Ref. 13. In fact, in the Wigner approach the heat flux is derived considering the time evolution of a local energy field $E(\boldsymbol{R}_l,t)=\frac{\hbar}{\mathcal{V}N_c}\sum_{qs}\Omega(\boldsymbol{q})_s n(\boldsymbol{R}_l,\boldsymbol{q},t)_{ss}$ where the matrix $n(\boldsymbol{R}_l,\boldsymbol{q},t)_{ss'}$ is a distribution obtained applying the Wigner transform to the density matrix, which generalizes the semiclassical phonon population appearing in the Peierls-Boltzmann formalism. The time-evolution of such quantity is regulated by the WTE, which is used to compute the time derivative of $E(\boldsymbol{R}_l,t)$. The (local) heat flux $\boldsymbol{J}(\boldsymbol{R}_l,t)$ obtained through the continuity equation $\frac{\partial}{\partial t}E(\boldsymbol{R}_l,t)=-\boldsymbol{\nabla}\cdot\boldsymbol{J}(\boldsymbol{R}_l,t)$ is related to the

expectation value of the total Wigner heat-flux operator $\hat{\boldsymbol{J}}$ presented here in Eq. (2.2.24) by $\frac{1}{N_c}\sum_{\boldsymbol{R}} \boldsymbol{J}(\boldsymbol{R}_l,t)=\mathrm{Tr}\left[\hat{\rho}(t)\hat{\boldsymbol{J}}\right]$ (cf. Sec. V.A of Ref. 13). This stands also as proof of consistency of the definition of the Wigner heat flux, obtained equivalently following the route of WTE as presented in Ref. 12,13 or Hardy's method introduced in Ref. 35 and outlined in Appendix 2.A.

The main difference between the two expressions for the heat-flux operator (2.2.15) and (2.2.24) is the lack in (2.2.24), derived from Wigner local energy, of the "anomalous" antiresonant term (2.2.18c). In addition, two different definitions of the velocity matrix are found. The one presented in (2.2.16) is the one originally discussed by Hardy and also the most commonly found in literature;[33,44,123,124,126] it consists of matrix elements of the gradient of the dynamical matrix, divided by the geometric mean of the frequencies of the modes involved. The velocity matrix defined in the Wigner formalism involves instead the matrix elements of the square root of the dynamical matrix. It can be shown that the latter satisfies the properties (2.2.17) (satisfied also by Hardy's velocity matrix), and that its diagonal elements are still the usual phonon group velocities $\boldsymbol{v}(\boldsymbol{q})_{ss}=\boldsymbol{\nabla}_{\boldsymbol{q}}\Omega(\boldsymbol{q})_s$. It can be also shown that the two velocity matrices (2.2.16) and (2.2.25) are related by

$$\boldsymbol{v}(\boldsymbol{q})_{ss'} = \frac{\Omega(\boldsymbol{q})_s+\Omega(\boldsymbol{q})_{s'}}{2\sqrt{\Omega(\boldsymbol{q})_s\Omega(\boldsymbol{q})_{s'}}}\boldsymbol{v}(\boldsymbol{q})_{ss'}. \tag{2.2.26}$$

From these remarks, we understand that the two definitions (2.2.15) and (2.2.24) of the harmonic heat flux are equal when considering diagonal ($s=s'$) or degenerate ($\Omega(\boldsymbol{q})_s=\Omega(\boldsymbol{q})_{s'}$ for $s\neq s'$) elements of the velocity matrices, and they both coincide to the second-quantization form of the heat flux (2.2.1) used in the LBTE formalism. Therefore, the differences between the heat-flux operators under scrutiny are solely in the off-diagonal and non-degenerate ($s\neq s'$ and $\Omega(\boldsymbol{q})_s\neq\Omega(\boldsymbol{q})_{s'}$) terms.

2.3 Derivation of thermal conductivity in a Green's function approach

In this Section we show how to derive the thermal conductivity using a many-body approach. The expressions of the heat flux in terms of the phonon creation and annihilation operators derived in Section 2.2 can now be used to compute the thermal conductivity in terms of interacting phonon Green's functions using standard methods of perturbation theory. The general procedure is independent from the choice of the heat flux, even though the final result depends on the structure of the heat-flux operator. We first present our expressions in terms of the full phonon spectral function (FSF) for both the Hardy and the Wigner heat-flux operators, and then we describe the expressions we get considering the LSFA.

To compute the correlation function at real frequencies we will use, instead of the retarded response function (2.1.3), its equivalent in the imaginary-time domain:

$$\chi^{\gamma\sigma}(\tau) = \langle \mathcal{T}_\tau \hat{J}^\gamma(\tau)\hat{J}^\sigma(0)\rangle\,. \tag{2.3.1}$$

We will then implement the standard many-body formalism of finite-temperature Green's functions[67] to compute the Fourier transform on Eq. (2.3.1) in Matsubara frequency, and from this by analytical continuation $\chi^{\alpha\beta}(\omega+i0^+)$. Given the structure of heat fluxes (2.2.15) and (2.2.24), the response function (2.3.1) is always expressed as a time-ordered product of

four phonon operators. By using the Matsubara-Wick theorem[135] the response function can be expressed in terms of products of two-particle operators or phonon Green's functions (see Appendix 2.C):

$$g(\boldsymbol{q},\tau)_s = -\langle \mathcal{T}_\tau \hat{a}(\boldsymbol{q},\tau)_s \hat{a}^\dagger(\boldsymbol{q},0)_s \rangle \tag{2.3.2}$$

where the time evolution of the operators is intended in the Heisenberg picture $\frac{\mathrm{d}\hat{a}(\boldsymbol{q},\tau)_s}{\mathrm{d}\tau} = [\hat{H}, \hat{a}(\boldsymbol{q},\tau)_s]$. As shown diagrammatically in Fig. 2.5 of Appendix 2.C, we consider explicitly the so-called "dressed-bubble" approximation, where only diagrams with two separated dressed Green's functions are included, hence neglecting vertex corrections (the implications of such choice will be discussed at the end of the present section). This approximation makes the analytical continuation straightforward, allowing us at the same time to recover in the LSFA the expression found with the WTE in Ref. 12 at the same level of approximation. Now, the rationale behind the decomposition (2.2.18b)-(2.2.18c) becomes evident: since the resonant and antiresonant heat-flux operators possess different numbers of creation-annihilation operators, we can neglect mixed terms $\langle \mathcal{T}_\tau \hat{\boldsymbol{J}}_R(\tau) \hat{\boldsymbol{J}}_A(0) \rangle$, assuming, as stated above, that no anomalous averages $\langle \mathcal{T}_\tau \hat{a}(\tau)\hat{a}(0) \rangle$ are present. Even if such averages cannot be discarded in the most general case, such terms are expected to be negligibly small with respect to the regular ones. This follows from the fact that anomalous averages do not posses a zero-th order term in the perturbative expansion, hence such terms will be always one order higher in the self-energy (defined below) with respect to the normal ones.[134,136,137]

The resulting expression for the current-current response function is then given by the product of two phonons Green's functions (2.3.2). For clarity, let us consider for example the response function obtained from the Wigner heat-flux operator (2.2.24):

$$\chi^{\gamma\sigma}(\tau) = \frac{\hbar^2}{N_c^2 \mathcal{V}^2} \sum_{\boldsymbol{q},ss'} \frac{(\Omega(\boldsymbol{q})_s + \Omega(\boldsymbol{q})_{s'})^2}{4} v^\gamma(\boldsymbol{q})_{ss'} v^\sigma(\boldsymbol{q})_{s's} g(\boldsymbol{q},\tau)_{s'} g(\boldsymbol{q},-\tau)_s. \tag{2.3.3}$$

Here $g(\boldsymbol{q},\tau)_s$ denotes the "dressed" phonon Green's functions, in which self-energy effects due to interactions such as anharmonicity or isotopic disorder are considered (*i.e.* intrinsic scattering sources). They can be encoded in the phonon spectral density, defined as:

$$b(\boldsymbol{q},\omega)_s = -\frac{\hbar}{\pi} \mathrm{Im} g(\boldsymbol{q}, i\omega_n)_s \Big|_{i\omega_n \to \hbar\omega + i0^+}. \tag{2.3.4}$$

The advantage of a formalism based on the spectral density is the direct connection with the phonon self-energy. In fact, the two are related through Eq. (2.3.4) via the relation

$$b(\boldsymbol{q},\omega)_s = \frac{1}{\pi} \frac{\gamma(\boldsymbol{q},\omega)_s}{(\omega - \Omega(\boldsymbol{q})_s - \Delta(\boldsymbol{q},\omega)_s)^2 + \gamma(\boldsymbol{q},\omega)_s^2} \tag{2.3.5}$$

where the phonon self-energy is defined as $\pi(\boldsymbol{q},\omega)_s/\hbar = \Delta(\boldsymbol{q},\omega) - i\gamma(\boldsymbol{q},\omega)_s$. Using the latter relation, scattering sources of different nature can be readily included in the calculation of thermal conductivity through the phonon self-energy. For example, in our test cases we consider anharmonicity — besides intrinsic isotope scattering — only at lowest perturbative order (3-phonon bubble, *i.e.* 3-phonon scattering), but Eq. (2.3.5) gives a precise and practical recipe on how to implement higher order anharmonicity such as 4-phonon scattering. This is relevant since it has been shown how quartic anharmonicity can change drastically diagonal thermal conductivity in certain materials,[60,138] while enhancing coherence effects and interband thermal conductivity in others.[5]

The full procedure to carry out the Fourier transform of Eq. (2.3.3) and to perform the analytical continuation is rather straightforward and it is outlined in Appendix 2.C. The final expression for the thermal conductivity is a function of the phonon spectral densities (2.3.5), with a structure depending on the details of the heat-flux operator. In the case of Hardy's heat-flux operator (2.2.15) the thermal conductivity is composed of two terms:

$$\kappa = \kappa_R + \kappa_A \,, \tag{2.3.6a}$$

$$\kappa_R^{\gamma\sigma} = \frac{\hbar^2\pi}{N_c\mathcal{V}T}\sum_{\boldsymbol{q},ss'}\frac{(\Omega(\boldsymbol{q})_s+\Omega(\boldsymbol{q})_{s'})^2}{4}v^{\gamma}(\boldsymbol{q})_{ss'}v^{\sigma}(\boldsymbol{q})_{s's}\int \mathrm{d}\omega\, b(\boldsymbol{q},\omega)_{s'}b(\boldsymbol{q},\omega)_s\left[-\frac{\partial n_T(\omega)}{\partial\hbar\omega}\right] \tag{2.3.6b}$$

$$\kappa_A^{\gamma\sigma} = \frac{\hbar^2\pi}{N_c\mathcal{V}T}\sum_{\boldsymbol{q},ss'}\frac{(\Omega(\boldsymbol{q})_s-\Omega(\boldsymbol{q})_{s'})^2}{4}v^{\gamma}(\boldsymbol{q})_{ss'}v^{\sigma}(\boldsymbol{q})_{s's}\int \mathrm{d}\omega\, b(\boldsymbol{q},\omega)_{s'}b(\boldsymbol{q},-\omega)_s\frac{\partial n_T(\omega)}{\partial\hbar\omega}\,. \tag{2.3.6c}$$

The result following from the Wigner definition of the heat-flux operator (2.2.24) is instead

$$\kappa^{\gamma\sigma} = \frac{\hbar^2\pi}{N_c\mathcal{V}T}\sum_{\boldsymbol{q},ss'}\frac{(\Omega(\boldsymbol{q})_s+\Omega(\boldsymbol{q})_{s'})^2}{4}v^{\gamma}(\boldsymbol{q})_{ss'}v^{\sigma}(\boldsymbol{q})_{s's}\int \mathrm{d}\omega\, b(\boldsymbol{q},\omega)_{s'}b(\boldsymbol{q},\omega)_s\left[-\frac{\partial n_T(\omega)}{\partial\hbar\omega}\right]. \tag{2.3.7}$$

The structure of thermal conductivity obtained with the Wigner heat-flux operator is completely analogous to the resonant term obtained in Hardy's formalism; the difference between (2.3.7) and (2.3.6b) resides only in the definition of the velocity matrices (see Eq. (2.2.16),(2.2.25) and (2.2.26)). Therefore, the difference between Eq. (2.3.6a) and Eq. (2.3.7) for the total thermal conductivity is due to the presence of the antiresonant term (2.3.6c) and due to the differences in the off-diagonal phonon velocities. This clearly mirrors the aforementioned discrepancies in the heat-flux operators.

Nonetheless, from both starting points, one can derive an expression of thermal conductivity in terms of an integral of the product of two FSFs. This analytical structure provides some physical intuition for interband transport in terms of phonon band mixing. For a perfectly harmonic crystal, the phonon spectral densities are δ-functions at the phonon frequencies $\Omega(\boldsymbol{q})_s$, *i.e.* $b(\boldsymbol{q},\Omega(\boldsymbol{q})_s)=\delta(\omega-\Omega(\boldsymbol{q})_s)$, while interactions have the effect of broadening such shapes and shifting the peaks (cf. Eq. (2.3.5)). If there is a non-zero overlap between spectral densities of two different modes $(\boldsymbol{q},s)\neq(\boldsymbol{q},s')$, the two phonon bands are mixed and can give a finite contribution to interband thermal conductivity.

Now we consider the LSFA for the expressions of the thermal conductivity discussed above. This consists in taking the limit where the probability of finding a vibrational excitation with energy ω, momentum $\boldsymbol{q}$ and band s is mostly concentrated around the non-interacting excitation energy, *i.e.* the harmonic frequency $\Omega(\boldsymbol{q})_s$, and the effect of the interaction is to introduce a finite linewidth to each harmonic phonon mode. This is equivalent to the assumption that the spectral density (2.3.5) has a Lorentzian lineshape, as one obtains by approximating the self-energy with its value at the harmonic phonon frequencies, and neglecting its real part, *i.e.* $\gamma(\boldsymbol{q},\omega)_s\simeq\gamma(\boldsymbol{q},\Omega(\boldsymbol{q})_s)_s\to\gamma(\boldsymbol{q})_s$ and $\Delta(\boldsymbol{q},\omega)_s\simeq 0$. If we further approximate the derivative of the Bose function with its value at the harmonic frequencies, we get that the spectral integrals in (2.3.6b),(2.3.6c),(2.3.7) consist in a convolution of two Lorentzians, that can be computed analytically. With this procedure, we get from Eq. (2.3.7), obtained using the Wigner heat-flux operator, the following expression for the

thermal conductivity in the LSFA

$$\kappa^{\gamma\sigma}=\frac{1}{N_c\mathcal{V}}\sum_{\boldsymbol{q},ss'}\frac{\Omega(\boldsymbol{q})_s+\Omega(\boldsymbol{q})_{s'}}{4}v^{\gamma}(\boldsymbol{q})_{ss'}v^{\sigma}(\boldsymbol{q})_{s's}\left[\frac{C(\boldsymbol{q})_s}{\Omega(\boldsymbol{q})_s}+\frac{C(\boldsymbol{q})_{s'}}{\Omega(\boldsymbol{q})_{s'}}\right] \tag{2.3.8}$$

$$\times\frac{\frac{1}{2}(\Gamma(\boldsymbol{q})_s+\Gamma(\boldsymbol{q})_{s'})}{(\Omega(\boldsymbol{q})_s-\Omega(\boldsymbol{q})_{s'})^2+\frac{1}{4}(\Gamma(\boldsymbol{q})_s+\Gamma(\boldsymbol{q})_{s'})^2} \tag{2.3.9}$$

where the modal heat capacity $C(\boldsymbol{q})_s$ has been defined in (2.2.2), and we have used the relation $\gamma(\boldsymbol{q})_s=\frac{1}{2}\Gamma(\boldsymbol{q})_s$ between the scattering rate $\Gamma(\boldsymbol{q})_s$ used in Boltzmann SMA (*i.e.* the linewidth) and the phonon self-energy $\gamma(\boldsymbol{q})_s$ (see e.g. Ref. 67, Sec. 8.1). This expression coincides exactly with the SMA of WTE obtained in Ref. 12, as further discussed below. Using the same procedure for the thermal conductivity (2.3.6a) obtained from Hardy heat flux we get

$$\kappa=\kappa_R+\kappa_A\,, \tag{2.3.10a}$$

$$\kappa_R^{\gamma\sigma}=\frac{1}{N_c\mathcal{V}}\sum_{\boldsymbol{q},ss'}\frac{\Omega(\boldsymbol{q})_s+\Omega(\boldsymbol{q})_{s'}}{4}v^{\gamma}(\boldsymbol{q})_{ss'}v^{\sigma}(\boldsymbol{q})_{s's}\left[\frac{C(\boldsymbol{q})_s}{\Omega(\boldsymbol{q})_s}+\frac{C(\boldsymbol{q})_{s'}}{\Omega(\boldsymbol{q})_{s'}}\right] \times\frac{\frac{1}{2}(\Gamma(\boldsymbol{q})_s+\Gamma(\boldsymbol{q})_{s'})}{(\Omega(\boldsymbol{q})_s-\Omega(\boldsymbol{q})_{s'})^2+\frac{1}{4}(\Gamma(\boldsymbol{q})_s+\Gamma(\boldsymbol{q})_{s'})^2}\,, \tag{2.3.10b}$$

$$\kappa_A^{\gamma\sigma}=\frac{1}{N_c\mathcal{V}}\sum_{\boldsymbol{q},ss'}\frac{\Omega(\boldsymbol{q})_s-\Omega(\boldsymbol{q})_{s'}}{4}v^{\gamma}(\boldsymbol{q})_{ss'}v^{\sigma}(\boldsymbol{q})_{s's}\left[\frac{C(\boldsymbol{q})_{s'}}{\Omega(\boldsymbol{q})_{s'}}-\frac{C(\boldsymbol{q})_s}{\Omega(\boldsymbol{q})_s}\right] \times\frac{\frac{1}{2}(\Gamma(\boldsymbol{q})_s+\Gamma(\boldsymbol{q})_{s'})}{(\Omega(\boldsymbol{q})_s+\Omega(\boldsymbol{q})_{s'})^2+\frac{1}{4}(\Gamma(\boldsymbol{q})_s+\Gamma(\boldsymbol{q})_{s'})^2}\,. \tag{2.3.10c}$$

The latter expressions elucidate the nomenclature for Hardy's heat-flux operator: the amplitude of the resonant thermal conductivity (2.3.10b) is maximum when the frequencies of the two modes resonate, *i.e.* when $\Omega(\boldsymbol{q})_s\simeq\Omega(\boldsymbol{q})_{s'}$, whereas the antiresonant (2.3.10c) term is maximum when $\Omega(\boldsymbol{q})_s\simeq-\Omega(\boldsymbol{q})_{s'}$. Since the phonon frequencies are positive definite, the condition that maximizes the antiresonant terms cannot be met, hence such terms are expected to be much smaller than the resonant ones. Once again, the resonant thermal conductivity (2.3.10b) resulting from Hardy's heat flux and the one derived from Wigner (2.3.8) share a common structure and they differ only in the non-degenerate interband $s\neq s'$ terms, due to the already discussed difference in the definition of the velocity matrices (2.2.26).

In order to discuss the differences between the expressions of thermal conductivity derived so far, it is instructive to consider different regimes for thermal transport. The two relevant quantities to be considered are the relative strength of the phonon linewidth $\Gamma(\boldsymbol{q})_s$ with respect to the harmonic frequencies $\Omega(\boldsymbol{q})_s$, and the magnitude of $\Gamma(\boldsymbol{q})_s$ with respect to the typical spacing among phonon branches, that can be roughly estimated as $\Delta\omega_{\text{avg}}=\frac{\Omega_{\text{max}}}{3N_{at}}$ (Ω_{max} is the maximum phonon frequency and $3N_{at}$ the number of phonon bands), see Fig. 2.2. In general, whenever $\Gamma(\boldsymbol{q})_s\ll\Omega(\boldsymbol{q})_s$ phonon states are well defined and one can safely approximate the phonon spectral function with a Lorentzian: this is the regime where the LFSA holds[139] (purple shaded section of Fig. 2.2). If $\Gamma(\boldsymbol{q})_s$ is also lower than $\Delta\omega_{\text{avg}}$, phonon branches do not overlap significantly and the Peierls-Boltzmann semiclassical theory becomes accurate (green shaded area in Fig. 2.2): phonons wavepackets propagate as particle of a gas, with well defined momentum $\boldsymbol{q}$ (the central momentum of the wavepacket), energy $\hbar\Omega(\boldsymbol{q})_s$, and scattering rate $\tau(\boldsymbol{q})_s=\frac{1}{\Gamma(\boldsymbol{q})_s}$. As the linewidth increases and overcomes $\Delta\omega_{\text{avg}}$, vibrational modes start to get mixed. In this regime, the wave-like nature

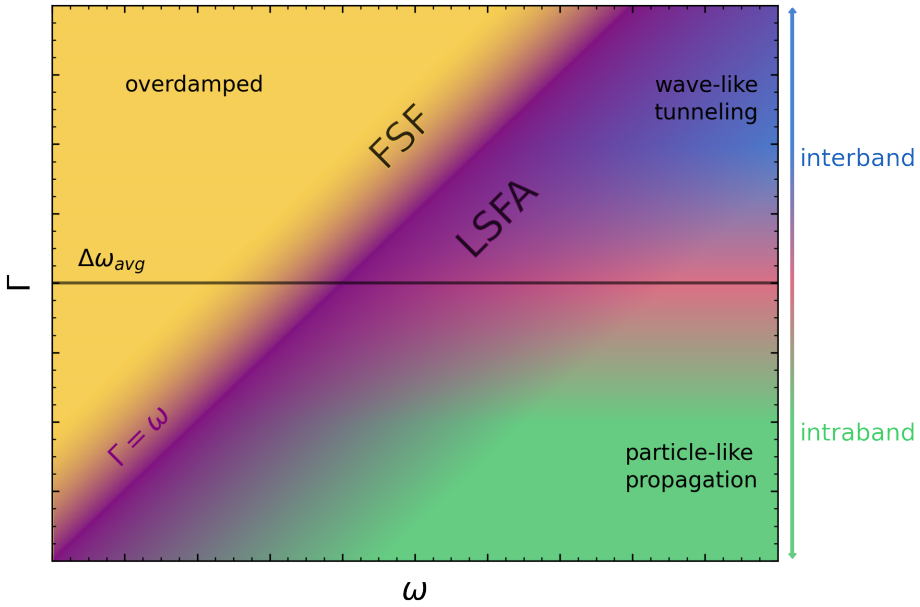

Figure 2.2. Diagram of the thermal transport regimes considering phonon linewidths (Γ) as a function of frequencies (ω). When the linewidths are larger than the frequencies, phonons are ill-defined and the vibrational modes are overdamped (gold area). In the latter regime, vibrational excitation must be discussed using full phonon spectral functions (FSF). When the linewidths are smaller than the frequencies (purple area), the Lorentzian spectral function approximation (LSFA) becomes feasible. The strength of phonon damping determines the transition from the particle-like regime (green area, where heat is mainly carried by phonon wavepackets that behave as particles of a gas), to the wave-like tunneling regime (blue area, where the effective overlap between phonon states allows them to interfere and enables interband tunneling transport). The transition from the particle-like to the wave-like regime is non-sharp (red shaded area), and phonons having a linewidth around the average interband spacing $\Delta\omega_{\text{avg}}$ (horizontal line) are at the center of this non-sharp crossover, behaving both particle- and wave-like. Both wave-like and particle-like conduction are well described in the LSFA, provided that heat hydrodynamics is negligible (see text).

of the atomic vibrations emerges, and heat conduction can also occur through the tunneling of phonons between overlapping bands. Note that there is no sharp separation between the two regimes: a phonon mode can contribute to thermal transport both in a particle-like and wave-like fashion, hence participating equally in intraband and interband conduction[12,13] (red shaded area of Fig. 2.2). This threshold has been denoted in Ref. 13 as the Wigner limit, and it has been shown that phonons around this threshold contribute comparably to the particle-like (intraband) and wave-like (interband) conductivity. On the other hand, the system enters a completely different regime when $\Gamma(\boldsymbol{q})_s \gtrsim \Omega(\boldsymbol{q})_s$ (gold-colored side of Fig. 2.2), since in this case the LSFA breaks down and the quasiparticle picture becomes invalid, with phonons losing their "identity" as heat carriers due to the strong interactions. In this regime the FSF must be used to compute thermal conductivity, considering the frequency dependence of the phonon self-energy. Also, in this case, the crossover to the overdamped regime is not defined by a sharp transition.

To summarize, while the expressions of thermal conductivity derived in this section in terms of the FSFs are valid throughout all the transport regimes regardless of phonon damping (within the limits of validity of perturbation theory), the expressions derived in the LSFA are correct only far from the overdamped regime. Nonetheless, even in the LSFA, the expression for the thermal conductivity we use consists of an extension of the BTE

considering the interband contribution to thermal transport.

However, we should mention that some care is needed in considering a general regime of validity of the dressed-bubble approximation. In fact, there is a transport regime where a theoretical justification of such approximation should not hold. This is the so-called hydrodynamical regime of thermal transport,[140] where momentum-conserving (normal) dominates over the resistive (Umklapp) scattering.[24] The Umklapp scatterings are 3-phonon scattering events where crystal momentum is not conserved.[36,119] The normal phonon scatterings are instead scattering events that conserve crystal momentum. In practice, Umklapp scattering limits heat conduction, while normal scattering do not degrade the heat flux but redistribute it across different phonon modes.[23,24] In a many-body language, it is known that in order to account for the fact that normal scatterings do not degrade the flux, one has to consider vertex corrections in the current-current response function, that are instead automatically included in the full solution of the BTE.[23,24,67,141,142] Neglecting such effects consists for the intraband conductivity (in the LSFA) in approximating the so-called transport relaxation time with the quasiparticle relaxation time (phonon self-energy). The validity of such an approximation scheme can be verified *a posteriori* by comparing the results for the thermal conductivity obtained with a LBTE approach obtained from a full diagonalization procedure with the ones obtained with SMA. However, it is generally understood[12,13,143] that heat hydrodynamics appears typically in materials with large values of thermal conductivity ($\gtrsim 10^3$ W/mK around room temperature for typical carbon-based materials[23,143,144]), in which it has been shown that accounting for phononic collective excitations with a full diagonalization procedure of LBTE overcomes the failure of the SMA in describing simple crystals.[25,142] Instead, for materials with ultralow thermal conductivity, the results obtained from the solution of the LBTE determined within the SMA approximation are practically indistinguishable from the exact solution of the LBTE.[13] Since the main interest of the presentChapter is to investigate the physics of interband thermal transport in ultralow-conductivity complex materials in temperature ranges where Umklapp scatterings are predominant, we do not expect to find any signature of heat hydrodynamics (*i.e.* vertex corrections effects) in our test cases and our approximation is expected to yield quantitatively reliable results. Anyhow, we have performed the abovementioned tests comparing our result for intraband thermal conductivity obtained via the dressed-bubble LSFA with the one obtained with a (computationally much more demanding) full-diagonalization procedure of the LBTE, finding no quantitatively relevant numerical differences for the materials under scrutiny.

In general, the LBTE and the WTE are able to describe the physics of intraband transport accounting also for the hydrodynamic regime of thermal transport, a feature missing in this work. On the other hand, interband transport is not taken into account by the LBTE and is described by the WTE only far from the overdamped regime, while here interband transport is treated in full generality in all the regimes including the overdamped one.

2.3.1 Comparison with other approaches

In this Section, we will discuss differences and analogies between the present expressions of thermal conductivity derived from the Hardy or Wigner heat fluxes with respect to the other results in the literature. Let us start by considering the comparison with the results derived using Hardy heat flux (2.2.15), as used both in older theoretical studies (Ref. 124, 145) and more recently in Ref. 33, 39. All these rely on a Green-Kubo approach, analogous to the one employed here, but with some differences that will be discussed below.

First of all, the present definition (2.3.2) of the phonon Green's function $g(\boldsymbol{q},\tau)_s$ is different from the one commonly found in literature,[67,131] corresponding to $G(\boldsymbol{q},\tau)_s = -\langle\mathcal{T}_\tau[\hat{a}(\boldsymbol{q},\tau)_s+\hat{a}^\dagger(-\boldsymbol{q},\tau)_s][\hat{a}(-\boldsymbol{q},0)_s+\hat{a}^\dagger(\boldsymbol{q},0)_s]\rangle$; the two are related simply by $G(\boldsymbol{q},\tau)_s = g(\boldsymbol{q},\tau)_s+g(\boldsymbol{q},-\tau)_s$ (further discussion in Appendix 2.D). The standard definition can be motivated by the fact that interaction terms for phonons depend only on the atomic displacement $\hat{u}\sim\hat{a}+\hat{a}^\dagger$. On the other hand, in the definition of the heat flux the momentum $\hat{P}$ of the atoms appears explicitly (cf. Eq. (2.2.10)). Since $\hat{u}$ and $\hat{P}$ are independent variables, we cannot express the correlations for the thermal current only in terms of the Green's function $G(\tau)\sim\langle\hat{u}(\tau)\hat{u}(0)\rangle$, but one must also consider an additional mixed Green's function such as $\tilde{G}(\tau)\sim\langle\hat{P}(\tau)\hat{u}(0)\rangle\sim g(\tau)-g(-\tau)$.[123,124]

The expressions (2.3.6a)-(2.3.6c) for the thermal conductivity derived from Hardy's heat flux (2.2.15) in terms of the FSF coincide with the results first proposed in Ref. 123 and Ref. 124. In Ref. 124 the thermal conductivity is obtained using a double-time Green's function approach,[124,146] employing a particular decoupling scheme — cf. Eq. (2.D.2) — to the heat-flux autocorrelation function (two-particle Green's function) directly in the time domain. We will show in Appendix 2.D how this decoupling scheme is equivalent to the present dressed-bubble approximation. Given such an equivalence, the present framework based on a diagrammatic expansion provides a transparent identification of the approximation used, and also shows how to systematically refine the results obtained by accounting for higher-order processes. The approach followed by Ref. 123 is more similar to the one presented here, but the approximation of the heat-flux autocorrelation is considered only for isotope scattering and without any diagrammatic interpretation. Both Ref. 123 and Ref. 124 rely on a formalism based on phonon displacement operators $\hat{A}(\boldsymbol{q})_s=\hat{a}(\boldsymbol{q})_s+\hat{a}^\dagger(-\boldsymbol{q})_s$, which leads to the definition of 4 kind of Green's functions (2 of which are independent).[123,124] Instead, here we only consider phonon operators $\hat{a}(\boldsymbol{q})_s$ and, as mentioned above, only one type of Green's function is needed, which greatly simplifies the notation. In this regard, we argue that the present formalism is more compact and consists of a more suitable choice for the treatment of lattice thermal transport in a many-body theoretical approach. Besides mathematical ease, the thermal conductivity (2.3.6a)-(2.3.6c) with this choice of the phonon Green's function features separate resonant and antiresonant contributions, whereas in the result proposed in both Ref. 123 and Ref. 124 those terms are mixed (see Appendix 2.D for details). As we shall see, the antiresonant terms are typically negligible with respect to the resonant ones, hence our expression (2.3.6a)-(2.3.6c) is more effective in highlighting leading order terms.

We can compare the present result for the thermal conductivity in the LSFA derived from the Hardy heat-flux operator (2.3.10a)-(2.3.10c) with the recent results of Refs. 33,39, obtained with a Green-Kubo approach where a constant scattering rate is assigned to each phonon mode. We note that the results for the thermal conductivity presented in Refs. 33,39 slightly differ from (2.3.10a)-(2.3.10c), in the fact that the interband conductivity of Refs.[33,39] features finite differences of the Bose-Einstein functions instead of the modal specific heats prefactors (related to the Bose-Einstein derivatives) featuring in (2.3.10a)-(2.3.10c). We give a possible explanation of this discrepancy — along with some more details on the comparison — in Appendix 2.D, where we argue that such differences stem from a subtlety in the derivation of thermal conductivity when considering phonon damping directly in the time-domain or in the frequency-domain expression of the phonon Green's functions. To our present knowledge, we find that this difference has only a formal valence since consistency is found in the numerical calculation of thermal conductivity for both test case materials considered in this work, as shown in Sec. 2.3.2.

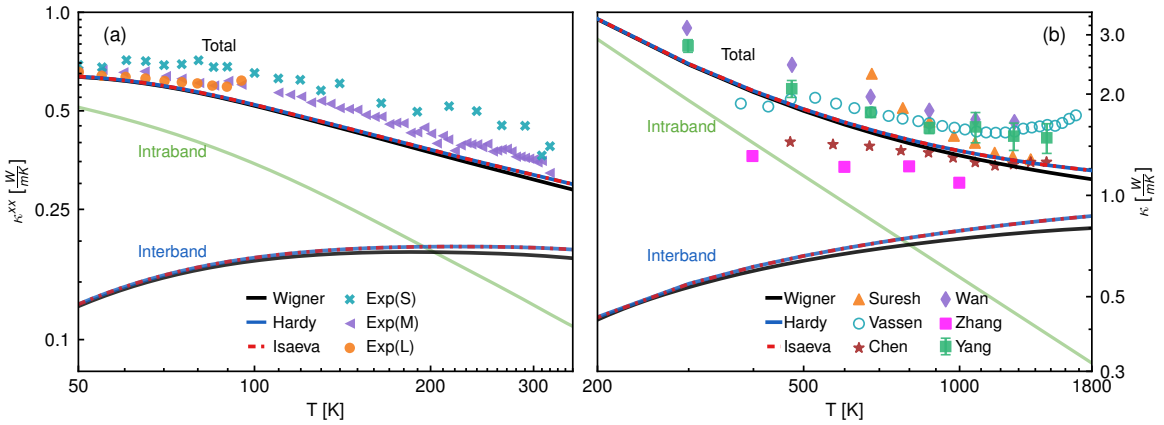

Figure 2.3. Lattice thermal conductivity of $CsPbBr_3$ (a) and $La_2Zr_2O_7$ (b). Experimental data for $CsPbBr_3$ are taken from Ref. 3 and "Exp(S)", "Exp(M)" and "Exp(L)" refer to measurements of κ^{xx} in nanowires of increasing section from smallest (S) to largest (L). Experimental data for $La_2Zr_2O_7$ are taken from Suresh *et al.*,[6] Vassen *et al.*,[7] Chen *et al.*,[8] Wan *et al.*,[9] Zhang *et al.*,[10] Yang *et al.*[11] Lines in different colors represents theoretical prediction from different formulations of thermal conductivity in the LSFA. For $CsPbBr_3$ we report the conductivity tensor component κ^{xx}, for $La_2Zr_2O_7$ we report a component of the isotropic conductivity tensor. Black, result from Wigner heat-flux from Eq. (2.3.8). Blue, result from Hardy heat-flux from Eq. (2.3.10a)-(2.3.10c). Red, result obtained following the approach of Ref. 33 (Isaeva *et al.*, reported in the Appendix in Eq. (2.D.11)). In the lower part of the figures the interband contributions to thermal conductivity are reported, which are obtained by considering only the off-diagonal and non-degenerate terms ($s\neq s'$ with $\Omega(\boldsymbol{q})_s\neq\Omega(\boldsymbol{q})_{s'}$) in the corresponding equations. The intraband term is reported in light green, it is obtained by considering only the diagonal ($s=s'$) or degenerate ($s\neq s'$ with $\Omega(\boldsymbol{q})_s=\Omega(\boldsymbol{q})_{s'}$) terms in the corresponding equations and in its the same in all the approaches considered. The results for the total conductivity (upper lines) are obtained by summing the corresponding interband term (lower lines) with the intraband part (light green).

Concerning the results obtained with Wigner heat flux (2.2.24), we emphasize that Eq. (2.3.7) represents a refinement of the WTE thermal conductivity formula in the SMA approximation[12,13] and is one of the main results of this work. In fact, besides reducing in the LSFA limit to the SMA of the WTE, it is valid in general for every shape of the spectral density, *i.e.* for every structure of the phonon self-energy. Therefore, the expression for interband thermal conductivity derived here can also be used in the overdamped regime where the spectral densities depart from the Lorentzian lineshape, e.g. near the edge of a structural phase transition.[49,147] On the other hand, the WTE result presented in[12] has the advantage of considering fully the LBTE result for the intraband conduction, hence being able to describe the hydrodynamic transport regime that we miss in the dressed-bubble approximation,[67] as stressed in the discussion of Fig. 2.2.

As mentioned, Eq. (2.3.8) derived as the LSFA of Eq. (2.3.7) coincides exactly with the SMA of the WTE obtained in Ref. 12. The result (2.3.8) proves how the same expression for thermal conductivity can be achieved using the Wigner transport equation or a Green-Kubo approach, thus consolidating the theoretical framework of the Wigner formulation of thermal transport while also clarifying how the results for thermal conductivity do not depend on the theoretical procedure employed to derive them.

Finally, we stress that when heat hydrodynamics can be neglected, all the formulations of thermal conductivity previously derived admit an intraband contribution which reduces in the semiclassical limit — *i.e.* neglecting interband terms in the LSFA — to the result from Peierls-Boltzmann transport equation in SMA.[119,148] In fact, if we take $s=s'$ both in (2.3.8)

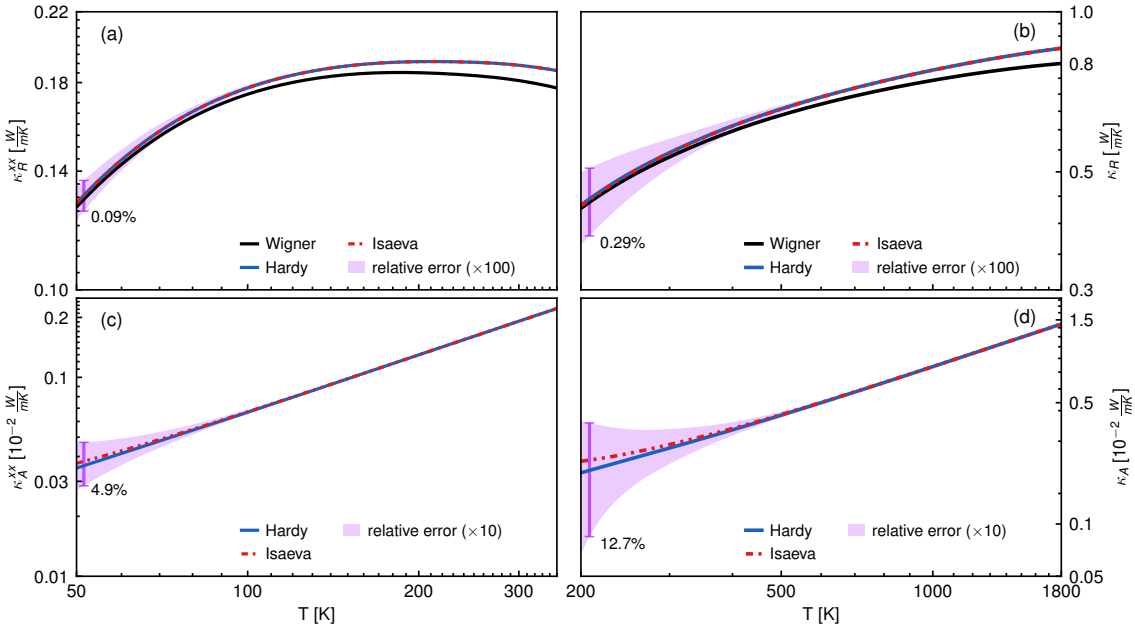

Figure 2.4. Comparison between the interband thermal conductivity obtained by means of the Hardy (blue, Eq. (2.3.10b)-(2.3.10c)) heat flux, the Wigner heat flux (black, Eq. (2.3.8)) and the Hardy heat flux in Ref. 33 (red, Isaeva *et al.*, reported in the Appendix in Eq. (2.D.11)). Left column: results for $CsPbBr_3$ (a-c). Right column: results for $La_2Zr_2O_7$ (b-d). For the case of the Hardy heat flux, we further distinguish between the resonant contribution (upper panels, a, b) and the antiresonant one (lower panels, c, d). The different scales in the latter plots elucidate how the antiresonant thermal conductivity is typically two orders of magnitude smaller than the resonant one, and it is mostly negligible. We also notice that in the LSFA the quantitative differences between the present results (2.3.10b)-(2.3.10c) and that those of Ref. 33 for the Hardy heat flux are numerically negligible. This is further evidenced by the pink shading, which represents the relative error between the blue and red lines, rescaled by a multiplicative factor for proper visualization. A single value of the relative error is reported as a percentage to set the scale.

and in (2.3.10a)-(2.3.10c) we get exactly the result for the BTE presented in Eq. (2.2.2).

2.3.2 Application to test cases $CsPbBr_3$ and $La_2Zr_2O_7$

We will now apply the result of thermal conductivity discussed and derived in the previous Section to two test case materials: $CsPbBr_3$ and $La_2Zr_2O_7$. $CsPbBr_3$ belongs to the family of lead-halide perovskite, interesting for their ultralow thermal conductivity and potential candidates for thermoelectric energy conversion.[3,4,28] $La_2Zr_2O_7$ is a pyrochlore bulk insulator characterized by thermal stability and ultralow thermal conductivity, thus it is of great interest for thermal barrier coating applications.[149] It is also an important test case for the calculations since interband lattice heat transport becomes predominant in this material at high temperatures (namely in the range that concerns applications). For the details of the vibrational properties of these materials such as phonon bands and linewidths, we refer the reader to Ref.[12] and Ref.[13] respectively for $CsPbBr_3$ and $La_2Zr_2O_7$.

For these systems we will implement the formulas for thermal conductivity obtained in the LSFA, namely (2.3.10a) from the Hardy heat flux and (2.3.8) for the Wigner heat flux (that coincides with that of Ref. 12). To enrich the comparison outlined in Sec. 2.3.1 between the present and previous results, we also implement the expression of the thermal conductivity presented in Ref. 33, derived using Hardy heat flux (the explicit expression is reported in the Appendix as Eq. (2.D.11)). We did not implement the expression of the thermal

conductivity proposed in Ref. 39 since it was derived using yet another definition for the heat-flux operator, which consists of a slight modification of Hardy heat flux (2.2.15), even though some plausible arguments on why the result for the thermal conductivity proposed in Ref. 39 should be similar to the one proposed in Ref. 33 for these systems are sketched in Appendix 2.D. The phonon scattering rates are computed considering the lowest-order 3-phonon scattering and the intrinsic isotopic scattering. Details of the numerical calculation can be found in Ref. 13.

The application of the LSFA to these test cases is motivated by the fact that in the temperature range considered the vast majority of vibrational modes of both $La_2Zr_2O_7$ and $CsPbBr_3$ feature linewidths well below the value of their harmonic frequencies (cf. Fig.8 of Ref. 13); hence we can treat both materials as safely far from the overdamped regime. It is worth noting that for the perovskite $CsPbBr_3$ a structural phase transition from the orthorhombic to the tetragonal phase is predicted for $T_c^{ot}{\sim}361\ K$, and another from tetragonal to cubic at $T_c^{tc}{\sim}403\ K$.[150] It has been shown recently in Ref. 147 how these two phases are characterized by extreme phonon damping, as evidenced by inelastic neutron scattering data signaling very broad phonon spectral profiles. The latter study testifies how even if the LSFA may hold for the orthorhombic phase, theoretical prediction for thermal conductivity of $CsPbBr_3$ at higher temperatures must be done with a formalism capable of describing overdamped phonon modes, considering the FSFs as in the present results of Eqs. (2.3.6a)-(2.3.6c) and (2.3.7).

The results are shown in Fig. 2.3. Here one sees that the different formulations for thermal conductivity give basically the same numerical results for the total thermal conductivity in both systems. In addition, the values for the thermal conductivity obtained are in good agreement with experimental data. As already mentioned, all the formulations studied lead to the same expression for the diagonal Peierls-Boltzmann conductivity, reported in light green and denoted as "intraband" in Fig. 2.3. This contribution, following the expected typical T^{-1} decay,[14] is however in broad disagreement with the experimental data. Such a disagreement is corrected by the interband terms, reported in the lower side of Fig. 2.3. The results presented in Fig. 2.3 show how the interband terms provide a sizeable contribution to the thermal conductivity especially at high temperatures, highlighting the importance of a correct description of interband transport in systems of this kind.

On the other hand, very small numerical differences are found between the Hardy and Wigner formulations of the heat flux. This is better seen in Fig. 2.4, where we provide a closer look at the interband contribution to the thermal conductivity as resulting from different formulations of the heat flux. In particular, the two results obtained starting from the Hardy heat flux are consistent with each other, with small discrepancies with the Wigner result when the temperature is increased. This is most likely a consequence of the fact that in these materials the phonon bands that build up most of the interband thermal conductivity are close in energy, *i.e.* $\Omega(\boldsymbol{q})_s{\simeq}\Omega(\boldsymbol{q})_{s'}$ in (2.3.10a). If this is the case, the differences between the velocities (2.2.26) are small, and the finite differences of the Bose functions well approximate the modal heat capacities which appear in our formulation. The antiresonant terms in Fig. 2.4(c-d) consist in less than 1% of total thermal conductivity through all the temperature ranges and are thus mostly negligible. The relative differences with the results from Ref[33] decrease when increasing temperature, especially for the antiresonant term. This can be understood from the fact that when the temperature is higher than the Debye temperature θ_D, (2.3.10a)-(2.3.10c) and Ref. 33 are the same, since for $T{\gg}\theta_D$ it holds $n(\Omega(\boldsymbol{q})_s){\simeq}k_BT/\hbar\Omega(\boldsymbol{q})_s\ \forall(\boldsymbol{q},s)$.

2.4 Heat flux and gauge invariance

In this Section, we comment on the numerical results of the thermal conductivity obtained from the different definitions of the heat flux in the LSFA presented in Sec. 2.3.2, discussing whether the agreement between the computed thermal conductivities could have been foreseen as a consequence of some broader invariance principle of thermal transport, that ensures consistency of transport coefficients regardless of the microscopic details. In fact, the real physical question triggered by the numerical correspondence between the results obtained with the Hardy and the Wigner heat flux concerns the role played by the freedom to partition the total energy in local contributions. In other words, do we have a guiding principle to decide what is the best choice of local energy to compute the thermal conductivity at a certain level of approximation?

As mentioned in the introduction, a possible way to reconcile results obtained with different definitions of heat flux has been outlined in Ref.[40] Here the authors show that whenever two choices of local energies differ by the divergence of a bounded vector field, the corresponding heat fluxes lead to the same thermal conductivity. The reason is that the corresponding heat fluxes, obtained from the continuity equation (1.2.16), differ by a total time-derivative term, which gives no contribution to thermal transport. Such a result, demonstrated in Ref. 40 by using a classical limit for the general formula (2.1.1), can be extended to the quantum case, as shown in Appendix 2.B. The basic mechanism can be easily understood from Eq. (2.1.6): since the thermal conductivity is defined as the $\omega \to 0$ limit of the current-current response function divided by ω, adding to the current a time derivative brings an additional factor ω^2 in the numerator, leading to a vanishing contribution in the zero-frequency limit. Such a result can be used for example to justify why we carried out the coarse-graining procedure outlined in Sec. 2.2 for the Hardy local energy using the equilibrium position $\boldsymbol{R}_l + \boldsymbol{\tau}_b$ instead that the instantaneous $\boldsymbol{R}_l + \boldsymbol{\tau}_b + \boldsymbol{u}(\boldsymbol{R}_l)_b$ atomic positions into the Δ_ℓ functions Eq. (2.2.8). Indeed, adding the local displacements $\boldsymbol{u}(\boldsymbol{R}_l)_b$ is equivalent to adding to the heat flux a total time derivative.

While very attractive and powerful, such gauge invariance does not answer the question posed. First, it provides a sufficient but not necessary condition for the equivalence between two different definitions of the heat flux. In other words, to the best of our knowledge, it has not been proven that all possible partitioning of the total energy must differ by a total derivative. More specifically, we could not prove that the two energy density operators derived from Hardy (2.2.7) and from Wigner (2.2.23) differ for the divergence of a bounded vector field. Thus, we cannot state that the two quantum heat-flux operators (2.2.15) and (2.2.24) differ by a total time derivative.

Secondly, the gauge-invariance principle is valid if the thermal conductivity is derived from the exact current-current correlation function, which is the one typically obtained from molecular dynamics simulations from a direct evaluation of the time integral of the heat-flux autocorrelation function.[59,127–129] However, we discussed here the derivation of the current-current correlation function in a certain diagrammatic approximation, and we further compared results obtained by different heat fluxes in the LSFA. The question then reduces to what is usually called a "conserving approximation" within the language of electrical transport, *i.e.* an approximate result that satisfies the gauge-invariant requirements of the theory. So far, it is not evident that also for thermal transport such an approach can be established. Nonetheless, we cannot help noting that the Hardy choice for the heat flux includes an antiresonant term for the heat-flux operator that is quantitatively irrelevant for

the thermal conductivity. As a consequence, the Wigner current has certainly the advantage to include from the beginning only the relevant interband processes for thermal transport, avoiding the computational effort to include irrelevant terms.

2.5 Conclusions

In summary, in this Chapter, we have shown how to derive an expression for the thermal conductivity with a full quantum-mechanical many-body formalism based on Green's functions and the Kubo formula. We have focused on two definitions of the energy field, that lead via the continuity equation to two different definitions of the heat flux. These two choices have been motivated by previous work in the literature. The first one corresponds to the heat flux originally proposed by Hardy,[35] which follows from a coarse-graining procedure implemented on the local harmonic Hamiltonian in real space. The second one corresponds to the Wigner heat flux implemented within the approach of Refs. 12, 13. Once the heat flux is defined in terms of creation and annihilation phonon operators, one can derive the thermal conductivity as the zero-frequency limit of a current-current response function, in close analogy with the usual diagrammatic approach implemented for electric transport.[67] Here, we compute the response function in the so-called dressed-bubble approximation, which neglects vertex corrections but accounts for all self-energy corrections of the phonon Greens' function due to interactions. Such an approximation allows us to derive an analytical expression for the thermal conductivity in terms of the exact phonon spectral density, that can be computed in principle at any perturbative order and extended to scattering sources of any nature. Thus, the present result based on the full phonon spectral density can also be used in the overdamped regime of thermal transport, where the quasiparticle picture of phonons breaks down.

The thermal conductivity is given, for both choices of the heat flux, by an intraband and an interband contribution. The former is independent of the choice of the heat flux, while the second displays some differences both in the definition of interband velocities and in the way interband processes are weighted, with the appearance in Hardy's formulation of antiresonant terms. The present expression of the thermal conductivity in terms of the full phonon spectral densities derived from Hardy's heat flux coincides with the one presented in the theoretical studies.[123,124] The analogous expression derived with Wigner heat flux is instead a novel and original result.

With the LSFA applied to the full quantum formula (2.3.7) with the Wigner heat flux we have recovered the results of the Wigner transport equation derived in Refs. 12, 13, thus proving the consistency of the Wigner formalism also in a fully quantum approach. On the other hand, in the case of the Hardy heat flux we have found formal differences with respect to the quantum derivation recently proposed in Ref. 33. We have argued that these differences originate from the procedure employed in Ref. 33, 39 to implement the limit of frequency-independent phonon lifetimes within the real-time Green's function, leading to some differences in the interband terms (the intraband are instead identical) that yield, however, no quantitative differences when computed numerically in the materials tested so far.

As benchmark examples, we have studied two systems with ultralow thermal conductivity, namely the perovskite $CsPbBr_3$ and the zirconate $La_2Zr_2O_7$. As discussed, we did not find so far a satisfactory general argument to understand the quantitative agreement between different formulations of the heat flux. On the other hand, we argued that the

Wigner formulation appears the most natural choice to compute the thermal conductivity in the dressed-bubble approximation, which reduces to the result from the Wigner transport equation in the LSFA. Indeed, it only includes the interband contributions which are actually relevant in this regime, at least for the systems tested so far. In the aforementioned test case materials, we have considered the effect of anharmonicity in the form of finite phonon lifetime due to 3-phonon and natural-abundance isotope scattering at the lowest perturbative order. In Ref. 13 it is presented a comparison between Raman scattering data for $CsPbBr_3$ and $La_2Zr_2O_7$ and simulated Raman spectra within the same approximation, *i.e.* considering lowest-order 3-phonon anharmonicity and no frequency renormalization, finding remarkable agreement between the two in the temperature range $100-300\,\mathrm{K}$. This gives us reason to believe that this level of approximation for the anharmonicity is accurate enough for the scope of the present study. In general, a comparison between the phonon frequencies and their linewidth obtained from ab-initio calculations and the phonon spectra obtained from inelastic neutron scattering[147] or electron energy loss spectroscopy,[151] could provide a quantitative evaluation of the accuracy of the approximation done in considering phonon anharmonicity at the lowest non-trivial order for the whole phonon dispersion (Raman scattering is limited to $\boldsymbol{q}=0$). As a possible future perspective, it would be interesting to consider the effect of higher-order anharmonicity such as 4-phonon scattering on the results for thermal conductivity for these materials.

Appendices of Chapter 2

2.A Details on the derivation of heat-flux operator

In this Appendix we show how to derive the expression for the heat flux associated with a given local energy operator, following Hardy's original procedure.[35] Its implementation for the Hardy local operator (2.2.7) has been detailed in Ref. 35. Here we will employ this procedure to derive the heat flux starting from the local energy operator emerging from the Wigner formalism. This will also serve us to show how the novel definition of the velocity matrix used in Wigner formalism follows from the derivation of the heat flux. Let us start by recalling the Wigner local energy given in Eq. (2.2.23)

$$\hat{h}(\boldsymbol{R}_l)_{b\alpha}=\frac{\hbar}{2}\sum_{\boldsymbol{R}_{l'}b'\alpha'}\sqrt{G}_{\boldsymbol{R}_l b\alpha,\boldsymbol{R}_{l'}b'\alpha'}\hat{a}^\dagger(\boldsymbol{R}_l)_{b\alpha}\hat{a}(\boldsymbol{R}_{l'})_{b'\alpha'}+\text{h.c.}, \tag{2.A.1}$$

which satisfies $\sum_{\boldsymbol{R}_l b\alpha}\hat{h}(\boldsymbol{R}_l)_{b\alpha}=\hat{\mathcal{H}}$ (without the zero-point-motion term, which does not affects the dynamics of the systems and thus does not provide any heat flux). To derive the heat flux from the continuity equation (1.2.16), one needs to define an energy density of continuous variable $h(\boldsymbol{x})$. This can be done convolving the discrete operator (2.A.1) with a continuous normalized distribution $\Delta_\ell(\boldsymbol{x}-\boldsymbol{R}_l-\boldsymbol{\tau}_b)$, such that $\hat{h}(\boldsymbol{x})=\sum_{\boldsymbol{R}_l b\alpha}\hat{h}(\boldsymbol{R}_l)_{b\alpha}\Delta_\ell(\boldsymbol{x}-\boldsymbol{R}_l-\boldsymbol{\tau}_b)$. It is easy to show that the continuous energy field satisfies $\int_V \mathrm{d}^3x\,\hat{h}(\boldsymbol{x})=\hat{\mathcal{H}}$. From the continuity equation (1.2.16), one has

$$-\nabla\cdot\hat{\boldsymbol{j}}(\boldsymbol{x})=\frac{d\hat{h}(\boldsymbol{x})}{dt}=-\frac{i}{\hbar}[\hat{h}(\boldsymbol{x}),\hat{\mathcal{H}}], \tag{2.A.2}$$

implying that the divergence of the energy flux operator can be computed from the commutator

$$\nabla\cdot\hat{\boldsymbol{j}}(\boldsymbol{x})=\frac{i}{\hbar}\sum_{\substack{\boldsymbol{R}_l b\alpha\\ \boldsymbol{R}_{l'}b'\alpha'}}\big[\Delta_\ell(\boldsymbol{x}-\boldsymbol{R}_l-\boldsymbol{\tau}_b)-\Delta_\ell(\boldsymbol{x}-\boldsymbol{R}_{l'}-\boldsymbol{\tau}_{b'})\big]\hat{h}(\boldsymbol{R}_l)_{b\alpha}\hat{h}(\boldsymbol{R}_{l'})_{b'\alpha'}. \tag{2.A.3}$$

Now the quantity in square bracket can be written in terms of the Taylor series of the distributions Δ_ℓ around the point $\boldsymbol{x}$:

$$\begin{aligned}\Delta_\ell(\boldsymbol{x}-\boldsymbol{R}-\boldsymbol{\tau}_b)-\Delta_\ell(\boldsymbol{x}-\boldsymbol{R}'-\boldsymbol{\tau}_{b'}) &= \sum_{|\gamma|}\tfrac{1}{\gamma!}\Big[\tfrac{\partial^\gamma}{\partial\boldsymbol{y}^\gamma}\Delta_\ell(\boldsymbol{y})\big|_{\boldsymbol{y}=\boldsymbol{x}}\Big](\boldsymbol{x}-\boldsymbol{R}-\boldsymbol{\tau}_b)^\gamma\\ &\quad-\sum_{|\gamma|}\tfrac{1}{\gamma!}\Big[\tfrac{\partial^\gamma}{\partial\boldsymbol{y}^\gamma}\Delta_\ell(\boldsymbol{y})\big|_{\boldsymbol{y}=\boldsymbol{x}}\Big](\boldsymbol{x}-\boldsymbol{R}'-\boldsymbol{\tau}_{b'})^\gamma\\ &=\sum_{|\gamma|\geq 1}\tfrac{1}{\gamma!}[(\boldsymbol{x}-\boldsymbol{R}-\boldsymbol{\tau}_b)^\gamma-(\boldsymbol{x}-\boldsymbol{R}'-\boldsymbol{\tau}_{b'})^\gamma]\tfrac{\partial^\gamma\Delta_\ell(\boldsymbol{x})}{\partial\boldsymbol{x}^\gamma},\end{aligned} \tag{2.A.4}$$

where γ is a multiindex used for multi-dimensional Taylor expansions, and clearly the zeroth order term of the resulting series is zero. It follows that Eq. (2.A.3) can be recast as

$$\nabla\cdot\hat{\boldsymbol{j}}(\boldsymbol{x})=\frac{i}{\hbar}\sum_{\substack{\boldsymbol{R}_l b\alpha\\ \boldsymbol{R}_{l'}b'\alpha'}}\hat{h}(\boldsymbol{R}_l)_{b\alpha}\hat{h}(\boldsymbol{R}_{l'})_{b'\alpha'}\sum_{|\gamma|\geq 1}\tfrac{1}{\gamma!}[(\boldsymbol{x}-\boldsymbol{R}_l-\boldsymbol{\tau}_b)^\gamma-(\boldsymbol{x}-\boldsymbol{R}_{l'}-\boldsymbol{\tau}_{b'})^\gamma]\tfrac{\partial^\gamma\Delta_\ell(\boldsymbol{x})}{\partial\boldsymbol{x}^\gamma}, \tag{2.A.5}$$

implying that the local heat-flux operator (*i.e.* the current density) reads

$$\hat{\boldsymbol{j}}(\boldsymbol{x})=\frac{i}{\hbar}\sum_{\substack{\boldsymbol{R}_l b\alpha\\ \boldsymbol{R}_{l'}b'\alpha'}}\hat{h}(\boldsymbol{R}_l)_{b\alpha}\hat{h}(\boldsymbol{R}_{l'})_{b'\alpha'}\Big\{(\boldsymbol{R}_{l'}+\boldsymbol{\tau}_{b'}-\boldsymbol{R}-\boldsymbol{\tau}_b)\Delta_\ell(\boldsymbol{x}) + \sum_{|\gamma|\geq 2}\frac{1}{\gamma!}[(\boldsymbol{x}-\boldsymbol{R}-\boldsymbol{\tau}_b)^\gamma-(\boldsymbol{x}-\boldsymbol{R'}-\boldsymbol{\tau}_{b'})^\gamma]\frac{\partial^{\gamma-1}\Delta_\ell(\boldsymbol{x})}{\partial\boldsymbol{x}^{\gamma-1}}\Big\}. \tag{2.A.6}$$

For the computation of the thermal conductivity one needs the total heat flux, obtained integrating the density and normalizing by the crystal's volume $V=\mathcal{V}N_c$ (where $\mathcal{V}$ is the volume of the primitive cell and N_c the number of primitive cell in the crystal)

$$\hat{\boldsymbol{J}}=\frac{1}{N_c\mathcal{V}}\int_V\hat{\boldsymbol{j}}(\boldsymbol{x})\mathrm{d}^3x. \tag{2.A.7}$$

When integrating Eq. (2.A.6) over the volume, one has that $\Delta_\ell(\boldsymbol{x})$ is non-zero only over a small region of space, so the volume integral of the derivatives can be neglected and one obtains the expression for the average heat flux:

$$\hat{\boldsymbol{J}}=\frac{-i}{\hbar N_c\mathcal{V}}\sum_{\substack{\boldsymbol{R}_l b\alpha\\ \boldsymbol{R}_{l'}b'\alpha'}}(\boldsymbol{R}_l+\boldsymbol{\tau}_b-\boldsymbol{R}_{l'}-\boldsymbol{\tau}_{b'})\hat{h}(\boldsymbol{R}_l)_{b\alpha}\hat{h}(\boldsymbol{R}_{l'})_{b'\alpha'}=\frac{-i}{\hbar N_c\mathcal{V}}\sum_{\boldsymbol{R}_l b\alpha}(\boldsymbol{R}_l+\boldsymbol{\tau}_b)[\hat{h}(\boldsymbol{R}_l)_{b\alpha},\hat{\mathcal{H}}]\,. \tag{2.A.8}$$

At this point we can plug in the commutator the definition of the local energy (2.A.1), obtaining

$$\begin{aligned}[\hat{h}(\boldsymbol{R}_l)_{b\alpha},\hat{\mathcal{H}}]=&\frac{\hbar^2}{2}\sum_{\substack{\boldsymbol{R}_l b'\alpha',\boldsymbol{R}_{l_1}b_1\alpha_1,\\ \boldsymbol{R}_{l_2}b_2\alpha_2}}\sqrt{G}_{\boldsymbol{R}_l b\alpha,\boldsymbol{R}_{l_1}b_1\alpha_1}\sqrt{G}_{\boldsymbol{R}_l b'\alpha',\boldsymbol{R}_{l_2}b_2\alpha_2}[\hat{\mathsf{a}}^\dagger(\boldsymbol{R}_l)_{b\alpha}\hat{\mathsf{a}}(\boldsymbol{R}_{l_1})_{b_1\alpha_1},\hat{\mathsf{a}}^\dagger(\boldsymbol{R}_{l'})_{b'\alpha'}\hat{\mathsf{a}}(\boldsymbol{R}_{l_2})_{b_2\alpha_2}]+\text{h.c.}\\ =&\frac{\hbar^2}{2}\sum_{\substack{\boldsymbol{R}_l b'\alpha',\boldsymbol{R}_{l_1}b_1\alpha_1,\\ \boldsymbol{R}_{l_2}b_2\alpha_2}}\sqrt{G}_{\boldsymbol{R}_l b\alpha,\boldsymbol{R}_{l_1}b_1\alpha_1}\sqrt{G}_{\boldsymbol{R}_l b'\alpha',\boldsymbol{R}_{l_2}b_2\alpha_2}\Big\{\hat{\mathsf{a}}^\dagger(\boldsymbol{R}_l)_{b\alpha}\hat{\mathsf{a}}(\boldsymbol{R}_{l_2})_{b_2\alpha_2}\delta_{\boldsymbol{R}_{l'}\boldsymbol{R}_{l_1}}\delta_{b'b_1}\delta_{\alpha'\alpha_1}\\ &-\hat{\mathsf{a}}^\dagger(\boldsymbol{R}_{l'})_{b'\alpha'}\hat{\mathsf{a}}(\boldsymbol{R}_{l_1})_{b_1\alpha_1}\delta_{\boldsymbol{R}_l\boldsymbol{R}_{l_2}}\delta_{bb_2}\delta_{\alpha\alpha_2}\Big\}+\text{h.c.}\,.\end{aligned} \tag{2.A.9}$$

Now we can plug the latter expression in the heat flux (2.A.8), and performing a relabelling $\boldsymbol{R}_{l_2}\to\boldsymbol{R}_{l_1}$ in the first term and $\boldsymbol{R}_l\leftrightarrow\boldsymbol{R}_{l'}$ in the second term of the last line of (2.A.9) we get

$$\hat{\boldsymbol{J}}=\frac{-i\hbar}{2N_c\mathcal{V}}\sum_{\substack{\boldsymbol{R}_l b\alpha,\boldsymbol{R}_{l'}b'\alpha',\\ \boldsymbol{R}_{l_1}b_1\alpha_1}}(\boldsymbol{R}_l+\boldsymbol{\tau}_b-\boldsymbol{R}_{l'}-\boldsymbol{\tau}_{b'})\sqrt{G}_{\boldsymbol{R}_l b\alpha,\boldsymbol{R}_{l'}b'\alpha'}\sqrt{G}_{\boldsymbol{R}_{l'}b'\alpha',\boldsymbol{R}_{l_1}b_1\alpha_1}\hat{\mathsf{a}}^\dagger(\boldsymbol{R}_l)_{b\alpha}\hat{\mathsf{a}}(\boldsymbol{R}_{l_1})_{b_1\alpha_1}+\text{h.c.} \tag{2.A.10}$$

Now we rewrite the bosonic operators in real space in terms of their Fourier transform,[13]

$$\hat{\mathsf{a}}(\boldsymbol{R}_l)_{b\alpha}=\frac{1}{\sqrt{N_c}}\sum_{\boldsymbol{q}}\hat{\mathsf{a}}(\boldsymbol{q})_{b\alpha}e^{+i\boldsymbol{q}\cdot(\boldsymbol{R}_l+\boldsymbol{\tau}_b)}, \tag{2.A.11}$$

obtaining

$$\begin{aligned}\hat{\boldsymbol{J}}=&\tfrac{-i\hbar}{2N_c\mathcal{V}}\sum_{\substack{\boldsymbol{q}\\ b\alpha,b'\alpha',\\ b_1\alpha_1}}\sum\hat{\mathsf{a}}^\dagger(\boldsymbol{q})_{b\alpha}\tfrac{1}{\sqrt{N_c}}\sum_{\boldsymbol{R}_{l'}\boldsymbol{R}_{l_1}}\hat{\mathsf{a}}(\boldsymbol{R}_{l_1})_{b_1\alpha_1}\sqrt{G}_{\boldsymbol{R}_{l'}b'\alpha',\boldsymbol{R}_{l_1}b_1\alpha_1}\\ &\times\sum_{\boldsymbol{R}_l}(\boldsymbol{R}_l+\boldsymbol{\tau}_b-\boldsymbol{R}_{l'}-\boldsymbol{\tau}_{b'})\sqrt{G}_{\boldsymbol{R}_lb\alpha,\boldsymbol{R}_{l'}b'\alpha'}e^{-i\boldsymbol{q}\cdot(\boldsymbol{R}_l+\boldsymbol{\tau}_b)}+\text{h.c.}\\ =&\tfrac{-i\hbar}{2N_c\mathcal{V}}\sum_{\substack{\boldsymbol{q}\\ b\alpha,b'\alpha',\\ b_1\alpha_1}}\sum\hat{\mathsf{a}}^\dagger(\boldsymbol{q})_{b\alpha}\tfrac{1}{\sqrt{N_c}}\sum_{\boldsymbol{R}_{l'}\boldsymbol{R}_{l_1}}\hat{\mathsf{a}}(\boldsymbol{R}_{l_1})_{b_1\alpha_1}\sqrt{G}_{\boldsymbol{R}_{l'}b'\alpha',\boldsymbol{R}_{l_1}b_1\alpha_1}e^{-i\boldsymbol{q}\cdot(\boldsymbol{R}_{l'}+\boldsymbol{\tau}_{b'})}\\ &\times\sum_{\boldsymbol{L}}(\boldsymbol{L}+\boldsymbol{\tau}_b-\boldsymbol{\tau}_{b'})\sqrt{G}_{\boldsymbol{L}b\alpha,0'b'\alpha'}e^{-i\boldsymbol{q}\cdot(\boldsymbol{L}+\boldsymbol{\tau}_b-\boldsymbol{\tau}_{b'})}+\text{h.c.}\\ =&\frac{\hbar}{2N_c\mathcal{V}}\sum_{\boldsymbol{q}}\sum_{\substack{b\alpha,b'\alpha',\\ b_1\alpha_1}}\boldsymbol{\nabla}_{\boldsymbol{q}}\sqrt{d(\boldsymbol{q})}_{b\alpha,b'\alpha'}\hat{\mathsf{a}}^\dagger(\boldsymbol{q})_{b\alpha}\frac{1}{\sqrt{N_c}}\sum_{\boldsymbol{R}_{l'}\boldsymbol{R}_{l_1}}\hat{\mathsf{a}}(\boldsymbol{R}_{l_1})_{b_1\alpha_1}\sqrt{G}_{\boldsymbol{R}_{l'}b'\alpha',\boldsymbol{R}_{l_1}b_1\alpha_1}e^{-i\boldsymbol{q}\cdot(\boldsymbol{R}_{l'}+\boldsymbol{\tau}_{b'})}+\text{h.c.}\end{aligned}\tag{2.A.12}$$

where we have multiplied and divided by $e^{-i\boldsymbol{q}\cdot(\boldsymbol{R}_{l'}+\boldsymbol{\tau}_{b'})}$ and used the symmetry property (2.2.5) of the matrix $\sqrt{G}_{\boldsymbol{R}_lb\alpha,\boldsymbol{R}_{l'}b'\alpha'}=\sqrt{G}_{\boldsymbol{R}_l-\boldsymbol{R}_{l'}b\alpha,0b'\alpha'}$ considering a change of summation index $\boldsymbol{R}_l\to\boldsymbol{L}=\boldsymbol{R}_l-\boldsymbol{R}_{l'}$ to introduce the gradient of the dynamical matrix from (2.2.12). In the same fashion we can recast $\hat{\mathsf{a}}(\boldsymbol{R}_{l_1})$ in terms of its reciprocal-space representation (2.A.11) to solve the summations in $\boldsymbol{R}_{l'}$, $\boldsymbol{R}_{l_1}$ obtaining

$$\hat{\boldsymbol{J}}=\frac{\hbar}{2N_c\mathcal{V}}\sum_{\boldsymbol{q}}\sum_{\substack{b\alpha,b'\alpha',\\ b_1\alpha_1}}\boldsymbol{\nabla}_{\boldsymbol{q}}\sqrt{d(\boldsymbol{q})}_{b\alpha,b'\alpha}\sqrt{d(\boldsymbol{q})}_{b'\alpha',b_1\alpha_1}\hat{\mathsf{a}}^\dagger(\boldsymbol{q})_{b\alpha}\hat{\mathsf{a}}(\boldsymbol{q})_{b_1\alpha_1}+\text{h.c.}\tag{2.A.13}$$

At this point we can pass to the normal mode basis (Eq. (2.2.11)) using the transformation $\hat{\mathsf{a}}(\boldsymbol{q})_{b\alpha}=\sum_s\varepsilon(\boldsymbol{q})_{s,b\alpha}\hat{a}(\boldsymbol{q})_s$ while considering the definition and properties of the velocity matrix (2.2.25), obtaining

$$\begin{aligned}\hat{\boldsymbol{J}}=&\frac{\hbar}{2N_c\mathcal{V}}\sum_{\boldsymbol{q},ss'}\{\Omega(\boldsymbol{q})_s\boldsymbol{v}(\boldsymbol{q})_{ss'}\hat{a}^\dagger(\boldsymbol{q})_s\hat{a}(\boldsymbol{q})_{s'}+\Omega(\boldsymbol{q})_s\boldsymbol{v}^*(\boldsymbol{q})_{ss'}\hat{a}^\dagger(\boldsymbol{q})_{s'}\hat{a}(\boldsymbol{q})_s\}\\ =&\frac{\hbar}{N_c\mathcal{V}}\sum_{\boldsymbol{q},ss'}\frac{\Omega(\boldsymbol{q})_s+\Omega(\boldsymbol{q})_{s'}}{2}\boldsymbol{v}(\boldsymbol{q})_{ss'}\hat{a}^\dagger(\boldsymbol{q})_s\hat{a}(\boldsymbol{q})_{s'}\end{aligned}\tag{2.A.14}$$

which is the heat-flux operator introduced in Eq. (2.2.24). As mentioned above, the procedure for the derivation of the heat flux from Hardy energy density (2.2.7) is completely analogous and it is reported in Hardy's original paper.[35]

2.B Gauge-invariance principle for the thermal conductivity: quantum considerations and implications on Hardy's derivation of the heat flux

In this Appendix we report some considerations on the application of the gauge-invariance principle for the thermal conductivity[40] in a quantum-mechanical framework, and we show how these allow to simplify the expression for the heat flux operator obtained following Hardy's approach. The starting point of the aforementioned work is the observation that energy's extensive character implies the energy density to be defined up to a divergence of

a bounded vector field, *i.e.* $\hat{h}'(\boldsymbol{x},t)=\hat{h}(\boldsymbol{x},t)+\boldsymbol{\nabla}\cdot\hat{\boldsymbol{\psi}}(\boldsymbol{x},t)$. Indeed, if $\hat{\boldsymbol{\psi}}(\boldsymbol{x},t)$ is bounded, the volume integral of $\hat{h}'(\boldsymbol{x},t)$ — *i.e.* the energy — differs from the volume integral of $\hat{h}(\boldsymbol{x})$ by a term that scales as a surface, hence is subextensive and does not contribute to the energy in the thermodynamical limit.[128] As a consequence, it follows an indeterminacy on the current density, since the two are related by the continuity equation (1.2.16). The indeterminacy on energy and current density thus acquire the structure of the gauge indeterminacy of vector and scalar potential of the electromagnetic field, namely

$$\begin{cases}\hat{h}'(\boldsymbol{x},t)=\hat{h}(\boldsymbol{x},t)+\boldsymbol{\nabla}\cdot\hat{\boldsymbol{\psi}}(\boldsymbol{x},t)\\ \hat{\boldsymbol{j}}'(\boldsymbol{x},t)=\hat{\boldsymbol{j}}(\boldsymbol{x},t)-\frac{\mathrm{d}}{\mathrm{d}t}\hat{\boldsymbol{\psi}}(\boldsymbol{x},t)\end{cases}\qquad \hat{\boldsymbol{J}}'(t)=\hat{\boldsymbol{J}}(t)-\frac{\mathrm{d}}{\mathrm{d}t}\hat{\boldsymbol{\Psi}}(t) \tag{2.B.1}$$

in which the last line describes the gauge transformation for the macroscopic heat flux, and $\hat{\boldsymbol{\Psi}}=\frac{1}{N_c\mathcal{V}}\int_V \mathrm{d}^3x\,\hat{\boldsymbol{\psi}}(\boldsymbol{x})$. The gauge invariance principle states that the indeterminacy (2.B.1) on the heat flux does not affect the thermal conductivity, so that

$$\kappa'=\frac{\mathcal{V}}{k_BT^2}\int_0^\infty \mathrm{d}t\,\langle\hat{\boldsymbol{J}}'(t)\cdot\hat{\boldsymbol{J}}'(0)\rangle=\frac{\mathcal{V}}{k_BT^2}\int_0^\infty \mathrm{d}t\,\langle\hat{\boldsymbol{J}}(t)\cdot\hat{\boldsymbol{J}}(0)\rangle=\kappa, \tag{2.B.2}$$

hence the thermal conductivity is well-defined regardless of the indeterminacy (2.B.1) on the microscopic energy and current density. The gauge invariance of thermal conductivity was proven originally in a classical statistical mechanics framework; in this Appendix we will extend such proof to the quantum mechanical picture and we will discuss its capabilities in the case of the Hardy heat-flux operator.

Quantum-mechanical considerations on the gauge invariance of thermal conductivity

To show the gauge invariance of thermal conductivity in quantum-mechanical picture, let us rephrase the Kubo formula (2.1.1) using the definition of the current-current correlation function introduced in Eq. (2.1.2). Inserting (2.1.2) in (2.1.1) without resorting to the fluctuation-dissipation theorem, we get

$$\kappa^{\gamma\sigma}=\frac{N_c\mathcal{V}}{k_BT^2}S^{\gamma\sigma}(\omega=0)=\frac{N_c\mathcal{V}}{k_BT^2}\int_{-\infty}^{+\infty}\mathrm{d}t\,\langle\hat{J}^\gamma(t)\hat{J}^\sigma(0)\rangle\,. \tag{2.B.3}$$

In order to have gauge invariance, we have to verify that the following condition is satisfied:

$$\kappa'^{\gamma\sigma}=\frac{N_c\mathcal{V}}{k_BT^2}\int_{-\infty}^{+\infty}\mathrm{d}t\,\langle[\hat{J}^\gamma(t)-\frac{\mathrm{d}\hat{\Psi}^\gamma(t)}{\mathrm{d}t}][\hat{J}^\sigma(0)-\frac{\mathrm{d}\hat{\Psi}^\sigma(0)}{\mathrm{d}t}]\rangle=\kappa^{\gamma\sigma}. \tag{2.B.4}$$

To this aim, we can show that any average that contains at least one total time derivative of an operator vanishes in (2.B.4). In fact, if we expand in the basis $\{|n\rangle\}$ of the eigenstates of the (full) Hamiltonian $\hat{H}$ defined such that $\hat{H}\,|n\rangle=E_n\,|n\rangle$, we get

$$\langle\hat{J}^\gamma(t)\frac{\mathrm{d}\hat{\Psi}^\sigma(0)}{\mathrm{d}t}\rangle=\sum_{nm}\frac{e^{-\beta E_n}}{\mathcal{Z}}\,\langle n|\hat{J}^\gamma(t)|m\rangle\,\langle m|\frac{\mathrm{d}\hat{\Psi}^\sigma(0)}{\mathrm{d}t}|n\rangle\,, \tag{2.B.5}$$

where $\mathcal{Z}=\mathrm{Tr}\left[e^{-\beta\hat{H}}\right]$ is the canonical partition function. In the latter expression we can now use the Heisenberg scheme for the evolution of operators $i\hbar\frac{\mathrm{d}}{\mathrm{d}t}\hat{A}(t)=[\hat{H},\hat{A}(t)]$, which yields

$$\langle\hat{J}^\gamma(t)\frac{\mathrm{d}\hat{\Psi}^\sigma(0)}{\mathrm{d}t}\rangle=\frac{i}{\hbar}\sum_{nm}\frac{e^{-\beta E_n}}{\mathcal{Z}}e^{-\frac{i}{\hbar}(E_n-E_m)t}(E_n-E_m) \times\langle n|\hat{J}^\gamma|m\rangle\langle m|\hat{\Psi}^\sigma|n\rangle\,. \tag{2.B.6}$$

Evidently, this term vanishes in the time integral of (2.B.4), since

$$\int_{-\infty}^{+\infty}\mathrm{d}t e^{-\frac{i}{\hbar}(E_n-E_m)t}\frac{(E_n-E_m)}{\hbar}=2\pi(E_n-E_m)\delta(E_n-E_m)=0$$

and this proves (2.B.4) and gauge invariance of thermal conductivity. Note that this result is valid with the assumption that the operator $\hat{\Psi}$ is bounded, which guarantees that every matrix element of $\hat{\Psi}$ in (2.B.6) is finite.
This is one of the key assumptions for the result of gauge invariance;[40] in fact, notice from Eq. (2.A.8) how the heat flux operator itself can be expressed as a total time derivative, namely the derivative of the first moment of the energy density $\hat{\boldsymbol{J}}=\frac{\mathrm{d}}{\mathrm{d}t}\sum_{\boldsymbol{R}_l b\alpha}(\boldsymbol{R}_l+\boldsymbol{\tau}_b)\hat{h}(\boldsymbol{R}_l)_{b\alpha}$. However, the latter expression features a time derivative of an operator which is clearly unbounded in the thermodynamical limit, and hence can yield a finite conductivity.

Gauge invariance and simplification of Hardy's derivation of the heat flux

Here we show how the gauge invariance properties of the thermal conductivity can be used to simplify significantly the structure of Hardy's heat-flux operator. Let us start by recalling the local energy operator used by Hardy,[35] introduced in Eq. (2.2.7)

$$\hat{h}(\boldsymbol{R}_l)_{b\alpha}=\frac{\hat{P}^2(\boldsymbol{R}_l)_{b\alpha}}{2M_b}+\hat{V}(\boldsymbol{R}_l)_{b\alpha} \tag{2.B.7}$$

where we have expressed for brevity the harmonic "on-site potential" as $\hat{V}(\boldsymbol{R}_l)_{b\alpha}=\frac{1}{2}\phi_{\boldsymbol{R}_l b\alpha,\boldsymbol{R}_{l'}b'\alpha'}\hat{u}(\boldsymbol{R}_l)_{b\alpha}\hat{u}(\boldsymbol{R}_{l'})_{b'\alpha'}$. As discussed in Sec. 2.2, the procedure to derive the heat-flux operator requires the convolution of the local-energy operator (2.2.7) with a smooth normalized distribution Δ_ℓ in order to define an energy density depending on a continuous variable, $\hat{h}(\boldsymbol{x})$. We anticipated in the main text that there is an ambiguity on where to center the coarse-graining functions Δ_ℓ. Hardy originally considered the center of the Δ_ℓ on the instantaneous position of the nuclei $\hat{\boldsymbol{r}}(\boldsymbol{R}_l)_b=\boldsymbol{R}_l+\boldsymbol{\tau}_b+\hat{\boldsymbol{u}}(\boldsymbol{R}_l)_b$ *i.e.* (the time dependence of the operators is omitted for brevity)

$$\hat{h}_{\text{Ref. 35}}(\boldsymbol{x})=\frac{1}{2}\sum_{\boldsymbol{R}_l b\alpha}\hat{h}(\boldsymbol{R}_l)_{b\alpha}\Delta_\ell(\boldsymbol{x}-\boldsymbol{R}_l-\boldsymbol{\tau}_b-\hat{\boldsymbol{u}}(\boldsymbol{R}_l)_{b\alpha})+\text{h.c.} \tag{2.B.8}$$

(h.c. stands for hermitian conjugate) whereas in this work we have centered such smoothening functions in the equilibrium position of the nuclei, as described in Eq. (2.2.8)

$$\hat{h}(\boldsymbol{x})=\sum_{\boldsymbol{R}_l b\alpha}\hat{h}(\boldsymbol{R}_l)_{b\alpha}\Delta_\ell(\boldsymbol{x}-\boldsymbol{R}_l-\boldsymbol{\tau}_b). \tag{2.B.9}$$

Using (2.B.9) in the procedure described in Appendix 2.A for the derivation of the heat flux leads to

$$\begin{aligned}\hat{\boldsymbol{J}}_{\text{Ref. 35}}=\frac{1}{2N_c\mathcal{V}}\sum_{\boldsymbol{R}_l b\alpha}\Big\{&\frac{\hat{\mathbf{p}}(\boldsymbol{R}_l)_b}{M_b}\big(\frac{\hat{p}(\boldsymbol{R}_l)^2_{b\alpha}}{2M_b}+\hat{V}(\boldsymbol{R}_l)_{b\alpha}\big)\\&+\sum_{\boldsymbol{R}_l b'\alpha'}(\hat{\boldsymbol{r}}(\boldsymbol{R}_l)_b-\hat{\boldsymbol{r}}(\boldsymbol{R}_{l'})_{b'})\frac{1}{i\hbar}\big[\frac{\hat{P}(\boldsymbol{R}_l)^2_{b\alpha}}{2M_b},\hat{V}(\boldsymbol{R}_{l'})_{b'\alpha'}\big]\Big\}+\text{ h.c.},\end{aligned}\tag{2.B.10}$$

which is the original structure of the heat flux proposed by Hardy in.[35] The latter has to be compared with the one we used in Eq. (2.2.10), which we recast as

$$\hat{\boldsymbol{J}}=\frac{1}{N_c\mathcal{V}}\sum_{\boldsymbol{R}_l b\alpha}(\boldsymbol{R}_l+\boldsymbol{\tau}_b-\boldsymbol{R}_{l'}-\boldsymbol{\tau}_{b'})\frac{1}{i\hbar}\big[\frac{\hat{P}(\boldsymbol{R}_l)^2_{b\alpha}}{2M_b},\hat{V}(\boldsymbol{R}_{l'})_{b'\alpha'}\big]\,.\tag{2.B.11}$$

Evidently, the structure of the heat-flux operator (2.B.10) is far more complicated than (2.B.11), and notably it features anharmonic $\mathcal{O}(p^3)$ and $\mathcal{O}(u^3)$ generated by an harmonic energy density such as (2.B.7). One could argue that (2.B.10) is a richer description of the heat flux in a lattice, but actually we can exploit the aforementioned properties of gauge invariance to prove that the heat fluxes (2.B.10) and (2.B.11) are related by a gauge transformation of the form (2.B.1), hence produce the same result for thermal conductivity. To this aim let us rephrase the convective part of the heat flux (2.B.10) as

$$\tfrac{1}{2N_c\mathcal{V}}\sum_{\boldsymbol{R}_l b\alpha}\tfrac{\hat{\mathbf{p}}(\boldsymbol{R}_l)_b}{M_b}\big(\tfrac{\hat{p}(\boldsymbol{R}_l)^2_{b\alpha}}{2M_b}+\hat{V}(\boldsymbol{R}_l)_{b\alpha}\big)=\tfrac{1}{2N_c\mathcal{V}}\sum_{\boldsymbol{R}_l b\alpha}\tfrac{d\hat{\boldsymbol{u}}(\boldsymbol{R}_l)_b}{dt}\hat{h}(\boldsymbol{R}_l)_{b\alpha}\tag{2.B.12}$$

while the conductive part of (2.B.10) can be recast as

$$\begin{aligned}&\tfrac{1}{2N_c\mathcal{V}}\sum_{\substack{\boldsymbol{R}_l b\alpha\\ \boldsymbol{R}_l b'\alpha'}}(\hat{\boldsymbol{r}}(\boldsymbol{R}_l)_b-\hat{\boldsymbol{r}}(\boldsymbol{R}_{l'})_{b'})\frac{1}{i\hbar}\big[\tfrac{\hat{P}(\boldsymbol{R}_l)^2_{b\alpha}}{2M_b},\hat{V}(\boldsymbol{R}_{l'})_{b'\alpha'}\big]\\&=\frac{1}{2}\hat{\boldsymbol{J}}+\tfrac{1}{2N_c\mathcal{V}}\sum_{\substack{\boldsymbol{R}_l b\alpha\\ \boldsymbol{R}_l b'\alpha'}}(\hat{\boldsymbol{u}}(\boldsymbol{R}_l)_b-\hat{\boldsymbol{u}}(\boldsymbol{R}_{l'})_{b'})\frac{1}{i\hbar}\big[\tfrac{\hat{P}(\boldsymbol{R}_l)^2_{b\alpha}}{2M_b},\hat{V}(\boldsymbol{R}_{l'})_{b'\alpha'}\big]\\&=\frac{1}{2}\hat{\boldsymbol{J}}+\frac{1}{2N_c\mathcal{V}}\sum_{\boldsymbol{R}_l b\alpha}\hat{\boldsymbol{u}}(\boldsymbol{R}_l)_b\frac{\mathrm{d}\hat{h}(\boldsymbol{R}_l)_{b\alpha}}{\mathrm{d}t}\,.\end{aligned}\tag{2.B.13}$$

Using (2.B.12)-(2.B.13) in (2.B.10) and solving the $\frac{1}{2}$ factors with the hermitian conjugate yields

$$\hat{\boldsymbol{J}}_{\text{Ref. 35}}=\hat{\boldsymbol{J}}+\frac{1}{2N_c\mathcal{V}}\frac{\mathrm{d}}{\mathrm{d}t}\big[\sum_{\boldsymbol{R}_l b\alpha}\hat{\boldsymbol{u}}(\boldsymbol{R}_l)_b\hat{h}(\boldsymbol{R}_l)_{b\alpha}\big]\tag{2.B.14}$$

which proves our point: centering the Δ_ℓ smoothening functions on the instantaneous position of the ions as in (2.B.9) or in their equilibrium position as in (2.B.7) leads to two heat-flux operators that differ by total time derivative of a bounded term. By virtue of the gauge invariance of thermal conductivity, the two heat fluxes describe the same physics of heat transport and can be thought as two "gauges" of the same heat flux.[33] Therefore, this invariance principle provides a solid theoretical reasoning to select the heat flux (2.B.11) over (2.B.10), choice that greatly simplifies the calculations.

Note that the identification $\frac{\hat{\boldsymbol{P}}(\boldsymbol{R}_l)_b}{M_b}=\frac{\mathrm{d}\hat{\boldsymbol{u}}(\boldsymbol{R}_l)_b}{\mathrm{d}t}$ that we used in (2.B.12) implies the important as-

sumption of no atomic diffusion, *i.e.* no drifting of the ionic equilibrium position $\frac{\mathrm{d}(\boldsymbol{R}_l+\boldsymbol{\tau}_b)}{\mathrm{d}t}=0$. This assumption, on which this whole proof holds, is typically met and causes no complications in a crystalline solid.

2.C Details on the derivation of thermal conductivity

In this Appendix we will describe how to derive the thermal conductivity expression discussed in 2.3 using the formalism of finite-temperature Green's function. We will follow the standard many-body approach for computing DC conductivities, outlined e.g. in Mahan's textbook.[67] Our goal is to compute thermal conductivity from the retarded response function, using the relation (2.1.6) derived from fluctuation-dissipation theorem

$$\kappa^{\gamma\sigma} = \frac{N_c\mathcal{V}}{T}\lim_{\omega\to 0}\frac{\mathrm{Im}\chi^{\gamma\sigma}(\omega+i0^+)}{\omega}\,. \tag{2.C.1}$$

As anticipated, the starting point is the time-ordered current-current response function in the imaginary time τ

$$\chi^{\gamma\sigma}(\tau) = \langle \mathcal{T}_\tau \hat{J}^\gamma(\tau)\hat{J}^\sigma(0)\rangle \tag{2.C.2}$$

which we shall rewrite in terms of the explicit expression of the heat flux chosen. We recap the expressions of the heat-flux operators in Wigner and Hardy formalism

Wigner

$$\hat{\boldsymbol{J}}=\frac{\hbar}{N_c\mathcal{V}}\sum_{\boldsymbol{q},ss'}\frac{\Omega(\boldsymbol{q})_s+\Omega(\boldsymbol{q})_{s'}}{2}\boldsymbol{v}(\boldsymbol{q})_{ss'}\hat{a}^\dagger(\boldsymbol{q})_s\hat{a}(\boldsymbol{q})_{s'} \tag{2.C.3a}$$

Hardy

$$\hat{\boldsymbol{J}} = \hat{\boldsymbol{J}}_R + \hat{\boldsymbol{J}}_A$$

$$\hat{\boldsymbol{J}}_R=\frac{\hbar}{N_c\mathcal{V}}\sum_{\boldsymbol{q},ss'}\frac{\Omega(\boldsymbol{q})_s+\Omega(\boldsymbol{q})_{s'}}{2}\boldsymbol{v}(\boldsymbol{q})_{ss'}\hat{a}^\dagger(\boldsymbol{q})_s\hat{a}(\boldsymbol{q})_{s'} \tag{2.C.3b}$$

$$\hat{\boldsymbol{J}}_A=\frac{\hbar}{N_c\mathcal{V}}\sum_{\boldsymbol{q},ss'}\frac{\Omega(\boldsymbol{q})_s-\Omega(\boldsymbol{q})_{s'}}{4}\boldsymbol{v}(\boldsymbol{q})_{ss'}\left[\hat{a}(-\boldsymbol{q})_s\hat{a}(\boldsymbol{q})_{s'}-\hat{a}^\dagger(\boldsymbol{q})_s\hat{a}^\dagger(-\boldsymbol{q})_{s'}\right]. \tag{2.C.3c}$$

As we will show, the structure of the final result only depends on the combination of phonon creation/annihilation operators appearing in the expression for the heat flux. Therefore the calculation of the response function (2.C.2) for the resonant part of the Hardy heat flux will be equal to one for the Wigner heat flux, apart from the prefactor of the velocity matrices. With this reasoning, we will only perform the calculation for Hardy heat flux (2.C.3b)-(2.C.3c), and the result for Wigner heat flux will follow. Using the expressions of Hardy heat flux in (2.C.2) yields

$$\begin{aligned}\chi^{\gamma\sigma}(\tau) =& \frac{\hbar^2}{N_c^2\mathcal{V}^2}\sum_{\boldsymbol{q},ss'}\sum_{\boldsymbol{k},zz'}\frac{\Omega(\boldsymbol{q})_s+\Omega(\boldsymbol{q})_{s'}}{2}\frac{\Omega(\boldsymbol{k})_z+\Omega(\boldsymbol{k})_{z'}}{2}v^\gamma(\boldsymbol{q})_{ss'}v^\sigma(\boldsymbol{k})_{zz'}\langle\mathcal{T}_\tau\hat{a}^\dagger(\boldsymbol{q},\tau)_s\hat{a}(\boldsymbol{q},\tau)_{s'}\hat{a}^\dagger(\boldsymbol{k})_z\hat{a}(\boldsymbol{k})_{z'}\rangle\\ &+\frac{\hbar^2}{N_c^2\mathcal{V}^2}\sum_{\boldsymbol{q},ss'}\sum_{\boldsymbol{k},zz'}\frac{\Omega(\boldsymbol{q})_s-\Omega(\boldsymbol{q})_{s'}}{4}\frac{\Omega(\boldsymbol{k})_z-\Omega(\boldsymbol{k})_{z'}}{4}v^\gamma(\boldsymbol{q})_{ss'}v^\sigma(\boldsymbol{k})_{zz'}\\ &\times\langle\mathcal{T}_\tau\left[\hat{a}(-\boldsymbol{q},\tau)_s\hat{a}(\boldsymbol{q},\tau)_{s'}-\hat{a}^\dagger(\boldsymbol{q},\tau)_s\hat{a}^\dagger(-\boldsymbol{q},\tau)_{s'}\right]\left[\hat{a}(-\boldsymbol{k})_z\hat{a}(\boldsymbol{k})_{z'}-\hat{a}^\dagger(\boldsymbol{k})_z\hat{a}^\dagger(-\boldsymbol{k})_{z'}\right]\rangle,\end{aligned} \tag{2.C.4}$$

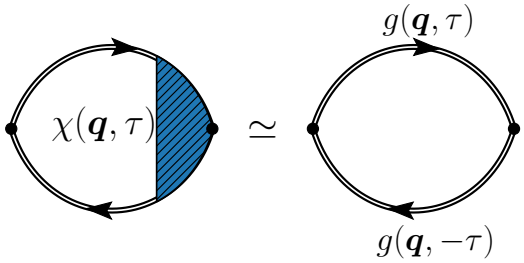

Figure 2.5. Diagramatic representation of dressed bubble approximation from Eq. (2.C.5). Left-hand side, full current-current correlation function $\chi(\boldsymbol{q},\tau)$. In the right-hand side, double solid lines represent interacting phonon Green's functions g from Eq. (2.C.6).

from which is evident how the response function is related to the two-particle phonon propagator.[67] The two terms in (2.C.4) represent respectively a resonant response function and an antiresonant response function, namely $\chi_R^{\gamma\sigma}(\tau) = \langle \mathcal{T}_\tau \hat{J}_R^\gamma(\tau)\hat{J}_R^\sigma(0)\rangle$ and $\chi_A^{\gamma\sigma}(\tau) = \langle \mathcal{T}_\tau \hat{J}_A^\gamma(\tau)\hat{J}_A^\sigma(0)\rangle$. This separation is made possible by the fact that the resonant and antiresonant heat fluxes posses a different number of creation/annihilation phonon operators, hence mixed $\langle T_\tau \hat{J}_R(\tau)\hat{J}_A(0)\rangle$ terms are zero (at least at the present level of approximation). More specifically, we will implement a dressed-bubble approximation, *i.e.* we will consider only bubble diagrams where the phonon lines are fully dressed by interaction, as diagramatically represented in Fig. 2.5. This amounts to neglecting vertex corrections and considering only self-energy effects in the phonon Green's functions, hence the two particle propagator is approximated as the product of two (interacting) phonon Green's functions, namely for the time-ordered product in the first term of (2.C.4)

$$\langle \mathcal{T}_\tau \hat{a}^\dagger(\boldsymbol{q},\tau)_s \hat{a}(\boldsymbol{q},\tau)_{s'} \hat{a}^\dagger(\boldsymbol{k})_z \hat{a}(\boldsymbol{k})_{z'}\rangle \simeq g(\boldsymbol{q},\tau)_{s'} g(\boldsymbol{q},-\tau)_s \delta_{\boldsymbol{q},\boldsymbol{k}} \delta_{sz'} \delta_{s'z}, \tag{2.C.5}$$

where the phonon Green's functions were introduced in (2.3.2) as

$$g(\boldsymbol{q},\tau)_s = -\langle \mathcal{T}_\tau \hat{a}(\boldsymbol{q},\tau)_s \hat{a}^\dagger(\boldsymbol{q},0)_s\rangle = \begin{cases} -\langle \hat{a}(\boldsymbol{q},\tau)_s \hat{a}^\dagger(\boldsymbol{q},0)_s\rangle & \tau > 0 \\ -\langle \hat{a}^\dagger(\boldsymbol{q},0)_s \hat{a}(\boldsymbol{q},\tau)_s\rangle & \tau < 0. \end{cases} \tag{2.C.6}$$

To be precise, we should also mention that the presence of $\delta_{ss'}$ in (2.C.5) consists in the additional approximation of neglecting branch mixed $\langle \hat{a}(\boldsymbol{q})_s \hat{a}^\dagger(\boldsymbol{q})_{s'}\rangle$ lines, since these are higher order in the self-energy.[145] Using the approximation (2.C.5) in (2.C.4) evaluating all the possible pairwise contractions we get

$$\begin{aligned} \chi^{\gamma\sigma}(\tau) = {} & \frac{\hbar^2}{N_c^2 \mathcal{V}^2} \sum_{\boldsymbol{q},ss'} \frac{(\Omega(\boldsymbol{q})_s + \Omega(\boldsymbol{q})_{s'})^2}{4} v^\gamma(\boldsymbol{q})_{ss'} v^\sigma(\boldsymbol{q})_{s's} g(\boldsymbol{q},\tau)_{s'} g(\boldsymbol{q},-\tau)_s \\ & + \frac{\hbar^2}{N_c^2 \mathcal{V}^2} \sum_{\boldsymbol{q},ss'} \frac{(\Omega(\boldsymbol{q})_s - \Omega(\boldsymbol{q})_{s'})^2}{4} v^\gamma(\boldsymbol{q})_{ss'} v^\sigma(\boldsymbol{q})_{s's} \tfrac{1}{2} \left[g(\boldsymbol{q},\tau)_{s'} g(\boldsymbol{q},\tau)_s + g(\boldsymbol{q},-\tau)_{s'} g(\boldsymbol{q},-\tau)_s \right] \end{aligned} \tag{2.C.7}$$

in which we have extensively used the property (2.2.25) of the velocity matrix to symmetrize the result (we stress that this property is verified by both Hardy's and Wigner's velocity matrices). Now we can take the Fourier transform of (2.C.8), passing from imaginary-time

to imaginary-frequency domain with $\chi^{\gamma\sigma}(i\Omega_n)=\int_0^{1/k_BT} \mathrm{d}\tau e^{i\Omega_n\tau}\chi^{\gamma\sigma}(\tau)$, which yields

$$\begin{aligned}\chi^{\gamma\sigma}(i\Omega_n) = \quad & \frac{\hbar^2 k_B T}{N_c^2\mathcal{V}^2}\sum_{\boldsymbol{q},ss'}\frac{(\Omega(\boldsymbol{q})_s+\Omega(\boldsymbol{q})_{s'})^2}{4}v^{\gamma}(\boldsymbol{q})_{ss'}v^{\sigma}(\boldsymbol{q})_{s's}\sum_{\omega_m} g(\boldsymbol{q},i\Omega_n+i\omega_m)_{s'}g(\boldsymbol{q},i\omega_m)_s \\ & +\frac{\hbar^2 k_B T}{N_c^2\mathcal{V}^2}\sum_{\boldsymbol{q},ss'}\frac{(\Omega(\boldsymbol{q})_s-\Omega(\boldsymbol{q})_{s'})^2}{4}v^{\gamma}(\boldsymbol{q})_{ss'}v^{\sigma}(\boldsymbol{q})_{s's} \\ & \times\sum_{\omega_m}\tfrac{1}{2}\left[g(\boldsymbol{q},i\Omega_n-i\omega_m)_{s'}g(\boldsymbol{q},i\omega_m)_s+g(\boldsymbol{q},-i\Omega_n-i\omega_m)_{s'}g(\boldsymbol{q},i\omega_m)_s\right],\end{aligned} \tag{2.C.8}$$

where the Matsubara bosonic frequencies are defined as $i\Omega_n=2\pi k_BTn,\ n\in\mathbb{Z}$. The next step consists in expressing the Green's function in terms of the spectral densities, using a Lehmann representation (see e.g. Mahan's textbook Ref. 67 sec. 3.3)

$$g(\boldsymbol{q},i\omega_l)_s = \int_{-\infty}^{+\infty}\mathrm{d}\omega\,\frac{b(\boldsymbol{q},\omega)_s}{i\omega_l-\hbar\omega}\,. \tag{2.C.9}$$

Using (2.C.9) in (2.C.8) yields an expression of the response function in the imaginary frequency domain in which the Matsubara frequency terms can be computed straightforwardly using standard summation techniques,[67] that will yield a combination of Bose-Einstein occupation functions. After having performed the Mastubara summation, we can consider the analytic continuation $i\Omega_n\to\hbar\omega+i0^+$ obtaining the finite frequency response function, whose imaginary part reads

$$\begin{aligned}\mathrm{Im}\chi^{\gamma\sigma}(\omega+i0^+)=&\tfrac{\hbar^2\pi}{N_c^2\mathcal{V}^2}\sum_{\boldsymbol{q},ss'}\tfrac{(\Omega(\boldsymbol{q})_s+\Omega(\boldsymbol{q})_{s'})^2}{4}v^{\gamma}(\boldsymbol{q})_{ss'}v^{\sigma}(\boldsymbol{q})_{s's}\iint\mathrm{d}\omega_1\mathrm{d}\omega_2\,b(\boldsymbol{q},\omega_1)_{s'}b(\boldsymbol{q},\omega_2)_s \\ & \times\delta(\omega_1-\omega_2-\omega)\tfrac{1}{\hbar}\left[-n_T(\omega_1)+n_T(\omega_2)\right] \\ & +\tfrac{\hbar^2\pi}{N_c^2\mathcal{V}^2}\sum_{\boldsymbol{q},ss'}\tfrac{(\Omega(\boldsymbol{q})_s-\Omega(\boldsymbol{q})_{s'})^2}{4}v^{\gamma}(\boldsymbol{q})_{ss'}v^{\sigma}(\boldsymbol{q})_{s's}\iint\mathrm{d}\omega_1\mathrm{d}\omega_2\,b(\boldsymbol{q},\omega_1)_{s'}b(\boldsymbol{q},\omega_2)_s \\ & \times\tfrac{1}{2\hbar}\left\{\delta(\omega_1+\omega_2+\omega)\left[n_T(-\omega_1)-n_T(\omega_2)\right]-\delta(\omega_1+\omega_2-\omega)\left[n_T(-\omega_2)-n_T(\omega_1)\right]\right\}.\end{aligned} \tag{2.C.10}$$

Finally from the latter expression, we can easily perform the static limit (2.C.1) to obtain thermal conductivity, which reads

$$\begin{aligned}\kappa^{\gamma\sigma} =&\frac{\hbar^2\pi}{N_c\mathcal{V}T}\sum_{\boldsymbol{q},ss'}\frac{(\Omega(\boldsymbol{q})_s+\Omega(\boldsymbol{q})_{s'})^2}{4}v^{\gamma}(\boldsymbol{q})_{ss'}v^{\sigma}(\boldsymbol{q})_{s's}\int\mathrm{d}\omega\,b(\boldsymbol{q},\omega)_{s'}b(\boldsymbol{q},\omega)_s\left[-\frac{\partial n_T(\omega)}{\partial\hbar\omega}\right] \\ &+\frac{\hbar^2\pi}{N_c\mathcal{V}T}\sum_{\boldsymbol{q},ss'}\frac{(\Omega(\boldsymbol{q})_s-\Omega(\boldsymbol{q})_{s'})^2}{4}v^{\gamma}(\boldsymbol{q})_{ss'}v^{\sigma}(\boldsymbol{q})_{s's}\int\mathrm{d}\omega\,b(\boldsymbol{q},\omega)_{s'}b(\boldsymbol{q},-\omega)_s\frac{\partial n_T(\omega)}{\partial\hbar\omega}\,.\end{aligned} \tag{2.C.11}$$

The first and second lines evidently coincide respectively with the resonant and antiresonant thermal conductivity obtained from Hardy heat flux, introduced in (2.3.6b)-(2.3.6c). The procedure for the Wigner heat flux current-current response function is exactly the same as for the resonant Hardy heat flux, hence one can repeat all the steps outlined so far using (2.C.3a) and verify that the only difference in the derivation consists in the definition of the velocity matrix. Therefore, the expression for thermal conductivity obtained from Wigner

definition of the heat-flux operator reads

$$\kappa^{\alpha\beta} = \frac{\hbar^2\pi}{N_c\mathcal{V}T}\sum_{\boldsymbol{q},ss'}\frac{(\Omega(\boldsymbol{q})_s+\Omega(\boldsymbol{q})_{s'})^2}{4}v^{\alpha}(\boldsymbol{q})_{ss'}v^{\beta}(\boldsymbol{q})_{s's}\int \mathrm{d}\omega\, b(\boldsymbol{q},\omega)_{s'}b(\boldsymbol{q},\omega)_s\left[-\frac{\partial n_T(\omega)}{\partial\hbar\omega}\right], \tag{2.C.12}$$

which is exactly (2.3.7). As a side note, let us discuss the spectral integrals featuring in (2.C.11),(2.C.12). In fact, one could question the definiteness of such integrals arguing that the derivative of the Bose function diverges as $\sim\omega^{-2}$ for $\omega\to 0$. However, it can be shown[67] that the bosonic spectral density must go to zero at least linearly for $\omega\to 0$, thus ensuring the convergence of the aforementioned integrals.

2.D Details on the comparison between different theoretical description of lattice thermal transport

In this Appendix, we provide a comparison between the present Green-Kubo approach to derive the expression for the thermal conductivity κ, and other derivations proposed in the literature. The thermal conductivity can be computed from the Kubo formula directly from its expressionin real-time domain (2.1.1), that we recall below

$$\kappa^{\gamma\sigma} = \lim_{\epsilon\to 0}\frac{N_c\mathcal{V}}{T}\int_0^{\infty}\mathrm{d}t\, e^{-\epsilon t}\int_0^{\beta}\mathrm{d}\lambda\,\langle\hat{J}^{\sigma}(0)\hat{J}^{\gamma}(t+i\hbar\lambda)\rangle\,. \tag{2.D.1}$$

In order to compute explicitly the conductivity, the so-called decoupling scheme[33,39,124,146,148] is employed, applied to the two-particle correlation function in real time domain, namely

$$\langle abcd\rangle \simeq \langle ab\rangle\langle cd\rangle + \langle ac\rangle\langle bd\rangle + \langle ad\rangle\langle bc\rangle, \tag{2.D.2}$$

where a,b,c,d are $a(\boldsymbol{q})/a^{\dagger}(\boldsymbol{q})$ operators. As we shall see here, employing the decoupling scheme (2.D.2) is formally equivalent to computing the response function in the dressed-bubble approximation (2.C.5), and will lead to the same expression of thermal conductivity in terms of the spectral densities (2.3.6a)-(2.3.7). To this aim, let's consider the case of the Hardy heat-flux operator (2.2.15). For the sake of brevity, we will just perform the calculation of the resonant thermal conductivity, hence considering only the resonant part of Hardy heat-flux operator (2.2.18b). Plugging the latter in (2.D.1) yields

$$\kappa_R^{\gamma\sigma} = \frac{\hbar^2}{N_c\mathcal{V}T}\int_0^{\infty}\mathrm{d}t\, e^{-\epsilon t}\int_0^{\beta}\mathrm{d}\lambda\sum_{\boldsymbol{q},ss'}\sum_{\boldsymbol{k},zz'}\frac{\Omega(\boldsymbol{q})_s+\Omega(\boldsymbol{q})_{s'}}{2}\frac{\Omega(\boldsymbol{k})_z+\Omega(\boldsymbol{k})_{z'}}{2}v^{\sigma}(\boldsymbol{k})_{zz'}v^{\gamma}(\boldsymbol{q})_{ss'}$$
$$\times\langle\hat{a}^{\dagger}(\boldsymbol{k})_z\hat{a}(\boldsymbol{k})_{z'}\hat{a}^{\dagger}(\boldsymbol{q},\bar{t})_s\hat{a}(\boldsymbol{q},\bar{t})_{s'}\rangle, \tag{2.D.3}$$

where for brevity we have reported $\bar{t}=t+i\hbar\lambda$ and omitted the $\epsilon\to 0$ limit. Now we can use the decoupling scheme (2.D.2) in the latter expression, obtaining (the decoupling scheme (2.D.2) carries the same combination of delta functions and coefficients as in the second line of Eq. (2.C.5))

$$\kappa_R^{\gamma\sigma} = \frac{\hbar^2}{N_c\mathcal{V}T}\sum_{\boldsymbol{q},ss'}\frac{(\Omega(\boldsymbol{q})_s+\Omega(\boldsymbol{q})_{s'})^2}{4}v^{\gamma}(\boldsymbol{q})_{ss'}v^{\sigma}(\boldsymbol{q})_{s's}\int_0^{\infty}\mathrm{d}t\, e^{-\epsilon t}\int_0^{\beta}\mathrm{d}\lambda\, c(\boldsymbol{q},\bar{t})_{s'}\tilde{c}(\boldsymbol{q},\bar{t})_s, \tag{2.D.4}$$

where we have introduced the correlation functions $c(\boldsymbol{q},t)_s = \langle \hat{a}(\boldsymbol{q},t)_s \hat{a}^\dagger(\boldsymbol{q})_s \rangle$ and $\tilde{c}(\boldsymbol{q},t)_s = \langle \hat{a}^\dagger(\boldsymbol{q},t)_s \hat{a}(\boldsymbol{q})_s \rangle$. At this point, we note in passing that the time-domain procedure can be quite useful to understand the interband conduction as an interference mechanism. To do so, let's take Eq. (D4) and let's focus only on the time-integration term. Let's consider for simplicity only two different non-degenerate modes s_1 and s_2, and neglect momentum dependence and quantum correlation (the integral $\int_0^\beta \mathrm{d}\lambda$ just yields a multiplicative β factor). The (classical) interband thermal conductivity is then proportional to $\kappa_R \propto \int_0^\infty \mathrm{d}t\, c_{s_1}(t)\tilde{c}_{s_2}(t)$. If we approximate the time-dependence of the correlation functions (for $t>0$) as the one of the damped harmonic modes $c_{s_1}(t) \propto e^{-\gamma_{s_1} t - i\Omega_{s_1} t}$, $\tilde{c}_{s_2}(t) \propto e^{-\gamma_{s_2} t + i\Omega_{s_2} t}$, we get that the interband conductivity is $\kappa_R \propto \int_0^\infty \mathrm{d}t \cos[(\Omega_{s_1} - \Omega_{s_2})t] e^{-(\gamma_{s_1}+\gamma_{s_2})t}$. From the latter expression, the interband conduction can be understood as interference between two different phonon modes, which of course follows from the wave-like nature of atomic oscillations. In fact, in molecular dynamics simulations, the interband contribution to thermal conductivity is deduced from the oscillatory behaviour of the heat-flux autocorrelation function.[39] This calculation is clearly qualitative, and only meets the purpose of a more clear physical interpretation.

In order to account rigorously for the effects of interactions, the real-time averages $c(\boldsymbol{q},t)_s, \tilde{c}(\boldsymbol{q},t)_s$ must be linked to the interacting phonon spectral densities (2.3.4). This can be done by means of the fluctuation-dissipation theorem.[117] Indeed one can show that

$$c(\boldsymbol{q},t)_s = -\!\!\int \mathrm{d}\omega\, e^{-i\omega t}\,[n_T(\omega)+1]\, b(\boldsymbol{q},\omega)_s, \tag{2.D.5a}$$

$$\tilde{c}(\boldsymbol{q},t)_s = -\!\!\int \mathrm{d}\omega\, e^{i\omega t} n_T(\omega) b(\boldsymbol{q},\omega)_s\,. \tag{2.D.5b}$$

We can then plug the latter relations into (2.D.4), and with straightforward integration of the phase factors of the correlation functions we get

$$\kappa_R^{\gamma\sigma} = \tfrac{\hbar^2\pi}{N_c \mathcal{V} T} \sum_{\boldsymbol{q},ss'} \tfrac{(\Omega(\boldsymbol{q})_s + \Omega(\boldsymbol{q})_{s'})^2}{4} v^\gamma(\boldsymbol{q})_{ss'} v^\sigma(\boldsymbol{q})_{s's} \iint \mathrm{d}\omega_1 \mathrm{d}\omega_2\, b(\boldsymbol{q},\omega_1)_{s'} b(\boldsymbol{q},\omega_2)_s \delta(\omega_1 - \omega_2) \times \frac{n_T(\omega_2)}{k_B T}\,[n_T(\omega_1)+1]\,, \tag{2.D.6}$$

which evidently coincides with the result from the resonant Hardy heat flux obtained in (2.3.6b) since $\frac{n_T(\omega)}{k_B T}\,[n_T(\omega)+1] = -\frac{\partial n_T(\omega)}{\partial \hbar\omega}$. The calculation outlined so far proves that the decoupling scheme (2.D.2) performed on real-time Green's functions coincides with the dressed-bubble approximation of the retarded response function discussed in (2.C.5) and employed in imaginary-time domain. It follows that, at this level of approximation, adopting one scheme or another is just a matter of taste. Nonetheless, we find that the general framework based on a diagrammatic expansion in the frequency domain makes the approximation used more transparent, and can be systematically extended to include additional effects due to vertex corrections.

The approach outlined in this Appendix basically consist in the procedure proposed in Ref. 124 to approximate the Kubo formula for thermal conductivity from its time domain expression (2.D.1). However, both in the latter work and in Ref. 123 the Green's functions are defined using the phonon displacement operators $\hat{A}(\boldsymbol{q})_s = \hat{a}(\boldsymbol{q})_s + \hat{a}^\dagger(-\boldsymbol{q})_s$ and $\hat{B}(\boldsymbol{q})_s = \hat{a}(\boldsymbol{q})_s - \hat{a}^\dagger(-\boldsymbol{q})_s$ as (in imaginary time-domain)

$$G(\boldsymbol{q},\tau)_s = -\langle \mathcal{T}_\tau \hat{A}(\boldsymbol{q},\tau)_s \hat{A}(-\boldsymbol{q},0)_s \rangle\,, \tag{2.D.7a}$$

$$\tilde{G}(\boldsymbol{q},\tau)_s = -\langle \mathcal{T}_\tau \hat{B}(\boldsymbol{q},\tau)_s \hat{A}(-\boldsymbol{q},0)_s \rangle\,. \tag{2.D.7b}$$

To match the expression (2.3.6a)-(2.3.6c) with the one presented in Ref. 123-,[124] one can notice the relation (valid when anomalous terms of the form $\langle \mathcal{T}_\tau \hat{a}(\tau)\hat{a}(0)\rangle$ are negligible[134,136,137]) with the Green's functions (2.D.7a)-(2.D.7b) and the one we use (2.C.6)

$$G(\boldsymbol{q},\tau)_s = g(\boldsymbol{q},\tau)_s + g(\boldsymbol{q},-\tau)_s\,, \tag{2.D.8a}$$
$$\tilde{G}(\boldsymbol{q},\tau)_s = g(\boldsymbol{q},\tau)_s - g(\boldsymbol{q},-\tau)_s\,, \tag{2.D.8b}$$

which imply that the relation between the spectral densities $B(\boldsymbol{q},\omega)_s = -\frac{\hbar}{\pi}\mathrm{Im}G(\boldsymbol{q}, i\omega_n \to \hbar\omega + i0^+)_s$ is

$$B(\boldsymbol{q},\omega)_s = b(\boldsymbol{q},\omega)_s - b(\boldsymbol{q},-\omega)_s\,, \tag{2.D.9a}$$
$$\tilde{B}(\boldsymbol{q},\omega)_s = b(\boldsymbol{q},\omega)_s + b(\boldsymbol{q},-\omega)_s\,. \tag{2.D.9b}$$

Using the latter relations to replace the spectral densities in the full thermal conductivity expression derived from Hardy heat flux (2.3.6a), and exploiting the properties of the velocity matrices (2.2.17), one gets

$$\kappa^{\gamma\sigma}_{\text{Ref. 123,124}} = \frac{\hbar^2\pi}{N_c\mathcal{V}T}\sum_{\boldsymbol{q},ss'} v^\gamma(\boldsymbol{q})_{ss'}v^\sigma(\boldsymbol{q})_{s's} \times \int \mathrm{d}\omega \left[\Omega(\boldsymbol{q})_s^2 B(\boldsymbol{q},\omega)_s B(\boldsymbol{q},\omega)_{s'} + \Omega(\boldsymbol{q})_s\Omega(\boldsymbol{q})_{s'}\tilde{B}(\boldsymbol{q},\omega)_s\tilde{B}(\boldsymbol{q},\omega)_{s'}\right]\left[-\frac{\partial n_T(\omega)}{\partial\hbar\omega}\right], \tag{2.D.10}$$

which is the expression presented in Eq.(46)-(47) of Ref. 124 and in Eq.(4.14) of Ref. 123. Notice how, as anticipated in the main text, the latter expression features no clear separation between resonant and antiresonant contributions, due to the representation of the Green's functions (2.D.8a)-(2.D.8b) that mixes such terms.

Instead for what concerns the comparison with Ref. 33, we note that the authors obtained a different result starting from the same Hardy flux operator (2.2.15) and implementing the Green-function method via the decoupling scheme (2.D.2). Specifically, the final result for conductivity presented in Ref. 33 is

$$\begin{aligned}\kappa^{\gamma\sigma}_{\text{Ref. 33}} = {}& \frac{\hbar^2}{N_c\mathcal{V}T}\sum_{\boldsymbol{q},ss'}\frac{(\Omega(\boldsymbol{q})_s+\Omega(\boldsymbol{q})_{s'})^2}{4}v^\gamma(\boldsymbol{q})_{ss'}v^\sigma(\boldsymbol{q})_{s's} \\ & \times \frac{n_T(\Omega(\boldsymbol{q})_s)-n_T(\Omega(\boldsymbol{q})_{s'})}{\hbar(\Omega(\boldsymbol{q})_{s'}-\Omega(\boldsymbol{q})_s)}\frac{\gamma(\boldsymbol{q})_s+\gamma(\boldsymbol{q})_{s'}}{(\Omega(\boldsymbol{q})_s-\Omega(\boldsymbol{q})_{s'})^2+(\gamma(\boldsymbol{q})_s+\gamma(\boldsymbol{q})_{s'})^2} \\ & + \frac{\hbar^2}{N_c\mathcal{V}T}\sum_{\boldsymbol{q},ss'}\frac{(\Omega(\boldsymbol{q})_s-\Omega(\boldsymbol{q})_{s'})^2}{4}v^\gamma(\boldsymbol{q})_{ss'}v^\sigma(\boldsymbol{q})_{s's} \\ & \times \frac{n_T(\Omega(\boldsymbol{q})_s)-n_T(-\Omega(\boldsymbol{q})_{s'})}{\hbar(\Omega(\boldsymbol{q})_{s'}+\Omega(\boldsymbol{q})_s)}\frac{\gamma(\boldsymbol{q})_s+\gamma(\boldsymbol{q})_{s'}}{(\Omega(\boldsymbol{q})_s+\Omega(\boldsymbol{q})_{s'})^2+(\gamma(\boldsymbol{q})_s+\gamma(\boldsymbol{q})_{s'})^2},\end{aligned} \tag{2.D.11}$$

which is to be compared with the present result from Hardy heat flux in the LSFA (2.3.10a)-(2.3.10c). As briefly mentioned in the main text, the difference resides in having derivatives of Bose-Einstein occupations with respect to frequency (which yield the modal specific heats) in Eqs. (2.3.10a)-(2.3.10c) and a "discretized" version of such derivative (the differences of Bose-Einstein occupations divided by the difference of the corresponding frequencies) in Eq. (2.D.11). The source of this discrepancy lies in the approximation scheme employed to reduce the spectral-density-based description to a quasiparticle picture, in which phonons have well-

defined energy ($\hbar\Omega(\boldsymbol{q})_s$) and lifetime ($[\Gamma(\boldsymbol{q})_s]^{-1}$). In the present derivation, we perform the dressed-bubble calculation and obtain the thermal conductivity expression (2.3.6a), which relates the thermal conductivity to the spectral densities. After having derived this general conductivity expression, which describes both the quasiparticle and the overdamped regime, we perform some approximations that allow one to recover a much simpler form, valid only in the regime where quasiparticles are well defined. Specifically, we employ the LSFA, discarding the self-energy's real part and approximating the self-energy's imaginary part with its value at the harmonic phonon frequency, so that the spectral function (2.3.5) becomes a Lorentzian centered at the phonon frequency $\Omega(\boldsymbol{q})_s$ and with a full width at half maximum equal to the phonon linewidth $\Gamma(\boldsymbol{q})_s$. Then we approximate the derivatives of the Bose distribution with their values at the phonon frequencies where the Lorentzian spectral functions are centered. This approximation yields an expression for the thermal conductivity (Eq. (2.3.8) or Eq. (2.3.10a)) that contains only quantities related to well-defined quasiparticles (*i.e.* frequencies, linewidths, velocities, and specific heat). In contrast, Ref. 33 employs the common approximation scheme (used e.g. also in Ref.[39]) that enforces the validity of the quasiparticle picture with a stronger condition and earlier in the derivation, assuming the correlation functions (2.D.5a)-(2.D.5b) to have the form $c(\boldsymbol{q},t)_s \simeq [n_T(\Omega(\boldsymbol{q})_s)+1]e^{i\Omega(\boldsymbol{q})_s t-\gamma(\boldsymbol{q})_s t}$ (that is anyway valid only for $t>0$). Clearly, performing this approximation on the correlation functions does not allow to obtain thermal conductivity expressions accounting for the full frequency dependence of the self-energy, as it is needed to describe transport in the overdamped regime. Moreover, inserting this approximation for the correlation function into (2.D.4), it is easy to see that the integral in the inverse-temperature-like variable λ (also called canonical correlation[117]) produces complex phase factors that depend on $\gamma(\boldsymbol{q})_s$ and must be neglected to recover the result (2.D.11). From a practical viewpoint, numerical results presented in Sec. 2.3.2 showed that no quantitative difference originates from this formal discrepancy in the expressions for the interband thermal conductivity, at least in the test case materials considered. From a formal viewpoint, the procedure employed in thisChapter has some useful features that are worth to be highlighted. In particular, it allows to: (i) obtain a thermal conductivity expression accounting for spectral functions and thus apt to describe also the overdamped regime of thermal transport; (ii) discuss in detail all the approximations required to extract from the spectral function a well-defined quasiparticle lifetime, thus to obtain a thermal conductivity expression including only quasiparticles' properties (frequencies, linewidths, velocities, specific heats).

In conclusion, it is worth mentioning that in Ref. 39, a Green-Kubo approach was used to derive a thermal conductivity expression employing yet another original formula for the heat flux. Specifically, the heat flux expression employed in Ref. 39 stems from a modification of Hardy on-site energy (2.2.7), and has an overall structure analogous to Hardy heat flux (2.2.15):

$$\hat{\boldsymbol{J}}''_{\text{Ref. 39}} = \hat{\boldsymbol{J}}''_R + \hat{\boldsymbol{J}}''_A \,, \tag{2.D.12a}$$

$$\hat{\boldsymbol{J}}''_R = \hat{\boldsymbol{J}}_R + \frac{\hbar}{N_c\mathcal{V}} \sum_{\boldsymbol{q},ss'} \frac{\Omega(\boldsymbol{q})_s - \Omega(\boldsymbol{q})_{s'}}{2} \boldsymbol{v}''(\boldsymbol{q})_{ss'} \hat{a}^\dagger(\boldsymbol{q})_s \hat{a}(\boldsymbol{q})_{s'} \,, \tag{2.D.12b}$$

$$\hat{\boldsymbol{J}}''_A = \hat{\boldsymbol{J}}_A + \frac{\hbar}{N_c\mathcal{V}} \sum_{\boldsymbol{q},ss'} \frac{\Omega(\boldsymbol{q})_s + \Omega(\boldsymbol{q})_{s'}}{4} \boldsymbol{v}''(\boldsymbol{q})_{ss'} \left[\hat{a}(-\boldsymbol{q})_s \hat{a}(\boldsymbol{q})_{s'} - \hat{a}^\dagger(\boldsymbol{q})_s \hat{a}^\dagger(-\boldsymbol{q})_{s'}\right], \tag{2.D.12c}$$

where the extra velocity matrix is defined as

$$\boldsymbol{v}''(\boldsymbol{q})_{ss'}=\frac{-i}{2\sqrt{\Omega(\boldsymbol{q})_s\Omega(\boldsymbol{q})_{s'}}}\sum_{\boldsymbol{R}_l}\frac{\phi_{\boldsymbol{R}_l b\alpha,0b'\alpha'}}{M_b}(\boldsymbol{R}_l+\boldsymbol{\tau}_b-\boldsymbol{\tau}_{b'})\varepsilon^*(\boldsymbol{q})_{s,b\alpha}\varepsilon(\boldsymbol{q})_{s',b'\alpha'}\ . \tag{2.D.13}$$

We did not perform the test to compare the result for interband conductivity proposed by Ref. 39. However, we expect small correction from the extra terms in the heat flux (2.D.12a). In fact, we have discussed how the resonant (antiresonant) current-current response function is peaked when $\Omega(\boldsymbol{q})_s-\Omega(\boldsymbol{q})_{s'}\simeq 0$ ($\Omega(\boldsymbol{q})_s+\Omega(\boldsymbol{q})_{s'}\simeq 0$), but the extra term in the resonant (antiresonant) heat flux (2.D.12b)((2.D.12c)) is proportional to $\Omega(\boldsymbol{q})_s-\Omega(\boldsymbol{q})_{s'}$ ($\Omega(\boldsymbol{q})_s+\Omega(\boldsymbol{q})_{s'}$), hence all the contributions from it to the thermal conductivity are expected to be small for the relevant coupling modes. Notice also that if the correction to the velocity matrix (2.D.13) is neglected, the final result for thermal conductivity presented in Ref. 39 coincides with the one presented in Ref. 33 and briefly discussed here in (2.D.11).

Chapter 3

Lattice thermal transport in self-consistent schemes

Introduction

Perturbative approaches are inapplicable in regimes of strong anharmonicity. In instances where the crystal structure is stabilized by thermal or quantum fluctuations, such as in the high-temperature phases of ferroelectric materials,[48,49] a standard perturbative calculation may yield imaginary phonon frequencies, giving a misleading indication of lattice instability. One of the most efficient solution to the limitations posed by perturbative approaches is the Self-Consistent Harmonic Approximation (SCHA).[50,56] This method, grounded in the quantum variational principle at finite temperatures, constrains the nuclei density matrix to the most general Gaussian in Cartesian coordinates. The interatomic force constant matrix and the equilibrium position of the ions are optimized to obtain the best estimate of the free energy of the fully anharmonic lattice of ions. As a result, the interatomic force constants acquire a temperature dependence, indicating the self-consistency of the model Hamiltonian that describes the system.

Nevertheless, as shown in Chapter 1, standard equations for thermal conductivity are derived within linear response, where the temperature variation is a small perturbation to a temperature-independent Hamiltonian.[44,57–59] Consequently, the common methodology of incorporating frequencies, scattering rates, and other lattice properties obtained from self-consistent schemes into the expressions for thermal conductivity based on linear response theory[49,60–64] lacks theoretical justification and thus predictive capabilities. Our goal is to formulate a theoretical approach suitable for studying thermal transport in strongly anharmonic systems within a self-consistent framework.

To formulate a theoretical approach suitable for studying thermal transport in strongly anharmonic crystals, in this chapter we rephrase the formalism introduced in Chapter 1 for a self-consistent framework. The maximum entropy principle and modified Liouville equation approach is particularly effective in treating self-consistent systems since it solely relies on manipulations of the density matrix and of the self-consistent Liouville operator that approximates the exact dynamics. We thus obtain a Kubo formula for thermal conductivity valid in time-dependent self-consistent dynamics. Then, we apply it to the dynamical extension of the self-consistent harmonic approximation, the time-dependent self-consistent harmonic approximation (TD-SCHA) introduced in Ref. 65 is to constrain the ionic density matrix to be the most general Gaussian in Cartesian coordinates with time-dependent free

parameters. We first reformulate the TD-SCHA in the Wigner formalism, where the density matrix becomes a function of position and momentum in quantum-phase space. This approach makes the TD-SCHA equations more compact and intuitive than the ones preesnted in the original formulation of Ref. 65. Most importantly, the Wigner formulation allows for a diagrammatic interpretation of the response functions obtained in TD-SCHA, allowing a clear understanding of the variety of anharmonic scatterings included in the theory and enabling easier comparisons with other existing theories of lattice dynamics. We use this diagrammatic picture to interpret thermal conductivity as a two-phonon response function. Finally, by applying our newly formulated Kubo expression for self-consistent schemes, we find that thermal conductivity diverges in TD-SCHA. This limitation stems from an intrinsic shortcoming of the TD-SCHA itself: in the approximate self-consistent dynamics, the dressed-bubble diagrams —responsible for the natural decay of the heat-flux autocorrelation function and the resulting finite conductivity— are absent.

Chapter Overview

This Chapter is organized as follows: in Sec. 3.1 we apply the maximum entropy principle plus modified Liouville equation approach to derive a Kubo formula valid for self-consistent systems. In Sec. 3.2 we derive the SCHA equations and thermal equilibrium state using the maximum entropy principle. In Sec. 3.3 we present the TD-SCHA approximation for the self-consistent ionic dynamics in Wigner formalism. In Sec. 3.4 we use the Kubo formula in self-consistent systems to compute an expression for thermal conductivity in TD-SCHA. In Sec. 3.5 we report some closing remarks.

Part of the content of this Chapter has been published in Phys. Rev. B 107, 174307 (2023).[152] The remaining part is in preparation to be submitted.

3.1 Reworking Kubo formula for thermal conductivity

In this Section, we derive the first-principles expression of thermal conductivity for self-consistent dynamics, thus applicable to strongly anharmonic systems. The advantage in working with self-consistent schemes is that the fully interacting system is mapped into a mean-field one where the coupling constants of the effective interactions are temperature dependent.

The modified Liouville equation approach introduced in Sec. 1.3 can be applied to temperature dependent Hamiltonians. In fact, in self-consistent schemes such as time-dependent density functional theory (TD-DFT),[75,153] time-dependent Hartree-Fock (TD-HF),[154] time-dependent self-consistent harmonic approximation (TDSCHA),[65,66] the exact dynamics is approximated with a self-consistent equation such as

$$\begin{aligned} &\frac{\partial \hat{\varrho}(t)}{\partial t} + \frac{i}{\hbar}\mathcal{L}_{sc}\hat{\varrho}(t) = 0 \\ &\frac{\partial \hat{\varrho}(t)}{\partial t} + \frac{i}{\hbar}[\hat{\mathcal{H}}[\varrho(t)], \hat{\varrho}(t)] = 0 \end{aligned} \tag{3.1.1}$$

where $\hat{\mathcal{H}}[\rho(t)]$ is the self-consistent Hamiltonian. The global equilibrium condition (*i.e.* with

constant temperature) in the self-consistent system is defined by the density matrix

$$\hat{\varrho}_0 = \frac{1}{\mathcal{Z}[\beta]} e^{-\beta \hat{\mathcal{H}}^{(0)}}, \quad \mathcal{Z}[\beta] = \mathrm{Tr}\left[e^{-\beta \hat{\mathcal{H}}^{(0)}}\right], \tag{3.1.2}$$

where with the subscript 0 we indicate self-consistent operators calculated at global thermal equilibrium

$$\hat{\mathcal{H}}^{(0)} \equiv \hat{\mathcal{H}}[\beta] = \int \mathrm{d}\boldsymbol{x}\, \hat{h}[\beta](\boldsymbol{x}) \equiv \int \mathrm{d}\boldsymbol{x}\, \hat{h}_0(\boldsymbol{x}) \,, \tag{3.1.3}$$

where $\hat{h}_0$ is the energy density associated with $\hat{\mathcal{H}}^{(0)}$. Eq. (3.1.2) defines the self-consistent relation between $\hat{\varrho}_0$ and $\hat{\mathcal{H}}_0$, and it is typically obtained from a variational principle (such as the minimization of the free energy) where the density matrix is constrained to assume a desired form, depending on the theory employed. In DFT, $\hat{\mathcal{H}}_0$ is the non-interacting Kohn-Sham Hamiltonian and $\hat{\varrho}_0$ is optimized to obtain the same (one-body) electronic density as the one of the interacting system at temperature $\frac{1}{k_B\beta}$.[155,156] In the SCHA, $\hat{\varrho}_0$ is a Gaussian density matrix and $\hat{\mathcal{H}}_0$ is a harmonic Hamiltonian whose interatomic force constant matrix and equilibrium position of the ions are optimized to minimize forces and to average the curvature of the Born-Oppenheimer energy surface for different ionic configurations.[50,56] The case of SCHA will be thouroughly discussed in Sec. 3.2.

3.1.1 Local equilibrium in self-consistent schemes

The procedure outlined in Sec. 1.3 is based on the Liouville equation Eq. (1.2.18) and on the definition of the local equilibrium operator $\hat{\rho}_{loc}$. Hence, by properly defining an expression of $\hat{\rho}_{loc}$ for the self-consistent case ($\hat{\varrho}_{loc}$), we can derive the steady-state solution of the modified version of the self-consistent Liouville equation

$$\frac{\partial \hat{\varrho}(t)}{\partial t} + \frac{i}{\hbar}\mathcal{L}_{sc}\hat{\varrho}(t) = -\epsilon[\hat{\varrho}(t) - \hat{\varrho}(t)] \,. \tag{3.1.4}$$

The derivation of the Kubo formula Eq. (1.3.10) relies on the fact that the energy density does not depend on the temperature field [cfr. Eq. (1.3.7)]. However, in a self-consistent scheme, the Hamiltonian depends on the state of the system through the density matrix, thereby introducing an additional temperature dependence and invalidating the derivation of Eq. (1.3.10).

In analogy with the coarse-graining assumption discussed in Eqs. (1.2.12)-(1.2.13), we build the local equilibrium density matrix by generalizing the equilbrium condition Eq. (3.1.2) to[108]

$$\begin{aligned} \hat{\varrho}_{loc} &= \frac{1}{\mathcal{Z}[\beta(\boldsymbol{x})]} e^{-\int \mathrm{d}\boldsymbol{x}\beta(\boldsymbol{x})\hat{h}[\beta(\boldsymbol{x})](\boldsymbol{x})}, \\ \mathcal{Z}[\beta(\boldsymbol{x})] &= \mathrm{Tr}\left[e^{-\int \mathrm{d}\boldsymbol{x}\beta(\boldsymbol{x})\hat{h}[\beta(\boldsymbol{x})](\boldsymbol{x})}\right] . \end{aligned} \tag{3.1.5}$$

Following the interpretation of Eq. (1.2.13) illustrated in Fig. 1.1, the self-consistent local equilibrium Eq. (3.1.5) can be seen in terms of coarse grains representing locally a self-consistent system with temperature $T_i = \frac{1}{k_B\beta_i}$ and a local Hamiltonian $\hat{h}_i[\beta_i]$.

The energy density thus depends on the density matrix, as it must satisfy the condition

$$\hat{\mathcal{H}}_{loc} \equiv \hat{\mathcal{H}}[\varrho_{loc}] = \int \mathrm{d}\boldsymbol{x}\, \hat{h}[\varrho_{loc}](\boldsymbol{x}). \tag{3.1.6}$$

Since $\hat{\mathcal{H}}$ depends on the temperature field through the density matrix, we denote

$$\hat{\mathcal{H}}_{loc}{=}\hat{\mathcal{H}}[\varrho_{loc}]{=}\hat{\mathcal{H}}[\beta(\boldsymbol{x})]\,. \tag{3.1.7}$$

It is important to highlight that the self-consistent energy density operator $\hat{h}(\boldsymbol{x})$ is different from $\hat{h}(\boldsymbol{x})$ associated with the Hamiltonian of the system $\hat{H}$, defined in Eq. (1.1.6).

3.1.2 Kubo formula for thermal conductivity in self-consistent schemes

Having defined the local equilibrium density matrix and the Liouville superoperator for the self-consistent systems, we can apply the modified Liouville equation approach to find the steady-state solution of (3.1.4) as presented in Sec. 1.3. For the self-consistent case, Eq. (1.3.6) becomes

$$\hat{\varrho}^{\epsilon}_{st} = -\int_0^{\infty} \mathrm{d}t'\, e^{-\epsilon t'} e^{-\frac{i}{\hbar}\mathcal{L}_{sc}t'} \frac{i}{\hbar}\mathcal{L}_{sc}\hat{\varrho}_{loc}\,. \tag{3.1.8}$$

From Eq. (3.1.8), we derive an expression of thermal conductivity retracing the procedure presented in Sec. 1.3. To do so, we have to evaluate the action of the self-consistent Liouville operator $\mathcal{L}_{sc}$ on the local equilibrium density matrix

$$\frac{i}{\hbar}\mathcal{L}_{sc}\hat{\varrho}_{loc} = \frac{i}{\hbar}[\hat{\mathcal{H}}[\varrho_{loc}], \hat{\varrho}_{loc}]\,. \tag{3.1.9}$$

We expand $\hat{\varrho}$ in the right side of Eq. (3.1.9) in $\beta(\boldsymbol{x}){=}\beta{+}\delta\beta(\boldsymbol{x})$; from Eq. (3.1.5), we expand as in Eq. (1.3.7), obtaining

$$\begin{aligned}\hat{\varrho}_{loc} &= \exp\left[-\beta\hat{\mathcal{H}}[\beta(\boldsymbol{x})] - \int \mathrm{d}\boldsymbol{x}\, \delta\beta(\boldsymbol{x})\hat{h}[\beta(\boldsymbol{x})](\boldsymbol{x})\right] \\ &\simeq e^{-\beta\hat{\mathcal{H}}_{loc}} {-} e^{-\beta\hat{\mathcal{H}}_{loc}} \int_0^{\beta} \mathrm{d}\lambda\, e^{\lambda\hat{\mathcal{H}}_{loc}} \int \mathrm{d}\boldsymbol{x}\, \frac{\delta\beta(\boldsymbol{x})}{\beta}\hat{h}[\beta(\boldsymbol{x})](\boldsymbol{x}) e^{-\lambda\hat{\mathcal{H}}_{loc}}\,.\end{aligned} \tag{3.1.10}$$

In intermediate steps, we neglect the normalization factor $\mathcal{Z}$ in Eq. (3.1.5) for brevity, restoring it at the end of the calculation. Discarding orders higher of $\mathcal{O}(\delta\beta)$, every quantity multiplied by $\delta\beta(\boldsymbol{x})$ must be computed at $\delta\beta(\boldsymbol{x}){=}0$, *i.e.* at the (global) equilibrium temperature β, hence

$$\hat{\varrho}_{loc} = e^{-\beta\hat{\mathcal{H}}_{loc}} - e^{-\beta\hat{\mathcal{H}}^{(0)}} \int_0^{\beta} \mathrm{d}\lambda\, e^{\lambda\hat{\mathcal{H}}^{(0)}} \int \mathrm{d}\boldsymbol{x}\, \frac{\delta\beta(\boldsymbol{x})}{\beta}\hat{h}^{(0)}(\boldsymbol{x}) e^{-\lambda\hat{\mathcal{H}}^{(0)}} + \mathcal{O}(\delta\beta)^2\,. \tag{3.1.11}$$

At variance with the expansion in Eq. (1.3.7), the first term of Eq. (3.1.11) still depends on $\delta\beta(\boldsymbol{x})$ through the self-consistency. Plugging the expansion Eq. (3.1.11) in Eq. (3.1.9) we get

$$\begin{aligned}\frac{i}{\hbar}\mathcal{L}_{sc}\hat{\varrho}_{loc} &= \frac{i}{\hbar}[\hat{\mathcal{H}}_{loc}, \hat{\varrho}_{loc}] \simeq \frac{i}{\hbar}[\hat{\mathcal{H}}_{loc}, e^{-\beta\hat{\mathcal{H}}_{loc}}] \\ &- \frac{i}{\hbar}[\hat{\mathcal{H}}_{loc}, e^{-\beta\hat{\mathcal{H}}^{(0)}} \int_0^{\beta} \mathrm{d}\lambda\, e^{\lambda\hat{\mathcal{H}}^{(0)}} \int \mathrm{d}\boldsymbol{x}\, \frac{\delta\beta(\boldsymbol{x})}{\beta}\hat{h}_0(\boldsymbol{x}) e^{-\lambda\hat{\mathcal{H}}^{(0)}}]\,.\end{aligned} \tag{3.1.12}$$

The first term of the last equality in Eq. (3.1.12) is not linear in $\delta\beta(\boldsymbol{x})$. The expansion of $\hat{\mathcal{H}}_{loc}$ at linear order in $\delta\beta(\boldsymbol{x})$ features complicated functional derivatives such as

$$\hat{\mathcal{H}}_{loc} \simeq \hat{\mathcal{H}}^{(0)} + \int \mathrm{d}\boldsymbol{x}\, \frac{\delta\hat{h}[\beta(\boldsymbol{x})]}{\delta\beta(\boldsymbol{x})}\bigg|_{\beta(\boldsymbol{x})=\beta} \delta\beta(\boldsymbol{x}). \tag{3.1.13}$$

However, it is clear that in Eq. (3.1.12) $[\hat{\mathcal{H}}_{loc}, e^{-\beta\hat{\mathcal{H}}_{loc}}]=0$: even if a nontrivial temperature dependence is present in $\hat{\mathcal{H}}_{loc}$, the same dependence appears in the self-consistent dynamics provided by $\mathcal{L}_{sc}$. The presence of terms like Eq. (3.1.13) due to a nontrivial temperature-ependent Hamiltonian $\hat{\mathcal{H}}$ challenges the applicability of the standard Kubo formula Eq. (1.3.10) in self-consistent systems. In the original Kubo formula derivation,[106] the temperature is treated as an imaginary time in the time-evolution operators, and temperature derivatives are related to time derivatives through a change of variables [see Ref. 106 (3.6)-(3.7) and Ref. 104 (3.426)]. However, such change of variables becomes invalid when the Hamiltonian depends on temperature.

From Eq. (3.1.12), we get at linear order in $\delta\beta(\boldsymbol{x})$

$$\frac{i}{\hbar}\mathcal{L}_{sc}\hat{\varrho}_{loc} = -e^{-\beta\hat{\mathcal{H}}^{(0)}}\int_0^\beta \mathrm{d}\lambda\, e^{\lambda\hat{\mathcal{H}}^{(0)}}\int\mathrm{d}\boldsymbol{x}\, \frac{\delta\beta(\boldsymbol{x})}{\beta}\frac{i}{\hbar}[\hat{\mathcal{H}}^{(0)}, \hat{h}^{(0)}(\boldsymbol{x})]e^{-\lambda\hat{\mathcal{H}}^{(0)}}\,. \tag{3.1.14}$$

Using the self-consistent Liouville equation Eq. (3.1.1), the commutator in Eq. (3.1.14) defines a self-consistent heat current through a self-consistent continuity equation Eq. (1.2.16)

$$\frac{i}{\hbar}[\hat{\mathcal{H}}^{(0)}, \hat{h}^{(0)}(\boldsymbol{x})] = -\boldsymbol{\nabla}\cdot\hat{\boldsymbol{j}}(\boldsymbol{x})\,. \tag{3.1.15}$$

The steady-state statistical operator then takes form

$$\hat{\varrho}^{\epsilon}_{st} = -\int_0^\infty \mathrm{d}t\, e^{-\epsilon t}e^{-\frac{i}{\hbar}\mathcal{L}_{sc}t}e^{-\beta\hat{\mathcal{H}}^{(0)}}\int_0^\beta \mathrm{d}\lambda\, e^{\lambda\hat{\mathcal{H}}^{(0)}}\int\mathrm{d}\boldsymbol{x}\, \frac{\delta\beta(\boldsymbol{x})}{\beta}\boldsymbol{\nabla}\cdot\hat{\boldsymbol{j}}(\boldsymbol{x})e^{-\lambda\hat{\mathcal{H}}^{(0)}} \tag{3.1.16}$$

that, as done for Eq. (1.3.9), we can recast as

$$\hat{\varrho}^{\epsilon}_{st} = \frac{V}{\beta}\boldsymbol{\nabla}\beta\cdot\int_0^\infty \mathrm{d}t\, e^{-\epsilon t}e^{-\frac{i}{\hbar}\mathcal{L}_{sc}t}e^{-\beta\hat{\mathcal{H}}^{(0)}}\int_0^\beta \mathrm{d}\lambda\, e^{\lambda\hat{\mathcal{H}}^{(0)}}\hat{\boldsymbol{\mathcal{J}}}e^{-\lambda\hat{\mathcal{H}}^{(0)}}, \tag{3.1.17}$$

where the self-consistent heat flux is $\hat{\boldsymbol{\mathcal{J}}}=\frac{1}{V}\int_V \mathrm{d}\boldsymbol{x}\,\hat{\boldsymbol{j}}(\boldsymbol{x})$. The thermal conductivity is obtained with the same procedure we used to get Eq. (1.3.10), hence

$$\kappa^{\gamma\sigma} = \lim_{\epsilon\to 0^+}\frac{V}{T}\int_0^\infty \mathrm{d}t\, e^{-\epsilon t}\int_0^\beta \mathrm{d}\lambda\,\mathrm{Tr}\left[\hat{J}^\gamma\hat{\varrho}_0 e^{-\frac{i}{\hbar}\mathcal{L}_{sc}t}e^{\lambda\hat{\mathcal{H}}^{(0)}}\hat{\mathcal{J}}^\sigma e^{-\lambda\hat{\mathcal{H}}^{(0)}}\right]. \tag{3.1.18}$$

Eq. (3.1.18) represents the generalization of the Kubo formula for thermal conductivity for self-consistent dynamics. A major difference between the self-consistent Liouville superoperator $\mathcal{L}_{sc}$ featuring the self-consistent Liouville equation (3.1.4) and the standard one $\mathcal{L}$ featuring in (1.3.2) is that $\mathcal{L}_{sc}$ is non linear. Thus the interpretation of $e^{\frac{i}{\hbar}\mathcal{L}_{sc}t}\hat{\varrho}$ as $\sim e^{-\frac{i}{\hbar}\hat{\mathcal{H}}^{(0)}}\hat{\varrho}e^{\frac{i}{\hbar}\hat{\mathcal{H}}^{(0)}}$ is not straightforward. Hence, the equivalence between Schrodinger and Heisenberg evolution of the operators is not granted in a self-consistent dynamics. However, from the

self-consistent Liouville equation (3.1.1) we can still define the infinitesimal evolution

$$\begin{aligned}\hat{\varrho}(t+dt) &= \hat{\varrho}(t) + \frac{\partial \hat{\varrho}(t)}{\partial t} dt = \hat{\varrho}(t) - \frac{i}{\hbar}[\hat{\mathcal{H}}[\varrho(t)], \hat{\varrho}(t)]dt \\ &= \hat{\varrho}(t) - \frac{i}{\hbar}\mathcal{L}_{sc}\hat{\varrho}(t)dt\end{aligned} \tag{3.1.19}$$

and the exponential $e^{i\mathcal{L}_{sc}t}$ is intendended in terms of its Taylor series. Integrating in t as done in Eq. (1.3.12), we can express Eq. (3.1.18) in terms of the self-consistent propagator

$$\kappa^{\gamma\sigma}(i\epsilon) = \frac{V}{T}\int_0^\beta \mathrm{d}\lambda \,\mathrm{Tr}\left[\hat{J}^\gamma \hat{\varrho}_0 \frac{i}{i\hbar\epsilon - \mathcal{L}_{sc}} e^{\lambda\hat{\mathcal{H}}^{(0)}} \hat{\mathcal{J}}^\nu e^{-\lambda\hat{\mathcal{H}}^{(0)}}\right]. \tag{3.1.20}$$

As per Eq. (1.3.12), the presence of the inverse self-consistent propagator $[i\hbar\epsilon - \mathcal{L}_{sc}]^{-1}$ computed at imaginary frequency $i\epsilon$ resembles the structure of the finite-frequency response function obtained in TD-SCHA[65,152] or in TD-DFT.[75] To be applied, Eqs. (3.1.18)-(3.1.20) require the definition of the action of the self-consistent Liouville superoperator $\mathcal{L}_{sc}$ on relevant operators, as done in TD-DFT[75] and TD-SCHA.[65,152] A key aspect of the self-consistent Kubo formula (3.1.18) or (3.1.20) for thermal conductivity is that it only depends on equilibrium quantities, in the same spirit of the standard Kubo formula and fluctuation-dissipation theorem.[117] In fact, to obtain the thermal condutivity using (3.1.18) or (3.1.20), we only need to define the global equilibrium self-consistent density matrix $\hat{\varrho}_0$ and Hamiltonian $\hat{\mathcal{H}}^{(0)}$, together with the self-consistent heat flux $\hat{\boldsymbol{\mathcal{J}}}$ from (3.1.15). Even if needed for the derivation, an explicit expression for the local equilibrium self-consistent density matrix $\hat{\varrho}_{loc}$ is not needed to obtain the linear transport coefficient (3.1.18).

3.1.3 Discussion of Kubo formula for self-consistent systems

Let us briefly discuss the fundamental aspects of Eq. (3.1.18), which consists of a novel result of this thesis. The thermal conductivity Eq. (3.1.18) can be represented as a Feynman diagram with two vertices connected by a propagator (cfr. Fig. 3.1).[104,110,141] The propagator is related to the time-evolution scheme, while the vertices are related to the heat flux operators $(\hat{\boldsymbol{\mathcal{J}}}, \hat{\boldsymbol{J}})$ appearing in the Kubo formula Eq. (3.1.18).

Details of the propagator are contained in the time-evolution superoperator $e^{-\frac{i}{\hbar}\mathcal{L}_{sc}t}$ (blue box in Fig. 3.1), that evolves the operators according to the self-consistent Liouville equation Eq. (3.1.1). Therefore, temperature and anharmonic effects are included in the dynamics through self-consistency at a quantum non-perturbative level. Conversely, the standard Kubo formula Eq. (1.3.10), which features the time-evolution $\hat{\boldsymbol{J}}(-t) = e^{-\frac{i}{\hbar}\mathcal{L}t}\hat{\boldsymbol{J}} = e^{-\frac{i}{\hbar}\hat{H}t}\hat{\boldsymbol{J}}e^{\frac{i}{\hbar}\hat{H}t}$, requires a perturbative truncation of the Hamiltonian $\hat{H}$ to a specific anharmonicity level. The present distinction is crucial, particularly in the context of lattice thermal transport, as it validates the theoretical description of strongly anharmonic crystals. In such systems, anharmonicity can not be regarded as a small correction to a lattice of harmonic oscillators, rendering thermal conductivity expressions reliant on perturbation theory such as Eq. (1.3.10) invalid.

While approaches like ab initio molecular dynamics (AIMD) circumvent the limitations of perturbative truncation of the anharmonic Hamiltonian, they are restricted to a classical treatment of the ions.[129,141,157–160] Therefore, in AIMD effects such as zero-point motion, Bose-Einstein population, and quantum anharmonicity are neglected. Self-consistent

theories, such as self-consistent phonon (SCP),[51] temperature-dependent effective potential (TDEP),[52] and SCHA,[50,56] can encompass all these effects in the calculation of phonon frequencies and related lattice properties. However, for the application of our thermal conductivity formula Eq. (3.1.18), a dynamical extension of the self-consistent theory is required. To our knowledge, among the cited methods, the SCHA is the only one with an ab initio dynamical extension in the form of the TD-SCHA.[65]

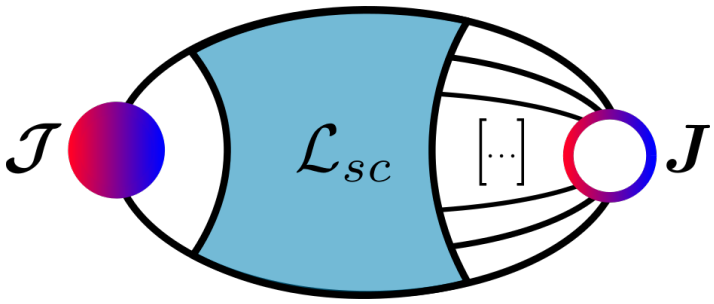

Figure 3.1. Diagrammatic representation of the Kubo formula for thermal conductivity in self-consistent schemes (Eq. (3.1.18)). The propagator (blue area) evolves the observables according to the self-consistent dynamics contained in $\mathcal{L}_{sc}$. It connects the self-consistent heat flux vertex $\mathcal{J}$ (full-circle)—assumed to be harmonic, *i.e.* derived from a two-phonon operator—, to the many-body heat flux vertex $\boldsymbol{J}$ (empty circle).

Another key difference of Eq. (3.1.18) with the standard Green-Kubo expression Eq. (1.3.10) is that it describes thermal conductivity as a quantum correlation function of two different heat fluxes. The first is the many-body heat flux $\hat{\boldsymbol{J}}$, that represents the flow of energy of the exact hamiltonian $\hat{H}$ [cfr. Eq. (1.2.16)]. As such, $\hat{\boldsymbol{J}}$ can encompass every level of anharmonicity, but it requires a perturbative truncation of the Hamiltonian $\hat{H}$. Moreover, being derived from the exact Hamiltonian $\hat{H}$, the heat flux vertex related to $\hat{\boldsymbol{J}}$ is inherently temperature independent. The heat flux operator $\hat{\mathcal{J}}$ in Eq. (3.1.18) is derived from the self-consistent Hamiltonian $\hat{\mathcal{H}}$ [cfr. Eq. (3.1.15)]. The structure of $\hat{\mathcal{J}}$ is thus given once the self-consistent Hamiltonian $\hat{\mathcal{H}}$ is specified. For example, in the SCHA since $\hat{\mathcal{H}}$ is a harmonic auxiliary Hamiltonian, $\hat{\mathcal{J}}$ consists in a harmonic self-consistent heat flux (discussed in detail in Sec. 3.2.3). Therefore, the heat flux vertex associated to $\hat{\mathcal{J}}$ features phonon properties (frequencies and velocities) that are temperature dependent through self-consistency. To be specific, if anharmonic terms are neglected in the approximation of $\hat{H}$, the heat flux $\hat{\boldsymbol{J}}$ would feature phonon frequencies and velocities obtained from standard perturbative techniques (*e.g.* DFPT[161] or finite differences[47]). Instead, the heat flux $\hat{\mathcal{J}}$ would feature phonon frequencies and velocity renormalized by self-consisitency.

The remainder of this Chapter will be devoted to obtain the definitions of $\hat{\varrho}_0, \hat{\mathcal{H}}^{(0)}, \hat{\mathcal{J}}, \mathcal{L}_{sc}$ in the context of the SCHA, to obain an expression of lattice thermal conductivity in a specific self-consistent picture.

3.2 Thermal equilibrium in the Self-Consistent Harmonic Approximation

In order to obtain the thermal conductivity in a self-consistent approach, we have to define the self-consistent Liouville superoperator $\mathcal{L}_{sc}$ that describes the approximated dynamics, and define the global equilibrium density matrix ϱ_0 in our self-consistent scheme. To discuss the property of strongly anharmonic crystals, the self-consistent harmonic approximation

(SCHA) is among the most advanced and popular theoretical approaches.[50,56] In the SCHA, the density matrix of the interacting lattice is approximated with a Gaussian density matrix, which characterize a system of harmonic oscillators. The interatomic force constant matrix and the equilibrium position of the ions (centroids) are optimized to obtain the best estimate of the free energy of the interacting system.[50,56]

In this Section, we outline the basic features of the SCHA method and discuss how to fit the SCHA in our MEP treatment of transport theory. We will first obtain the global equilibrium density matrix, thus the SCHA density matrix maximizing the entropy with the constraint of a fixed expectation value of the energy

$$\tilde{S}[\beta] = -\operatorname{Tr}[\hat{\varrho}\log\hat{\varrho}] - \beta\left(\operatorname{Tr}\left[\hat{\varrho}\hat{H}\right] - E\right) , \tag{3.2.1}$$

where $\hat{H}$ is the Born-Oppenheimer Hamiltonian

$$\hat{H} = \sum_{a=1}^{3N} \frac{\hat{P}_a^2}{2m_a} + \hat{V}_{BO}(\vec{\boldsymbol{R}}) . \tag{3.2.2}$$

For brevity, in this chapter we indicate with $a{=}(i,\alpha)$ a composite index with the atomic index i and Cartesian index α, $m_a{=}m_i$ is the mass of atom i, and $\vec{\boldsymbol{R}} = (\boldsymbol{R}_1,..,\boldsymbol{R}_N)$ is the collection of all position operators with eigenstates $\left|\vec{\boldsymbol{R}}\right\rangle = |\boldsymbol{R}_1,..,\boldsymbol{R}_N\rangle$. The variation of $\tilde{S}$ will be done by taking $\hat{\varrho}$ as a gaussian density matrix.

Next, having obtain the equilibrium SCHA density matrix at fixed temperature $\hat{\varrho}_0$ and associated self-consistent Hamiltonian $\hat{\mathcal{H}}^{(0)}$, we will obtain an expression for the self-consistent heat flux $\hat{\boldsymbol{\mathcal{J}}}$ in SCHA .

3.2.1 Foundations of the SCHA method

The SCHA consist in approximating the density matrix describing the oscillating ions in a crystal as a gaussian. In particular, considering the most generic quadratic Hamiltonian

$$\hat{\mathcal{H}}_{\vec{\boldsymbol{\mathcal{R}}},\overleftrightarrow{\boldsymbol{\Phi}}} = \sum_{a=1}^{3N} \frac{\hat{P}_a^2}{2m_a} + \mathcal{V}_{\vec{\boldsymbol{\mathcal{R}}},\overleftrightarrow{\boldsymbol{\Phi}}}(\vec{\boldsymbol{R}}) \tag{3.2.3a}$$

$$\mathcal{V}_{\vec{\boldsymbol{\mathcal{R}}},\overleftrightarrow{\boldsymbol{\Phi}}}(\vec{\boldsymbol{R}}) = \frac{1}{2}\sum_{ab}\left(\hat{R}_a - \mathcal{R}_a\right)\Phi_{ab}\left(\hat{R}_b - \mathcal{R}_b\right) \tag{3.2.3b}$$

the SCHA density matrix is build by setting the Bloch equation[162]

$$\frac{\partial\hat{\varrho}}{\partial\beta} = -\hat{\mathcal{H}}_{\vec{\boldsymbol{\mathcal{R}}},\overleftrightarrow{\boldsymbol{\Phi}}}\hat{\varrho} \tag{3.2.4}$$

along with the normalization condition $\operatorname{Tr}[\hat{\varrho}]{=}1$ and the boundary condition $\hat{\varrho}{=}\mathbb{I}$ for $\beta{=}0$. The notation $\overleftrightarrow{\circ}$ indicates a $3N{\times}3N$ matrix. The centroids $\vec{\boldsymbol{\mathcal{R}}}$ and the effective force constant matrix $\overleftrightarrow{\boldsymbol{\Phi}}$ in Eqs. (3.2.3a)-(3.2.3b) are parameters of the SCHA density matrix (3.2.4). Eq. (3.2.4) is solved by

$$\hat{\varrho}_{\vec{\boldsymbol{\mathcal{R}}},\overleftrightarrow{\boldsymbol{\Phi}}} = \frac{e^{-\beta\hat{\mathcal{H}}_{\vec{\boldsymbol{\mathcal{R}}},\overleftrightarrow{\boldsymbol{\Phi}}}}}{\mathcal{Z}_{\vec{\boldsymbol{\mathcal{R}}},\overleftrightarrow{\boldsymbol{\Phi}}}[\beta]} , \qquad \mathcal{Z}_{\vec{\boldsymbol{\mathcal{R}}},\overleftrightarrow{\boldsymbol{\Phi}}}[\beta] = \operatorname{Tr}\left[e^{-\beta\hat{\mathcal{H}}_{\vec{\boldsymbol{\mathcal{R}}},\overleftrightarrow{\boldsymbol{\Phi}}}}\right], \tag{3.2.5}$$

which is of the from (3.1.2). The matrix Φ_{ab} is positive definite and defines the SCHA dynamical matrix as

$$D_{ab} = \frac{\Phi_{ab}}{\sqrt{m_a m_b}} = \sum_{\mu=1}^{3N} \omega_\mu^2 e_{\mu,a} e_{\nu,b} \tag{3.2.6}$$

where ω_μ are the SCHA phonon frequencies and $e_{\mu,a}$ are the SCHA phonon polarization vectors. We stress that the frequencies ω_μ do not correspond to experimentally observable phonons but only to auxiliary quantities, just like the Kohn-Sham bands in DFT.

We show in Appendix 3.A that the SCHA density matrix in the Schrodinger representation has a gaussian form

$$\left\langle \vec{\boldsymbol{R}} \right| \hat{\varrho}_{\vec{\boldsymbol{\mathcal{R}}}, \overleftrightarrow{\boldsymbol{\Phi}}} \left| \vec{\boldsymbol{R}}' \right\rangle = \varrho_{\vec{\boldsymbol{\mathcal{R}}}, \overleftrightarrow{\boldsymbol{\Phi}}}(\vec{\boldsymbol{R}}, \vec{\boldsymbol{R}}') = \sqrt{\det\left(\frac{\overleftrightarrow{\boldsymbol{\Upsilon}}}{2\pi}\right)} \exp\left(-\frac{1}{4} \sum_{ab=1}^{3N} \Theta_{ab}(R_a - \mathcal{R}_a)(R_b - \mathcal{R}_b) \right.$$
$$\left. -\frac{1}{4} \sum_{ab=1}^{3N} \Theta_{ab}(R'_a - \mathcal{R}_a)(R'_b - \mathcal{R}_b) + \sum_{ab=1}^{3N} A_{ab}(R_a - \mathcal{R}_a)(R'_b - \mathcal{R}_b) \right) \tag{3.2.7}$$

where $\overleftrightarrow{\boldsymbol{\Theta}}$ and $\overleftrightarrow{\boldsymbol{A}}$ are symmetric tensors and $\overleftrightarrow{\boldsymbol{\Upsilon}} = \overleftrightarrow{\boldsymbol{\Theta}} - 2\overleftrightarrow{\boldsymbol{A}}$ is positive definite. The matrix $\overleftrightarrow{\boldsymbol{\Upsilon}}$ is the inverse covariance matrix, featuring in the diagonal elements of the densty matrix as

$$\varrho_{\vec{\boldsymbol{\mathcal{R}}}, \overleftrightarrow{\boldsymbol{\Phi}}}(\vec{\boldsymbol{R}}, \vec{\boldsymbol{R}}) = \sqrt{\det\left(\frac{\boldsymbol{\Upsilon}}{2\pi}\right)} e^{-\frac{1}{2}\sum_{ab=1}^{3N}(R_a - \mathcal{R}_a)\Upsilon_{ab}(R'_b - \mathcal{R}_b)} \tag{3.2.8}$$

The density matrix $\hat{\varrho}_{\vec{\boldsymbol{\mathcal{R}}}, \overleftrightarrow{\boldsymbol{\Phi}}}$ solves $\hat{\mathcal{H}}_{\vec{\boldsymbol{\mathcal{R}}}, \overleftrightarrow{\boldsymbol{\Phi}}}$, so $\overleftrightarrow{\boldsymbol{\Upsilon}}$ and $\overleftrightarrow{\boldsymbol{A}}$ are not free parameters but depend on the SCHA phonons $\{\omega_\mu, e_\mu\}$ (Eq. (3.2.6))

$$\Upsilon_{ab} = \sum_{\mu=1}^{3N} \frac{2\omega_\mu}{\hbar(1+2n_\mu)} e_{\mu,a} e_{\mu,b} = \sum_{\mu=1}^{3N} \xi_\mu^{-2} e_{\mu,a} e_{\mu,b} \tag{3.2.9a}$$

$$A_{ab} = \sum_{\mu=1}^{3N} \frac{2\omega_\mu n_\mu(n_\mu+1)}{\hbar(1+2n_\mu)} e_{\mu,a} e_{\mu,b}. \tag{3.2.9b}$$

where n_μ is the Bose-Einstein occupation number $n_\mu = [e^{\beta\hbar\omega_\mu} - 1]^{-1}$ and we have introduced the SCHA thermal length ξ_μ which reads

$$\xi_\mu^2 = \frac{\hbar}{2\omega_\mu}(1+2n_\mu) = \frac{\hbar}{2\omega_\mu} \coth\left(\tfrac{1}{2}\omega_\mu\beta\right). \tag{3.2.10}$$

The best estimate for the parameters $\vec{\boldsymbol{\mathcal{R}}}, \overleftrightarrow{\boldsymbol{\Phi}}$ are obtained by a free energy minimization procedure.[50] By virtue of Bogoliubov variational principle, the exact free energy

$$F[\rho] = \mathrm{Tr}\left[\hat{\rho}\hat{H}\right] - k_B T S[\rho] \tag{3.2.11}$$

and the one computed with the SCHA density matrix (3.2.4)

$$F[\varrho_{\vec{\boldsymbol{\mathcal{R}}}, \overleftrightarrow{\boldsymbol{\Phi}}}] = F_{\vec{\boldsymbol{\mathcal{R}}}, \overleftrightarrow{\boldsymbol{\Phi}}} = \mathrm{Tr}\left[\hat{\varrho}_{\vec{\boldsymbol{\mathcal{R}}}, \overleftrightarrow{\boldsymbol{\Phi}}} \hat{H}\right] - k_B T S[\varrho_{\vec{\boldsymbol{\mathcal{R}}}, \overleftrightarrow{\boldsymbol{\Phi}}}] \tag{3.2.12}$$

are related by $F[\rho] \leq F_{\vec{\mathcal{R}},\Phi}$. The best SCHA estimate for the free energy is obtained as

$$F_{best} = \min_{\vec{\mathcal{R}},\overleftrightarrow{\Phi}} F[\varrho_{\vec{\mathcal{R}},\overleftrightarrow{\Phi}}] \,. \tag{3.2.13}$$

The stationarity condition of the free energy $\delta F{=}0$ results in the self-consistent equation for the best parameters $(\boldsymbol{\mathcal{R}}^{(0)}, \boldsymbol{\Phi}^{(0)})$

$$\left\langle -\frac{\partial \hat{V}_{BO}(\vec{\boldsymbol{R}})}{\partial R_a} \right\rangle_{\varrho_{\vec{\mathcal{R}}^{(0)},\overleftrightarrow{\Phi}^{(0)}}} = 0 \,, \tag{3.2.14a}$$

$$\left\langle \frac{\partial^2 \hat{V}_{BO}(\vec{\boldsymbol{R}})}{\partial R_a \partial R_b} \right\rangle_{\varrho_{\vec{\mathcal{R}}^{(0)},\overleftrightarrow{\Phi}^{(0)}}} = \Phi^{(0)}_{ab} \tag{3.2.14b}$$

where we have used the shorthand notation $\langle \hat{O} \rangle_{\varrho_{\vec{\mathcal{R}},\overleftrightarrow{\Phi}}} = \mathrm{Tr}\left[\hat{O}\hat{\varrho}_{\vec{\mathcal{R}},\overleftrightarrow{\Phi}}\right]$. Eqs. (3.2.14) renormalize the SCHA phonons, defined from $\overleftrightarrow{\Phi}^{(0)}$, and the average atomic positions, $\vec{\mathcal{R}}^{(0)}$, by anharmonicty and quantum fluctuations at finite temperature.[56] Indeed, contrary to the harmonic approximation, the SCHA force constant is not the curvature of the BO energy surface at the minimum. SCHA averages the potential with a distribution that has a finite width so there are additional anharmonic terms due to quantum-thermal Gaussian fluctuations.[56,152] We will show in what follows that the SCHA equations (3.2.14) can be obtained from the MEP with a constrained maximization that enforces the density matrix to be a Gaussian of the form (3.2.4).

Before proceeding, let us note some useful relations in the SCHA formalism. One of the most important feature of the SCHA is that since the density matrix is a Gaussian, its derivatives possess an analytic expression. Such property can be exploited to compute derivatives of observables using the integration by parts. For example, for the expecatation value of an observable diagonal in the Schrodinger representation, we can compute its derivative with respect to a parameter λ as (proven in Appendix 3.A)

$$\frac{\partial}{\partial \lambda} \left\langle O(\vec{\boldsymbol{R}}) \right\rangle_{\varrho_{\vec{\mathcal{R}},\overleftrightarrow{\Phi}}} = \sum_a \frac{\partial \mathcal{R}_a}{\partial \lambda} \left\langle \frac{\partial O(\vec{\boldsymbol{R}})}{\partial \hat{R}_a} \right\rangle_{\varrho_{\vec{\mathcal{R}},\overleftrightarrow{\Phi}}} + \frac{1}{2} \sum_{ab} \frac{\partial \Upsilon^{-1}_{ab}}{\partial \lambda} \left\langle \frac{\partial^2 O(\vec{\boldsymbol{R}})}{\partial \hat{R}_a \partial \hat{R}_b} \right\rangle_{\varrho_{\vec{\mathcal{R}},\overleftrightarrow{\Phi}}} . \tag{3.2.15}$$

Another remarkable result of the SCHA is that the harmonic free energy, defined as the functional

$$\mathcal{F}_{\vec{\mathcal{R}},\vec{\Phi}}[\rho] = \mathrm{Tr}\left[\hat{\rho}\hat{\mathcal{H}}_{\vec{\mathcal{R}},\vec{\Phi}}\right] + k_B T \,\mathrm{Tr}[\hat{\rho}\log\hat{\rho}] \tag{3.2.16}$$

associated with the state (3.2.7) can be computed analytically in the normal mode basis (proven in Appendix 3.A) as

$$\mathcal{F}_{\vec{\mathcal{R}},\vec{\Phi}}[\varrho_{\vec{\mathcal{R}},\overleftrightarrow{\Phi}}] = -\frac{1}{\beta}\log \mathcal{Z}_{\vec{\mathcal{R}},\vec{\Phi}}[\beta] = \frac{1}{\beta}\sum_\mu \log[2\sinh\left(\tfrac{1}{2}\hbar\omega_\mu\beta\right)] \tag{3.2.17}$$

The expectation value of the harmonic energy (3.2.3a) reads

$$\left\langle \hat{\mathcal{H}} \right\rangle_{\varrho_{\vec{\mathcal{R}},\overleftrightarrow{\Phi}}} = \sum_{ab} \Phi_{ab}\Upsilon^{-1}_{ab} = \sum_\mu \omega_\mu^2 \xi_\mu^2 = \sum_\mu \hbar\omega_\mu(n_\mu + \tfrac{1}{2}) \tag{3.2.18}$$

which is the expected result for a system of N harmonic oscillators in 3D. Combining (3.2.17) and (3.2.18), we get the entropy associated with the Gaussian density matrix (3.2.7) as

$$\begin{aligned} S[\varrho_{\vec{\mathcal{R}},\overleftrightarrow{\Phi}}] &= -\operatorname{Tr}\left(\hat{\varrho}_{\vec{\mathcal{R}},\overleftrightarrow{\Phi}} \log \hat{\varrho}_{\vec{\mathcal{R}},\overleftrightarrow{\Phi}}\right) = \frac{1}{\beta}[\left\langle \hat{\mathcal{H}} \right\rangle_{\varrho_{\vec{\mathcal{R}},\overleftrightarrow{\Phi}}} - \mathcal{F}_{\vec{\mathcal{R}},\vec{\Phi}}] \\ &= \frac{1}{2}\sum_{\mu}\left[\beta\hbar\omega_\mu \coth\left(\tfrac{1}{2}\beta\hbar\omega_\mu\right) - 2\log\left(\sinh\left(\tfrac{1}{2}\beta\hbar\omega_\mu\right)\right)\right] . \end{aligned} \tag{3.2.19}$$

3.2.2 Global equilibrium in SCHA

As first step to the application of the SCHA to the problem of thermal transport, we want to employ the MEP to derive the global equilibrium SCHA density matrix. In such condition, we search for the SCHA density matrix that maximizes the entropy under the constraint of a constant expectation value of the Hamiltonian $\hat{H}$. As per (1.2.6), we want to maximize the entropy functional

$$\tilde{S}[\varrho] = -\operatorname{Tr}\left[\hat{\varrho}\log\hat{\varrho}\right] - \beta\left(\operatorname{Tr}\left[\hat{H}\hat{\varrho}\right] - E\right) \tag{3.2.20}$$

restricting our constrained maximization to the class of Gaussian density matrices of the form. Let us first take a step back analyzing the definition of the Gaussian density matrix. The assumption of a Gaussian structure of the density matrix traces back to the definition of the Bloch equation (3.2.4). From the derivation of the canonical ensemble density matrix from the MEP done in (1.2.6), we understand that the solution of the Bloch equation (3.2.4) is the density matrix that maximizes the entropy of a system of harmonic oscillators with fixed expectation value E of the harmonic Hamiltonian $\hat{\mathcal{H}}_{\vec{\mathcal{R}},\vec{\Phi}}$, *i.e.*

$$\tilde{\mathcal{S}}[\varrho_{\vec{\mathcal{R}},\overleftrightarrow{\Phi}}] = -\operatorname{Tr}\left[\hat{\varrho}_{\vec{\mathcal{R}},\overleftrightarrow{\Phi}}\log\hat{\varrho}_{\vec{\mathcal{R}},\overleftrightarrow{\Phi}}\right] - \eta\left(\operatorname{Tr}\left[\hat{\mathcal{H}}_{\vec{\mathcal{R}},\vec{\Phi}}\hat{\varrho}_{\vec{\mathcal{R}},\overleftrightarrow{\Phi}}\right] - E\right) . \tag{3.2.21}$$

From the discussion above and from (3.2.21), we understand that the temperature associated with the extremal solution of (3.2.21) is in general different from the temperature associated with the maximum of the entropy (3.2.20). In fact, the temperature of the system T is associated with the Lagrangian multiplier β. Being Langrangian multipliers of two different constrained maximizations, respectively of S in (3.2.20) and of $\tilde{\mathcal{S}}$ in (3.2.21), in principle η and β are different. From the argument just elucidated, we shall consider as the density matrix that approximates the exact one as a Gaussian density matrix with an "effective" temperature η as

$$\hat{\varrho}_{\eta,\vec{\mathcal{R}},\overleftrightarrow{\Phi}} = \frac{e^{-\eta\hat{\mathcal{H}}_{\boldsymbol{R},\vec{\Phi}}}}{\operatorname{Tr}\left[e^{-\eta\hat{\mathcal{H}}_{\boldsymbol{R},\vec{\Phi}}}\right]} \tag{3.2.22}$$

to be considered as an extra variational parameter. The reasoning behind (3.2.22) can be understood as follows. In the SCHA, the exact density matrix of the fully interacting lattice of ions is approximated by the density matrix of a system of harmonic oscillators. When measuring a property such as the energy, $\operatorname{Tr}\left[\hat{H}\hat{\varrho}_\eta\right]$, of the fully interacting system, the result will include contributions from both harmonic and anharmonic terms (interactions of all orders). On the other hand, the energy associated with the harmonic oscillator system, $\operatorname{Tr}\left[\hat{\mathcal{H}}\hat{\varrho}_\eta\right]$, is purely harmonic by construction. To balance this difference, a system of harmonic oscillators with, for instance, a higher effective temperature η can reproduce the observables of the fully interacting system at a lower temperature β. This adjustment accounts for the additional anharmonic contributions present in the interacting system.

To find the global equilibrium SCHA density matrix, we thus maximize the entropy functional

$$\tilde{S}[\varrho_{\eta,\boldsymbol{\mathcal{R}},\boldsymbol{\Phi}}] = -\operatorname{Tr}\left[\hat{\varrho}_{\eta,\vec{\boldsymbol{\mathcal{R}}},\overleftrightarrow{\boldsymbol{\Phi}}} \log \hat{\varrho}_{\eta,\vec{\boldsymbol{\mathcal{R}}},\overleftrightarrow{\boldsymbol{\Phi}}}\right] - \beta\left(\operatorname{Tr}\left[\hat{H}\hat{\varrho}_{\eta,\vec{\boldsymbol{\mathcal{R}}},\overleftrightarrow{\boldsymbol{\Phi}}}\right] - E\right) \tag{3.2.23}$$

where we restrict the constraint maximization to the space of the density matrix of the form (3.2.22). The entropy functional (3.2.23) depends on β and the stationarity with respect to β fixes the expectation value of the BO Hamiltonian (3.2.2), while the variation of the functional with respect to the density matrix (3.2.22) can be recast as variation with respect to the parameters $(\eta, \vec{\boldsymbol{\mathcal{R}}}, \overleftrightarrow{\boldsymbol{\Phi}})$. The stationarity of the functional (3.2.23) can be expressed as

$$\delta\tilde{S} = \sum_a \frac{\partial \tilde{S}}{\partial \mathcal{R}_a}\delta\mathcal{R}_a + \sum_{ab}\frac{\partial\tilde{S}}{\partial\Phi_{ab}}\delta\Phi_{ab} + \frac{\partial\tilde{S}}{\partial\eta}\delta\eta = 0\,. \tag{3.2.24}$$

Being independent parameters, by a simple argument of variational calculus we can recast (3.2.24) as

$$\begin{cases} \frac{\partial\tilde{S}}{\partial\mathcal{R}_a} &= 0\,, \\ \frac{\partial\tilde{S}}{\partial\Phi_{ab}} &= 0\,, \\ \frac{\partial\tilde{S}}{\partial\eta} &= 0\,. \end{cases} \tag{3.2.25}$$

The condition (3.2.25) consist in a set of coupled equations, to be solved for every choice of $(\eta, \vec{\boldsymbol{\mathcal{R}}}, \overleftrightarrow{\boldsymbol{\Phi}})$. In Appendix 3.B we prove that the solution of (3.2.25) is

$$\left\langle -\frac{\partial\hat{V}_{BO}(\vec{\boldsymbol{R}})}{\partial R_a}\right\rangle_{\varrho_{\eta^{(0)},\vec{\boldsymbol{\mathcal{R}}}^{(0)},\boldsymbol{\Phi}^{(0)}}} = 0\,, \tag{3.2.26a}$$

$$\left\langle \frac{\partial^2\hat{V}_{BO}(\vec{\boldsymbol{R}})}{\partial R_a\partial R_b}\right\rangle_{\varrho_{\eta^{(0)},\vec{\boldsymbol{\mathcal{R}}}^{(0)},\boldsymbol{\Phi}^{(0)}}} = \Phi^{(0)}_{ab}\,, \tag{3.2.26b}$$

$$\eta^{(0)} = \beta\,. \tag{3.2.26c}$$

The relations (3.2.26) consist in a novel result of this thesis. Eqs. (3.2.26a)-(3.2.26b) are the standard SCHA equations (3.2.14), that can be equivalently obtained from the condition of minimization of the free energy (3.2.13). The derivation of the SCHA equation from the MEP extends the standard discussion of the SCHA to a larger parameter space, in which the temperature of the trial density matrix is not specified but considered as an extra variational parameter. Nonetheless, the third equation (3.2.26c) implies that the best possible estimate for the temperature η of the approximated Gaussian density matrix is equal to the temperature of the system β.

The conditions (3.2.26) provide the parameters $(\eta^{(0)}, \vec{\boldsymbol{\mathcal{R}}}^{(0)}, \overleftrightarrow{\boldsymbol{\Phi}}^{(0)})$, from which we can define the SCHA equilibrium density matrix and Hamiltonian as

$$\hat{\varrho}^{(0)} = \frac{e^{-\beta\hat{\mathcal{H}}^{(0)}}}{\mathcal{Z}[\beta]} \tag{3.2.27a}$$

$$\hat{\mathcal{H}}^{(0)} = \sum_a \frac{\hat{p}_a^2}{2m_a} + \frac{1}{2}\sum_{ab}\left\langle\frac{\partial^2\hat{V}_{BO}(\vec{\boldsymbol{R}})}{\partial R_a\partial R_b}\right\rangle_{\varrho^{(0)}}(\hat{R}_a - \mathcal{R}_a^{(0)})(\hat{R}_b - \mathcal{R}_b^{(0)})\,. \tag{3.2.27b}$$

Eqs. (3.2.27) give us a specific example for the case of the SCHA of the general discussion of the self-consistent global equilibrium condition discussed in Eq. (3.1.2). The expression of

the self-consistent equilibrium density matrix (3.2.27a) consist in the first ingredient needed to compute the thermal conductivity from the Kubo formula for self-consistent systems introduced in (3.1.18).

3.2.3 Heat flux in SCHA

In order to apply the Kubo formula (3.1.18) and obtain the thermal conductivity in SCHA, we need to obtain an expression for the heat flux operator $\hat{\boldsymbol{\mathcal{J}}}$. As discussed in Sec. (2.2), the procedure to obtain the heat flux operator starts with the definition of the on-site energy density. The energy density in SCHA can be obtained from the equilibrium Hamiltonian (3.2.27b) as

$$\hat{\mathcal{H}}^{(0)} = \sum_a \hat{h}_a \tag{3.2.28}$$

which is the self-consistent version of (2.2.6). As thoroughly discussed in Sec. (2.2), the extensivity relation (3.2.28) leaves space to different definition of the on-site self-consistent energy density $\hat{h}_a$. In this thesis, we adopt a Hardy[35] convention for the SCHA on-site energy, obtaining

$$\hat{h}_a = \frac{\hat{p}_a^2}{2m_a} + \frac{1}{2}\sum_b \Phi_{ab}^{(0)}(\hat{R}_a - \mathcal{R}_a^{(0)})(\hat{R}_b - \mathcal{R}_b^{(0)})\,, \tag{3.2.29}$$

which is the self-consistent analogue of the Hardy on-site energy defined in (2.2.7). Using the continuity equation (3.1.15), we can define the microscopic current density $\hat{\boldsymbol{j}}(\boldsymbol{x})$ from the on-site energy (3.2.29) and obtained the self-consistent heat flux $\hat{\boldsymbol{\mathcal{J}}}$ with a procedure completely equivalent to the one outlined in Sec. 2.2.1 and developed in Ref. 35. This amounts in substituting $\hat{u}\to\hat{R}-\mathcal{R}^{(0)}$, $\phi_{ab}^{(0)}\to\Phi_{ab}^{(0)}$, $\hat{H}_0\to\hat{\mathcal{H}}^{(0)}$ in the expression of the Hardy heat flux (2.2.10). In doing so, we get the expression of the heat flux in SCHA

$$\hat{\mathcal{J}}^{\sigma} = \frac{1}{2V}\sum_{ab}^{N}(\mathcal{R}_a^{\sigma\,(0)} - \mathcal{R}_b^{\sigma\,(0)}) \sum_{\alpha\beta}^{x,y,z} \Phi_{a,b}^{\alpha,\beta\,(0)}\delta\hat{R}_a^{\alpha\,(0)}\frac{\hat{P}_b^{\beta}}{m_b} \tag{3.2.30}$$

where $\delta\vec{\boldsymbol{R}}^{(0)}=\vec{\boldsymbol{R}}-\vec{\boldsymbol{\mathcal{R}}}^{(0)}$. Greek letters as superscript will denote cartesian directions . In fact, note that since the heat flux is a Cartesian vector, to express the $\sigma=x,y,z$ component of $\hat{\boldsymbol{\mathcal{J}}}$ in (3.2.30) we have separated the summation over the N atoms and the x,y,z Cartesian coordinates. We also stress that the SCHA heat flux $\hat{\boldsymbol{\mathcal{J}}}$ at variance with the harmonic "perturbative" $\hat{\boldsymbol{J}}$ obtained in (2.2.10) depends on self-consistent quantities $(\vec{\boldsymbol{\mathcal{R}}}^{(0)}, \overleftrightarrow{\boldsymbol{\Phi}}^{(0)})$. By virtue of (3.2.26), $\hat{\boldsymbol{\mathcal{J}}}$ possess an implicit temperature dependence, in $\overleftrightarrow{\boldsymbol{\Phi}}^{(0)}$ and $\vec{\boldsymbol{R}}^{(0)}$. In terms of phonons, the self-consistent heat flux (3.2.30) if expressed in the phonon basis features self-consistent phonons frequency and velocities obtained from the SCHA dynamical matrix $\boldsymbol{D}$ defined in Eq. (3.2.6).

3.3 Time dependent self-consistent harmonic approximation (TD-SCHA)

The remaining ingredient we need to obtain an expression of thermal conductivity in SCHA is the explicit definition of the Liouville self-consistent superoperator $\mathcal{L}_{sc}$ that encodes the approximated dynamics. This consists in the most articulate object to obtain, since it necessitates to extend the SCHA to a time-dependent framework.

Refs. 65,66 introduced the time-dependent self-consistent harmonic approximation (TD-SCHA) for describing finite-temperature nuclear dynamics with quantum and anharmonic fluctuations beyond perturbative approaches. The idea of TD-SCHA is to constrain the nuclear density matrix to be the most general Gaussian (in Cartesian coordinates) with time-dependent parameters. Ref. 65 used the first quantization formalism to derive the equations of motion by minimizing the quantum action at T=0 K. Then, these equations are extended to finite temperatures.[65]

The TD-SCHA Liouville equation reads

$$\frac{\partial \hat{\varrho}(t)}{\partial t} + \frac{i}{\hbar}\mathcal{L}_{sc}\hat{\varrho}(t) = \frac{\partial \hat{\varrho}(t)}{\partial t} + \frac{i}{\hbar}[\hat{\mathcal{H}}[\hat{\varrho}(t)], \varrho(t)] = 0 \tag{3.3.1}$$

where the self-consistent time-dependent Hamiltonian $\hat{\mathcal{H}}[\varrho(t)]$ is an effective quadratic Hamiltonian that depends on the Gaussian density matrix $\hat{\varrho}(t)$ as

$$\hat{\mathcal{H}}[\varrho(t)] = \sum_a \frac{\hat{p}_a^2}{2m_a} + \sum_a \left\langle \frac{\partial \hat{V}_{\text{tot}}(\vec{\boldsymbol{R}}, t)}{\partial R_a} \right\rangle_{\varrho(t)} (\hat{R}_a - \mathcal{R}(t)_a) + \frac{1}{2}\sum_{ab} \left\langle \frac{\partial^2 \hat{V}_{\text{tot}}(\vec{\boldsymbol{R}}, t)}{\partial R_a \partial R_b} \right\rangle_{\varrho(t)} (\hat{R}_a - \mathcal{R}(t)_a)(\hat{R}_b - \mathcal{R}(t)_b). \tag{3.3.2}$$

Eq. (3.3.2) features a time-dependent potential containing both the internal static interaction given by the BO potential and an external time-dependent perturbation

$$\hat{V}_{\text{tot}}(t) = \hat{V}_{\text{BO}}(\vec{\boldsymbol{R}}) + \hat{V}_{\text{ext}}(\vec{\boldsymbol{R}}, t)\ , \tag{3.3.3}$$

and $\vec{\boldsymbol{\mathcal{R}}}(t)$ are time varying equilibrium position of the ions. Thanks to self-consistency, the TD-SCHA goes beyond harmonic/perturbative methods. No approximations are made on the total potential, so anharmonic effects are included exactly when the BO energy surfaced is sampled. However, the exceptional complexity of the original TD-SCHA formulation hampers its physical interpretations.[50,66] In this chapter we reformulate the TD-SCHA in the Wigner language. In doing so, we rephrase the self-consistent dynamical theory of ionic motions in terms a diagramatic picture, resulting in a formalism of easier interpretation and comparison with other established approaches.

3.3.1 Wigner-Gaussian dynamics: time-dependent response of quantum anharmonic nuclei

The Wigner formalism describes the quantum nuclear evolution in terms of position and momentum degrees of freedom, in a way analogous to the classical Liouville propagation. The Wigner quasi-distribution,[163] obtained as a Fourier transform of the density operator $\hat{\varrho}(t)$, is the quantum analogue of the classical phase-space probability distribution

$$\rho_{\text{w}}(\vec{\boldsymbol{R}}, \vec{\boldsymbol{P}}, t) = \int_{-\infty}^{+\infty} \frac{d\vec{\boldsymbol{R}}' e^{-\frac{i}{\hbar}\vec{\boldsymbol{P}}\cdot\vec{\boldsymbol{R}}'}}{(2\pi\hbar)^{3N}} \left\langle \vec{\boldsymbol{R}} + \frac{\vec{\boldsymbol{R}}'}{2} \middle| \hat{\varrho}(t) \middle| \vec{\boldsymbol{R}} - \frac{\vec{\boldsymbol{R}}'}{2} \right\rangle . \tag{3.3.4}$$

We remark that Eq. (3.3.4) is normalized,

$$\int_{-\infty}^{+\infty} d\vec{\boldsymbol{R}} \int_{-\infty}^{+\infty} d\vec{\boldsymbol{P}} \rho_{\text{w}}(\vec{\boldsymbol{R}}, \vec{\boldsymbol{P}}, t) = 1 \tag{3.3.5}$$

but, in general, it is not positive-definite,[164] hence it can not be interpreted as a probability distribution. Still, it encodes all the information on the system. Similarly, the Wigner expression for an operator $\hat{O}$ is defined as

$$O_{\mathrm{w}}(\vec{\boldsymbol{R}},\vec{\boldsymbol{P}}) = \int_{-\infty}^{+\infty} d\vec{\boldsymbol{R}}' e^{-\frac{i}{\hbar}\vec{\boldsymbol{P}}\cdot\vec{\boldsymbol{R}}'} \left\langle \vec{\boldsymbol{R}} + \frac{\vec{\boldsymbol{R}}'}{2} \middle| \hat{O} \middle| \vec{\boldsymbol{R}} - \frac{\vec{\boldsymbol{R}}'}{2} \right\rangle, \tag{3.3.6}$$

so that quantum averages in the Wigner formalism have the same expression as the classical ones

$$\left\langle \hat{O} \right\rangle_{\rho_{\mathrm{w}}} = \int_{-\infty}^{+\infty} d\vec{\boldsymbol{R}} \int_{-\infty}^{+\infty} d\vec{\boldsymbol{P}} O_{\mathrm{w}}(\vec{\boldsymbol{R}},\vec{\boldsymbol{P}}) \rho_{\mathrm{w}}(\vec{\boldsymbol{R}},\vec{\boldsymbol{P}},t). \tag{3.3.7}$$

The TD-SCHA constrains the quantum density matrix as the most general time-dependent Gaussian.[65] Since the Wigner transformation is equivalent to a Fourier transform, also the corresponding Wigner quasi-distribution is a Gaussian

$$\begin{aligned}\varrho(\vec{\boldsymbol{R}},\vec{\boldsymbol{P}},t) = \mathcal{N}(t) \exp\Bigg[&-\frac{1}{2}\sum_{ab=1}^{3N} (R_a - \mathcal{R}(t)_a)\alpha(t)_{ab}(R_b - \mathcal{R}(t)_b) \\ &-\frac{1}{2}\sum_{ab=1}^{3N} (P_a - \mathcal{P}(t)_a)\beta(t)_{ab}(P_b - \mathcal{P}(t)_b) + \sum_{ab=1}^{3N} (R_a - \mathcal{R}(t)_a)\gamma(t)_{ab}(P - \mathcal{P}(t)_b)\Bigg],\end{aligned}$$

where $\mathcal{N}(t)$ is the normalization, defined such that

$$\int_{-\infty}^{+\infty} d\vec{\boldsymbol{R}} \int_{-\infty}^{+\infty} d\vec{\boldsymbol{P}} \varrho(\vec{\boldsymbol{R}},\vec{\boldsymbol{P}},t) = 1. \tag{3.3.8}$$

$\vec{\boldsymbol{\mathcal{R}}}(t)$, $\vec{\boldsymbol{\mathcal{P}}}(t)$, $\overleftrightarrow{\boldsymbol{\alpha}}(t)$, $\overleftrightarrow{\boldsymbol{\beta}}(t)$, $\overleftrightarrow{\boldsymbol{\gamma}}(t)$ are the time-dependent free parameters of the distribution. In contrast to the general Wigner distribution, Eq. (3.3.8) is positive-definite and can be interpreted as the quantum probability distribution. The position and momentum centroids $\vec{\boldsymbol{\mathcal{R}}}(t)$ and $\vec{\boldsymbol{\mathcal{P}}}(t)$ are $3N$ real vectors and represent, respectively, the average instantaneous position and momentum of the ions

$$\vec{\boldsymbol{\mathcal{R}}}(t) = \left\langle \vec{\boldsymbol{R}} \right\rangle_{\varrho(t)}, \qquad \vec{\boldsymbol{\mathcal{P}}}(t) = \left\langle \vec{\boldsymbol{P}} \right\rangle_{\varrho(t)} \tag{3.3.9}$$

where the TD-SCHA averages of Wigner observables are

$$\left\langle \hat{O} \right\rangle_{\varrho(t)} = \int_{-\infty}^{+\infty} d\vec{\boldsymbol{R}} \int_{-\infty}^{+\infty} d\vec{\boldsymbol{P}} \varrho(\vec{\boldsymbol{R}},\vec{\boldsymbol{P}},t) O(\boldsymbol{R},\boldsymbol{P}) \tag{3.3.10}$$

$\overleftrightarrow{\boldsymbol{\alpha}}(t)$, $\overleftrightarrow{\boldsymbol{\beta}}(t)$ and $\overleftrightarrow{\boldsymbol{\gamma}}(t)$ are $3N \times 3N$ real tensors ($\overleftrightarrow{\boldsymbol{\alpha}}(t)$ and $\overleftrightarrow{\boldsymbol{\beta}}(t)$ are symmetric).

The dynamics of the Wigner distribution can be obtained by transforming the time-dependent equation (3.3.1) of the TD-SCHA[65,66] in the Wigner basis. Using the definition of the Wigner transform of a commutator[163]

$$[\hat{A},\hat{B}]_{\mathrm{w}}(\vec{\boldsymbol{R}},\vec{\boldsymbol{P}}) = 2iA_{\mathrm{w}}(\vec{\boldsymbol{R}},\vec{\boldsymbol{P}}) \sin\left(\frac{\hbar}{2}\hat{\boldsymbol{\Lambda}}\right) B_{\mathrm{w}}(\vec{\boldsymbol{R}},\vec{\boldsymbol{P}}) \tag{3.3.11}$$

where the Poisson bracket operator is defined as

$$\hat{\mathbf{\Lambda}} = \overleftarrow{\boldsymbol{\nabla}}_{\boldsymbol{R}} \cdot \overrightarrow{\boldsymbol{\nabla}}_{\boldsymbol{P}} - \overleftarrow{\boldsymbol{\nabla}}_{\boldsymbol{P}} \cdot \overrightarrow{\boldsymbol{\nabla}}_{\boldsymbol{R}} \,, \tag{3.3.12}$$

Eq. (3.3.1) can be recast in Wigner basis with a self-consistent Wigner-Liouville equation

$$\frac{\partial}{\partial t}\varrho(\vec{\boldsymbol{R}}, \vec{\boldsymbol{P}}, t) + i\mathcal{L}_{sc}\varrho(\vec{\boldsymbol{R}}, \vec{\boldsymbol{P}}, t) = 0 \,. \tag{3.3.13}$$

The self-consistent TD-SCHA Liouville operator acts as

$$i\mathcal{L}_{sc}\varrho(\vec{\boldsymbol{R}}, \vec{\boldsymbol{P}}, t) = \Big\{\mathcal{H}[\varrho], \varrho(\vec{\boldsymbol{R}}, \vec{\boldsymbol{P}}, t)\Big\} \tag{3.3.14}$$

where the brackets indicate the classical Poisson brackets

$$\{A, B\} = \sum_{a=1}^{3N} \left(\frac{\partial A}{\partial R_a}\frac{\partial B}{\partial P_a} - \frac{\partial A}{\partial P_a}\frac{\partial B}{\partial R_a} \right). \tag{3.3.15}$$

In (3.3.14), $\mathcal{H}[\varrho]$ is a quadratic time-dependent Hamiltonian that depends self-consistently on $\varrho(t)$

$$\begin{aligned} \mathcal{H}[\varrho] = &\sum_{a=1}^{3N} \frac{P_a^2}{2m_a} + \sum_{a=1}^{3N} \delta R_a(t) \left\langle \frac{\partial V_{\text{tot}}(\vec{\boldsymbol{R}}, t)}{\partial R_a} \right\rangle_{\varrho(t)} \\ &+ \frac{1}{2}\sum_{ab=1}^{3N} \delta R_a(t) \left\langle \frac{\partial^2 V_{\text{tot}}(\vec{\boldsymbol{R}}, t)}{\partial R_a \partial R_b} \right\rangle_{\varrho(t)} \delta R_b(t). \end{aligned} \tag{3.3.16}$$

where $\delta\vec{\boldsymbol{R}}(t) = \vec{\boldsymbol{R}} - \vec{\boldsymbol{\mathcal{R}}}(t)$. Inserting the Wigner-TD-SCHA distribution, Eq. (3.3.8), in Eq. (3.3.13) we get (details in Appendix 3.C)

$$\frac{d}{dt}\vec{\vec{\boldsymbol{\mathcal{R}}}}(t) = \vec{\vec{\boldsymbol{\mathcal{P}}}}(t) \tag{3.3.17a}$$

$$\frac{d}{dt}\vec{\vec{\boldsymbol{\mathcal{P}}}}(t) = -\left\langle \frac{\partial V_{\text{tot}}}{\partial \vec{\vec{\boldsymbol{R}}}} \right\rangle_{\varrho(t)} \tag{3.3.17b}$$

$$\frac{d}{dt}\overleftrightarrow{\tilde{\boldsymbol{\alpha}}}(t) = -\left\langle \frac{\partial^2 V_{\text{tot}}}{\partial \vec{\vec{\boldsymbol{R}}} \partial \vec{\vec{\boldsymbol{R}}}} \right\rangle_{\varrho(t)} \cdot \overleftrightarrow{\tilde{\boldsymbol{\gamma}}}^T(t) - \overleftrightarrow{\tilde{\boldsymbol{\gamma}}}(t) \cdot \left\langle \frac{\partial^2 V_{\text{tot}}}{\partial \vec{\vec{\boldsymbol{R}}} \partial \vec{\vec{\boldsymbol{R}}}} \right\rangle_{\varrho(t)} \tag{3.3.17c}$$

$$\frac{d}{dt}\overleftrightarrow{\tilde{\boldsymbol{\beta}}}(t) = \overleftrightarrow{\tilde{\boldsymbol{\gamma}}}^T(t) + \overleftrightarrow{\tilde{\boldsymbol{\gamma}}}(t) \tag{3.3.17d}$$

$$\frac{d}{dt}\overleftrightarrow{\tilde{\boldsymbol{\gamma}}}(t) = \overleftrightarrow{\tilde{\boldsymbol{\alpha}}}(t) - \left\langle \frac{\partial^2 V_{\text{tot}}}{\partial \vec{\vec{\boldsymbol{R}}} \partial \vec{\vec{\boldsymbol{R}}}} \right\rangle_{\varrho(t)} \cdot \overleftrightarrow{\tilde{\boldsymbol{\beta}}}(t) \tag{3.3.17e}$$

where to compact the notation, we drop the explicit time and position dependence of $\hat{V}_{\text{tot}}$ and the $\widetilde{\circ}$ indicates a mass-rescaled variable like

$$\widetilde{R}_a = \sqrt{m_a} R_a, \qquad \widetilde{P}_a = \frac{P_a}{\sqrt{m_a}}. \tag{3.3.18}$$

In (3.C.5), we have expressed with the dot product the matrix multiplication

$$(\overleftrightarrow{\boldsymbol{A}} \cdot \overleftrightarrow{\boldsymbol{B}})_{ab} = \sum_c A_{ac} B_{cb} \,. \tag{3.3.19}$$

and in the derivatives with respect to $3N$ vectors as

$$\left(\frac{\partial V}{\partial \vec{\boldsymbol{R}}}\right)_a = \frac{\partial V}{\partial R_a}, \quad \left(\frac{\partial^2 V}{\partial \vec{\boldsymbol{R}} \partial \vec{\boldsymbol{R}}}\right)_{ab} = \frac{\partial^2 V}{\partial R_a \partial R_b}. \tag{3.3.20}$$

In addition, we have the equation for the normalization

$$\frac{d}{dt}\mathcal{N}(t) = 0 \tag{3.3.21}$$

which is automatically satisfied by Eqs (3.C.5). As a consequence, the TD-SCHA dynamics is closed, so if $\varrho(t)$ is initially prepared as a Gaussian, then $\varrho(t)$ will preserve its shape during the evolution. The TD-SCHA dynamics of Eq. (3.C.5) is more straightforward than the original derivation using the standard formalism of operators in quantum mechanics. An interesting feature of the Wigner formulation of TD-SCHA is that Eqs (3.3.13)-(3.C.5) do not contain $\hbar$. The implications of such founding are thouroughly investigated in Ref. 152.

SCHA equilibrium as static limit of TDSCHA

A particular solution of Eq. (3.C.5) is the equilibrium state in the absence of a time-dependent perturbation ($V_{\text{ext}} = 0$). From Eqs (3.C.5), we get

$$\left\langle \frac{\partial V_{\text{BO}}}{\partial \vec{\vec{\boldsymbol{R}}}} \right\rangle_{(0)} = 0 \tag{3.3.22a}$$

$$\left\langle \vec{\vec{\boldsymbol{P}}} \right\rangle_{(0)} = 0 \tag{3.3.22b}$$

$$\overleftrightarrow{\vec{\vec{\gamma}}}^{(0)} = 0 \tag{3.3.22c}$$

$$\overleftrightarrow{\vec{\vec{\alpha}}}^{(0)} \cdot \overleftrightarrow{\vec{\vec{\beta}}}^{(0)-1} = \left\langle \frac{\partial^2 V_{\text{BO}}}{\partial \vec{\vec{\boldsymbol{R}}} \partial \vec{\vec{\boldsymbol{R}}}} \right\rangle_{(0)} \tag{3.3.22d}$$

where (0) indicates that the averages are performed on $\varrho^{(0)}$, the equilibrium Wigner distribution that solve self-consistently Eq. (3.C.5). Since the average momentum is zero (Eq. 3.3.22c), we set $\delta\vec{\boldsymbol{P}} = \vec{\boldsymbol{P}}$, and the Wigner distribution becomes

$$\varrho^{(0)}(\vec{\boldsymbol{R}}, \vec{\boldsymbol{P}}) = \mathcal{N}^{(0)} \exp\left(-\frac{1}{2}\vec{\vec{\boldsymbol{P}}} \cdot \overleftrightarrow{\vec{\vec{\beta}}}^{(0)} \cdot \vec{\vec{\boldsymbol{P}}} - \frac{1}{2}\delta\vec{\vec{\boldsymbol{R}}} \cdot \overleftrightarrow{\vec{\vec{\alpha}}}^{(0)} \cdot \delta\vec{\vec{\boldsymbol{R}}}\right). \tag{3.3.23}$$

Eq. (3.3.22a) is clearly equivalent to the SCHA equilibrium condition on the forces (3.2.26a), while (3.3.22d) is equivalent to the self-consistent equation (3.2.26b) that defines the SCHA phonons. In fact, it is clear from the structure of (3.3.23) that $\widetilde{\boldsymbol{\alpha}}^{(0)} \cdot \overleftrightarrow{\vec{\vec{\beta}}}^{(0)-1} = \boldsymbol{D}$, where the SCHA dynamical matrix define the non-interacting self-consistent phonons

$$D_{ab} = \left\langle \frac{\partial^2 V_{\text{BO}}}{\partial \widetilde{R}_a \partial \widetilde{R}_b} \right\rangle_{(0)} = \sum_{\mu=1}^{3N} \omega_\mu^2 e_\mu^a e_\mu^b. \tag{3.3.24}$$

Eq. (3.3.23) is a static solution of the Wigner TD-SCHA equations. Among all distributions, the equilibrium one satisfy

$$\widetilde{\alpha}^{(0)}_{ab} = \Upsilon^{-1}_{ab} = \sum_{\mu=1}^{3N} \frac{\hbar(1+2n_\mu)}{2\omega_\mu} e^a_\mu e^b_\mu \tag{3.3.25a}$$

$$\widetilde{\beta}^{(0)}_{ab} = \sum_{\mu=1}^{3N} \frac{\hbar\omega_\mu(1+2n_\mu)}{2} e^a_\mu e^b_\mu \,. \tag{3.3.25b}$$

The equilibrium solution (3.3.23) is crucial since it can be used as an initial condition to solve the linearized version of the TD-SCHA equations of motion (3.C.5).

Diagramatic intepretation of SCHA phonons and connection with perturbation theory

Here we present a diagrammatic expansion of the SCHA (static solution of the TD-SCHA) in a quartic potential to clarify the anharmonic processes involved in the theory and to highlight the differences between SCHA and standard perturbation theory used in Chapter 2.

We define the SCHA propagator from Eq. (3.3.24)

$$\overleftrightarrow{\boldsymbol{\mathcal{G}}}^{(0)}(\omega)^{-1} = \omega^2 \overleftrightarrow{\mathbb{I}} - \overleftrightarrow{\boldsymbol{D}} \xrightarrow{\omega=0} -\overleftrightarrow{\boldsymbol{D}}. \tag{3.3.26}$$

Note that the SCHA is a static theory so it is defined through $\omega{=}0$ quantities. Similarly, one defines the harmonic propagator as

$$\overleftrightarrow{\boldsymbol{G}}^{(0)}(\omega)^{-1} = \omega^2 \overleftrightarrow{\mathbb{I}} - \frac{\partial^2 V_{\mathrm{BO}}}{\partial \vec{\widetilde{\boldsymbol{R}}} \partial \vec{\widetilde{\boldsymbol{R}}}}\bigg|_{\boldsymbol{R}=\vec{\boldsymbol{\mathcal{R}}}_{\mathrm{BO}}} \xrightarrow{\omega=0} -\frac{\partial^2 V_{\mathrm{BO}}}{\partial \vec{\widetilde{\boldsymbol{R}}} \partial \vec{\widetilde{\boldsymbol{R}}}}\bigg|_{\boldsymbol{R}=\vec{\boldsymbol{\mathcal{R}}}_{\mathrm{BO}}} \tag{3.3.27}$$

$\vec{\boldsymbol{\mathcal{R}}}_{\mathrm{BO}}$ is the minimum of $V_{\mathrm{BO}}(\vec{\boldsymbol{R}})$

$$\frac{\partial V_{\mathrm{BO}}}{\partial \vec{\widetilde{\boldsymbol{R}}}}\bigg|_{\vec{\boldsymbol{R}}=\vec{\boldsymbol{\mathcal{R}}}_{\mathrm{BO}}} = 0. \tag{3.3.28}$$

Note the difference in notation with respect to Chapter 2. In Chapter 2, we have indicated the minimum of the Born-Oppenheimer potential $\vec{\boldsymbol{\mathcal{R}}}_{\mathrm{BO}}$ as $\vec{\boldsymbol{R}}_l$ in the definition of the displacement operator $\hat{u}(\boldsymbol{R}_l)_{b\alpha}$ in (2.2.3). Here, the tag BO is explicity expressed to avoid confusion with the ionic configuration $\vec{\boldsymbol{R}}$.

In the harmonic approximation, the lattice normal modes are the eigenvalues of the second-order expansion of the BO potential around its minimum $\vec{\boldsymbol{\mathcal{R}}}_{\mathrm{BO}}$

$$\frac{\partial^2 V_{\mathrm{BO}}}{\partial \widetilde{R}_a \partial \widetilde{R}_b}\bigg|_{\boldsymbol{R}=\vec{\boldsymbol{\mathcal{R}}}_{\mathrm{BO}}} = \sum_{\mu=1}^{3N} \Omega^2_\mu \varepsilon^a_\mu \varepsilon^b_\nu. \tag{3.3.29}$$

The latter expression represents the lowest order expansion of the BO potential $\boldsymbol{d}$ used in standard harmonic approximation of the BO Hamiltonian, such as (2.2.3). Notice that the harmonic Green's function $\overleftrightarrow{\boldsymbol{G}}^{(0)}$ are different from the one defined in (2.3.2), [cfr. Appendix 2.D] and are proportional to the Green's functions defined in (2.D.7a). In what follows we use $\overleftrightarrow{\boldsymbol{G}}^{(0)}$ (harmonic) and $\overleftrightarrow{\boldsymbol{\mathcal{G}}}^{(0)}$ (SCHA) to denote the static limit ($\omega = 0$) of the propagators introduced in Eqs. (3.3.26), (3.3.27).

To connect the SCHA with perturbation theory, we expand the BO energy landscape $V_{\mathrm{BO}}(\vec{\boldsymbol{R}})$ in a Taylor series around the positions $\vec{\boldsymbol{\mathcal{R}}}_{\mathrm{BO}}$. All the SCHA equations contain

Gaussian averages of BOES derivatives

$$\left\langle \frac{\partial^k V^{(\mathrm{BO})}}{\partial \widetilde{R}_{b_1} .. \partial \widetilde{R}_{b_k}} \right\rangle_{(0)} = \sum_{n=0}^{\infty} \frac{1}{n!} \sum_{a_1..a_n=1}^{3N} \overset{(k+n)}{d}_{b_1..b_k a_1..a_n} \left\langle \left(\delta\widetilde{R} + \widetilde{\delta}\right)_{a_1} .. \left(\delta\widetilde{R} + \widetilde{\delta}\right)_{a_n} \right\rangle_{(0)} \tag{3.3.30}$$

where the anharmonic vertices in Eq. (3.3.30) are evaluated at the minimum of the BO energy landscape

$$\overset{(n)}{d}_{a_1 \dots a_n} = \left. \frac{\partial^n V^{(\mathrm{BO})}}{\partial \widetilde{R}_{a_1} \dots \partial \widetilde{R}_{a_n}} \right|_{\boldsymbol{R}=\vec{\boldsymbol{\mathcal{R}}}_{\mathrm{BO}}} \tag{3.3.31}$$

and $\vec{\widetilde{\boldsymbol{\delta}}}$ is the difference between the minimum of the BO potential and the equilibrium centroids of the SCHA

$$\vec{\widetilde{\boldsymbol{\delta}}} = \vec{\widetilde{\boldsymbol{\mathcal{R}}}}^{(0)} - \vec{\widetilde{\boldsymbol{\mathcal{R}}}}_{\mathrm{BO}}. \tag{3.3.32}$$

The SCHA distribution is a Gaussian, so the averages in Eq. (3.3.30) can be evaluated analytically up to any order using the Wick theorem. In a perturbative expansion, we assume that each anharmonic vertex scales as

$$\overset{(n)}{\boldsymbol{d}} \sim \mathcal{O}(\xi^{n-2}) \tag{3.3.33}$$

where ξ is the perturbative parameter and can be estimated as the ratio of the thermal length and the average bond distance.[56] In what follows, we truncate the BO potential to the fourth-order, setting

$$\overset{(n)}{\boldsymbol{d}} = 0 \quad n \geq 5. \tag{3.3.34}$$

Substituting the Taylor expansion into the first SCHA equation, Eq. (3.3.22a), we obtain a self-consistent equation for $\widetilde{\vec{\boldsymbol{\delta}}}$ that takes into account quantum and anharmonic effects on the atomic positions shift

$$\delta_a = \sum_{bcd=1}^{3N} \frac{g^{(0)}_{ab}}{2} \left[\left(\overset{(3)}{d}_{bcd} + \frac{1}{3} \sum_{e=1}^{3N} \overset{(4)}{d}_{bcde} \delta_e \right) \delta_c \delta_d - \left(\overset{(3)}{d}_{bcd} + \sum_{e=1}^{3N} \overset{(4)}{d}_{bcde} \delta_e \right) \mathcal{G}^{(0)}(t=0^-)_{cd} \right], \tag{3.3.35}$$

where, in analogy with many-body theory, $\overleftrightarrow{\boldsymbol{\mathcal{G}}}^{(0)}(t{=}0^-)$ is the SCHA (mass-reduced) position-position correlator

$$\mathcal{G}^{(0)}(t{=}0^-)_{ab} = -\left\langle (\widetilde{R} - \widetilde{\mathcal{R}}^{(0)})_a (\widetilde{R} - \widetilde{\mathcal{R}}^{(0)})_b \right\rangle_{(0)}, \tag{3.3.36}$$

where $t{=}0^-$ is the many-body analytical continuation in time.[104] Similarly, the second SCHA equation (Eq. 3.3.24) results in a self-consistent expression for the self-energy

$$\mathcal{G}^{(0)}{}^{-1}_{ab} = G^{(0)}{}^{-1}_{ab} - \Pi^{(0)}_{ab}, \tag{3.3.37}$$

$$\Pi^{(0)}_{ab} = \sum_{c=1}^{3N} \overset{(3)}{d}_{abc} \delta_c - \sum_{cd=1}^{3N} \frac{\overset{(4)}{d}_{abcd}}{2} \left(\mathcal{G}^{(0)}(t=0^-)_{cd} - \delta_c \delta_d \right). \tag{3.3.38}$$

Self-consistent phonon (SCP) methods[51,165] solves Eqs (3.3.35) (3.3.38) (3.3.37) by fitting the anharmonic force constants.[166] Often, Eq. (3.3.35) is ignored, and $\widetilde{\vec{\boldsymbol{\delta}}}$ is assumed to be zero, which is valid only if all the atomic coordinates are constrained by symmetry.[41] On the contrary, the SCHA can go beyond the SCP method, including all the anharmonic vertices

with $n \geq 5$ and polarization mixing. Indeed, the stochastic sampling of the potential[50] includes these effects automatically. The SCHA and SCP methods are static theories: the self-energy is real, and the phonons defined in Eq. (3.3.37) are non-interacting excitations with an infinite lifetime.

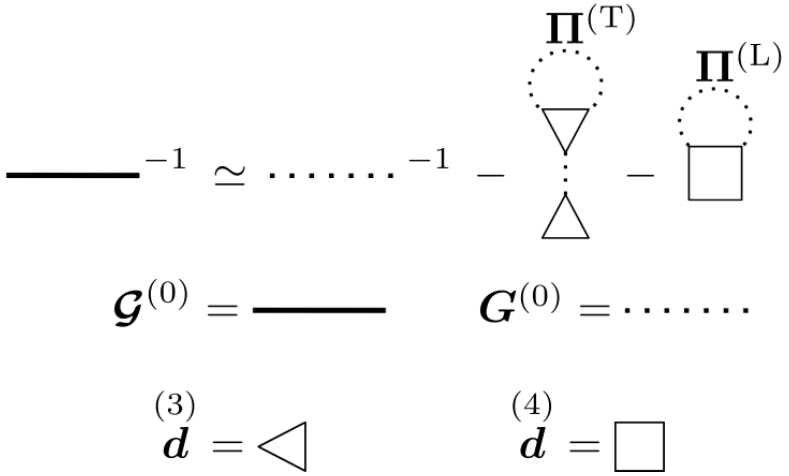

Figure 3.2. Diagrammatic expression for the SCHA one-phonon propagator at lowest perturbative order ξ^2 (see Ref. 56). The single solid line is the static SCHA propagator $\overleftrightarrow{\boldsymbol{\mathcal{G}}}^{(0)}$ Eq. (3.3.26). The thin dotted line is the static harmonic propagator $\boldsymbol{g}^{(0)}$ Eq. (3.3.27). The scattering vertices are defined in Eq. (3.3.31) with n=3 (triangle) and n=4(square). The tadpole and loop diagram are defined in Eq. (3.3.41)

Expressing both the SCHA propagator and the position shift as a series of $\mathcal{O}(\xi^n)$ corrections

$$\overleftrightarrow{\boldsymbol{\mathcal{G}}}^{(0)} = \overleftrightarrow{\boldsymbol{\mathcal{G}}}^{(0)\xi=0} + \overleftrightarrow{\boldsymbol{\mathcal{G}}}^{(0)\xi=1} + .. \qquad \overleftrightarrow{\boldsymbol{\mathcal{G}}}^{(0)\xi=n} \sim \mathcal{O}(\xi^n) \tag{3.3.39a}$$

$$\vec{\tilde{\boldsymbol{\delta}}} = \vec{\tilde{\boldsymbol{\delta}}}^{\xi=0} + \vec{\tilde{\boldsymbol{\delta}}}^{\xi=1} + .. \qquad \vec{\tilde{\boldsymbol{\delta}}}^{\xi=n} \sim \mathcal{O}(\xi^n) \tag{3.3.39b}$$

one can solve order by order in ξ Eqs (3.3.35) (3.3.38) (3.3.37) to systematically obtain all the corrections to the SCHA propagator with a cubic-quartic potential. Ref. 56 solved Eqs. (3.3.35), (3.3.38), (3.3.37) up to $\mathcal{O}(\xi^2)$ and showed that

$$\left(\mathcal{G}^{(0)}\right)^{-1}_{ab} \simeq \left(G^{(0)}\right)^{-1}_{ab} - \left(\Pi^{(\mathrm{L})}_{ab} + \Pi^{(\mathrm{T})}_{ab}\right) \tag{3.3.40}$$

where $\overleftrightarrow{\boldsymbol{\Pi}}^{(\mathrm{L})}$ and $\overleftrightarrow{\boldsymbol{\Pi}}^{(\mathrm{T})}$ are respectively the loop (L) and tadpole (T) diagram (cf. Fig. 3.2),

$$\Pi^{(\mathrm{L})}_{ab} = -\frac{1}{2}\sum_{cd=1}^{3N} \overset{(4)}{d}_{abcd} G^{(0)}(t{=}0^-)_{cd}, \tag{3.3.41a}$$

$$\Pi^{(\mathrm{T})}_{ab} = -\frac{1}{2}\sum_{cdef=1}^{3N} \overset{(3)}{d}_{abc} g^{(0)}_{cd} \overset{(3)}{d}_{def} G^{(0)}(t{=}0^-)_{ef}\ , \tag{3.3.41b}$$

here $\overleftrightarrow{\boldsymbol{G}}^{(0)}(t{=}0^-)$ is the harmonic counterpart of $\overleftrightarrow{\boldsymbol{\mathcal{G}}}^{(0)}(t{=}0^-)$, Eq. (3.3.36). The loop diagram, Eq. (3.3.41a), comes from quantum/anharmonic fluctuations at fixed positions by setting $\vec{\tilde{\boldsymbol{\delta}}} = \mathbf{0}$ in Eq. (3.3.38). On the other hand, the tadpole diagram, Eq. (3.3.41b), comes from the renormalization of atomic positions, Eq. (3.3.35). Note that the SCHA self-energy contains

a subclass of diagrams, called instant phonons, which do not carry energy and do not have imaginary part (infinite lifetime).[145]

3.3.2 Linearized equations of motion and response function in TDSCHA

When an external time-dependent potential couples to phonons without causing irreversible changes in the material, the system is in the linear response regime. In these cases the external perturbation $V_{\text{ext}}(\vec{\boldsymbol{R}}, t)$ is in the form

$$V_{\text{ext}}(\vec{\boldsymbol{R}}, t) = \mathcal{B}(\vec{\boldsymbol{R}})\mathcal{V}(t). \tag{3.3.42}$$

In this regime, the SCHA distribution $\varrho^{(0)}(\vec{\boldsymbol{R}})$ (See appendix 3.D) is perturbed by $\varrho^{(1)}(\vec{\boldsymbol{R}}, t)$

$$\varrho(\vec{\boldsymbol{R}}, t) = \varrho^{(0)}(\vec{\boldsymbol{R}}) + \varrho^{(1)}(\vec{\boldsymbol{R}}, t). \tag{3.3.43}$$

The probability distribution change leads to the emergence of time-dependent correction (denoted by (1)) to the static parameters. So the free parameters of $\varrho^{(1)}(\vec{\boldsymbol{R}}, t)$ are

$$\widetilde{\mathcal{R}}(t)_\mu = \widetilde{\mathcal{R}}^{(0)}_\mu + \widetilde{\mathcal{R}}^{(1)}_\mu, \tag{3.3.44a}$$
$$\widetilde{\alpha}(t)_{\mu\nu} = \widetilde{\alpha}^{(0)}_\mu \delta_{\mu,\nu} + \widetilde{\alpha}^{(1)}(t)_{\mu\nu}, \tag{3.3.44b}$$
$$\widetilde{\beta}_{\mu\nu}(t) = \widetilde{\beta}^{(0)}_\mu \delta_{\mu,\nu} + \widetilde{\beta}^{(1)}(t)_{\mu\nu}, \tag{3.3.44c}$$

where we express the tensors in the SCHA polarization basis $\{e_\mu\}$ of Eq. (3.3.24). In Appendix 3.E, we express the dynamics of the average momentum $\vec{\vec{\mathcal{P}}}^{(1)}$ and of the mixed matrix $\overleftrightarrow{\widetilde{\gamma}}^{(1)}$ in those of the variables of Eqs (3.3.44). So Eqs (3.3.44) define the dynamics unambiguously.

To obtain the linearized equations of motion, we plug the perturbed correlators (Eqs (3.3.44)) into the equations of motion (Eq. (3.C.5)). Additionally, we use Eq. (3.3.43) to compute the averages of the total potential. This procedure (see appendix 3.E for details) leads to the linear system in the frequency domain

$$\left(\boldsymbol{\mathcal{L}}' + \omega^2\right) \cdot \begin{bmatrix} \vec{\vec{\mathcal{R}}}^{(1)} \\ \overleftrightarrow{\widetilde{\alpha}}^{(1)} \\ \overleftrightarrow{\widetilde{\beta}}^{(1)} \end{bmatrix} = \boldsymbol{p}' \mathcal{V}(\omega). \tag{3.3.45}$$

The perturbation vector $\boldsymbol{p}'$ depends, in general, on equilibrium (SCHA) averages of first and second derivatives of $\mathcal{B}(\vec{\boldsymbol{R}})$.

The external potential modifies the SCHA equilibrium state, defined by Eq. (**??**). The response function encodes how the observable $\mathcal{A}(\vec{\boldsymbol{R}})$ changes when the system is (slightly) out of equilibrium. In the linear response regime, this modification depends only on equilibrium quantities. The TD-SCHA response function is obtained expanding $\langle \mathcal{A} \rangle_{\varrho^{(0)}+\varrho^{(1)}}$ (see Eq. (3.3.43)) in the perturbed parameters of Eqs (3.3.44) around the equilibrium value $\langle \mathcal{A} \rangle_{(0)}$. In appendix 3.E, we show that the first-order correction in the frequency domain is a simple

scalar product in the space of the correlators (Eq. (3.3.44))

$$\langle \mathcal{A} \rangle_{(1)}(\omega) = \boldsymbol{r}'^{\dagger} \cdot \begin{bmatrix} \vec{\vec{\mathcal{R}}}^{(1)} \\ \overleftrightarrow{\alpha}^{(1)} \\ \overleftrightarrow{\beta}^{(1)} \end{bmatrix}, \tag{3.3.46}$$

where the response vector $\boldsymbol{r}'$, similarly to $\boldsymbol{p}'$, contains equilibrium averages of position-derivatives of $\mathcal{A}(\vec{\boldsymbol{R}})$. Finally, inverting the linearized equations of motion, Eq. (3.3.45), we get

$$\langle \mathcal{A} \rangle_{(1)}(\omega) = \boldsymbol{r}'^{\dagger} \cdot \left(\boldsymbol{\mathcal{L}}' + \omega^2 \right)^{-1} \cdot \boldsymbol{p}' \mathcal{V}(\omega), \tag{3.3.47}$$

where $\circ^{-1}$ denotes the inverse. The TD-SCHA general response function of an observable $\mathcal{A}(\vec{\boldsymbol{R}})$ to an external perturbation $\mathcal{B}(\vec{\boldsymbol{R}})$ is

$$\chi(\omega)_{\mathcal{A},\mathcal{B}} = \boldsymbol{r}'^{\dagger} \cdot \left(\boldsymbol{\mathcal{L}}' + \omega^2 \right)^{-1} \cdot \boldsymbol{p}'. \tag{3.3.48}$$

This expression has the same form as the one presented in Ref. 65, where the standard description of quantum mechanics is adopted. The Wigner formalism enormously simplifies the equations, allowing for a clear connection with many-body propagators, contrary to previous formulations.[65,66]

3.3.3 Diagrammatic interpretation of linear response in TDSCHA

In this section, we provide an exhaustive interpretation in terms of Feynman diagrams of Eq. (3.3.48). To do this, we introduce a new basis (see Appendix 3.F and Appendix 3.G for details), which consists in a linear combination of the matrices $\overleftrightarrow{\alpha}^{(1)}, \overleftrightarrow{\beta}^{(1)}$ featuring in Eqs (3.3.44b) (3.3.44c). So, the general response function (Eq. (3.3.48)) takes the form

$$\chi(\omega)_{\mathcal{A},\mathcal{B}} = \boldsymbol{r} \cdot \boldsymbol{\mathcal{L}}(\omega)^{-1} \cdot \boldsymbol{p}, \tag{3.3.49}$$

where the response vector $\boldsymbol{r}$ and the perturbation vector $\boldsymbol{p}$ have a simple expression in terms of equilibrium averages of $\mathcal{A}(\vec{\boldsymbol{R}})$ and $\mathcal{B}(\vec{\boldsymbol{R}})$

$$\boldsymbol{p} = \begin{bmatrix} \left\langle \frac{\partial \mathcal{B}}{\partial \widetilde{R}_\mu} \right\rangle_{(0)} \\ \left\langle \frac{\partial^2 \mathcal{B}}{\partial \widetilde{R}_\mu \partial \widetilde{R}_\nu} \right\rangle_{(0)} \\ \left\langle \frac{\partial^2 \mathcal{B}}{\partial \widetilde{R}_\mu \partial \widetilde{R}_\nu} \right\rangle_{(0)} \end{bmatrix}, \qquad \boldsymbol{r} = \begin{bmatrix} \left\langle \frac{\partial \mathcal{A}}{\partial \widetilde{R}_\mu} \right\rangle_{(0)} \\ \left\langle \frac{\partial^2 \mathcal{A}}{\partial \widetilde{R}_\mu \partial \widetilde{R}_\nu} \right\rangle_{(0)} \\ \left\langle \frac{\partial^2 \mathcal{A}}{\partial \widetilde{R}_\mu \partial \widetilde{R}_\nu} \right\rangle_{(0)} \end{bmatrix}. \tag{3.3.50}$$

$\boldsymbol{\mathcal{L}}(\omega)$ propagates the perturbation caused by $\boldsymbol{p}$ in the system and encodes the information on how the latter affects $\boldsymbol{r}$, which defines how the observable changes. Indeed, its multiplication by a vector representing the status of the system, as $\boldsymbol{r}$ or $\boldsymbol{p}$ (3.3.50), gives the anharmonic scattering processes that further dress the SCHA Green's function introducing a finite lifetime

(see section 3.3.4). In the new basis, $\boldsymbol{\mathcal{L}}(\omega)$ of Eq. (3.3.49) has a simple symmetric form

$$\boldsymbol{\mathcal{L}}(\omega)=\begin{bmatrix} \overleftrightarrow{\boldsymbol{\mathcal{G}}}^{(0)}(\omega)^{-1} & -\overset{(3)}{\boldsymbol{D}} & -\overset{(3)}{\boldsymbol{D}} \\ -\overset{(3)}{\boldsymbol{D}} & \boldsymbol{\chi}_{-}^{(0)}(\omega)^{-1}-\overset{(4)}{\boldsymbol{D}} & -\overset{(4)}{\boldsymbol{D}} \\ -\overset{(3)}{\boldsymbol{D}} & -\overset{(4)}{\boldsymbol{D}} & -\boldsymbol{\chi}_{+}^{(0)}(\omega)^{-1}-\overset{(4)}{\boldsymbol{D}} \end{bmatrix}, \tag{3.3.51}$$

$$\boldsymbol{\mathcal{L}}(\omega)=\boldsymbol{\mathcal{L}}(\omega)^{\dagger}. \tag{3.3.52}$$

The harmonic and anharmonic contributions to $\boldsymbol{\mathcal{L}}(\omega)$ are

$$\boldsymbol{\mathcal{L}}_{\text{harm}}(\omega)=\begin{bmatrix} \overleftrightarrow{\boldsymbol{\mathcal{G}}}^{(0)}(\omega)^{-1} & \mathbf{0} & \mathbf{0} \\ \mathbf{0} & \boldsymbol{\chi}_{-}^{(0)}(\omega)^{-1} & \mathbf{0} \\ \mathbf{0} & \mathbf{0} & -\boldsymbol{\chi}_{+}^{(0)}(\omega)^{-1} \end{bmatrix}, \tag{3.3.53}$$

$$\boldsymbol{\mathcal{L}}_{\text{anh}}(\omega)=\begin{bmatrix} \mathbf{0} & -\overset{(3)}{\boldsymbol{D}} & -\overset{(3)}{\boldsymbol{D}} \\ -\overset{(3)}{\boldsymbol{D}} & -\overset{(4)}{\boldsymbol{D}} & -\overset{(4)}{\boldsymbol{D}} \\ -\overset{(3)}{\boldsymbol{D}} & -\overset{(4)}{\boldsymbol{D}} & -\overset{(4)}{\boldsymbol{D}} \end{bmatrix}. \tag{3.3.54}$$

We report in Fig. 3.3 a graphical expression for Eq. (3.3.51). To construct a diagrammatic representation, we associate each tensor in $\boldsymbol{\mathcal{L}}(\omega)$ with a symbol that possesses a number of extremities equal to the rank of the tensor. The single solid line in Fig. 3.3 represents the

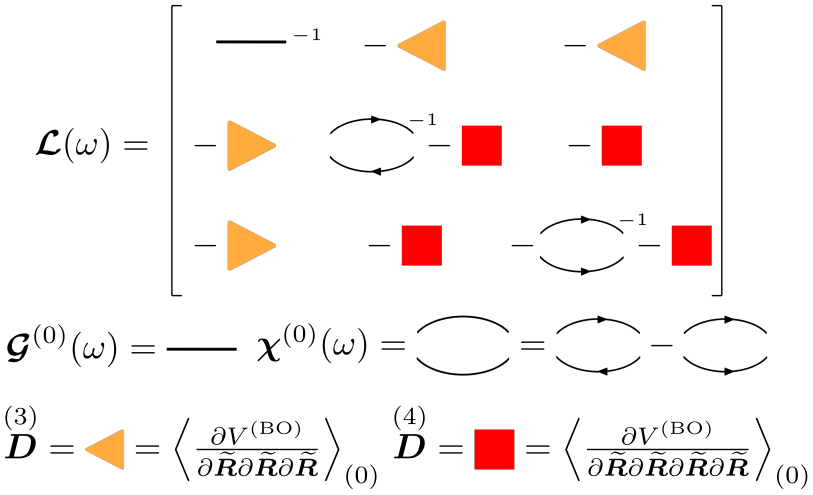

Figure 3.3. Graphical expression for Eq. (3.3.51) in terms of the free SCHA propagators (single and double solid line Eqs (3.3.55) (3.3.56)) and the third and fourth order scattering vertex (orange triangle and red square defined in Eqs (3.3.58) (3.3.59)).

equilibrium SCHA Green's function $\overleftrightarrow{\boldsymbol{\mathcal{G}}}^{(0)}(\omega)$

$$\mathcal{G}^{(0)}(\omega)_{\mu\nu}=\frac{\delta_{\mu\nu}}{\omega^2-\omega_{\mu}^2}, \tag{3.3.55}$$

where $\{\omega_\mu\}$ are the SCHA frequencies defined in Eq. (3.3.24). The double single solid line in Fig. 3.3 is the two-phonon SCHA propagator $\boldsymbol{\chi}^{(0)}(\omega)$

$$\chi^{(0)}(\omega)_{\mu\nu\eta\lambda} = \chi^{(0)}_{-}(\omega)_{\mu\nu\eta\lambda} - \chi^{(0)}_{+}(\omega)_{\mu\nu\eta\lambda} \tag{3.3.56}$$

which contains a resonant $\boldsymbol{\chi}^{(0)}_{-}(\omega)$ and an anti-resonant term $\boldsymbol{\chi}^{(0)}_{+}(\omega)$

$$\chi^{(0)}_{-}(\omega)_{\mu\nu\eta\lambda} = \delta_{\mu\eta}\delta_{\nu\lambda}\frac{\hbar\left[\omega_\mu - \omega_\nu\right]\left[n_\mu - n_\nu\right]}{4\omega_\mu\omega_\nu[(\omega_\mu - \omega_\nu)^2 - \omega^2]}, \tag{3.3.57a}$$

$$\chi^{(0)}_{+}(\omega)_{\mu\nu\eta\lambda} = \delta_{\mu\eta}\delta_{\nu\lambda}\frac{\hbar\left[\omega_\mu + \omega_\nu\right]\left[1 + n_\mu + n_\nu\right]}{4\omega_\mu\omega_\nu[(\omega_\mu + \omega_\nu)^2 - \omega^2]}. \tag{3.3.57b}$$

The anti-resonant part $\boldsymbol{\chi}^{(0)}_{+}(\omega)$ describes the absorption/emission processes of a phonon pair (double solid line with both arrows in the same directions in Fig. 3.3) while the resonant $\boldsymbol{\chi}^{(0)}_{-}(\omega)$ the case in which one phonon is absorbed, and the other one is emitted (double solid line with arrows pointing in opposite directions in Fig. 3.3).

The first row of Eq. (3.3.51) relates the propagation of single phonon excitation $\overleftrightarrow{\boldsymbol{\mathcal{G}}}^{(0)}(\omega)$ to two-phonon $\boldsymbol{\chi}^{(0)}_{\pm}(\omega)$. The process is mediated by the three-phonon scattering vertex (orange triangle of Fig. 3.3)

$$\overset{(3)}{D}_{\mu\nu\eta} = \left\langle \frac{\partial^3 V^{(\mathrm{BO})}}{\partial\widetilde{R}_\mu\partial\widetilde{R}_\nu\partial\widetilde{R}_\eta} \right\rangle_{(0)}. \tag{3.3.58}$$

The second and third rows of Eq. (3.3.51) show that double excitations interact with each other via the fourth-order scattering vertex (red square of Fig. 3.3)

$$\overset{(4)}{D}_{\mu\nu\eta\lambda} = \left\langle \frac{\partial^4 V^{(\mathrm{BO})}}{\partial\widetilde{R}_\mu\partial\widetilde{R}_\nu\partial\widetilde{R}_\eta\partial\widetilde{R}_\lambda} \right\rangle_{(0)}, \tag{3.3.59}$$

or can decay in a single phonon via the three-phonon scattering vertex, Eq. (3.3.58). As a guide for the reader, in Table 3.1, we report a summary of all the symbols used.

Inspecting the expression of $\boldsymbol{\mathcal{L}}(\omega)$, we understand that in TD-SCHA only single and double excitations are dressed by anharmonicity and that only single phonons can decay in a higher-order phonon propagation. The scattering vertices, Eqs (3.3.58) (3.3.59), included in the dynamical response have an interesting diagrammatic expression (see also Ref. 167). In general, they do not coincide with the derivatives of the BO potential evaluated at the equilibrium SCHA positions $\vec{\boldsymbol{\mathcal{R}}}^{(0)}$ but they contain extra corrections due to quantum-thermal fluctuations. All of these terms are included in the TD-SCHA. Expanding Eqs (3.3.58) (3.3.59) in $\vec{\boldsymbol{R}} - \vec{\boldsymbol{\mathcal{R}}}^{(0)}$, we get the following series, as reported in appendix 3.H,

$$\begin{aligned}\overset{(3)}{D}_{\mu\nu\eta} = &\sum_{n=0}^{+\infty}\frac{(-1)^n}{2^n n!}\sum_{\alpha_1..\alpha_{2n}=1}^{3N}\overset{(3+2n)}{D}{}^{(0)}_{\mu\nu\eta\alpha_1..\alpha_{2n-1}\alpha_{2n}} \\ &\mathcal{G}^{(0)}(t=0^-)_{\alpha_1\alpha_2}..\mathcal{G}^{(0)}(t=0^-)_{\alpha_{2n-1}\alpha_{2n}},\end{aligned} \tag{3.3.60a}$$

$$\begin{aligned}\overset{(4)}{D}_{\mu\nu\eta\lambda} = &\sum_{n=0}^{+\infty}\frac{(-1)^n}{2^n n!}\sum_{\alpha_1..\alpha_{2n}=1}^{3N}\overset{(4+2n)}{D}{}^{(0)}_{\mu\nu\eta\lambda\alpha_1\alpha_2..\alpha_{2n-1}\alpha_{2n}} \\ &\mathcal{G}^{(0)}(t=0^-)_{\alpha_1\alpha_2}..\mathcal{G}^{(0)}(t=0^-)_{\alpha_{2n-1}\alpha_{2n}},\end{aligned} \tag{3.3.60b}$$

Notation	Diagram	Formula	Description	Eq.
$\mathcal{G}^{(0)}(\omega)_{\mu\nu}$		$\frac{\delta_{\mu\nu}}{\omega^2-\omega_\mu^2}$	Bare one-phonon SCHA propagator	(3.3.26)
$g^{(0)}(\omega)_{\mu\nu}$		$\frac{\delta_{\mu\nu}}{\omega^2-\Omega_\mu^2}$	Bare perturbative one-phonon propagator	(3.3.27)
$\chi^{(0)}(\omega)_{\mu\nu\eta\lambda}$	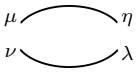	$\chi_-^{(0)}(\omega)_{\mu\nu\eta\lambda} - \chi_+^{(0)}(\omega)_{\mu\nu\eta\lambda}$	Bare two-phonon SCHA propagator	(3.3.56)
$\chi_-^{(0)}(\omega)_{\mu\nu\eta\lambda}$	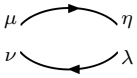	$\delta_{\mu\eta}\delta_{\nu\lambda}\frac{\hbar[\omega_\mu-\omega_\nu][n_\mu-n_\nu]}{4\omega_\mu\omega_\nu[(\omega_\mu-\omega_\nu)^2-\omega^2]}$	Resonant two-phonon SCHA propagator	(3.3.57a)
$\chi_+^{(0)}(\omega)_{\mu\nu\eta\lambda}$	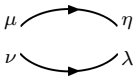	$\delta_{\mu\eta}\delta_{\nu\lambda}\frac{\hbar[\omega_\mu+\omega_\nu][1+n_\mu+n_\nu]}{4\omega_\mu\omega_\nu[(\omega_\mu+\omega_\nu)^2-\omega^2]}$	Antiresonant two-phonon SCHA propagator	(3.3.57b)
$\overset{(4)}{D}_{\mu\nu\eta\lambda}$	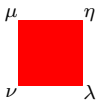	$\left\langle \frac{\partial^4 V^{(\mathrm{BO})}}{\partial\widetilde{R}_\mu\partial\widetilde{R}_\nu\partial\widetilde{R}_\eta\partial\widetilde{R}_\lambda} \right\rangle_{(0)}$	Four-phonon SCHA vertex	(3.3.59)
$\overset{(4)}{D}{}^{(0)}_{\mu\nu\eta\lambda}$	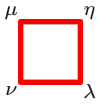	$\left.\frac{\partial^4 V^{(\mathrm{BO})}}{\partial\widetilde{R}_\mu\partial\widetilde{R}_\nu\partial\widetilde{R}_\eta\partial\widetilde{R}_\lambda}\right\vert_{\boldsymbol{R}=\vec{\boldsymbol{\mathcal{R}}}^{(0)}}$	Perturbative four-phonon vertex at the SCHA positions	(3.3.61)
$\overset{(4)}{d}_{\mu\nu\eta\lambda}$	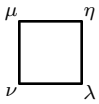	$\left.\frac{\partial^4 V^{(\mathrm{BO})}}{\partial\widetilde{R}_\mu\partial\widetilde{R}_\nu\partial\widetilde{R}_\eta\partial\widetilde{R}_\lambda}\right\vert_{\boldsymbol{R}=\vec{\boldsymbol{\mathcal{R}}}_{\mathrm{BO}}}$	Perturbative four-phonon scattering vertex	(3.3.31)
$\overset{(3)}{D}_{\mu\nu\eta}$	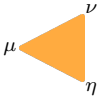	$\left\langle \frac{\partial^3 V^{(\mathrm{BO})}}{\partial\widetilde{R}_\mu\partial\widetilde{R}_\nu\partial\widetilde{R}_\eta} \right\rangle_{(0)}$	Three-phonon SCHA vertex	(3.3.58)
$\overset{(3)}{D}{}^{(0)}_{\mu\nu\eta}$	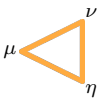	$\left.\frac{\partial^3 V^{(\mathrm{BO})}}{\partial\widetilde{R}_\mu\partial\widetilde{R}_\nu\partial\widetilde{R}_\eta}\right\vert_{\boldsymbol{R}=\vec{\boldsymbol{\mathcal{R}}}^{(0)}}$	Perturbative three-phonon vertex at SCHA positions	(3.3.61)
$\overset{(3)}{d}_{\mu\nu\eta}$	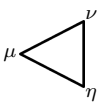	$\left.\frac{\partial^3 V^{(\mathrm{BO})}}{\partial\widetilde{R}_\mu\partial\widetilde{R}_\nu\partial\widetilde{R}_\eta}\right\vert_{\boldsymbol{R}=\vec{\boldsymbol{\mathcal{R}}}_{\mathrm{BO}}}$	Perturbative three-phonon vertex	(3.3.31)

Table 3.1. Collection of symbols frequently used in the main text. First column: the notation used. Second column: graphical expression with indexes. Third column: mathematical definition. Fourth column: description of the symbol. Fifth column: first labeled equation where the symbol appears.

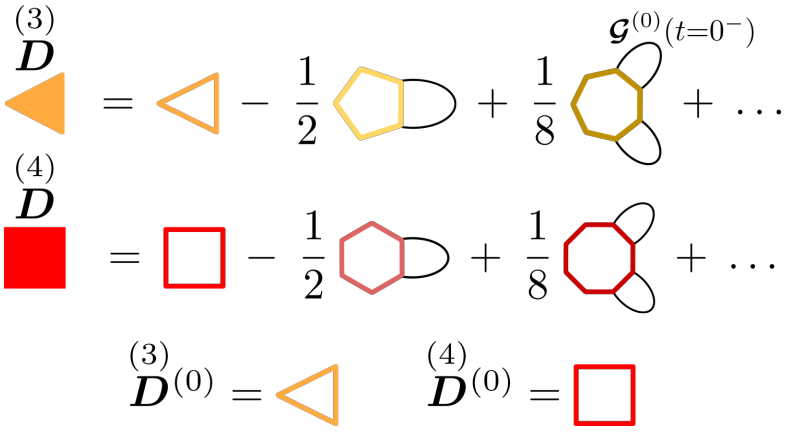

Figure 3.4. Diagrammatic expression for the SCHA scattering tensors Eqs (3.3.58) (3.3.59) as presented in Eqs (3.3.60). Each SCHA propagator is contracted with a higher order derivative of the anharmonic tensor Eq. (3.3.61) evaluated at the SCHA positions, i.e., they do not coincide with Eq. (3.3.31). These are represented as $n = 3, 5, 7..$ and $n = 4, 6, 8..$ regular polygons.

where the anharmonic vertices in the series are

$$\overset{(n)}{D}{}^{(0)}_{\alpha_1..\alpha_n} = \frac{\partial^n V^{(\mathrm{BO})}}{\partial \widetilde{R}_{\alpha_1}..\partial \widetilde{R}_{\alpha_n}}\bigg|_{\boldsymbol{R}=\vec{\boldsymbol{\mathcal{R}}}^{(0)}}. \tag{3.3.61}$$

These differ in general from $\overset{(n)}{\boldsymbol{d}}$, see Eq. (3.3.31), since the minimum of the Born-Oppenheimer potential $\vec{\boldsymbol{\mathcal{R}}}_{\mathrm{BO}}$ does not coincide with the SCHA centroid $\vec{\boldsymbol{\mathcal{R}}}^{(0)}$. In Fig. 3.4, we report the diagrammatic expansion for Eqs (3.3.60). Each anharmonic tensor in Eq. (3.3.61) with $n > 3, 4$ has a pair of indexes contracted with a SCHA propagator $\overleftrightarrow{\boldsymbol{\mathcal{G}}}^{(0)}(t{=}0^-)$ (Eq. (3.3.61)). This indicates that quantum-thermal fluctuations result in the renormalization of the anharmonic vertices.

3.3.4 Anharmonic propagators

In this Section, we discuss the TD-SCHA interacting propagators. Specifically, we present two-phonon processes neglected in previous works.[65,66] In TD-SCHA, the one-phonon $\mathcal{G}(\omega)_{\mu\nu}$, two-phonon $\chi(\omega)_{\mu\nu\eta\lambda}$, and the one-two phonon $\Gamma(\omega)_{\mu\eta\lambda}$ interacting propagators are obtained as response functions by setting in $\chi(\omega)_{\mathcal{A},\mathcal{B}}$ (Eq. (3.3.49))

$$\mathcal{A}_{\mathcal{G}} = \delta\widetilde{R}^{(0)}_{\mu} \qquad \mathcal{B}_{\mathcal{G}} = \delta\widetilde{R}^{(0)}_{\nu}, \tag{3.3.62a}$$

$$\mathcal{A}_{\chi} = \frac{1}{2}\delta\widetilde{R}^{(0)}_{\mu}\delta\widetilde{R}^{(0)}_{\nu} \qquad \mathcal{B}_{\chi} = \frac{1}{2}\delta\widetilde{R}^{(0)}_{\eta}\delta\widetilde{R}^{(0)}_{\lambda}, \tag{3.3.62b}$$

$$\mathcal{A}_{\Gamma} = \delta\widetilde{R}^{(0)}_{\mu} \qquad \mathcal{B}_{\Gamma} = \frac{1}{2}\delta\widetilde{R}^{(0)}_{\eta}\delta\widetilde{R}^{(0)}_{\lambda}. \tag{3.3.62c}$$

The response and perturbation vectors (see Eqs (3.3.50)) corresponding to Eqs (3.3.62) are as follows

$$\boldsymbol{r}_{\mathcal{G}} = \begin{bmatrix} \vec{\delta}_\mu \\ \mathbf{0} \\ \mathbf{0} \end{bmatrix} \qquad \boldsymbol{p}_{\mathcal{G}} = \begin{bmatrix} \vec{\delta}_\nu \\ \mathbf{0} \\ \mathbf{0} \end{bmatrix}, \tag{3.3.63a}$$

$$\boldsymbol{r}_{\chi} = \begin{bmatrix} \mathbf{0} \\ \overleftrightarrow{S}_{\mu\nu} \\ \overleftrightarrow{S}_{\mu\nu} \end{bmatrix} \qquad \boldsymbol{p}_{\chi} = \begin{bmatrix} \mathbf{0} \\ \overleftrightarrow{S}_{\eta\lambda} \\ \overleftrightarrow{S}_{\eta\lambda} \end{bmatrix}, \tag{3.3.63b}$$

$$\boldsymbol{r}_{\Gamma} = \begin{bmatrix} \vec{\delta}_\mu \\ \mathbf{0} \\ \mathbf{0} \end{bmatrix} \qquad \boldsymbol{p}_{\Gamma} = \begin{bmatrix} \mathbf{0} \\ \overleftrightarrow{S}_{\eta\lambda} \\ \overleftrightarrow{S}_{\eta\lambda} \end{bmatrix}, \tag{3.3.63c}$$

where $\vec{\delta}_\mu$ is a $3N$ vector with 1 in the mode index μ and zero elsewhere and $\overleftrightarrow{S}_{\eta\lambda}$ is a $3N \times 3N$ matrix with $1/2$ on the mode indexes η and λ and zeros elsewhere. The choice of $\mathcal{A}/\mathcal{B}$, as in Eqs (3.3.62), is not arbitrary. In the non-interacting case, $\boldsymbol{\mathcal{L}}(\omega)$ is diagonal, so the response function simplifies to

$$\begin{aligned} \chi(\omega)_{\mathcal{A},\mathcal{B}} =& \boldsymbol{r}_i \begin{bmatrix} \overleftrightarrow{\mathcal{G}}^{(0)}(\omega) & \mathbf{0} & \mathbf{0} \\ \mathbf{0} & \boldsymbol{\chi}_-^{(0)}(\omega) & \mathbf{0} \\ \mathbf{0} & \mathbf{0} & -\boldsymbol{\chi}_+^{(0)}(\omega) \end{bmatrix} \boldsymbol{p}_i \\ i =& \mathcal{G}, \chi, \Gamma. \end{aligned} \tag{3.3.64}$$

From Eq. (3.3.64), we recover the one and two phonon free propagators (Eqs (3.3.55) (3.3.56)) and no cross terms connecting single to double excitations. These results are consistent with the standard linear response theory, which is treated with the many-body formalism in the non-interacting case. This shows that Eqs (3.3.63) recover physically relevant quantities. To get the interacting Green's function, we plug $\boldsymbol{r}$ and $\boldsymbol{p}$ of Eqs (3.3.63) in the expression of $\chi(\omega)_{\mathcal{A},\mathcal{B}}$, Eq. (3.3.49), and we invert $\boldsymbol{\mathcal{L}}(\omega)$ following Refs[65,168,169] (see also appendix 3.F). To do this, we consider $\boldsymbol{\mathcal{L}}(\omega)$, Eq. (3.3.51), as a 3×3 block-matrix (as represented in Fig. 3.3) where each block itself is a tensor. The same applies to $\boldsymbol{r}$ and $\boldsymbol{p}$, Eqs (3.3.50), which are understood as 3 components vectors. From the non-interacting case (Eq. (3.3.64)), we learn that the first component of $\boldsymbol{p}/\boldsymbol{r}$ controls the single-mode propagation while the second and third the two-phonon channel. The inversion process mixes the matrix elements of $\boldsymbol{\mathcal{L}}(\omega)$, adding interactions (non-zero self-energies) to the free propagators, which are expressed as diagrammatic series. The representation of Fig. 3.3 is a graphical aid to visualize the building blocks of these diagrams. In Appendix 3.G, we report the details of all the results presented. In the calculations we always reduce the inversion of $\boldsymbol{\mathcal{L}}(\omega)$ to a 2×2 block-matrix with the

following form

$$\begin{bmatrix} \boldsymbol{A} & \boldsymbol{C} \\ \boldsymbol{C}^\dagger & \boldsymbol{B} \end{bmatrix} \tag{3.3.65}$$

which can be easily inverted (see appendix 3.F)

$$\begin{bmatrix} \boldsymbol{D}^{-1} & -\boldsymbol{D}^{-1}\cdot\boldsymbol{C}\cdot\boldsymbol{B}^{-1} \\ -\boldsymbol{B}^{-1}\cdot\boldsymbol{C}^\dagger\cdot\boldsymbol{D}^{-1} & \boldsymbol{B}^{-1}\cdot\left(\mathbf{1}+\boldsymbol{C}^\dagger\cdot\boldsymbol{D}^{-1}\cdot\boldsymbol{C}\cdot\boldsymbol{B}^{-1}\right) \end{bmatrix} \tag{3.3.66}$$

where $\boldsymbol{D} = \boldsymbol{A} - \boldsymbol{C}\cdot\boldsymbol{B}^{-1}\cdot\boldsymbol{C}^\dagger$.

First, we discuss the one-phonon propagator. Because only the first component of both $\boldsymbol{p}_{\mathcal{G}}$ and $\boldsymbol{r}_{\mathcal{G}}$, Eq. (3.3.63a), is non-zero, the response calculation is simplified. In particular, we compact the 2×2 two-phonon sector of $\boldsymbol{\mathcal{L}}(\omega)$ (*i.e.* $\boldsymbol{\mathcal{L}}(\omega)_{ij}$ with $i,j>1$) in a 1×1 block matrix. As shown in appendix 3.G, $\boldsymbol{\mathcal{L}}(\omega)$ is reduced to a 2×2 block-matrix $\boldsymbol{\mathcal{L}}_{1\text{ph}}(\omega)$, so that the one-phonon propagator is given by

$$\overleftrightarrow{\boldsymbol{\mathcal{G}}}(\omega) = \boldsymbol{r}_{\mathcal{G}}\cdot\boldsymbol{\mathcal{L}}(\omega)^{-1}\cdot\boldsymbol{p}_{\mathcal{G}} = \left(\boldsymbol{\mathcal{L}}_{1\text{ph}}(\omega)^{-1}\right)_{11} \tag{3.3.67}$$

where

$$\boldsymbol{\mathcal{L}}_{1\text{ph}}(\omega) = \begin{bmatrix} \overleftrightarrow{\boldsymbol{\mathcal{G}}}^{(0)}(\omega)^{-1} & \overset{(3)}{-\boldsymbol{D}} \\ \overset{(3)}{-\boldsymbol{D}} & \boldsymbol{\chi}^{(0)}(\omega)^{-1} - \overset{(4)}{\boldsymbol{D}} \end{bmatrix}. \tag{3.3.68}$$

Note that $\left(\boldsymbol{\mathcal{L}}_{1\text{ph}}(\omega)\right)_{22}$ represents the anharmonic two-phonon channel in which single modes can decay through the three-phonon vertex, $\left(\boldsymbol{\mathcal{L}}_{1\text{ph}}(\omega)\right)_{12}$. Graphically Eq. (3.3.67) corresponds to

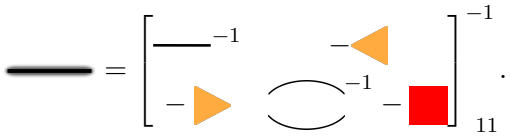

(3.3.69)

In Eq. (3.3.67), we apply the general result of Eq. (3.3.66) to obtain the interacting Green's function

$$\overleftrightarrow{\boldsymbol{\mathcal{G}}}(\omega) = \overleftrightarrow{\boldsymbol{\mathcal{G}}}^{(0)}(\omega) + \overleftrightarrow{\boldsymbol{\mathcal{G}}}^{(0)}(\omega)\cdot\overleftrightarrow{\boldsymbol{\Pi}}(\omega)\cdot\overleftrightarrow{\boldsymbol{\mathcal{G}}}(\omega), \tag{3.3.70}$$

where the self-energy $\overleftrightarrow{\boldsymbol{\Pi}}(\omega)$ coincides with the one reported in Refs[56,65,66]

$$\overleftrightarrow{\boldsymbol{\Pi}}(\omega) = \overset{(3)}{\boldsymbol{D}} : \left(\mathbf{1} - \boldsymbol{\chi}^{(0)}(\omega) : \overset{(4)}{\boldsymbol{D}}\right)^{-1} : \boldsymbol{\chi}^{(0)}(\omega) : \overset{(3)}{\boldsymbol{D}}, \tag{3.3.71}$$

where $\boldsymbol{A} : \boldsymbol{B} = \sum_{\mu\nu=1}^{3N} A_{..\mu\nu}B_{\mu\nu..}$. The definition of the non-interacting two-phonon propagator $\boldsymbol{\chi}^{(0)}(\omega)$ (Eq. (3.3.56)) is one reported by Ref. 56 in Eq. (72) multiplied by $-1/2$ so that all the definitions are consistent. Physical phonon frequencies and lifetimes are determined by real and imaginary parts of $\overleftrightarrow{\boldsymbol{\mathcal{G}}}(\omega+i0^+)$, Eq. (3.3.70), as discussed in Ref. 50. In addition, we remark that the polarization vectors can also change when adding dynamical effects, so polarization-mixing is automatically included in Eq. (3.3.70). The bubble diagram is the

lowest-order approximation for the self-energy,

$$\overleftrightarrow{\mathbf{\Pi}}(\omega) = \overset{(3)}{\boldsymbol{D}} : \boldsymbol{\chi}^{(0)}(\omega) : \overset{(3)}{\boldsymbol{D}} \tag{3.3.72}$$

as described in Eq. (3.3.71), and is incorporated in many self-consistent phonon (SCP) calculations within the improved SCP (ISCP) framework.[165,170–172] TD-SCHA provides a solid first-principle justification to the application of Eq. (3.3.72) and provides a path to move beyond the bubble approximation.

For the two-phonon case, we proceed as before. We use the definition of $\boldsymbol{r}_\chi/\boldsymbol{p}_\chi$ (Eq. (3.3.63b)) to reabsorb the one-phonon sector of $\boldsymbol{\mathcal{L}}(\omega)$ (*i.e.* the row $\boldsymbol{\mathcal{L}}(\omega)_{1j}$ and column $\boldsymbol{\mathcal{L}}(\omega)_{j1}$ with $j = 1, 2, 3$) into the two-phonon sector. So we solve

$$\boldsymbol{\chi}(\omega) = \boldsymbol{r}_\chi \cdot \boldsymbol{\mathcal{L}}(\omega)^{-1} \cdot \boldsymbol{p}_\chi = \sum_{ij}^{1,2} \left(\boldsymbol{\mathcal{L}}_{2\text{ph}}(\omega)^{-1}\right)_{ij} \tag{3.3.73}$$

where $\boldsymbol{\mathcal{L}}_{2\text{ph}}(\omega)$ is a 2×2 block-matrix

$$\boldsymbol{\mathcal{L}}_{2\text{ph}}(\omega) = \begin{bmatrix} \boldsymbol{\chi}_-^{(0)}(\omega)^{-1} - \boldsymbol{\Sigma}(\omega) & -\boldsymbol{\Sigma}(\omega) \\ -\boldsymbol{\Sigma}(\omega) & -\boldsymbol{\chi}_+^{(0)}(\omega)^{-1} - \boldsymbol{\Sigma}(\omega) \end{bmatrix}. \tag{3.3.74}$$

$\boldsymbol{\Sigma}(\omega)$ is the two-phonon self-energy

$$\boldsymbol{\Sigma}(\omega) = \boldsymbol{\Sigma}(\omega)^\dagger = \overset{(4)}{\boldsymbol{D}} + \overset{(3)}{\boldsymbol{D}} \cdot \overleftrightarrow{\boldsymbol{\mathcal{G}}}^{(0)}(\omega) \cdot \overset{(3)}{\boldsymbol{D}} \tag{3.3.75}$$

where single phonon excitations enter in $\boldsymbol{\Sigma}(\omega)$ via the three-phonon vertex. Graphically, Eq. (3.3.73) corresponds to

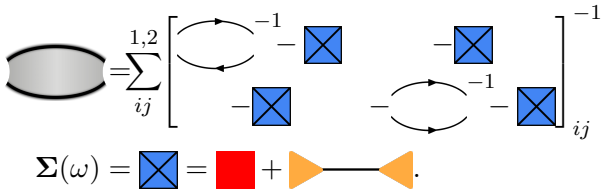

(3.3.76)

Again we use Eq. (3.3.66) to invert Eq. (3.3.74) and we end up with the interacting two-phonon propagator

$$\boldsymbol{\chi}(\omega) = \boldsymbol{\chi}^{(0)}(\omega) + \boldsymbol{\chi}^{(0)}(\omega) : \boldsymbol{\Sigma}(\omega) : \boldsymbol{\chi}(\omega) \tag{3.3.77}$$

with $\boldsymbol{\Sigma}(\omega)$, Eq. (3.3.75), being the TD-SCHA two-phonon self-energy. We find that, in the two-phonon propagation, there is the possibility of either decay in a single phonon through the third-order scattering vertex or in another pair through the fourth-order scattering vertex. There are no higher-order decay processes. For the mixed propagator, we proceed as before. The form of $\boldsymbol{p}_\Gamma/\boldsymbol{r}_\Gamma$ (Eq. (3.3.63c)) allows single phonon excitations to be triggered by two-phonon propagation via the three-phonon vertex, leading to a non-zero one-two phonon propagation

$$\boldsymbol{\Gamma}(\omega) = \overleftrightarrow{\boldsymbol{\mathcal{G}}}^{(0)}(\omega) \cdot \overset{(3)}{\boldsymbol{D}} : \boldsymbol{\chi}(\omega). \tag{3.3.78}$$

We demonstrate that Eqs. (3.3.70) (3.3.77) are the fundamental components of the TD-SCHA response. The relationship between these two propagators becomes clear when

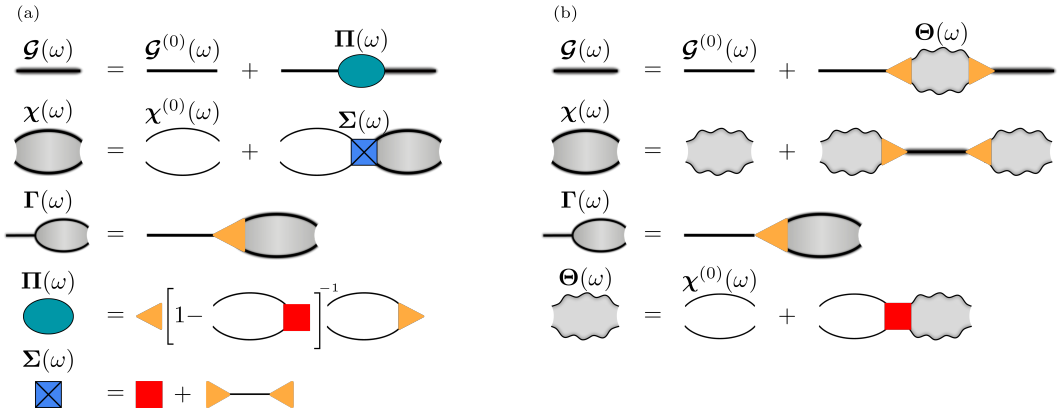

Figure 3.5. In a) we report the diagrammatic expression of the interacting one, two and one-two phonon Green's functions, Eqs (3.3.70) (3.3.77) (3.3.78). In b) we show Eqs (3.3.79). Thinner solid lines represent the non-interacting SCHA propagators $\overleftrightarrow{\mathcal{G}}^{(0)}(\omega)$ and $\boldsymbol{\chi}^{(0)}(\omega)$, defined in Eqs (3.3.70) (3.3.77). The three/four-phonon scattering vertices are defined in Eqs (3.3.58) (3.3.59) and represented as orange triangles and red squares.

expressed in terms of the partially screened two-phonon propagator $\boldsymbol{\Theta}(\omega)=\boldsymbol{\chi}(\omega)|_{\overset{(3)}{\boldsymbol{D}}=0}$ in which a phonon pair propagates only through the four phonon scattering vertex. Note that $\boldsymbol{\Theta}(\omega)$ generalizes in the dynamical regime Eq. (26) of Ref. 56. As proved in appendix 3.G, the new expressions for the propagators are

$$\overleftrightarrow{\mathcal{G}}(\omega) = \overleftrightarrow{\mathcal{G}}^{(0)}(\omega) + \overleftrightarrow{\mathcal{G}}^{(0)}(\omega) \cdot \overset{(3)}{\boldsymbol{D}} : \boldsymbol{\Theta}(\omega) : \overset{(3)}{\boldsymbol{D}} \cdot \overleftrightarrow{\mathcal{G}}(\omega), \tag{3.3.79a}$$

$$\boldsymbol{\chi}(\omega) = \boldsymbol{\Theta}(\omega) + \boldsymbol{\Theta}(\omega) : \overset{(3)}{\boldsymbol{D}} \cdot \overleftrightarrow{\mathcal{G}}(\omega) \cdot \overset{(3)}{\boldsymbol{D}} : \boldsymbol{\Theta}(\omega), \tag{3.3.79b}$$

$$\boldsymbol{\Theta}(\omega) = \boldsymbol{\chi}^{(0)}(\omega) + \boldsymbol{\chi}^{(0)}(\omega) : \overset{(4)}{\boldsymbol{D}} : \boldsymbol{\Theta}(\omega). \tag{3.3.79c}$$

Now, only $\overleftrightarrow{\mathcal{G}}(\omega)$ and $\boldsymbol{\Theta}(\omega)$ have a Dyson form, whereas $\boldsymbol{\chi}(\omega)$ has a different structure where single and double propagations are disentangled. Fig. 3.5 summarizes the diagrammatic expressions for the interacting propagators. In panel a) we report Eqs (3.3.70) (3.3.77) (3.3.78), while panel b) shows Eqs (3.3.79).

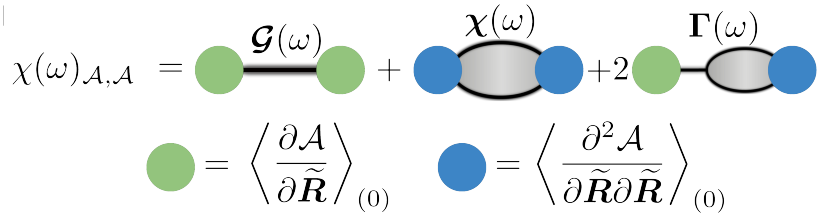

Figure 3.6. Diagrammatic expression of the processes included in the fully interacting response, Eq. (3.3.49), if $\mathcal{A} = \mathcal{B}$. The interacting TD-SCHA Green's functions are reported in Eqs (3.3.70) (3.3.77) (3.3.78). The green vertex is related to the first entry of $\boldsymbol{p}/\boldsymbol{r}$ while the blue vertex is to the second and third entries of $\boldsymbol{p}/\boldsymbol{r}$, see Eqs. (3.3.50).

By computing all the TD-SCHA interacting propagators, we gain a complete comprehension of the diagrammatic expression summarized in Fig. 3.6 for the TD-SCHA response function $\chi(\omega)_{\mathcal{A},\mathcal{A}}$ (Eq. (3.3.49)). In fact, Eq. (3.3.49) can be decomposed into the interacting propagators. One-phonon processes $\overleftrightarrow{\mathcal{G}}(\omega)$ are coupled to first-order position derivatives

of the perturbation, first entry of $\boldsymbol{p}/\boldsymbol{r}$ Eqs (3.3.50). On the other hand, two-phonon excitations $\boldsymbol{\chi}(\omega)$ and $\boldsymbol{\Gamma}(\omega)$ are triggered by non-zero second-order position derivatives of the perturbation, second and third entries of $\boldsymbol{p}/\boldsymbol{r}$ Eqs. (3.3.50).

3.3.5 Multiple excitations in TD-SCHA

The Gaussian approximation defines a hierarchy of diagrams that is truncated at the two-phonon level. In this Section, we demonstrate that, in TD-SCHA, all higher-order phonon propagators are related to the Green's functions of Eqs (3.3.70) (3.3.77) (3.3.78).

For example, the three-phonon propagator is obtained setting in Eq. (3.3.49) a tensor-like perturbation/response functions

$$\mathcal{A} = \delta\widetilde{R}^{(0)}_{\alpha}\delta\widetilde{R}^{(0)}_{\beta}\delta\widetilde{R}^{(0)}_{\gamma} \qquad \mathcal{B} = \delta\widetilde{R}^{(0)}_{\mu}\delta\widetilde{R}^{(0)}_{\nu}\delta\widetilde{R}^{(0)}_{\eta}. \tag{3.3.80}$$

In this case, only the first entries of $\boldsymbol{p}/\boldsymbol{r}$, i.e. $\left\langle \partial\mathcal{A}/\partial\widetilde{\boldsymbol{R}}\right\rangle_{(0)}$, are non-zero. This means that in the case of Eq. (3.3.80) we have a one-phonon response, as the one obtained for $\boldsymbol{\mathcal{G}}(\omega)$ (Eq. (3.3.63a)). As computed in Appendix 3.G, the three-phonon response is

$$\begin{aligned}\chi^{\alpha\beta\gamma}_{\mu\nu\eta}(\omega) &= \mathcal{G}^{(0)}(t{=}0^-)_{\beta\gamma}\mathcal{G}^{(0)}(t{=}0^-)_{\nu\eta}\mathcal{G}(\omega)_{\alpha\mu} \\ &+ \text{permutations of } (\alpha\beta\gamma) \text{ and } (\mu\nu\eta)\end{aligned} \tag{3.3.81}$$

and in Fig. 3.7 we report its diagrammatic structure. This contains the one-phonon Green's function $\boldsymbol{\mathcal{G}}(\omega)$, Eq. (3.3.70), and a disconnected part, $\boldsymbol{\mathcal{G}}^{(0)}(t=0^-)$ which comes from the averages $\left\langle \delta\widetilde{\boldsymbol{R}}\delta\widetilde{\boldsymbol{R}}\right\rangle_{(0)}$ (Eq. (3.3.36)) in $\left\langle \partial\mathcal{A}/\partial\widetilde{\boldsymbol{R}}\right\rangle_{(0)}$.

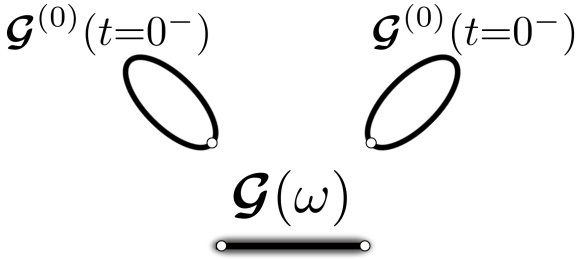

Figure 3.7. Diagrammatic expression for the TDSCHA interacting three-phonon Green's function obtained as a response to a cubic perturbation, Eq. (3.3.80). In TDSCHA, the tree-phonons propagator is a disconnected diagram.

In this case, the SCHA correction, $\boldsymbol{\mathcal{G}}^{(0)}(t=0^-)$, does not enter the phonon propagation but it dresses the interaction with the external probe. This means that if we take a scalar perturbation

$$\mathcal{A} = \mathcal{B} = \frac{1}{3}\sum_{\alpha\beta\gamma=1}^{3N} K_{\alpha\beta\gamma}\delta\widetilde{R}^{(0)}_{\alpha}\delta\widetilde{R}^{(0)}_{\beta}\delta\widetilde{R}^{(0)}_{\gamma}, \tag{3.3.82}$$

with $K_{\alpha\beta\gamma}$ a tensor that does not depend on atomic positions, $\boldsymbol{\mathcal{G}}^{(0)}(t=0^-)$ is contracted with $\boldsymbol{K}$.

Similarly, all the higher-order propagators, i.e. those obtained with

$$\mathcal{A} \sim \left(\delta\widetilde{R}^{(0)}\right)^{n-2} \qquad \mathcal{B} \sim \left(\delta\widetilde{R}^{(0)}\right)^{m-2} \qquad m,n>2, \tag{3.3.83}$$

give disconnected diagrams. In all these cases we will get a $\chi_{\mathcal{A},\mathcal{B}}(\omega)$ that contains only one of the TDSCHA propagators (Eqs (3.3.70) (3.3.77) (3.3.78)) along witha disconnected part that depends only on $\boldsymbol{\mathcal{G}}^{(0)}(t=0^-)$, Eq. (3.3.36).

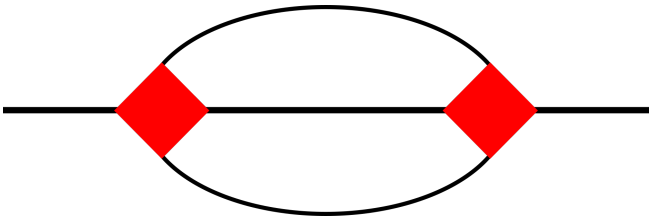

Figure 3.8. Diagrammatic expression for the Saturn diagram with a three SCHA phonon propagation (solid lines are the propagators of Eq. (3.3.55)). The red vertex is the four-phonon scattering vertex Eq. (3.3.59) which leads to three phonon excitations. This class of diagrams is missed by TDSCHA where we can not connect a single SCHA line to the four-phonon scattering vertex.

Hence, the TD-SCHA can not capture processes beyond a two-phonon mechanism: the propagators of Eqs. (3.3.70) (3.3.77) (3.3.78) serve as the building blocks of the response. This means that there are general rules in the symbolic inversion of $\boldsymbol{\mathcal{L}}(\omega)$ (see Eq. (3.3.51)). In Fig. 3.3 the solid line (one-phonon SCHA propagator of Eq. (3.3.56)) is always attached to one extremity of the orange triangle (Eq. (3.3.58)). The double solid line (two-phonon SCHA propagator Eq. (3.3.56)) is connected to two extremities either of the red square (four phonon vertex Eq. (3.3.59)) or of the orange triangle (three phonon vertex Eq. (3.3.58)).

We do not get three or more SCHA phonon resonances. One example is the 'Saturn' diagram (Fig. 3.8) which is missed by our method. This diagram would correspond to a single SCHA propagator attached to the four-phonon vertex and this is not contained in TDSCHA. Notably, the TDSCHA diagrams arise from the stationary action principle of quantum mechanics,[65,66] ensuring that there is no double counting and that the theory is consistent. The inclusion of new scattering mechanisms, such as Fig. 3.8, must be approached with extreme care to avoid compromising the internal coherence and overcounting some anharmonic processes.

3.4 Thermal transport in TD-SCHA

Let us briefly recap our discussion so far. In Sec. 3.1 using the MEP and the modified Liouville equation, we have derived a generalization for the Kubo formula for thermal conductivity applicable in self-consistent systems (3.1.20). The ingredients needed to calculate thermal conductivity in a self-consistent scheme are the self-consistent heat flux $\hat{\boldsymbol{\mathcal{J}}}$, the self-consistent global equilbrium density matrix $\hat{\varrho}^{(0)}$ and the self-consistent Liouville superoperator $\mathcal{L}_{sc}$. Throughout this Chapter, we have obtained the definitions of $\hat{\varrho}^{(0)}$ [Eq. (3.2.27a)], $\hat{\boldsymbol{\mathcal{J}}}$ [Eq. (3.2.30)] in SCHA and of $\mathcal{L}_{sc}$ [Eq. (3.3.51)] in TD-SCHA. We are thus ready to combine those ingredients to obtain an expression of the lattice thermal conductivity in TD-SCHA.

However, we have discussed in Sec. 3.3.2 how the dynamical response function in TD-SCHA is completely determined once the response and perturbation vectors $\boldsymbol{r}/\boldsymbol{p}$ are determined. Moreover, the TD-SCHA Liouville operator $\mathcal{L}_{sc}$ possess a compact formulation only when expressed in terms of the linear operator that determines the equations of motion of the parameters $(\vec{\boldsymbol{\mathcal{R}}}^{(1)}, \overleftrightarrow{\boldsymbol{\alpha}}^{(1)}, \overleftrightarrow{\boldsymbol{\beta}}^{(1)})$ (cf. Eq. (3.3.45). Since $\boldsymbol{p}$ only depend on the external potential $\hat{V}_{\text{ext}}$ (3.3.42), the most convenient way to obtain the thermal conductivity in TD-SCHA is to reconstruct a "thermal" potential from the modified Liouville equation approach of Sec. 3.1.

In other words, we want to express the thermal conductivity (3.1.18) as a response function computed in TD-SCHA formalism as in Eq. (3.3.49), *i.e.*

$$\kappa(i\epsilon)^{xy} \sim \boldsymbol{r}^x \cdot \boldsymbol{\mathcal{L}}(i\epsilon)^{-1} \cdot \boldsymbol{p}^y \tag{3.4.1}$$

We have discussed in Sec. 1.2 the conceptual differences between the mechanical and the maximum entropy approaches to derive the equations for thermal conductivity, and how the two can coincide in linear response if the sign of the thermal potential (1.1.9) is flipped.

Let us take few steps back in the derivation of the self-consistent conductivity (3.1.18). Performing the time integral in the steady-state solution of the modified self-consistent Liouville equation Eq. (3.1.8), we get

$$\hat{\varrho}^{\epsilon}_{st} = \frac{1}{\hbar i\epsilon - \mathcal{L}_{sc}} \mathcal{L}_{sc}\hat{\varrho}_{loc} \,. \tag{3.4.2}$$

If we use the Kubo identity (1.A.7), we get from Eq. (3.1.14) that

$$\mathcal{L}_{sc}\hat{\varrho}_{loc} = [-\int \mathrm{d}\boldsymbol{x}\, \frac{\delta\beta(\boldsymbol{x})}{\beta} \hat{h}^{(0)}(\boldsymbol{x}), \hat{\varrho}^{(0)}], \tag{3.4.3}$$

so that

$$\hat{\varrho}^{\epsilon}_{st} = \frac{1}{\hbar i\epsilon - \mathcal{L}_{sc}} [-\int \mathrm{d}\boldsymbol{x}\, \frac{\delta\beta(\boldsymbol{x})}{\beta} \hat{h}^{(0)}(\boldsymbol{x}), \hat{\varrho}^{(0)}]. \tag{3.4.4}$$

Instead, if we consider the TD-SCHA Liouville equation for the induced density matrix $\hat{\varrho}^{(1)}$ at linear order in $\hat{V}_{\text{ext}}$, we get in frequency domain (cf. Eq. 65 of Ref. 65)

$$\hat{\varrho}^{(1)}(\omega) = \frac{1}{\hbar\omega - \mathcal{L}_{sc}} [\hat{V}_{\text{ext}}(\omega), \hat{\varrho}_0] \,. \tag{3.4.5}$$

Comparing (3.4.4) and (3.4.5) and with the identification $\omega \to i\epsilon$, we can identify the term in (3.4) as the static limit of a thermal self-consistent potential to be used in TD-SCHA calculations, *i.e.*

$$\hat{V}_{\text{ext}}(\omega)\Big|_{\omega=0} = -\int \mathrm{d}\boldsymbol{x}\, \frac{\delta\beta(\boldsymbol{x})}{\beta} \hat{h}^{(0)}(\boldsymbol{x}) \,. \tag{3.4.6}$$

In fact, we have already discussed in Sec. (1.2), how the pre-ϵ-limit $\hat{\varrho}^{\epsilon}_{st}$ plays the role of the induced density matrix $\hat{\rho}^{(1)}$ usually considered in adiabatic switching-on procedure. Notice the sign change in the TD-SCHA thermal potential consistent with the discussion of (1.1.9). Our procedure then consist in considering the mechanical proxy for the self-consistent thermal potential

$$\hat{V}_{\text{ext}}(\omega) = -\int \mathrm{d}\boldsymbol{x}\, \frac{\delta\beta(\boldsymbol{x})}{\beta} \hat{h}^{(0)}(\boldsymbol{x},\omega) \simeq -\frac{V}{\beta} \sum_{\sigma}^{x,y,z} \boldsymbol{\nabla}^{\sigma} \beta \frac{\hat{\mathcal{J}}^{\sigma}(\omega)}{i\omega} \tag{3.4.7}$$

and compute the expectation value of the heat-flux operator $\hat{\boldsymbol{J}}$ in the spirit of (3.3.47) in terms of "thermal" (th) response and perturbation vectors

$$\langle \hat{J}^{\gamma} \rangle_{\varrho^{(1)}(\omega)} \sim -\sum_{\sigma}^{x,y,z} \boldsymbol{r}^{\gamma}_{\text{th}} \cdot \boldsymbol{\mathcal{L}}(\omega)^{-1} \cdot \boldsymbol{p}^{\sigma}_{\text{th}} \boldsymbol{\nabla}^{\sigma} T \,, \tag{3.4.8}$$

using the established TD-SCHA procedure. The precise structure of the frequency dependent

heat flux (3.4.8) is still to be defined. We then obtain the thermal conductivity as

$$\kappa^{xy} = -\lim_{\epsilon\to 0^+}\lim_{\omega\to 0}\frac{\partial\langle\hat{J}^x\rangle_{\varrho^{(1)}(\omega+i\epsilon)}}{\partial\boldsymbol{\nabla}^y T}\,. \tag{3.4.9}$$

It is important to stress that even if the adiabatic switching-on of a thermal potential can provide an equivalent expression of thermal conductivity obtain with the MEP and the modified Liouville equation in the perturbative approaches discussed in Chapter 1 (if the sign of the thermal potential is changed, cf. Appendix 1.A), it is not interchangeable with our procedure for self-consistent schemes. In fact, in the adiabatic switching-on approach, the thermal potential is identified from the expansion of the local equilibrium operator $\hat{\rho}_{loc}$ at linear order in the temperature field,[44] as discussed in (1.1.9). In self-consistent schemes, the expansion of the local equilibrium density matrix $\hat{\varrho}_{loc}$ does not provide a straighforward derivation of a thermal potential, as discussed in Eqs. (3.1.10)-(3.1.13). Instead, the identification of a thermal self-consistent potential is possible when studying $\mathcal{L}_{sc}\hat{\varrho}_{loc}$, featuring in the expression of the steady-state self-consistent density matrix , obtained from the modified Liouville approach developed in Sec. 3.1.

3.4.1 Thermal potential in TD-SCHA and perturbation vector

The definition (3.3.50) of the perturbation and response vectors $\boldsymbol{r}/\boldsymbol{p}$ is slightly modified in the case of thermal transport. Let us start from the definition of $\boldsymbol{p}$. The perturbation vector in (3.3.50) is derived from the assumption that the external potential (3.3.42) only depends on the ionic position $\vec{\boldsymbol{R}}$. The thermal potential (3.4.7) features the heat flux $\hat{\boldsymbol{\mathcal{J}}}$ defined in (3.2.30), which depends both on the ionic positions and momenta $\vec{\boldsymbol{R}}, \vec{\boldsymbol{P}}$. Thus, the thermal potential (3.4.11a) is not in the form (3.3.42).

Using the definition of the self-consistent heat flux (3.2.30), and considering that the Wigner transform of a product of operators (Moyal product[13,163]) is

$$(\hat{A}\hat{B})_{\mathrm{w}}(\vec{\boldsymbol{R}},\vec{\boldsymbol{P}}) = A_{\mathrm{w}}(\vec{\boldsymbol{R}},\vec{\boldsymbol{P}})e^{-\frac{\hbar}{2i}\hat{\boldsymbol{\Lambda}}}B_{\mathrm{w}}(\vec{\boldsymbol{R}},\vec{\boldsymbol{P}})\,, \tag{3.4.10}$$

the Wigner transform of the thermal TD-SCHA potential is

$$V_{\mathrm{ext}}(\vec{\boldsymbol{R}},\vec{\boldsymbol{P}},\omega) = -\frac{V}{\beta}\sum_{\sigma}^{x,y,z}\boldsymbol{\nabla}\beta^{\sigma}\frac{\mathcal{J}^{\sigma}(\vec{\boldsymbol{R}},\vec{\boldsymbol{P}},\omega)}{i\omega} \tag{3.4.11a}$$

$$\mathcal{J}^{y}(\vec{\boldsymbol{R}},\vec{\boldsymbol{P}},\omega) = \sum_{\mu\nu}\mathcal{J}^{y}_{\mu\nu}\delta\widetilde{R}^{(0)}_{\mu}\widetilde{P}_{\nu}\,. \tag{3.4.11b}$$

where the self-consistent heat flux in the SCHA eigenmode basis reads in Eq. (3.4.11b) features the self-consistent heat flux matrix

$$\mathcal{J}^{y}_{\mu\nu} = \frac{1}{2V}\sum_{ab}^{N}(\mathcal{R}^{y(0)}_{a}-\mathcal{R}^{y(0)}_{b})\sum_{\alpha\beta}^{x,y,z}D^{\alpha,\beta}_{a,b}e^{\alpha}_{a,\mu}e^{\beta}_{b,\nu}\,, \tag{3.4.12}$$

which has the dimensions of a phonon velocity times a phonon frequency, and it is anti-symmetric $\mathcal{J}^{y}_{\mu\nu}=-\mathcal{J}^{y}_{\nu\mu}$. In Appendix 3.E we derive the expression of the perturbation vector in presence of a potential of the form (3.4.11). Its expression in the basis $(\vec{\boldsymbol{\mathcal{R}}}^{(1)}, \overleftrightarrow{\boldsymbol{a}}^{(1)}, \overleftrightarrow{\boldsymbol{b}}^{(1)})$ in

which the Liouville operator $\mathcal{L}(\omega)$ has the form (3.3.51) is

$$-\sum_{\sigma}^{x,y,z} \boldsymbol{p}^{\sigma}_{\mathrm{th},\mu\nu} \boldsymbol{\nabla}^{\sigma} T = -\sum_{\sigma}^{x,y,z} \frac{V}{T} \begin{bmatrix} 0 \\ \frac{1}{c_{\mu\nu}} \mathcal{J}^{\sigma}_{\mu\nu} \\ c_{\mu\nu} \mathcal{J}^{\sigma}_{\mu\nu} \end{bmatrix} \boldsymbol{\nabla}^{\sigma} T \tag{3.4.13}$$

where

$$c_{\mu\nu} = \frac{\omega_{\nu} - \omega_{\mu}}{\omega_{\mu} + \omega_{\nu}}. \tag{3.4.14}$$

The component of the perturbation vector $\boldsymbol{p}_{\mathrm{th},\mu\nu}$ related to $\boldsymbol{\mathcal{R}}^{(1)}$ is zero, *i.e.* the perturbation vector has the form (3.3.63b). This signals that the thermal conductivity only depends on the two-phonon Green's function, as expected from the many-body formulation of thermal transport discussed in Chapter 2.

3.4.2 Response vector in thermal TD-SCHA

The response vector $\boldsymbol{r}$ is related to the physical quantity we want to observe when the system is perturbed by the external potential. The definition of $\boldsymbol{r}$ presented in Eq. (3.3.50) assumes that the observable we study depends only on the ionic positions $\vec{\boldsymbol{R}}$. In thermal transport, we want to study the expectation value of the heat flux $\hat{\boldsymbol{J}}$, to deduce the thermal conductivity via Eq. (3.4.9). In general, the heat flux operator depends both on the ionic position and momenta.

As discussed in Sec. 3.1.3, the heat flux $\hat{\boldsymbol{J}}$ describing the flow of energy of the exact Hamiltonian $\hat{H}$ necessitates a perturbative truncation of the full Hamiltonian $\hat{H}$. In this thesis, we limit ourself to the evaluation of the thermal conductivity due to the harmonic heat flux of the form (2.2.10). In the notation adopted in this Chapter, the harmonic perturbative heat flux reads

$$\hat{J}^{x} = \frac{1}{2V} \sum_{ab}^{N} (\mathcal{R}_{\mathrm{BO}a}^{x} - \mathcal{R}_{\mathrm{BO}b}^{x}) \sum_{\alpha\beta}^{x,y,z} d_{a,b}^{\alpha,\beta} \delta \hat{R}_{\mathrm{BO}a}^{\alpha\,(0)} \frac{\hat{P}_{b}^{\beta}}{m_b}. \tag{3.4.15}$$

where the definitions of $\vec{\boldsymbol{\mathcal{R}}}_{\mathrm{BO}}$ and $\boldsymbol{d}$ where given in Sec. 3.3.1. By generalizing the expansion (3.E.19) to an operator that depends on the product $\hat{R}\hat{P}$ as (3.4.15), it is straightforward to show that the expectation value of $\hat{J}$ in TD-SCHA linear response is

$$\left\langle \hat{J}^{x} \right\rangle_{\rho^{(1)}(\omega)} = \sum_{\mu\nu} \frac{1}{\widetilde{\alpha}_{\mu}^{(0)} \widetilde{\beta}_{\nu}^{(0)}} J^{x}_{\mu\nu} \widetilde{\gamma}^{(1)}_{\mu\nu}(\omega) \tag{3.4.16}$$

where, as per (3.4.12), the (perturbative) heat flux matrix elements are defined as

$$\begin{aligned} J^{x}_{\mu\nu} &= \frac{1}{2V} \sum_{ab}^{N} (\mathcal{R}_{\mathrm{BO}a}^{x} - \mathcal{R}_{\mathrm{BO}b}^{x}) \sum_{\alpha\beta}^{x,y,z} d_{a,b}^{\alpha,\beta} e^{\alpha}_{a,\mu} e^{\beta}_{b,\nu} \,. \\ &= \frac{1}{V} \sqrt{\omega_{\mu}\omega_{\nu}} v^{x}_{\mu\nu} \,, \end{aligned} \tag{3.4.17}$$

where $v^{x}_{\mu\nu}$ corresponds to the definition of Hardy velocity matrix (2.2.16) in the (SCHA) phonon eigenmode basis. As discussed in the derivation of the dynamical equations in 3.E, the evolution of the matrix $\overleftrightarrow{\widetilde{\gamma}}^{(1)}(\omega)$ can be absorbed in the evolution of the parameters

$(\vec{\vec{\boldsymbol{\mathcal{R}}}}^{(1)}, \overleftrightarrow{\tilde{\boldsymbol{\alpha}}}^{(1)}, \overleftrightarrow{\tilde{\boldsymbol{\beta}}}^{(1)})$, or equivalently in the basis $(\vec{\vec{\boldsymbol{\mathcal{R}}}}^{(1)}, \overleftrightarrow{\tilde{\boldsymbol{a}}}^{(1)}, \overleftrightarrow{\tilde{\boldsymbol{b}}}^{(1)})$ used to define the diagrammatic expression of the TD-SCHA response (3.3.51)

$$\overleftrightarrow{\tilde{\gamma}}^{(1)}(\omega) = \frac{\partial \overleftrightarrow{\tilde{\gamma}}^{(1)}}{\partial \vec{\vec{\boldsymbol{\mathcal{R}}}}^{(1)}} \cdot \vec{\vec{\boldsymbol{\mathcal{R}}}}^{(1)}(\omega) + \frac{\partial \overleftrightarrow{\tilde{\gamma}}^{(1)}}{\partial \overleftrightarrow{\tilde{\boldsymbol{a}}}^{(1)}} : \overleftrightarrow{\tilde{\boldsymbol{a}}}^{(1)}(\omega) + \frac{\partial \overleftrightarrow{\tilde{\gamma}}^{(1)}}{\partial \overleftrightarrow{\tilde{\boldsymbol{b}}}^{(1)}} : \overleftrightarrow{\tilde{\boldsymbol{b}}}^{(1)}(\omega) \,. \tag{3.4.18}$$

Moreover, since the $\boldsymbol{\mathcal{R}}$ entry of the perturbation vector (3.4.13) is 0, the dynamics of $\vec{\vec{\boldsymbol{\mathcal{R}}}}^{(1)}$ can be expressed in terms of $(\overleftrightarrow{\tilde{\boldsymbol{a}}}^{(1)}, \overleftrightarrow{\tilde{\boldsymbol{b}}}^{(1)})$, as proven in Appendix (3.G). Henceforth, Eq. (3.G.22) can be plugged in Eq. (3.4.18) to obtain

$$\overleftrightarrow{\tilde{\gamma}}^{(1)}(\omega) = \left[\frac{\partial \overleftrightarrow{\tilde{\gamma}}^{(1)}}{\partial \vec{\vec{\boldsymbol{\mathcal{R}}}}^{(1)}} \cdot \overleftrightarrow{\boldsymbol{\mathcal{G}}}^{(0)}(\omega) \cdot \overset{(3)}{\boldsymbol{D}} + \frac{\partial \overleftrightarrow{\tilde{\gamma}}^{(1)}}{\partial \overleftrightarrow{\tilde{\boldsymbol{a}}}^{(1)}}\right] : \overleftrightarrow{\tilde{\boldsymbol{a}}}^{(1)}(\omega) + \left[\frac{\partial \overleftrightarrow{\tilde{\gamma}}^{(1)}}{\partial \vec{\vec{\boldsymbol{\mathcal{R}}}}^{(1)}} \cdot \overleftrightarrow{\boldsymbol{\mathcal{G}}}^{(0)}(\omega) \cdot \overset{(3)}{\boldsymbol{D}} + \frac{\partial \overleftrightarrow{\tilde{\gamma}}^{(1)}}{\partial \overleftrightarrow{\tilde{\boldsymbol{b}}}^{(1)}}\right] : \overleftrightarrow{\tilde{\boldsymbol{b}}}^{(1)}(\omega) \,. \tag{3.4.19}$$

The derivatives of $\overleftrightarrow{\tilde{\gamma}}^{(1)}(\omega)$ can be explicitly computed exploiting its dynamical equation (3.E.2d). In doing so and plugging (3.4.19) in (3.4.16), we obtain the expression of the response vector

$$\frac{1}{-i\omega}\boldsymbol{r}_{\mathrm{th},\mu\nu}(\omega)^x = \sum_{\eta\lambda} \frac{1}{-i\omega} J^x_{\mu\nu} c_{\mu\nu}(\omega_\mu + \omega_\nu)^2 \begin{bmatrix} 0 \\ \delta_{\mu\nu}\delta_{\eta\lambda} + \chi^{(0)}(0)_{\mu\nu\mu\nu}\Sigma(\omega)_{\mu\nu\eta\lambda} \\ \delta_{\mu\nu}\delta_{\eta\lambda} + \chi^{(0)}(0)_{\mu\nu\mu\nu}\Sigma(\omega)_{\mu\nu\eta\lambda} \end{bmatrix}, \tag{3.4.20}$$

where $\boldsymbol{\Sigma}(\omega)$ is the two-phonon self-energy (3.3.75), while

$$\chi_0(\omega{=}0)_{\mu\nu\mu\nu} = \frac{1}{2}\frac{\xi_\mu^2 - \xi_\nu^2}{\omega_\mu^2 - \omega_\nu^2} = \frac{1}{2}\frac{\partial \Upsilon_\mu^{-1}}{\partial \Phi_\nu} \tag{3.4.21}$$

is the static limit of the bare two-phonon propagator in SCHA.[56] In the case of thermal TD-SCHA, the response vector acquires a frequency dependence through the two-phonon self-energy $\boldsymbol{\Sigma}(\omega)$. Note that the $\frac{1}{i\omega}$ factor in (3.4.20) follows from the integration of the equation of motion of $\overleftrightarrow{\tilde{\gamma}}^{(1)}(\omega)$.

3.4.3 Thermal conductivity in TD-SCHA

Combining the definitions of the perturbation and response vectors obtained in (3.4.13) and (3.4.20), we can compute the thermal conductivity in TD-SCHA from (3.4.9), obtaining

$$\kappa^{xy} = \lim_{\epsilon\to 0^+}\lim_{\omega\to 0} \frac{1}{-i\omega}\boldsymbol{r}_{\mathrm{th}}(\omega)^x \cdot \boldsymbol{\mathcal{L}}_{2\mathrm{ph}}(\omega)^{-1} \cdot \boldsymbol{p}^y_{\mathrm{th}}\Big|_{\omega=\omega+i\epsilon}, \tag{3.4.22}$$

where the presence of the two-phonon progapator defined in (3.3.74) follows from the structure of $\boldsymbol{r}_{\mathrm{th}}/\boldsymbol{p}_{\mathrm{th}}$. It is interesting to note that, since the response and the pertubation vectors both feature matrix elements of heat-flux operators, Eq. (3.4.22) is reminiscent of the static limit of the current current correlation function divided by ω, used in (2.1.5) to obtain thermal conductivity in a many-body approach. As per (2.1.5), the evaluation of the thermal conductivity (3.4.22) in TD-SCHA can be seen as a static limit of a retarded response function,

analytically extended in the complex frequency $z=\omega+i\epsilon$. By virtue of the analytic properties of the retarded response functions, the limits in (3.4.22) can be inverted

$$\kappa^{xy} = \lim_{\omega\to 0} \frac{1}{-i\omega} \boldsymbol{r}_{\text{th}}(\omega+i0^+)^x \cdot \boldsymbol{\mathcal{L}}_{\text{2ph}}(\omega+i0^+)^{-1} \cdot \boldsymbol{p}^y_{\text{th}} \,. \tag{3.4.23}$$

Eq. (3.4.23) is a remarkable result since it is the exact analogue of the expression (2.1.5) obtained using the fluctuation-dissipation theorem but derived from a completely different perspective. The explicit expression of (3.4.23) is quite complicated. We will first consider it in the harmonic case, *i.e.* by turning off all the anharmonic scattering vertices. Then, we will present some consideration on the fully anharmonic case.

Harmonic limit of the TD-SCHA thermal conductivity

The harmonic limit of TD-SCHA can be obtained by assuming that the BO energy surface is perfectly quadratic, *i.e.* the derivatives $\overset{(n)}{\boldsymbol{d}}$ of the BO potential defined in (3.3.31) are 0 for $n>2$. Clearly, this approximation also results in $\boldsymbol{D}=\boldsymbol{d}$, $\overset{(3)}{\boldsymbol{D}}=\overset{(4)}{\boldsymbol{D}}=\boldsymbol{\Sigma}=0$, and $\boldsymbol{J}=\boldsymbol{\mathcal{J}}$. In this case, the two-phonon propagator (3.3.74) is diagonal, and the harmonic thermal conductivity obtained from (3.4.22) reads

$$\kappa^0(\omega)^{xy} = \frac{V}{T} \sum_{\mu\nu\eta\lambda\xi\zeta} \frac{1}{-i\omega} J^x_{\mu\nu} c_{\mu\nu} (\omega_\mu + \omega_\nu)^2 \begin{bmatrix} \delta_{\mu\nu}\delta_{\eta\lambda} \\ \delta_{\mu\nu}\delta_{\eta\lambda} \end{bmatrix} \begin{bmatrix} \boldsymbol{\chi}^{(0)}_-(\omega) & 0 \\ 0 & -\boldsymbol{\chi}^{(0)}_+(\omega) \end{bmatrix}_{\eta\lambda\xi\zeta} \begin{bmatrix} c^{-1}_{\xi\zeta} \\ c_{\xi\zeta} \end{bmatrix} J^y_{\xi\zeta} \,. \tag{3.4.24}$$

In the TD-SCHA formulation, the thermal conductivity naturally appears as a sum of a resonant and a antiresonant term (within the adopted convention of the heat flux). We have thoroughly discussed in Chapter 2 how the antiresonant contribution to thermal conductivity is typically negligible with respect to the resonant term[110,173] (cf. Fig. 2.4). Thus, we focus on the analysis of the resonant part of (3.4.24), which reads

$$\kappa^0_{\text{R}}(\omega)^{xy} = \sum_{\mu\nu} (\omega_\mu + \omega_\nu)^2 J^x_{\mu\nu} \frac{\chi^{(0)}_-(\omega)_{\mu\nu\mu\nu}}{-i\omega} J^y_{\mu\nu} \,, \tag{3.4.25}$$

having exploited the Kronecker deltas featuring in the expression of $\boldsymbol{\chi}_-$ [Eq. (3.3.57a)]. In a procedure similar to the calculation done in (2.C.10), it is possible to show that

$$\lim_{\omega\to 0} \frac{\chi^{(0)}_-(\omega+i0^+)_{\mu\nu\mu\nu}}{-i\omega} = \frac{\hbar}{4\omega_\mu\omega_\nu} [-\frac{\partial n_\mu}{\partial \hbar\omega_\mu}] \pi\delta(\omega_\mu - \omega_\nu) \tag{3.4.26}$$

and, using the relation between $\boldsymbol{J}_{\mu\nu}$ and the velocity matrix $\boldsymbol{v}_{\mu\nu}$ (3.4.17), the expression (3.4.25) yields

$$\kappa^{0\,xy}_{\text{R}} = \frac{\hbar^2}{VT} \sum_{\mu\nu} \frac{(\omega_\mu + \omega_\nu)^2}{4} v^x_{\mu\nu} v^y_{\mu\nu} [-\frac{\partial n_\mu}{\partial \hbar\omega_\mu}] \pi\delta(\omega_\mu - \omega_\nu) \,. \tag{3.4.27}$$

The Dirac delta in (3.4.27) signals the divergence of the thermal conductivity, as expected for a harmonic crystal.

Eq. (3.4.25) consists in a fundamental result of this thesis. It corresponds precisely to the harmonic $\Gamma\to 0$ limit of the resonant thermal conductivity (2.3.10b) computed in Chapter 2 from a many-body Green's function approach.[110] Thus, from a completely different

framework based on the MEP, modified Liouville equation and the dynamical generalization of the SCHA, we are able to recover in the harmonic limit the result obtained from a well-established theoretical approach based on perturbation theory. Such discussion is a proof of validity of our novel first-principle approach to tackle thermal transport in self-consistent systems.

Anharmonic TD-SCHA thermal conductivity

Considering the explicit definition of the two-phonon propagator (3.3.74), we can express the thermal conductivity (3.4.22)

$$\begin{aligned}\kappa(\omega)^{xy}=&\frac{V}{T}\sum_{\substack{\mu\nu\eta\\ \lambda\xi\zeta}}\frac{1}{-i\omega}J^x_{\mu\nu}c_{\mu\nu}(\omega_\mu+\omega_\nu)^2\\ &\times\begin{bmatrix}\boldsymbol{S}+\boldsymbol{\chi}^{(0)}(0):\boldsymbol{\Sigma}(\omega)\\ \boldsymbol{S}+\boldsymbol{\chi}^{(0)}(0):\boldsymbol{\Sigma}(\omega)\end{bmatrix}\begin{bmatrix}\boldsymbol{\chi}^{(0)}_-(\omega)^{-1}-\boldsymbol{\Sigma}(\omega) & -\boldsymbol{\Sigma}(\omega)\\ -\boldsymbol{\Sigma}(\omega) & -\boldsymbol{\chi}^{(0)}_+(\omega)^{-1}-\boldsymbol{\Sigma}(\omega)\end{bmatrix}^{-1}_{\substack{\mu\nu\eta\lambda\\ \eta\lambda\xi\zeta}}\begin{bmatrix}\frac{1}{c_{\xi\zeta}}\\ c_{\xi\zeta}\end{bmatrix}\mathcal{J}^y_{\xi\zeta}\,.\end{aligned}\tag{3.4.28}$$

By noting that the response vector has equal entries, we can exploit the property of the symbolic inversion proven in (3.G.27) to separate Eq. (3.4.28) explicitly in a resonant and antiresonant conductivity

$$\kappa(\omega)^{xy}=\kappa_R(\omega)^{xy}+\kappa_A(\omega)^{xy}\tag{3.4.29a}$$

$$\kappa_R(\omega)^{xy}=\frac{V}{T}\sum_{\substack{\mu\nu\eta\\ \lambda\xi\zeta}}J^x_{\mu\nu}c_{\mu\nu}(\omega_\mu+\omega_\nu)^2\left[\boldsymbol{S}+\boldsymbol{\chi}^{(0)}(0):\boldsymbol{\Sigma}(\omega)\right]_{\mu\nu\eta\lambda}\left[\frac{1}{1-\boldsymbol{\chi}^{(0)}(\omega):\boldsymbol{\Sigma}(\omega)}:\frac{\boldsymbol{\chi}^{(0)}_-(\omega)}{-i\omega}\right]_{\eta\lambda\xi\sigma}\frac{1}{c_{\xi\zeta}}\mathcal{J}^y_{\xi\zeta}\tag{3.4.29b}$$

$$\kappa_A(\omega)^{xy}=\frac{V}{T}\sum_{\substack{\mu\nu\eta\\ \lambda\xi\zeta}}J^x_{\mu\nu}c_{\mu\nu}(\omega_\mu+\omega_\nu)^2\left[\boldsymbol{S}+\boldsymbol{\chi}^{(0)}(0):\boldsymbol{\Sigma}(\omega)\right]_{\mu\nu\eta\lambda}\left[\frac{1}{1-\boldsymbol{\chi}^{(0)}(\omega):\boldsymbol{\Sigma}(\omega)}:\frac{\boldsymbol{\chi}^{(0)}_+(\omega)}{i\omega}\right]_{\eta\lambda\xi\sigma}c_{\xi\zeta}\mathcal{J}^y_{\xi\zeta}\tag{3.4.29c}$$

Eqs. (3.4.29) is in one of the key results of this thesis. It consists in the first expression for the anharmonic thermal conductivity obtained from first principles in a fully self-consistent theoretical framework. Even if it is still a quite formal expression, it posses some important features that can be discussed. Let us analyze the resonant conductivity $\kappa_R(\omega)$ (3.4.29b). As expected in the discussion of the Kubo formula (3.1.18) for self-consistent systems, the thermal conductivity $\kappa_R(\omega)$ features two heat flux vertices $(\boldsymbol{J},\boldsymbol{\mathcal{J}})$. The heat flux vertex $\boldsymbol{J}$ is related to the operator $\hat{\boldsymbol{J}}$ introuced in Eq. (3.4.17) which is obtained from a perturbative truncation of the BO Hamiltonian at the harmonic level [Eq. (2.2.3)]. As such, it features bare phonon frequencies and velocities without any anharmonic renormalization. Instead, the self-consistent heat flux vertices $\boldsymbol{\mathcal{J}}$ would be associated with SCHA frequencies and velocities. We have discussed in Sec. (3.3.1) how the SCHA phonons can be intended as renormalized perturbative phonons considering an infinite set of specific diagrams (check Fig. 3.2).

The essential feature of Eq. (3.4.29b) is the term $\frac{\boldsymbol{\chi}^{(0)}_-(\omega)}{-i\omega}$. In fact, to obtain the expression of thermal conductivity, we still have to perform the static limit $\omega\to 0$. Comparing $\kappa_R(\omega)^{xy}$ with its harmonic counterpart $\kappa^0_R(\omega)^{xy}$ in Eq. (3.4.25), we note that even if the structure of the

vertices is different, both the harmonic and the anharmonic resonant thermal conductivities feature the bare resonant propagator $\chi_{-}^{(0)}(\omega)$ divided by ω. It follows from (3.4.26) that the static limit of $\frac{\chi_{-}^{(0)}(\omega)}{-i\omega}$ will be proportional to a Dirac delta and results in a divergent anharmonic thermal conductivity. Such shortcoming is an intrinsic limitation of the TD-SCHA. From the diagramatic interpretation presented in Sec. 3.3.3, we have a clear picture of the class of anharmonic scatterings included in the TD-SCHA phonon Green's functions. The two-phonon Green's function $\boldsymbol{\chi}(\omega)$ is renormalized by the self-energy $\boldsymbol{\Sigma}(\omega)$, which is purely real and do not provide any lifetime. As such, the TD-SCHA does not provide any decay channel for the current-current correlation function, and the thermal conductivity is infinite.

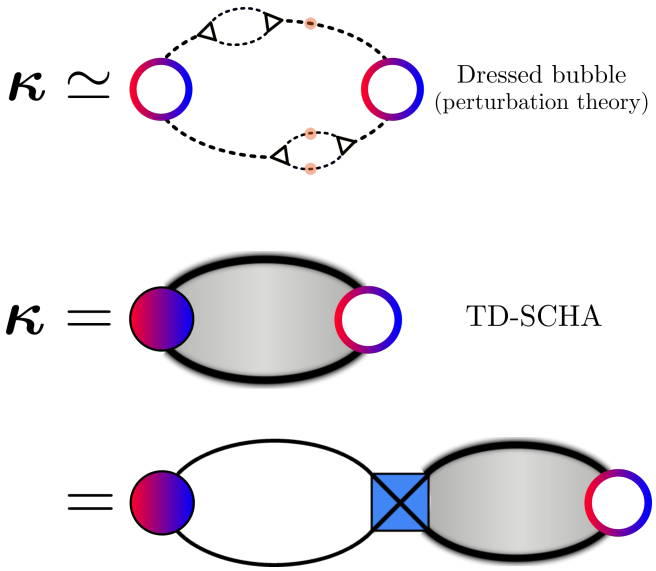

Figure 3.9. Diagrammatic comparison of thermal conductivity obtained in a (lowest-order) dressed-bubble approximation following from perturbation theory and in TD-SCHA [Eq. (3.4.29)]. The renormalization of the two-phonon Green's function in TD-SCHA does not account for dressed-bubble diagrams, and this results in a infinite conductivity. The meaning of the symbols were already presented in Fig. 3.1 for the heat flux vertices, in Fig. 3.2 for the phonon quantities obtained in perturbation theory, and in Fig. 3.5 for the TD-SCHA two-phonon Dyson equation. The vertically aligned orange dots in the upper half elucidate how a the dressed-bubble diagram features three-phonon lines at the same time. Such process can be understood as a three-phonon excitation, which is absent in TD-SCHA.

In the many-body approach to lattice thermal transport developed in Chapter 2, we obtained a finite heat-flux autocorrelation by accounting for anharmonicity in a dressed-bubble approximation [*cf. e.g.* Eq. (2.3.3)]. In the dressed-bubble approximation, the full two-phonon Green's function is approximated with a product of two interacting phonon Green's functions. Thus, the one-phonon self-energy accounting for the decay of the single-phonon Green's function enters in the two-phonon autocorrelation function and provides a finite anharmonic thermal conductivity. However, dressed-bubble diagrams that are present in the exact two-phonon Green's function are absent in the TD-SCHA scheme.

Such deficiency follows from the fundamental difference between perturbative and self-consistent approaches. In a perturbative approach, the fully interacting phonon Green's function can be approximated by selecting any given diagram among the ones allowed by the interaction considered, typically computed at the lowest nontrivial order. Instead, in a self-consistent approach, one does not have such freedom of choice, since only a particular

class of diagrams are included in the dynamics, depending on the self-consistent scheme. The advantage is that the special class of diagrams considered are included at all orders of anharmonicity. In the case of TD-SCHA, the diagrams included in the ionic dynamics are summarized in Fig. 3.5. A diagrammatic comparison between the thermal conductivity obtained in a dressed-bubble approximation and in TD-SCHA is presented in Fig. 3.9. A physical insight on why TD-SCHA can not provide a finite thermal conductivity can be understood by comparing the diagrammatic expressions in Fig. 3.9. In the dressed-bubble approximation, the anharmonicity is accounted in the self-energy of the one-phonon Green's functions. However, from the perspective of the two-phonon Green's function self-energy, the dressed-bubble can be seen as a three-phonon process. As elucidated by the orange dots in Fig. 3.9, a dressed-bubble diagram features three phonon lines at the same time. Such process can be understood in terms of a two-phonon self-energy originating from a three-phonon propagator. As discussed in Sec. 3.3.5, the TD-SCHA does not account for processes that feature more than two phonons and a dressed-bubble diagram is simply not included in the TD-SCHA two-phonon dynamics.

The term $[\boldsymbol{S}+\boldsymbol{\chi}^{(0)}(0):\boldsymbol{\Sigma}(\omega)]\,[1-\boldsymbol{\chi}^{(0)}(\omega):\boldsymbol{\Sigma}(\omega)]^{-1}$ that originates from the inversion of the interacting anharmonic propagator can be interpreted as a "anharmonic screening" of the perturbative heat flux vertex. As will be discussed in Chapter 4, the screening of the vertices of a response function due to the interacting propagator is typical of self-consistent time-dependent schemes, such as TD-HF or TD-DFT.

3.5 Conclusions

This Chapter is the core of this thesis. By reworking the maximum entropy and modified Liouville equation approach presented in Chapter 1, we have devised a novel first-principles methodology to obtain an expression of thermal conductivity valid in self-consistent schemes. To describe solids in presence of strong anharmonicity, we have adopted nonperturbative approach provided by the SCHA. We have derived the equilibrium state in the SCHA from the maximum entropy principle, expanding the variational space for the Gaussians used to approximate the exact density matrix. To discuss the self-consistent dynamics, we have employed the scheme of the TD-SCHA. Reformulating such theory in the Wigner representation of quantum mechanics, we have obtained a clear interpretation in terms of Feynman diagrams both of the response functions and of the anharmonic scattering included in the phonon dynamics in the TD-SCHA. Then we fitted the TD-SCHA linear response scheme in the framework of thermal transport by defining a TD-SCHA "thermal-potential" from the self-consistent Kubo formula for thermal conductivity we developed. This procedure allowed us to interpet the thermal conductivity in a form similar to a static limit of a current-current response function, as done in Chapter 2. The harmonic limit of the TD-SCHA thermal conductivity coincides exactly with the result obtained from many-body perturbation theory. Such consistency supports the validity of our approach to thermal transport in TD-SCHA. Computing the static limit of the full anharmonic current-current correlation function, we realize that the thermal conductivity in TD-SCHA diverges. We have discussed how this shortcoming follows from an intrinsic limitation of the approximation. In the TD-SCHA, the dressed-bubble diagrams that renormalize the two-phonon correlation and provide a finite conductivity are absent. Thus, while the TD-SCHA represents on of the most advanced first-principles approach to lattice dynamics, it still does not offer a fully nonperturbative model for thermal transport.

Appendices of Chapter 3

3.A Review of SCHA relations

In this Appendix, we prove some useful relations obtained in the SCHA formalism.

Density matrix of harmonic oscillators

Density matrix of a free particle in 1D

The hamiltonian for a free particle of mass m in 1D along the axis x is

$$\hat{H}_x = \frac{-\hbar^2}{2m}\frac{\partial^2}{\partial x^2} \tag{3.A.1}$$

hence its density matrix satisfies the Bloch equation (3.2.4)

$$-\frac{\partial}{\partial\beta}\rho(x,x';\beta) = -\frac{\hbar^2}{2m}\frac{\partial^2}{\partial x^2}\rho(x,x';\beta). \tag{3.A.2}$$

This differential equation describes a gaussian density matrix

$$\rho(x,x';\beta) = \sqrt{\frac{m}{2\pi\hbar^2\beta}}e^{-\frac{m}{2\hbar^2\beta}(x-x')^2} \tag{3.A.3}$$

normalized by the thermal wavelength of the particle $\lambda^2 = \frac{2\pi\hbar^2\beta}{m} = 2\pi\sigma^2$. To verify it, we can directly compute

$$\begin{aligned} -\frac{\partial}{\partial\beta}\rho(x,x';\beta) &= -\frac{\partial}{\partial\beta}\left(\frac{1}{\lambda}e^{-\frac{(x-x')^2}{\lambda^2/\pi}}\right) \\ = \frac{1}{\lambda}\frac{\partial\lambda}{\partial\beta}\rho(x,x';\beta) &+ \frac{\partial}{\partial\beta}\left(\frac{\pi}{\lambda^2}\right)(x-x')^2\rho(x,x';\beta) \end{aligned} \tag{3.A.4}$$

whereas

$$\begin{aligned} -\frac{\hbar^2}{2m}\frac{\partial}{\partial x}\frac{\partial}{\partial x}\rho(x,x';\beta) &= \frac{\lambda^2}{4\pi\beta}\frac{\partial}{\partial x}\frac{\pi}{\lambda^2}2(x-x')\rho(x,x';\beta) \\ &= \frac{1}{2\beta}\rho(x,x';\beta) - \frac{1}{\beta}\frac{\pi}{\lambda^2}(x-x')^2\rho(x,x';\beta) \end{aligned} \tag{3.A.5}$$

which are equal since $\frac{1}{\lambda}\frac{\partial\lambda}{\partial\beta} = \frac{1}{2\beta}$ and $\frac{\partial}{\partial\beta}\frac{1}{\lambda^2} = -\frac{1}{\beta\lambda^2}$. From this we can compute the partition function and the free energy as

$$\begin{aligned} \mathcal{Z} = \mathrm{Tr}\{\hat{\rho}_U\} = \int dx\, \langle x|\hat{\rho}(\beta)_U|x\rangle = \sqrt{\frac{m}{2\pi\hbar^2\beta}} \\ F = -\frac{1}{\beta}\log\mathcal{Z} = -\frac{1}{\beta}\log\sqrt{\frac{m}{2\pi\hbar^2\beta}} \end{aligned} \tag{3.A.6}$$

where the subscript U denotes unnormalized density matrix.

Density matrix of 1D harmonic oscillator

The hamiltonian of a 1D oscillator is

$$\hat{\mathcal{H}} = \frac{\hat{p}^2}{2m} + \frac{1}{2}m\omega^2\hat{x}^2 \tag{3.A.7}$$

which in position representation reads

$$\mathcal{H}_x = -\frac{\hbar^2}{2m}\boldsymbol{\nabla}_x^2 + \frac{1}{2}m\omega^2 x^2. \tag{3.A.8}$$

Let us impose the differential equation on the density matrix:

$$-\frac{\partial}{\partial\beta}\rho(x,x';\beta) = \mathcal{H}_x\rho(x,x';\beta) = -\frac{\hbar^2}{2m}\frac{\partial^2}{\partial x^2}\rho(x,x';\beta) + \frac{1}{2}m\omega^2x^2\rho(x,x';\beta) \tag{3.A.9}$$

Let us now introduce the following change of variables

$$s = \sqrt{\frac{m\omega}{\hbar}}x \quad ; \quad f = \frac{\hbar\omega}{2}\beta \tag{3.A.10}$$

that can be used to recast the differential equation for the density matrix; dividing the latter by $\hbar\omega$ we get

$$\begin{aligned} -\frac{1}{2}\frac{\partial}{\partial\frac{\hbar\omega}{2}\beta}\rho(x,x';\beta) &= -\frac{1}{2}\frac{\partial^2}{\partial\frac{m\omega}{\hbar}x^2}\rho(x,x';\beta) + \frac{1}{2}\frac{m\omega}{\hbar}x^2\rho(x,x';\beta) \\ \frac{\partial}{\partial f}\rho(s,s';f) &= -\frac{\partial^2}{\partial s^2}\rho(s,s';f) + s^2\rho(s,s';f). \end{aligned} \tag{3.A.11}$$

Now the idea is that for $\beta \to 0, f \to 0 \iff T \to \infty$ the kinetic energy is bigger than the potential energy $K \gg V$ and the harmonic oscillator behaves as a free particle. This sets the high temperature gaussian (free particle) limit

$$\rho(x,x';\beta) \to \sqrt{\frac{m}{2\pi\hbar^2\beta}}e^{-\frac{m}{2\hbar^2\beta}(x-x')^2} = \sqrt{\frac{m\omega}{4\pi\hbar f}}e^{-\frac{(s-s')^2}{4f^2}} \qquad \text{for} \quad T\to\infty \tag{3.A.12}$$

and the following "generalized" gaussian structure is proposed (for the diagonal element)

$$\begin{aligned} \rho(s,s;f) =& Ne^{-[a(f)s^2+b(f)s+c(f)]} \\ \rho(s,s';0) = \delta(x-x') &= \sqrt{\frac{m\omega}{\hbar}}\delta(s-s') \end{aligned} \tag{3.A.13}$$

If we plug this into the differential equation, a set of coupled differential equations for the coefficient are produced

$$\begin{aligned} a'(f) &= -4a^2(f) + 1 \\ b'(f) &= -4a(f)b(f) \\ c'(f) &= 2a(f) - b^2(f) \end{aligned} \tag{3.A.14}$$

This set of equation can be solved analytically, yielding

$$\begin{aligned} a(f) &= \frac{1}{2}\coth 2f \\ b(f) &= \frac{A}{\sinh 2f} \\ c(f) &= \frac{1}{2}\log\sinh 2f + \frac{A^2}{2}\coth 2f - \log B \end{aligned} \tag{3.A.15}$$

with A,B as free parameters. Comparing to the free particle limit, the parameters can be set to $B = \sqrt{\frac{m\omega}{2\pi\hbar}}$ and $A = -s'$. From this we can deduce the final form of the density matrix of a 1D oscillator

$$\rho(s, s'; \beta) = \sqrt{\frac{m\omega}{2\pi\hbar\sinh 2f}} e^{-\frac{1}{2\sinh 2f}[(s^2+s'^2)\cosh 2f - 2ss']} \tag{3.A.16}$$

that we can express back in x, x' as

$$\rho(x, x'; \beta) = \sqrt{\frac{m\omega}{2\pi\hbar\sinh 2f}} e^{-\frac{m\omega}{2\hbar\sinh 2f}[(x^2+x'^2)\cosh 2f - 2xx']} \tag{3.A.17}$$

where we recall $f = \frac{\hbar\omega}{2}\beta$. For the diagonal element we use the hyperbolic duplication formula $\sinh(2f) = 2\sinh(f)\cosh(f)$ and $\cosh(2f) - 1 = 2\sinh^2(f)$ from which we get

$$\rho(x, x; b) = \sqrt{\frac{m\omega}{2\pi\hbar\sinh 2f}} e^{-\frac{m\omega}{\hbar}\tanh(f)x^2} \, . \tag{3.A.18}$$

This density matrix is still unnormalized. From the latter we can access the partition function as

$$\begin{aligned} \mathcal{Z}(\beta) = \mathrm{Tr}\{\hat{\rho}(\beta)\} &= \int \mathrm{d}x \, \rho(x, x'; \beta) = \int \mathrm{d}x \sqrt{\frac{m\omega}{2\pi\hbar\sinh 2f}} e^{-\frac{m\omega}{\hbar}\tanh(f)x^2} \\ &= \sqrt{\frac{1}{2\pi\sinh(2f)\tanh(f)}} \int \mathrm{d}x \sqrt{\frac{m\omega}{\hbar}} \sqrt{\tanh(x)} e^{-\frac{m\omega}{\hbar}\tanh(f)x^2} \\ &= \sqrt{\frac{1}{4\pi\sinh(f)\cosh(f)\tanh(f)}} \int \mathrm{d}s \, e^{-s^2} = \frac{1}{2\sinh(f)}. \end{aligned} \tag{3.A.19}$$

The free energy of the harmonic oscillator is then

$$\begin{aligned} \mathcal{F}(\beta) = -\frac{1}{\beta}\log\mathcal{Z}(\beta) = \frac{1}{\beta}\log(2\sinh(f)) = \frac{1}{\beta}\log\Big(e^{\frac{\hbar\omega}{2}\beta} - e^{-\frac{\hbar\omega}{2}\beta}\Big) \\ = \frac{\hbar\omega}{2} + \frac{1}{\beta}\log\Big(1 - e^{-\beta\hbar\omega}\Big) = \frac{\hbar\omega}{2} - \frac{1}{\beta}\log(n(\omega)+1) = \langle U\rangle - T\langle S\rangle \end{aligned} \tag{3.A.20}$$

where $n(\omega)$ is the Bose-Einstein population. Now let's normalize the density matrix; considering only the prefactor of $\rho/\mathcal{Z}$ we have

$$\sqrt{\frac{m\omega}{2\pi\hbar}} \frac{2\sinh(f)}{\sqrt{\sinh(2f)}} = \sqrt{\frac{m\omega}{2\pi\hbar}} \sqrt{\frac{4\sinh^2(f)}{2\cosh(f)\sinh(f)}} = \sqrt{\frac{2m\omega}{2\pi\hbar\coth(f)}} \tag{3.A.21}$$

and the $\coth(f)$ can be recast as

$$\coth\left(\frac{\hbar\omega}{2}\beta\right) = \frac{e^{\frac{\hbar\omega}{2}\beta} + e^{-\frac{\hbar\omega}{2}\beta}}{e^{\frac{\hbar\omega}{2}\beta} - e^{-\frac{\hbar\omega}{2}\beta}} = \frac{e^{\beta\hbar\omega}+1}{e^{\beta\hbar\omega}-1} = \frac{e^{\beta\hbar\omega}}{e^{\beta\hbar\omega}-1} + n(\omega) = -n(-\omega) + n(\omega) = 1 + 2n(\omega). \tag{3.A.22}$$

The normalized density matrix of a 1D oscillator is

$$\rho(x, x'; \beta) = \sqrt{\frac{m}{2\pi\frac{\hbar}{2\omega}(1+2n(\omega))}} e^{-\frac{m\omega}{2\hbar\sinh(\beta\hbar\omega)}\left[(x^2+x'^2)\cosh(\beta\hbar\omega) - 2xx'\right]} \tag{3.A.23}$$

rewritten in this way to highlight the factor $\xi^2 = \frac{\hbar}{2\omega}(1+2n(\omega)) = \frac{\hbar}{2\omega}\coth\left(\frac{\beta\hbar\omega}{2}\right)$ that will be introduced in SCHA notation.

Density matrix of N oscillators in 3D

The hamiltonian of N harmonic oscillators in 3D reads

$$\hat{\mathcal{H}} = \sum_a \frac{\hat{p}_a^2}{2m_a} + \frac{1}{2}\sum_{ab}\Phi_{ab}(\hat{R}_a - \mathcal{R}_a)(\hat{R}_b - \mathcal{R}_b) = \sum_a \frac{\hat{p}_a^2}{2m_a} + \frac{1}{2}\sum_{ab}\Phi_{ab}\hat{u}_a\hat{u}_b \tag{3.A.24}$$

where the indices a, b spans both the Cartesian directions and the number of the oscillators. The operator $\hat{u}_a = \hat{R}_a - \hat{\mathcal{R}}_a$ indicate the displacement from the equilibrium position of the ion a. The dynamical matrix can be introduced as (2.2.12)

$$\frac{\Phi_{ab}}{\sqrt{m_a m_b}} = D_{ab} = \sum_\mu \omega_\mu^2 e_{\mu,a} e_{\mu,b} \quad . \tag{3.A.25}$$

Let us introduce the transformation in normal mode coordinates

$$\begin{aligned} \hat{u}_a &= \sum_\mu \frac{e_{\mu,a}}{\sqrt{m_a}}\hat{q}_\mu \\ \hat{p}_a &= \sum_\mu \sqrt{m_a} e_{\mu,a}\hat{p}_\mu \end{aligned} \tag{3.A.26}$$

that diagonalizes the Hamiltonian

$$\hat{\mathcal{H}} = \sum_\mu \left(\frac{\hat{p}_\mu^2}{2} + \frac{\omega_\mu^2\hat{q}_\mu^2}{2}\right). \tag{3.A.27}$$

This Hamiltonian appears as a sum of 1D harmonic oscillators, for which the density matrix is (3.A.23). Notice the slight difference in the masses, reabsorbed in the normal mode coordinates; the substitution we have to perform from the 1D case is $\sqrt{m}x \to u$. The density matrix will then be

$$\hat{\varrho} = \frac{e^{-\beta\hat{\mathcal{H}}}}{\mathcal{Z}} = \prod_\mu \frac{e^{-\beta\mathcal{H}_\mu}}{\mathcal{Z}_\mu} \tag{3.A.28}$$

and the density matrix would be

$$\varrho(\vec{\boldsymbol{q}}, \vec{\boldsymbol{q}}') = \prod_\mu \sqrt{\frac{1}{2\pi\frac{\hbar}{2\omega_\mu}(1+2n_\mu)}} e^{-\frac{\omega_\mu}{2\hbar\sinh(\beta\hbar\omega_\mu)}\left[(q_\mu^2 + q_\mu'^{\,2})\cosh(\beta\hbar\omega_\mu) - 2q_\mu q_\mu'\right]} \tag{3.A.29}$$

and we can introduce $\xi_\mu^2 = \frac{\hbar}{2\omega_\mu}(1+2n_\mu) = \frac{\hbar}{2\omega_\mu}\coth\left(\frac{1}{2}\beta\hbar\omega_\mu\right)$ SCHA (thermal lengths), where for brevity $n_\mu = n(\omega_\mu)$. The diagonal elements are

$$\begin{aligned}\varrho(\vec{\boldsymbol{q}},\vec{\boldsymbol{q}}) &= \prod_\mu \sqrt{\frac{1}{2\pi\xi_\mu^2}} e^{-\frac{\omega_\mu}{\hbar}\tanh\left(\frac{\beta\hbar\omega_\mu}{2}\right)q_\mu^2} = \prod_\mu \sqrt{\frac{1}{2\pi\xi_\mu^2}} e^{-\frac{q_\mu^2}{2\xi_\mu^2}} \\ &= \prod_\mu (\sqrt{\frac{1}{2\pi\xi_\mu^2}}) \prod_\mu e^{-\frac{q_\mu^2}{2\xi_\mu^2}} = \prod_\mu (\sqrt{\frac{1}{2\pi\xi_\mu^2}}) e^{-\sum_\mu \frac{q_\mu^2}{2\xi_\mu^2}}\end{aligned} \tag{3.A.30}$$

which describes a product of 3N gaussian matrices in the normal mode coordinates. Now we want to go back to real space displacements using

$$q_\mu = \sum_a \sqrt{m_a} e_{\mu,a} u_a \tag{3.A.31}$$

and with this trasformation the quadratic form in the gaussian exponent becomes

$$\sum_\mu \sum_{ab} \sqrt{m_a} e_{\mu,a} u_a \sqrt{m_b} e_{\mu,b} u_b \frac{q_\mu^2}{2\xi_\mu^2} = \sum_{ab} \Upsilon_{ab} u_a u_b \tag{3.A.32}$$

introducing the matrix

$$\Upsilon_{ab} = \sum_\mu \frac{\sqrt{m_a m_b}}{\xi_\mu^2} e_{\mu,a} e_{\mu,b} = \sum_\mu \frac{\sqrt{m_a m_b}}{\hbar(1+2n_\mu)} 2\omega_\mu e_{\mu,a} e_{\mu,b}. \tag{3.A.33}$$

In order to pass from q to u, since the density matrix is normalized, we have to multiply times the jacobian of the transformation

$$|J_\mu^a| = \det\left(\frac{\partial q_\mu}{\partial u_a}\right) = \det(\sqrt{m_a} e_{\mu,a}). \tag{3.A.34}$$

This comes from the trasformation of the probability distributions $p(x)dx{=}p(y)dy$. Using this we can express the density matrix in displacement coordinates as

$$\varrho(\vec{\boldsymbol{R}},\vec{\boldsymbol{R}}) = \det(\sqrt{m_a} e_{\mu,a}) \det\left(\sqrt{\frac{1}{2\pi\xi_\mu\xi_{\mu'}}}\delta_{\mu,\mu'}\right) e^{-\frac{1}{2}\sum_{ab}\Upsilon_{ab}u_a u_b}. \tag{3.A.35}$$

Now using $\sqrt{\det(A^2)} = \sqrt{\det(A)\det(A)} = \sqrt{\det(A)^2} = \det(A)$, we can rewrite the prefactor as

$$\begin{aligned}\det(\sqrt{m_a} e_{\mu,a}) \det\left(\sqrt{\frac{\delta_{\mu,\mu'}}{2\pi\xi_\mu\xi_{\mu'}}}\right) &= \sqrt{\det(\sqrt{m_a} e_{\mu,a}) \det(\sqrt{m_b} e_{\mu',b}) \det\left(\frac{\delta_{\mu,\mu'}}{2\pi\xi_\mu\xi_{\mu'}}\right)} \\ &= \sqrt{\det\left(\sqrt{m_a m_b} e_{\mu,a} e_{\mu',b} \frac{\delta_{\mu,\mu'}}{2\pi\xi_\mu\xi_{\mu'}}\right)} = \sqrt{\det\left(\frac{\Upsilon}{2\pi}\right)}\end{aligned} \tag{3.A.36}$$

from which we have the expression of the diagonal elements in the Schrodinger representation of the Gaussian density matrix (3.2.8)

$$\varrho(\vec{\boldsymbol{R}}, \vec{\boldsymbol{R}}) = \sqrt{\det\left(\frac{\overleftrightarrow{\boldsymbol{\Upsilon}}}{2\pi}\right)} e^{-\frac{1}{2}\sum_{ab} \Upsilon_{ab} u_a u_b} . \tag{3.A.37}$$

With a slightly more cumbersome but formally equivalent procedure, the structure of the full density matrix (3.2.7) can be obtained from (3.A.29).

Using the argument (3.A.28), we get that the free energy of 3N oscillators can be obtained by addition of the single modes free energy (3.A.20), i.e.

$$\mathcal{F} = \frac{1}{\beta} \sum_{\mu} \log[2 \sinh\left(\tfrac{1}{2}\hbar\omega_\mu \beta\right)] \tag{3.A.38}$$

which is the expression introduced in (3.2.17).

SCHA equilibrium energy

Here we compute the expectation value of the harmonic Hamiltonian $\hat{\mathcal{H}}_{\vec{\boldsymbol{\mathcal{R}}},\vec{\boldsymbol{\Phi}}}$ introduced in (3.2.3a), that we rewrite as a kinetic plus a harmonic potential as

$$\hat{\mathcal{H}}_{\vec{\boldsymbol{\mathcal{R}}},\vec{\boldsymbol{\Phi}}} = \hat{K} + \hat{\mathcal{V}}_{\vec{\boldsymbol{\mathcal{R}}},\vec{\boldsymbol{\Phi}}}(\vec{\boldsymbol{R}}) \tag{3.A.39}$$

on the Gaussian density matrix (3.2.7).

Kinetic energy

To calculate the kinetic energy in the SCHA, we must consider the matrix elements of the density operator in the Schrodinger representation (3.2.7)

$$\varrho(\vec{\boldsymbol{R}}, \vec{\boldsymbol{R}}') = \frac{1}{\sqrt{\det\left(2\pi \overleftrightarrow{\boldsymbol{\Upsilon}}^{-1}\right)}} \exp\left[-\sum_{ab} \frac{\Theta_{ab}}{4}(u_a u_b + u'_a u'_b) + \sum_{ab} A_{ab} u_a u'_b\right] , \tag{3.A.40}$$

where $u_a = R_a - \mathcal{R}_a$. The kinetic energy is computed as

$$\begin{aligned} \left\langle \hat{K} \right\rangle_{\varrho} &= -\sum_c \frac{\hbar^2}{2m_c} \int \mathrm{d}\vec{\boldsymbol{R}}\, \mathrm{d}\vec{\boldsymbol{R}}' \left\langle \vec{\boldsymbol{R}} \middle| \varrho \middle| \vec{\boldsymbol{R}}' \right\rangle \left\langle \vec{\boldsymbol{R}}' \middle| \frac{\partial^2}{\partial R_c^2} \middle| \vec{\boldsymbol{R}} \right\rangle \\ &= -\sum_c \frac{\hbar^2}{2m_c} \int \mathrm{d}\vec{\boldsymbol{R}}\, \mathrm{d}\vec{\boldsymbol{R}}' \left(\frac{\partial^2}{\partial R_c^2} \left\langle \vec{\boldsymbol{R}} \middle| \varrho \middle| \vec{\boldsymbol{R}}' \right\rangle\right) \delta(\vec{\boldsymbol{R}} - \vec{\boldsymbol{R}}') \end{aligned} \tag{3.A.41}$$

and we can compute the derivatives from (3.A.40) as

$$\begin{aligned} \frac{\partial}{\partial R_c} \varrho(\vec{\boldsymbol{R}}, \vec{\boldsymbol{R}}') &= -\varrho(\vec{\boldsymbol{R}}, \vec{\boldsymbol{R}}') \sum_d \left[\frac{\Theta_{cd}}{2} u_d - A_{cd} u'_d\right] \\ \frac{\partial^2}{\partial R_c^2} \varrho(\vec{\boldsymbol{R}}, \vec{\boldsymbol{R}}') &= \varrho(\vec{\boldsymbol{R}}, \vec{\boldsymbol{R}}') \left[\sum_d \frac{\Theta_{cd}}{2} u_d - A_{cd} u'_d\right]^2 - \varrho(\vec{\boldsymbol{R}}, \vec{\boldsymbol{R}}') \frac{\Theta_{cc}}{2} . \end{aligned} \tag{3.A.42}$$

So the kinetic energy can be computed as

$$\begin{aligned}
\left\langle \hat{K} \right\rangle_{\varrho} &= \sum_c \frac{\hbar^2}{4m_c} \Theta_{cc} \int \mathrm{d}\vec{\boldsymbol{R}}\, \varrho(\vec{\boldsymbol{R}}) - \sum_c \frac{\hbar^2}{2m_c} \int \mathrm{d}\vec{\boldsymbol{R}}\, \varrho(\vec{\boldsymbol{R}}) (\frac{1}{2} \sum_d [\Theta_{cd} - 2A_{cd}] u_d)^2 \\
&= \sum_c \frac{\hbar^2}{2m_c} \frac{\Theta_{cc}}{2} - \frac{1}{4} \sum_c \frac{\hbar^2}{2m_c} \sum_{df} \Upsilon_{cd} \Upsilon_{cf} \int \mathrm{d}\vec{\boldsymbol{R}}\, \varrho(\vec{\boldsymbol{R}}) u_f u_d \\
&= \sum_c \frac{\hbar^2}{2m_c} \frac{\Theta_{cc}}{2} - \frac{1}{4} \sum_c \frac{\hbar^2}{2m_c} \sum_{df} \Upsilon_{cd} \Upsilon_{cf} \Upsilon^{-1}_{fd} \\
\left\langle \hat{K} \right\rangle_{\varrho} &= \frac{\hbar^2}{2} \mathrm{Tr}\left(\frac{\tilde{\Theta}}{2}\right) - \frac{\hbar^2}{2} \mathrm{Tr}\left(\frac{\tilde{\Upsilon}}{4}\right) = \frac{\hbar^2}{2} \mathrm{Tr}\left(\frac{\tilde{\Theta}}{4}\right) + \frac{\hbar^2}{2} \mathrm{Tr}\left(\frac{\tilde{A}}{2}\right) = \frac{\hbar^2}{2} \mathrm{Tr}\left(\frac{\tilde{\Upsilon}}{4}\right) + \frac{\hbar^2}{2} \mathrm{Tr}\left(\tilde{A}\right)
\end{aligned} \tag{3.A.43}$$

where the mass reduced matrix are defined as $\tilde{\Theta}_{ab} = \frac{\Theta_{ab}}{\sqrt{m_a m_b}}$. In the third line of the last calculation we have used the result

$$\langle \hat{u}_a \hat{u}_b \rangle_{\varrho} = \int \mathrm{d}\vec{\boldsymbol{R}}\, \varrho(\vec{\boldsymbol{R}}) u_a u_b = \Upsilon^{-1}_{ab} \tag{3.A.44}$$

Harmonic potential energy and equipartition theorem

The expectation value of the harmonic potential is straightforward

$$\left\langle \hat{\mathcal{V}}_{\vec{\boldsymbol{\mathcal{R}}}, \vec{\boldsymbol{\Phi}}} \right\rangle_{\varrho} = \frac{1}{2} \sum_{ab} \Phi_{ab} \langle \hat{u}_a \hat{u}_b \rangle_{\varrho} = \frac{1}{2} \sum_{ab} \Phi_{ab} \Upsilon^{-1}_{ab} = \frac{1}{2} \mathrm{Tr}\left[\Phi \Upsilon^{-1}\right] = \frac{1}{2} \sum_{\mu} \omega_\mu^2 \xi_\mu^2 \tag{3.A.45}$$

and if we work out the kinetic energy we see that

$$\begin{aligned}
\left\langle \hat{K} \right\rangle_{\varrho} &= \frac{\hbar^2}{2} \mathrm{Tr}\left(\frac{\tilde{\Theta}}{4}\right) + \frac{\hbar^2}{2} \mathrm{Tr}\left(\frac{\tilde{A}}{2}\right) = \frac{\hbar^2}{4} \sum_\mu \left[\frac{\tilde{\Theta}_\mu}{2} + \tilde{A}_\mu\right] \\
&= \frac{\hbar^2}{4} \sum_\mu \frac{\omega_\mu}{\hbar} \left[\coth(\hbar\omega_\mu\beta) + \frac{1}{\sinh(\hbar\omega_\mu\beta)}\right] = \frac{\hbar^2}{4} \sum_\mu \frac{\omega_\mu}{\hbar} \coth\left(\tfrac{1}{2}\hbar\omega_\mu\beta\right) \\
\left\langle \hat{K} \right\rangle_{\varrho} &= \frac{1}{2} \sum_\mu \omega_\mu^2 \frac{\hbar}{2\omega_\mu} \coth\left(\tfrac{1}{2}\hbar\omega_\mu\beta\right) = \frac{1}{2} \sum_\mu \omega_\mu^2 \xi_\mu^2 = \left\langle \hat{\mathcal{V}} \right\rangle_{\varrho}
\end{aligned} \tag{3.A.46}$$

which consist in the equipartition (virial) theorem for a harmonic system. So we have that

$$\left\langle \hat{\mathcal{H}}_{\vec{\boldsymbol{\mathcal{R}}}, \vec{\boldsymbol{\Phi}}} \right\rangle_{\varrho} = \sum_\mu \omega_\mu^2 \xi_\mu^2 \tag{3.A.47}$$

Derivatives of SCHA expectation values

Here we prove the relation introduced in (3.2.15) for the derivatives of observables diagonal in Schrodinger representation

$$\frac{\partial}{\partial \lambda} \left\langle O(\vec{\boldsymbol{R}}) \right\rangle_{\varrho_{\vec{\boldsymbol{\mathcal{R}}}, \overleftrightarrow{\boldsymbol{\Phi}}}} = \sum_a \frac{\partial \mathcal{R}_a}{\partial \lambda} \left\langle \frac{\partial O(\vec{\boldsymbol{R}})}{\partial \hat{R}_a} \right\rangle_{\varrho_{\vec{\boldsymbol{\mathcal{R}}}, \overleftrightarrow{\boldsymbol{\Phi}}}} + \frac{1}{2} \sum_{ab} \frac{\partial \Upsilon^{-1}_{ab}}{\partial \lambda} \left\langle \frac{\partial^2 O(\vec{\boldsymbol{R}})}{\partial \hat{R}_a \partial \hat{R}_b} \right\rangle_{\varrho_{\vec{\boldsymbol{\mathcal{R}}}, \overleftrightarrow{\boldsymbol{\Phi}}}}. \tag{3.A.48}$$

Let us first define the matrix L_μ^a which is useful for the calculations

$$\begin{aligned} \Upsilon_{ab}^{-1} &= \sum_\mu L_\mu^a L_\mu^b \,, \\ L_\mu^a &= \xi^\mu \frac{e_\mu^a}{\sqrt{m_a}} \,. \end{aligned} \tag{3.A.49}$$

Using the definition (3.2.8), the average of an operator can be computed in SCHA as

$$\left\langle O(\vec{\boldsymbol{R}}) \right\rangle_{\varrho_{\vec{\boldsymbol{\mathcal{R}}},\overleftrightarrow{\boldsymbol{\Phi}}}} = \det\left(\frac{\overleftrightarrow{\boldsymbol{\Upsilon}}}{2\pi}\right) \int \mathrm{d}\vec{\boldsymbol{R}}\, O(\vec{\boldsymbol{R}}) e^{-\frac{1}{2}\sum_{ab}(R_a-\mathcal{R}_a)\Upsilon_{ab}(R_b-\mathcal{R}_b)}. \tag{3.A.50}$$

To recast the latter integral as a Gaussian integral we can perform the change of variable $\vec{\boldsymbol{R}} = \vec{\boldsymbol{\mathcal{R}}} + \vec{\boldsymbol{u}}$, obtaining

$$\left\langle O(\vec{\boldsymbol{R}}) \right\rangle_{\varrho_{\vec{\boldsymbol{\mathcal{R}}},\overleftrightarrow{\boldsymbol{\Phi}}}} = \frac{1}{\sqrt{\det\left(2\pi\overleftrightarrow{\boldsymbol{\Upsilon}}^{-1}\right)}} \int \mathrm{d}\boldsymbol{u}\, O(\vec{\boldsymbol{\mathcal{R}}} + \vec{\boldsymbol{u}}) e^{-\frac{1}{2}\sum_{ab} u_a \Upsilon_{ab} u_b}. \tag{3.A.51}$$

We can proceed by transforming

$$y_\mu = \sum_a \frac{\sqrt{m_a}}{\xi_\mu} e_{\mu,a} u_a \,, \qquad u_a = \sum_\mu \frac{\xi_\mu}{\sqrt{m_a}} e_{\mu,a} y_\mu = \sum_\mu L_\mu^a y_\mu \tag{3.A.52}$$

from which it is clear that the jacobian is $|J_\mu^a| = \det\left(\frac{\partial u^a}{\partial y_\mu}\right) = \det\left(L_\mu^a\right)$. The exponent can be recast using $\sum_{ab} u_a \Upsilon_{ab} u_b = \sum_\mu \sum_{ab} u_a e_{\mu,a} \frac{\sqrt{m_a m_b}}{\xi_\mu^2} e_{\mu,b} u_b = \sum_\mu y_\mu^2$ and using the fact $\det\left(\overleftrightarrow{\boldsymbol{\Upsilon}}^{-1}\right) = \det^2(\overleftrightarrow{\boldsymbol{L}})$ we get

$$\left\langle O(\vec{\boldsymbol{R}}) \right\rangle_{\varrho_{\vec{\boldsymbol{\mathcal{R}}},\overleftrightarrow{\boldsymbol{\Phi}}}} = \int \mathrm{d}\vec{\boldsymbol{y}} \frac{e^{-\frac{1}{2}\sum_\mu y_\mu^2}}{\sqrt{2\pi}} O(\vec{\boldsymbol{\mathcal{R}}} + \overleftrightarrow{\boldsymbol{L}}\vec{\boldsymbol{y}}) = \int [dy] O(\vec{\boldsymbol{\mathcal{R}}} + \overleftrightarrow{\boldsymbol{L}}\vec{\boldsymbol{y}}) \tag{3.A.53}$$

where we define the gaussian measure as $[dy] = \prod_\mu e^{-\frac{y_\mu}{2}} \frac{\mathrm{d}y_\mu}{\sqrt{2\pi}}$. Now we can compute the derivatives of the expectation value. From (3.A.53) we can express the derivative with respect to a parameter λ as derivative with respect to the spatial argument $O(\vec{\boldsymbol{\mathcal{R}}} + \overleftrightarrow{\boldsymbol{L}}\vec{\boldsymbol{y}})$ and apply the chain rule

$$\frac{\partial}{\partial\lambda}\left\langle O(\vec{\boldsymbol{R}}) \right\rangle_{\varrho_{\vec{\boldsymbol{\mathcal{R}}},\overleftrightarrow{\boldsymbol{\Phi}}}} = \sum_c \frac{\partial\mathcal{R}_c}{\partial\lambda} \int [dy] \frac{\partial O}{\partial R_c} + \int [dy] \sum_c \frac{\partial O}{\partial R_c} \sum_\mu \frac{\partial L_\mu^c}{\partial\lambda} y_\mu \,. \tag{3.A.54}$$

The first term in the right-hand side of (3.A.54) is the first term of (3.A.48), i.e.

$$\sum_c \frac{\partial\mathcal{R}_c}{\partial\lambda} \int [dy] \frac{\partial O}{\partial R_c} = \sum_c \frac{\partial\mathcal{R}_c}{\partial\lambda} \left\langle \frac{\partial O(\vec{\boldsymbol{R}})}{\partial \hat{R}_c} \right\rangle \tag{3.A.55}$$

The second term in (3.A.54) can be computed using the property of Gaussian measure $\frac{\partial}{\partial y_\mu}[dy] = \prod_\mu \cdots \frac{\partial}{\partial y_\mu} e^{-y_\mu^2/2} = -y_\mu[dy]$, yielding

$$\begin{aligned}\frac{\partial}{\partial\lambda}\left\langle \hat{O}\right\rangle_{\tilde{\rho}_{\boldsymbol{\mathcal{R}},\boldsymbol{\Phi}}} &= \sum_{c,\mu}\frac{\partial L^c_\mu}{\partial\lambda}\int -\frac{\partial}{\partial y_\mu}[dy]\frac{\partial}{\partial R^c}O(\vec{\boldsymbol{\mathcal{R}}}+\overleftrightarrow{\boldsymbol{L}}\vec{\boldsymbol{y}}) = \sum_{c,\mu}\frac{\partial L^c_\mu}{\partial\lambda}\int[dy]\frac{\partial}{\partial R^c}\frac{\partial}{\partial y_\mu}O(\vec{\boldsymbol{\mathcal{R}}}+\overleftrightarrow{\boldsymbol{L}}\vec{\boldsymbol{y}}) \\ &= \sum_{c,\mu}\frac{\partial L^c_\mu}{\partial\lambda}\int[dy]\frac{\partial}{\partial R^c}\sum_d\frac{\partial O}{\partial R^d}\frac{\partial}{\partial y_\mu}\sum_\nu L^d_\nu y_\nu = \sum_{cd}\sum_\mu\frac{\partial L^c_\mu}{\partial\lambda}L^d_\mu\int[dy]\frac{\partial^2 O(\vec{\boldsymbol{\mathcal{R}}}+\overleftrightarrow{\boldsymbol{L}}\vec{\boldsymbol{y}})}{\partial R^c\partial R^d} \\ &= \sum_{cd}\sum_\mu\frac{1}{2}\frac{\partial}{\partial\lambda}\left(L^c_\mu L^d_\mu\right)\left\langle\frac{\partial^2 O}{\partial R^c\partial R^d}\right\rangle_{\tilde{\rho}_{\boldsymbol{\mathcal{R}},\boldsymbol{\Phi}}} = \frac{1}{2}\sum_{cd}\frac{\partial\Upsilon^{-1}_{cd}}{\partial\lambda}\left\langle\frac{\partial^2 O}{\partial R^c\partial R^d}\right\rangle_{\tilde{\rho}_{\boldsymbol{\mathcal{R}},\boldsymbol{\Phi}}}.\end{aligned} \tag{3.A.56}$$

The last equality proves together with (3.A.55) the general result (3.A.48).

3.B Details of maximum entropy principle for SCHA equilibrium

Here we give extended proof of the variation of the entropy functional (3.2.23) with respect to the parameters of the density matrix $(\eta, \boldsymbol{\mathcal{R}}, \Phi)$. The variaton with respect to the Lagrangian multiplier β fixes the expectation value of the energy, which is a consequence of bath coupling, and represents the absolute temperature of the bath in the canonical ensemble. We must then set

$$\delta\tilde{S} = \sum_a \delta\mathcal{R}_a\frac{\partial\tilde{S}}{\partial\mathcal{R}_a} + \sum_{ab}\delta\Phi_{ab}\frac{\partial\tilde{S}}{\partial\Phi_{ab}} + \delta\eta\frac{\partial\tilde{S}}{\partial\eta} = 0 \tag{3.B.1}$$

computing all the variations and setting them separately to zero. For brevity, in intermediate calculations we drop the parameters subscript $\varrho_{\eta,\boldsymbol{\mathcal{R}},\boldsymbol{\Phi}}\to\varrho$, $\hat{\mathcal{H}}_{\eta,\boldsymbol{\mathcal{R}},\vec{\boldsymbol{\Phi}}}\to\hat{\mathcal{H}}$.

Variations in $\delta\mathcal{R}$

From (3.B.1), we set

$$\begin{aligned}-\frac{\partial\tilde{S}}{\partial\mathcal{R}_a} &= \frac{\partial}{\partial\mathcal{R}_a}\operatorname{Tr}[\hat{\varrho}\log\hat{\varrho}] + \beta\frac{\partial}{\partial\mathcal{R}_a}\operatorname{Tr}\left[\hat{\varrho}\hat{H}\right] = 0 \\ \operatorname{Tr}\left[\frac{\partial\hat{\varrho}}{\partial\mathcal{R}_a}\log\hat{\varrho}\right] &+ \operatorname{Tr}\left[\frac{\partial\hat{\varrho}}{\partial\mathcal{R}_a}\right] = -\beta\operatorname{Tr}\left[\frac{\partial\hat{\varrho}}{\partial\mathcal{R}_a}\hat{H}\right].\end{aligned} \tag{3.B.2}$$

Using the property of the density matrix (3.2.5)

$$\frac{\partial}{\partial\mathcal{R}_a}\hat{\varrho} = -\frac{\partial}{\partial\hat{R}_a}\hat{\varrho} = -\frac{1}{i\hbar}[\hat{\varrho},\hat{p}_a], \tag{3.B.3}$$

we can use the cyclic property of trace to move the derivative (integration by parts)

$$\operatorname{Tr}\left[\frac{\partial\hat{\varrho}}{\partial\hat{R}_a}\hat{O}\right] = \operatorname{Tr}\left[\frac{1}{i\hbar}[\hat{\varrho},\hat{p}_a]\hat{O}\right] = \operatorname{Tr}\left[\hat{\varrho}\frac{1}{i\hbar}[\hat{p}_a,\hat{O}]\right] = -\operatorname{Tr}\left[\hat{\varrho}\frac{\partial\hat{O}}{\partial\hat{R}_a}\right]. \tag{3.B.4}$$

Hence, the left-hand side of (3.B.2) is

$$\begin{aligned} &\mathrm{Tr}\left[\frac{\partial\hat{\varrho}}{\partial\mathcal{R}_a}\log\hat{\varrho}\right]+\mathrm{Tr}\left[\frac{\partial\hat{\varrho}}{\partial\mathcal{R}_a}\right]=-\mathrm{Tr}\left[\frac{\partial\hat{\varrho}}{\partial\hat{R}_a}\log\hat{\varrho}\right]-\mathrm{Tr}\left[\frac{\partial\hat{\varrho}}{\partial\hat{R}_a}\right] \\ &=\mathrm{Tr}\left[\hat{\varrho}\frac{\partial\log\hat{\varrho}}{\partial\hat{R}_a}\right]-\mathrm{Tr}\left[\frac{\partial\hat{\varrho}}{\partial\hat{R}_a}\right]=\mathrm{Tr}\left[\hat{\varrho}\hat{\varrho}^{-1}\frac{\partial\hat{\varrho}}{\partial\hat{R}_a}\right]-\mathrm{Tr}\left[\frac{\partial\hat{\varrho}}{\partial\hat{R}_a}\right]=0 \end{aligned} \tag{3.B.5}$$

and we are left with

$$\frac{\partial\tilde{S}}{\partial\mathcal{R}_a}=\beta\,\mathrm{Tr}\left[\frac{\partial\hat{\varrho}}{\partial\mathcal{R}_a}\hat{H}\right]=\beta\,\mathrm{Tr}\left[\hat{\varrho}\frac{\partial\hat{H}}{\partial\hat{R}_a}\right]=0 \tag{3.B.6}$$

that is precisely the first SCHA equilibrium condition (3.2.26a)

$$-\left\langle\frac{\partial\hat{V}_{BO}}{\partial R_a}\right\rangle_{\varrho}=0\,. \tag{3.B.7}$$

Variations in $\delta\Phi$

To compute the variation in Φ of (3.B.1), we compute

$$\frac{\partial\tilde{S}}{\partial\Phi_{ab}}=-\frac{\partial}{\partial\Phi_{ab}}\mathrm{Tr}[\hat{\varrho}\log\hat{\varrho}]-\beta\frac{\partial}{\partial\Phi_{ab}}\mathrm{Tr}\left[\hat{\varrho}\hat{H}\right]=0 \tag{3.B.8}$$

To compute the harmonic entropy, we exploit

$$-\mathrm{Tr}(\hat{\varrho}\log\hat{\varrho})=\eta[\left\langle\hat{\mathcal{H}}\right\rangle_{\varrho}-\mathcal{F}] \tag{3.B.9}$$

where $\mathcal{F}$ is the harmonic free energy. Now the derivative of the harmonic free energy was calculated in Ref. 56 (eq A14):

$$\frac{\partial\mathcal{F}}{\partial\Phi_{ab}}=\frac{1}{2}\Upsilon^{-1}_{ab}\,. \tag{3.B.10}$$

The derivative of the harmonic energy is obtained from (3.A.47):

$$\frac{\partial}{\partial\Phi_{ab}}\left\langle\hat{\mathcal{H}}\right\rangle_{\varrho}=\frac{\partial}{\partial\Phi_{ab}}\sum_{cd}\Phi_{cd}\Upsilon^{-1}_{cd}=\Upsilon^{-1}_{ab}+\sum_{cd}\Phi_{cd}\frac{\partial\Upsilon^{-1}_{cd}}{\partial\Phi_{ab}} \tag{3.B.11}$$

so that

$$\frac{\partial}{\partial\Phi_{ab}}[-\mathrm{Tr}[\varrho\log\varrho]]=\frac{\eta}{2}\Upsilon^{-1}_{ab}+\eta\sum_{cd}\Phi_{cd}\frac{\partial\Upsilon^{-1}_{cd}}{\partial\Phi_{ab}}\,. \tag{3.B.12}$$

The other term to be derived is

$$\begin{aligned} \frac{\partial}{\partial\Phi_{ab}}\left\langle\hat{H}\right\rangle_{\varrho}&=\frac{\partial}{\partial\Phi_{ab}}\left\langle\hat{K}\right\rangle_{\varrho}+\frac{\partial}{\partial\Phi_{ab}}\left\langle\hat{V}_{BO}\right\rangle_{\varrho}=\frac{\partial}{\partial\Phi_{ab}}\frac{1}{2}\sum_{cd}\Phi_{cd}\Upsilon^{-1}_{cd}+\frac{\partial}{\partial\Phi_{ab}}\left\langle\hat{V}_{BO}\right\rangle_{\varrho} \\ &=\frac{1}{2}\Upsilon^{-1}_{ab}+\frac{1}{2}\sum_{cd}\Phi_{cd}\frac{\partial\Upsilon^{-1}_{cd}}{\partial\Phi_{ab}}+\frac{1}{2}\sum_{cd}\frac{\partial\Upsilon^{-1}_{cd}}{\partial\Phi_{ab}}\left\langle\frac{\partial^2V_{BO}}{\partial R_c\partial R_d}\right\rangle_{\varrho} \end{aligned} \tag{3.B.13}$$

obtained from the harmonic kinetic energy (3.A.46) and the SCHA derivation trick (3.2.15). So we have for the derivative of the entropy functional

$$\begin{aligned}\frac{\partial \tilde{S}}{\partial \Phi_{ab}} &= -\frac{\partial}{\partial \Phi_{ab}} \operatorname{Tr}[\varrho \log \varrho] - \beta \frac{\partial}{\partial \Phi} \langle H \rangle_{\varrho} = 0 \\ &= \frac{\eta}{2} \Upsilon^{-1}_{ab} + \eta \sum_{cd} \Phi_{cd} \frac{\partial \Upsilon^{-1}_{cd}}{\partial \Phi_{ab}} - \frac{\beta}{2} \Upsilon^{-1}_{ab} - \frac{\beta}{2} \sum_{cd} \Phi_{cd} \frac{\partial \Upsilon^{-1}_{cd}}{\partial \Phi_{ab}} - \frac{\beta}{2} \sum_{cd} \frac{\partial \Upsilon^{-1}_{cd}}{\partial \Phi_{ab}} \left\langle \frac{\partial^2 \hat{V}_{BO}}{\partial R_c \partial R_d} \right\rangle_{\varrho} \\ &= \frac{1}{2}(\eta - \beta) \Upsilon^{-1}_{ab} + (\eta - \frac{\beta}{2}) \sum_{cd} \Phi_{cd} \frac{\partial \Upsilon^{-1}_{cd}}{\partial \Phi_{ab}} - \frac{\beta}{2} \sum_{cd} \frac{\partial \Upsilon^{-1}_{cd}}{\partial \Phi_{ab}} \left\langle \frac{\partial^2 \hat{V}_{BO}}{\partial R_c \partial R_d} \right\rangle_{\varrho} = 0 \,.\end{aligned} \tag{3.B.14}$$

Variations in $\delta\eta$

From (3.B.1), we set the derivative of the entropy function with respect to η to zero, yielding

$$\frac{\partial \tilde{S}}{\partial \eta} = \frac{\partial}{\partial \eta} \operatorname{Tr}[\hat{\varrho} \log \hat{\varrho}] + \beta \frac{\partial}{\partial \eta} \operatorname{Tr}\left[\hat{\varrho} \hat{H}\right] = 0 \,. \tag{3.B.15}$$

We compute the derivative of the entropy directly from (3.2.19), obtaining

$$\begin{aligned}\frac{\partial}{\partial \eta}[-\operatorname{Tr}(\hat{\varrho} \log \hat{\varrho})] &= \frac{\partial}{\partial \eta} \left[\frac{1}{2} \sum_{\mu} \left[\eta \hbar \omega_{\mu} \coth\left(\tfrac{1}{2} \eta \hbar \omega_{\mu}\right) - 2 \log\left(\sinh\left(\tfrac{1}{2} \eta \hbar \omega_{\mu}\right)\right) \right] \right] \\ &= -\frac{\eta}{4} \sum_{\mu} \frac{\hbar^2 \omega_{\mu}^2}{\sinh^2(\frac{1}{2} \eta \hbar \omega_{\mu})}\end{aligned} \tag{3.B.16}$$

Let's rearrange the last term by noting the relation

$$\frac{\partial}{\partial \eta} \xi_{\mu}^2 = \frac{\partial}{\partial \eta} \left(\frac{\hbar}{2\omega_{\mu}} \coth\left(\tfrac{1}{2} \eta \hbar \omega_{\mu}\right) \right) = -\frac{\hbar^2}{4} \frac{1}{\sinh^2(\frac{1}{2} \eta \hbar \omega_{\mu})} \tag{3.B.17}$$

hence

$$\frac{\partial}{\partial \eta}[-\operatorname{Tr}(\hat{\varrho} \log \hat{\varrho})] = -\frac{\eta}{4} \sum_{\mu} \frac{\hbar^2 \omega_{\mu}^2}{\sinh^2(\frac{1}{2} \hbar \omega_{\mu} \eta)} = \eta \sum_{\mu} \omega_{\mu}^2 \frac{\partial \xi_{\mu}^2}{\partial \eta} = \eta \sum_{ab} \Phi_{ab} \frac{\partial \Upsilon^{-1}_{ab}}{\partial \eta} \tag{3.B.18}$$

The other term to be calculated is $\frac{\partial}{\partial \eta} \left\langle \hat{H} \right\rangle_{\varrho} = \frac{\partial}{\partial \eta} \left\langle \hat{K} + \hat{V}_{BO} \right\rangle_{\rho}$. To compute it we exploit the expressions of the average kinetic energy (3.A.46)

$$\frac{\partial}{\partial \eta} \langle K \rangle_{\varrho} = \frac{1}{2} \sum_{ab} \Phi_{ab} \frac{\partial \Upsilon^{-1}_{ab}}{\partial \eta} \tag{3.B.19}$$

and the SCHA derivation result (3.2.15)

$$\frac{\partial}{\partial \eta} \left\langle \hat{V}_{BO} \right\rangle_{\varrho} = \sum_{a} \frac{\partial \mathcal{R}_a}{\partial \eta} \left\langle \frac{\partial \hat{V}_{BO}}{\partial R_a} \right\rangle_{\varrho} + \frac{1}{2} \sum_{ab} \frac{\partial \Upsilon^{-1}_{ab}}{\partial \eta} \left\langle \frac{\partial^2 \hat{V}_{BO}}{\partial R_a \partial R_b} \right\rangle_{\varrho}. \tag{3.B.20}$$

Overall we have

$$\frac{\partial \tilde{S}}{\partial \eta} = (\eta - \frac{\beta}{2}) \sum_{ab} \Phi_{ab} \frac{\partial \Upsilon^{-1}_{ab}}{\partial \eta} - \beta \sum_{a} \frac{\partial \mathcal{R}_a}{\partial \eta} \left\langle \frac{\partial \hat{V}_{BO}}{\partial R_a} \right\rangle_{\varrho} - \frac{\beta}{2} \sum_{ab} \frac{\partial \Upsilon^{-1}_{ab}}{\partial \eta} \left\langle \frac{\partial^2 \hat{V}_{BO}}{\partial R_a \partial R_b} \right\rangle_{\varrho} = 0. \tag{3.B.21}$$

Coupled equations for the entropy maximization in SCHA

Combining Eqs. (3.B.7),(3.B.14), (3.B.21), we get a system of coupled equations

$$\begin{aligned} -\left\langle \frac{\partial \hat{V}_{BO}}{\partial R_a} \right\rangle_{\varrho} &= 0 \,, \\ \frac{1}{2}(\eta-\beta)\Upsilon^{-1}_{ab} + (\eta-\frac{\beta}{2})\sum_{cd}\Phi_{cd}\frac{\partial \Upsilon^{-1}_{cd}}{\partial \Phi_{ab}} - \frac{\beta}{2}\sum_{cd}\frac{\partial \Upsilon^{-1}_{cd}}{\partial \Phi_{ab}}\left\langle \frac{\partial^2 \hat{V}_{BO}}{\partial R_c \partial R_d}\right\rangle_{\varrho} &= 0 \,, \\ (\eta-\frac{\beta}{2})\sum_{ab}\Phi_{ab}\frac{\partial \Upsilon^{-1}_{ab}}{\partial \eta} - \beta\sum_{a}\frac{\partial \mathcal{R}_a}{\partial \eta}\left\langle \frac{\partial \hat{V}_{BO}}{\partial R_a}\right\rangle_{\varrho} - \frac{\beta}{2}\sum_{ab}\frac{\partial \Upsilon^{-1}_{ab}}{\partial \eta}\left\langle \frac{\partial^2 \hat{V}_{BO}}{\partial R_a \partial R_b}\right\rangle_{\varrho} &= 0 \,. \end{aligned} \tag{3.B.22}$$

The first equation can be readily substituted into the third to get

$$\begin{aligned} \frac{1}{2}(\eta-\beta)\Upsilon^{-1}_{ab} + (\eta-\frac{\beta}{2})\sum_{cd}\Phi_{cd}\frac{\partial \Upsilon^{-1}_{cd}}{\partial \Phi_{ab}} - \frac{\beta}{2}\sum_{cd}\frac{\partial \Upsilon^{-1}_{cd}}{\partial \Phi_{ab}}\left\langle \frac{\partial^2 \hat{V}_{BO}}{\partial R_c \partial R_d}\right\rangle_{\varrho} &= 0 \,, \\ (\eta-\frac{\beta}{2})\sum_{ab}\Phi_{ab}\frac{\partial \Upsilon^{-1}_{ab}}{\partial \eta} - \frac{\beta}{2}\sum_{ab}\frac{\partial \Upsilon^{-1}_{ab}}{\partial \eta}\left\langle \frac{\partial^2 \hat{V}_{BO}}{\partial R_a \partial R_b}\right\rangle_{\varrho} &= 0 \,. \end{aligned} \tag{3.B.23}$$

which can be rewritten as

$$\begin{aligned} (\eta-\beta)[\Upsilon^{-1}_{ab} + \sum_{cd}\Phi_{cd}\frac{\partial \Upsilon^{-1}_{cd}}{\partial \Phi_{ab}}] + \sum_{cd}\left(\eta\Phi_{cd} - \beta\left\langle \frac{\partial^2 \hat{V}_{BO}}{\partial R_c \partial R_d}\right\rangle_{\varrho}\right)\frac{\partial \Upsilon^{-1}_{cd}}{\partial \Phi_{cd}} &= 0 \\ \sum_{ab}\left(-\beta\left\langle \frac{\partial^2 \hat{V}_{BO}}{\partial R_a \partial R_b}\right\rangle_{\varrho} + (2\eta-\beta)\Phi_{ab}\right)\frac{\partial \Upsilon^{-1}_{ab}}{\partial \eta} &= 0 \,. \end{aligned} \tag{3.B.24}$$

Since Υ is positive definite and, being a temperature, $\eta{>}0$, the last equation implies

$$\beta\left\langle \frac{\partial^2 \hat{V}_{BO}}{\partial R_a \partial R_b}\right\rangle_{\varrho} = (2\eta-\beta)\Phi_{ab} \,. \tag{3.B.25}$$

The latter relation can be used in the first equation of (3.B.24), obtaining

$$\begin{aligned} (\eta-\beta)[\Upsilon^{-1}_{ab} + \sum_{cd}\Phi_{cd}\frac{\partial \Upsilon^{-1}_{cd}}{\partial \Phi_{ab}}] + \sum_{cd}(\eta\Phi_{cd} - (2\eta-\beta)\Phi_{cd})\frac{\partial \Upsilon^{-1}_{cd}}{\partial \Phi_{cd}} &= 0 \\ (\eta-\beta)\Upsilon^{-1}_{ab} + (\eta-\beta)\sum_{cd}\Phi_{cd}\frac{\partial \Upsilon^{-1}_{cd}}{\partial \Phi_{ab}} + (\beta-\eta)\sum_{cd}\Phi_{cd}\frac{\partial \Upsilon^{-1}_{cd}}{\partial \Phi_{cd}} &= 0 \\ (\eta-\beta)\Upsilon^{-1}_{ab} &= 0 \end{aligned} \tag{3.B.26}$$

which finally implies

$$\eta = \beta \tag{3.B.27}$$

that combined with (3.B.25) yields

$$\left\langle \frac{\partial^2 \hat{V}_{BO}}{\partial R_a \partial R_b}\right\rangle_{\rho} = \Phi_{ab} \,. \tag{3.B.28}$$

Eqs. (3.B.7),(3.B.27),(3.B.28) prove the SCHA equations (3.2.26) obtained from the MEP.

3.C TD-SCHA equations of motion

In this Appendix, we prove the Wigner-TD-SCHA equations of motion Eqs (**??**). For compactness, we define the mass-rescaled free parameters

$$\begin{aligned}
&\widetilde{\alpha}(t)_{ab} = \frac{\alpha(t)_{ab}}{\sqrt{m_a m_b}} \quad \widetilde{\beta}(t)_{ab} = \sqrt{m_a m_b}\beta(t)_{ab} \quad \widetilde{\gamma}(t)_{ab} = \sqrt{\frac{m_b}{m_a}}\gamma(t)_{ab} \\
&\widetilde{R}_a = \sqrt{m_a}R_a \quad \widetilde{\mathcal{R}}(t)_a = \sqrt{m_a}\mathcal{R}(t)_a \\
&\widetilde{P}_a = \frac{P_a}{\sqrt{m_a}} \quad \widetilde{\mathcal{P}}(t)_a = \frac{\mathcal{P}(t)_a}{\sqrt{m_a}}
\end{aligned} \tag{3.C.1}$$

The equation of motion for the free parameters $\overleftrightarrow{\widetilde{\boldsymbol{\alpha}}}(t), \overleftrightarrow{\widetilde{\boldsymbol{\beta}}}(t), \overleftrightarrow{\widetilde{\boldsymbol{\gamma}}}(t), \vec{\widetilde{\boldsymbol{\mathcal{R}}}}(t), \vec{\widetilde{\boldsymbol{\mathcal{P}}}}(t)$ are found with Eq. (3.3.13) (we drop the arrows above matrices and vectors in intermediate steps):

$$\begin{aligned}
\frac{\partial \varrho(\boldsymbol{R},\boldsymbol{P},t)}{\partial t} =& \frac{\partial \mathcal{H}[\varrho]}{\partial \widetilde{\boldsymbol{R}}} \cdot \frac{\partial \varrho(\boldsymbol{R},\boldsymbol{P},t)}{\partial \widetilde{\boldsymbol{P}}} - \frac{\partial \mathcal{H}[\varrho]}{\partial \widetilde{\boldsymbol{P}}} \cdot \frac{\partial \varrho(\boldsymbol{R},\boldsymbol{P},t)}{\partial \widetilde{\boldsymbol{R}}} = \\
=& \left(\left\langle \frac{\partial V_{\text{tot}}}{\partial \widetilde{\boldsymbol{R}}} \right\rangle_{\varrho(t)} + \delta\widetilde{\boldsymbol{R}}(t) \cdot \left\langle \frac{\partial^2 V_{\text{tot}}}{\partial \widetilde{\boldsymbol{R}} \partial \widetilde{\boldsymbol{R}}} \right\rangle_{\varrho(t)} \right) \cdot \frac{\partial \varrho(\boldsymbol{R},\boldsymbol{P},t)}{\partial \widetilde{\boldsymbol{P}}} \\
&- \left(\delta\widetilde{\boldsymbol{P}}(t) + \widetilde{\boldsymbol{\mathcal{P}}}(t) \right) \cdot \frac{\partial \varrho(\boldsymbol{R},\boldsymbol{P},t)}{\partial \widetilde{\boldsymbol{R}}}
\end{aligned} \tag{3.C.2}$$

with $\delta\widetilde{\boldsymbol{R}}(t) = \widetilde{\boldsymbol{R}} - \widetilde{\boldsymbol{\mathcal{R}}}(t)$ and $\delta\widetilde{\boldsymbol{P}}(t) = \widetilde{\boldsymbol{P}} - \widetilde{\boldsymbol{\mathcal{P}}}(t)$. The gradient of $\varrho(\boldsymbol{R},\boldsymbol{P},t)$, defined in Eq. (3.3.8), is

$$\frac{\partial \log\left(\varrho(\boldsymbol{R},\boldsymbol{P},t)\right)}{\partial \widetilde{\boldsymbol{P}}} = -\widetilde{\boldsymbol{\beta}}(t) \cdot \delta\widetilde{\boldsymbol{P}}(t) + \widetilde{\boldsymbol{\gamma}}^T(t) \cdot \delta\widetilde{\boldsymbol{R}}(t), \tag{3.C.3a}$$

$$\frac{\partial \log\left(\varrho(\boldsymbol{R},\boldsymbol{P},t)\right)}{\partial \widetilde{\boldsymbol{R}}} = -\widetilde{\boldsymbol{\alpha}}(t) \cdot \delta\widetilde{\boldsymbol{R}}(t) + \widetilde{\boldsymbol{\gamma}}(t) \cdot \delta\widetilde{\boldsymbol{P}}(t). \tag{3.C.3b}$$

The time derivative of $\varrho(\boldsymbol{R},\boldsymbol{P},t)$ gives

$$\begin{aligned}
&\frac{\partial \log\left(\varrho(\boldsymbol{R},\boldsymbol{P},t)\right)}{\partial t} = \frac{\dot{\mathcal{N}}(t)}{\mathcal{N}(t)} \\
&- \frac{1}{2}\delta\widetilde{\boldsymbol{R}}(t) \cdot \dot{\widetilde{\boldsymbol{\alpha}}}(t) \cdot \delta\widetilde{\boldsymbol{R}}(t) - \frac{1}{2}\delta\widetilde{\boldsymbol{P}}(t) \cdot \dot{\widetilde{\boldsymbol{\beta}}}(t) \cdot \delta\boldsymbol{P}(t) \\
&+ \delta\widetilde{\boldsymbol{R}}(t) \cdot \dot{\widetilde{\boldsymbol{\gamma}}}(t) \cdot \delta\widetilde{\boldsymbol{P}}(t) + \\
&+ \dot{\widetilde{\boldsymbol{\mathcal{R}}}}(t) \cdot \boldsymbol{\alpha}(t) \cdot \delta\widetilde{\boldsymbol{R}}(t) + \dot{\widetilde{\boldsymbol{\mathcal{P}}}}(t) \cdot \widetilde{\boldsymbol{\beta}}(t) \cdot \delta\widetilde{\boldsymbol{P}}(t) - \dot{\widetilde{\boldsymbol{\mathcal{R}}}}(t) \cdot \widetilde{\boldsymbol{\gamma}}(t) \cdot \delta\widetilde{\boldsymbol{P}}(t) \\
&- \dot{\widetilde{\boldsymbol{\mathcal{P}}}}(t) \cdot \widetilde{\boldsymbol{\gamma}}^T(t) \cdot \delta\widetilde{\boldsymbol{R}}(t),
\end{aligned} \tag{3.C.4}$$

where $\dot{\circ}$ denotes the time derivative. With Eqs (3.C.3) and Eq. (3.C.4) the Wigner-Liouville equation Eq. (3.C.2) becomes a polynomial in $\delta\widetilde{\boldsymbol{R}}(t)\,\delta\widetilde{\boldsymbol{P}}(t)$ then, setting to zero the coefficients,

we get the equations of motion for the free parameters

$$\frac{d}{dt}\vec{\vec{\mathcal{R}}}(t) = \vec{\vec{\mathcal{P}}}(t) \tag{3.C.5a}$$

$$\frac{d}{dt}\vec{\vec{\mathcal{P}}}(t) = -\left\langle \frac{\partial V_{\text{tot}}}{\partial \vec{\vec{R}}} \right\rangle_{\varrho(t)} \tag{3.C.5b}$$

$$\frac{d}{dt}\overleftrightarrow{\alpha}(t) = -\left\langle \frac{\partial^2 V_{\text{tot}}}{\partial \vec{\vec{R}} \partial \vec{\vec{R}}} \right\rangle_{\varrho(t)} \cdot \overleftrightarrow{\gamma}^T(t) - \overleftrightarrow{\gamma}(t) \cdot \left\langle \frac{\partial^2 V_{\text{tot}}}{\partial \vec{\vec{R}} \partial \vec{\vec{R}}} \right\rangle_{\varrho(t)} \tag{3.C.5c}$$

$$\frac{d}{dt}\overleftrightarrow{\beta}(t) = \overleftrightarrow{\gamma}^T(t) + \widetilde{\gamma}(t) \tag{3.C.5d}$$

$$\frac{d}{dt}\overleftrightarrow{\gamma}(t) = \overleftrightarrow{\alpha}(t) - \left\langle \frac{\partial^2 V_{\text{tot}}}{\partial \vec{\vec{R}} \partial \vec{\vec{R}}} \right\rangle_{\varrho(t)} \cdot \overleftrightarrow{\beta}(t) \tag{3.C.5e}$$

where $\circ^\dagger$ denotes the hermitian conjugate of a matrix. The equations of motion for the tensors keep the distribution normalized.

3.D Linear expansion of the TD-SCHA density matrix

In this Appendix, we show how to expand at first order the TD-SCHA position probability distribution and how the anharmonic vertices, Eqs (3.3.58) (3.3.59), emerge. All the free parameters are perturbed with respect to their static value (denoted by (0))

$$\vec{\mathcal{R}}(t) = \vec{\mathcal{R}}^{(0)} + \vec{\mathcal{R}}^{(1)}(t) \tag{3.D.1a}$$

$$\vec{\mathcal{P}}(t) = \vec{\mathcal{P}}^{(1)}(t) \tag{3.D.1b}$$

$$\overleftrightarrow{\alpha}(t) = \overleftrightarrow{\alpha}^{(0)} + \overleftrightarrow{\alpha}^{(1)}(t) \tag{3.D.1c}$$

$$\overleftrightarrow{\beta}(t) = \overleftrightarrow{\beta}^{(0)} + \overleftrightarrow{\beta}^{(1)}(t) \tag{3.D.1d}$$

$$\overleftrightarrow{\gamma}(t) = \overleftrightarrow{\gamma}^{(1)}(t) \tag{3.D.1e}$$

The first thing to do is to expand at first order the position probability distribution in the perturbative free parameters, *i.e.* those denoted by the superscript (1). Before performing the expansion, we report the full position probability distribution obtained from Eq. (3.3.8)

$$\begin{aligned} \varrho(\vec{R}, t) = & \sqrt{\det\left(\frac{\overleftrightarrow{\alpha}(t) - \overleftrightarrow{\gamma}(t) \cdot \overleftrightarrow{\beta}^{-1}(t) \cdot \overleftrightarrow{\gamma}(t)^T}{2\pi}\right)} \\ & \times \exp\left[-\frac{1}{2}(\vec{R} - \vec{\mathcal{R}}(t)) \cdot \left(\overleftrightarrow{\alpha}(t) - \overleftrightarrow{\gamma}(t) \cdot \overleftrightarrow{\beta}^{-1}(t) \cdot \overleftrightarrow{\gamma}(t)^T\right) \cdot (\vec{R} - \vec{\mathcal{R}}(t))\right]. \end{aligned} \tag{3.D.2}$$

The leading order is controlled by $\overleftrightarrow{\alpha}^{(0)} + \overleftrightarrow{\alpha}^{(1)}(t)$. We define the displacements with respect the equilibrium position as $\delta\vec{\vec{R}}^{(0)} = \vec{\vec{R}} - \vec{\vec{\mathcal{R}}}^{(0)}$. The expansion gives

$$\varrho(\vec{R}, t) = \varrho^{(0)}(\vec{R}) + \varrho^{(1)}(\vec{R}, t), \tag{3.D.3}$$

where $\varrho^{(0)}(\vec{\boldsymbol{R}})$ is the equilibrium probability distribution (see Eq. (**??**))

$$\varrho^{(0)}(\vec{\boldsymbol{R}}) = \sqrt{\det\left(\frac{\overleftrightarrow{\boldsymbol{\alpha}}^{(0)}}{2\pi}\right)} \exp\left(-\frac{1}{2}\delta\vec{\tilde{\boldsymbol{R}}}^{(0)} \cdot \overleftrightarrow{\tilde{\boldsymbol{\alpha}}}^{(0)} \cdot \delta\vec{\tilde{\boldsymbol{R}}}^{(0)}\right). \tag{3.D.4}$$

The explicit expression for $\varrho^{(1)}(\vec{\boldsymbol{R}}, t)$ in Eq. (3.D.3), following,[50] is

$$\begin{aligned}\varrho^{(1)}(\vec{\boldsymbol{R}}, t) =& \varrho^{(0)}(\vec{\boldsymbol{R}}) \left\{ \frac{1}{2} \operatorname{Tr}\left[\overleftrightarrow{\boldsymbol{\alpha}}^{(0)-1} \cdot \overleftrightarrow{\boldsymbol{\alpha}}^{(1)}(t)\right] - \frac{1}{2}\delta\vec{\boldsymbol{R}}^{(0)} \cdot \overleftrightarrow{\boldsymbol{\alpha}}^{(1)}(t) \cdot \delta\vec{\boldsymbol{R}}^{(0)} \right. \\ & \left. + \delta\vec{\boldsymbol{R}}^{(0)} \cdot \overleftrightarrow{\boldsymbol{\alpha}}^{(0)} \cdot \vec{\boldsymbol{\mathcal{R}}}^{(1)}(t) \right\}.\end{aligned} \tag{3.D.5}$$

Next, we derive an expression for the perturbed averages of a position-dependent observable $O(\vec{\boldsymbol{R}})$. Using the expression for $\varrho^{(1)}(\vec{\boldsymbol{R}}, t)$, Eq. (3.D.5), and integration by parts we get

$$\begin{aligned}\left\langle \hat{O} \right\rangle_{(1)}(t) =& \int d\vec{\boldsymbol{R}} \varrho^{(1)}(\vec{\boldsymbol{R}}, t) O(\vec{\boldsymbol{R}}) \\ =& -\frac{1}{2} \sum_{ab=1}^{3N} \tilde{\alpha}^{(1)}(t)_{ab} \left(\left\langle \delta\tilde{R}_a^{(0)} \delta\tilde{R}_b^{(0)} \hat{O} \right\rangle_{(0)} - (\tilde{\alpha}^{(0)})^{-1}_{ba} \left\langle \hat{O} \right\rangle_{(0)} \right) \\ & + \sum_{a=1}^{3N} \tilde{\mathcal{R}}_a^{(1)}(t) \left\langle \frac{\partial \hat{O}}{\partial \tilde{R}_a} \right\rangle_{(0)}.\end{aligned} \tag{3.D.6}$$

Note that now all the averages have to be performed on the equilibrium ensemble. We introduce the equilibrium three and four phonon scattering vertices as in[56]

$$\begin{aligned}\overset{(3)}{D}_{abc} =& \left\langle \frac{\partial V_{\text{BO}}}{\partial\tilde{R}_a \partial\tilde{R}_b \partial\tilde{R}_c} \right\rangle_{(0)} = \sum_{mn=1}^{3N} \tilde{\alpha}_{an}^{(0)} \tilde{\alpha}_{bm}^{(0)} \left\langle \delta\tilde{R}_n \delta\tilde{R}_m \frac{\partial V_{\text{BO}}}{\partial\tilde{R}_c} \right\rangle_{(0)} \\ & - \tilde{\alpha}_{ab}^{(0)} \left\langle \frac{\partial V_{\text{BO}}}{\partial\tilde{R}_c} \right\rangle_{(0)}\end{aligned} \tag{3.D.7a}$$

$$\begin{aligned}\overset{(4)}{D}_{abcd} =& \left\langle \frac{\partial V_{\text{BO}}}{\partial\tilde{R}_a \partial\tilde{R}_b \partial\tilde{R}_c \partial\tilde{R}_d} \right\rangle_{(0)} = \sum_{nm=1}^{3N} \tilde{\alpha}_{an}^{(0)} \tilde{\alpha}_{bm}^{(0)} \left\langle \delta\tilde{R}_n \delta\tilde{R}_m \frac{\partial^2 V_{\text{BO}}}{\partial\tilde{R}_c \partial\tilde{R}_d} \right\rangle_{(0)} \\ & - \tilde{\alpha}_{ab}^{(0)} \left\langle \frac{\partial^2 V_{\text{BO}}}{\partial\tilde{R}_c \partial\tilde{R}_d} \right\rangle_{(0)}.\end{aligned} \tag{3.D.7b}$$

It is convenient also to introduce the potential $\mathbb{V}(\vec{\boldsymbol{R}})$ as the difference between the BO potential and the harmonic auxiliary potential obtained at equilibrium

$$\mathbb{V}(\vec{\boldsymbol{R}}) = V_{\text{BO}}(\vec{\boldsymbol{R}}) - \frac{1}{2}\delta\vec{\tilde{\boldsymbol{R}}}^{(0)} \cdot \overleftrightarrow{\boldsymbol{D}} \cdot \delta\vec{\tilde{\boldsymbol{R}}}^{(0)}, \tag{3.D.8}$$

where $\overleftrightarrow{\boldsymbol{D}}$ defines the SCHA phonons, Eq. (3.3.24). Using Eq. (3.D.6), we relate the perturbed averages of $\mathbb{V}(\vec{\boldsymbol{R}})$ to the scattering vertices of Eqs (3.D.7)

$$\left\langle \frac{\partial \mathbb{V}}{\partial \widetilde{R}_a} \right\rangle_{(1)} = \frac{1}{2} \sum_{bcde=1}^{3N} \widetilde{\alpha}^{(1)}(t)_{de} (\widetilde{\alpha}^{(0)-1})_{db} (\widetilde{\alpha}^{(0)-1})_{ec} \overset{(3)}{D}_{abc}; \tag{3.D.9a}$$

$$\left\langle \frac{\partial^2 \mathbb{V}}{\partial \widetilde{R}_a \partial \widetilde{R}_b} \right\rangle_{(1)} = \sum_{c=1}^{3N} \overset{(3)}{D}_{abc} \widetilde{\mathcal{R}}^{(1)}(t)_c - \frac{1}{2} \sum_{cdef=1}^{3N} \widetilde{\alpha}^{(1)}(t)_{ef} (\widetilde{\alpha}^{(0)-1})_{ec} (\widetilde{\alpha}^{(0)-1})_{fd} \overset{(4)}{D}_{abcd}. \tag{3.D.9b}$$

At this point it is straightforward to get the following perturbed averages for the BO potential:

$$\left\langle \frac{\partial \mathbb{V}}{\partial \widetilde{R}_a} \right\rangle_{(1)} = \left\langle \frac{\partial V_{\text{BO}}}{\partial \widetilde{R}_a} \right\rangle_{(1)} - \sum_{b=1}^{3N} D_{ab} \widetilde{\mathcal{R}}^{(1)}_b(t), \tag{3.D.10a}$$

$$\left\langle \frac{\partial^2 \mathbb{V}}{\partial \widetilde{R}_a \partial \widetilde{R}_b} \right\rangle_{(1)} = \left\langle \frac{\partial^2 V_{\text{BO}}}{\partial \widetilde{R}_a \partial \widetilde{R}_b} \right\rangle_{(1)}. \tag{3.D.10b}$$

3.E Derivation of the linearized TD-SCHA equations

In this Appendix, we prove the linearized equations of motion discussed in Section 3.3.2. To do this we write all the supercell tensors in the static equilibrium polarization basis $\{\boldsymbol{e}_\mu\}$ defined in Eq. (3.3.24). So a multi-indices tensor $A(t)_{a_1,..,a_N}$ defined in the supercell can be written in the polarization basis as

$$A(t)_{\mu_1,..,\mu_N} = \sum_{a_1,..,a_N=1}^{3N} e_{\mu_1,a_1} .. e_{\mu_N,a_N} A(t)_{a_1,..,a_N}. \tag{3.E.1}$$

From now on all the quantities are written in this basis.

All the supercell tensors are written in the equilibrium polarization basis, see Eq. (3.E.1). The equations of motion (Eqs (3.C.5)) expanded at first order are

$$\frac{d^2}{dt^2} \widetilde{\mathcal{R}}^{(1)}(t)_\alpha = -\omega_\alpha^2 \widetilde{\mathcal{R}}^{(1)}(t)_\alpha - \left\langle \frac{\partial \mathbb{V}}{\partial \widetilde{R}_\alpha} \right\rangle_{(1)} - \left\langle \frac{\partial V_{\text{ext}}(t)}{\partial \widetilde{R}_\alpha} \right\rangle_{(0)}; \tag{3.E.2a}$$

$$\frac{d}{dt} \widetilde{\alpha}^{(1)}(t)_{\alpha\beta} = -2 \sum_{\mu\nu=1}^{3N} S_{\alpha\beta\mu\nu} \left(\widetilde{\gamma}^{(1)}(t)_{\mu\nu} \omega_\nu^2 \right); \tag{3.E.2b}$$

$$\frac{d}{dt} \widetilde{\beta}^{(1)}(t)_{\alpha\beta} = 2 \sum_{\mu\nu=1}^{3N} S_{\alpha\beta\mu\nu} \left(\widetilde{\gamma}^{(1)}(t)_{\mu\nu} \right); \tag{3.E.2c}$$

$$\frac{d}{dt} \widetilde{\gamma}^{(1)}(t)_{\alpha\beta} = \widetilde{\alpha}^{(1)}(t)_{\alpha\beta} - \omega_\alpha^2 \widetilde{\beta}^{(1)}(t)_{\alpha\beta} - \left[\left\langle \frac{\partial^2 V_{\text{ext}}(t)}{\partial \widetilde{R}_\alpha \partial \widetilde{R}_\beta} \right\rangle_{(0)} + \left\langle \frac{\partial^2 \mathbb{V}}{\partial \widetilde{R}_\alpha \partial \widetilde{R}_\beta} \right\rangle_{(1)} \right] \widetilde{\beta}^{(0)}_{\alpha\beta}, \tag{3.E.2d}$$

where

$$S_{\alpha\beta\mu\nu} = \frac{1}{2} (\delta_{\alpha\mu}\delta_{\beta\nu} + \delta_{\alpha\nu}\delta_{\beta\mu}) \tag{3.E.3}$$

and $\mathbb{V}(\vec{\boldsymbol{R}})$ is the difference between the exact BO energy surface and the SCHA auxiliary

potential, Eq. (3.D.8). The averages of $\mathbb{V}(\vec{\boldsymbol{R}})$ are defined in Eqs. (3.D.9) and contain anharmonic corrections. Now, we derive with respect to time Eqs (3.E.2) to delete the equation for $\overleftrightarrow{\widetilde{\gamma}}^{(1)}(t)$ since the perturbed averages do not depend on this parameter, see Eq. (3.D.6). Next, we take the Fourier transform of the second order set of differential equations for $\vec{\widetilde{\boldsymbol{\mathcal{R}}}}^{(1)}(t)$ $\overleftrightarrow{\widetilde{\alpha}}^{(1)}(t)$ and $\overleftrightarrow{\widetilde{\beta}}^{(1)}(t)$. Finally, we perform a change of variables. Instead of using the basis $\{\overleftrightarrow{\widetilde{\boldsymbol{\alpha}}}^{(1)}(\omega), \overleftrightarrow{\widetilde{\boldsymbol{\beta}}}^{(1)}(\omega)\}$, we work with $\{\overleftrightarrow{\widetilde{\boldsymbol{a}}}'^{(1)}(\omega), \overleftrightarrow{\widetilde{\boldsymbol{b}}}'^{(1)}(\omega)\}$ which is defined as a linear combination of the original free parameters

$$\begin{bmatrix} \widetilde{a}'^{(1)}(\omega)_{\mu\nu} \\ \widetilde{b}'^{(1)}(\omega)_{\mu\nu} \end{bmatrix} = M_{\mu\nu} \begin{bmatrix} \widetilde{\alpha}^{(1)}(\omega)_{\mu\nu} \\ \widetilde{\beta}^{(1)}(\omega)_{\mu\nu} \end{bmatrix}, \tag{3.E.4}$$

where we define $\boldsymbol{M}$ as

$$M_{\mu\nu} = \begin{bmatrix} \frac{K^-_{\mu\nu}}{\omega_\mu \omega_\nu} & K^-_{\mu\nu} \\ \\ -\frac{K^+_{\mu\nu}}{\omega_\mu \omega_\nu} & K^+_{\mu\nu} \end{bmatrix}. \tag{3.E.5}$$

The coefficients in Eqs (3.E.5) are functions of the equilibrium auxiliary frequencies $\{\omega_\mu^2\}$ defined in Eq. (3.3.24) and

$$K^\pm_{\mu\nu} = \frac{\hbar^2 n_{\mu\nu}}{2X^\pm_{\mu\nu}}, \tag{3.E.6a}$$

$$X^\pm_{\mu\nu} = \sqrt{\pm\frac{1}{2}\frac{\hbar\left[\omega_\mu \pm \omega_\nu\right]\left[(1\pm 1) + 2(n_\mu \pm n_\nu)\right]}{4\omega_\mu\omega_\nu}}, \tag{3.E.6b}$$

$$n_{\mu\nu} = \frac{1}{8}(1+2n_\nu)(1+2n_\mu). \tag{3.E.6c}$$

Using the basis defined in Eq. (3.E.5) we get the following equations of motion for $\{\vec{\widetilde{\boldsymbol{\mathcal{R}}}}^{(1)}(\omega), \overleftrightarrow{\widetilde{\boldsymbol{a}}}'^{(1)}(\omega), \widetilde{\boldsymbol{b}}'^{(1)}(\omega)\}$:

$$\left(\omega^2 - \omega_\alpha^2\right)\widetilde{\mathcal{R}}^{(1)}(\omega)_\alpha - \left\langle \frac{\partial \mathbb{V}}{\partial \widetilde{R}_\alpha} \right\rangle_{(1)} = \left\langle \frac{\partial V_{\text{ext}}(\omega)}{\partial \widetilde{R}_\alpha} \right\rangle_{(0)}, \tag{3.E.7a}$$

$$\left(\omega^2 - \omega^{-2}_{\alpha\beta}\right)\widetilde{a}'^{(1)}(\omega)_{\alpha\beta} + X^-_{\alpha\beta}\left\langle \frac{\partial^2 \mathbb{V}}{\partial \widetilde{R}_\alpha \partial \widetilde{R}_\beta} \right\rangle_{(1)} = -X^-_{\alpha\beta}\left\langle \frac{\partial^2 V_{\text{ext}}(\omega)}{\partial \widetilde{R}_\alpha \partial \widetilde{R}_\beta} \right\rangle_{(0)}, \tag{3.E.7b}$$

$$\left(\omega^2 - \omega^{+2}_{\alpha\beta}\right)\widetilde{b}'^{(1)}(\omega)_{\alpha\beta} - X^+_{\alpha\beta}\left\langle \frac{\partial^2 \mathbb{V}}{\partial \widetilde{R}_\alpha \partial \widetilde{R}_\beta} \right\rangle_{(1)} = X^+_{\alpha\beta}\left\langle \frac{\partial^2 V_{\text{ext}}(\omega)}{\partial \widetilde{R}_\alpha \partial \widetilde{R}_\beta} \right\rangle_{(0)}, \tag{3.E.7c}$$

where ω^2 comes from the Fourier transform of a second order derivative with respect to time.

Eqs. (3.E.7) are written in terms of a matrix vector product in the space of the perturbative free parameters. Recalling the definition of $V_{\text{ext}}(\vec{\boldsymbol{R}}, \omega) = \mathcal{B}(\boldsymbol{R})\mathcal{V}(\omega)$, we write the linearized

equations of motion as a matrix-vector product

$$(\omega^2 \mathbf{1} + \boldsymbol{\mathcal{L}}') \cdot \begin{bmatrix} \vec{\widetilde{\boldsymbol{\mathcal{R}}}}^{(1)}(\omega) \\ \overleftrightarrow{\widetilde{\boldsymbol{a}}}'^{(1)}(\omega) \\ \overleftrightarrow{\widetilde{\boldsymbol{b}}}'^{(1)}(\omega) \end{bmatrix} = \begin{bmatrix} \left\langle \frac{\partial \mathcal{B}}{\partial \vec{\widetilde{\boldsymbol{R}}}} \right\rangle_{(0)} \\ -\overset{(4)}{\boldsymbol{X}}^{-} : \left\langle \frac{\partial^2 \mathcal{B}}{\partial \vec{\widetilde{\boldsymbol{R}}} \partial \vec{\widetilde{\boldsymbol{R}}}} \right\rangle_{(0)} \\ \overset{(4)}{\boldsymbol{X}}^{+} : \left\langle \frac{\partial^2 \mathcal{B}}{\partial \vec{\widetilde{\boldsymbol{R}}} \partial \vec{\widetilde{\boldsymbol{R}}}} \right\rangle_{(0)} \end{bmatrix} \mathcal{V}(\omega), \tag{3.E.8}$$

where

$$\overset{(4)}{X}{}^{\pm}{}_{\alpha\beta\mu\nu} = X^{\pm}_{\alpha\beta} S_{\alpha\beta\mu\nu} \tag{3.E.9}$$

with $X^{\pm}_{\alpha\beta}$ defined in Eq. (3.E.6b) and $S_{\alpha\beta\mu\nu}$ in Eq. (3.E.3). We define the RHS vector as the perturbation vector $\boldsymbol{p}'$

$$\boldsymbol{p}'^{\dagger} = \left[\left\langle \frac{\partial \mathcal{B}}{\partial \vec{\widetilde{\boldsymbol{R}}}} \right\rangle_{(0)}, \quad -\overset{(4)}{\boldsymbol{X}}^{-} : \left\langle \frac{\partial^2 \mathcal{B}}{\partial \vec{\widetilde{\boldsymbol{R}}} \partial \vec{\widetilde{\boldsymbol{R}}}} \right\rangle_{(0)}, \quad \overset{(4)}{\boldsymbol{X}}^{+} : \left\langle \frac{\partial^2 \mathcal{B}}{\partial \vec{\widetilde{\boldsymbol{R}}} \partial \vec{\widetilde{\boldsymbol{R}}}} \right\rangle_{(0)} \right]. \tag{3.E.10}$$

The matrix $\boldsymbol{\mathcal{L}}'$ acts in the space of the perturbative parameters. It is symmetric and contains two terms, the harmonic and anharmonic contribution

$$\boldsymbol{\mathcal{L}}' = \boldsymbol{\mathcal{L}}'_{\text{harm}} + \boldsymbol{\mathcal{L}}'_{\text{anh}}. \tag{3.E.11}$$

The harmonic part $\boldsymbol{\mathcal{L}}'_{\text{harm}}$ is diagonal in our basis

$$\boldsymbol{\mathcal{L}}'_{\text{harm}} \cdot \begin{bmatrix} \vec{\widetilde{\boldsymbol{\mathcal{R}}}}^{(1)}(\omega) \\ \overleftrightarrow{\widetilde{\boldsymbol{a}}}'^{(1)}(\omega) \\ \overleftrightarrow{\widetilde{\boldsymbol{b}}}'^{(1)}(\omega) \end{bmatrix} = - \begin{bmatrix} \overleftrightarrow{\boldsymbol{D}} \cdot & 0 & 0 \\ 0 & \overset{(4)}{\boldsymbol{\omega}}{}^{2}_{-} : & 0 \\ 0 & 0 & \overset{(4)}{\boldsymbol{\omega}}{}^{2}_{+} : \end{bmatrix} \begin{bmatrix} \vec{\widetilde{\boldsymbol{\mathcal{R}}}}^{(1)}(\omega) \\ \overleftrightarrow{\widetilde{\boldsymbol{a}}}'^{(1)}(\omega) \\ \overleftrightarrow{\widetilde{\boldsymbol{b}}}'^{(1)}(\omega) \end{bmatrix}. \tag{3.E.12}$$

The matrix $\boldsymbol{\mathcal{L}}'_{\text{harm}}$ depends only on the equilibrium auxiliary frequencies of Eq. (3.3.24). We introduced a four indices tensor

$$\overset{(4)}{\omega}{}^{2}_{\pm\alpha\beta\mu\nu} = (\omega^{\pm}_{\alpha\beta})^2 S_{\alpha\beta\mu\nu}, \tag{3.E.13}$$

with $\overleftrightarrow{\boldsymbol{S}}$ defined in Eq. (3.E.3) and

$$\omega^{\pm}_{\mu\nu} = \omega_\mu \pm \omega_\nu. \tag{3.E.14}$$

The right-hand side of Eq. (3.E.12) should be read as a standard matrix-vector product. The matrix element contains also information on how to contract the indices, the operation $\cdot$ is defined in general as the contraction of the last and first index of two tensors

$$\boldsymbol{A} \cdot \boldsymbol{B} = \sum_{\mu=1}^{3N} A_{\ldots\mu} B_{\mu\ldots} \tag{3.E.15}$$

and : is defined as

$$\boldsymbol{Q} : \boldsymbol{Q}' = \sum_{\mu\nu=1}^{3N} Q_{\ldots\mu\nu} Q'_{\mu\nu\ldots} \tag{3.E.16}$$

The application of $\boldsymbol{\mathcal{L}}'_{\text{anh}}$ gives

$$\boldsymbol{\mathcal{L}}'_{\text{anh}} \cdot \begin{bmatrix} \vec{\widetilde{\boldsymbol{\mathcal{R}}}}^{(1)}(\omega) \\ \overleftrightarrow{\widetilde{\boldsymbol{a}}}'^{(1)}(\omega) \\ \overleftrightarrow{\widetilde{\boldsymbol{b}}}'^{(1)}(\omega) \end{bmatrix} = \begin{bmatrix} -\left\langle \frac{\partial \mathbb{V}}{\partial \vec{\widetilde{\boldsymbol{R}}}} \right\rangle_{(1)} \\ \overset{(4)}{\boldsymbol{X}}{}^{-} : \left\langle \frac{\partial^2 \mathbb{V}}{\partial \vec{\widetilde{\boldsymbol{R}}} \partial \vec{\widetilde{\boldsymbol{R}}}} \right\rangle_{(1)} \\ -\overset{(4)}{\boldsymbol{X}}{}^{+} : \left\langle \frac{\partial^2 \mathbb{V}}{\partial \vec{\widetilde{\boldsymbol{R}}} \partial \vec{\widetilde{\boldsymbol{R}}}} \right\rangle_{(1)} \end{bmatrix}. \tag{3.E.17}$$

Writing the perturbed averages of $\mathbb{V}(\vec{\boldsymbol{R}})$ in terms of the scattering tensors, as in Eq. (3.D.9), and using the change of variables of Eq. (3.E.5), it is trivial to prove that in the new basis $\boldsymbol{\mathcal{L}}'_{\text{anh}}$ is symmetric and has the following form

$$\boldsymbol{\mathcal{L}}'_{\text{anh}} = \begin{bmatrix} 0 & \overset{(3)}{\boldsymbol{D}} : \overset{(4)}{\boldsymbol{X}}{}^{-} & -\overset{(3)}{\boldsymbol{D}} : \overset{(4)}{\boldsymbol{X}}{}^{+} \\ \overset{(4)}{\boldsymbol{X}}{}^{-} : \overset{(3)}{\boldsymbol{D}} & -\overset{(4)}{\boldsymbol{X}}{}^{-} : \overset{(4)}{\boldsymbol{D}} : \overset{(4)}{\boldsymbol{X}}{}^{-} & \overset{(4)}{\boldsymbol{X}}{}^{-} : \overset{(4)}{\boldsymbol{D}} : \overset{(4)}{\boldsymbol{X}}{}^{+} \\ -\overset{(4)}{\boldsymbol{X}}{}^{+} : \overset{(3)}{\boldsymbol{D}} & \overset{(4)}{\boldsymbol{X}}{}^{+} : \overset{(4)}{\boldsymbol{D}} : \overset{(4)}{\boldsymbol{X}}{}^{-} & -\overset{(4)}{\boldsymbol{X}}{}^{+} : \overset{(4)}{\boldsymbol{D}} : \overset{(4)}{\boldsymbol{X}}{}^{+} \end{bmatrix}. \tag{3.E.18}$$

This term contains information on the anharmonicity of the system through the third and fourth phonon scattering tensors, defined in Eq. (3.D.7).

Now that we have the linearized equations of motion, we present the general response function Eq. (3.3.48). To do this we need the correction of a position-dependent observable $\mathcal{A}(\vec{\boldsymbol{R}})$ in the new basis Eq. (3.E.5)

$$\begin{aligned} \langle \mathcal{A} \rangle_{(1)}(\omega) &= \sum_{\alpha=1}^{3N} \frac{\partial \langle \mathcal{A} \rangle_{(0)}}{\partial \widetilde{\mathcal{R}}_\alpha} \widetilde{\mathcal{R}}^{(1)}(\omega)_\alpha + \sum_{\alpha\beta=1}^{3N} \frac{\partial \langle \mathcal{A} \rangle_{(0)}}{\partial \widetilde{a}'^{(0)}_{\alpha\beta}} \widetilde{a}'^{(1)}(\omega)_{\alpha\beta} + \sum_{\alpha\beta=1}^{3N} \frac{\partial \langle \mathcal{A} \rangle_{(0)}}{\partial \widetilde{b}'^{(0)}_{\alpha\beta}} \widetilde{b}'^{(1)}(\omega)_{\alpha\beta} \\ &= \sum_{\alpha=1}^{3N} \left\langle \frac{\partial \mathcal{A}}{\partial \widetilde{R}_\alpha} \right\rangle_{(0)} \widetilde{\mathcal{R}}^{(1)}(\omega)_\alpha - \sum_{\alpha\beta=1}^{3N} X^-_{\alpha\beta} \left\langle \frac{\partial^2 \mathcal{A}}{\partial \widetilde{R}_\alpha \partial \widetilde{R}_\beta} \right\rangle_{(0)} \widetilde{a}'^{(1)}(\omega)_{\alpha\beta} \\ &\quad + \sum_{\alpha\beta=1}^{3N} X^+_{\alpha\beta} \left\langle \frac{\partial^2 \mathcal{A}}{\partial \widetilde{R}_\alpha \partial \widetilde{R}_\beta} \right\rangle_{(0)} \widetilde{b}'^{(1)}(\omega)_{\alpha\beta}. \end{aligned} \tag{3.E.19}$$

The previous expression can be demonstrated using the change of variable definition, Eq. (3.E.5), the chain rule and the following relations in the original basis (i.e. the one used in appendix 3.D)

$$\frac{\partial \langle \mathcal{A} \rangle_{(0)}}{\partial \widetilde{\mathcal{R}}^{(0)}_\alpha} = \left\langle \frac{\partial \mathcal{A}}{\partial \widetilde{R}_\alpha} \right\rangle_{(0)}, \tag{3.E.20a}$$

$$\frac{\partial \langle \mathcal{A} \rangle_{(0)}}{\partial \widetilde{\alpha}^{(0)}_{\alpha\beta}} = -\frac{1}{2\widetilde{\alpha}^{(0)}_{\alpha\alpha}\widetilde{\alpha}^{(0)}_{\beta\beta}} \left\langle \frac{\partial^2 \mathcal{A}}{\partial \widetilde{R}_\alpha \partial \widetilde{R}_\beta} \right\rangle_{(0)}, \tag{3.E.20b}$$

$$\frac{\partial \langle \mathcal{A} \rangle_{(0)}}{\partial \widetilde{\beta}^{(0)}_{\alpha\beta}} = 0. \tag{3.E.20c}$$

The derivative with respect to $\widetilde{\alpha}^{(0)}_{\alpha\beta}$ is obtained using the formalism of Ref. 56 ($\boldsymbol{\alpha}^{(0)} = \boldsymbol{\Upsilon}^{-1}$ in the standard SCHA notation).

We define the response vector $\boldsymbol{r}'$ similarly to $\boldsymbol{p}'$ (Eq. (3.E.10))

$$\boldsymbol{r}'^{\dagger} = \left[\left\langle \frac{\partial \mathcal{A}}{\partial \vec{\tilde{\boldsymbol{R}}}} \right\rangle_{(0)}, \quad -\overset{(4)}{\boldsymbol{X}}{}^{-} : \left\langle \frac{\partial^2 \mathcal{A}}{\partial \vec{\tilde{\boldsymbol{R}}} \partial \vec{\tilde{\boldsymbol{R}}}} \right\rangle_{(0)}, \quad \overset{(4)}{\boldsymbol{X}}{}^{+} : \left\langle \frac{\partial^2 \mathcal{A}}{\partial \vec{\tilde{\boldsymbol{R}}} \partial \vec{\tilde{\boldsymbol{R}}}} \right\rangle_{(0)} \right] \tag{3.E.21}$$

so from Eq. (3.E.19) we can extract the response formula (Eq. (3.3.48))

$$\frac{\langle \mathcal{A} \rangle_{(1)}(\omega)}{\mathcal{V}(\omega)} = \frac{1}{\mathcal{V}(\omega)} \boldsymbol{r}' \cdot \begin{bmatrix} \vec{\tilde{\boldsymbol{\mathcal{R}}}}^{(1)}(\omega) \\ \overleftrightarrow{\tilde{\boldsymbol{a}}}'^{(1)}(\omega) \\ \overleftrightarrow{\tilde{\boldsymbol{b}}}'^{(1)}(\omega) \end{bmatrix} = \boldsymbol{r}' \cdot \left(\boldsymbol{\mathcal{L}}' + \omega^2 \right)^{-1} \cdot \boldsymbol{p}' = \chi(\omega)_{\mathcal{A},\mathcal{B}} \tag{3.E.22}$$

where $\langle \mathcal{A} \rangle_{(1)}(\omega)$ is expressed as a scalar product in the space of the perturbative parameters.

Modification of the linearized equations for a thermal potential

Here we show how the set of linearized equations (3.E.2) gets modified if the external potential depends also on the ionic momenta $\vec{\boldsymbol{P}}$. In particular, we will consider the case of a external potential of the form

$$\begin{aligned} V_{\text{ext}}(\vec{\boldsymbol{R}}, \vec{\boldsymbol{P}}, t) = C^0(t) + \vec{\boldsymbol{C}}^{(1)}(t) \cdot \boldsymbol{\delta}\vec{\boldsymbol{R}} + \vec{\boldsymbol{C}}^{(2)}(t) \cdot \boldsymbol{\delta}\vec{\boldsymbol{P}} + \tfrac{1}{2} \boldsymbol{\delta}\vec{\boldsymbol{R}} \cdot \overleftrightarrow{\boldsymbol{C}}^{(3)}(t) \cdot \boldsymbol{\delta}\vec{\boldsymbol{R}} \\ + \tfrac{1}{2} \boldsymbol{\delta}\vec{\boldsymbol{P}} \cdot \overleftrightarrow{\boldsymbol{C}}^{(4)}(t) \cdot \boldsymbol{\delta}\vec{\boldsymbol{P}} + \boldsymbol{\delta}\vec{\boldsymbol{R}} \cdot \overleftrightarrow{\boldsymbol{C}}^{(5)}(t) \cdot \boldsymbol{\delta}\vec{\boldsymbol{P}} \end{aligned} \tag{3.E.23}$$

so that

$$\begin{aligned} C_a^{(1)} = \left. \frac{\partial V_{\text{ext}}}{\partial R_a} \right|_{(\delta\vec{\boldsymbol{R}}, \delta\vec{\boldsymbol{P}})=0}; \; C_a^{(2)} = \left. \frac{\partial V_{\text{ext}}}{\partial P_a} \right|_{(\delta\vec{\boldsymbol{R}}, \delta\vec{\boldsymbol{P}})=0} \\ C_{ab}^{(3)} = \left. \frac{\partial^2 V_{\text{ext}}}{\partial R_a \partial R_b} \right|_{(\delta\vec{\boldsymbol{R}}, \delta\vec{\boldsymbol{P}})=0}; \; C_{ab}^{(4)} = \left. \frac{\partial^2 V_{\text{ext}}}{\partial P_a \partial P_b} \right|_{(\delta\vec{\boldsymbol{R}}, \delta\vec{\boldsymbol{P}})=0}; \; C_{ab}^{(5)} = \left. \frac{\partial^2 V_{\text{ext}}(t)}{\partial R_a \partial P_b} \right|_{(\delta\vec{\boldsymbol{R}}, \delta\vec{\boldsymbol{P}})=0}. \end{aligned} \tag{3.E.24}$$

The linear order of TD-SCHA Liouville equation (3.3.13) reads

$$\frac{\partial}{\partial t} \varrho^{(1)}(\vec{\boldsymbol{R}}, \vec{\boldsymbol{P}}, t) = \{ \mathcal{H}^{(0)}[\varrho^{(1)}(t)], \varrho^{(0)}(\vec{\boldsymbol{R}}, \vec{\boldsymbol{P}}) \} + \{ \mathcal{H}^{(0)}[\varrho^{(1)}(t)], \varrho^{(0)}(\vec{\boldsymbol{R}}, \vec{\boldsymbol{P}}) \} + \{ V_{\text{ext}}(\vec{\boldsymbol{R}}, \vec{\boldsymbol{P}}), \varrho^{(0)}(\vec{\boldsymbol{R}}, \vec{\boldsymbol{P}}) \} \tag{3.E.25}$$

where $\mathcal{H}^{(0)}[\varrho]$ is the Hamiltonian (3.3.16) without any external perturbation. The first two terms in (3.E.25) lead to the system of equations (3.C.5) for the first order correction of the parameters with $V_{\text{ext}} = 0$. So to account for the correction due to the potential (3.E.23), we compute

$$\begin{aligned} \{ V_{\text{ext}}(\vec{\boldsymbol{R}}, \vec{\boldsymbol{P}}), \varrho^{(0)}(\vec{\boldsymbol{R}}, \vec{\boldsymbol{P}}) \} = \Bigg[- \sum_{ac} C_c^{(2)} \alpha_{ca}^{(0)} \delta R_a + \sum_{ac} C_c^{(1)} \beta_{ca}^{(0)} \delta P_a - \sum_{abc} \tfrac{1}{2} (C_{ac}^{(5)} \alpha_{bc}^{(0)} - C_{bc}^{(5)} \alpha_{ca}^{(0)}) \delta R_a \delta R_b \\ + \sum_{abc} \tfrac{1}{2} (\beta_{bc}^{(0)} C_{ca}^{(5)} - \beta_{ac}^{(0)} C_{cb}^{(5)}) \delta P_a \delta P_b - \sum_{abc} (\alpha_{ac}^{(0)} C_{cb}^{(4)} - C_{ac}^{(3)} \beta_{cb}^{(0)}) \delta R_a \delta P_b \Bigg] \varrho^{(0)}(\vec{\boldsymbol{R}}, \vec{\boldsymbol{P}}) \, . \end{aligned} \tag{3.E.26}$$

Considering (3.E.26) and the polynomial expansion carried out in Sec 3.C, the system of

equation (3.C.5) at linear order results in

$$\frac{d}{dt}\vec{\vec{\mathcal{R}}}^{(1)}(t) = \vec{\vec{\mathcal{P}}}^{(1)}(t) + \frac{\partial V_{\text{ext}}(t)}{\partial \vec{\vec{P}}} \tag{3.E.27a}$$

$$\frac{d}{dt}\vec{\vec{\mathcal{P}}}^{(1)}(t) = -\left\langle \frac{\partial V_{\text{BO}}}{\partial \vec{\vec{R}}} \right\rangle_{\varrho^{(1)}(t)} - \frac{\partial V_{\text{ext}}(t)}{\partial \vec{\vec{R}}} \tag{3.E.27b}$$

$$\frac{d}{dt}\overleftrightarrow{\vec{\alpha}}^{(1)}(t) = -\overleftrightarrow{\vec{\Phi}} \cdot \overleftrightarrow{\vec{\gamma}}^{(1)T}(t) - \overleftrightarrow{\vec{\gamma}}^{(1)}(t) \cdot \overleftrightarrow{\vec{\Phi}} - \frac{\partial^2 V_{\text{ext}}(t)}{\partial \vec{\vec{R}} \partial \vec{\vec{P}}} \cdot \overleftrightarrow{\vec{\alpha}}^{(0)} - \overleftrightarrow{\vec{\alpha}}^{(0)} \cdot \frac{\partial^2 V_{\text{ext}}(t)}{\partial \vec{\vec{R}} \partial \vec{\vec{P}}} \tag{3.E.27c}$$

$$\frac{d}{dt}\overleftrightarrow{\vec{\beta}}^{(1)}(t) = \overleftrightarrow{\vec{\gamma}}^{(1)T}(t) + \overleftrightarrow{\vec{\gamma}}^{(1)}(t) + \frac{\partial^2 V_{\text{ext}}(t)}{\partial \vec{\vec{R}} \partial \vec{\vec{P}}} \cdot \overleftrightarrow{\vec{\beta}}^{(0)} + \overleftrightarrow{\vec{\beta}}^{(0)} \cdot \frac{\partial^2 V_{\text{ext}}(t)}{\partial \vec{\vec{R}} \partial \vec{\vec{P}}} \tag{3.E.27d}$$

$$\begin{aligned}\frac{d}{dt}\overleftrightarrow{\vec{\gamma}}^{(1)}(t) =& \overleftrightarrow{\vec{\alpha}}^{(1)}(t) - \overleftrightarrow{\vec{\Phi}} \cdot \overleftrightarrow{\vec{\beta}}^{(1)}(t) - \left\langle \frac{\partial^2 V_{\text{BO}}}{\partial \vec{\vec{R}} \partial \vec{\vec{R}}} \right\rangle_{\varrho^{(1)}(t)} \cdot \overleftrightarrow{\vec{\beta}}^{(0)} \\ &- \frac{\partial^2 V_{\text{ext}}(t)}{\partial \vec{\vec{R}} \partial \vec{\vec{R}}} \cdot \overleftrightarrow{\vec{\beta}}^{(0)} + \overleftrightarrow{\vec{\alpha}}^{(0)} \cdot \frac{\partial^2 V_{\text{ext}}(t)}{\partial \vec{\vec{P}} \partial \vec{\vec{P}}}\end{aligned} \tag{3.E.27e}$$

For the specific case of a thermal potential expressed in terms of a harmonic current as (3.4.11), the only nonzero term is $\frac{\partial^2 V_{\text{ext}}(t)}{\partial \vec{\vec{R}} \partial \vec{\vec{P}}}$. In this case, we can express the second order system of equations as

$$\frac{d^2}{dt^2}\vec{\vec{\mathcal{R}}}^{(1)}(t) = -\left\langle \frac{\partial V_{\text{BO}}}{\partial \vec{\vec{R}}} \right\rangle_{\varrho^{(1)}(t)} \tag{3.E.28a}$$

$$\begin{aligned}\frac{d^2}{dt^2}\overleftrightarrow{\vec{\alpha}}^{(1)}(t) =& -\overleftrightarrow{\vec{\Phi}} \cdot \left[\overleftrightarrow{\vec{\alpha}}^{(1)}(t) - \overleftrightarrow{\vec{\Phi}} \cdot \overleftrightarrow{\vec{\beta}}^{(1)}(t) - \left\langle \frac{\partial^2 V_{\text{BO}}}{\partial \vec{\vec{R}} \partial \vec{\vec{R}}} \right\rangle_{\varrho^{(1)}(t)} \cdot \overleftrightarrow{\vec{\beta}}^{(0)} \right]^T \\ &- \left[\overleftrightarrow{\vec{\alpha}}^{(1)}(t) - \overleftrightarrow{\vec{\Phi}} \cdot \overleftrightarrow{\vec{\beta}}^{(1)}(t) - \left\langle \frac{\partial^2 V_{\text{BO}}}{\partial \vec{\vec{R}} \partial \vec{\vec{R}}} \right\rangle_{\varrho^{(1)}(t)} \cdot \overleftrightarrow{\vec{\beta}}^{(0)} \right] \cdot \overleftrightarrow{\vec{\Phi}} - \frac{\partial}{\partial t} \frac{\partial^2 V_{\text{ext}}(t)}{\partial \vec{\vec{R}} \partial \vec{\vec{P}}} \cdot \overleftrightarrow{\vec{\alpha}}^{(0)} - \overleftrightarrow{\vec{\alpha}}^{(0)} \cdot \frac{\partial}{\partial t} \frac{\partial^2 V_{\text{ext}}(t)}{\partial \vec{\vec{R}} \partial \vec{\vec{P}}}\end{aligned} \tag{3.E.28b}$$

$$\begin{aligned}\frac{d^2}{dt^2}\overleftrightarrow{\vec{\beta}}^{(1)}(t) =& 2\overleftrightarrow{\vec{\alpha}}^{(1)}(t) - \overleftrightarrow{\vec{\beta}}^{(1)}(t) \cdot \overleftrightarrow{\vec{\Phi}} - \overleftrightarrow{\vec{\Phi}} \cdot \overleftrightarrow{\vec{\beta}}^{(1)}(t) - \overleftrightarrow{\vec{\beta}}^{(0)} \cdot \left\langle \frac{\partial^2 V_{\text{BO}}}{\partial \vec{\vec{R}} \partial \vec{\vec{R}}} \right\rangle_{\varrho^{(1)}(t)} \\ &- \left\langle \frac{\partial^2 V_{\text{BO}}}{\partial \vec{\vec{R}} \partial \vec{\vec{R}}} \right\rangle_{\varrho^{(1)}(t)} \cdot \overleftrightarrow{\vec{\beta}}^{(0)} + \frac{\partial}{\partial t} \frac{\partial^2 V_{\text{ext}}(t)}{\partial \vec{\vec{R}} \partial \vec{\vec{P}}} \cdot \overleftrightarrow{\vec{\beta}}^{(0)} + \overleftrightarrow{\vec{\beta}}^{(0)} \cdot \frac{\partial}{\partial t} \frac{\partial^2 V_{\text{ext}}(t)}{\partial \vec{\vec{R}} \partial \vec{\vec{P}}}\end{aligned} \tag{3.E.28c}$$

Comparing the system just derived with (3.E.7), we understand that the system of equation in presence of a harmonic thermal potential is the equivalent to the case discussed in (3.E.2) with the substitution $\frac{\partial^2 V_{\text{ext}}(t)}{\partial \widetilde{R}_\alpha \partial \widetilde{R}_\beta} \to \frac{\partial}{\partial t} \frac{\partial^2 V_{\text{ext}}(t)}{\partial \widetilde{R}_a \partial \widetilde{P}_b}$. The presence of the time-derivative is crucial since, in frequency domain, it eliminates the $\frac{1}{i\omega}$ factor in the definition of the thermal vector potential (3.4.11). Plugging (3.4.11) in (3.E.28), we obtain the thermal perturbation vector in the subspace of the parameters $(\vec{\boldsymbol{\mathcal{R}}}^{(1)}, \overleftrightarrow{\vec{\alpha}}^{(1)}, \overleftrightarrow{\vec{\beta}}^{(1)})$ (denoted $''$)

$$\boldsymbol{p}''_{\text{th},\mu\nu}{}^{\sigma} = -\frac{V}{\beta} \begin{bmatrix} 0 \\ \left(\tilde{\alpha}^{(0)}_{\mu} - \tilde{\alpha}^{(0)}_{\nu}\right) \mathcal{J}^{\sigma}_{\mu\nu} \\ \left(\tilde{\beta}^{(0)}_{\mu} - \tilde{\beta}^{(0)}_{\nu}\right) \mathcal{J}^{\sigma}_{\mu\nu} \end{bmatrix}, \tag{3.E.29}$$

having expressed explicitly the matrix elements in the phonon basis, and the Cartesian component σ of the temperature gradient to which $\boldsymbol{p}$ couples (cf. (3.4.8)). Eq. (3.E.29) allows the application of the established TD-SCHA theory for the case of thermal transport.

3.F Symbolic inversion

In this appendix we describe the symbolic inversion of a symmetric square super-tensor with this form

$$\boldsymbol{L} = \begin{bmatrix} \boldsymbol{A} & \boldsymbol{C} \\ \boldsymbol{C}^\dagger & \boldsymbol{B} \end{bmatrix} \tag{3.F.1}$$

where $\boldsymbol{A}, \boldsymbol{B}, \boldsymbol{C}, \boldsymbol{C}^\dagger$ are tensors. Using Gaussian reduction we get the inverse

$$\boldsymbol{L}^{-1} = \begin{bmatrix} \boldsymbol{D}^{-1} & -\boldsymbol{D}^{-1} \cdot \boldsymbol{C} \cdot \boldsymbol{B}^{-1} \\ -\boldsymbol{B}^{-1} \cdot \boldsymbol{C}^\dagger \cdot \boldsymbol{D}^{-1} & \boldsymbol{B}^{-1} + \boldsymbol{B}^{-1} \cdot \boldsymbol{C}^\dagger \cdot \boldsymbol{D}^{-1} \cdot \boldsymbol{C} \cdot \boldsymbol{B}^{-1}. \end{bmatrix} \tag{3.F.2}$$

where $\boldsymbol{D} = \boldsymbol{A} - \boldsymbol{C} \cdot \boldsymbol{B}^{-1} \cdot \boldsymbol{C}^\dagger$. It is trivial to check that $\boldsymbol{L} \cdot \boldsymbol{L}^{-1} = \boldsymbol{L}^{-1} \cdot \boldsymbol{L} = \mathbf{1}$. For what follows we need $\boldsymbol{C} = \mathbf{1}$ so Eq. (3.F.2) becomes

$$\boldsymbol{L}^{-1} = \begin{bmatrix} \boldsymbol{A}^{-1} - \boldsymbol{A}^{-1} \cdot (1 - \boldsymbol{A} \cdot \boldsymbol{B})^{-1} & (1 - \boldsymbol{B} \cdot \boldsymbol{A})^{-1} \\ (1 - \boldsymbol{A} \cdot \boldsymbol{B})^{-1} & -\boldsymbol{A} \cdot (1 - \boldsymbol{B} \cdot \boldsymbol{A})^{-1}. \end{bmatrix} \tag{3.F.3}$$

Again, for our purposes (see next appendix 3.G), we need to find a formula for the sum of entries of Eq. (3.F.3). Summing the coefficients of Eq. (3.F.3) we get

$$\begin{aligned} &\boldsymbol{L}_{11}^{-1} + \boldsymbol{L}_{21}^{-1} + \boldsymbol{L}_{12}^{-1} + \boldsymbol{L}_{22}^{-1} = \\ &\boldsymbol{A}^{-1} - \boldsymbol{A}^{-1} \cdot (1 - \boldsymbol{A} \cdot \boldsymbol{B})^{-1} + (\mathbf{1} - \boldsymbol{B} \cdot \boldsymbol{A})^{-1} + (\mathbf{1} - \boldsymbol{A} \cdot \boldsymbol{B})^{-1} - \boldsymbol{A} \cdot (\mathbf{1} - \boldsymbol{B} \cdot \boldsymbol{A})^{-1} \\ &= \boldsymbol{A}^{-1} \cdot [(\mathbf{1} - \boldsymbol{A} \cdot \boldsymbol{B}) - (\mathbf{1} - \boldsymbol{A})] \cdot (1 - \boldsymbol{A} \cdot \boldsymbol{B})^{-1} + (1 - \boldsymbol{A}) \cdot (\mathbf{1} - \boldsymbol{B} \cdot \boldsymbol{A})^{-1} \\ &= \boldsymbol{A}^{-1} \cdot [\boldsymbol{A} \cdot (\mathbf{1} - \boldsymbol{B})] \cdot (1 - \boldsymbol{A} \cdot \boldsymbol{B})^{-1} + (1 - \boldsymbol{A}) \cdot (\mathbf{1} - \boldsymbol{B} \cdot \boldsymbol{A})^{-1} \\ &= (1 - \boldsymbol{B}) \cdot (1 - \boldsymbol{A} \cdot \boldsymbol{B})^{-1} + (1 - \boldsymbol{A}) \cdot (\mathbf{1} - \boldsymbol{B} \cdot \boldsymbol{A})^{-1}. \end{aligned} \tag{3.F.4}$$

Now we set $\boldsymbol{A} = \mathbf{1} + \widetilde{\boldsymbol{A}}$ and $\boldsymbol{B} = \mathbf{1} + \widetilde{\boldsymbol{B}}$ so we have that Eq. (3.F.4) is

$$\begin{aligned} &\widetilde{\boldsymbol{B}} \cdot \left(\widetilde{\boldsymbol{A}} + \widetilde{\boldsymbol{B}} + \widetilde{\boldsymbol{A}} \cdot \widetilde{\boldsymbol{B}}\right)^{-1} + \widetilde{\boldsymbol{A}} \cdot \left(\widetilde{\boldsymbol{A}} + \widetilde{\boldsymbol{B}} + \widetilde{\boldsymbol{B}} \cdot \widetilde{\boldsymbol{A}}\right)^{-1} \\ &= \left(1 + \widetilde{\boldsymbol{A}} \cdot \widetilde{\boldsymbol{B}}^{-1} + \widetilde{\boldsymbol{A}}\right)^{-1} + \left(1 + \widetilde{\boldsymbol{B}} \cdot \widetilde{\boldsymbol{A}}^{-1} + \widetilde{\boldsymbol{B}}\right)^{-1} \\ &= \left(\widetilde{\boldsymbol{A}}^{-1} + \widetilde{\boldsymbol{B}}^{-1} + \mathbf{1}\right)^{-1} \cdot \widetilde{\boldsymbol{A}} + \left(\widetilde{\boldsymbol{B}}^{-1} + \widetilde{\boldsymbol{A}}^{-1} + \mathbf{1}\right)^{-1} \cdot \widetilde{\boldsymbol{B}} \\ &= \left(1 + \widetilde{\boldsymbol{B}}^{-1} + \widetilde{\boldsymbol{A}}^{-1}\right)^{-1} \cdot (\widetilde{\boldsymbol{A}}^{-1} + \widetilde{\boldsymbol{B}}^{-1}). \end{aligned} \tag{3.F.5}$$

We will use this formula in appendix 3.G.

3.G Derivation of the interacting Green's function in TD-SCHA

The easiest way to get the interacting Green's function is to use another change of variables in Eqs (3.E.2)

$$\begin{bmatrix} \widetilde{a}^{(1)}_{\mu\nu}(\omega) \\ \widetilde{b}^{(1)}_{\mu\nu}(\omega) \end{bmatrix} = -\frac{\hbar^2 n_{\mu\nu}}{2} \begin{bmatrix} \frac{1}{\omega_\mu \omega_\nu} & 1 \\ \frac{1}{\omega_\mu \omega_\nu} & -1 \end{bmatrix} \begin{bmatrix} \widetilde{\alpha}^{(1)}_{\mu\nu}(\omega) \\ \widetilde{\beta}^{(1)}_{\mu\nu}(\omega) \end{bmatrix} \tag{3.G.1}$$

where $n_{\mu\nu}$ is defined in Eq. (3.E.6c) and $\{\omega_\mu^2\}$ in Eq. (3.3.24). As done in appendix 3.E, we write Eqs (3.E.2) in this new basis switching to second-order time-derivatives

$$\begin{aligned} &\begin{bmatrix} \left(\overleftrightarrow{\mathcal{G}}^{(0)}(\omega)\right)^{-1} \cdot & 0 & 0 \\ 0 & \left(\boldsymbol{\chi}_-^{(0)}(\omega)\right)^{-1} : & 0 \\ 0 & 0 & -\left(\boldsymbol{\chi}_+^{(0)}(\omega)\right)^{-1} : \end{bmatrix} \begin{bmatrix} \vec{\widetilde{\boldsymbol{\mathcal{R}}}}^{(1)}(\omega) \\ \overleftrightarrow{\widetilde{\boldsymbol{a}}}^{(1)}(\omega) \\ \overleftrightarrow{\widetilde{\boldsymbol{b}}}^{(1)}(\omega) \end{bmatrix} \\ &= \begin{bmatrix} \left\langle \frac{\partial \mathbb{V}}{\partial \vec{\widetilde{\boldsymbol{R}}}} \right\rangle_{(1)} \\ \left\langle \frac{\partial^2 \mathbb{V}}{\partial \vec{\widetilde{\boldsymbol{R}}} \partial \vec{\widetilde{\boldsymbol{R}}}_\beta} \right\rangle_{(1)} \\ \left\langle \frac{\partial^2 \mathbb{V}}{\partial \vec{\widetilde{\boldsymbol{R}}} \partial \vec{\widetilde{\boldsymbol{R}}}_\beta} \right\rangle_{(1)} \end{bmatrix} + \begin{bmatrix} \left\langle \frac{\partial V_{\text{ext}}}{\partial \vec{\widetilde{\boldsymbol{R}}}} \right\rangle_{(0)} \\ \left\langle \frac{\partial^2 V_{\text{ext}}}{\partial \vec{\widetilde{\boldsymbol{R}}} \partial \vec{\widetilde{\boldsymbol{R}}}} \right\rangle_{(0)} \\ \left\langle \frac{\partial^2 V_{\text{ext}}}{\partial \vec{\widetilde{\boldsymbol{R}}} \partial \vec{\widetilde{\boldsymbol{R}}}} \right\rangle_{(0)} \end{bmatrix} \end{aligned} \tag{3.G.2}$$

where we recognize the resonant and anti-resonant terms of the two-phonon propagator

$$\begin{aligned} \chi_-^{(0)}(\omega)_{\mu\nu\sigma\pi} &= \delta_{\mu\sigma}\delta_{\nu\pi} \frac{\hbar\left[\omega_\mu - \omega_\nu\right]\left[n_\mu - n_\nu\right]}{4\omega_\mu\omega_\nu[(\omega_\mu - \omega_\nu)^2 - \omega^2]}; \\ \chi_+^{(0)}(\omega)_{\mu\nu\sigma\pi} &= \delta_{\mu\sigma}\delta_{\nu\pi} \frac{\hbar\left[\omega_\mu + \omega_\nu\right]\left[1 + n_\mu + n_\nu\right]}{4\omega_\mu\omega_\nu[(\omega_\mu + \omega_\nu)^2 - \omega^2]}. \end{aligned} \tag{3.G.3}$$

The anharmonic vector in this basis is simply

$$\begin{bmatrix} \left\langle \frac{\partial \mathbb{V}}{\partial \vec{\widetilde{\boldsymbol{R}}}} \right\rangle_{(1)} \\ \left\langle \frac{\partial^2 \mathbb{V}}{\partial \vec{\widetilde{\boldsymbol{R}}} \partial \vec{\widetilde{\boldsymbol{R}}}_\beta} \right\rangle_{(1)} \\ \left\langle \frac{\partial^2 \mathbb{V}}{\partial \vec{\widetilde{\boldsymbol{R}}} \partial \vec{\widetilde{\boldsymbol{R}}}_\beta} \right\rangle_{(1)} \end{bmatrix} = \begin{bmatrix} 0 & \overset{(3)}{\boldsymbol{D}} : & \overset{(3)}{\boldsymbol{D}} : \\ \overset{(3)}{\boldsymbol{D}} \cdot & \overset{(4)}{\boldsymbol{D}} : & \overset{(4)}{\boldsymbol{D}} : \\ \overset{(3)}{\boldsymbol{D}} \cdot & \overset{(4)}{\boldsymbol{D}} : & \overset{(4)}{\boldsymbol{D}} : \end{bmatrix} \begin{bmatrix} \vec{\widetilde{\boldsymbol{\mathcal{R}}}}^{(1)} \\ \overleftrightarrow{\widetilde{\boldsymbol{a}}}^{(1)} \\ \overleftrightarrow{\widetilde{\boldsymbol{b}}}^{(1)} \end{bmatrix}. \tag{3.G.4}$$

In a compact form, the linearized equations of motion are

$$\boldsymbol{\mathcal{L}}(\omega) \cdot \begin{bmatrix} \vec{\widetilde{\boldsymbol{\mathcal{R}}}}^{(1)}(\omega) \\ \overleftrightarrow{\widetilde{\boldsymbol{a}}}^{(1)}(\omega) \\ \overleftrightarrow{\widetilde{\boldsymbol{b}}}^{(1)}(\omega) \end{bmatrix} = \begin{bmatrix} \left\langle \frac{\partial V_{\text{ext}}}{\partial \vec{\widetilde{\boldsymbol{R}}}} \right\rangle_{(0)} \\ \left\langle \frac{\partial^2 V_{\text{ext}}}{\partial \vec{\widetilde{\boldsymbol{R}}} \partial \vec{\widetilde{\boldsymbol{R}}}} \right\rangle_{(0)} \\ \left\langle \frac{\partial^2 V_{\text{ext}}}{\partial \vec{\widetilde{\boldsymbol{R}}} \partial \vec{\widetilde{\boldsymbol{R}}}} \right\rangle_{(0)} \end{bmatrix} \tag{3.G.5}$$

The tensor $\boldsymbol{\mathcal{L}}(\omega)$ describes the evolution in the linear regime and it is

$$\boldsymbol{\mathcal{L}}(\omega) = \begin{bmatrix} \left(\overleftrightarrow{\boldsymbol{\mathcal{G}}}^{(0)}(\omega)\right)^{-1} & \overset{(3)}{-\boldsymbol{D}} & \overset{(3)}{-\boldsymbol{D}} \\ \overset{(3)}{-\boldsymbol{D}} & \left(\boldsymbol{\chi}_{-}^{(0)}(\omega)\right)^{-1} - \overset{(4)}{\boldsymbol{D}} & \overset{(4)}{-\boldsymbol{D}} \\ \overset{(3)}{-\boldsymbol{D}} & \overset{(4)}{-\boldsymbol{D}} & -\left(\boldsymbol{\chi}_{+}^{(0)}(\omega)\right)^{-1} - \overset{(4)}{\boldsymbol{D}} \end{bmatrix} \tag{3.G.6}$$

The correction to the average of an observable $\mathcal{A}$ is

$$\langle \mathcal{A} \rangle_{(1)} = \left\langle \frac{\partial \mathcal{A}}{\partial \vec{\tilde{\boldsymbol{R}}}} \right\rangle_{(0)} \cdot \vec{\tilde{\boldsymbol{\mathcal{R}}}}^{(1)}(\omega) + \left\langle \frac{\partial^2 \mathcal{A}}{\partial \vec{\tilde{\boldsymbol{R}}} \partial \vec{\tilde{\boldsymbol{R}}}} \right\rangle_{(0)} : \overleftrightarrow{\boldsymbol{S}} : \overleftrightarrow{\tilde{\boldsymbol{a}}}^{(1)}(\omega) + \left\langle \frac{\partial^2 \mathcal{A}}{\partial \vec{\tilde{\boldsymbol{R}}} \partial \vec{\tilde{\boldsymbol{R}}}} \right\rangle_{(0)} : \overleftrightarrow{\boldsymbol{S}} : \overleftrightarrow{\tilde{\boldsymbol{b}}}^{(1)}(\omega) \tag{3.G.7}$$

where $\overleftrightarrow{\boldsymbol{S}}$ is defined in Eq. (3.E.3). So, following the procedure described in appendix 3.E, the response function is

$$\chi_{\mathcal{A},\mathcal{B}}(\omega) = \boldsymbol{r}^{\dagger} \cdot \boldsymbol{\mathcal{L}}(\omega)^{-1} \cdot \boldsymbol{p} \tag{3.G.8}$$

defining the response vector $\boldsymbol{r}$ as

$$\boldsymbol{r}^{\dagger} = \left[\left\langle \frac{\partial \mathcal{A}}{\partial \vec{\tilde{\boldsymbol{R}}}} \right\rangle_{(0)}, \quad \left\langle \frac{\partial^2 \mathcal{A}}{\partial \vec{\tilde{\boldsymbol{R}}} \partial \vec{\tilde{\boldsymbol{R}}}} \right\rangle_{(0)}, \quad \left\langle \frac{\partial^2 \mathcal{A}}{\partial \vec{\tilde{\boldsymbol{R}}} \partial \vec{\tilde{\boldsymbol{R}}}} \right\rangle_{(0)} \right], \tag{3.G.9}$$

and the perturbation vector $\boldsymbol{p}$ as

$$\boldsymbol{p}^{\dagger} = \left[\left\langle \frac{\partial \mathcal{B}}{\partial \vec{\tilde{\boldsymbol{R}}}} \right\rangle_{(0)}, \quad \left\langle \frac{\partial^2 \mathcal{B}}{\partial \vec{\tilde{\boldsymbol{R}}} \partial \vec{\tilde{\boldsymbol{R}}}} \right\rangle_{(0)}, \quad \left\langle \frac{\partial^2 \mathcal{B}}{\partial \vec{\tilde{\boldsymbol{R}}} \partial \vec{\tilde{\boldsymbol{R}}}} \right\rangle_{(0)} \right]. \tag{3.G.10}$$

First we discuss the non-interacting case setting $\overset{(3)}{\boldsymbol{D}} = \boldsymbol{0}$ $\overset{(4)}{\boldsymbol{D}} = \boldsymbol{0}$. Using $\mathcal{A}$ and $\mathcal{B}$ as in Eq. (3.3.62a) we get

$$\boldsymbol{r}^{\dagger} = \begin{bmatrix} \vec{\boldsymbol{\delta}} & \boldsymbol{0} & \boldsymbol{0} \end{bmatrix} \qquad \boldsymbol{p}^{\dagger} = \begin{bmatrix} \vec{\boldsymbol{\delta}} & \boldsymbol{0} & \boldsymbol{0} \end{bmatrix}. \tag{3.G.11}$$

with $\vec{\boldsymbol{\delta}} = \vec{\boldsymbol{\delta}}_{\mu}$ as in Eq. (3.3.63a). The free phonon propagator is

$$\mathcal{G}^{(0)}(\omega)_{\mu\nu} = \frac{\delta_{\mu\nu}}{\omega^2 - \omega_{\mu}^2}. \tag{3.G.12}$$

Then we chose $\mathcal{A}$ and $\mathcal{B}$ according to Eq. (3.3.62b) so

$$\boldsymbol{r}^{\dagger} = \begin{bmatrix} \boldsymbol{0} & \overleftrightarrow{\boldsymbol{S}} & \overleftrightarrow{\boldsymbol{S}} \end{bmatrix} \qquad \boldsymbol{p}^{\dagger} = \begin{bmatrix} \boldsymbol{0} & \overleftrightarrow{\boldsymbol{S}} & \overleftrightarrow{\boldsymbol{S}} \end{bmatrix}, \tag{3.G.13}$$

where $\overleftrightarrow{\boldsymbol{S}}$ is defined in Eq. (3.E.3). The two-phonon free propagator is

$$\chi^{(0)}(\omega)_{\mu\nu\sigma\pi} = -\left(\chi_{+}^{(0)}(\omega)_{\mu\nu\sigma\pi} - \chi_{-}^{(0)}(\omega)_{\mu\nu\sigma\pi}.\right) \tag{3.G.14}$$

We chose $\mathcal{A}$ and $\mathcal{B}$ according to Eq. (3.3.62c)

$$\boldsymbol{r}^{\dagger} = \begin{bmatrix} \vec{\boldsymbol{\delta}} & \boldsymbol{0} & \boldsymbol{0} \end{bmatrix} \quad \boldsymbol{p}^{\dagger} = \begin{bmatrix} \boldsymbol{0} & \overleftrightarrow{\boldsymbol{S}} & \overleftrightarrow{\boldsymbol{S}} \end{bmatrix} \tag{3.G.15}$$

$\boldsymbol{\mathcal{L}}(\omega)$ is diagonal in the case $\overset{(3)}{\boldsymbol{D}} = \mathbf{0}$ $\overset{(4)}{\boldsymbol{D}} = \mathbf{0}$ so we get that the one-two phonon free propagator is zero

$$\Gamma^{(0)}(\omega)_{\mu\sigma\pi} = 0. \tag{3.G.16}$$

One-phonon Green's function

Now we derive the one-phonon interacting Green's function ($\overset{(3)}{\boldsymbol{D}} \neq \mathbf{0}$ $\overset{(4)}{\boldsymbol{D}} \neq \mathbf{0}$). Following[65] we chose the observables $\mathcal{A}$ and $\mathcal{B}$ as in Eq. (3.3.62a)

$$\overset{\leftrightarrow}{\boldsymbol{\mathcal{G}}}(\omega) = \begin{bmatrix} \vec{\boldsymbol{\delta}} & \mathbf{0} & \mathbf{0} \end{bmatrix} \cdot \boldsymbol{\mathcal{L}}(\omega)^{-1} \cdot \begin{bmatrix} \vec{\boldsymbol{\delta}} \\ \mathbf{0} \\ \mathbf{0} \end{bmatrix} = \left(\boldsymbol{\mathcal{L}}(\omega)^{-1}\right)_{11}. \tag{3.G.17}$$

We use Eq (3.F.2) to get

$$\begin{aligned} \overset{\leftrightarrow}{\boldsymbol{\mathcal{G}}}(\omega)^{-1} &= \overset{\leftrightarrow}{\boldsymbol{\mathcal{G}}}^{(0)}(\omega)^{-1} \\ &- \begin{bmatrix} \overset{(3)}{\boldsymbol{D}} : & \overset{(3)}{\boldsymbol{D}} : \end{bmatrix} \begin{bmatrix} \left(\boldsymbol{\chi}_{-}^{(0)}(\omega) : \overset{(4)}{\boldsymbol{D}}\right)^{-1} - \mathbf{1} & -\mathbf{1} \\ -\mathbf{1} & -\left(\boldsymbol{\chi}_{+}^{(0)}(\omega) : \overset{(4)}{\boldsymbol{D}}\right)^{-1} - \mathbf{1} \end{bmatrix}^{-1} \begin{bmatrix} : \overset{(4)}{\boldsymbol{D}}^{-1} & : \overset{(3)}{\boldsymbol{D}} \\ : \overset{(4)}{\boldsymbol{D}}^{-1} & : \overset{(3)}{\boldsymbol{D}} \end{bmatrix} \end{aligned} \tag{3.G.18}$$

now Eq. (3.F.5) comes in help since we just need the sum of the inverse tensor's entries

$$\begin{aligned} \overset{\leftrightarrow}{\boldsymbol{\mathcal{G}}}(\omega)^{-1} &= \overset{\leftrightarrow}{\boldsymbol{\mathcal{G}}}^{(0)}(\omega)^{-1} - \overset{(3)}{\boldsymbol{D}} : \left[\mathbf{1} - \boldsymbol{\chi}^{(0)}(\omega) : \overset{(4)}{\boldsymbol{D}}\right]^{-1} : \left(\boldsymbol{\chi}^{(0)}(\omega) : \overset{(4)}{\boldsymbol{D}}\right) : \overset{(4)}{\boldsymbol{D}}^{-1} : \overset{(3)}{\boldsymbol{D}} \\ &= \overset{\leftrightarrow}{\boldsymbol{\mathcal{G}}}^{(0)}(\omega)^{-1} - \overset{\leftrightarrow}{\boldsymbol{\Pi}}(\omega) \end{aligned} \tag{3.G.19}$$

where $\overset{\leftrightarrow}{\boldsymbol{\Pi}}(\omega)$ coincides with the one presented in Ref. 56, 65, 66.

Two-phonons Green's function

Now we derive the two phonons interacting Green's function $\boldsymbol{\chi}(\omega)$ which is obtained by choosing $\mathcal{A}$ and $\mathcal{B}$ according to Eq. (3.3.62b). In this basis this means computing

$$\boldsymbol{\chi}(\omega) = \begin{bmatrix} \mathbf{0} & \overset{\leftrightarrow}{\boldsymbol{S}} & \overset{\leftrightarrow}{\boldsymbol{S}} \end{bmatrix} \cdot \boldsymbol{\mathcal{L}}(\omega)^{-1} \cdot \begin{bmatrix} \mathbf{0} \\ \overset{\leftrightarrow}{\boldsymbol{S}} \\ \overset{\leftrightarrow}{\boldsymbol{S}} \end{bmatrix}. \tag{3.G.20}$$

The perturbation $\mathcal{B}$ chosen (Eq. (3.3.62b)) leads to the following linearized equations of motion (see Eq. (3.G.5))

$$\boldsymbol{\mathcal{L}}(\omega) \cdot \begin{bmatrix} \vec{\boldsymbol{\mathcal{R}}}^{(1)}(\omega) \\ \overset{\leftrightarrow}{\boldsymbol{a}}^{(1)}(\omega) \\ \overset{\leftrightarrow}{\boldsymbol{b}}^{(1)}(\omega) \end{bmatrix} = \begin{bmatrix} \mathbf{0} \\ \overset{\leftrightarrow}{\boldsymbol{S}} \\ \overset{\leftrightarrow}{\boldsymbol{S}} \end{bmatrix}. \tag{3.G.21}$$

Using the expression of $\boldsymbol{\mathcal{L}}(\omega)$, Eq. (3.G.6), we find that the first free parameter is related to the other two

$$\vec{\widetilde{\boldsymbol{\mathcal{R}}}}^{(1)}(\omega) = \overset{\leftrightarrow}{\boldsymbol{\mathcal{G}}}^{(0)}(\omega) \cdot \overset{(3)}{\boldsymbol{D}} : \left(\overset{\leftrightarrow}{\widetilde{\boldsymbol{a}}}^{(1)}(\omega) + \overset{\leftrightarrow}{\widetilde{\boldsymbol{b}}}^{(1)}(\omega) \right). \tag{3.G.22}$$

So instead of having to invert the full $\boldsymbol{\mathcal{L}}(\omega)$ we reduce Eq. (3.G.20) to

$$\begin{aligned}
\boldsymbol{\chi}(\omega) &= \begin{bmatrix} \overset{\leftrightarrow}{\boldsymbol{S}} : & \overset{\leftrightarrow}{\boldsymbol{S}} : \end{bmatrix} \begin{bmatrix} + \left(\boldsymbol{\chi}_{-}^{(0)}(\omega) \right)^{-1} - \overset{(4)}{\boldsymbol{D}} - \overset{(3)}{\boldsymbol{D}} \cdot \overset{\leftrightarrow}{\boldsymbol{\mathcal{G}}}^{(0)}(\omega) \cdot \overset{(3)}{\boldsymbol{D}} & - \overset{(4)}{\boldsymbol{D}} - \overset{(3)}{\boldsymbol{D}} \cdot \overset{\leftrightarrow}{\boldsymbol{\mathcal{G}}}^{(0)}(\omega) \cdot \overset{(3)}{\boldsymbol{D}} \\ - \overset{(4)}{\boldsymbol{D}} - \overset{(3)}{\boldsymbol{D}} \cdot \overset{\leftrightarrow}{\boldsymbol{\mathcal{G}}}^{(0)}(\omega) \cdot \overset{(3)}{\boldsymbol{D}} & + \left(\boldsymbol{\chi}_{+}^{(0)}(\omega) \right)^{-1} - \overset{(4)}{\boldsymbol{D}} - \overset{(3)}{\boldsymbol{D}} \cdot \overset{\leftrightarrow}{\boldsymbol{\mathcal{G}}}^{(0)}(\omega) \cdot \overset{(3)}{\boldsymbol{D}} \end{bmatrix}^{-1} \begin{bmatrix} : \overset{\leftrightarrow}{\boldsymbol{S}} \\ : \overset{\leftrightarrow}{\boldsymbol{S}} \end{bmatrix} \\
&= \begin{bmatrix} \overset{\leftrightarrow}{\boldsymbol{S}} : & \overset{\leftrightarrow}{\boldsymbol{S}} : \end{bmatrix} \begin{bmatrix} + \left(\boldsymbol{\chi}_{-}^{(0)}(\omega) \right)^{-1} - \boldsymbol{\Sigma}(\omega) & - \boldsymbol{\Sigma}(\omega) \\ - \boldsymbol{\Sigma}(\omega) & + \left(\boldsymbol{\chi}_{+}^{(0)}(\omega) \right)^{-1} - \boldsymbol{\Sigma}(\omega) \end{bmatrix}^{-1} \begin{bmatrix} : \overset{\leftrightarrow}{\boldsymbol{S}} \\ : \overset{\leftrightarrow}{\boldsymbol{S}} \end{bmatrix} \\
&= - \begin{bmatrix} \overset{\leftrightarrow}{\boldsymbol{S}} : & \overset{\leftrightarrow}{\boldsymbol{S}} : \end{bmatrix} \begin{bmatrix} + \mathbf{1} - \left(\boldsymbol{\chi}_{-}^{(0)}(\omega) : \boldsymbol{\Sigma}(\omega) \right)^{-1} & \mathbf{1} \\ \mathbf{1} & \left(\boldsymbol{\chi}_{+}^{(0)}(\omega) : \boldsymbol{\Sigma}(\omega) \right)^{-1} + \mathbf{1} \end{bmatrix}^{-1} \begin{bmatrix} : \boldsymbol{\Sigma}(\omega)^{-1} : \overset{\leftrightarrow}{\boldsymbol{S}} \\ : \boldsymbol{\Sigma}(\omega)^{-1} : \overset{\leftrightarrow}{\boldsymbol{S}} \end{bmatrix}
\end{aligned} \tag{3.G.23}$$

where we define the two phonon self-energy $\boldsymbol{\Sigma}(\omega)$ as in Eq. (3.3.75)

$$\boldsymbol{\Sigma}(\omega) = \overset{(4)}{\boldsymbol{D}} + \overset{(3)}{\boldsymbol{D}} \cdot \overset{\leftrightarrow}{\boldsymbol{\mathcal{G}}}^{(0)}(\omega) \cdot \overset{(3)}{\boldsymbol{D}}. \tag{3.G.24}$$

Again we can use Eq. (3.F.5) to get the two-phonon interacting Green's function

$$\begin{aligned}
\boldsymbol{\chi}(\omega) &= \overset{\leftrightarrow}{\boldsymbol{S}} : \left[\mathbf{1} - \boldsymbol{\chi}^{(0)}(\omega) : \boldsymbol{\Sigma}(\omega) \right]^{-1} : \boldsymbol{\chi}^{(0)}(\omega) : \boldsymbol{\Sigma}(\omega) : \boldsymbol{\Sigma}^{-1}(\omega) : \overset{\leftrightarrow}{\boldsymbol{S}} \\
&= \left[\mathbf{1} - \boldsymbol{\chi}^{(0)}(\omega) : \boldsymbol{\Sigma}(\omega) \right]^{-1} : \boldsymbol{\chi}^{(0)}(\omega) \\
&= \boldsymbol{\chi}^{(0)}(\omega) : \left[\mathbf{1} - \boldsymbol{\Sigma}(\omega) : \boldsymbol{\chi}^{(0)}(\omega) \right]^{-1}
\end{aligned} \tag{3.G.25}$$

proving Eq. (3.3.77).

On passing, we note the following simplification of the two phonon propagator

$$\begin{bmatrix} \overset{\leftrightarrow}{\boldsymbol{S}} : & \overset{\leftrightarrow}{\boldsymbol{S}} : \end{bmatrix} \begin{bmatrix} \boldsymbol{\mathcal{L}}_{\text{2ph}}(\omega)_{11}^{-1} & \boldsymbol{\mathcal{L}}_{\text{2ph}}(\omega)_{12}^{-1} \\ \boldsymbol{\mathcal{L}}_{\text{2ph}}(\omega)_{21}^{-1} & \boldsymbol{\mathcal{L}}_{\text{2ph}}(\omega)^{-1}{}_{22} \end{bmatrix} = \overset{\leftrightarrow}{\boldsymbol{S}} : \left[\boldsymbol{\mathcal{L}}_{\text{2ph}}(\omega)_{11}^{-1} + \boldsymbol{\mathcal{L}}_{\text{2ph}}(\omega)_{21}^{-1}, \boldsymbol{\mathcal{L}}_{\text{2ph}}(\omega)_{12}^{-1} + \boldsymbol{\mathcal{L}}_{\text{2ph}}(\omega)_{22}^{-1} \right] \tag{3.G.26}$$

and using the symbolic invertion (3.F.3) on the two phonon propagator (3.3.74), we get

$$\begin{bmatrix} \overset{\leftrightarrow}{\boldsymbol{S}} : & \overset{\leftrightarrow}{\boldsymbol{S}} : \end{bmatrix} \begin{bmatrix} \boldsymbol{\mathcal{L}}_{\text{2ph}}(\omega)_{11}^{-1} & \boldsymbol{\mathcal{L}}_{\text{2ph}}(\omega)_{12}^{-1} \\ \boldsymbol{\mathcal{L}}_{\text{2ph}}(\omega)_{21}^{-1} & \boldsymbol{\mathcal{L}}_{\text{2ph}}(\omega)^{-1}{}_{22} \end{bmatrix} = \overset{\leftrightarrow}{\boldsymbol{S}} : \frac{1}{1 - \boldsymbol{\chi}^{(0)}(\omega) : \boldsymbol{\Sigma}(\omega)} : \left[\boldsymbol{\chi}_{-}^{(0)}(\omega), -\boldsymbol{\chi}_{+}^{(0)}(\omega) \right] \tag{3.G.27}$$

which greatly simplies the expression of the two phonon propagator when the response vector has equal entries.

One-two phonon Green's function

The last Green's function to discuss is the one-two phonon $\mathbf{\Gamma}(\omega)$ obtained setting $\mathcal{A}$ and $\mathcal{B}$ as in Eq. (3.3.62c)

$$\mathbf{\Gamma}(\omega) = \begin{bmatrix} \vec{\boldsymbol{\delta}} \\ \mathbf{0} \\ \mathbf{0} \end{bmatrix} \cdot \boldsymbol{\mathcal{L}}(\omega)^{-1} \cdot \begin{bmatrix} \mathbf{0} \\ \overleftrightarrow{\boldsymbol{S}} \\ \overleftrightarrow{\boldsymbol{S}} \end{bmatrix}. \tag{3.G.28}$$

We simplify this inversion using again Eq. (3.G.22). Now $\overleftrightarrow{\tilde{\boldsymbol{a}}}^{(1)}(\omega) + \overleftrightarrow{\tilde{\boldsymbol{b}}}^{(1)}(\omega)$ are found considering the reduced linear system extracted from Eq. (3.G.21)

$$\begin{aligned} &\mathbf{\Sigma}(\omega) : \begin{bmatrix} +\left(\boldsymbol{\chi}_{-}^{(0)}(\omega) : \mathbf{\Sigma}(\omega)\right)^{-1} - \mathbf{1} & -\mathbf{1} \\ -\mathbf{1} & -\left(\boldsymbol{\chi}_{+}^{(0)}(\omega) : \mathbf{\Sigma}(\omega)\right)^{-1} - \mathbf{1} \end{bmatrix} \begin{bmatrix} : \overleftrightarrow{\tilde{\boldsymbol{a}}}^{(1)}(\omega) \\ : \overleftrightarrow{\tilde{\boldsymbol{b}}}^{(1)}(\omega) \end{bmatrix} = \begin{bmatrix} \overleftrightarrow{\boldsymbol{S}} \\ \overleftrightarrow{\boldsymbol{S}} \end{bmatrix} \\ &\begin{bmatrix} \overleftrightarrow{\tilde{\boldsymbol{a}}}^{(1)}(\omega) \\ \overleftrightarrow{\tilde{\boldsymbol{b}}}^{(1)}(\omega) \end{bmatrix} = - \begin{bmatrix} \mathbf{1} - \left(\boldsymbol{\chi}_{-}^{(0)}(\omega) : \mathbf{\Sigma}(\omega)\right)^{-1} & \mathbf{1} \\ \mathbf{1} & \mathbf{1} + \left(\boldsymbol{\chi}_{+}^{(0)}(\omega) : \mathbf{\Sigma}(\omega)\right)^{-1} \end{bmatrix}^{-1} \begin{bmatrix} : \mathbf{\Sigma}^{-1}(\omega) \\ : \mathbf{\Sigma}^{-1}(\omega) \end{bmatrix} \end{aligned} \tag{3.G.29}$$

From Eq. (3.G.29) we get the sum $\overleftrightarrow{\tilde{\boldsymbol{a}}}^{(1)}(\omega) + \overleftrightarrow{\tilde{\boldsymbol{b}}}^{(1)}(\omega)$

$$\begin{aligned} &\overleftrightarrow{\tilde{\boldsymbol{a}}}^{(1)}(\omega) + \overleftrightarrow{\tilde{\boldsymbol{b}}}^{(1)}(\omega) = \\ &- \begin{bmatrix} \overleftrightarrow{\boldsymbol{S}} : & \overleftrightarrow{\boldsymbol{S}} : \end{bmatrix} \begin{bmatrix} \mathbf{1} - \left(\boldsymbol{\chi}_{-}^{(0)}(\omega) : \mathbf{\Sigma}(\omega)\right)^{-1} & \mathbf{1} \\ \mathbf{1} & \mathbf{1} + \left(\boldsymbol{\chi}_{+}^{(0)}(\omega) : \mathbf{\Sigma}(\omega)\right)^{-1} \end{bmatrix}^{-1} \begin{bmatrix} : \overleftrightarrow{\boldsymbol{S}} : \mathbf{\Sigma}^{-1}(\omega) \\ : \overleftrightarrow{\boldsymbol{S}} : \mathbf{\Sigma}^{-1}(\omega) \end{bmatrix} \end{aligned} \tag{3.G.30}$$

Again Eq. (3.F.5) comes in help so

$$\overleftrightarrow{\tilde{\boldsymbol{a}}}^{(1)}(\omega) + \overleftrightarrow{\tilde{\boldsymbol{b}}}^{(1)}(\omega) = \left[\mathbf{1} - \boldsymbol{\chi}^{(0)}(\omega) : \mathbf{\Sigma}(\omega)\right]^{-1} : \boldsymbol{\chi}^{(0)}(\omega) : \mathbf{\Sigma}(\omega) : \mathbf{\Sigma}^{-1}(\omega) = \boldsymbol{\chi}(\omega) \tag{3.G.31}$$

Since the response vector $\boldsymbol{r}$ is just $[\vec{\boldsymbol{\delta}} \quad \mathbf{0} \quad \mathbf{0}]$ the one-two phonon Green's function $\mathbf{\Gamma}(\omega)$ is given by $\vec{\boldsymbol{\mathcal{R}}}^{(1)}(\omega)$ (see Eq. (3.G.7)), so, with Eq. (3.G.22), we end up with

$$\mathbf{\Gamma}(\omega) = \vec{\boldsymbol{\mathcal{R}}}^{(1)}(\omega) = \overleftrightarrow{\boldsymbol{\mathcal{G}}}^{(0)}(\omega) \cdot \overset{(3)}{\boldsymbol{D}} : \boldsymbol{\chi}(\omega). \tag{3.G.32}$$

This proves Eq. (3.3.78).

Two-phonon reduced Dyson equation

In closing, we present the proof of Eqs (3.3.79). The Dyson equations for the one and two-phonon Green's functions in TD-SCHA are respectively

$$\overleftrightarrow{\mathcal{G}}(\omega)^{-1} = \overleftrightarrow{\mathcal{G}}^{(0)}(\omega)^{-1} - \overset{(3)}{\boldsymbol{D}} : \left(\mathbf{1} - \boldsymbol{\chi}^{(0)}(\omega) : \overset{(4)}{\boldsymbol{D}}\right)^{-1} : \boldsymbol{\chi}^{(0)}(\omega) : \overset{(3)}{\boldsymbol{D}} \tag{3.G.33}$$

and

$$\boldsymbol{\chi}(\omega)^{-1} = \boldsymbol{\chi}^{(0)}(\omega)^{-1} - \overset{(4)}{\boldsymbol{D}} - \overset{(3)}{\boldsymbol{D}} \cdot \overleftrightarrow{\mathcal{G}}^{(0)}(\omega) \cdot \overset{(3)}{\boldsymbol{D}} \,. \tag{3.G.34}$$

We rewrite the above definitions using the partially screened two-phonon propagator, defined as

$$\boldsymbol{\Theta}(\omega)^{-1} = \boldsymbol{\chi}^{(0)}(\omega)^{-1} - \overset{(4)}{\boldsymbol{D}}. \tag{3.G.35}$$

One sees immediately that the full two-phonon propagator is

$$\boldsymbol{\chi}(\omega)^{-1} = \boldsymbol{\Theta}(\omega)^{-1} - \overset{(3)}{\boldsymbol{D}} \cdot \overleftrightarrow{\mathcal{G}}^{(0)}(\omega) \cdot \overset{(3)}{\boldsymbol{D}} \tag{3.G.36}$$

and that the one phonon propagator is

$$\overleftrightarrow{\mathcal{G}}(\omega)^{-1} = \overleftrightarrow{\mathcal{G}}^{(0)}(\omega)^{-1} - \overset{(3)}{\boldsymbol{D}} : \left(\boldsymbol{\chi}^{(0)}(\omega)^{-1} - \overset{(4)}{\boldsymbol{D}}\right)^{-1} : \overset{(3)}{\boldsymbol{D}} = \overleftrightarrow{\mathcal{G}}^{(0)}(\omega)^{-1} - \overset{(3)}{\boldsymbol{D}} : \boldsymbol{\Theta}(\omega) : \overset{(3)}{\boldsymbol{D}}. \tag{3.G.37}$$

Below we show that the two phonon propagator Eq. (3.G.36) is given by

$$\boldsymbol{\chi}(\omega) = \boldsymbol{\Theta}(\omega) + \boldsymbol{\Theta}(\omega) : \overset{(3)}{\boldsymbol{D}} \cdot \overleftrightarrow{\mathcal{G}}(\omega) \cdot \overset{(3)}{\boldsymbol{D}} : \boldsymbol{\Theta}(\omega) \,. \tag{3.G.38}$$

We express the one phonon propagator as

$$\begin{aligned} \overleftrightarrow{\mathcal{G}}(\omega) &= \left(\overleftrightarrow{\mathcal{G}}^{(0)}(\omega)^{-1} - \overset{(3)}{\boldsymbol{D}} : \boldsymbol{\Theta}(\omega) : \overset{(3)}{\boldsymbol{D}}\right)^{-1} \\ &= \left\{ \overset{(3)}{\boldsymbol{D}} : \left[\left(\overset{(3)}{\boldsymbol{D}} \cdot \overleftrightarrow{\mathcal{G}}^{(0)}(\omega) \cdot \overset{(3)}{\boldsymbol{D}} \right)^{-1} - \boldsymbol{\Theta}(\omega) \right] : \overset{(3)}{\boldsymbol{D}} \right\}^{-1} \end{aligned} \tag{3.G.39}$$

and plugging the latter expression in Eq. (3.G.38) we get

$$\begin{aligned} \boldsymbol{\chi}(\omega) &= \boldsymbol{\Theta}(\omega) + \boldsymbol{\Theta}(\omega) : \left[\left(\overset{(3)}{\boldsymbol{D}} \cdot \overleftrightarrow{\mathcal{G}}^{(0)}(\omega) \cdot \overset{(3)}{\boldsymbol{D}} \right)^{-1} - \boldsymbol{\Theta}(\omega) \right]^{-1} : \boldsymbol{\Theta}(\omega) \\ &= \boldsymbol{\Theta}(\omega) + \boldsymbol{\Theta}(\omega) : \left(\mathbf{1} - \overset{(3)}{\boldsymbol{D}} \cdot \overleftrightarrow{\mathcal{G}}^{(0)}(\omega) \cdot \overset{(3)}{\boldsymbol{D}} : \boldsymbol{\Theta}(\omega) \right)^{-1} : \overset{(3)}{\boldsymbol{D}} \cdot \overleftrightarrow{\mathcal{G}}^{(0)}(\omega) \cdot \overset{(3)}{\boldsymbol{D}} : \boldsymbol{\Theta}(\omega) \\ &= \boldsymbol{\Theta}(\omega) + \left(\boldsymbol{\Theta}(\omega)^{-1} - \overset{(3)}{\boldsymbol{D}} \cdot \overleftrightarrow{\mathcal{G}}^{(0)}(\omega) \cdot \overset{(3)}{\boldsymbol{D}} \right)^{-1} : \overset{(3)}{\boldsymbol{D}} \cdot \overleftrightarrow{\mathcal{G}}^{(0)}(\omega) \cdot \overset{(3)}{\boldsymbol{D}} : \boldsymbol{\Theta}(\omega) \\ &= \boldsymbol{\Theta}(\omega) + \boldsymbol{\chi}(\omega) : \overset{(3)}{\boldsymbol{D}} \cdot \overleftrightarrow{\mathcal{G}}^{(0)}(\omega) \cdot \overset{(3)}{\boldsymbol{D}} : \boldsymbol{\Theta}(\omega). \end{aligned} \tag{3.G.40}$$

Now moving the last term on the left-hand side and inverting we get

$$\begin{aligned}
&\boldsymbol{\chi}(\omega) : (\mathbf{1} - \overset{(3)}{\boldsymbol{D}} \cdot \overset{\leftrightarrow}{\boldsymbol{\mathcal{G}}}^{(0)}(\omega) \cdot \overset{(3)}{\boldsymbol{D}} : \boldsymbol{\Theta}(\omega)) = \boldsymbol{\Theta}(\omega), \\
&\boldsymbol{\chi}(\omega) = \boldsymbol{\Theta}(\omega) : \left(\mathbf{1} - \overset{(3)}{\boldsymbol{D}} \cdot \overset{\leftrightarrow}{\boldsymbol{\mathcal{G}}}^{(0)}(\omega) \cdot \overset{(3)}{\boldsymbol{D}} : \boldsymbol{\Theta}(\omega)\right)^{-1}, \\
&\boldsymbol{\chi}(\omega) = \left(\boldsymbol{\Theta}(\omega)^{-1} - \overset{(3)}{\boldsymbol{D}} \cdot \overset{\leftrightarrow}{\boldsymbol{\mathcal{G}}}^{(0)}(\omega) \cdot \overset{(3)}{\boldsymbol{D}}\right)^{-1},
\end{aligned} \tag{3.G.41}$$

and finally, we recover the standard expression for the two phonon propagator

$$\boldsymbol{\chi}(\omega) = \left(\boldsymbol{\chi}^{(0)}(\omega)^{-1} - \overset{(4)}{\boldsymbol{D}} - \overset{(3)}{\boldsymbol{D}} \cdot \overset{\leftrightarrow}{\boldsymbol{\mathcal{G}}}^{(0)}(\omega) \cdot \overset{(3)}{\boldsymbol{D}}\right)^{-1} \tag{3.G.42}$$

which proves that Eq. (3.G.36) and Eq. (3.G.38) are equivalent expressions of the anharmonic two-phonon propagator.

Three-phonon Green's function

We discuss also the three phonon Green's function obtained with $\mathcal{A}$ and $\mathcal{B}$ as in Eq. (3.3.80)

$$\mathcal{A} = \delta\widetilde{R}^{(0)}_{\alpha}\delta\widetilde{R}^{(0)}_{\beta}\delta\widetilde{R}^{(0)}_{\gamma} \qquad \mathcal{B} = \delta\widetilde{R}^{(0)}_{\alpha'}\delta\widetilde{R}^{(0)}_{\beta'}\delta\widetilde{R}^{(0)}_{\gamma'} \tag{3.G.43}$$

In this case we have

$$\left\langle \frac{\partial^2 \mathcal{A}}{\partial\widetilde{\boldsymbol{R}}\partial\widetilde{\boldsymbol{R}}} \right\rangle_{(0)} = \left\langle \frac{\partial^2 \mathcal{B}}{\partial\widetilde{\boldsymbol{R}}\partial\widetilde{\boldsymbol{R}}} \right\rangle_{(0)} = \mathbf{0} \tag{3.G.44}$$

and

$$\left\langle \frac{\partial \mathcal{A}}{\partial\widetilde{R}_{\mu}} \right\rangle_{(0)} = \delta_{\mu\alpha}\left(\widetilde{\alpha}^{(0)-1}\right)_{\beta\gamma} + \delta_{\mu\beta}\left(\widetilde{\alpha}^{(0)-1}\right)_{\alpha\gamma} + \delta_{\mu\gamma}\left(\widetilde{\alpha}^{(0)-1}\right)_{\alpha\beta} \tag{3.G.45}$$

so only the first entries of $\boldsymbol{r}'$ and $\boldsymbol{p}'$ are non zero. The response calculation is formally identical to the one-phonon interacting Green's function one Eq. (3.G.17). Using, Eq. (3.G.8), we get the three phonon propagator

$$\begin{aligned}
\chi_{3\text{ph}}(\omega) = \sum_{\mu\nu=1}^{3N} &\left(\delta_{\mu\alpha}\left(\widetilde{\alpha}^{(0)-1}\right)_{\beta\gamma} + \delta_{\mu\beta}\left(\widetilde{\alpha}^{(0)-1}\right)_{\alpha\gamma} + \delta_{\mu\gamma}\left(\widetilde{\alpha}^{(0)-1}\right)_{\alpha\beta}\right)\mathcal{G}(\omega)_{\mu\nu} \\
&\left(\delta_{\nu\alpha'}\left(\widetilde{\alpha}^{(0)-1}\right)_{\beta'\gamma'} + \delta_{\nu\beta'}\left(\widetilde{\alpha}^{(0)-1}\right)_{\alpha'\gamma'} + \delta_{\nu\gamma'}\left(\widetilde{\alpha}^{(0)-1}\right)_{\alpha'\beta'}\right)
\end{aligned} \tag{3.G.46}$$

The diagrammatic interpretation is straightforward once we use Eq. (3.3.36). The three-phonon response is

$$\begin{aligned}
\chi_{3\text{ph}}(\omega) =& \mathcal{G}^{(0)}(t=0^-)_{\beta\gamma}\mathcal{G}^{(0)}(t=0^-)_{\beta'\gamma'}\mathcal{G}(\omega)_{\alpha\alpha'} \\
&+ \text{permutations of } (\alpha\beta\gamma) \text{ and } (\alpha'\beta'\gamma') \text{ separately}
\end{aligned} \tag{3.G.47}$$

This proves the diagrammatic expression of Fig. 3.7.

3.H Scattering vertices

In this appendix, we present the diagrammatic expression of the scattering vertices in TD-SCHA, Eqs (3.3.58) (3.3.59). We consider first the three-phonon term Eq. (3.3.58) since the same holds for Eq. (3.3.59).

We average the third-derivative of the BO potential on the equilibrium SCHA distribution $\varrho^{(0)}(\vec{\boldsymbol{R}})$ (see Eq. (3.3.23))

$$\overset{(3)}{D}_{ijk} = \int d\vec{\boldsymbol{R}} \varrho^{(0)}(\vec{\boldsymbol{R}}) \frac{\partial^3 V_{\mathrm{BO}}(\vec{\boldsymbol{R}})}{\partial \widetilde{R}_i \partial \widetilde{R}_j \partial \widetilde{R}_k}. \tag{3.H.1}$$

Starting from Eq. (3.H.1) we perform the change of variables $\widetilde{u}_a = \widetilde{R}_a - \widetilde{\mathcal{R}}_a^{(0)}$ and we expand in $\vec{\boldsymbol{u}}$

$$\overset{(3)}{D}_{ijk} = \int \mathrm{d}\vec{\boldsymbol{u}}\, \varrho^{(0)}(\boldsymbol{u}) \left[\sum_{n=0}^{+\infty} \frac{1}{n!} \sum_{a_1..a_n} \overset{(3+n)}{D^{(0)}}_{ijka_1..a_n} \widetilde{u}_{a_1} ... \widetilde{u}_{a_n} \right], \tag{3.H.2}$$

where $\overset{(n)}{\boldsymbol{D}}^{(0)}$ is defined in Eq. (3.3.61). Note that $\overset{(n)}{\boldsymbol{D}}^{(0)}$ differs in general from $\overset{(n)}{\boldsymbol{d}}$, see Eq. (3.3.31), since the minimum of the Born-Oppenheimer potential $\vec{\boldsymbol{\mathcal{R}}}_{\mathrm{BO}}$ does not coincide with the SCHA centroid $\vec{\boldsymbol{\mathcal{R}}}^{(0)}$.

Only even terms in Eq. (3.H.2) are non-zero

$$\begin{aligned}
\overset{(3)}{D}_{ijk} &= \sum_{n=0}^{+\infty} \frac{1}{(2n)!} \sum_{a_1..a_{2n}} \overset{(3+2n)}{D^{(0)}}_{ijka_1..a_{2n}} \langle \widetilde{u}_{a_1} ... \widetilde{u}_{a_{2n}} \rangle_{(0)} \\
&= \sum_{n=0}^{+\infty} \frac{1}{(2n)!} \sum_{a_1..a_{2n}} \overset{(3+2n)}{D^{(0)}}_{ijka_1..a_{2n}} \sum_P P \left[\left(\widetilde{\alpha}^{(0)-1}\right)_{a_1a_2} ... \left(\widetilde{\alpha}^{(0)-1}\right)_{a_{2n-1}a_{2n}} \right] \\
&= \sum_{n=0}^{+\infty} \frac{1}{2^n n!} \sum_{a_1..a_{2n}} \overset{(3+2n)}{D^{(0)}}_{ijka_1..a_{2n}} \left(\widetilde{\alpha}^{(0)-1}\right)_{a_1a_2} ... \left(\widetilde{\alpha}^{(0)-1}\right)_{a_{2n-1}a_{2n}}
\end{aligned} \tag{3.H.3}$$

where P denotes the permutations of the indices according to the Wick theorem. In the last line, we use the symmetry properties of the anharmonic vertices and the fact that the number of contractions for a $2n$ multivariate Gaussian expectation value is $(2n-1)!!$, where !! is the double factorial. In polarization the final result is

$$\overset{(3)}{D}_{\mu\nu\phi} = \sum_{n=0}^{+\infty} \frac{(-1)^n}{2^n n!} \sum_{\alpha_1..\alpha_{2n}} \overset{(3+2n)}{D^{(0)}}_{\mu\nu\phi\alpha_1..\alpha_{2n}} \underbrace{\mathcal{G}^{(0)}(t=0^-)_{\alpha_1\alpha_2} ... \mathcal{G}^{(0)}(t=0^-)_{\alpha_{2n-1}\alpha_{2n}}}_{\mathrm{n}}, \tag{3.H.4}$$

where we use $\overset{\leftrightarrow}{\widetilde{\boldsymbol{\alpha}}}^{(0)-1} = \overset{\leftrightarrow}{\boldsymbol{\Upsilon}}^{-1} = \left\langle \delta\vec{\vec{\boldsymbol{R}}} \delta\vec{\vec{\boldsymbol{R}}} \right\rangle_{(0)}$, see Eq. (3.A.44) and Eq. (3.3.36). The same holds for the fourth-order scattering vertex

$$\overset{(4)}{D}_{\mu\nu\phi\psi} = \sum_{n=0}^{+\infty} \frac{(-1)^n}{2^n n!} \sum_{\alpha_1..\alpha_{2n}} \overset{(4+2n)}{D^{(0)}}_{\mu\nu\phi\psi\alpha_1..\alpha_{2n}} \underbrace{\mathcal{G}^{(0)}(t=0^-)_{\alpha_1\alpha_2} ... \mathcal{G}^{(0)}(t=0^-)_{\alpha_{2n-1}\alpha_{2n}}}_{\mathrm{n}}. \tag{3.H.5}$$

Eq. (3.H.4) Eq. (3.H.5) give a diagrammatic expression for the TD-SCHA scattering vertices, see Fig. 3.4.

Chapter 4

Variational formulation of dynamical electronic response functions beyond DFT

Introduction

In the last Chapter of this thesis, we shift our focus on the calculation of the electronic response function in self-consistent approaches. Following linear response theory,[67,68] the electronic response functions can be written in terms of a dressed (or screened) vertex and a bare (or unscreened) one. We refer to this formulation as 'bare-screen'.

Nonetheless, if some approximations for the vertices are performed, the bare-screen structure yields results that are not the closest to the exact solution. Let's take the example of the phonon self-energy, which can be seen as a response function where the vertices are represented by the electron-phonon couplings. In this case, it has been shown in Ref. 69 for static perturbations, extended to time-dependent perturbations in Ref. 70 and recently confirmed in Ref. 71, that an exact rewriting of the response function in terms of dressed vertices corresponds to a variational formulation in terms of the electronic density. It is thus clear that any approximation of the self-consistent density, and hence of the self-consistent vertices, affects the value of the response function to the second order, contrary to the bare-screen case which is affected to the first order. We refer to this variational formulation as the 'screen-screen' approach. This functional formulation is closely related to that used for the static dielectric tensors by Gonze et al. in Ref. 174 within the Kohn-Sham, time-independent density-functional-theory frameworks.

In this Chapter, we extend the results of the Refs.[69] and [70] for a generic response function, and for a wider class of problems. In particular, we consider systems that can be described via generalized Kohn-Sham equations,[72] i.e. containing nonlocal electronic interactions. We operate neglecting retardation effects in the screening of the electronic interactions, as per the adiabatic approximation of time-dependent density functional theory (TD-DFT).[73–75]

Several theoretical schemes can be recovered as particular cases of our framework, such as time-dependent Hartree-Fock[76,77] (TD-HF), TD-DFT[73,74] with (global[78,79] or range separated[80–83] hybrid functionals), and the Bethe-Salpeter equation[84–86] (BSE) within the static-screened exchange (SX) approximation.[87]

The central achievement of this chapter consists in obtaining an exact rewriting of the response function in terms of screened electronic vertices, that is variational with respect to

the one-body electronic density-matrix. Our result is in close analogy to the screen-screen approach of Ref. 70, but valid for a wider class of electronic interactions and any linear response. In fact, the generality of this response formalism enables the investigation of virtually any type of electronic response, including the interatomic force constants used to compute phonons, and the electronic polarizability used to obtain optical or finite momentum transfer properties.

We complement our study by presenting another formulation, referred to as 'screen*-screen', first introduced in Ref. 88 for DFT-like formalisms, and recently extended to the exact many-body response in Ref. 89. Here, the response function is rewritten exactly in terms of two vertices that are one the complex conjugate of the other. We show that the screen*-screen formulation is not variational in the density matrix, but it allows the rewriting of the imaginary part of the response function exactly as a generalized Fermi Golden Rule. Being positive definite, it can be used to justify semiclassical Boltzmann equation approaches, where the dissipation is viewed as a scattering probability.

We implement a computational procedure based on a set of self-consistent equations for the electronic density matrix to determine the response functions. The level of our approximation is equivalent to the SX+BSE methods, as developed e.g. in Refs.[90,91] We illustrate our developments with an application to graphene, where excitonic effects are relevant in the description of several spectroscopic features, such as the logarithmic divergence of the group velocity near Dirac point,[92,93] and the $\pi-\pi^*$ plasmon peak features in optics[94,95] and low momentum-transfer electron-energy loss spectroscopy.[96] Also, excitonic effects are expected to be important to determine the steepening of the Kohn anomaly and the enhancement of the electron-phonon coupling for phonons at zone border.[97–100] In this chapter, we focus on the optical conductivity in the various formulations for the response function. We numerically demonstrate that the screen-screen approach is variational with respect to the electronic density matrix, while the others are not.

As further proof, we compute the optical conductivity at a generic frequency ω by using the self-consistent density matrix obtained at a fixed frequency ω_0. For $\omega \simeq \omega_0$, we obtain that the screen-screen approach approximates the exact optical conductivity with an error that is quadratic in the frequency, while bare-screen and screen*-screen display a linear error.

Chapter overview

This chapter is organized as follows: in Sec. 4.1 we introduce the generalized Kohn-Sham equations and the linear response formalism used throughout the Chapter. In Sec. 4.2, we formulate the response functions in terms of the screened vertices. We introduce the bare-screen, the screen-screen and the screen*-screen response functions. We show that the screen-screen response function can be seen as a stationary point of a functional of the density matrix, and it is thus variational in the density matrix. We show that the screen*-screen formulation allows an exact rewriting of the imaginary part of the response as a generalized Fermi Golden Rule. In Sec. 4.5, we present the application of our formalism, where we demonstrate the variationality of the screen-screen formulation computing the optical conductivity of graphene. Finally, in Sec. 4.6 we draw the conclusions of this chapter.

The content of this Chapter has been submitted to Physical Review B and uploaded on Cornell University arxiv/cond-mat as arXiv:2410.22889.[175]

4.1 Electronic linear response functions with nonlocal exchange interaction

In this Section, we summarize the linear response formalism that we use to describe the response equations of an electronic system subject to an external perturbation where nonlocal exchange interactions are included.

We consider a class of systems for which the single-particle orbitals $\{|\psi_{i\sigma}\rangle\}$ subject to a external time-dependent potential $\hat{V}_{\text{ext}}(t)$ evolve according to the generalized time-dependent Kohn-Sham equations[75,176,177]

$$i\hbar\frac{\partial}{\partial t}|\psi_{i\sigma}(t)\rangle=\left[-\frac{\hbar^2\boldsymbol{\nabla}^2}{2m}+\hat{V}_{\text{scf}}(t)\right]|\psi_{i\sigma}(t)\rangle, \tag{4.1.1}$$

$$\hat{V}_{\text{scf}}(t)=\hat{V}_{\text{Hxc}}(t)+\hat{V}_{\text{ext}}(t). \tag{4.1.2}$$

$\hat{V}_{\text{Hxc}}(t)$ is the self-consistent Hartree+exchange-correlation potential; i,σ indicate respectively the electronic and spin state. In this chapter, we only consider spin independent Hamiltonians, hence we drop the σ spin subscript for brevity. In the following, we express the matrix elements of nonlocal operators in Schrodinger representation as

$$\langle\boldsymbol{r}|\hat{O}(t)|\boldsymbol{r}'\rangle=O(\boldsymbol{r},\boldsymbol{r}',t). \tag{4.1.3}$$

The generalized potential $\hat{V}_{\text{Hxc}}(t)$ depends self-consistently on the electronic wavefunctions. It is useful to introduce the one-body electron density matrix, defined as

$$n(\boldsymbol{r},\boldsymbol{r}',t)=\sum_i f_i\psi_i(\boldsymbol{r}',t)^*\psi_i(\boldsymbol{r},t). \tag{4.1.4}$$

where $\psi_i(\boldsymbol{r},t)=\langle\boldsymbol{r}|\psi_i(t)\rangle$ and f_i is the Fermi-Dirac occupation of the state $|\psi_i\rangle$. We define the electronic density as twice the diagonal part of the density matrix

$$\rho(\boldsymbol{r},t)=2n(\boldsymbol{r},\boldsymbol{r},t), \tag{4.1.5}$$

where the factor 2 follows from spin degeneracy. In analogy with common applications of TD-DFT,[75,176] we retain the adiabatic approximation in which

$$\hat{V}_{\text{Hxc}}(t)\simeq\hat{V}_{\text{Hxc}}[\hat{n}(t)]. \tag{4.1.6}$$

In considering the time dependence of $\hat{V}_{\text{Hxc}}(t)$ only through the density matrix at the same time, we neglect memory effects in the electronic interaction.[178] This amounts in considering a frequency independent approximation of the interaction kernel.

At variance with the TD-DFT approach, we consider a generalized nonlocal Hamiltonian $\hat{V}_{\text{Hxc}}[\hat{n}(t)]$. We call 'local' $\hat{V}^{\text{loc}}_{\text{Hxc}}$ the part of the Hamiltonian that depends on the electronic density as in TD-DFT, while the remainder is referred to as 'nonlocal', i.e.

$$V_{\text{Hxc}}(\boldsymbol{r},\boldsymbol{r}',t)=V^{\text{loc}}_{\text{Hxc}}(\boldsymbol{r},t)\delta(\boldsymbol{r}-\boldsymbol{r}')+V^{\text{nloc}}_{\text{xc}}(\boldsymbol{r},\boldsymbol{r}',t), \tag{4.1.7}$$

$$V^{\text{loc}}_{\text{Hxc}}(\boldsymbol{r},t)=\frac{\partial E_{\text{Hxc}}[\rho]}{\partial\rho(\boldsymbol{r})}\Big|_{\rho(\boldsymbol{r})=\rho(\boldsymbol{r},t)}. \tag{4.1.8}$$

In Eq. (4.1.8), $E_{\text{Hxc}}[\rho]$ is the static DFT functional in which, if hybrid functionals are used, the

double-counting terms associated to the exact exchange are removed. The potential $V_{\rm Hxc}^{\rm loc}(\boldsymbol{r},t)$ in Eq. (4.1.7) contains both the Hartree and the local part of the exchange-correlation potential. For the nonlocal part of the Hamiltonian, we select the following form

$$V_{\rm xc}^{\rm nloc}(\boldsymbol{r},\boldsymbol{r}',t) = -n(\boldsymbol{r},\boldsymbol{r}',t)W(\boldsymbol{r},\boldsymbol{r}'). \tag{4.1.9}$$

Depending on the choice of $W(\boldsymbol{r},\boldsymbol{r}')$ in Eq. (4.1.9), we encompass different approximations of the electronic interaction. If $W(\boldsymbol{r},\boldsymbol{r}')=v(\boldsymbol{r}-\boldsymbol{r}')$, where $v(\boldsymbol{r}-\boldsymbol{r}')=e^2/(|\boldsymbol{r}-\boldsymbol{r}'|)$ is the Coulomb interaction, we recover the exchange potential used in Hartree-Fock schemes. Range-separated hybrid functionals[82] are obtained through $W(\boldsymbol{r},\boldsymbol{r}')=\alpha(\boldsymbol{r}-\boldsymbol{r}')v(\boldsymbol{r}-\boldsymbol{r}')$, where $\alpha(\boldsymbol{r}-\boldsymbol{r}')$ is a well suited function used to separate and tune the ratio between short and long range parts of the exchange.[80,81] Finally, the SX approximation is obtained by setting $W(\boldsymbol{r},\boldsymbol{r}')=\int \mathrm{d}\boldsymbol{r}_1\, \epsilon^{-1}(\boldsymbol{r},\boldsymbol{r}_1)v(\boldsymbol{r}_1-\boldsymbol{r}')$ where ϵ^{-1} is the static inverse dielectric function in the random-phase approximation (RPA).

From now on, integration over spatial variables with numbers as subscript is always implicit, i.e. we adopt the following convention:

$$f(\boldsymbol{r},\boldsymbol{r}',\boldsymbol{r}_1,\boldsymbol{r}_2)g(\boldsymbol{r}_1,\boldsymbol{r}_2)=\int \mathrm{d}\boldsymbol{r}_1\mathrm{d}\boldsymbol{r}_2 f(\boldsymbol{r},\boldsymbol{r}',\boldsymbol{r}_1,\boldsymbol{r}_2)g(\boldsymbol{r}_1,\boldsymbol{r}_2), \tag{4.1.10}$$

where the spatial integrals are performed over the whole volume of the system. We express the analytic continuation of Fourier transforms of retarded quantities in complex frequency $z=\omega+i\eta$ as

$$f(z) = \int_{-\infty}^{\infty} \mathrm{d}t\, e^{izt} f(t). \tag{4.1.11}$$

The expression is well defined for $\eta>0$ due to the causality condition of $f(t)$, i.e. $f(t)=0$ for $t<0$. Physical observables are obtained in the limit $\eta\to 0^+$, to be considered after the thermodynamical limit.[113]

4.1.1 Linear response

4.1.2 Linear response

We suppose that the external potential is differentiable with respect to two independent time-varying parameters $a(t), b(t)$, which contain all the time-dependence of the external potential. We consider the completely general expansion

$$\hat{V}_{\rm ext}[a(t),b(t)] = \hat{V}_{\rm ext}^{{\rm nl}\,(a)}a(t)+\hat{V}_{\rm ext}^{{\rm nl}\,(b)}b(t)+\frac{1}{2}\begin{bmatrix}a(t), b(t)\end{bmatrix}\cdot\begin{bmatrix}\hat{V}_{\rm ext}^{{\rm nl}\,(a,a)} & \hat{V}_{\rm ext}^{{\rm nl}\,(a,b)}\\ \hat{V}_{\rm ext}^{{\rm nl}\,(a,b)} & \hat{V}_{\rm ext}^{{\rm nl}\,(b,b)}\end{bmatrix}\cdot\begin{bmatrix}a(t)\\ b(t)\end{bmatrix}+\dots . \tag{4.1.12}$$

In particular, we consider the case of external operators that are non local ('nl') in Schrodinger representation, i.e. $[\hat{V}_{\rm ext}^{{\rm nl}\,(a)},\hat{\boldsymbol{r}}]\neq 0$. In this framework, we can define four-points response functions. Further, we can include practical situations where the effective perturbation is nondiagonal in space, as in the case of the ionic motion in a nonlocal pseudopotential picture.[179]

In linear response, the density matrix induced by the presence of the perturbation that

couples to $b(t)$ is

$$2n(\boldsymbol{r},\boldsymbol{r}',t)=\int_{-\infty}^{+\infty}\mathrm{d}t'\,L(\boldsymbol{r},\boldsymbol{r}',\boldsymbol{r}_1,\boldsymbol{r}_2,t')V_{\mathrm{ext}}^{\mathrm{nl}\,(b)}(\boldsymbol{r}_1,\boldsymbol{r}_2)b(t-t'), \tag{4.1.13}$$

where the factor 2 takes into account spin degeneracy, and L is the retarded interacting electron-hole propagator, i.e. $L(t)=0$ for $t<0$.

We now indicate $n^{(b)}(\boldsymbol{r},\boldsymbol{r}',t)$ as the retarded response to the specific perturbation $b(t)=\delta(t)$. Its expression in frequency domain is

$$2n^{(b)}(\boldsymbol{r},\boldsymbol{r}',z) = L(\boldsymbol{r},\boldsymbol{r}',\boldsymbol{r}_1,\boldsymbol{r}_2,z)V_{\mathrm{ext}}^{\mathrm{nl}\,(b)}(\boldsymbol{r}_1,\boldsymbol{r}_2). \tag{4.1.14}$$

For a generic perturbation $b(t)$, the density response in frequency domain can be deduced as $n(\boldsymbol{r},\boldsymbol{r}',z) = n^{(b)}(\boldsymbol{r},\boldsymbol{r}',z)b(z)$, where $b(z)$ is the Fourier transform of $b(t)$. For the remainder of this Chapter, we will only deal with linear response. Therefore, we will use the term electronic density matrix to address the induced density matrix rather than the exact ground-state density matrix introduced in Eq. (4.1.4).

Expanding at linear order in the external field the self-consistent potential of Eq. (4.1.7) we get

$$V_{\mathrm{scf}}^{(b)}(\boldsymbol{r},\boldsymbol{r}',z) = V_{\mathrm{ext}}^{\mathrm{nl}\,(b)}(\boldsymbol{r},\boldsymbol{r}')+K(\boldsymbol{r},\boldsymbol{r}',\boldsymbol{r}_1,\boldsymbol{r}_2)n^{(b)}(\boldsymbol{r}_1,\boldsymbol{r}_2,z). \tag{4.1.15}$$

The nonlocal kernel of the interaction K is defined as

$$K(\boldsymbol{r},\boldsymbol{r}',\boldsymbol{r}'',\boldsymbol{r}''') =\frac{\delta V_{\mathrm{Hxc}}(\boldsymbol{r},\boldsymbol{r}')}{\delta n(\boldsymbol{r}'',\boldsymbol{r}''')} \tag{4.1.16}$$

$$=2f_{\mathrm{Hxc}}(\boldsymbol{r},\boldsymbol{r}'')\delta(\boldsymbol{r}-\boldsymbol{r}')\delta(\boldsymbol{r}''-\boldsymbol{r}''') - W(\boldsymbol{r},\boldsymbol{r}')\delta(\boldsymbol{r}-\boldsymbol{r}'')\delta(\boldsymbol{r}'-\boldsymbol{r}'''), \tag{4.1.17}$$

where

$$f_{\mathrm{Hxc}}(\boldsymbol{r},\boldsymbol{r}'') = \frac{e^2}{|\boldsymbol{r}-\boldsymbol{r}''|} + \frac{\delta V_{\mathrm{xc}}^{\mathrm{loc}}(\boldsymbol{r})}{\delta\rho(\boldsymbol{r}'')} \tag{4.1.18}$$

is the adiabatic Hartree plus exchange-correlation ('Hxc') kernel. Using the linear response theory for time-dependent generalized Kohn-Sham equations,[180] the linear order expansion of the density of Eq. (4.1.4) is instead written as (see Appendix 4.A for a derivation):

$$2n^{(b)}(\boldsymbol{r},\boldsymbol{r}',z)=L^0(\boldsymbol{r},\boldsymbol{r}',\boldsymbol{r}_1,\boldsymbol{r}_2,z)V_{\mathrm{scf}}^{(b)}(\boldsymbol{r}_1,\boldsymbol{r}_2,z). \tag{4.1.19}$$

In Eq. (4.1.19), L^0 is the bare electron-hole propagator, defined as

$$L^0(\boldsymbol{r},\boldsymbol{r}',\boldsymbol{r}'',\boldsymbol{r}''',z) = 2\sum_{ij}\frac{f_j^{(0)}-f_i^{(0)}}{\hbar z-(\varepsilon_i^{(0)}-\varepsilon_j^{(0)})}\psi_i^{(0)}(\boldsymbol{r})\psi_j^{(0)}(\boldsymbol{r}')^* \times\psi_i^{(0)}(\boldsymbol{r}'')^*\psi_j^{(0)}(\boldsymbol{r}'''), \tag{4.1.20}$$

where the superscript $^{(0)}$ indicates quantities computed without external perturbations, and the factor 2 accounts for spin degeneracy.

A diagrammatic representation of Eqs. (4.1.15), (4.1.17), and (4.1.19) is given in Table 4.1. In particular, the coupled expressions of Eqs. (4.1.15), (4.1.19) represent the generalization of the TD-DFT equations to the case of nonlocal kernel[90,91,153] . They can be solved with

an iterative method. The process starts from the 'unscreened' density matrix $n_0^{(b)}=L^0V_{\rm ext}^{{\rm nl}\,(b)}$ and updates the potential $V_{\rm scf}^{(b)}$ through the application of the interaction kernel K, as for the Sternheimer equations,[161] until self consistency is achieved.

It is also interesting to express the interacting electron-hole propagator L in terms of the bare one, $L^{(0)}$. Using Eqs. (4.1.15) and (4.1.19) in Eq. (4.1.14), we get

$$L(\boldsymbol{r},\boldsymbol{r}',\boldsymbol{r}'',\boldsymbol{r}''',z) = L^0(\boldsymbol{r},\boldsymbol{r}',\boldsymbol{r}'',\boldsymbol{r}''',z)+\tfrac{1}{2}L^0(\boldsymbol{r},\boldsymbol{r}',\boldsymbol{r}_1,\boldsymbol{r}_2,z)K(\boldsymbol{r}_1,\boldsymbol{r}_2,\boldsymbol{r}_3,\boldsymbol{r}_4)L(\boldsymbol{r}_3,\boldsymbol{r}_4,\boldsymbol{r}'',\boldsymbol{r}''',z). \tag{4.1.21}$$

Eq. (4.1.21) is the Dyson equation for the interacting electron-hole propagator L in the screened exchange approximation for the generalized Hxc functional (see Eq. (14.25) of Ref. 87 or Ref. 90).

We finally discuss the properties that will be used to define and to characterize the screened formulations of the response functions. The bare electron-hole propagator satisfies the properties:

$$L^0(\boldsymbol{r},\boldsymbol{r}',\boldsymbol{r}'',\boldsymbol{r}''',z)^* = L^0(\boldsymbol{r}'',\boldsymbol{r}''',\boldsymbol{r},\boldsymbol{r}',z^*) \tag{4.1.22}$$

$$L^0(\boldsymbol{r},\boldsymbol{r}',\boldsymbol{r}'',\boldsymbol{r}''',-z) = L^0(\boldsymbol{r}''',\boldsymbol{r}'',\boldsymbol{r}',\boldsymbol{r},z) \tag{4.1.23}$$

which can be proven directly from Eq. (4.1.20). Instead, from the definition Eq. (4.1.17) follows that:

$$K(\boldsymbol{r},\boldsymbol{r}',\boldsymbol{r}'',\boldsymbol{r}''') = K(\boldsymbol{r}'',\boldsymbol{r}''',\boldsymbol{r},\boldsymbol{r}'), \tag{4.1.24}$$

$$K(\boldsymbol{r},\boldsymbol{r}',\boldsymbol{r}'',\boldsymbol{r}''') = K(\boldsymbol{r}''',\boldsymbol{r}'',\boldsymbol{r}',\boldsymbol{r}), \tag{4.1.25}$$

which can be proven exploiting the symmetries of the delta functions and the fact that in the SX approximation $W(\boldsymbol{r},\boldsymbol{r}')=W(\boldsymbol{r}',\boldsymbol{r})$. Combining these equations with Eq. (4.1.21), we obtain:

$$L(\boldsymbol{r},\boldsymbol{r}',\boldsymbol{r}'',\boldsymbol{r}''',z)^* = L(\boldsymbol{r}'',\boldsymbol{r}''',\boldsymbol{r},\boldsymbol{r}',z^*), \tag{4.1.26}$$

$$L(\boldsymbol{r},\boldsymbol{r}',\boldsymbol{r}'',\boldsymbol{r}''',-z) = L(\boldsymbol{r}''',\boldsymbol{r}'',\boldsymbol{r}',\boldsymbol{r},z). \tag{4.1.27}$$

Eqs. (4.1.26)-(4.1.27) show that the symmetry properties of the bare electron hole propagator $L^{(0)}$ Eqs. (4.1.22)-(4.1.23) are inherited by the interacting propagator L.

4.1.3 Examples of response functions

In the examples considered below, for simplicity we will consider a local external potential, i.e.

$$\langle\boldsymbol{r}|\hat{V}_{\rm ext}^{{\rm nl}\,(a)}|\boldsymbol{r}'\rangle=V_{\rm ext}^{(a)}(\boldsymbol{r})\delta(\boldsymbol{r}-\boldsymbol{r}'). \tag{4.1.28}$$

At this point, we introduce the retarded response function that describes the variation of the observable tied to the perturbation $\hat{V}_{\rm ext}^{(a)}$ due to the presence of the perturbation $\hat{V}_{\rm ext}^{(b)}$. It is expressed in Fourier space as

$$C_{ab}(z) = 2V_{\rm ext}^{(a)}(\boldsymbol{r}_1)n^{(b)}(\boldsymbol{r}_1,\boldsymbol{r}_1,z) \tag{4.1.29}$$

or equivalently, using Eq. (4.1.14), as

$$C_{ab}(z) = V^{(a)}_{\text{ext}}(\boldsymbol{r}_1)L(\boldsymbol{r}_1,\boldsymbol{r}_1,\boldsymbol{r}_2,\boldsymbol{r}_2,z)V^{(b)}_{\text{ext}}(\boldsymbol{r}_2). \tag{4.1.30}$$

Eq. (4.1.30) is valid for a general external perturbation. Depending on the nature of the parameters a, b, we obtain different response functions, that correspond to different physical observables. In this Section, we present some notable examples of response functions which are of wide use in the study of molecular and crystalline systems.

In particular, from the knowledge of the retarded interacting electron-hole propagator L, that is defined for clamped nuclei at the equilibrium positions, we can obtain the phonon Green's function and the vibrational spectra (see e.g. 88, 181–183). Notice that the clamped nuclei hypothesis corresponds to disregarding electron-phonon effects on the electron dynamics, such as the terms neglected leveraging the Migdal theorem[184] (cf. Fig. 1(b) of[182]) and electron-phonon insertions in the electron Green function (cf. Fig. (1)c of[182]).

To this purpose, for a molecule, we consider the displacements $u_{s\alpha}(t)/u_{r\beta}(t')$ of the atoms s/r along the Cartesian coordinates α/β. In Eq. (4.1.30), we take

$$V^{(a)}_{\text{ext}}(\boldsymbol{r}_1) = \frac{\partial V_{\text{ext}}(\boldsymbol{r}_1)}{\partial u_{s\alpha}} = V^{(s\alpha)}_{\text{ext}}(\boldsymbol{r}_1), \tag{4.1.31}$$

$$V^{(b)}_{\text{ext}}(\boldsymbol{r}_2) = \frac{\partial V_{\text{ext}}(\boldsymbol{r}_2)}{\partial u_{r\beta}} = V^{(r\beta)}_{\text{ext}}(\boldsymbol{r}_2). \tag{4.1.32}$$

In this case, the response function (4.1.30) corresponds to the nontrivial contribution to the frequency-dependent interatomic force constant matrix $C_{s\alpha,r\beta}$,[70,71,181,185,186] which reads

$$C_{s\alpha,r\beta}(z) = V^{(s\alpha)}_{\text{ext}}(\boldsymbol{r}_1)L(\boldsymbol{r}_1,\boldsymbol{r}_1,\boldsymbol{r}_2,\boldsymbol{r}_2,z)V^{(r\beta)}_{\text{ext}}(\boldsymbol{r}_2). \tag{4.1.33}$$

The corresponding dynamical matrix $D_{s\alpha,r\beta}$ is defined as

$$D_{s\alpha,r\beta}(z) = \frac{C_{s\alpha,r\beta}(z) + V^{(s\alpha,r\beta)}_{\text{ext}}(\boldsymbol{r}_1)\rho^{(0)}(\boldsymbol{r}_1)}{\sqrt{M_s M_r}}, \tag{4.1.34}$$

where M_s represent the mass of the atom s. Notice that, in order to define the dynamical matrix in Eq. (4.1.34) that determines the motions of the atoms, the second order term in the potential expansion in Eq. (4.1.12) is needed, even though it enters in a term of trivial evaluation.[70] $D_{s\alpha,r\beta}$ can be used to define the displacement-displacement (divided by the nuclear masses) Green's function [71] as:

$$G^{-1}{}_{s\alpha,r\beta}(z) = z^2 - D_{s\alpha,r\beta}(z). \tag{4.1.35}$$

The phonon spectral weight is defined as:

$$A(\omega) = -\lim_{\eta\to 0^+}\sum_{s\alpha}\text{Im}\left[\frac{\omega+i\eta}{\pi}G_{s\alpha,s\alpha}(\omega+i\eta)\right]. \tag{4.1.36}$$

The peaks of the spectral weight define the vibrational frequencies, while the vibrational self energy can be obtained from $D_{s\alpha,r\beta}$.

To define the density-density response in the context of periodic crystals, we consider a system with unit cell Ω and a periodic perturbation of wavevector $\boldsymbol{q}$. We suppose that $\boldsymbol{q}$ is commensurate with a Born-Von Karman supercell of dimensions $N\Omega$ which has the

same periodicity of the perturbation. In this case, the density-density response function is obtained by considering Eq. (4.1.30) with

$$V_{\text{ext}}^{(a)}(\boldsymbol{r}) = e^{-i\boldsymbol{q}\cdot\boldsymbol{r}}, \quad V_{\text{ext}}^{(b)}(\boldsymbol{r}) = e^{i\boldsymbol{q}\cdot\boldsymbol{r}}. \tag{4.1.37}$$

The response in Eq. (4.1.30) now depends on $(\boldsymbol{q}, z)$. The density-density response function therefore reads

$$\chi(\boldsymbol{q}, z) = \int_{N\Omega} \frac{d\boldsymbol{r}}{N\Omega} e^{-i\boldsymbol{q}\cdot\boldsymbol{r}} L(\boldsymbol{r}, \boldsymbol{r}, \boldsymbol{r}_1, \boldsymbol{r}_1, z) e^{i\boldsymbol{q}\cdot\boldsymbol{r}_1}, \tag{4.1.38}$$

where the integral over $\boldsymbol{r}$ runs over the N cells of the supercell and the implicit one over $\boldsymbol{r}_1$ on the full crystal. In Sec. 4.5, we compute the density-density response function to obtain the optical conductivity $\sigma(\boldsymbol{q}, z)$ of graphene.

Finally, we also define the linear response to a monochromatic displacement of ions (i.e. phonons), in which the response function becomes the Fourier transform of the dynamical matrix. For the crystal case, we consider the atoms to be situated at $u_{s\alpha}^{\boldsymbol{R}} = R_\alpha + \tau_{s\alpha}$, $\boldsymbol{R}$ being a direct Bravais lattice vector and $\boldsymbol{\tau}_s$ the coordinate relative to the unit cell origin. We take

$$V_{\text{ext}}^{(a)}(\boldsymbol{r}) = \sum_{\boldsymbol{R}} e^{-i\boldsymbol{q}\cdot(\boldsymbol{R}+\boldsymbol{\tau}_s)} \frac{\partial V_{\text{ext}}(\boldsymbol{r})}{\partial u_{s\alpha}^{\boldsymbol{R}}} = U_{\text{ext}}^{(s\alpha,-\boldsymbol{q})}(\boldsymbol{r}) e^{-i\boldsymbol{q}\cdot\boldsymbol{r}}, \tag{4.1.39}$$

$$V_{\text{ext}}^{(b)}(\boldsymbol{r}) = \sum_{\boldsymbol{R}} e^{i\boldsymbol{q}\cdot(\boldsymbol{R}+\boldsymbol{\tau}_r)} \frac{\partial V_{\text{ext}}(\boldsymbol{r})}{\partial u_{r\beta}^{\boldsymbol{R}}} = U_{\text{ext}}^{(r\beta,\boldsymbol{q})}(\boldsymbol{r}) e^{i\boldsymbol{q}\cdot\boldsymbol{r}}, \tag{4.1.40}$$

where $U_{\text{ext}}^{(r\beta,\boldsymbol{q})}(\boldsymbol{r}_2)$ are cell-periodic potentials and the sum over $\boldsymbol{R}$ runs over the full crystal. Eq. (4.1.30) becomes

$$C_{s\alpha,r\beta}(\boldsymbol{q}, z) = \frac{1}{N} \int_{N\Omega} d\boldsymbol{r}\, U_{\text{ext}}^{(s\alpha,-\boldsymbol{q})}(\boldsymbol{r}) e^{-i\boldsymbol{q}\cdot\boldsymbol{r}} L(\boldsymbol{r}, \boldsymbol{r}, \boldsymbol{r}_2, \boldsymbol{r}_2, z) U_{\text{ext}}^{(r\beta,\boldsymbol{q})}(\boldsymbol{r}_2) e^{i\boldsymbol{q}\cdot\boldsymbol{r}_2}. \tag{4.1.41}$$

For any wavevector $\boldsymbol{q}$, the dynamical matrix and the Green's function are obtained in the same way as for Eqs. (4.1.34) and (4.1.35).

4.2 Response functions in terms of screened vertices

In this Section, we present three different but equivalent rewritings of the response functions in the case of a nonlocal interaction potential, starting from Eq. (4.1.29). The first formulation is the bare-screen, which is the most common formulation. In the static DFT framework, it is equivalent to the Sternheimer approach of Ref.[161] Next, we introduce the screen-screen approach, extending the approach of Ref. 70 to the case of nonlocal interactions. We show that this formulation is variational with respect to the electron density matrix. Thus, an approximation of the density matrix results in a quadratic error in the response function. Finally, we introduce the screen*-screen formulation, that provides an expression for the imaginary part of the response function in the form of a generalized Fermi Golden Rule, extending the approach of Ref. 88 to the case of nonlocal interactions. We stress that the three proposed formulations are exactly equivalent. They differ only whenever one performs an approximation on the electronic density matrix, as proved numerically in Sec. 4.5.

4.2.1 Bare-screen response

We start from Eq. (4.1.29). We use the relation between the density and the potential given by Eq. (4.1.19), to reformulate the response function C_{ab} as

$$C^{\text{bs}}_{ab}(z)=V^{(a)}_{\text{ext}}(\boldsymbol{r}_1)L^0(\boldsymbol{r}_1,\boldsymbol{r}_1,\boldsymbol{r}_2,\boldsymbol{r}_3,z)V^{(b)}_{\text{scf}}(\boldsymbol{r}_2,\boldsymbol{r}_3,z). \tag{4.2.1}$$

Eq. (4.2.1) can be interpreted diagramatically as a response function composed by the two vertices $V^{(a)}_{\text{ext}}$ and $V^{(b)}_{\text{scf}}$ connected by the propagator L^0 (cf. Table 4.1). The external potential $V^{(a)}_{\text{ext}}$ does not depend on the electronic density matrix. The bare electron-hole propagator L^0 describes the response of noninteracting particles, as explicitly shown by Eq. (4.1.20). Thus, the screening of the response due to the electronic interactions is only contained in the self-consistent potential. Accordingly, we refer to $V^{(b)}_{\text{scf}}$ and $V^{(a)}_{\text{ext}}$ respectively as a screened and a bare vertex. We call the formulation Eq. (4.2.1) the bare-screen response C^{bs}_{ab}.

Eq. (4.2.1) is linear in the electronic density matrix. To show it, we introduce the functional

$$\mathcal{F}_{ab}[\lambda,z] = V^{(a)}_{\text{ext}}(\boldsymbol{r}_1)L^0(\boldsymbol{r}_1,\boldsymbol{r}_1,\boldsymbol{r}_2,\boldsymbol{r}_3,z)\left[V^{(b)}_{\text{ext}}(\boldsymbol{r}_2)\delta(\boldsymbol{r}_2-\boldsymbol{r}_3)+K(\boldsymbol{r}_2,\boldsymbol{r}_3,\boldsymbol{r}_4,\boldsymbol{r}_5)\lambda(\boldsymbol{r}_4,\boldsymbol{r}_5)\right], \tag{4.2.2}$$

that satisfies the relation

$$C^{\text{bs}}_{ab}(z) = \mathcal{F}_{ab}[\lambda=n^{(b)}(z),z]. \tag{4.2.3}$$

From Eq. (4.2.2), it follows that

$$\left.\frac{\delta\mathcal{F}_{ab}[\lambda,z]}{\delta\lambda(\boldsymbol{r}_i,\boldsymbol{r}_j)}\right|_{\lambda=n^{(b)}(z)} = V^{(a)}_{\text{ext}}(\boldsymbol{r}_1)L^0(\boldsymbol{r}_1,\boldsymbol{r}_1,\boldsymbol{r}_2,\boldsymbol{r}_3,z)K(\boldsymbol{r}_2,\boldsymbol{r}_3,\boldsymbol{r}_i,\boldsymbol{r}_j). \tag{4.2.4}$$

The above derivative does not depend on the electronic density matrix. Therefore, an error of $\delta n^{(b)}(\boldsymbol{r},\boldsymbol{r}',z)$ on the density matrix results in an error of order $\delta n^{(b)}(\boldsymbol{r},\boldsymbol{r}',z)$ in the bare-screen response, thus proving its linearity with respect to changes in the electronic density matrix.

4.2.2 Screen-screen response

To obtain the screen-screen response we manipulate Eq. (4.2.1) by expressing the external potential $V^{(a)}_{\text{ext}}$ in terms of the self-consistent potential $V^{(a)}_{\text{scf}}$. Therefore, we rewrite Eq. (4.2.1) using the relation between the screened potential and the external potential, Eq. (4.1.15). $C_{ab}(z)$ then becomes

$$C_{ab}(z)=[V^{(a)}_{\text{scf}}(\boldsymbol{r}_2,\boldsymbol{r}_1,-z)-K(\boldsymbol{r}_2,\boldsymbol{r}_1,\boldsymbol{r}_3,\boldsymbol{r}_4)n^{(a)}(\boldsymbol{r}_3,\boldsymbol{r}_4,-z)]L^0(\boldsymbol{r}_1,\boldsymbol{r}_2,\boldsymbol{r}_5,\boldsymbol{r}_6,z)V^{(b)}_{\text{scf}}(\boldsymbol{r}_5,\boldsymbol{r}_6,z). \tag{4.2.5}$$

Further, we use the connection between the bare electron-hole propagator L^0 and the induced density, given by Eq. (4.1.19), and the symmetry properties of the kernel expressed in Eqs. (4.1.24) and (4.1.25). With these ingredients, Eq. (4.2.5) is rewritten as

$$\begin{aligned}C^{\text{ss}}_{ab}(z)=&V^{(a)}_{\text{scf}}(\boldsymbol{r}_2,\boldsymbol{r}_1,-z)L^0(\boldsymbol{r}_1,\boldsymbol{r}_2,\boldsymbol{r}_3,\boldsymbol{r}_4,z)V^{(b)}_{\text{scf}}(\boldsymbol{r}_3,\boldsymbol{r}_4,z)\\ &-2n^{(a)}(\boldsymbol{r}_2,\boldsymbol{r}_1,-z)K(\boldsymbol{r}_1,\boldsymbol{r}_2,\boldsymbol{r}_3,\boldsymbol{r}_4)n^{(b)}(\boldsymbol{r}_3,\boldsymbol{r}_4,z).\end{aligned} \tag{4.2.6}$$

The first term in Eq. (4.2.6) is made up of two screened vertices $V^{(a)}_{\text{scf}}, V^{(b)}_{\text{scf}}$, connected by the bare electron-hole propagator L^0. The second term in Eq. (4.2.6) removes double-counting

terms that occur in the first term (cfr. Table 4.1 for the diagramatic representation). We refer to the formulation in Eq. (4.2.6) as the screen-screen response function $C^{\mathrm{ss}}_{ab}(z)$.

Eq. (4.2.6) represents the generalization of the result obtained in Ref. 70 in the case of a nonlocal interaction potential, and is the main result of this chapter. Closely to the result obtained in the aforementioned work, we show in the following section that the response function in Eq. (4.2.6) is variational with respect to the density matrix.

Eq.	Expression	Diagramatic representation
(4.1.15)	$V^{(b)}_{\mathrm{scf}} = V^{(b)}_{\mathrm{ext}} + Kn^{(b)}$	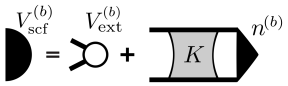
(4.1.17)	$K = 2f_{\mathrm{Hxc}} - W$	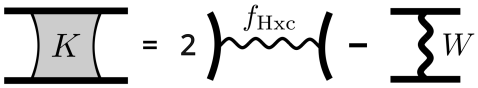
(4.1.19)	$2n^{(b)} = L^0 V^{(b)}_{\mathrm{scf}}$	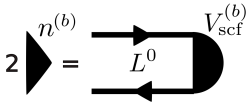
(4.2.1)	$C^{\mathrm{bs}}_{ab} = V^{(a)}_{\mathrm{ext}} L^0 V^{(b)}_{\mathrm{scf}}$	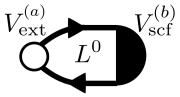
(4.2.6)	$C^{\mathrm{ss}}_{ab} = V^{(a)}_{\mathrm{scf}} L^0 V^{(b)}_{\mathrm{scf}} - 2n^{(a)} K n^{(b)}$	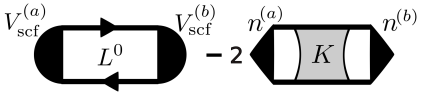
(4.2.13)	$C^{\mathrm{s^*s}}_{ab} = V^{(a)*}_{\mathrm{scf}} L^0 V^{(b)}_{\mathrm{scf}} - 2n^{(a)*} K n^{(b)}$	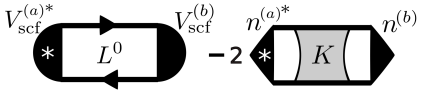

Table 4.1. Diagramatic representation of the the self-consistent equations for the screened vertex, kernel, density matrix and different formulations of the response functions. The full black semicircle represent the screened vertex V_{scf}, while an empty circle symbolizes the bare (local) vertex V_{ext}. The bare electron-hole propagator L^0 is represented as two lines, while the shaded grey block is the interaction kernel K. The density matrix is sketched with a full black triangle. The star symbolizes complex conjugation. The Hartree plus exchange-correlation kernel f_{Hxc} and screened Coulomb interaction W are represented by thin and thick wavy lines respectively. Notice that the diagrams contained in the interaction kernel depend on the particular approximation scheme adopted. In the case of the SX approximation, $f_{\mathrm{Hxc}} = v$, where v is the bare Coulomb interaction, and $W = \epsilon^{-1}v$ is the Coulomb interaction screened by the RPA inverse dielectric constant.

Stationary response functional

To demonstrate the variationality of the screen-screen response, we introduce the response functional

$$F_{ab}[\lambda,\lambda',z]=\Big[V^{(a)}_{\rm ext}(\boldsymbol{r}_1)\delta(\boldsymbol{r}_1-\boldsymbol{r}_2)+K(\boldsymbol{r}_2,\boldsymbol{r}_1,\boldsymbol{r}_5,\boldsymbol{r}_6)\lambda(\boldsymbol{r}_5,\boldsymbol{r}_6)\Big]\,L^0(\boldsymbol{r}_1,\boldsymbol{r}_2,\boldsymbol{r}_3,\boldsymbol{r}_4,z)$$
$$\times\Big[V^{(b)}_{\rm ext}(\boldsymbol{r}_3)\delta(\boldsymbol{r}_3-\boldsymbol{r}_4)+K(\boldsymbol{r}_3,\boldsymbol{r}_4,\boldsymbol{r}_7,\boldsymbol{r}_8)\lambda'(\boldsymbol{r}_7,\boldsymbol{r}_8)\Big]-2\lambda(\boldsymbol{r}_2,\boldsymbol{r}_1)K(\boldsymbol{r}_1,\boldsymbol{r}_2,\boldsymbol{r}_3,\boldsymbol{r}_4)\lambda'(\boldsymbol{r}_3,\boldsymbol{r}_4), \tag{4.2.7}$$

that satisfies the relation

$$C^{\rm ss}_{ab}(z)=F_{ab}[\lambda{=}n^{(a)}(-z),\lambda'{=}n^{(b)}(z),z]. \tag{4.2.8}$$

The functional $F_{ab}[\lambda,\lambda',z]$ in Eq. (4.2.7) satisfies

$$\frac{\delta F_{ab}[\lambda,\lambda',z]}{\delta\lambda(\boldsymbol{r}_i,\boldsymbol{r}_j)}\Big|_{\substack{\lambda=n^{(a)}(-z),\\ \lambda'=n^{(b)}(z)}}=0,\qquad \frac{\delta F_{ab}[\lambda,\lambda',z]}{\delta\lambda'(\boldsymbol{r}_i,\boldsymbol{r}_j)}\Big|_{\substack{\lambda=n^{(a)}(-z),\\ \lambda'=n^{(b)}(z)}}=0. \tag{4.2.9}$$

In fact, let us consider the derivative of $F_{ab}[\lambda,\lambda',z]$ with respect to λ, which reads

$$\frac{\delta F_{ab}[\lambda,\lambda',z]}{\delta\lambda(\boldsymbol{r}_i,\boldsymbol{r}_j)}\Big|_{\substack{\lambda=n^{(a)}(-z)\\ \lambda'=n^{(b)}(z)}}=K(\boldsymbol{r}_2,\boldsymbol{r}_1,\boldsymbol{r}_i,\boldsymbol{r}_j)L^0(\boldsymbol{r}_1,\boldsymbol{r}_2,\boldsymbol{r}_3,\boldsymbol{r}_4,z)V^{(b)}_{\rm scf}(\boldsymbol{r}_3,\boldsymbol{r}_4,z)-K(\boldsymbol{r}_j,\boldsymbol{r}_i,\boldsymbol{r}_1,\boldsymbol{r}_2)2n^{(b)}(\boldsymbol{r}_1,\boldsymbol{r}_2,z). \tag{4.2.10}$$

Using Eq. (4.1.14), we recast Eq. (4.2.10) as

$$\frac{\delta F_{ab}[\lambda,\lambda',z]}{\delta\lambda(\boldsymbol{r}_i,\boldsymbol{r}_j)}\Big|_{\substack{\lambda=n^{(a)}(-z)\\ \lambda'=n^{(b)}(z)}}=\left[K(\boldsymbol{r}_2,\boldsymbol{r}_1,\boldsymbol{r}_i,\boldsymbol{r}_j)-K(\boldsymbol{r}_j,\boldsymbol{r}_i,\boldsymbol{r}_1,\boldsymbol{r}_2)\right]2n^{(b)}(\boldsymbol{r}_1,\boldsymbol{r}_2,z)=0. \tag{4.2.11}$$

where the term in square brackets in Eq. (4.2.11) is zero due to the symmetries of the kernel expressed in Eqs. (4.1.24) and (4.1.25). Instead, the derivative with respect λ' reads

$$\frac{\delta F_{ab}[\lambda,\lambda',z]}{\delta\lambda'(\boldsymbol{r}_i,\boldsymbol{r}_j)}\Big|_{\substack{\lambda=n^{(a)}(-z)\\ \lambda'=n^{(b)}(z)}}=\Big[V^{(a)}_{\rm scf}(\boldsymbol{r}_2,\boldsymbol{r}_1,-z)L^0(\boldsymbol{r}_1,\boldsymbol{r}_2,\boldsymbol{r}_3,\boldsymbol{r}_4,z)-2n^{(a)}(\boldsymbol{r}_4,\boldsymbol{r}_3,-z)\Big]\,K(\boldsymbol{r}_3,\boldsymbol{r}_4,\boldsymbol{r}_i,\boldsymbol{r}_j)=0. \tag{4.2.12}$$

The term in square brackets of Eq. (4.2.12) vanishes using the symmetry property (4.1.23) of the bare electron-hole propagator L^0 in its relation with the density matrix (4.1.19).

Eq. (4.2.9) implies that the screen-screen response function of Eq. (4.2.6) is an extremal point of the functional $F_{ab}[\lambda,\lambda',z]$, in both λ and λ'. In other words, an error of $\delta n^{(b/a)}(\boldsymbol{r},\boldsymbol{r}',\pm z)$ on the density matrix results in an error of order $\left[\delta n^{(b/a)}(\boldsymbol{r},\boldsymbol{r}',\pm z)\right]^2$ in the screen-screen response.

4.2.3 Screen*-screen response

In Sec. 4.2.1 and 4.2.2 we have discussed respectively the definitions of the bare-screen and screen-screen response functions. As anticipated in the introduction, we now introduce another possible formulation of the electronic response, from which a generalization of the Fermi Golden Rule for the imaginary part of the response function can be demonstrated.

Performing the same passages as for the screen-screen response, but with $-z^*$ instead of

$-z$, we rewrite the response function of Eq. (4.1.29) as

$$C_{ab}^{\mathrm{s^*s}}(z)=V_{\mathrm{scf}}^{(a)}(\boldsymbol{r}_2,\boldsymbol{r}_1,-z^*)L^0(\boldsymbol{r}_1,\boldsymbol{r}_2,\boldsymbol{r}_3,\boldsymbol{r}_4,z)V_{\mathrm{scf}}^{(b)}(\boldsymbol{r}_3,\boldsymbol{r}_4,z) \\ -2n^{(a)}(\boldsymbol{r}_2,\boldsymbol{r}_1,-z^*)K(\boldsymbol{r}_1,\boldsymbol{r}_2,\boldsymbol{r}_3,\boldsymbol{r}_4)n^{(b)}(\boldsymbol{r}_3,\boldsymbol{r}_4,z). \tag{4.2.13}$$

It is interesting to notice that Eq. (4.2.13) determines the holomorphic quantity $C_{ab}^{\mathrm{s^*s}}(z)$ by summing two separately nonholomorphic terms. The screen*-screen response in Eq. (4.2.13) can be obtained from the functional in Eq. (4.2.7), as

$$C_{ab}^{\mathrm{s^*s}}(z) = F_{ab}[\lambda{=}n^{(a)}(-z^*), \lambda'{=}n^{(b)}(z), z]. \tag{4.2.14}$$

However, $C_{ab}^{\mathrm{s^*s}}(z)$ is not a stationary point of the functional $F[\lambda,\lambda',z]$:

$$\frac{\delta F_{ab}[\lambda,\lambda',z]}{\delta\lambda'(\boldsymbol{r}_i,\boldsymbol{r}_j)}\bigg|_{\substack{\lambda=n^{(a)}(-z^*)\\ \lambda'=n^{(b)}(z)}} {=}K(\boldsymbol{r}_3,\boldsymbol{r}_4,\boldsymbol{r}_i,\boldsymbol{r}_j)\left[V_{\mathrm{scf}}^{(a)}(\boldsymbol{r}_2,\boldsymbol{r}_1,-z^*)L^0(\boldsymbol{r}_1,\boldsymbol{r}_2,\boldsymbol{r}_3,\boldsymbol{r}_4,z)-2n^{(a)}(\boldsymbol{r}_4,\boldsymbol{r}_3,-z^*)\right]. \tag{4.2.15}$$

The term in square brackets in Eq. (4.2.15) is zero only in the nonresonant case in which $\eta{=}0, z{=}\omega$ and the screen-screen and screen*-screen formulations coincide. Therefore, an error of $\delta n^{(b)}(\boldsymbol{r},\boldsymbol{r}',z)$ on the density matrix results in an error of order $\delta n^{(b)}(\boldsymbol{r},\boldsymbol{r}',z)$ in the screen*-screen response, thus proving its linearity with respect to changes in the electronic density matrix.

Generalized Fermi Golden Rule

Let us consider the particular case where:

$$V_{\mathrm{ext}}^{(a)}(\boldsymbol{r}) = V_{\mathrm{ext}}^{(b)}(\boldsymbol{r})^*. \tag{4.2.16}$$

This correspond to the diagonal response function of a perturbation, either real, or modulated by a wavevector $\boldsymbol{q}$, as that of a phonon with quasimomentum $\hbar\boldsymbol{q}$. For the present case, the properties Eqs. (4.1.26)-(4.1.27) and Eqs. (4.1.22)-(4.1.23) respectively of the interacting and bare electron-hole propagators L and L^0 can be leveraged in the definitions of the density matrix Eq. (4.1.14) and Eq. (4.1.19) to show that

$$n^{(a)}(\boldsymbol{r}',\boldsymbol{r},-z^*) = n^{(b)}(\boldsymbol{r},\boldsymbol{r}',z)^*, \tag{4.2.17}$$

$$V_{\mathrm{scf}}^{(a)}(\boldsymbol{r}',\boldsymbol{r},-z^*) = V_{\mathrm{scf}}^{(b)}(\boldsymbol{r},\boldsymbol{r}',z)^*. \tag{4.2.18}$$

Using Eq. (4.2.17) and Eq. (4.2.18), and the properties Eq. (4.1.24) of K and Eq. (4.1.26) of L^0, we obtain:

$$\mathrm{Im}C_{ab}^{\mathrm{s^*s}}(z){=}V_{\mathrm{scf}}^{(b)}(\boldsymbol{r}_1,\boldsymbol{r}_2,z)^*V_{\mathrm{scf}}^{(b)}(\boldsymbol{r}_3,\boldsymbol{r}_4,z)\frac{1}{2i}[L^0(\boldsymbol{r}_1,\boldsymbol{r}_2,\boldsymbol{r}_3,\boldsymbol{r}_4,z){-}L^0(\boldsymbol{r}_1,\boldsymbol{r}_2,\boldsymbol{r}_3,\boldsymbol{r}_4,z^*)], \tag{4.2.19}$$

Passing from the real space representation to the Dirac one, we get

$$\mathrm{Im}C_{ab}^{\mathrm{s^*s}}(z){=}2\sum_{ij}|\langle\psi_i^{(0)}|\hat{V}_{\mathrm{scf}}^{(b)}(z)|\psi_j^{(0)}\rangle|^2\mathrm{Im}\left[\frac{f_j^{(0)}-f_i^{(0)}}{\hbar z{-}(\varepsilon_i^{(0)}{-}\varepsilon_j^{(0)})}\right]. \tag{4.2.20}$$

Supposing that the matrix elements $\langle\psi_i^{(0)}|\hat{V}_{\text{scf}}^{(b)}(z)|\psi_j^{(0)}\rangle$ remain finite in the $\eta\to0^+$ limit, and that $C_{ab}^{\text{s*s}}(z)$ represents a self-energy, it follows that

$$\Gamma(\omega)=-\frac{1}{\hbar}\lim_{\eta\to0^+}2\text{Im}C_{ab}^{\text{s*s}}(z)=\frac{2\pi}{\hbar}2\sum_{ij}(f_j^{(0)}-f_i^{(0)})|\langle\psi_i^{(0)}|\hat{V}_{\text{scf}}^{(b)}(\omega)|\psi_j^{(0)}\rangle|^2\delta(\varepsilon_i^{(0)}-\varepsilon_j^{(0)}-\hbar\omega). \tag{4.2.21}$$

Eq. (4.2.21) consists in the generalization of the Fermi Golden Rule[187] to the case of self-consistent Hamiltonians. When computed e.g. at the frequency of the phonon, it corresponds to the full width at half maximum and it is widely used to compute phonon scattering rates. The combination of the square modulus of the screened vertices, the Fermi-Dirac populations, and the Dirac delta in Eq. (4.2.21) clearly makes $\Gamma(\omega)$ a positive definite quantity. This property allows for a probabilistic interpretation of Γ; much like in semiclassical Boltzmann-Equation approaches, the imaginary part of the response function associated with dissipation can be interpreted in terms of scattering processes.

As for the standard Fermi Golden Rule, Eq. (4.2.21) is only valid when the summation over states i,j forms a continuum, and ω is taken within this continuum. In solids this is generally obtained considering a Born–von Karman periodic cell of volume $V=N\Omega$ and performing the $V\to\infty$ thermodynamic limit before the $\eta\to0^+$ one. Moreover, assuming that the matrix elements of the screened potential are finite, to obtain Eq. (4.2.21) we neglected the contributions from the electronic excitations generated by the electron-electron interaction decoupled from an underlined continuum, such as undamped plasmons or bounded excitons. In this cases, $\langle\psi_i^{(0)}|\hat{V}_{\text{scf}}^{(b)}(\omega)|\psi_j^{(0)}\rangle$ diverges for $\eta\to0^+$ at resonance, even in the thermodynamic limit. These contributions are instead fully included in Eq. (4.2.20), that remains valid in the $\eta\to0^+$ also in presence of undamped plasmons or excitons.

It is important to stress that the bare-screen [see Eq. (4.2.1)], the screen-screen [see Eq. (4.2.6)] and the screen*-screen [see Eq. (4.2.13)] are equivalent formulations of the same physical observable. Thus, the generalized Fermi Golden Rule holds for each formulation as $\text{Im}C_{ab}^{\text{s*s}}(z)=\text{Im}C_{ab}^{\text{ss}}(z)=\text{Im}C_{ab}^{\text{bs}}(z)$, where the $\eta\to0^+$ limit is given by Eq. (4.2.21), when the screened matrix elements remain finite.

4.3 Response functions in terms of partially screened vertices

So far, we expressed the linear response in term of either the external unscreened potential, $V_{\text{ext}}^{(b)}$, or the interacting, fully screened potential, $V_{\text{scf}}^{(b)}$. However, there are instances where it is advantageous to introduce and use a partially screened potential, that we call $V_{\text{p}}^{(b)}$, where the $V_{\text{ext}}^{(b)}$ is dressed by only a part of the interacting kernel K. In this section, we reformulate the response function in terms of partially screened vertices and propagators.

4.3.1 Partial screening of the vertices

We introduce partial screening effects, by partitioning the kernel of the interaction in Eq. (4.4.1) as:

$$K(\boldsymbol{r},\boldsymbol{r}',\boldsymbol{r}'',\boldsymbol{r}''')=K^{\text{p}}(\boldsymbol{r},\boldsymbol{r}',\boldsymbol{r}'',\boldsymbol{r}''')+K^{\text{c}}(\boldsymbol{r},\boldsymbol{r}',\boldsymbol{r}'',\boldsymbol{r}''') \tag{4.3.1}$$

assuming that the partial kernel K^{p} is real (as K and thus K^{c}) and has the same symmetry properties

$$K^{\mathrm{p}}(\boldsymbol{r},\boldsymbol{r}',\boldsymbol{r}'',\boldsymbol{r}''') = K^{\mathrm{p}}(\boldsymbol{r}'',\boldsymbol{r}''',\boldsymbol{r},\boldsymbol{r}'), \tag{4.3.2}$$
$$K^{\mathrm{p}}(\boldsymbol{r},\boldsymbol{r}',\boldsymbol{r}'',\boldsymbol{r}''') = K^{\mathrm{p}}(\boldsymbol{r}''',\boldsymbol{r}'',\boldsymbol{r}',\boldsymbol{r}). \tag{4.3.3}$$

From these properties of K^{p} and the analogous ones of K, it follows that:

$$K^{\mathrm{c}}(\boldsymbol{r},\boldsymbol{r}',\boldsymbol{r}'',\boldsymbol{r}''') = K^{\mathrm{c}}(\boldsymbol{r}'',\boldsymbol{r}''',\boldsymbol{r},\boldsymbol{r}'), \tag{4.3.4}$$
$$K^{\mathrm{c}}(\boldsymbol{r},\boldsymbol{r}',\boldsymbol{r}'',\boldsymbol{r}''') = K^{\mathrm{c}}(\boldsymbol{r}''',\boldsymbol{r}'',\boldsymbol{r}',\boldsymbol{r}). \tag{4.3.5}$$

Using the repartion of the interaction in Eq. (4.3.1), we define a partially screened potential

$$V_{\mathrm{p}}^{(b)}(\boldsymbol{r},\boldsymbol{r}',z) = V_{\mathrm{ext}}^{\mathrm{nl}\,(b)}(\boldsymbol{r},\boldsymbol{r}')+K^{\mathrm{p}}(\boldsymbol{r},\boldsymbol{r}',\boldsymbol{r}_1,\boldsymbol{r}_2)n^{(b)}(\boldsymbol{r}_1,\boldsymbol{r}_2,z). \tag{4.3.6}$$

Using Eq. (4.3.1), we get from Eq. (4.1.15) the relation between the self-consistent induced potential and the partially screened potential

$$V_{\mathrm{scf}}^{(b)}(\boldsymbol{r},\boldsymbol{r}',z) = V_{\mathrm{p}}^{(b)}(\boldsymbol{r},\boldsymbol{r}',z) + K^{\mathrm{c}}(\boldsymbol{r},\boldsymbol{r}',\boldsymbol{r}_1,\boldsymbol{r}_2)n^{(b)}(\boldsymbol{r}_1,\boldsymbol{r}_2,z). \tag{4.3.7}$$

In analogy with Eqs. (4.1.14) and (4.1.19), we define the induced density matrix in terms of a partially interacting propagator L^{c}

$$2n^{(b)}(\boldsymbol{r},\boldsymbol{r}',z)=L^{\mathrm{c}}(\boldsymbol{r},\boldsymbol{r}',\boldsymbol{r}_1,\boldsymbol{r}_2,z)V_{\mathrm{p}}^{(b)}(\boldsymbol{r}_1,\boldsymbol{r}_2,z). \tag{4.3.8}$$

To elucidate its differences with the interacting electron-hole propagator L defined in Eq. (4.1.21), we derive the Dyson equation of the partially interacting propagator L^{c}. Using Eq. (4.3.7) in the definition of the density matrix in terms of the self-consistent potential Eq. (4.1.19), we get

$$2n^{(b)}(\boldsymbol{r},\boldsymbol{r}',z) = L^{0}(\boldsymbol{r},\boldsymbol{r}',\boldsymbol{r}_1,\boldsymbol{r}_2,z)\left[V_{\mathrm{p}}^{(b)}(\boldsymbol{r}_1,\boldsymbol{r}_2,z) + K^{\mathrm{c}}(\boldsymbol{r}_1,\boldsymbol{r}_2,\boldsymbol{r}_3,\boldsymbol{r}_4)n^{(b)}(\boldsymbol{r}_3,\boldsymbol{r}_4,z)\right]. \tag{4.3.9}$$

By rewriting the density in terms of partially screened quantities as in Eq. (4.3.8), we recast Eq. (4.3.9) as

$$\begin{aligned} L^{\mathrm{c}}(\boldsymbol{r},\boldsymbol{r}',\boldsymbol{r}_1,\boldsymbol{r}_2,z)V_{\mathrm{p}}^{(b)}(\boldsymbol{r}_1,\boldsymbol{r}_2,z) = L^{0}(\boldsymbol{r},\boldsymbol{r}',\boldsymbol{r}_1,\boldsymbol{r}_2,z)\big[\delta(\boldsymbol{r}_1-\boldsymbol{r}_5)\delta(\boldsymbol{r}_2-\boldsymbol{r}_6) \\ + \tfrac{1}{2}K^{\mathrm{c}}(\boldsymbol{r}_1,\boldsymbol{r}_2,\boldsymbol{r}_3,\boldsymbol{r}_4)L^{\mathrm{c}}(\boldsymbol{r}_3,\boldsymbol{r}_4,\boldsymbol{r}_5,\boldsymbol{r}_6,z)\big]V_{\mathrm{p}}^{(b)}(\boldsymbol{r}_5,\boldsymbol{r}_6,z), \end{aligned} \tag{4.3.10}$$

from which it follows that

$$L^{\mathrm{c}}(\boldsymbol{r},\boldsymbol{r}',\boldsymbol{r}'',\boldsymbol{r}''',z) = L^{0}(\boldsymbol{r},\boldsymbol{r}',\boldsymbol{r}'',\boldsymbol{r}''',z)+\tfrac{1}{2}L^{0}(\boldsymbol{r},\boldsymbol{r}',\boldsymbol{r}_1,\boldsymbol{r}_2,z)K^{\mathrm{c}}(\boldsymbol{r}_1,\boldsymbol{r}_2,\boldsymbol{r}_3,\boldsymbol{r}_4)L^{\mathrm{c}}(\boldsymbol{r}_3,\boldsymbol{r}_4,\boldsymbol{r}'',\boldsymbol{r}''',z). \tag{4.3.11}$$

Eq. (4.3.11) is the Dyson equation for the partially interacting propagator.

For completeness, we also express the relation between the partially interacting propagator L^{c} and the fully interacting propagator L. We plug the relation Eq. (4.3.6) in Eq. (4.3.8), obtaining

$$2n^{(b)}(\boldsymbol{r},\boldsymbol{r}',z) = L^{\mathrm{c}}(\boldsymbol{r},\boldsymbol{r}',\boldsymbol{r}_1,\boldsymbol{r}_2,z)\left[V_{\mathrm{ext}}^{(b)}(\boldsymbol{r}_1,\boldsymbol{r}_2,z) + K^{\mathrm{p}}(\boldsymbol{r}_1,\boldsymbol{r}_2,\boldsymbol{r}_3,\boldsymbol{r}_4)n^{(b)}(\boldsymbol{r}_3,\boldsymbol{r}_4,z)\right]. \tag{4.3.12}$$

Expressing the density matrix in Eq. (4.3.12) in terms of the interacting electron-hole propagator L from Eq. (4.1.14), we get

$$L(\boldsymbol{r},\boldsymbol{r}',\boldsymbol{r}_1,\boldsymbol{r}_2,z)V^{(b)}_{\rm ext}(\boldsymbol{r}_1,\boldsymbol{r}_2,z) = L^{\rm c}(\boldsymbol{r},\boldsymbol{r}',\boldsymbol{r}_1,\boldsymbol{r}_2,z)\big[\delta(\boldsymbol{r}_1-\boldsymbol{r}_5)\delta(\boldsymbol{r}_2-\boldsymbol{r}_6) + \tfrac{1}{2}K^{\rm p}(\boldsymbol{r}_1,\boldsymbol{r}_2,\boldsymbol{r}_3,\boldsymbol{r}_4)L(\boldsymbol{r}_3,\boldsymbol{r}_4,\boldsymbol{r}_5,\boldsymbol{r}_6,z)\big]V^{(b)}_{\rm ext}(\boldsymbol{r}_5,\boldsymbol{r}_6,z), \tag{4.3.13}$$

from which it follows that

$$L(\boldsymbol{r},\boldsymbol{r}',\boldsymbol{r}'',\boldsymbol{r}''',z) = L^{\rm c}(\boldsymbol{r},\boldsymbol{r}',\boldsymbol{r}'',\boldsymbol{r}''',z)+\tfrac{1}{2}L^{\rm c}(\boldsymbol{r},\boldsymbol{r}',\boldsymbol{r}_1,\boldsymbol{r}_2,z)K^{\rm p}(\boldsymbol{r}_1,\boldsymbol{r}_2,\boldsymbol{r}_3,\boldsymbol{r}_4)L(\boldsymbol{r}_3,\boldsymbol{r}_4,\boldsymbol{r}'',\boldsymbol{r}''',z). \tag{4.3.14}$$

From Eq. (4.3.14) it is clear that to obtain the fully interacting electron-hole propagator L, one must incorporate into the partially interacting propagator $L^{\rm c}$ the remainder of the interaction comprised in $K^{\rm p}$.

Using the properties of the bare propagator expressed in Eqs. (4.1.22)-(4.1.23) and of the complementary part of the retarded kernel $K^{\rm c}$ in Eqs. (4.3.4)-(4.3.5), it follows from Eq. (4.3.11) that the partially interacting propagator satisfies

$$L^{\rm c}(\boldsymbol{r},\boldsymbol{r}',\boldsymbol{r}'',\boldsymbol{r}''',z)^* = L^{\rm c}(\boldsymbol{r}'',\boldsymbol{r}''',\boldsymbol{r},\boldsymbol{r}',z^*) \tag{4.3.15}$$

$$L^{\rm c}(\boldsymbol{r},\boldsymbol{r}',\boldsymbol{r}'',\boldsymbol{r}''',-z) = L^{\rm c}(\boldsymbol{r}''',\boldsymbol{r}'',\boldsymbol{r}',\boldsymbol{r},z) \tag{4.3.16}$$

4.3.2 Partial screen - partial screen response

As done in Sec. 4.2, we express the response functions in terms of the partially screened quantities defined in Sec. 4.3.1. First, we assume for simplicity that the external potential in Eq. (4.3.6) is local, i.e. satisfies Eq. (4.1.28). In this case, the response function $C_{ab}(z)$ is expressed as in Eq. (4.1.29). Using (4.3.8), we recast the response function as

$$C_{ab}(z) = V^{(a)}_{\rm ext}(\boldsymbol{r}_1)L^{\rm c}(\boldsymbol{r}_1,\boldsymbol{r}_1,\boldsymbol{r}_2,\boldsymbol{r}_3,z)V^{(b)}_{\rm p}(\boldsymbol{r}_2,\boldsymbol{r}_3,z). \tag{4.3.17}$$

To obtain the partially screened-partially screened response, we manipulate Eq. (4.3.17) by expressing the external potential $V^{(a)}_{\rm ext}$ in terms of the partially screened potential $V^{(a)}_{\rm p}$. Therefore, we rewrite Eq. (4.3.17) using the relation between the partially screened potential and the external potential, Eq. (4.3.6). $C_{ab}(z)$ then becomes

$$C_{ab}(z)=\big[V^{(a)}_{\rm p}(\boldsymbol{r}_2,\boldsymbol{r}_1,-z)-K^{\rm p}(\boldsymbol{r}_1,\boldsymbol{r}_2,\boldsymbol{r}_3,\boldsymbol{r}_4)n^{(a)}(\boldsymbol{r}_3,\boldsymbol{r}_4,-z)\big] \times L^{\rm c}(\boldsymbol{r}_1,\boldsymbol{r}_2,\boldsymbol{r}_5,\boldsymbol{r}_6,z)V^{(b)}_{\rm p}(\boldsymbol{r}_5,\boldsymbol{r}_6,z). \tag{4.3.18}$$

Further we use the connection between the partially interacting propagator $L^{\rm c}$ and the induced density, given by Eq. (4.3.8), and the symmetry property of $K^{\rm c}$ expressed in Eqs. (4.3.4)-(4.3.5). With these ingredients, Eq. (4.3.18) is rewritten as

$$C^{\rm pp}_{ab}(z)=V^{(a)}_{\rm p}(\boldsymbol{r}_2,\boldsymbol{r}_1,-z)L^{\rm c}(\boldsymbol{r}_1,\boldsymbol{r}_2,\boldsymbol{r}_3,\boldsymbol{r}_4,z)V^{(b)}_{\rm p}(\boldsymbol{r}_3,\boldsymbol{r}_4,z) -2n^{(a)}(\boldsymbol{r}_2,\boldsymbol{r}_1,-z)K^{\rm p}(\boldsymbol{r}_1,\boldsymbol{r}_2,\boldsymbol{r}_3,\boldsymbol{r}_4)n^{(b)}(\boldsymbol{r}_3,\boldsymbol{r}_4,z). \tag{4.3.19}$$

The first term in Eq. (4.3.19) is made up of two partially screened vertices $V^{(a)}_{\rm p}$, $V^{(b)}_{\rm p}$, connected by the partially interacting propagator $L^{\rm c}$. We refer to the formulation in Eq. (4.3.19) as the 'partial screen-partial screen' response function, denoted $C^{\rm pp}_{ab}(z)$.

Eq. (4.3.19) represents a further equivalent rewriting of the response function. In close analogy with the screen-screen formulation presented in Sec. 4.2.2, we show that the partial screen-partial screen response function is variational with respect to the density matrix.

Stationary response functional

To demonstrate the variationality of the partial screen-partial screen response, we introduce the response functional

$$F^{\mathrm{pp}}_{ab}[\lambda,\lambda',z]=\Big[V^{(a)}_{\mathrm{ext}}(\boldsymbol{r}_1)\delta(\boldsymbol{r}_1-\boldsymbol{r}_2)+K^{\mathrm{p}}(\boldsymbol{r}_2,\boldsymbol{r}_1,\boldsymbol{r}_5,\boldsymbol{r}_6)\lambda(\boldsymbol{r}_5,\boldsymbol{r}_6)\Big]\,L^{\mathrm{c}}(\boldsymbol{r}_1,\boldsymbol{r}_2,\boldsymbol{r}_3,\boldsymbol{r}_4,z)$$
$$\times\Big[V^{(b)}_{\mathrm{ext}}(\boldsymbol{r}_3)\delta(\boldsymbol{r}_3-\boldsymbol{r}_4)+K^{\mathrm{p}}(\boldsymbol{r}_3,\boldsymbol{r}_4,\boldsymbol{r}_7,\boldsymbol{r}_8)\lambda'(\boldsymbol{r}_7,\boldsymbol{r}_8)\Big]-2\lambda(\boldsymbol{r}_2,\boldsymbol{r}_1)K^{\mathrm{p}}(\boldsymbol{r}_1,\boldsymbol{r}_2,\boldsymbol{r}_3,\boldsymbol{r}_4)\lambda'(\boldsymbol{r}_3,\boldsymbol{r}_4), \tag{4.3.20}$$

that satisfies the relation

$$C^{\mathrm{pp}}_{ab}(z)=F^{\mathrm{pp}}_{ab}[\lambda{=}n^{(a)}(-z),\lambda'{=}n^{(b)}(z),z]. \tag{4.3.21}$$

This functional can be obtained replacing into the functional $F_{ab}[\lambda,\lambda',z]$ used for $C^{\mathrm{ss}}_{ab}(z)$, Eq. (4.2.7), L^0 with L^{c} and K with K^{p}. Since the substituted objects share the same properties of the original ones, we can follow the proof presented in Sec. 4.2.2, obtaining:

$$\frac{\delta F^{\mathrm{pp}}_{ab}[\lambda,\lambda',z]}{\delta\lambda(\boldsymbol{r}_i,\boldsymbol{r}_j)}\Big|_{\substack{\lambda=n^{(a)}(-z),\\ \lambda'=n^{(b)}(z)}} = 0, \tag{4.3.22}$$

$$\frac{\delta F^{\mathrm{pp}}_{ab}[\lambda,\lambda',z]}{\delta\lambda'(\boldsymbol{r}_i,\boldsymbol{r}_j)}\Big|_{\substack{\lambda=n^{(a)}(-z),\\ \lambda'=n^{(b)}(z)}} = 0. \tag{4.3.23}$$

Eqs. (4.3.22)-(4.3.23) imply that the partial screen-partial screen response function of Eq. (4.3.19) is also an extremal point of the functional $F^{\mathrm{pp}}_{ab}[\lambda,\lambda',z]$, in both λ and λ'. In other words, an error of $\delta n^{(b/a)}(\boldsymbol{r},\boldsymbol{r}',z)$ on the density matrix results in an error of order $\left[\delta n^{(b/a)}(\boldsymbol{r},\boldsymbol{r}',\pm z)\right]^2$ in the partial screen-partial screen response.

Example of a partial screening approach

Here we present an example of a particular choice for the separation of the interaction kernel (4.3.1). We work in the BSE framework, that corresponds to setting $\delta V^{\mathrm{loc}}_{\mathrm{xc}}/\delta\rho{=}0$ in Eq. (4.1.18). In this picture, we separate the kernel in Hartree and exchange contribution, selecting for K^{p} the Hartree kernel i.e.

$$K^{\mathrm{p}}(\boldsymbol{r},\boldsymbol{r}',\boldsymbol{r}'',\boldsymbol{r}''')=K^{\mathrm{H}}(\boldsymbol{r},\boldsymbol{r}',\boldsymbol{r}'',\boldsymbol{r}''')=2\frac{e^2}{|\boldsymbol{r}-\boldsymbol{r}''|}\delta(\boldsymbol{r}{-}\boldsymbol{r}')\delta(\boldsymbol{r}''{-}\boldsymbol{r}''') \tag{4.3.24}$$

while the complementary part K^{c} is the screened-exchange term featuring W, i.e.

$$K^{\mathrm{c}}(\boldsymbol{r},\boldsymbol{r}',\boldsymbol{r}'',\boldsymbol{r}''')=K^{W}(\boldsymbol{r},\boldsymbol{r}',\boldsymbol{r}'',\boldsymbol{r}''')=-W(\boldsymbol{r},\boldsymbol{r}')\delta(\boldsymbol{r}{-}\boldsymbol{r}'')\delta(\boldsymbol{r}'{-}\boldsymbol{r}'''). \tag{4.3.25}$$

Considering the Dyson equation (4.3.11) for the partially interacting electron-hole propagator L^{c} with the partial kernel Eq. (4.3.25), we get

Eq.	Expression	Diagramatic representation
(4.3.26)	$L^{\rm c} = L_0 - \frac{1}{2} L_0 W L^{\rm c}$	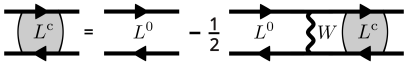
(4.3.27)	$L^{\rm lad}(\boldsymbol{r},\boldsymbol{r}') = L^{\rm c}(\boldsymbol{r},\boldsymbol{r},\boldsymbol{r}',\boldsymbol{r}')$	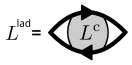
(4.1.21)	$L = L_0 + L_0 v L - \frac{1}{2} L_0 W L$	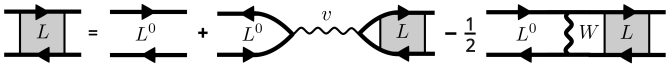

Table 4.2. Diagramatic representation of the the self-consistent equations for the Dyson equation of the interacting electon hole propagators $L^{\rm c}$, $L^{\rm lad}$ and L, in the BSE framework where $\delta V_{\rm xc}^{\rm loc}/\delta\rho{=}0$. The bare electron-hole propagator L^0 is represented as two lines. The unscreened and screened Coulomb interactions, v and W respectively, are represented by thin and thick wavy lines.

$$L^{\rm c}(\boldsymbol{r},\boldsymbol{r}',\boldsymbol{r}'',\boldsymbol{r}''',z) = L^0(\boldsymbol{r},\boldsymbol{r}',\boldsymbol{r}'',\boldsymbol{r}''',z) - \tfrac{1}{2} L^0(\boldsymbol{r},\boldsymbol{r}',\boldsymbol{r}_1,\boldsymbol{r}_2,z) W(\boldsymbol{r}_1,\boldsymbol{r}_2) L^{\rm c}(\boldsymbol{r}_1,\boldsymbol{r}_2,\boldsymbol{r}'',\boldsymbol{r}''',z). \tag{4.3.26}$$

where it is evident that $L^{\rm c}$ includes only ladder diagrams. Moreover, since the partially screened potential is in the present case local, we just need in $F^{\rm pp}_{ab}$ the diagonal elements of $L^{\rm c}$, that we call the ladder-bubble diagram:

$$L^{\rm lad}(\boldsymbol{r},\boldsymbol{r}',z) = L^{\rm c}(\boldsymbol{r},\boldsymbol{r},\boldsymbol{r}',\boldsymbol{r}',z). \tag{4.3.27}$$

A diagrammatic representation of the Dyson equation (4.3.26) of $L^{\rm c}$ and of Eq. (4.3.27) is presented in Table 4.2.

The choice of the partial screening Eq. (4.3.24) bears the important consequence that the partial screened-partial screen response $C^{\rm pp}_{ab}(z)$ in Eq. (4.3.19) only depends on the electronic densities, and not on the whole density matrix. Moreover, if we use approximated densities $\rho^{\rm (b)}_{\rm ap}(\boldsymbol{r},z)$ and $\rho^{\rm (a)}_{\rm ap}(\boldsymbol{r},-z)$ in the variational functional $F^{\rm pp}_{ab}$, we obtain a variationally approximated expression of $C^{\rm pp}_{ab}(z)$ as:

$$C^{\rm pp}_{ab,{\rm ap}}(z){=}V^{(a)}_{\rm extH,ap}(\boldsymbol{r}_1,-z) L^{\rm lad}(\boldsymbol{r}_1,\boldsymbol{r}_2,z)\, V^{(b)}_{\rm extH,ap}(\boldsymbol{r}_2,z) {-} \rho^{(a)}_{\rm ap}(\boldsymbol{r}_1,-z) \frac{e^2}{|\boldsymbol{r}_1{-}\boldsymbol{r}_2|} \rho^{(b)}_{\rm ap}(\boldsymbol{r}_2,z), \tag{4.3.28}$$

where the approximated partially screened potential is

$$V^{(b)}_{\rm extH,ap}(\boldsymbol{r},z) = V^{(b)}_{\rm ext}(\boldsymbol{r}) {+} \frac{e^2}{|\boldsymbol{r}-\boldsymbol{r}_1|} \rho^{(b)}_{\rm ap}(\boldsymbol{r}_1,z), \tag{4.3.29}$$

and the analogous expression is used for $V^{(a)}_{\rm extH,ap}(\boldsymbol{r},-z)$. Note that, with this choice of K^p, the variational response (4.3.28) is similar to the formulation proposed in Ref. 89, cf. Eq. (6) of the v2 version of the preprint.

We obtain the exact response $C^{\rm pp}_{ab}(z){=}C_{ab}(z)$ using in Eqs. (4.3.28) and (4.3.29) the non-

approximated densities:

$$\rho^{(b)}(\boldsymbol{r},z) = L(\boldsymbol{r},\boldsymbol{r},\boldsymbol{r}_1,\boldsymbol{r}_1,z)V^{(b)}_{\rm ext}(\boldsymbol{r}_1), \tag{4.3.30}$$

$$\rho^{(a)}(\boldsymbol{r},-z) = L(\boldsymbol{r},\boldsymbol{r},\boldsymbol{r}_1,\boldsymbol{r}_1,-z)V^{(a)}_{\rm ext}(\boldsymbol{r}_1), \tag{4.3.31}$$

where $L(\boldsymbol{r},\boldsymbol{r},\boldsymbol{r}',\boldsymbol{r}',z)$ is the full BSE bubble diagram, obtained from the interacting-electron hole propagator L. The BSE for L is reported in Table 4.2.

By virtue of the variationality of the partial screen-partial screen response Eq. (4.3.22)-(4.3.23), we have that the error on the response is quadratic in the error on the density:

$$C^{\rm pp}_{ab,{\rm ap}}(z) - C_{ab}(z) = O\left(\left(\rho^{(b/a)}_{\rm ap}(\pm z) - \rho^{(b/a)}(\pm z)\right)^2\right). \tag{4.3.32}$$

As we will show in a following paper,[188] the approximated scheme given by Eqs. (4.3.28) and (4.3.29), is particularly appealing, if we want to devise a practical scheme to evaluate the BSE corrections to the phonon self-energy on top of a standard static phonon calculation, based on DFT linear response theory.[185,186] In this case, we can leverage the fact that both the dynamical and BSE effects produce small relative-corrections to the static DFT electronic densities $\rho^{(b/a)}_{\rm DFT}$ in the range of frequencies corresponding to the phonon scale (typically up to 10-100 meV). Thus, in Eqs. (4.3.28) and (4.3.29), we can safely use:

$$\rho^{(b)}_{\rm ap}(\boldsymbol{r},z) = \rho^{(b)}_{\rm DFT}(\boldsymbol{r}), \tag{4.3.33}$$

$$\rho^{(a)}_{\rm ap}(\boldsymbol{r},-z) = \rho^{(a)}_{\rm DFT}(\boldsymbol{r}), \tag{4.3.34}$$

keeping the resulting error on the phonon self-energy under control, thanks to the variational properties of the $F^{\rm pp}_{ab}$ functional.

In Ref. 188 we will leverage the variationality of the partial screen-partial screen response to effectively approximate the phonon dispersion of graphene including exchange effects. We report here the formal derivation of the partial screen-partial screen formulation in order to focus more on physical insights of our findings in Ref. 188

4.4 Memory effects in the full or partial interaction kernel

In the framework used throughout all our manuscript, we have neglected memory effects in the electronic interaction, i.e. we have worked in the adiabatic approximation Eq. (4.1.6). In this Section, we discuss briefly how to overcome such an approximation.

To relax the adiabiatic approximation for the exchange and correlation potential, introduced in Eq. (4.1.6), we generalize the nonlocal kernel of the interaction introduced in Eq. (4.1.17) accounting for memory effects in the Hartree-exchange-correlation part as

$$K(\boldsymbol{r},\boldsymbol{r}',\boldsymbol{r}'',\boldsymbol{r}''',z) = 2f_{\rm Hxc}(\boldsymbol{r},\boldsymbol{r}'',z)\delta(\boldsymbol{r}-\boldsymbol{r}')\delta(\boldsymbol{r}''-\boldsymbol{r}''') - W(\boldsymbol{r},\boldsymbol{r}')\delta(\boldsymbol{r}-\boldsymbol{r}'')\delta(\boldsymbol{r}'-\boldsymbol{r}'''), \tag{4.4.1}$$

where $f_{\rm Hxc}(\boldsymbol{r},\boldsymbol{r}'',z)$ is the retarded Hartree plus exchange-correlation kernel, which is holomorphic for ${\rm Im}z>0$. A formal expression for $f_{\rm Hxc}(\boldsymbol{r},\boldsymbol{r}'',z)$ is presented e.g. in Ref. 189. For the present discussion, we do not discuss a specific expression for $f_{\rm Hxc}(\boldsymbol{r},\boldsymbol{r}'',z)$ analogous to (4.1.18). We only use the property (see Eq. (6) of Ref. 189)

$$f_{\rm Hxc}(\boldsymbol{r},\boldsymbol{r}'',z) = f_{\rm Hxc}(\boldsymbol{r}'',\boldsymbol{r},-z). \tag{4.4.2}$$

From Eq. (4.4.2), it follows that the retarded kernel of the interaction satisfies[180,189]

$$K(\boldsymbol{r},\boldsymbol{r}',\boldsymbol{r}'',\boldsymbol{r}''',z) = K(\boldsymbol{r}''',\boldsymbol{r}'',\boldsymbol{r}',\boldsymbol{r},-z) \tag{4.4.3}$$

This property can be leveraged to generalize the formalism developed in Secs. 4.2 and 4.3 including memory effects in the Hxc part of the electronic interaction. Specifically, the bare-screen [Eq. (4.2.1)], the screen-screen [Eq. (4.2.6)], the screen*-screen [Eq. (4.2.13)] and the partial screen-partial screen [Eq. (4.3.19)] response can be directly generalized including a frequency dependent kernel, of the form Eq. (4.4.1). Using the symmetry property Eq. (4.4.3), it is straightforward to show that the variationality of the screen-screen and of the partial screen-partial screen formulations still hold, while the bare-screen and the screen*-screen formulations are not.

Notice however that the screen*-screen formulation with a retarded kernel does not posses the generalized Fermi Golden Rule structure as in Eq. (4.2.21). In fact, the imaginary part of the screen*-screen response function [Eq. (4.2.20)] acquires a finite contribution associated with the imaginary part of the retarded kernel.

In conclusion, we mention that the partition of the electronic interaction discussed in Sec. 4.3 can be performed considering memory in the partial and complementary kernels that sum up to a frequency independent kernel, i.e.

$$K(\boldsymbol{r},\boldsymbol{r}',\boldsymbol{r}'',\boldsymbol{r}''')=K^{\mathrm{p}}(\boldsymbol{r},\boldsymbol{r}',\boldsymbol{r}'',\boldsymbol{r}''',z)+K^{\mathrm{c}}(\boldsymbol{r},\boldsymbol{r}',\boldsymbol{r}'',\boldsymbol{r}''',z)\,. \tag{4.4.4}$$

It is straightforward to show that the variationality of the partial screen-partial screen response still holds if the partial retarded kernels satisfy the properties

$$K^{\mathrm{p}}(\boldsymbol{r},\boldsymbol{r}',\boldsymbol{r}'',\boldsymbol{r}''',z) = K^{\mathrm{p}}(\boldsymbol{r}''',\boldsymbol{r}'',\boldsymbol{r}',\boldsymbol{r},-z), \tag{4.4.5}$$

$$K^{\mathrm{c}}(\boldsymbol{r},\boldsymbol{r}',\boldsymbol{r}'',\boldsymbol{r}''',z) = K^{\mathrm{c}}(\boldsymbol{r}''',\boldsymbol{r}'',\boldsymbol{r}',\boldsymbol{r},-z)\,. \tag{4.4.6}$$

A separation of the form Eq. (4.4.4) can be useful in instances where the memory effects are included in the individual parts of the electronic screening, but cancel out when summed in the fully interacting kernel.

4.5 Application: optical conductivity of graphene

In this Section, we apply the linear response formalism developed in the previous sections to the calculation of optical conductivity of graphene. As detailed in Ref. 190, the diagonal element of the optical conductivity tensor in the direction of the unitary vector $\hat{\boldsymbol{q}}=\boldsymbol{q}/q$ can be computed as

$$\sigma_{\hat{\boldsymbol{q}}}(z) = \lim_{q\to 0} \frac{iz\bar{\chi}(\boldsymbol{q},z)}{q^2}\,. \tag{4.5.1}$$

In Eq. (4.5.1), $\boldsymbol{q}$ is the momentum of the external scalar potential, and $\bar{\chi}$ is the macroscopic density-density response computed in the condition of null macroscopic electric field (this condition is indicated with a bar over the symbol representing the physical quantity, to be consistent with the notations introduced in Refs.[190–194]). In the small $\boldsymbol{q}$ regime considered in this Section, the null macroscopic field condition is imposed by removing the macroscopic component of the Coulomb kernel in the Hartree term of Eq. (4.1.17), $\bar{v}_{\boldsymbol{G}=0}(\boldsymbol{q})=0$, where $v_{\boldsymbol{G}}(\boldsymbol{q})$ is the Fourier transform of the Coulomb potential and $\boldsymbol{G}$ are the reciprocal lattice vectors.

In the following, we present the formulas for χ and $\bar{\chi}$ and we show the results for σ, which can be directly linked to an experimental measure, e.g. optical absorption.

4.5.1 Density-density response in periodic systems

The eigenstates of $\hat{H}^{(0)}$ are Bloch states $|\psi^{(0)}_{m\boldsymbol{k}}\rangle$ of quasimomentum $\boldsymbol{f}k$, normalized on the Born–von Karman supercell of volume $N\Omega$, containing N unit cells. If $V^{(b)}_{\text{ext}}(\boldsymbol{r})=V^{(\boldsymbol{q})}_{\text{ext}}(\boldsymbol{r})=e^{i\boldsymbol{q}\cdot\boldsymbol{r}}$, we can write $\hat{n}^{(\boldsymbol{q})}$ and $\hat{V}^{(\boldsymbol{q})}_{\text{scf}}$ in the basis of the unperturbed states as:

$$\langle\psi^{(0)}_{n\boldsymbol{k}'}|\hat{n}^{(\boldsymbol{q})}(z)|\psi^{(0)}_{m\boldsymbol{k}}\rangle=\delta_{\boldsymbol{k}',\boldsymbol{k}+\boldsymbol{q}}\langle\psi^{(0)}_{n\boldsymbol{k}+\boldsymbol{q}}|\hat{n}^{(\boldsymbol{q})}(z)|\psi^{(0)}_{m\boldsymbol{k}}\rangle, \tag{4.5.2}$$

$$\langle\psi^{(0)}_{n\boldsymbol{k}'}|\hat{V}^{(\boldsymbol{q})}_{\text{scf}}(z)|\psi^{(0)}_{m\boldsymbol{k}}\rangle=\delta_{\boldsymbol{k}',\boldsymbol{k}+\boldsymbol{q}}\langle\psi^{(0)}_{n\boldsymbol{k}+\boldsymbol{q}}|\hat{V}^{(\boldsymbol{q})}_{\text{scf}}(z)|\psi^{(0)}_{m\boldsymbol{k}}\rangle. \tag{4.5.3}$$

In this representation, Eqs. (4.1.19) and (4.1.20) express the relation between the nonzero matrix elements of $\hat{n}^{(\boldsymbol{q})}$ and $\hat{V}^{(\boldsymbol{q})}_{\text{scf}}$ as

$$2\langle\psi^{(0)}_{n\boldsymbol{k}+\boldsymbol{q}}|\hat{n}^{(\boldsymbol{q})}(z)|\psi^{(0)}_{m\boldsymbol{k}}\rangle = L^0_{n\boldsymbol{k}+\boldsymbol{q},m\boldsymbol{k}}(z)\langle\psi^{(0)}_{n\boldsymbol{k}+\boldsymbol{q}}|\hat{V}^{(\boldsymbol{q})}_{\text{scf}}(z)|\psi^{(0)}_{m\boldsymbol{k}}\rangle, \tag{4.5.4}$$

where

$$L^0_{n\boldsymbol{k}+\boldsymbol{q},m\boldsymbol{k}}(z) = 2\frac{f^{(0)}_{m\boldsymbol{k}} - f^{(0)}_{n\boldsymbol{k}+\boldsymbol{q}}}{\hbar z - (\varepsilon^{(0)}_{n\boldsymbol{k}+\boldsymbol{q}} - \varepsilon^{(0)}_{m\boldsymbol{k}})}. \tag{4.5.5}$$

Eqs. (4.1.15) and (4.1.17) become:

$$\langle\psi^{(0)}_{n\boldsymbol{k}+\boldsymbol{q}}|\hat{V}^{(\boldsymbol{q})}_{\text{scf}}(z)|\psi^{(0)}_{m\boldsymbol{k}}\rangle = \langle\psi^{(0)}_{n\boldsymbol{k}+\boldsymbol{q}}|\hat{V}^{(\boldsymbol{q})}_{\text{ext}}|\psi^{(0)}_{m\boldsymbol{k}}\rangle+\frac{1}{N}\sum_{\boldsymbol{k}'sl}K^{n\boldsymbol{k}+\boldsymbol{q},m\boldsymbol{k}}_{s\boldsymbol{k}'+\boldsymbol{q},l\boldsymbol{k}'}\langle\psi^{(0)}_{s\boldsymbol{k}'+\boldsymbol{q}}|\hat{n}^{(\boldsymbol{q})}(z)|\psi^{(0)}_{l\boldsymbol{k}'}\rangle, \tag{4.5.6}$$

where, in the BSE framework

$$\begin{aligned}K^{n\boldsymbol{k}+\boldsymbol{q},m\boldsymbol{k}}_{s\boldsymbol{k}'+\boldsymbol{q},l\boldsymbol{k}'} = N\int_{N\Omega}\mathrm{d}\boldsymbol{r}\,\Big[&\psi^{(0)}_{n\boldsymbol{k}+\boldsymbol{q}}(\boldsymbol{r})^*\psi^{(0)}_{m\boldsymbol{k}}(\boldsymbol{r})2v(\boldsymbol{r}-\boldsymbol{r}_1)\;\psi^{(0)}_{s\boldsymbol{k}'+\boldsymbol{q}}(\boldsymbol{r}_1)\psi^{(0)}_{l\boldsymbol{k}'}(\boldsymbol{r}_1)^*\\ &-\psi^{(0)}_{n\boldsymbol{k}+\boldsymbol{q}}(\boldsymbol{r})^*\psi^{(0)}_{m\boldsymbol{k}}(\boldsymbol{r}_1)\;W(\boldsymbol{r},\boldsymbol{r}_1)\psi^{(0)}_{s\boldsymbol{k}'+\boldsymbol{q}}(\boldsymbol{r})\psi^{(0)}_{l\boldsymbol{k}'}(\boldsymbol{r}_1)^*\Big],\end{aligned} \tag{4.5.7}$$

where, as usual, the integral over $\boldsymbol{r}$ runs over the N cells of the supercell and the implicit one over $\boldsymbol{r}_1$ on the full crystal.

Usually, the most difficult (i.e. the most computationally time consuming) quantities to be evaluated with accuracy are the self-consistent electronic density matrix and potential, since they need to be determined via the self-consistent set of Eqs. (4.5.4), (4.5.6). On the contrary, $L^0_{n\boldsymbol{k}+\boldsymbol{q},m\boldsymbol{k}}(z)$ has a very simple explicit form, that only requires the knowledge of energies and wavefunctions of the unperturbed Hamiltonian $\hat{H}^{(0)}$. In the evaluation of $\bar{\chi}$, it is convenient to use an approximated density matrix:

$$\langle\psi^{(0)}_{n\boldsymbol{k}+\boldsymbol{q}}|\hat{n}^{(\boldsymbol{q})}(z)|\psi^{(0)}_{m\boldsymbol{k}}\rangle_{\text{ap}}. \tag{4.5.8}$$

From this approximated density matrix, we define a corresponding approximated self-

consistent potential as:

$$\langle\psi^{(0)}_{n\boldsymbol{k}+\boldsymbol{q}}|\hat{V}^{(\boldsymbol{q})}_{\rm scf}(z)|\psi^{(0)}_{m\boldsymbol{k}}\rangle_{\rm ap}=\langle\psi^{(0)}_{n\boldsymbol{k}+\boldsymbol{q}}|\hat{V}^{(\boldsymbol{q})}_{\rm ext}|\psi^{(0)}_{m\boldsymbol{k}}\rangle+\frac{1}{N}\sum_{\boldsymbol{k}'sl}K^{n\boldsymbol{k}+\boldsymbol{q},m\boldsymbol{k}}_{s\boldsymbol{k}'+\boldsymbol{q},l\boldsymbol{k}'}\langle\psi^{(0)}_{s\boldsymbol{k}'+\boldsymbol{q}}|\hat{n}^{(\boldsymbol{q})}(z)|\psi^{(0)}_{l\boldsymbol{k}'}\rangle_{\rm ap}. \tag{4.5.9}$$

Notice that, in general, for the approximated quantities Eq. (4.5.4) does not hold.

Within the functional formulation defined in Section 4.2, we obtain the approximated expressions of χ by using Eqs. (4.2.3), (4.2.8), (4.2.14), where in place of λ and λ' we use the approximated density matrix (Eq. (4.5.8)), obtaining:

$$\chi^{\rm bs}_{\rm ap}(\boldsymbol{q},z)=\frac{1}{N}\sum_{\boldsymbol{k}nm}\langle\psi^{(0)}_{m\boldsymbol{k}}|\hat{V}^{(-\boldsymbol{q})}_{\rm ext}|\psi^{(0)}_{n\boldsymbol{k}+\boldsymbol{q}}\rangle L^0_{n\boldsymbol{k}+\boldsymbol{q},m\boldsymbol{k}}(z)\langle\psi^{(0)}_{n\boldsymbol{k}+\boldsymbol{q}}|\hat{V}^{(\boldsymbol{q})}_{\rm scf}(z)|\psi^{(0)}_{m\boldsymbol{k}}\rangle_{\rm ap}. \tag{4.5.10}$$

Instead, the screen-screen and the screen*-screen density-density response read

$$\begin{aligned}\chi^{\rm ss}_{\rm ap}(\boldsymbol{q},z) &= \frac{1}{N}\sum_{\boldsymbol{k}nm}\langle\psi^{(0)}_{m\boldsymbol{k}}|\hat{V}^{(-\boldsymbol{q})}_{\rm scf}(-z)|\psi^{(0)}_{n\boldsymbol{k}+\boldsymbol{q}}\rangle_{\rm ap}L^0_{n\boldsymbol{k}+\boldsymbol{q},m\boldsymbol{k}}(z)\langle\psi^{(0)}_{n\boldsymbol{k}+\boldsymbol{q}}|\hat{V}^{(\boldsymbol{q})}_{\rm scf}(z)|\psi^{(0)}_{m\boldsymbol{k}}\rangle_{\rm ap}\\ &\quad-\frac{2}{N^2}\sum_{\substack{\boldsymbol{k}nm\\ \boldsymbol{k}'ls}}\langle\psi^{(0)}_{m\boldsymbol{k}}|\hat{n}^{(-\boldsymbol{q})}(-z)|\psi^{(0)}_{n\boldsymbol{k}+\boldsymbol{q}}\rangle_{\rm ap}K^{n\boldsymbol{k}+\boldsymbol{q},m\boldsymbol{k}}_{s\boldsymbol{k}'+\boldsymbol{q},l\boldsymbol{k}'}\langle\psi^{(0)}_{s\boldsymbol{k}'+\boldsymbol{q}}|\hat{n}^{(\boldsymbol{q})}(z)|\psi^{(0)}_{l\boldsymbol{k}'}\rangle_{\rm ap},\end{aligned} \tag{4.5.11}$$

$$\begin{aligned}\chi^{\rm s^*s}_{\rm ap}(\boldsymbol{q},z) &= \frac{1}{N}\sum_{\boldsymbol{k}nm}\langle\psi^{(0)}_{m\boldsymbol{k}}|\hat{V}^{(-\boldsymbol{q})}_{\rm scf}(-z^*)|\psi^{(0)}_{n\boldsymbol{k}+\boldsymbol{q}}\rangle_{\rm ap}L^0_{n\boldsymbol{k}+\boldsymbol{q},m\boldsymbol{k}}(z)\langle\psi^{(0)}_{n\boldsymbol{k}+\boldsymbol{q}}|\hat{V}^{(\boldsymbol{q})}_{\rm scf}(z)|\psi^{(0)}_{m\boldsymbol{k}}\rangle_{\rm ap}\\ &\quad-\frac{2}{N^2}\sum_{\substack{\boldsymbol{k}nm\\ \boldsymbol{k}'ls}}\langle\psi^{(0)}_{m\boldsymbol{k}}|\hat{n}^{(-\boldsymbol{q})}(-z^*)|\psi^{(0)}_{n\boldsymbol{k}+\boldsymbol{q}}\rangle_{\rm ap}K^{n\boldsymbol{k}+\boldsymbol{q},m\boldsymbol{k}}_{s\boldsymbol{k}'+\boldsymbol{q},l\boldsymbol{k}'}\langle\psi^{(0)}_{s\boldsymbol{k}'+\boldsymbol{q}}|\hat{n}^{(\boldsymbol{q})}(z)|\psi^{(0)}_{l\boldsymbol{k}'}\rangle_{\rm ap}.\end{aligned} \tag{4.5.12}$$

Notice that in Eqs. (4.5.11),(4.5.12), the first matrix elements can be obtained from the relations:

$$\langle\psi^{(0)}_{m\boldsymbol{k}}|\hat{V}^{(-\boldsymbol{q})}_{\rm scf}(-z)|\psi^{(0)}_{n\boldsymbol{k}+\boldsymbol{q}}\rangle_{\rm ap}=\langle\psi^{(0)}_{n\boldsymbol{k}+\boldsymbol{q}}|\hat{V}^{(\boldsymbol{q})}_{\rm scf}(z^*)|\psi^{(0)}_{m\boldsymbol{k}}\rangle^*_{\rm ap}, \tag{4.5.13}$$

$$\langle\psi^{(0)}_{m\boldsymbol{k}}|\hat{V}^{(-\boldsymbol{q})}_{\rm scf}(-z^*)|\psi^{(0)}_{n\boldsymbol{k}+\boldsymbol{q}}\rangle_{\rm ap}=\langle\psi^{(0)}_{n\boldsymbol{k}+\boldsymbol{q}}|\hat{V}^{(\boldsymbol{q})}_{\rm scf}(z)|\psi^{(0)}_{m\boldsymbol{k}}\rangle^*_{\rm ap}, \tag{4.5.14}$$

and that analogous relations holds for the matrix elements of the density matrix.

If no approximation are used, the three formulations provide the exact result $\chi(\boldsymbol{q},z)$. Instead if $\langle\psi^{(0)}_{n\boldsymbol{k}+\boldsymbol{q}}|\hat{n}^{(\boldsymbol{q})}(z)|\psi^{(0)}_{m\boldsymbol{k}}\rangle_{\rm ap}\neq\langle\psi^{(0)}_{n\boldsymbol{k}+\boldsymbol{q}}|\hat{n}^{(\boldsymbol{q})}(z)|\psi^{(0)}_{m\boldsymbol{k}}\rangle$, the three formulation will provide three distinct estimations of $\chi(\boldsymbol{q},z)$. Since the screen-screen formulation is variational with respect to the density matrix [Eq. (4.2.11)], while the bare-screen and screen*-screen formulations are not [Eqs. (4.2.4) and (4.2.15)], we have that:

$$\chi^{\rm bs}_{\rm ap}(\boldsymbol{q},z)-\chi(\boldsymbol{q},z)=O\left(\hat{n}^{(\boldsymbol{q})}_{\rm ap}(z)-\hat{n}^{(\boldsymbol{q})}(z)\right), \tag{4.5.15}$$

$$\chi^{\rm ss}_{\rm ap}(\boldsymbol{q},z)-\chi(\boldsymbol{q},z)=O\left(\left(\hat{n}^{(\boldsymbol{q})}_{\rm ap}(z)-\hat{n}^{(\boldsymbol{q})}(z)\right)^2\right), \tag{4.5.16}$$

$$\chi^{\rm s^*s}_{\rm ap}(\boldsymbol{q},z)-\chi(\boldsymbol{q},z)=O\left(\hat{n}^{(\boldsymbol{q})}_{\rm ap}(z)-\hat{n}^{(\boldsymbol{q})}(z)\right). \tag{4.5.17}$$

Namely, for small deviations of the approximated density matrix from the exact one, the screen-screen formulation provides the best estimation of the exact values, as we demonstrate numerically in the next Sections.

4.5.2 Electron-electron interaction in the density density response of graphene

To account for the effects of the electron-electron interaction in the response of graphene, we follow the approach thoroughly described in Ref. 190. We include the interaction in $\hat{H}^{(0)}$ by the static-screened exchange approximation, and in the density-density response by solving the BSE for $\bar{\chi}(\boldsymbol{q}, z)$, with $\hbar z{=}\hbar\omega{+}i\eta$. In both calculations, we use the same static $W(\boldsymbol{r}, \boldsymbol{r}')$. We work within the π-orbitals subspace using a tight-binding model. We obtain the optical conductivity $\sigma(z)$ from Eq. (4.5.1) using a finite but small value of $|\boldsymbol{q}|$. Due to the symmetries of graphene, the conductivity is independent of the direction $\hat{\boldsymbol{q}}$ and we can drop from σ such subscript. To obtain the required $\bar{\chi}(\boldsymbol{q}, z)$, we eliminate the long-range component of the Hartree kernel. This is done replacing in all the Eqs. of the previous subsection $K^{n\boldsymbol{k}+\boldsymbol{q},m\boldsymbol{k}}_{s\boldsymbol{k}'+\boldsymbol{q},l\boldsymbol{k}'}$ by $\bar{K}^{n\boldsymbol{k}+\boldsymbol{q},m\boldsymbol{k}}_{s\boldsymbol{k}'+\boldsymbol{q},l\boldsymbol{k}'}$, as detailed in Appendix 4.B.

In the present work, the self-consistent system of Eqs. (4.5.4) and (4.5.6) is solved using an iterative procedure. Namely, we call $\langle\psi^{(0)}_{n\boldsymbol{k}+\boldsymbol{q}}|\hat{n}^{(\boldsymbol{q})}(z)|\psi^{(0)}_{m\boldsymbol{k}}\rangle_\tau$ the density matrix at the iteration τ. By inserting this density matrix in Eq. (4.5.6) together with $\bar{K}^{n\boldsymbol{k}+\boldsymbol{q},m\boldsymbol{k}}_{s\boldsymbol{k}'+\boldsymbol{q},l\boldsymbol{k}'}$, we obtain the self-consistent potential $\langle\psi^{(0)}_{n\boldsymbol{k}+\boldsymbol{q}}|\hat{V}^{(\boldsymbol{q})}_{\text{scf}}(z)|\psi^{(0)}_{m\boldsymbol{k}}\rangle_\tau$ at the same iteration τ. At the first iteration ($\tau{=}0$), we use:

$$2\langle\psi^{(0)}_{n\boldsymbol{k}+\boldsymbol{q}}|\hat{n}^{(\boldsymbol{q})}(z)|\psi^{(0)}_{m\boldsymbol{k}}\rangle_0 = L^0_{n\boldsymbol{k}+\boldsymbol{q},m\boldsymbol{k}}(z)\langle\psi^{(0)}_{n\boldsymbol{k}+\boldsymbol{q}}|\hat{V}^{(\boldsymbol{q})}_{\text{ext}}|\psi^{(0)}_{m\boldsymbol{k}}\rangle. \tag{4.5.18}$$

The density matrix at the iteration $\tau{+}1$ is obtained by summing the density matrix at the step τ, with a weight $(1{-}x)$, with that obtained inserting the self-consistent potential at the iteration τ in Eq. (4.5.4), with a weight x. Typical values of $x{\simeq}0.2$ assures the convergence of the iterative solution to its fixed point. In Appendix 4.B, we summarize other details of the calculation.

In Fig. 4.1, we show the remarkable agreement between the measured optical conductivity and that predicted by our BSE approach, for $\hbar\omega{<}5.5$ eV. The measured rise for $\hbar\omega{>}7$ eV and the plateau between 5.5 and 7 eV are missing in the theoretical results, since they are associated to transitions involving σ-bands, neglected in our approach. In Fig. 4.1, we also show the large impact of the excitonic interaction, i.e. the ladder corrections with W (cf. Table 4.1). Indeed, if we neglect the screening of the vertices, by setting to zero $\bar{K}^{n\boldsymbol{k}+\boldsymbol{q},m\boldsymbol{k}}_{s\boldsymbol{k}'+\boldsymbol{q},l\boldsymbol{k}'}$ in the calculation, we overestimate the position of the $\pi{-}\pi^*$ plasmon peak (at $\sim$4.6 eV in experiments). Moreover, we do not reproduce the expected asymmetric shape of the peak, as proven in Refs.[94,95]

4.5.3 Exploiting variationality

In the following, we consider two exemplary kinds of errors in the evaluation of the electronic density matrix. The first example regards the error that naturally arises when performing the self-consistent cycle described in Sec. 4.5.2 in terms of τ. The second instead regards the case where the exact electronic density matrix vertex is computed for some given frequency $\omega{=}\omega_0$, and then such density matrix is used as an approximation to determine the response function across the entire frequency range.

Convergence of the optical conductivity within the iterative approach

We investigate the convergence of the electronic density matrix within the iteration cycle described in Sec. 4.5.2. Referring to the notation of the previous section, we now perform

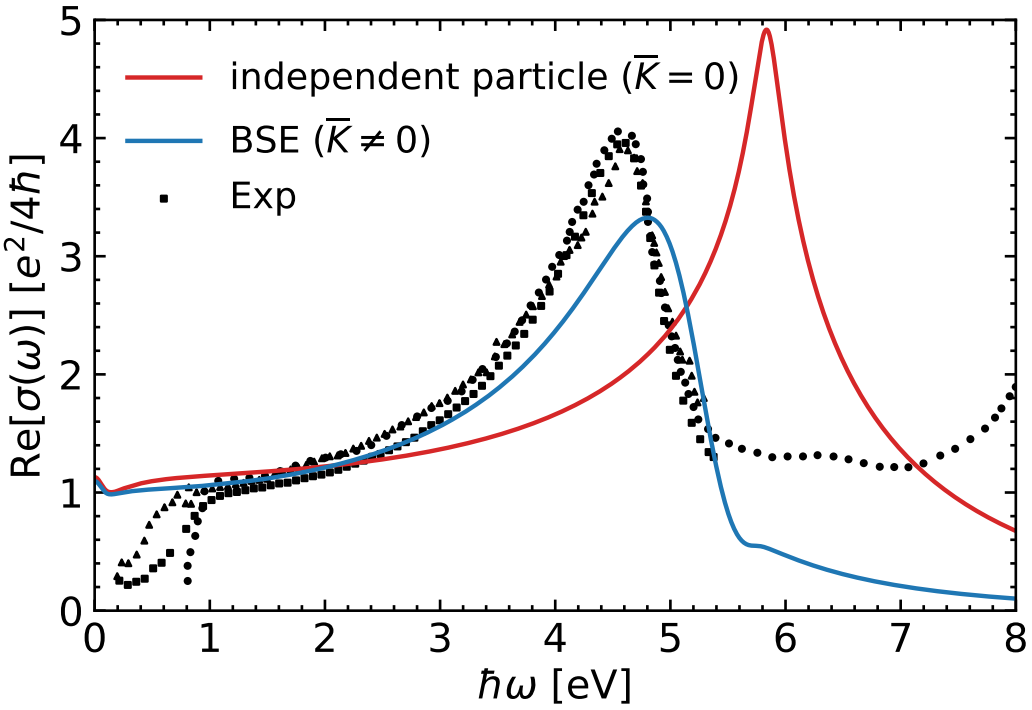

Figure 4.1. Optical conductivity of freestanding graphene obtained with the independent particle approximation (red), i.e. by setting the kernel $\bar{K} = 0$, and by solving the BSE (blue), compared within experimental results (black symbols). Black triangles, squares and dots are experimental data obtained from Refs. 195, 196 and 197 respectively.

the following identification

$$\langle\psi^{(0)}_{n\boldsymbol{k}+\boldsymbol{q}}|\hat{n}^{(\boldsymbol{q})}(z)|\psi^{(0)}_{m\boldsymbol{k}}\rangle_{\text{ap}} = \langle\psi^{(0)}_{n\boldsymbol{k}+\boldsymbol{q}}|\hat{n}^{(\boldsymbol{q})}(z)|\psi^{(0)}_{m\boldsymbol{k}}\rangle_{\tau}, \tag{4.5.19}$$

and the same for all the other quantities for which 'ap'→'τ'.

It is clear that the scaling properties of $\bar{\chi}(z)$ with respect to the density are reflected on $\sigma(z)$ via Eq. (4.5.1). Henceforth, we now show numerical results proving Eqs. (4.5.15), (4.5.16) and (4.5.17), but studying the optical conductivity. We introduce the counterparts of the density-density responses obtained via Eq. (4.5.1) as $\sigma^{\text{bs}}_{\tau}(z)$, $\sigma^{\text{ss}}_{\tau}(z)$ and $\sigma^{\text{s*s}}_{\tau}(z)$, with obvious meaning of the symbols. We verified numerically that:

$$\sigma^{\text{bs}}_{\infty}(z) = \sigma^{\text{ss}}_{\infty}(z) = \sigma^{\text{s*s}}_{\infty}(z) = \sigma(z). \tag{4.5.20}$$

For each formulation, we report the values of the error as a function of the iteration step in Fig. 4.2, for the frequency $\hbar\omega$=4.8 eV. In the semi-logarithmic scale of Fig. 4.2, all the formulations converge linearly with respect to the iterations number, meaning that $\sigma_{\tau}(z)$ converges exponentially with the number of iterations τ. Also, we notice that in semi-logarithmic scale $\sigma^{\text{ss}}_{\tau}$ converges twice as fast with respect to both $\sigma^{\text{bs}}_{\tau}$ and $\sigma^{\text{s*s}}_{\tau}$, confirming the advantageous variational property of the screen-screen formulation.

Fixed frequency approximation of optical conductivity

In this section we treat the case where the (numerically) exact electronic density matrices known for some given frequency ω_0 (namely, for z_0=ω_0+$i\eta$ and z_0^*=ω_0−$i\eta$) and then used to

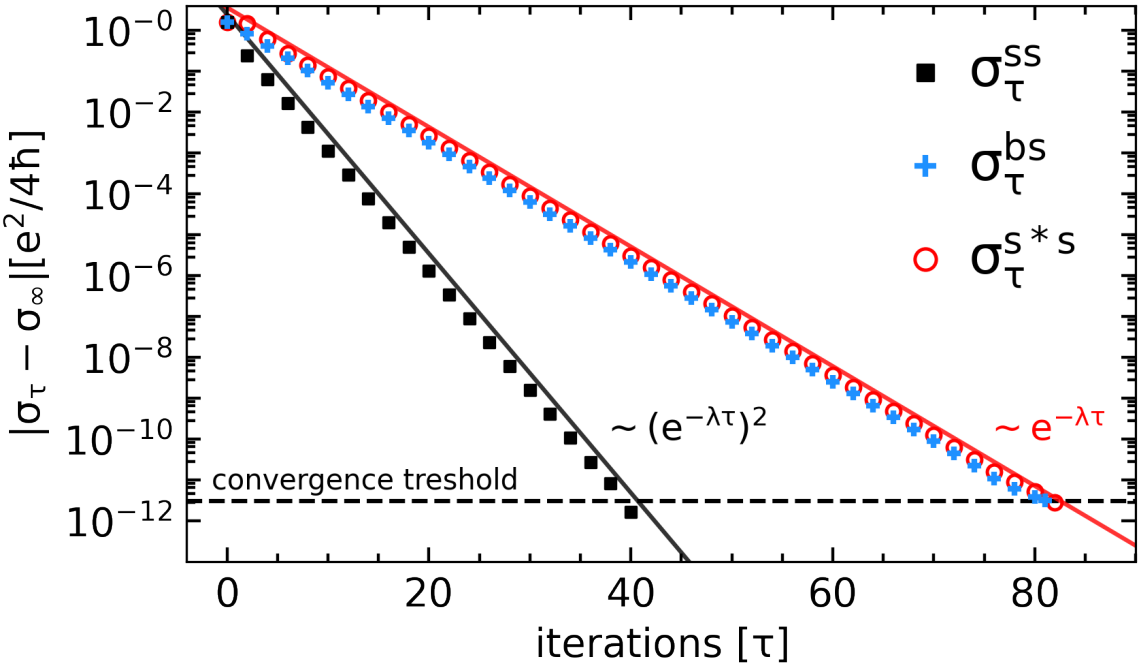

Figure 4.2. Convergence behavior of the conductivity $\sigma(z)$ at ($\hbar\omega$=4.8 eV, $\hbar\eta$=0.1 eV) as a function of the iteration step τ of the self-consistent scheme explained in Sec. 4.5.2, for the three different formulations described in Sec. 4.2 (screen-screen in red, bare-screen in blue, screen*-screen in green). Scatter points indicate the error $|\sigma_\tau - \sigma_\infty|$. The cycle is terminated when $|\sigma_\tau - \sigma_\infty|$ is below a given convergence threshold (black dashed line). Lines indicate linear fits of the convergence trend, that in semi-log scale indicate exponential convergence. The screen-screen response convergences twice as fast with respect to the other formulations, thus proving the variationality of the screen-screen formulation.

determine the response function across the entire frequency range. Such an approximation clearly comes with great numerical advantage, in terms of time saved avoiding repeating the self consistent routine for every frequency. This is often the case of phonon calculations, where the electron-phonon vertexes are known only in the static case ($z_0 = z_0^* = 0$).

In this case, we pose:

$$\langle \psi^{(0)}_{n\boldsymbol{k}+\boldsymbol{q}} | \hat{n}^{(\boldsymbol{q})}(z) | \psi^{(0)}_{m\boldsymbol{k}} \rangle_{\text{ap}} = \langle \psi^{(0)}_{n\boldsymbol{k}+\boldsymbol{q}} | \hat{n}^{(\boldsymbol{q})}(z_0) | \psi^{(0)}_{m\boldsymbol{k}} \rangle, \tag{4.5.21}$$

$$\langle \psi^{(0)}_{n\boldsymbol{k}+\boldsymbol{q}} | \hat{V}^{(\boldsymbol{q})}_{\text{scf}}(z) | \psi^{(0)}_{m\boldsymbol{k}} \rangle_{\text{ap}} = \langle \psi^{(0)}_{n\boldsymbol{k}+\boldsymbol{q}} | \hat{V}^{(\boldsymbol{q})}_{\text{scf}}(z_0) | \psi^{(0)}_{m\boldsymbol{k}} \rangle \tag{4.5.22}$$

and similarly for all the z^* quantities. Using the definitions in Eqs. (4.5.21) and (4.5.22), we get

$$\bar{\chi}^{\text{bs}}_{\text{ap}}(\boldsymbol{q}, z_0) = \bar{\chi}^{\text{ss}}_{\text{ap}}(\boldsymbol{q}, z_0) = \bar{\chi}^{\text{s*s}}_{\text{ap}}(\boldsymbol{q}, z_0) = \bar{\chi}(\boldsymbol{q}, z_0) \tag{4.5.23}$$

and the second summations in Eqs. (4.5.11) and (4.5.12) do not depend anymore on z.

Therefore, we obtain that: widetext

$$\bar{\chi}^{\mathrm{bs}}_{z_0}(\boldsymbol{q},z) = \bar{\chi}(\boldsymbol{q},z_0) + \frac{1}{N}\sum_{\boldsymbol{k}nm} \langle\psi^{(0)}_{m\boldsymbol{k}}|\hat{V}^{(-\boldsymbol{q})}_{\mathrm{ext}}|\psi^{(0)}_{n\boldsymbol{k}+\boldsymbol{q}}\rangle \Delta L^0_{n\boldsymbol{k}+\boldsymbol{q},m\boldsymbol{k}}(z,z_0)\langle\psi^{(0)}_{n\boldsymbol{k}+\boldsymbol{q}}|\hat{V}^{(\boldsymbol{q})}_{\mathrm{scf}}(z_0)|\psi^{(0)}_{m\boldsymbol{k}}\rangle, \tag{4.5.24}$$

$$\bar{\chi}^{\mathrm{ss}}_{z_0}(\boldsymbol{q},z) = \bar{\chi}(\boldsymbol{q},z_0) + \frac{1}{N}\sum_{\boldsymbol{k}nm} \langle\psi^{(0)}_{m\boldsymbol{k}}|\hat{V}^{(-\boldsymbol{q})}_{\mathrm{scf}}(-z_0)|\psi^{(0)}_{n\boldsymbol{k}+\boldsymbol{q}}\rangle \Delta L^0_{n\boldsymbol{k}+\boldsymbol{q},m\boldsymbol{k}}(z,z_0)\langle\psi^{(0)}_{n\boldsymbol{k}+\boldsymbol{q}}|\hat{V}^{(\boldsymbol{q})}_{\mathrm{scf}}(z_0)|\psi^{(0)}_{m\boldsymbol{k}}\rangle, \tag{4.5.25}$$

$$\bar{\chi}^{\mathrm{s^*s}}_{z_0}(\boldsymbol{q},z) = \bar{\chi}(\boldsymbol{q},z_0) + \frac{1}{N}\sum_{\boldsymbol{k}nm} \langle\psi^{(0)}_{m\boldsymbol{k}}|\hat{V}^{(-\boldsymbol{q})}_{\mathrm{scf}}(-z_0^*)|\psi^{(0)}_{n\boldsymbol{k}+\boldsymbol{q}}\rangle \Delta L^0_{n\boldsymbol{k}+\boldsymbol{q},m\boldsymbol{k}}(z,z_0)\langle\psi^{(0)}_{n\boldsymbol{k}+\boldsymbol{q}}|\hat{V}^{(\boldsymbol{q})}_{\mathrm{scf}}(z_0)|\psi^{(0)}_{m\boldsymbol{k}}\rangle, \tag{4.5.26}$$

where, for notation clarity, we replaced the "ap" subscript in the approximated $\bar{\chi}$ with "z_0" and

$$\Delta L^0_{n\boldsymbol{k}+\boldsymbol{q},m\boldsymbol{k}}(z,z_0) = L^0_{n\boldsymbol{k}+\boldsymbol{q},m\boldsymbol{k}}(z) - L^0_{n\boldsymbol{k}+\boldsymbol{q},m\boldsymbol{k}}(z_0). \tag{4.5.27}$$

Due to the different variational properties of the three approaches, the error of the screen-screen formulation is predicted to be the smallest for z close to z_0, and:

$$\bar{\chi}^{\mathrm{bs}}_{z_0}(\boldsymbol{q},z) - \bar{\chi}(\boldsymbol{q},z) = O\left(z-z_0\right), \tag{4.5.28}$$

$$\bar{\chi}^{\mathrm{ss}}_{z_0}(\boldsymbol{q},z) - \bar{\chi}(\boldsymbol{q},z) = O\left((z-z_0)^2\right), \tag{4.5.29}$$

$$\bar{\chi}^{\mathrm{s^*s}}_{z_0}(\boldsymbol{q},z) - \bar{\chi}(\boldsymbol{q},z) = O\left(z-z_0\right). \tag{4.5.30}$$

In particular, Eq. (4.5.29), assures that $\bar{\chi}^{\mathrm{ss}}_{z_0}(\boldsymbol{q},z)$ and $\bar{\chi}(\boldsymbol{q},z)$ are tangent to each other in z_0:

$$\frac{\partial\bar{\chi}^{\mathrm{ss}}_{z_0}(\boldsymbol{q},z_0)}{\partial z} = \frac{\partial\bar{\chi}(\boldsymbol{q},z_0)}{\partial z} \tag{4.5.31}$$

Interestingly, by Eq. (4.5.25), we reformulate the response as that of an effective noninteracting electronic system (with, eventually, complex matrix elements). Such formulation does not require the expensive evaluation of the double-counting correction term, that involves a double summation (see second line of Eq. (4.5.11)). Moreover, the fixed-frequency vertices are suitable for fast Wannier-function[198,199] or other matrix-element interpolation schemes even in the present BSE approach. Finally, the presence of the differential operator ΔL^0 localizes the contributions of interband transitions around the resonances with z and z_0. This allows the restriction of the calculation to a limited number of bands near the Fermi-level, namely, to a low-energy model of the system.

We now discuss the numerical results. Let us call $\sigma^{\mathrm{bs}}_{z_0}(z)$, $\sigma^{\mathrm{ss}}_{z_0}(z)$ and $\sigma^{\mathrm{s^*s}}_{z_0}(z)$ the optical conductivity obtained with approximated vertices at $z{=}z_0$. Here, the aim is to compare numerically these three approximated expressions with respect to the exact $\sigma(z)$. Therefore, we select four representative frequency values $\hbar\omega_0{=}\{0.25, 4.3, 4.80, 5.20\}$ eV, and represent the three different approximated conductivities in Fig. 4.3(a)-(b)-(c)-(d) respectively. The numerical results confirm the validity of Eq. (4.5.31). This is most evident in Fig. 4.3(c) and (d). All the three formulations have the same value at the reference frequency, but only $\sigma^{\mathrm{ss}}_{z_0}(z)$ is tangent to the exact calculation. In Fig. 4.3(c), $\hbar\omega_0$ coincides with the maximum of reflectivity and the screen-screen approximation is in good agreement with the self-consistent calculation in frequency range of order $\simeq$100 meV. In Fig. 4.3(a)-(b)-(d) instead, $\sigma^{\mathrm{ss}}_{z_0}(z)$ is in remarkable good agreement with $\sigma(z)$ for a much wider range of frequencies, of order of some

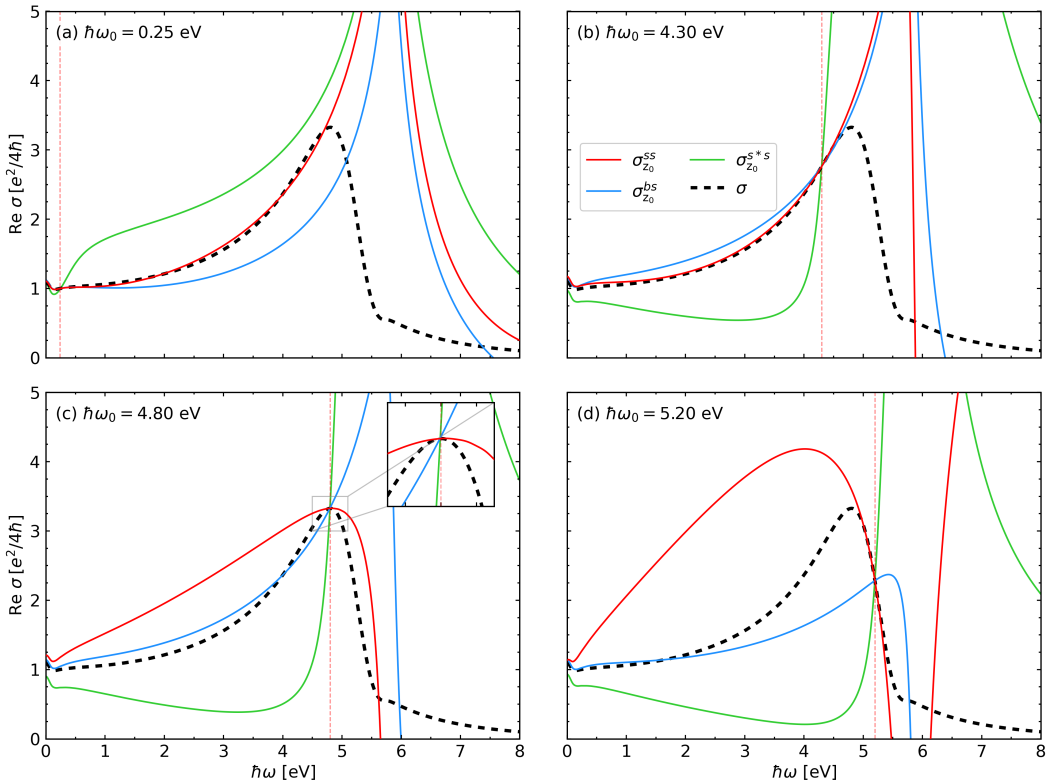

Figure 4.3. Fixed frequency approximation of the optical conductivity of graphene. The exact reference $\sigma(z)$ is indicated by black dashed line. The screen-screen, bare-screen, screen*-screen approximated conductivities $\sigma_{z_0}(z)$ (red, blue and green respectively) are obtained using Eqs. (4.5.24), (4.5.25), and (4.5.26), where the screened vertexes are computed at a fixed reference value of $z_0{=}\omega_0{+}i\eta$. In each panel we indicate the $\hbar\omega_0$ in digits and by a vertical orange dashed lines. The screen-screen conductivity is always tangent to the exact one in $\hbar\omega_0$, in contrast to the other approximated conductivities. Moreover, in all cases, but the one of panel (c), where $\hbar\omega_0$ coincides with the peak, the screen-screen conductivity closely follows the exact one on a wide range of energies.

eV, while $\sigma^{\mathrm{bs}}_{z_0}(z)$ and $\sigma^{\mathrm{s^*s}}_{z_0}(z)$ perform much worse. We associate the good agreement with the full self-consistent calculation of the screen-screen approximation in Fig. 4.3(a) with the fact that the selected frequency lies in a range where the conductivity is sufficiently far from both the Drude and the plasmon peak. Thus, where the conductivity is sufficiently flat, the screen-screen approximation works well since it posses exact first order derivative by construction. Such consistency showcases the possibility of employing the screen-screen approximation to obtain precise calculations for a fraction of the computational cost. Moreover, the fixed frequency approximation could be extended approximating the density matrix on a "coarse-grid" in frequency space. By repeating the self-consistent calculation only in a small set of frequencies, different trends of the conductivity pertaining to different part of the optical spectrum can be captured. In this way, the fully self-consistent the optical conductivity can be reconstructed more precisely by "patching up" few fixed-frequency approximations.

4.6 Conclusions

In the context of systems that can be described via a generalized Kohn-Sham equation, we have introduced three equivalent formulations for any electronic dynamical response function, referred to as bare-screen, screen-screen, and screen*-screen. We have shown that

all the three rewritings of the response function can be expressed as values of appropriate functionals of the one-body electronic density matrix, but only the screen-screen response represents a stationary point of its functional. This implies that the error in the screen-screen response function is quadratic with respect to the error in the density matrix, while the bare-screen and screen*-screen formulations are instead linear. The variational character of the screen-screen response function is the central result of this chapter. It extends the findings of Ref. 70 obtained for nonadiabatic phonons within TD-DFT to any type of response function to incorporate the effect of nonlocal exchange-correlation effects. The screen*-screen formulation also holds considerable physical significance, as we show that its imaginary part can be interpreted as a generalized Fermi Golden Rule. Moreover, we have showed how the variational screen-screen formulation can be extended by including part of the interaction to the partially screened vertices and the rest to a partially interacting electron-hole propagator. The partial screen-partial screen reformulation of the response function so obtained can be advantageous to evaluate the BSE corrections to the phonon self-energy on top of a standard static phonon calculation, as we will show in Ref. 188. Even if all our derivations were carried out neglecting memory effects in the electronic interaction, we have showed that such an assumption can be relaxed and our results can be generalized including memory effects in the Hartree-exchange correlation part of the kernel.

We validated our findings using a tight-binding model of graphene within the SX approximation of the electronic interaction. To provide numerical evidence of variationality, we studied the convergence trends of the optical conductivity $\sigma(\omega)$ within a self-consistent iterative procedure. The different formulations of the response function exhibit distinct convergence behaviors. In particular, the screen-screen response decays quadratically with the distance from the converged solution for the density matrix, while the bare-screen and the screen*-screen formulations converge only linearly. The variationality of the screen-screen response function can also be used to perform approximate calculations more efficiently. To demonstrate such capabilities, we have devised a fixed-frequency approximation of the density matrix and applied it to compute the optical conductivity of graphene. Such an approximation consists in determining the density matrix self-consistently at a specific frequency ω_0, and then use it for all other frequencies, avoiding the costly self-consistent routine at all frequencies. Our results show that the screen-screen approximation is the closest to the full self-consistent calculation among the formulations considered, and it is the only one that matches the first order derivative of the optical conductivity at ω_0, consistently with its variational nature. The quality of the approximation in a wider neighborhood of ω_0 depends on the form of the function near the reference frequency: where the optical conductivity is quite flat, we find remarkable agreement in an interval of frequency of the order of several eV; where it is more peaked, the approximation is valid in a smaller neighborhood, of the order of $\simeq$100 meV. In contrast, the quality of the bare-screen and screen*-screen approximations rapidly deteriorates with the distance from ω_0.

The core value of the results obtained with the fixed frequency approximation reside in the fundamental proof of concept of the variationality of the screen-screen formulation rather than an appealing cheap numerical implementation. However, the variational formulation of the response function opens the door to more advanced approximations that could significantly reduce computational costs when applied in other contexts. For instance, it could be used to compute the response function using a density matrix approximated at a high electronic temperature or on a coarse k-grid.[70] The latter is among the main bottlenecks for BSE approaches, and our method could result in a drastic speedup in the calculations.

Appendices of Chapter 4

4.A Derivation of the induced density in time-dependent linear response

In this Appendix, we derive the expression of the induced density Eq. (4.1.14) in terms of the bare electron-hole propagator L^0 from linear response theory. At linear order in the external field, the time-dependent generalized Kohn-Sham equation [Eq. (4.1.1)] can be recast in a Liouville equation for the induced density matrix $\hat{n}^{(1)}$[75]

$$i\hbar\frac{\partial}{\partial t}\hat{n}^{(1)}(t) = [\hat{H}^{(0)}, \hat{n}^{(1)}(t)] + [\hat{V}^{(1)}_{\text{scf}}(t), \hat{n}^{(0)}] \tag{4.A.1}$$

where $\hat{H}^{(0)}$ is the Hamiltonian in absence of the external field and $\hat{n}^{(0)}$ reads

$$\hat{n}^{(0)} = \sum_i f_i^{(0)} |\psi_i^{(0)}\rangle\langle\psi_i^{(0)}| \tag{4.A.2}$$

By using the evolution in the interaction picture

$$\hat{\tilde{O}}(t) = e^{\frac{i}{\hbar}\hat{H}^{(0)}t} O(t) e^{-\frac{i}{\hbar}\hat{H}^{(0)}t}, \tag{4.A.3}$$

Eq. (4.A.1) can be recast as

$$i\hbar\frac{\partial}{\partial t}\hat{\tilde{n}}^{(1)}(t) = [\hat{\tilde{V}}^{(1)}_{\text{scf}}(t), \hat{\tilde{n}}^{(0)}], \tag{4.A.4}$$

where $\hat{n}^{(0)}{=}\hat{\tilde{n}}^{(0)}$. We can evaluate the right-hand side of Eq. (4.A.4) using Eq. (4.A.2) as

$$[\hat{\tilde{V}}^{(1)}_{\text{scf}}(t), \hat{\tilde{n}}^{(0)}] = \sum_{ij} e^{i\omega_{ij}t}(f_j^{(0)} - f_i^{(0)})\langle\psi_i^{(0)}|\hat{V}^{(1)}_{\text{scf}}(t)|\psi_j^{(0)}\rangle|\psi_i^{(0)}\rangle\langle\psi_j^{(0)}| \tag{4.A.5}$$

where $\omega_{ij} = (\epsilon_i^{(0)} - \epsilon_j^{(0)})/\hbar$.

We integrate Eq. (4.A.4) in time from $-\infty$ to t, considering that $\hat{V}^{(1)}_{\text{scf}}(t){=}0$, for $t{<}t_0$, where t_0 is the starting time of the perturbation, and we obtain

$$\hat{n}^{(1)}(t){=}\frac{1}{i\hbar}e^{-\frac{i}{\hbar}\hat{H}^{(0)}t}\int_{-\infty}^{t}\mathrm{d}t'\,[\hat{\tilde{V}}^{(1)}_{\text{scf}}(t'), \hat{\tilde{n}}^{(0)}]e^{\frac{i}{\hbar}\hat{H}^{(0)}t}. \tag{4.A.6}$$

Using Eq. (4.A.5) and taking the Fourier transform as in (4.1.11), we have from (4.A.6)

$$\begin{aligned}\hat{n}^{(1)}(z) \;=\; & \sum_{ij}\frac{f_j^{(0)}-f_i^{(0)}}{i\hbar}|\psi_i^{(0)}\rangle\langle\psi_j^{(0)}|\int_{-\infty}^{\infty}\mathrm{d}t\, e^{i(z-\omega_{ij})t} \\ & \times\int_{-\infty}^{t}\mathrm{d}t'\, e^{i\omega_{ij}t'}\langle\psi_i^{(0)}|\hat{V}^{(1)}_{\text{scf}}(t')|\psi_j^{(0)}\rangle.\end{aligned} \tag{4.A.7}$$

The integral in t in Eq. (4.A.7) can be solved integrating by parts, obtaining:

$$\hat{n}^{(1)}(z) = \sum_{ij}\frac{f_j^{(0)}-f_i^{(0)}}{i\hbar}|\psi_i^{(0)}\rangle\langle\psi_j^{(0)}|\int_{-\infty}^{\infty}\mathrm{d}t\,\frac{ie^{i(z-\omega_{ij})t}}{(z-\omega_{ij})}e^{i\omega_{ij}t}\langle\psi_i^{(0)}|\hat{V}^{(1)}_{\text{scf}}(t)|\psi_j^{(0)}\rangle.$$

In fact, the lower extremal value of the primitive is 0 since $V_{\rm scf}(t)=0$ for $t<t_0$, while the upper one is zero since for retarded quantities it holds $\mathrm{Im}z>0$. From Eq. (4.A.8) it follows

$$\hat{n}^{(1)}(z)=\sum_{ij}\frac{(f_j^{(0)}-f_i^{(0)})|\psi_i^{(0)}\rangle\langle\psi_j^{(0)}|\langle\psi_i^{(0)}|\hat{V}_{\rm scf}^{(1)}(z)|\psi_j^{(0)}\rangle}{\hbar z-(\epsilon_i^{(0)}-\epsilon_j^{(0)})}. \tag{4.A.8}$$

Considering the matrix elements in Schrodinger representation of Eq. (4.A.8) with the identification $(1)\to(b)$, we obtain Eqs. (4.1.19) and (4.1.20).

4.B Details of numerical implementation on tight-binding model of graphene

In this Appendix, we give some details about the numerical implementation of the density-density response functions described in Sec. 4.5. We have employed a tight-binding model of graphene, thoroughly described in Ref. 190.

By Fourier transforming v and W in Eq. (4.5.7), and exploiting the symmetries of the crystal, we evaluated the interaction kernel as

$$\begin{aligned}K^{n\boldsymbol{k}+\boldsymbol{q},m\boldsymbol{k}}_{s\boldsymbol{k}'+\boldsymbol{q},l\boldsymbol{k}'}&=\frac{2}{A}\sum_{\boldsymbol{G}}\langle\psi^{(0)}_{n\boldsymbol{k}+\boldsymbol{q}}|e^{i(\boldsymbol{q}+\boldsymbol{G})\cdot\boldsymbol{r}}|\psi^{(0)}_{m\boldsymbol{k}}\rangle v^{\rm 2D}_{\boldsymbol{G}}(\boldsymbol{q})\langle\psi^{(0)}_{l\boldsymbol{k}'}|e^{-i(\boldsymbol{q}+\boldsymbol{G})\cdot\boldsymbol{r}'}|\psi^{(0)}_{s\boldsymbol{k}'+\boldsymbol{q}}\rangle\\&-\frac{1}{A}\sum_{\boldsymbol{G}\boldsymbol{G}'}\langle\psi^{(0)}_{n\boldsymbol{k}+\boldsymbol{q}}|e^{i(\boldsymbol{k}-\boldsymbol{k}'+\boldsymbol{G})\cdot\boldsymbol{r}}|\psi^{(0)}_{s\boldsymbol{k}'+\boldsymbol{q}}\rangle W^{\rm 2D}_{\boldsymbol{G}\boldsymbol{G}'}(\boldsymbol{k}-\boldsymbol{k}')\langle\psi^{(0)}_{l\boldsymbol{k}'}|e^{-i(\boldsymbol{k}-\boldsymbol{k}'+\boldsymbol{G}')\cdot\boldsymbol{r}'}|\psi^{(0)}_{m\boldsymbol{k}}\rangle\ ,\end{aligned} \tag{4.B.1}$$

where A is the area of graphene unit cell and $\{\boldsymbol{G}\}$ are graphene reciprocal lattice vectors. For graphene, the vectors $\boldsymbol{q}$, $\boldsymbol{k}$, $\boldsymbol{k}'$, $\boldsymbol{G}$ lie in the (x,y) plane. The matrix elements are calculated with a tight-binding model, while $v^{\rm 2D}$ and $W^{\rm 2D}$ are effective 2D bare and screened Coulomb interactions. Within the rectangular orbital approximation, the z dependence of the single particle states ψ is approximated as

$$\psi_{n\boldsymbol{k}}(\boldsymbol{r}_\parallel,z)\approx\psi_{n\boldsymbol{k}}(\boldsymbol{r}_\parallel)\frac{\Theta(|z|-d/2)}{\sqrt{d}} \tag{4.B.2}$$

where $\boldsymbol{r}_\parallel=(x,y)$, d is graphene thickness and Θ is the Heaviside function. Such kind of approximations, where the orbital shape is simplified, are usually accurate for response functions where $|\boldsymbol{q}|d\ll 1$, as our case. Within the rectangular orbital approximation, the effective 2D bare interaction can be written as

$$\begin{aligned}v^{\rm 2D}_{\boldsymbol{G}}(\boldsymbol{q})&=\frac{1}{d^2}\int_{-d/2}^{d/2}\mathrm{d}z\int_{-d/2}^{d/2}\mathrm{d}z'\int d(\boldsymbol{r}_\parallel-\boldsymbol{r}'_\parallel)\frac{e^{-i(\boldsymbol{q}+\boldsymbol{G})\cdot(\boldsymbol{r}_\parallel-\boldsymbol{r}'_\parallel)}}{\varepsilon_r\sqrt{(z-z')^2+(\boldsymbol{r}_\parallel-\boldsymbol{r}'_\parallel)^2}}\\&=\frac{2\pi}{\varepsilon_r|\boldsymbol{q}+\boldsymbol{G}|}F(|\boldsymbol{q}+\boldsymbol{G}|d)\ ,\end{aligned} \tag{4.B.3}$$

where ε_r is the relative dielectric constant of an eventual uniform background and

$$F(x)=\frac{2}{x}\left(1+\frac{e^{-x}-1}{x}\right)\ . \tag{4.B.4}$$

The screened 2D effective Coulomb interaction can be written as

$$W^{\mathrm{2D}}_{\boldsymbol{G}\boldsymbol{G}'}(\boldsymbol{q}) = \frac{1}{d^2}\int_{-d/2}^{d/2}\mathrm{d}z\int_{-d/2}^{d/2}\mathrm{d}z'\int d\boldsymbol{r}_\parallel\int d\boldsymbol{r}'_\parallel e^{-i(\boldsymbol{q}+\boldsymbol{G})\cdot\boldsymbol{r}_\parallel}W(\boldsymbol{r},\boldsymbol{r}')e^{i(\boldsymbol{q}+\boldsymbol{G}')\cdot\boldsymbol{r}'_\parallel} = \varepsilon^{-1,\mathrm{2D}}_{\boldsymbol{G}\boldsymbol{G}'}(\boldsymbol{q})v^{\mathrm{2D}}_{\boldsymbol{G}'}(\boldsymbol{q})\,, \tag{4.B.5}$$

where $\varepsilon^{-1,\mathrm{2D}}_{\boldsymbol{G}\boldsymbol{G}'}(\boldsymbol{q})$ is the effective 2D static inverse dielectric constant

$$\varepsilon^{-1,\mathrm{2D}}_{\boldsymbol{G}\boldsymbol{G}'}(\boldsymbol{q}) = \frac{1}{d^2}\int_{-d/2}^{d/2}\mathrm{d}z\int_{-d/2}^{d/2}\mathrm{d}z'\int\mathrm{d}\boldsymbol{r}_\parallel\int\mathrm{d}\boldsymbol{r}'_\parallel\, e^{-i(\boldsymbol{q}+\boldsymbol{G})\cdot\boldsymbol{r}_\parallel}\varepsilon^{-1}(\boldsymbol{r},\boldsymbol{r}')e^{i(\boldsymbol{q}+\boldsymbol{G}')\cdot\boldsymbol{r}'_\parallel}\,. \tag{4.B.6}$$

The procedure to obtain the dielectric function $\varepsilon^{-1,\mathrm{2D}}_{\boldsymbol{G}\boldsymbol{G}'}(\boldsymbol{q})$, within the random-phase approximation and self-consistently with the SX band structure is detailed in Ref. 190. As in Ref. 190, we suppose that the screened interaction is well approximated by that of an uniform system, i.e. $W^{\mathrm{2D}}_{\boldsymbol{G}\boldsymbol{G}'}(\boldsymbol{k}-\boldsymbol{k}') \approx \delta_{\boldsymbol{G}\boldsymbol{G}'}W^{\mathrm{2D}}(\boldsymbol{k}-\boldsymbol{k}'+\boldsymbol{G})$. Finally, the density-density response computed in the condition of null macroscopic electric field is obtained using $\bar{K}^{n\boldsymbol{k}+\boldsymbol{q},m\boldsymbol{k}}_{s\boldsymbol{k}'+\boldsymbol{q},l\boldsymbol{k}'}$, that is given by Eq. (4.B.3), where in the first summation (in the Hartree contribution) the $\boldsymbol{G}=\boldsymbol{0}$ term is omitted.

In order to obtain the density-density response function $\bar{\chi}(\boldsymbol{q},z)$ [Eq. (4.5.10)], we need to compute the density matrix $n^{(\boldsymbol{q})}(z)$ on a set of ω points at fixed η. In our implementation of a tight-binding model of graphene, we solve numerically the reciprocal space expression for the self-consistent Eqs. (4.5.4) and (4.5.6). The electron energies $\{\epsilon^{(0)}_{n\boldsymbol{k}}\}$ and wavefunctions $\{\psi^{(0)}_{n\boldsymbol{k}}\}$ are obtained in a tight-binding model with parameters fitted to DFT ab-initio calculations, then employing many-body perturbation theory within the SX approximation to include nonlocal exchange effects. The band indices $\{n,m,l,s\}$ in Eqs. (4.5.4), (4.5.6) and (4.5.7) indicate either π/π^* bands. In the calculation of the kernel, we selected the $\boldsymbol{G}$ vectors satisfying the condition $|\boldsymbol{G}|^2/2 < 2.5$ Ry, that corresponds to include $\boldsymbol{G}=(0,0)$ and the first shell of the six $\boldsymbol{G}$ vectors with lower modulus. We used also a cutoff in the screened interaction $W^{\mathrm{2D}}(\boldsymbol{k}-\boldsymbol{k}'+\boldsymbol{G})$, such that $W^{\mathrm{2D}}(\boldsymbol{k}-\boldsymbol{k}'+\boldsymbol{G})=0$ if $|\boldsymbol{k}-\boldsymbol{k}'+\boldsymbol{G}|<|\mathrm{K}|$, where K is the Dirac point. We have performed our calculations reported in Sec. 4.5 using a 361×361 Monkhorst-Pack grid in reciprocal space, and electronic smearing of η=100 meV. The optical conductivities are obtained for a small but finite wavevector, of value $\boldsymbol{q}=(10^{-3},0)2\pi/a$ in Cartesian coordinates, where $a=2.46$ Å is the lattice parameter of graphene, and the x axis is along the ΓK direction. We verified numerically that the same converge trends are shown at larger momentum transfer, at $\boldsymbol{q}=(0.1,0)2\pi/a$. For the convergence study presented in Sec. 4.5.3, the reference conductivity $\sigma(z)$ is taken as $\sigma^{\mathrm{ss}}_{\tau_\infty}(z)$, where τ_∞=41 is the number of steps needed to achieve self-consistency in the screen-screen calculation.

In Ref. 190, we have presented the numerical details of the solution of the BSE with a pseudo-Hermitian Lanczos algorithm. In both the implentation we presented in Ref. 190 and the one presented here, an iterative routine is employed to calculate the response function. The cycle is stopped when the relative error on response function [in this case, the optical conductivity $\sigma_\tau(z)$] between two consecutive steps is below a certain convergence threshold. The pseudo-Hermitian Lanczos algorithm has the advantage with respect to the method presented here that the full ω spectrum can be computed with just one iterative cycle.

However, the self-consistent procedure presented here possess two features that could be advantageous with respect to the one we used in Ref. 190. First, it is more accurate

for a single frequency calculation. In fact, we tested that with the same parameters (k grid and η), we reached a converge threshold of 10^{-16} on the relative error of the response with our procedure, while with the Lanczos algorithm we are not able to increase over a convergence threshold of $10^{-5}-10^{-8}$ (depending on the calculations parameters) due to numerical instabilities. Hence, the procedure devised in these work can be beneficial when the response function at a single frequency is needed, as it is the case for the calculation of phonon self-energy from the dynamical interatomic force constant matrix.[188] Secondly, even if implemented on a simple tight-binding model with only two bands (π/π^*), the self-consistent routine presented here is fitted for a more sophisticated implementation where empty states are not explicitly considered. In fact, resembling the TD-DFT routine, Eqs. (4.5.4) can be rephrased in terms of projectors into occupied states as per the Sternheimer equations, thus obtaining the set of equations adopted in ab-initio implementations,[161] which is not as straightforward in the pseudo-Hermitian Lanczos approach. We also note that both our self-consistent routine and the pseudo Hermitian Lanczos algorithm scale as N_k^4, where N_k is the linear dimension of the k grid, while the exact diagonalization of the electron-hole Hamiltonian in the BSE scales as N_k^6 (see Ref.[190] for a formal definition of the BSE Hamiltonian).

Conclusions and outlooks

In this thesis, we have confronted the complicated problems of thermal transport in strongly anharmonic crystals and the response of interacting electronic systems including exchange effects.

To the former is devoted large part of our work. In Chapter 1, we have presented the formalism of maximum entropy principle (MEP) n approach developed in the works by Zubarev.[102,103] Such framewowrk consist in a very powerful and versatile theoretical tool to describe the quantum mechanical statistical operator of a system in a nonequilibrium condition. We used the MEP to derive the steady state in which constant heat flux is present, and obtained a Kubo formula for thermal conductivity. A key step in our procedure is to show that the steady state obtained from the MEP can also be written as the static solution of a modified Liouville equation. This result will allow us to extend in a compact and elegant way the same formalism to the case of the self-consistent approach to interacting systems, discussed in Chapter 3. Our formalism can also be extended straightforwardly to study mass and charge transport.[2,101] Moreover, we have showed how our formalism differs from standard derivation of the DC conductivity based on the adiabatic switching-on of an external "mechanical" potential that simulates the effects of a temperature field.[44,57,104] The main difference consists, at linear order in $\boldsymbol{\nabla} T$, in an expression of conductivity derived from standard response theory in a negative sign for thermal conductivity. Even if apparently overlooked in most of the previous derivations,[44,57,104] we have discussed how this sign change bears an interesting physical insight regarding the flow of entropy. In fact, while apt for the description of transport process where the currents are stimulated by mechanical forces, hence are driven in the direction of the minimum of the energy, the standard procedure of the adiabatic switching-on of the perturbation does not reproduce the evolution of the system in which entropy is produced.

In Chapter 2, we have employed a full quantum-mechanical many-body formalism based on Green's functions to derive an expression for the thermal conductivity that accounts for interband heat conduction in complex crystals. We have focused on two definitions of the energy field, that lead via the continuity equation to two different definitions of the heat flux: the Hardy[35] and the Wigner heat flux.[12,13] These two choices have been motivated by previous work in the literature. We have computed the response function in the so-called dressed-bubble approximation, which neglects vertex corrections but accounts for all self-energy corrections of the phonon Greens' function. Such an approximation allows us to derive an analytical expression for the thermal conductivity in terms of the exact phonon spectral density, that can be computed in principle at any perturbative order and extended to scattering sources of any nature. Neglecting vertex corrections in the dressed-bubble approximation is the main limitation of our many-body approach, that in principle cannot be applied in the hydrodynamic regime of thermal transport, in which heat is mainly carried

by collective excitation of phonon.[25] Modeling hydrodynamic thermal transport requires to account for repopulation terms in the description of scattering,[23–25,142] and is a possible future development of the work done so far. The thermal conductivity is given, for both choices of the heat flux, by an intraband and an interband contribution. The former is independent of the choice of the heat flux, while the second displays some differences. We have argued that these differences originate from the procedure employed to approximate the Green's fucntions in established approaches.[33,39] Such difference yield no quantitative differences when computed numerically in the materials tested so far, namely the perovskite $CsPbBr_3$ and the zirconate $La_2Zr_2O_7$. It may be interesting to search for a test case in which the details of different formulations of thermal conductivity might provide appreciable quantitative differences. Indeed, the identification of such discrepancies could help to understand the differences between the various formulations. From a broader perspective, it would be interesting to test the general quantum formula of thermal conductivity in terms of the full phonon spectral densities (2.3.6a)-(2.3.7). In the overdamped regime of lattice heat conduction, strong interactions may result in very broad (or non-Lorentzian) profiles for the spectral densities.[49,147] This could lead to significant mixing and coherence effects between many phonon bands far apart in energy. In this case, the difference between the definition of the off-diagonal velocity (2.2.26) — that constitute most of the difference between the results from Hardy and Wigner heat fluxes — should be enhanced, and the different formulations of interband thermal conductivity must reflect that in a clear discrepancy. The recent work of Ref. 126 goes in this direction, even if the results for thermal conductivity obtained implementing the expression derived in Ref. 124 for the test case GeTe differ less than 15% from the result of thermal conductivity computed with BTE in the SMA, whereas in complex crystals such discrepancy is typically far more remarkable, consisting up to 70% of total conductivity for the materials we tested. An improvement on the topic of interband transport, specifically concerning the calculation of lattice thermal conductivity in the overdamped regime was reported in our work submitted to Physical Review B and uploaded on arxiv as arXiv:2410.13485,[200] but was not presented in this thesis.

In Chapter 3, we have faced our most ambitious quest tha consisted in the developement of a nonperturbative theoretical framework for lattice thermal transport. By reworking the maximum entropy and modified Liouville equation approach presented in Chapter 1, we have devised a novel first-principles methodology to obtain an expression of thermal conductivity valid in self-consistent schemes. To describe solids in presence of strong anharmonicity, we have adopted nonperturbative approach provided by the SCHA. We have derived the equilibrium state in the SCHA from the maximum entropy principle, expanding the variational space for the Gaussians used to approximate the exact density matrix. To discuss the self-consistent dynamics, we have employed the scheme of the TD-SCHA. Reformulating such theory in the Wigner representation of quantum mechanics, we have obtained a clear interpretation in terms of Feynman diagrams both of the response functions and of the anharmonic scattering included in the phonon dynamics in the TD-SCHA. Then we fitted the TD-SCHA linear response scheme in the framework of thermal transport by defining a TD-SCHA "thermal-potential" from the self-consistent Kubo formula for thermal conductivity we developed. This procedure allowed us to describe the thermal conductivity in terms of a current-current response function, as done in Chapter 2. The harmonic limit of the TD-SCHA thermal conductivity coincides exactly with the result obtained from many-body perturbation theory. Such consistency supports the validity of our approach to thermal

transport in TD-SCHA. Computing the static limit of the full anharmonic current-current correlation function, we realize that the thermal conductivity in TD-SCHA diverges. We have discussed how this shortcoming follows from an intrinsic limitation of the approximation. In the TD-SCHA, the dressed-bubble diagrams that renormalize the two-phonon correlation and provide a finite conductivity are absent.

Nonetheless, our expression of the thermal conductivity within TD-SCHA retains features of significant physical insight. Specifically, the presence of a self-consistent heat flux derived from the approximate Hamiltonian sheds light on the quasiparticles that act as the primary carriers of heat in a self-consistent framework. Moreover, the exact inversion of the Liouville operator in TD-SCHA can be understood as a "anharmonic" screening of the thermal response, analogous to what is observed in other time-dependent self-consistent approaches like time-dependent density functional theory (TD-DFT)[73,74] and time-dependent Hartree-Fock (TD-HF).[76,77] Our findings therefore suggest parallels between lattice thermal transport and electron transport theory, where self-consistent methods are far more advanced. By situating the description of thermal conductivity within this broader framework, advances in lattice thermal transport could emerge by learning from established methods in electron transport theory.[201] Overall, our derivation of thermal conductivity in TD-SCHA represents one of the few recent efforts[12,33,129,142,173] to deepen the theoretical understanding of thermal transport from first principles.

In Chapter 4, we applied our work on linear response theory within self-consistent frameworks to establish a variational formulation of the dynamical response function in electronic systems within generalized TD-DFT with hybrid functionals, TD-HF, and Bethe-Salpeter equation methods. For systems governed by a generalized Kohn-Sham equation, we introduced three equivalent forms for the electronic dynamical response functions: bare-screen, screen-screen, and screen-screen*. Although all three are expressed as functionals of the one-body electronic density matrix, only the screen-screen response is a stationary point, leading to a quadratic dependence on density matrix errors, unlike the linear dependence seen in the other two. This variational property of the screen-screen response function, extending findings by Ref. 70 on nonadiabatic phonons in TD-DFT, is the central result of the Chapter, generalizing their findings to any response function with nonlocal exchange-correlation effects. Notably, the screen*-screen formulation is also physically meaningful, as its imaginary part provides a generalized Fermi Golden Rule. We validated our approach using a tight-binding model of graphene under the SX approximation for electronic interactions. Examining the variational property through the convergence trends of optical conductivity $\sigma(\omega)$ in a self-consistent iterative scheme, we observed that the screen-screen response exhibits quadratic convergence with respect to density matrix accuracy, in contrast to the linear convergence of the other formulations. This property also enables more efficient approximate calculations: we developed a fixed-frequency approximation where the density matrix, determined self-consistently at a reference frequency ω_0, is applied to other frequencies, avoiding repeated self-consistent calculations. The screen-screen approximation aligns closely with full self-consistent results, uniquely matching the first derivative of $\sigma(\omega)$ at ω_0, consistent with its variational nature. The approximation's accuracy depends on the behavior of $\sigma(\omega)$: in flatter regions, it holds over several eV; in more peaked areas, it's valid within around 100 meV. Even though implemented on a simple model, our self-consistent approach and screen-screen approximations are adaptable for more advanced ab initio applications. A more detailed discussion of the efficiency of a tight-binding model of

graphene in reproducing ab initio results for spectroscopic properties was reported in our work uploaded on arxiv as arXiv:2409.17645[190] and submitted to Physical Review B, but it was not presented in this thesis.

Bibliography

[1] Din Zubarev and D Zubarev. Nonequilibrium statistical thermodynamics. Springer, 1974.

[2] Dmitrii N Zubarev, Vladimir Morozov, and Gerd Ropke. Statistical Mechanics of Nonequilibrium Processes, Volume 1 (See 3527400834): Basic Concepts, Kinetic Theory, volume 1. Wiley-VCH, 1996.

[3] Yuxi Wang, Renxing Lin, Pengchen Zhu, Qinghui Zheng, Qianjin Wang, Deyu Li, and Jia Zhu. Cation dynamics governed thermal properties of lead halide perovskite nanowires. Nano letters, 18(5):2772–2779, 2018.

[4] Andrea Pisoni, Jacim Jacimovic, Osor S Barisic, Massimo Spina, Richard Gaál, László Forró, and Endre Horváth. Ultra-low thermal conductivity in organic–inorganic hybrid perovskite ch3nh3pbi3. The journal of physical chemistry letters, 5(14):2488–2492, 2014.

[5] Yi Xia, Vidvuds Ozoliņš, and Chris Wolverton. Microscopic mechanisms of glasslike lattice thermal transport in cubic cu 12 sb 4 s 13 tetrahedrites. Physical review letters, 125(8):085901, 2020.

[6] Girija Suresh, G Seenivasan, MV Krishnaiah, and P Srirama Murti. Investigation of the thermal conductivity of selected compounds of gadolinium and lanthanum. Journal of Nuclear Materials, 249(2-3):259–261, 1997.

[7] Robert Vassen, Xueqiang Cao, Frank Tietz, Debabrata Basu, and Detlev St"over. Zirconates as new materials for thermal barrier coatings. Journal of the American Ceramic Society, 83(8):2023–2028, 2000.

[8] Hongfei Chen, Yanfeng Gao, Shunyan Tao, Yun Liu, and Hongjie Luo. Thermophysical properties of lanthanum zirconate coating prepared by plasma spraying and the influence of post-annealing. Journal of alloys and compounds, 486(1-2):391–399, 2009.

[9] Chunlei Wan, Wei Zhang, Yifeng Wang, Zhixue Qu, Aibing Du, Ruifen Wu, and Wei Pan. Glass-like thermal conductivity in ytterbium-doped lanthanum zirconate pyrochlore. Acta materialia, 58(18):6166–6172, 2010.

[10] Dongbo Zhang, Kai Liao, Yue Yu, Zhongyuan Tian, and Yue Cao. Microstructure and thermal & mechanical properties of la2zr2o7@ ysz composite ceramic. Ceramics International, 46(4):4737–4747, 2020.

[11] Jun Yang, Chunlei Wan, Meng Zhao, Muhammad Shahid, and Wei Pan. Effective blocking of radiative thermal conductivity in la2zr2o7/lapo4 composites for high temperature thermal insulation applications. Journal of the European Ceramic Society, 36(15):3809–3814, 2016.

[12] Michele Simoncelli, Nicola Marzari, and Francesco Mauri. Unified theory of thermal transport in crystals and glasses. Nature Physics, 15(8):809–813, 2019.

[13] Michele Simoncelli, Nicola Marzari, and Francesco Mauri. Wigner formulation of thermal transport in solids. Physical Review X, 12(4):041011, 2022.

[14] Rudolf Peierls. Zur kinetischen theorie der w"armeleitung in kristallen. Annalen der Physik, 395(8):1055–1101, 1929.

[15] David A Broido, Michael Malorny, Gerd Birner, Natalio Mingo, and DA Stewart. Intrinsic lattice thermal conductivity of semiconductors from first principles. Applied Physics Letters, 91(23):231922, 2007.

[16] Jivtesh Garg, Nicola Bonini, Boris Kozinsky, and Nicola Marzari. Role of Disorder and Anharmonicity in the Thermal Conductivity of Silicon-Germanium Alloys: A First-Principles Study. Phys. Rev. Lett., 106:045901, Jan 2011.

[17] Keivan Esfarjani, Gang Chen, and Harold T. Stokes. Heat transport in silicon from first-principles calculations. Phys. Rev. B, 84:085204, Aug 2011.

[18] Maria N. Luckyanova, Jivtesh Garg, Keivan Esfarjani, Adam Jandl, Mayank T. Bulsara, Aaron J. Schmidt, Austin J. Minnich, Shuo Chen, Mildred S. Dresselhaus, Zhifeng Ren, Eugene A. Fitzgerald, and Gang Chen. Coherent phonon heat conduction in superlattices. Science, 338(6109):936–939, 2012.

[19] David G. Cahill, Paul V. Braun, Gang Chen, David R. Clarke, Shanhui Fan, Kenneth E. Goodson, Pawel Keblinski, William P. King, Gerald D. Mahan, Arun Majumdar, Humphrey J. Maris, Simon R. Phillpot, Eric Pop, and Li Shi. Nanoscale thermal transport. ii. 2003–2012. Appl. Phys. Rev., 1(1):011305, 2014.

[20] Alan JH McGaughey, Ankit Jain, Hyun-Young Kim, and Bo Fu. Phonon properties and thermal conductivity from first principles, lattice dynamics, and the Boltzmann transport equation. J. Appl. Phys., 125(1):011101, 2019.

[21] Lorenzo Paulatto, Ion Errea, Matteo Calandra, and Francesco Mauri. First-principles calculations of phonon frequencies, lifetimes, and spectral functions from weak to strong anharmonicity: The example of palladium hydrides. Phys. Rev. B, 91:054304, Feb 2015.

[22] Giorgia Fugallo, Michele Lazzeri, Lorenzo Paulatto, and Francesco Mauri. Ab initio variational approach for evaluating lattice thermal conductivity. Phys. Rev. B, 88:045430, Jul 2013.

[23] Giorgia Fugallo, Andrea Cepellotti, Lorenzo Paulatto, Michele Lazzeri, Nicola Marzari, and Francesco Mauri. Thermal conductivity of graphene and graphite: collective excitations and mean free paths. Nano letters, 14(11):6109–6114, 2014.

[24] Andrea Cepellotti, Giorgia Fugallo, Lorenzo Paulatto, Michele Lazzeri, Francesco Mauri, and Nicola Marzari. Phonon hydrodynamics in two-dimensional materials. Nature communications, 6(1):1–7, 2015.

[25] Andrea Cepellotti and Nicola Marzari. Thermal transport in crystals as a kinetic theory of relaxons. Physical Review X, 6(4):041013, 2016.

[26] Davide Donadio and Giulia Galli. Atomistic Simulations of Heat Transport in Silicon Nanowires. Phys. Rev. Lett., 102:195901, May 2009.

[27] Wu Li and Natalio Mingo. Ultralow lattice thermal conductivity of the fully filled skutterudite $YbFe_4Sb_{12}$ due to the flat avoided-crossing filler modes. Phys. Rev. B, 91:144304, Apr 2015.

[28] Woochul Lee, Huashan Li, Andrew B Wong, Dandan Zhang, Minliang Lai, Yi Yu, Qiao Kong, Elbert Lin, Jeffrey J Urban, Jeffrey C Grossman, et al. Ultralow thermal conductivity in all-inorganic halide perovskites. Proceedings of the National Academy of Sciences, 114(33):8693–8697, 2017.

[29] Xi Chen, Annie Weathers, Jesús Carrete, Saikat Mukhopadhyay, Olivier Delaire, Derek A. Stewart, Natalio Mingo, Steven N. Girard, Jie Ma, Douglas L. Abernathy, Jiaqiang Yan, Raman Sheshka, Daniel P. Sellan, Fei Meng, Song Jin, Jianshi Zhou, and Li Shi. Twisting phonons in complex crystals with quasi-one-dimensional substructures. Nat. Commun., 6:6723, 2015.

[30] Annie Weathers, Jesús Carrete, John P. DeGrave, Jeremy M. Higgins, Arden L. Moore, Jaehyun Kim, Natalio Mingo, Song Jin, and Li Shi. Glass-like thermal conductivity in nanostructures of a complex anisotropic crystal. Phys. Rev. B, 96:214202, Dec 2017.

[31] Pierre-François Lory, Stéphane Pailhès, Valentina M Giordano, Holger Euchner, Hong Duong Nguyen, Reiner Ramlau, Horst Borrmann, Marcus Schmidt, Michael Baitinger, Matthias Ikeda, et al. Direct measurement of individual phonon lifetimes in the clathrate compound Ba 7.81 Ge 40.67 Au 5.33. Nat. Commun., 8(1):491, 2017.

[32] Saikat Mukhopadhyay, David S Parker, Brian C Sales, Alexander A Puretzky, Michael A McGuire, and Lucas Lindsay. Two-channel model for ultralow thermal conductivity of crystalline tl3vse4. Science, 360(6396):1455–1458, 2018.

[33] Leyla Isaeva, Giuseppe Barbalinardo, Davide Donadio, and Stefano Baroni. Modeling heat transport in crystals and glasses from a unified lattice-dynamical approach. Nature communications, 10(1):1–6, 2019.

[34] Yixiu Luo, Xiaolong Yang, Tianli Feng, Jingyang Wang, and Xiulin Ruan. Vibrational hierarchy leads to dual-phonon transport in low thermal conductivity crystals. Nature communications, 11(1):1–10, 2020.

[35] Robert J Hardy. Energy-flux operator for a lattice. Physical Review, 132(1):168, 1963.

[36] Rudolf Ernst Peierls. Quantum theory of solids. Oxford Classics Series, 2001.

[37] Philip B. Allen and Joseph L. Feldman. Thermal Conductivity of Glasses: Theory and Application to Amorphous Si. Phys. Rev. Lett., 62:645–648, Feb 1989.

[38] Michele Simoncelli, Francesco Mauri, and Nicola Marzari. Thermal conductivity of glasses: First-principles theory and applications. npj Computational Materials, 9(1):106, 2023.

[39] Andrey Pereverzev and Tommy Sewell. Theoretical analysis of oscillatory terms in lattice heat-current time correlation functions and their contributions to thermal conductivity. Physical Review B, 97(10):104308, 2018.

[40] Loris Ercole, Aris Marcolongo, Paolo Umari, and Stefano Baroni. Gauge invariance of thermal transport coefficients. Journal of Low Temperature Physics, 185(1):79–86, 2016.

[41] Michele Lazzeri, Matteo Calandra, and Francesco Mauri. Anharmonic phonon frequency shift in mgb 2. Physical Review B, 68(22):220509, 2003.

[42] José Menéndez and Manuel Cardona. Temperature dependence of the first-order raman scattering by phonons in si, ge, and α- s n: Anharmonic effects. Physical Review B, 29(4):2051, 1984.

[43] Shobhana Narasimhan and David Vanderbilt. Anharmonic self-energies of phonons in silicon. Physical Review B, 43(5):4541, 1991.

[44] Philip B Allen and Joseph L Feldman. Thermal conductivity of disordered harmonic solids. Physical Review B, 48(17):12581, 1993.

[45] Lorenzo Paulatto, Francesco Mauri, and Michele Lazzeri. Anharmonic properties from a generalized third-order ab initio approach: Theory and applications to graphite and graphene. Physical Review B, 87(21):214303, 2013.

[46] Wu Li, Jesús Carrete, Nebil A Katcho, and Natalio Mingo. Shengbte: A solver of the boltzmann transport equation for phonons. Computer Physics Communications, 185(6):1747–1758, 2014.

[47] Atsushi Togo. First-principles phonon calculations with phonopy and phono3py. J. Phys. Soc. Jpn., 92(1):012001, 2023.

[48] Guilherme AS Ribeiro, Lorenzo Paulatto, Raffaello Bianco, Ion Errea, Francesco Mauri, and Matteo Calandra. Strong anharmonicity in the phonon spectra of pbte and snte from first principles. Physical Review B, 97(1):014306, 2018.

[49] Unai Aseginolaza, Raffaello Bianco, Lorenzo Monacelli, Lorenzo Paulatto, Matteo Calandra, Francesco Mauri, Aitor Bergara, and Ion Errea. Phonon collapse and second-order phase transition in thermoelectric snse. Physical review letters, 122(7):075901, 2019.

[50] Lorenzo Monacelli, Raffaello Bianco, Marco Cherubini, Matteo Calandra, Ion Errea, and Francesco Mauri. The stochastic self-consistent harmonic approximation: calculating vibrational properties of materials with full quantum and anharmonic effects. Journal of Physics: Condensed Matter, 33(36):363001, 2021.

[51] Terumasa Tadano and Shinji Tsuneyuki. First-principles lattice dynamics method for strongly anharmonic crystals. Journal of the Physical Society of Japan, 87(4):041015, 2018.

[52] O. Hellman, I. A. Abrikosov, and S. I. Simak. Lattice dynamics of anharmonic solids from first principles. Phys. Rev. B, 84:180301, Nov 2011.

[53] Petros Souvatzis, Olle Eriksson, MI Katsnelson, and SP Rudin. The self-consistent ab initio lattice dynamical method. Computational materials science, 44(3):888–894, 2009.

[54] Bartomeu Monserrat, ND Drummond, and RJ Needs. Anharmonic vibrational properties in periodic systems: energy, electron-phonon coupling, and stress. Physical Review B, 87(14):144302, 2013.

[55] Thierry Dauxois, Michel Peyrard, and AR Bishop. Dynamics and thermodynamics of a nonlinear model for dna denaturation. Physical Review E, 47(1):684, 1993.

[56] Raffaello Bianco, Ion Errea, Lorenzo Paulatto, Matteo Calandra, and Francesco Mauri. Second-order structural phase transitions, free energy curvature, and temperature-dependent anharmonic phonons in the self-consistent harmonic approximation: Theory and stochastic implementation. Physical Review B, 96(1):014111, 2017.

[57] JM Luttinger. Theory of thermal transport coefficients. Physical Review, 135(6A):A1505, 1964.

[58] GV Chester. The theory of irreversible processes. Reports on Progress in Physics, 26(1):411, 1963.

[59] Stefano Baroni, Riccardo Bertossa, Loris Ercole, Federico Grasselli, and Aris Marcolongo. Heat transport in insulators from ab initio green-kubo theory. Handbook of materials modeling: Applications: Current and emerging materials, pages 809–844, 2020.

[60] Yi Xia, Vinay I Hegde, Koushik Pal, Xia Hua, Dale Gaines, Shane Patel, Jiangang He, Muratahan Aykol, and Chris Wolverton. High-throughput study of lattice thermal conductivity in binary rocksalt and zinc blende compounds including higher-order anharmonicity. Physical Review X, 10(4):041029, 2020.

[61] Đorđe Dangić, Olle Hellman, Stephen Fahy, and Ivana Savić. The origin of the lattice thermal conductivity enhancement at the ferroelectric phase transition in gete. npj Computational Materials, 7(1):57, 2021.

[62] Terumasa Tadano and Wissam A Saidi. First-principles phonon quasiparticle theory applied to a strongly anharmonic halide perovskite. Physical Review Letters, 129(18):185901, 2022.

[63] Tongcai Yue, Yinchang Zhao, Jun Ni, Sheng Meng, and Zhenhong Dai. Strong quartic anharmonicity, ultralow thermal conductivity, high band degeneracy and good thermoelectric performance in na2tlsb. npj Computational Materials, 9(1):17, 2023.

[64] Johan Klarbring, Olle Hellman, Igor A Abrikosov, and Sergei I Simak. Anharmonicity and ultralow thermal conductivity in lead-free halide double perovskites. Physical Review Letters, 125(4):045701, 2020.

[65] Lorenzo Monacelli and Francesco Mauri. Time-dependent self-consistent harmonic approximation: Anharmonic nuclear quantum dynamics and time correlation functions. Physical Review B, 103(10):104305, 2021.

[66] Jae-Mo Lihm and Cheol-Hwan Park. Gaussian time-dependent variational principle for the finite-temperature anharmonic lattice dynamics. Physical Review Research, 3(3):L032017, 2021.

[67] Gerald D Mahan. Many-particle physics. Springer Science & Business Media, 2013.

[68] G. Giuliani and G. Vignale. Quantum Theory of the Electron Liquid. Masters Series in Physics and Astronomy. Cambridge University Press, 2005.

[69] Stefano Piscanec, Michele Lazzeri, Francesco Mauri, Andrea Carlo Ferrrari, and John Robertson. Kohn anomalies and electron-phonon interactions in graphite. Phys. Rev. Lett., 93(18):185503, 2004.

[70] Matteo Calandra, Gianni Profeta, and Francesco Mauri. Adiabatic and nonadiabatic phonon dispersion in a Wannier function approach. Physical Review B, 82(16):165111, 2010.

[71] Jan Berges, Nina Girotto, Tim Wehling, Nicola Marzari, and Samuel Poncé. Phonon self-energy corrections: To screen, or not to screen. Physical Review X, 13(4):041009, 2023.

[72] Roi Baer and Leeor Kronik. Time-dependent generalized Kohn-Sham theory. The European Physical Journal B, 91(7):170, Jul 2018.

[73] Carsten A Ullrich. Time-dependent density-functional theory: concepts and applications. Oxford University Press, Oxford, 2011.

[74] Miguel A.L. Marques, Neepa T. Maitra, Fernando M.S. Nogueira, E. K. U. Gross, and Angel Rubio. Fundamentals of Time-Dependent Density Functional Theory. Lecture Notes in Physics book series. Springer, Berlin, Heidelberg, 2012.

[75] Dario Rocca, Ralph Gebauer, Yousef Saad, and Stefano Baroni. Turbo charging time-dependent density-functional theory with lanczos chains. The Journal of Chemical Physics, 128(15), 2008.

[76] A. D. McLachlan and M. A. Ball. Time-dependent Hartree—Fock theory for molecules. Rev. Mod. Phys., 36:844–855, Jul 1964.

[77] Leonardo Bernasconi, Ross Webster, Stanko Tomić, and Nicholas M Harrison. Optical response of extended systems from time-dependent Hartree-Fock and time-dependent density-functional theory. Journal of Physics: Conference Series, 367(1):012001, may 2012.

[78] Axel D. Becke. A new mixing of Hartree–Fock and local density-functional theories. The Journal of Chemical Physics, 98(2):1372–1377, 01 1993.

[79] John P. Perdew, Matthias Ernzerhof, and Kieron Burke. Rationale for mixing exact exchange with density functional approximations. The Journal of Chemical Physics, 105(22):9982–9985, 12 1996.

[80] Akinaga Yoshinobu and Ten-no Seiichiro. Range-separation by the Yukawa potential in long-range corrected density functional theory with gaussian-type basis functions. Chemical Physics Letters, 462(4):348–351, 2008.

[81] Michael Seth and Tom Ziegler. Range-separated exchange functionals with slater-type functions. Journal of Chemical Theory and Computation, 8(3):901–907, 2012. PMID: 26593352.

[82] Jiawei Zhan, Marco Govoni, and Giulia Galli. Nonempirical range-separated hybrid functional with spatially dependent screened exchange. Journal of Chemical Theory and Computation, 19(17):5851–5862, 2023.

[83] Stefano Paolo Villani, Marco Campetella, Paolo Barone, and Francesco Mauri. Giant piezoelectricity driven by thouless pump in conjugated polymers. npj Computational Materials, 10(1):81, 2024.

[84] Lars Hedin. New method for calculating the one-particle Green's function with application to the electron-gas problem. Phys. Rev., 139:A796–A823, Aug 1965.

[85] Giancarlo Strinati. Application of the Green's functions method to the study of the optical properties of semiconductors. La Rivista del Nuovo Cimento (1978-1999), 11(12):1–86, 1988.

[86] Giovanni Onida, Lucia Reining, and Angel Rubio. Electronic excitations: density-functional versus many-body Green's-function approaches. Rev. Mod. Phys., 74:601–659, Jun 2002.

[87] Richard M Martin, Lucia Reining, and David M Ceperley. Interacting electrons. Cambridge University Press, 2016.

[88] P.B. Allen. Dynamical Properties of Solids Vol 3: Metals, Superconductors, Magnetic Materials, Liquids, chapter Phonons and the Superconducting Transition Temperature. North-Holland Publishing Company, Amsterdam, 1980.

[89] Gianluca Stefanucci and Enrico Perfetto. Phonon linewidths with two screened electron-phonon couplings are not overscreened.

[90] Dario Rocca, Deyu Lu, and Giulia Galli. Ab initio calculations of optical absorption spectra: Solution of the Bethe–Salpeter equation within density matrix perturbation theory. The Journal of Chemical Physics, 133(16):164109, 10 2010.

[91] Dario Rocca, Yuan Ping, Ralph Gebauer, and Giulia Galli. Solution of the Bethe-Salpeter equation without empty electronic states: Application to the absorption spectra of bulk systems. Phys. Rev. B, 85:045116, Jan 2012.

[92] David A Siegel, Cheol-Hwan Park, Choongyu Hwang, Jack Deslippe, Alexei V Fedorov, Steven G Louie, and Alessandra Lanzara. Many-body interactions in quasi-freestanding graphene. Proceedings of the National Academy of Sciences, 108(28):11365–11369, 2011.

[93] Alberto Guandalini, Dario A. Leon, Pino D'Amico, Claudia Cardoso, Andrea Ferretti, Massimo Rontani, and Daniele Varsano. Efficient GW calculations via interpolation of the screened interaction in momentum and frequency space: The case of graphene. Phys. Rev. B, 109:075120, Feb 2024.

[94] Li Yang, Jack Deslippe, Cheol-Hwan Park, Marvin L. Cohen, and Steven G. Louie. Excitonic effects on the optical response of graphene and bilayer graphene. Phys. Rev. Lett., 103:186802, Oct 2009.

[95] Li Yang. Excitons in intrinsic and bilayer graphene. Phys. Rev. B, 83:085405, Feb 2011.

[96] Alberto Guandalini, Ryosuke Senga, Yung-Chang Lin, Kazu Suenaga, Andrea Ferretti, Daniele Varsano, Andrea Recchia, Paolo Barone, Francesco Mauri, Thomas Pichler, and Christian Kramberger. Excitonic effects in energy-loss spectra of freestanding graphene. Nano Letters, 23(24):11835–11841, 2023.

[97] D. M. Basko and I. L. Aleiner. Interplay of coulomb and electron-phonon interactions in graphene. Phys. Rev. B, 77:041409, Jan 2008.

[98] Tommaso Venanzi, Lorenzo Graziotto, Francesco Macheda, Simone Sotgiu, Taoufiq Ouaj, Elena Stellino, Claudia Fasolato, Paolo Postorino, Vaidotas Mišeikis, Marvin Metzelaars, Paul K"ogerler, Bernd Beschoten, Camilla Coletti, Stefano Roddaro, Matteo Calandra, Michele Ortolani, Christoph Stampfer, Francesco Mauri, and Leonetta Baldassarre. Probing enhanced electron-phonon coupling in graphene by infrared resonance Raman spectroscopy. Phys. Rev. Lett., 130:256901, Jun 2023.

[99] Lorenzo Graziotto, Francesco Macheda, Tommaso Venanzi, Guglielmo Marchese, Simone Sotgiu, Taoufiq Ouaj, Elena Stellino, Claudia Fasolato, Paolo Postorino, Marvin Metzelaars, Paul K"ogerler, Bernd Beschoten, Matteo Calandra, Michele Ortolani, Christoph Stampfer, Francesco Mauri, and Leonetta Baldassarre. Infrared resonance Raman of bilayer graphene: Signatures of massive fermions and band structure on the 2D peak. Nano Lett., 24(6):1867–1873, February 2024.

[100] Lorenzo Graziotto, Francesco Macheda, Thibault Sohier, Matteo Calandra, and Francesco Mauri. Theory of infrared double-resonance Raman spectrum in graphene: The role of the zone-boundary electron-phonon enhancement. Phys. Rev. B, 109:075420, Feb 2024.

[101] Sadao Nakajima. On quantum theory of transport phenomena: steady diffusion. Progress of Theoretical Physics, 20(6):948–959, 1958.

[102] Dmitrii Nikolaevich Zubarev. Boundary conditions for statistical operators in the theory of nonequilibrium processes and quasiaverages. Teoreticheskaya i Matematicheskaya Fizika, 3(2):276–286, 1970.

[103] Dmitrii Nikolaevich Zubarev and Vladimir Petrovich Kalashnikov. Construction of statistical operators for nonequilibrium processes. Teoreticheskaya i Matematicheskaya Fizika, 3(1):126–134, 1970.

[104] Gerald D Mahan. Many-particle physics. Springer Science & Business Media, 2000.

[105] Murray Gell-Mann and ML Goldberger. The formal theory of scattering. Physical Review, 91(2):398, 1953.

[106] Ryogo Kubo. Statistical-mechanical theory of irreversible processes. i. general theory and simple applications to magnetic and conduction problems. Journal of the Physical Society of Japan, 12(6):570–586, 1957.

[107] WT Grandy Jr. Principle of maximum entropy and irreversible processes. Physics Reports, 62(3):175–266, 1980.

[108] Florian G Eich, M Di Ventra, and G Vignale. Density-functional theory of thermoelectric phenomena. Physical review letters, 112(19):196401, 2014.

[109] Mattia Udina, Jacopo Fiore, Tommaso Cea, Claudio Castellani, Goetz Seibold, and Lara Benfatto. Thz non-linear optical response in cuprates: predominance of the bcs response over the higgs mode. Faraday Discussions, 237:168–185, 2022.

[110] Giovanni Caldarelli, Michele Simoncelli, Nicola Marzari, Francesco Mauri, and Lara Benfatto. Many-body green's function approach to lattice thermal transport. Phys. Rev. B, 106:024312, Jul 2022.

[111] Walter T Grandy Jr. Entropy and the time evolution of macroscopic systems, volume 10. Oxford University Press on Demand, 2008.

[112] DJ Scalapino. A look back: Early applications of maximum entropy estimation to quantum statistical mechanics. 1993.

[113] Ryogo Kubo, Morikazu Toda, and Natsuki Hashitsume. Statistical physics II: nonequilibrium statistical mechanics, volume 31. Springer Science & Business Media, 2012.

[114] Ryogo Kubo, Mario Yokota, and Sadao Nakajima. Statistical-mechanical theory of irreversible processes. ii. response to thermal disturbance. Journal of the Physical Society of Japan, 12(11):1203–1211, 1957.

[115] Roberto Luzzi and Aurea R Vasconcellos. On the nonequilibrium statistical operator method. Fortschritte der Physik/Progress of Physics, 38(11):887–922, 1990.

[116] Giorgio Parisi and Ramamurti Shankar. Statistical field theory. 1988.

[117] Ryogo Kubo. The fluctuation-dissipation theorem. Reports on progress in physics, 29(1):255, 1966.

[118] Edwin T. Jaynes. Where do we stand on maximum entropy. 1979.

[119] John M Ziman. Electrons and phonons: the theory of transport phenomena in solids. Oxford university press, 2001.

[120] Joseph L Feldman, Mark D Kluge, Philip B Allen, and Frederick Wooten. Thermal conductivity and localization in glasses: Numerical study of a model of amorphous silicon. Physical Review B, 48(17):12589, 1993.

[121] J. L. Feldman and Mark D. Kluge. Realistic model calculations based on the kubo theory for the thermal conductivity of amorphous insulators. Philos. Mag. B, 71(4):641–647, 1995.

[122] Philip B. Allen, Joseph L. Feldman, Jaroslav Fabian, and Frederick Wooten. Diffusons, locons and propagons: Character of atomie yibrations in amorphous Si. Philos. Mag. B, 79(11-12):1715–1731, 1999.

[123] AA Maradudin. The lattice thermal conductivity of an isotopically disordered crystal. Journal of the American Chemical Society, 86(17):3405–3413, 1964.

[124] BS Semwal and PK Sharma. Thermal conductivity of an anharmonic crystal. Physical Review B, 5(10):3909, 1972.

[125] Alberto Debernardi, Stefano Baroni, and Elisa Molinari. Anharmonic phonon lifetimes in semiconductors from density-functional perturbation theory. Physical review letters, 75(9):1819, 1995.

[126] Đorđe Dangić, Olle Hellman, Stephen Fahy, and Ivana Savić. The origin of the lattice thermal conductivity enhancement at the ferroelectric phase transition in GeTe. Npj Comput. Mater., 7(1):57, 2021.

[127] Patrick K Schelling, Simon R Phillpot, and Pawel Keblinski. Comparison of atomic-level simulation methods for computing thermal conductivity. Physical Review B, 65(14):144306, 2002.

[128] Aris Marcolongo, Paolo Umari, and Stefano Baroni. Microscopic theory and quantum simulation of atomic heat transport. Nature Physics, 12(1):80–84, 2016.

[129] Christian Carbogno, Rampi Ramprasad, and Matthias Scheffler. Ab initio green-kubo approach for the thermal conductivity of solids. Physical review letters, 118(17):175901, 2017.

[130] Lars Onsager. Reciprocal relations in irreversible processes. i. Physical review, 37(4):405, 1931.

[131] Aleksei Alekseevich Abrikosov, Lev Petrovich Gorkov, and Igor Ekhielevich Dzyaloshinski. Methods of quantum field theory in statistical physics. Courier Corporation, 2012.

[132] Duane C Wallace. Thermodynamics of crystals. American Journal of Physics, 40(11):1718–1719, 1972.

[133] Stefano Lepri, Roberto Livi, and Antonio Politi. Thermal conduction in classical low-dimensional lattices. Physics reports, 377(1):1–80, 2003.

[134] B Deo and SN Behera. Calculation of thermal conductivity by the kubo formula. Physical Review, 141(2):738, 1966.

[135] Takeo Matsubara. A new approach to quantum-statistical mechanics. Progress of theoretical physics, 14(4):351–378, 1955.

[136] SN Behera and B Deo. Substitutional defects and resonant modes in solids. Physical Review, 153(3):728, 1967.

[137] Qingping Meng, Lijun Wu, David O Welch, and Yimei Zhu. Lattice vibrations in the frenkel-kontorova model. ii. thermal conductivity. Physical Review B, 91(22):224306, 2015.

[138] Sheng Li, Qiye Zheng, Yinchuan Lv, Xiaoyuan Liu, Xiqu Wang, Pinshane Y Huang, David G Cahill, and Bing Lv. High thermal conductivity in cubic boron arsenide crystals. Science, 361(6402):579–581, 2018.

[139] Evgenii Mikhailovich Lifshitz and Lev Petrovich Pitaevskii. Statistical physics: theory of the condensed state, volume 9. Elsevier, 2013.

[140] RA Guyer and JA Krumhansl. Thermal conductivity, second sound, and phonon hydrodynamic phenomena in nonmetallic crystals. Physical Review, 148(2):778, 1966.

[141] Tao Sun and Philip B Allen. Lattice thermal conductivity: Computations and theory of the high-temperature breakdown of the phonon-gas model. Physical Review B, 82(22):224305, 2010.

[142] Michele Simoncelli, Nicola Marzari, and Andrea Cepellotti. Generalization of fourier's law into viscous heat equations. Physical Review X, 10(1):011019, 2020.

[143] Lucas Lindsay. First principles peierls-boltzmann phonon thermal transport: a topical review. Nanoscale and Microscale Thermophysical Engineering, 20(2):67–84, 2016.

[144] Alistair Ward, DA Broido, Derek A Stewart, and Gernot Deinzer. Ab initio theory of the lattice thermal conductivity in diamond. Physical Review B, 80(12):125203, 2009.

[145] AA Maradudin and AE Fein. Scattering of neutrons by an anharmonic crystal. Physical Review, 128(6):2589, 1962.

[146] KN Pathak. Theory of anharmonic crystals. Physical Review, 139(5A):A1569, 1965.

[147] T Lanigan-Atkins, X He, MJ Krogstad, DM Pajerowski, DL Abernathy, Guangyong NMN Xu, Zhijun Xu, D-Y Chung, MG Kanatzidis, S Rosenkranz, et al. Two-dimensional overdamped fluctuations of the soft perovskite lattice in cspbbr 3. Nature materials, pages 1–7, 2021.

[148] Gyaneshwar P Srivastava. The physics of phonons. Routledge, 2019.

[149] Jing Zhang, Xingye Guo, Yeon-Gil Jung, Li Li, and James Knapp. Lanthanum zirconate based thermal barrier coatings: A review. Surface and Coatings Technology, 323:18–29, 2017.

[150] Shunsuke Hirotsu, Jimpei Harada, Masashi Iizumi, and Kazuo Gesi. Structural phase transitions in cspbbr3. Journal of the Physical Society of Japan, 37(5):1393–1398, 1974.

[151] Ryosuke Senga, Kazu Suenaga, Paolo Barone, Shigeyuki Morishita, Francesco Mauri, and Thomas Pichler. Position and momentum mapping of vibrations in graphene nanostructures. Nature, 573(7773):247–250, 2019.

[152] Antonio Siciliano, Lorenzo Monacelli, Giovanni Caldarelli, and Francesco Mauri. Wigner gaussian dynamics: Simulating the anharmonic and quantum ionic motion. Physical Review B, 107(17):174307, 2023.

[153] Erich Runge and Eberhard KU Gross. Density-functional theory for time-dependent systems. Physical review letters, 52(12):997, 1984.

[154] Tie-cheng Li and Pei-qing Tong. Hohenberg-kohn theorem for time-dependent ensembles. Physical Review A, 31(3):1950, 1985.

[155] N David Mermin. Thermal properties of the inhomogeneous electron gas. Physical Review, 137(5A):A1441, 1965.

[156] Aurora Pribram-Jones, Stefano Pittalis, EKU Gross, and Kieron Burke. Thermal density functional theory in context. In Frontiers and Challenges in Warm Dense Matter, pages 25–60. Springer, 2014.

[157] Florian Knoop, Matthias Scheffler, and Christian Carbogno. Ab initio green-kubo simulations of heat transport in solids: method and implementation. Physical Review B, 107(22):224304, 2023.

[158] Susumu Fujii, Masato Yoshiya, and Craig AJ Fisher. Quantifying anharmonic vibrations in thermoelectric layered cobaltites and their role in suppressing thermal conductivity. Scientific Reports, 8(1):11152, 2018.

[159] Yifan Zhu, Yi Xia, Yancheng Wang, Ye Sheng, Jiong Yang, Chenguang Fu, Airan Li, Tiejun Zhu, Jun Luo, Christopher Wolverton, et al. Violation of the t- 1 relationship in the lattice thermal conductivity of mg3sb2 with locally asymmetric vibrations. Research, 2020.

[160] Zezhu Zeng, Cunzhi Zhang, Yi Xia, Zheyong Fan, Chris Wolverton, and Yue Chen. Nonperturbative phonon scatterings and the two-channel thermal transport in tl 3 vse 4. Physical Review B, 103(22):224307, 2021.

[161] Stefano Baroni, Stefano De Gironcoli, Andrea Dal Corso, and Paolo Giannozzi. Phonons and related crystal properties from density-functional perturbation theory. Reviews of modern Physics, 73(2):515, 2001.

[162] Richard P Feynman. Statistical mechanics: A set of lectures. 2018.

[163] Kaya Imre, Erc"ument "Ozizmir, Marcos Rosenbaum, and PF Zweifel. Wigner method in quantum statistical mechanics. Journal of Mathematical Physics, 8(5):1097–1108, 1967.

[164] Marcel Novaes. Wigner and husimi functions in the double-well potential. Journal of Optics B: Quantum and Semiclassical Optics, 5(3):S342–S348, jun 2003.

[165] Terumasa Tadano and Shinji Tsuneyuki. Self-consistent phonon calculations of lattice dynamical properties in cubic $\mathrm{srtio_3}$ with first-principles anharmonic force constants. Phys. Rev. B, 92:054301, Aug 2015.

[166] T Tadano, Y Gohda, and S Tsuneyuki. Anharmonic force constants extracted from first-principles molecular dynamics: applications to heat transfer simulations. Journal of Physics: Condensed Matter, 26(22):225402, may 2014.

[167] W. G"otze and K. H. Michel. Elastic constants of nonionic anharmonic crystals. Zeitschrift f"ur Physik A Hadrons and nuclei, 217(2):170–187, April 1968.

[168] Francesco Macheda, Paolo Barone, and Francesco Mauri. Electron-phonon interaction and longitudinal-transverse phonon splitting in doped semiconductors. Phys. Rev. Lett., 129:185902, Oct 2022.

[169] Francesco Macheda, Thibault Sohier, Paolo Barone, and Francesco Mauri. Electron-phonon interaction and phonon frequencies in two-dimensional doped semiconductors. Physical Review B, 107(9):094308, 2023.

[170] Yusuke Oba, Terumasa Tadano, Ryosuke Akashi, and Shinji Tsuneyuki. First-principles study of phonon anharmonicity and negative thermal expansion in $\mathrm{scf_3}$. Phys. Rev. Materials, 3:033601, Mar 2019.

[171] V. V. Goldman, G. K. Horton, and M. L. Klein. An improved self-consistent phonon approximation. Phys. Rev. Lett., 21:1527–1529, Nov 1968.

[172] N. R. Werthamer. Self-consistent phonon formulation of anharmonic lattice dynamics. Phys. Rev. B, 1:572–581, Jan 1970.

[173] Alfredo Fiorentino and Stefano Baroni. From green-kubo to the full boltzmann kinetic approach to heat transport in crystals and glasses. Physical Review B, 107(5):054311, 2023.

[174] Xavier Gonze, Douglas C. Allan, and Michael P. Teter. Dielectric tensor, effective charges, and phonons in α-quartz by variational density-functional perturbation theory. Phys. Rev. Lett., 68:3603–3606, Jun 1992.

[175] Giovanni Caldarelli, Alberto Guandalini, Francesco Macheda, and Francesco Mauri. Variational formulation of dynamical electronic response functions in bethe-salpeter,(screened) hartree-fock, hybrid-dft approaches. arXiv preprint arXiv:2410.22889, 2024.

[176] R"udiger Bauernschmitt and Reinhart Ahlrichs. Treatment of electronic excitations within the adiabatic approximation of time dependent density functional theory. Chemical Physics Letters, 256(4-5):454–464, 1996.

[177] Roi Baer and Leeor Kronik. Time-dependent generalized kohn–sham theory. The European Physical Journal B, 91:170, 2018.

[178] Kieron Burke, Jan Werschnik, and EKU Gross. Time-dependent density functional theory: Past, present, and future. The Journal of chemical physics, 123(6), 2005.

[179] R.M. Martin. Electronic Structure: Basic Theory and Practical Methods. Cambridge University Press, 2020.

[180] Mark E Casida, DP Chong, et al. Recent advances in density functional methods, 1995.

[181] E. G. Maximov. A self-consistent description of the electron-phonon system in metals and the problem of lattice stability. Sov. Phys.-JETP, 42(6):1138, 1975.

[182] W. H. Buttler, F. J. Pinski, and P. B. Allen. Phonon linewidths and electron-phonon interaction in Nb. Physical Review B, 19(7):3708, 1979.

[183] Feliciano Giustino. Electron-phonon interactions from first principles. Rev. Mod. Phys., 89:015003, Feb 2017.

[184] A. B. Migdal. Interaction between electrons and lattice vibrations in a normal metal. Sov. Phys.-JETP, 6:996, 1958.

[185] Paolo Giannozzi, Stefano De Gironcoli, Pasquale Pavone, and Stefano Baroni. Ab initio calculation of phonon dispersions in semiconductors. Physical Review B, 43(9):7231, 1991.

[186] Xavier Gonze and Changyol Lee. Dynamical matrices, born effective charges, dielectric permittivity tensors, and interatomic force constants from density-functional perturbation theory. Physical Review B, 55(16):10355, 1997.

[187] Enrico Fermi. Nuclear physics: a course given by Enrico Fermi at the University of Chicago. University of Chicago press, 1950.

[188] Alberto Guandalini, Giovanni Caldarelli, Francesco Macheda, and Francesco Mauri. In preparation.

[189] EKU Gross and Walter Kohn. Local density-functional theory of frequency-dependent linear response. Physical review letters, 55(26):2850, 1985.

[190] Alberto Guandalini, Giovanni Caldarelli, Francesco Macheda, and Francesco Mauri. High- and low-energy many-body effects of graphene in a unified approach. arXiv:2409.17645, 2024.

[191] Francesco Macheda, Paolo Barone, and Francesco Mauri. Electron-phonon interaction and longitudinal-transverse phonon splitting in doped semiconductors. Phys. Rev. Lett., 129:185902, Oct 2022.

[192] Massimiliano Stengel. Flexoelectricity from density-functional perturbation theory. Phys. Rev. B, 88:174106, Nov 2013.

[193] Francesco Macheda, Thibault Sohier, Paolo Barone, and Francesco Mauri. Electron-phonon interaction and phonon frequencies in two-dimensional doped semiconductors. Phys. Rev. B, 107:094308, Mar 2023.

[194] Francesco Macheda, Paolo Barone, and Francesco Mauri. First-principles calculations of dynamical Born effective charges, quadrupoles, and higher order terms from the charge response in large semiconducting and metallic systems. Phys. Rev. B, 110:094306, Sep 2024.

[195] Kin Fai Mak, Long Ju, Feng Wang, and Tony F Heinz. Optical spectroscopy of graphene: From the far infrared to the ultraviolet. Solid state communications, 152(15):1341–1349, 2012.

[196] You-Chia Chang, Chang-Hua Liu, Che-Hung Liu, Zhaohui Zhong, and Theodore B Norris. Extracting the complex optical conductivity of mono-and bilayer graphene by ellipsometry. Applied Physics Letters, 104(26), 2014.

[197] Wei Li, Guangjun Cheng, Yiran Liang, Boyuan Tian, Xuelei Liang, Lianmao Peng, AR Hight Walker, David J Gundlach, and Nhan V Nguyen. Broadband optical properties of graphene by spectroscopic ellipsometry. Carbon, 99:348–353, 2016.

[198] Giovanni Marini, Guglielmo Marchese, Gianni Profeta, Jelena Sjakste, Francesco Macheda, Nathalie Vast, Francesco Mauri, and Matteo Calandra. Epiq: an open-source software for the calculation of electron-phonon interaction related properties. Computer Physics Communications, 295:108950, 2024.

[199] Hyungjun Lee, Samuel Poncé, Kyle Bushick, Samad Hajinazar, Jon Lafuente-Bartolome, Joshua Leveillee, Chao Lian, Jae-Mo Lihm, Francesco Macheda, Hitoshi Mori, Hari Paudyal, Weng Hong Sio, Sabyasachi Tiwari, Marios Zacharias, Xiao Zhang, Nicola Bonini, Emmanouil Kioupakis, Elena R. Margine, and Feliciano Giustino. Electron–phonon physics from first principles using the epw code. npj Computational Materials, 9(1):156, Aug 2023.

[200] Đorđe Dangić, Giovanni Caldarelli, Raffaello Bianco, Ivana Savić, and Ion Errea. Lattice thermal conductivity in the anharmonic overdamped regime. arXiv preprint arXiv:2410.13485, 2024.

[201] Guglielmo Marchese, Francesco Macheda, Luca Binci, Matteo Calandra, Paolo Barone, and Francesco Mauri. Born effective charges and vibrational spectra in superconducting and bad conducting metals. Nature Physics, 20(1):88–94, 2024.